

A group of approximately 30 people, including men and women of various ages, are standing on a balcony of a modern building. The building features a prominent glass facade with a grid pattern and a section with a textured stone or brick facade. The sky is clear and blue. The text is overlaid on the top left of the image.

Reliability *and* Optimization of Structural Systems

Editors:

Armen Der Kiureghian

Aram Hajian

AUA Press
Yerevan, Armenia

Proceedings of the sixteenth working conference of the International Federation of Information Processing (IFIP) Working Group 7.5 on Reliability and Optimization of Structural Systems, Yerevan, Armenia, June 24-27, 2012

Reliability and Optimization of Structural Systems

Editors

A. Der Kiureghian

*Department of Civil and Environmental Engineering
University of California, Berkeley*


A. Hajian

*College of Science and Engineering
American University of Armenia, Yerevan*

624.17
INT

American University of Armenia Press
Yerevan, Armenia

© 2012 American University of Armenia, Yerevan, Armenia

Printed and bound in Yerevan, Armenia, by  "Printinfo", www.printinfo.am

Photos: (front cover and on pages v, vi) by Artak Hambarian, AUA, Armenia;
(pages vii, viii) by Nikolay Dimitrov, DTU, Denmark.

All rights reserved. No part of this publication or the information contained herein may be reproduced, stored in a retrieval system, or transmitted in any form or by any means, electronic, mechanical, by photocopying, recording or otherwise, without written prior permission from the publisher.

Although all care is taken to ensure integrity and quality of this publication and the information herein, no responsibility is assumed by the publisher nor the editors for any damage to the property or persons as a result of operation or use of this publication and/or the information contained herein.

Published by: American University of Armenia
40 Baghramyan Avenue
Yerevan 0019, Republic of Armenia
www.aua.am
e-mail: ifip2012@aua.am

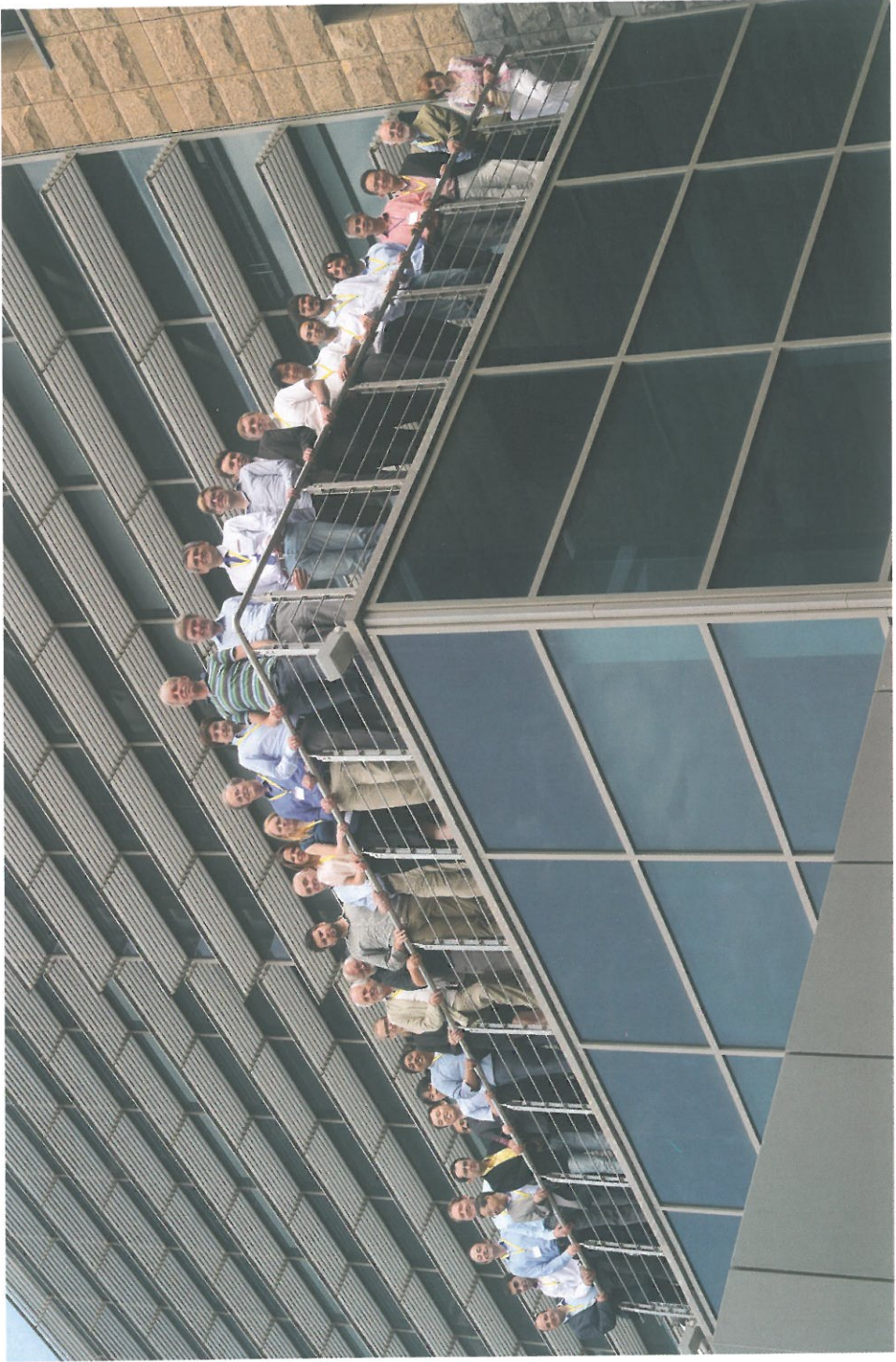
ISBN: 978-0-9657429-0-0

Table of Contents

Preface

Reliability-based design optimization with uncertain cost <i>T. Haukaas & M. Mahsuli</i>	1
Sequential selection of an optimal operating window <i>M.A. Maes & A. Naess</i>	9
Life-cycle cost based optimal design of fluid viscous dampers <i>A.A. Taflanidis & I. Gidaris</i>	17
Optimization of sequential decisions by least squares Monte Carlo method <i>K. Nishijima & A. Anders</i>	25
Enhanced least squares Monte Carlo method for real-time decision optimizations for evolving natural hazards <i>A. Anders & K. Nishijima</i>	33
Sensitivity analysis methods for reliability problems <i>K.W. Breitung</i>	41
slangTNG – Scriptable software for stochastic structural analysis <i>C. Bucher & S. Wolff</i>	49
Reliability analysis of structure using metaheuristic method <i>K. Nakatsu, H. Furuta, K. Takahashi, K. Ishibashi & K. Ando</i>	57
Designing for wind actions based on time-domain analysis: Accounting for statistical uncertainty <i>D. Straub, I. Papaioannou & A. Michalski</i>	65
Adaptive importance sampling using nonparametric density function <i>N. Kutz & J. Song</i>	75
Enhancing meta-model-based importance sampling by subset simulation <i>B. Sudret, V. Dubourg & J.-M. Bourinet</i>	83
Assessment of MCMC algorithms for subset simulation <i>I. Papaioannou, K. Zwirgmaier & D. Straub</i>	91
Identification and reliability of reinforced concrete structural systems for model updating purposes <i>S. Sessa, F. Marmo & N. Valoroso</i>	103
Reliability analysis for adhesive bonded composite stepped lap joints loaded in fatigue <i>A. Kimiaeifar, J.D. Sørensen, E. Lund & O.T. Thomsen</i>	111
Multi-dimensional risk interdependence analysis for buildings and building users <i>G. Ginda & M. Maślak</i>	119
Truck load modeling for reliability based code calibration <i>G. Fu, P. Yen, J. You & L. Liu</i>	127

Structural reliability methods for wind power converter system component reliability assessment <i>E.E. Kostandyan & J.D. Sørensen</i>	135
Reliability of offshore wind turbines subject to seismic loading <i>M. Mardfekri & P. Gardoni</i>	143
Reduction of the random variables of the turbulent wind field <i>M.T. Sichani & S.R.K. Nielsen</i>	151
Some observations on the subset simulation related to the wind turbine mechanics <i>M.T. Sichani, S.R.K. Nielsen & P. Thoft-Christensen</i>	159
Fatigue reliability of offshore wind turbine systems <i>S. Márquez-Domínguez & J.D. Sørensen</i>	167
Maintenance optimization for offshore wind turbines using POMDP <i>J.S. Nielsen & J.D. Sørensen</i>	175
System reliability effects in wind turbine blades <i>N. Dimitrov, P. Friis-Hansen & C. Berggreen</i>	183
Bayesian network with Gaussian variables for post-earthquake emergency management <i>M. Pozzi, A. Der Kiureghian, Y. Yue & D. Zonta</i>	191
Probabilistic modeling of networked systems for risk assessment <i>J. Qin & M.H. Faber</i>	199
Fragility curves for bridges under differential support motions <i>K. Konakli</i>	207
Bridge management system for a large number of bridges using genetic algorithms <i>K. Nakatsu, H. Furuta, K. Takahashi, K. Ishibashi & T. Umekage</i>	215
Short-term instability in stochastic systems <i>M.F. Dimentberg, C. Bucher, A. Hera & A. Naess</i>	223
Tolling contracts <i>H. Kechejian & V.K. Ohanyan</i>	231
An alternative linear response surface method for stochastic dynamic analysis <i>U. Alibrandi</i>	237
FORM in high dimensions for stochastic dynamic analysis <i>S.D. Koduru & A. Der Kiureghian</i>	245
Discretization of stochastic processes in time domain by <i>sinc</i> basis functions and application in TELM analysis <i>M. Broccardo & A. Der Kiureghian</i>	253
Author index	261



Conference participants on the terrace of AUA Paramaz Avedisian Building



Conference participants at Ashtaraki Dzor



Participants at Garni Temple (1st century AD)



Participants at Genocide Memorial

Preface

These are the proceedings of the sixteenth working conference of the International Federation of Information Processing (IFIP) Working Group 7.5 on Reliability and Optimization of Structural Systems, which took place at the American University of Armenia, Yerevan, on June 24-27, 2012. This volume contains 32 papers presented at the conference.

The conference was supported by IFIP TC-7, IFIP's technical committee on Modeling and Optimization, the University of California at Berkeley, and the American University of Armenia (AUA). This support is greatly acknowledged. AUA is a young university founded in 1991, in affiliation with the University of California, through the efforts of three American-Armenian academics, including the first co-editor of this volume. AUA provided excellent facilities in its new Paramaz Avedisian Building and superb logistical support for this gathering.

The purpose of the Working Group 7.5 is to promote modern theories and methods of structural and system reliability and optimization; to stimulate research, development and application of structural and system reliability and optimization theories; to further the dissemination and exchange of information on reliability and optimization of structural systems; and to encourage education in structural and system reliability and optimization theories.

The main themes of the conference were structural and system reliability methods, probabilistic models, engineering risk analysis and decision making, stochastic systems, reliability-based optimal design, and applications in various civil engineering domains, including infrastructure systems, wind turbines, bridges, natural hazards, and seismic analysis. The conference was marked by lively discussions and noteworthy participation of several young researchers, who presented valuable contributions to the field and brought new viewpoints to the discussion.

As of June 2012, the IFIP Working Group 7.5 has the membership listed below. Also listed are members of the Scientific Committee and the local Organizing Committee. Many of the researchers and practitioners listed below played active roles in the scientific program of the conference.

- | | |
|----------------------------------|--|
| U. Alibrandi, Italy | A. Nowak, USA |
| A. Anders, Denmark | V. Ohanyan, Armenia |
| K. Ando, Japan | M.D. Panday, Canada |
| A.H.-S. Ang, USA | I. Papaioannou, Germany |
| G. Augusti, Italy | M. Pozzi, USA |
| F. Biondini, Italy | J. Qin, Switzerland |
| F. Bontempi, Italy | J.O. Royset, USA |
| A. Borri, Italy | S. Ruiz, Mexico |
| K. Breitung, Germany | M. Sakano, Japan |
| M. Broccardo, USA | T. Sato, Japan |
| C. Bucher, Austria | S. Sessa, Italy |
| J. Casas, Spain | N. Shetty, UK |
| H.N. Cho, South Korea | W. Shiraki, Japan |
| M. Ciampoli, Italy | M.T. Sichani, Denmark |
| R. Corotis, USA | P. Sniady, Poland |
| D. De Leon, Mexico | J. Song, USA |
| A. Der Kiureghian, USA | J. Sørensen, Denmark |
| M. Dimentberg, USA | D. Straub, Germany (Vice-chair) |
| N. Dimitrov, Denmark | B. Sudret, France |
| O. Ditlevsen, Denmark | M.M. Szerszen, USA |
| M. Dogaki, Japan | A. Taflanidis, USA |
| H. Ellis, USA | N.J. Tarp-Johansen, Denmark |
| L. Esteva, Mexico (Former Chair) | P. Thoft-Christensen, Denmark (former Chair) |
| M.H. Faber, Switzerland (Chair) | T. Umekage, Japan |
| D.M. Frangopol, USA | P. Waarts, The Netherlands |

G. Fu, USA
 H. Furuta, Japan
 P. Gardoni, USA
 G. Ginda, Poland
 M. Gioffre, Italy
 M. Grigoriu, USA
 C. Guedes-Soares, Portugal
 T. Haukaas, Canada
 E. Heredia-Zavoni, Mexico
 H. Hong, Canada
 J. Li, China
 M. Kawatani, Japan
 C.W. Kim, Japan
 A. Kimiaefar, Denmark
 S. Koduru, Canada
 N. Kogiso, Japan
 K. Konakli, Denmark
 E.E. Kostandyan, Denmark
 M. Lemaire, France
 M.A. Maes, Canada
 K. Marti, Germany
 S. Márquez-Dominguez, Denmark
 M. Máslak, Poland
 R. Melchers, Australia
 Y. Murotsu, Japan
 A. Naess, Norway
 J.J. Nielson, Denmark
 S.R.K. Nielson, Denmark
 K. Nishijima, Denmark

W.-K. Wen, USA
 Z. Zembaty, Poland
 Y. Zhao, Japan

Scientific Committee

A. H.-S. Ang, USA
 C. Bucher, Austria
 A. Der Kiureghian, USA
 L. Esteva, Mexico
 M.H. Faber, Denmark
 D. Frangopol, USA
 H. Furuta, Japan
 A. Naess, Norway
 A. Nowak, USA
 R. Melchers, Australia
 M. Panday, Canada
 J.O. Royset, USA
 J. Song, USA
 J.D. Sørensen, Denmark
 D. Straub, Germany
 B. Sudret, France

Organizing Committee

Armen Der Kiureghian, Chair
 Rubina Danilova, Secretary
 Aram Hajian
 Suren Khachatryan
 Sargis Zeytounyan

Results from previous conferences have been published in the following proceedings:

1. Reliability and optimization of structural systems. Proceedings of the first IFIP WG 7.5 working conference, Aalborg, Denmark, May 6- 8, 1987 (ed. P. Thoft-Christensen). Lecture notes in engineering, Vol. 33, Springer-Verlag Berlin Heidelberg New York.
2. Reliability and optimization of structural systems. Proceedings of the second IFIP WG 7.5 working conference, London, UK, Sept. 26- 28, 1988 (ed. P. Thoft-Christensen). Lecture notes in engineering, Vol. 48, Springer-Verlag Berlin Heidelberg New York.
3. Reliability and optimization of structural systems. Proceedings of the third IFIP WG 7.5 working conference, Berkeley, California, USA, Mar. 26- 27, 1990 (eds. A. Der Kiureghian and P. Thoft-Christensen). Lecture notes in engineering, Vol. 61 , Springer-Verlag Berlin Heidelberg New York.
4. Reliability and optimization of structural systems. Proceedings of the fourth IFIP WG 7.5 working conference, Munich, Germany, Sept. 11 - 13, 1991 (eds. R. Rackwitz and P. Thoft-Christensen). Lecture notes in engineering, Vol. 76, Springer-Verlag Berlin Heidelberg New York.
5. Reliability and optimization of structural systems. Proceedings of the fifth IFIP WG 7.5 working conference, Takamatsu, Kagawa, Japan, March 22- 26, 1993 (eds. P. Thoft-Christensen and H. Ishikawa). IFIP transactions B-12, Applications in technology, Elsevier Science Publishers B. V, Amsterdam.

6. Reliability and optimization of structural systems. Proceedings of the sixth IFIP WG 7.5 working conference, Assisi, Italy, Sept. 7- 9, 1994 (eds. R. Rackwitz, G. Augusti , A. Bori), 1995 Chapman & Hall, London.
7. Reliability and optimization of structural systems. Proceedings of the seventh IFIP WG 7.5 working Conference, Boulder, CO, USA, April 2--4, 1996 (eds. D.M. Frangopol, R.B. Corotis, and R. Rackwitz).
8. Reliability and optimization of structural systems. Proceedings of the eighth IFIP WG 7.5 working conference, Krakow, Poland, May 11 - 13, 1998 (eds. A.S. Nowak and M.M. Szerszen), University of Michigan, Ann Arbor, MI, USA.
9. Reliability and optimization of structural systems. Proceedings of the ninth IFIP WG 7.5 working conference, University of Ann Arbor, Michigan, Sept. 25- 27, 2000 (eds. A.S. Nowak and M.M. Szerszen), University of Michigan, Ann Arbor, MI, USA.
10. Reliability and optimization of structural systems. Proceedings of the tenth IFIP WG 7.5 working conference, Kansai University, Osaka, Japan, Mar. 25- 27, 2002 (eds. H. Furuta, M. Dogaki and M. Sakano), A.A. Balkema Publishers.
11. Reliability and optimization of structural systems. Proceedings of the eleventh IFIP WG 7.5 working conference, Banff, Canada, Nov. 2- 5, 2003 (eds. M. Maes and L. Huysse), A. A. Balkema Publishers.
12. Advances in Reliability and Optimization of Structural Systems. Proceedings of the twelfth IFIP WG 7.5 working conference, Aalborg, Denmark, May 22-25, 2005 (eds. J.D. Sørensen and D.M. Frangopol), Taylor and Francis/Balkema.
13. Reliability and Optimization of Structural Systems. Proceedings of the thirteenth IFIP WG 7.5 working conference, Kobe, Japan, Oct 11-14, 2006 (eds. D.M. Frangopol, M. Kawatani and C.-W. Kim), Taylor and Francis/Balkema.
14. Reliability and Optimization of Structural Systems. Proceedings of the fourteenth IFIP WG 7.5 working conference, Toluca, Mexico, Aug 6-9, 2008 (CD version; ed. L. Esteva), Institute of Engineering, National University of Mexico, lestevam@iingen.unam.mx).
15. Reliability and Optimization of Structural Systems. Proceedings of the fifteenth IFIP WG 7.5 working conference, Technical University of Munich, Germany, April 7-10, 2010 (ed. D. Straub), CRC Press, Taylor & Francis Group.

The editors wish to thank their team and the many other AUA staff members who helped with the organization of the conference and publication of this volume. We also express our thanks to the authors of the published papers and other participants of the conference. Without their excellent contributions, the Yerevan conference would not have been successful.

Armen Der Kiureghian

Aram Hajian

American University of Armenia, Yerevan

Reliability-based design optimization with uncertain cost

T. Haukaas & M. Mahsuli

University of British Columbia, Vancouver, Canada

ABSTRACT: This paper presents techniques for estimation of seismic losses, followed by a discussion of how to define and minimize the associated seismic risk. The backdrop for the developments is a new computer program, called *Rt*, which runs reliability analyses in conjunction with many probabilistic models. A library of probabilistic models for hazards, response, damage, and loss is implemented in *Rt*. These models are employed in this paper for seismic loss estimation. Upon computing the all-important cost exceedance probability curve, risk measures are defined and minimized. A numerical example is presented, in which 622 buildings are subjected to multiple sources of seismic hazard. The cost of retrofit of the building stock is included in the probability curve, which facilitates the computation of the optimum level of retrofit.

1 INTRODUCTION

The context for this paper is seismic loss estimation, and the ultimate objective is to minimize the total cost associated with earthquakes. In the application considered here, the cost stems from repair of buildings that are damaged by earthquakes. However, the definition of cost and the proposed optimization approach are intended to have broader applicability. Given appropriate models, the cost may include other direct and indirect contributions, such as cost associated with business interruption during repair. In fact, the cost should be interpreted as a general measure of negative utility. Furthermore, the developments related to optimization, i.e. minimization of risk, are related to a broad class of problems where the outcome of a scalar utility measure is both uncertain and dependent on decision variables. From this viewpoint, relevant applications are found as far afield as in the financial sector.

The fact that the cost of earthquakes is modeled as a random variable does not imply that a simple standard distribution suffices to characterize its uncertainty. On the contrary, an array of probabilistic models is required to evaluate the total cost. Even when employing analytical methods to evaluate repair cost and other performance metrics, separate models are required for hazard, structure, damage, and performance (Baker and Cornell 2008; Cornell and Krawinkler 2000). The present study places particular emphasis on modeling, for several reasons. One obvious motive is that engineers continually strive to improve the models that form the basis for design and retrofit decisions. Another reason is the aspiration to employ the power and versatility of reliability methods to compute cost probabilities (Haukaas 2008). Importantly, the reliability-based approach provides the opportunity to develop new and powerful models with Bayesian techniques.

The problem addressed in this paper has five ingredients: probabilistic models, reliability methods, a cost exceedance probability curve (EP curve), risk measures, and optimization methods. These ingredients are described in subsequent sections, but a few general observations are first made: It is noted that probabilistic models are at the heart of the computations, and the

quality of the results depends on the quality of the modeling. The models serve to predict the outcome of physical quantities related to hazard, response, damage, and cost, with due account of uncertainties. In turn, reliability methods utilize the probabilistic models to compute the EP curve, or points on that curve. The EP curve is essentially the probability distribution of the cost associated with a building or a region. Provided the EP curve, the next question is how decisions will affect it. To quantify this, it is useful to introduce scalar surrogate measures based on the EP curve, called risk measures. Finally, optimization is carried out to reduce the value of those risk measures. The following sections discuss these ingredients in greater detail, starting with the computer program that is tailored to carry out this type of analysis.

2 COMPUTER PROGRAM

Software applications for structural reliability analysis have been developed since the early 1980's. In fact, a variety of computer programs are presently available for structural reliability computations (Pellissetti and Schuëller 2006). Although several of these programs are capable of handling multiple limit-state functions and even complex finite element models, a new challenge is posed in this study: Reliability analysis with many advanced probabilistic models requires a new type of computer program to orchestrate multi-model analysis. The new computer program Rt has been developed for this purpose (Mahsuli and Haukaas 2012).

Rt is freely downloadable at www.inrisk.ubc.ca, together with examples and tutorials to help the user get started. The primary objective with Rt is to run reliability and optimization analysis in which limit-state functions, objective functions, and constraint functions require the evaluation of many probabilistic models. A typical example is seismic risk analysis, which warrants an array of models for hazard, response, damage, and cost. The key novelties in Rt are in the module that contains the models, parameters, and function. Conversely, the analysis methods in Rt, such as FORM, SORM, and optimization algorithms, are similar to those found in most other reliability and optimization software.

3 PROBABILISTIC MODELS

Rt contains a steadily growing collection of probabilistic models. The responses from a model enter either as input to another model or as input to a function, and all responses are physical measurable quantities. In other words, the models simulate physical phenomena, and no model produces a probability as output, as is the case for fragility curves and other conditional probability models used elsewhere.

This paper presents the results of a comprehensive seismic risk analysis of the 622 buildings on the campus of the University of British Columbia in Vancouver, Canada. The types of models that are employed to model this problem range from earthquake magnitude to building damage and repair cost. The region is subjected to three sources of seismicity: Shallow crustal earthquakes, deep subcrustal earthquakes, and megathrust subduction earthquakes. The first two are modeled as area sources, while subduction earthquakes originate from a line source. In turn, each building is associated with a separate model for displacement response, acceleration response, damage, and repair cost. In short, a total of 4,389 instances of 14 model types are utilized to model the problem in Rt. Furthermore, 8,097 response objects are employed to convey responses from one model to another, and ultimately to the function that represents repair cost. All uncertainty, except the uncertainty in earthquake occurrence times that is described by Poisson point processes, is described by a total of 281 random variables, which enter into the computations in each model.

4 RELIABILITY METHODS

The objective of the probabilistic analysis in this paper is to determine the probability of exceedance at different cost thresholds. Two analysis options are available in Rt for this purpose. Both are capable of multi-hazard analysis, which is required in the considered example due to

the presence of multiple earthquake sources. One of the analysis options is based on Monte Carlo sampling, and the other is based on FORM in conjunction with the load coincidence method (Wen 1990). For the purpose of the subsequent discussions, the exceedance probabilities from Monte Carlo sampling for a 50-year time period is shown by the solid line in Figure 1. It is noted that the cost-exceedance probabilities diminish rapidly as the cost threshold increases. For example, the probability of exceeding \$100M is 0.0365, while the probability of exceeding \$500 is 0.0071. These two results are associated with 1.62% and 3.74% coefficient of variation, respectively, and are obtained by Monte Carlo sampling with 100,000 samples.

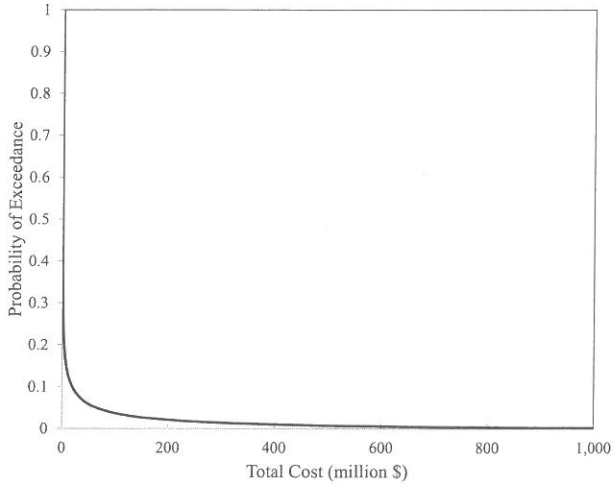


Figure 1: Exceedance probability curve for the UBC campus obtained by scenario sampling.

5 MEASURES OF RISK

A long-standing tenet of decision-making under uncertainty is to base decisions on expected cost, or more generally, on expected utility. This approach is the foundation for reliability-based design optimization, where the expected cost of failure is defined as the product of the failure probability and the failure cost. However, the computation of the entire EP curve in contemporary earthquake engineering and other fields renders vastly more information available than the mean cost. This fact, together with the possibility of incorporating risk averseness, as well as possible applications in the insurance industry and the financial sector, motivates the exploration of risk measures beyond expected cost. In fact, in spite of steadfast consensus in the engineering community that decisions under uncertainty should be risk-based, specific definitions of risk are often elusive. Beyond expected cost, a variety of definitions and interpretations of risk emerge. A large body of literature is available, and it is apparent that convergence to an omnipotent risk measure is either an oxymoron or far away (Aven 2012; Bernstein 1998). This implies that the basis for risk-based decisions, i.e. the definition of risk, must be carefully examined on a case-by-case basis.

Coherency requirements for risk measures have received significant attention in recent years (Artzner et al. 1999; Rockafellar and Royset 2010; Rockafellar 2007). These requirements constitute a useful mathematical framework, but it is also necessary to examine each potential risk measure from another perspective: How does it reflect the preferences of the decision maker? For example, some decision makers may be concerned primarily with the mean annual cost, while others may be concerned with the costs in the far tail of the EP curve. Furthermore, a risk measure that encompasses the entire EP curve and facilitates minimization of the cost probability at all cost levels may be of interest, regardless of its satisfaction of the mathematical coherency requirements. Another example of the complexity involved in selecting a risk measure is that minimization of tail cost can actually increase the mean cost (Haukaas 2008).

In the following, scalar risk measures extracted from the EP curve are denoted by r . The random variable that represents the cost is denoted C , and its realizations are denoted c . The probability density function is denoted $f(c)$, the cumulative distribution function is denoted $F(c)$, and the EP curve, which essentially is the complementary cumulative distribution function, is denoted $G(c)$. From elementary statistics it is understood that the probability density function and the EP curve have the relationship

$$f(c) = -\frac{dG(c)}{dc} \Leftrightarrow G(c) = \int_c^{\infty} f(c)dc \quad (1)$$

The inverse cumulative distribution function is denoted $F^{-1}(p)$, and similarly the inverse EP curve is denoted $G^{-1}(p)$. As a result, $G^{-1}(p)$ is the cost that has probability p of being exceeded. Following this notation, several risk measures are expressed below in terms of the EP curve. Perhaps the most basic risk measure is the mean seismic cost:

$$r_1 = \mu_C = -\int_{-\infty}^{\infty} c \cdot \frac{dG(c)}{dc} dc \quad (2)$$

and the standard deviation:

$$r_2 = \sigma_C = -\int_{-\infty}^{\infty} (c - \mu_C)^2 \cdot \frac{dG(c)}{dc} dc \quad (3)$$

In terms of measures that address the tail of the EP curve, two basic risk measures are defined as (Haukaas 2008)

$$r_3(p) = G^{-1}(p) \quad (4)$$

and

$$r_4(c) = G(c) \quad (5)$$

A reduction in r_3 implies a reduction in the cost that has probability p of being exceeded, while a reduction in r_4 implies a reduction in the probability of exceeding the cost c . Another risk measure is

$$r_5(\tau) = -\int_{\tau}^{\infty} c \cdot \frac{dG(c)}{dc} dc \quad (6)$$

which is the expectation of the costs that lie above the threshold τ .

The tail-measures presented so far require the selection of the value of p , c , or τ . Furthermore, because the measures r_3 , r_4 , and r_5 are defined in the tail, it can be argued that none of them employ all the information contained in the EP curve. An alternative that remedies this problem, while also circumventing the selection of an *ad hoc* parameter value, is the second moment of the cost:

$$r_6 = E[C^2] = \sigma_C^2 + \mu_C^2 = -\int_{-\infty}^{\infty} c^2 \cdot \frac{dG(c)}{dc} dc \quad (7)$$

A reduction in r_6 implies that the tail of the EP curve is “pulled” downwards. This is an appealing property because it implies that the highest costs are penalized the most. In fact, the higher the order of the moment, the more the costs in the tail are penalized. Thus, r_6 and perhaps higher moments appear to be an appealing class of risk measures in the context of minimizing overall costs due to earthquakes.

6 OPTIMIZATION

So far, the discussion in this paper has focused on the computation of the EP curve, and the extraction of risk measures from it. However, the ultimate objective is to make decisions that min-

imize the seismic risk. To facilitate such optimization, this study introduces a decision variable that influences the cost. This is one reason why the word cost is preferred in this paper instead of the narrower meaning of the word loss. Importantly, the cost of changing the value of the decision variable is included in the total cost. To this end, reconsider the portfolio of buildings that was described earlier. To estimate the optimal amount of retrofit needed for this portfolio, the building strength parameter, d , is introduced. To understand its definition it is necessary to examine the building response model and the construction cost model that are employed in the analysis example. The displacement response of each building, measured as peak drift ratio, δ_p , is modeled by

$$\ln(\delta_p) = \theta_1 + \theta_2 \ln(\delta_y) + \theta_3 \ln(\delta_u) - \theta_4 \ln((1+d) \cdot V) - \theta_5 \ln(\kappa) + \theta_6 \ln(Sa) + \theta_7 Sa + \varepsilon \quad (8)$$

where δ_y =yield drift ratio, δ_u =ultimate drift ratio, V =lateral strength-to-weight ratio, κ =degradation factor, Sa =5%-damped spectral acceleration at the building period computed at the building location, and ε is the model error. It is observed that d is a dimensionless measure that affects the lateral seismic strength of the building. Practically, an increase in d is achieved by adding shear walls to a structure, or similar retrofit measures. Because d enters in the multiplication factor $(1+d)$ it is clear that $d=0$ implies no retrofit while $d>0$ implies a strengthening. The latter results in a reduction in δ_p and thus a reduction in ensuing damage and repair costs. It is also noted that an increase in strength is usually accompanied by an increase in stiffness. However, under the assumption that strength and stiffness increase proportionally, the parameters δ_y and δ_u remain unchanged, because they depend solely on the strength-to-stiffness ratio.

The decision variable also enters the model that predicts incremental construction cost associated with retrofit, which reads

$$c_o = d \cdot (\gamma \cdot C_s \cdot A) \cdot \left(\frac{7-\alpha}{4} \right) \cdot \varepsilon_o \quad (9)$$

where γ =ratio of the cost of the lateral force resisting system to the total structural cost, C_s =structural cost per unit floor area, A =total floor area, α =code-level factor that expresses the strength of the building prior to retrofit, and ε_o =model error factor. α is defined so that $\alpha=1$ for buildings that are built prior to seismic standards, $\alpha=2$ for low-code, $\alpha=3$ for moderate code, and $\alpha=4$ for building built to high seismic standards. The fraction in Eq. (9) is included because it is assumed that buildings built to high standards cost 25% less to retrofit than the moderate code level, while pre-code buildings cost 50% more to retrofit than the moderate code level.

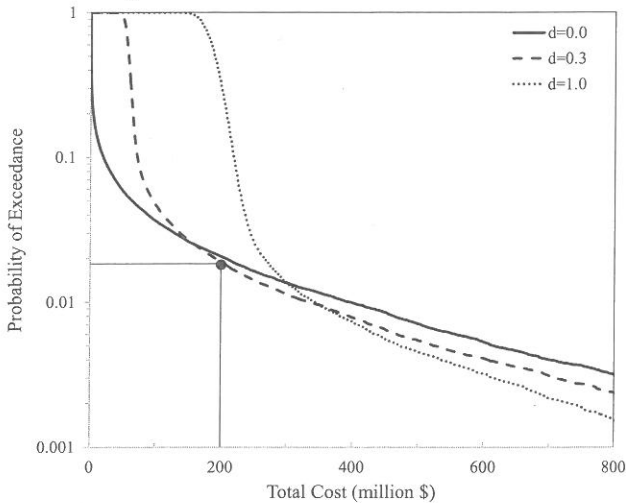


Figure 2: EP curves for three different values of d .

The ultimate objective in the numerical example is to determine the optimum value of d , i.e. the optimum amount of retrofit. First, the risk measure $r_4(c)$ with $c=\$200\text{M}$ is considered. The use of $r_4(\$200\text{M})$ implies that the decision maker is concerned about the probability that the cost exceeds $\$200\text{M}$, including money spent on retrofit. To expose the nature of this problem, a graphical approach is explored. As a starting point, reconsider Figure 1, which shows the EP curve for the portfolio of 622 buildings for $d=0$, i.e. no retrofit. In order to study the tail probabilities, the EP curve is reproduced in a logarithmic scale in Figure 2. The solid line in Figure 2 is the same as the solid line in Figure 1. Careful inspection reveals that $r_4(\$200\text{M})=0.0207$ for $d=0$.

Next, several new analyses are carried out with values of d varying from no retrofit ($d=0$) to comprehensive retrofit ($d=1$). The significant difference in the EP curve for these two alternatives is exposed in Figure 2, where they are plotted as solid and dotted lines, respectively. Next, consider Figure 3, which shows the “EP surface” that is obtained by continuously varying d from 0 to 1. It is observed that the dotted line in Figure 2, which tracks the value of $r_4(\$200\text{M})$, exhibits the bath-tub variation that is characteristic for most objective functions. This means that the cost exceedance probability first tends to decrease when d is increased from 0. At around $d=0.3$, however, the construction cost outweighs the gain from reduced damage and the trend is reversed. In other words, $d^*=0.3$ for $r_4(\$200\text{M})$. The EP curve for $d=0.3$ is shown as a dashed line in Figure 2, which confirms that this optimum, shown as a solid dot, is indeed associated with smaller probability than both $d=0$ and $d=1$. To be precise, the thin straight lines in Figure 2 reveal that the value of $r_4(\$200\text{M})$ at the optimum is 0.0189.

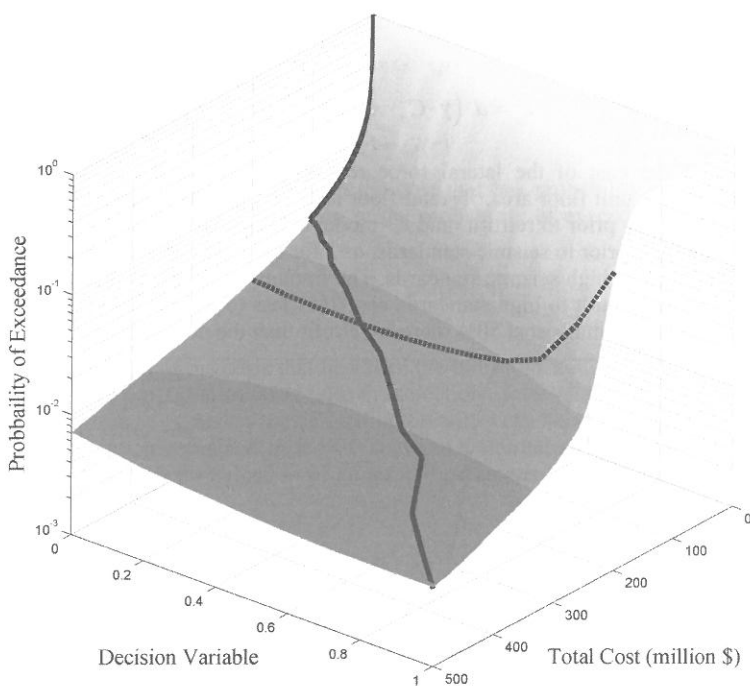


Figure 3: EP surface.

The discussion in the previous paragraph is predicated on the threshold $c=\$200\text{M}$ in $r_4(c)$. This value of c is arbitrarily chosen. It is therefore of interest to broaden the discussion to other cost thresholds in $r_4(c)$. To this end, it is first observed from the curvature of the surface in Fig-

ure 3 that d^* appears to be relatively low for low values of c , while d^* appears to increase when c increases. This is confirmed by the solid line in Figure 3, which traces d^* for different values of the cost threshold c . It is understood from above that the intersection between the solid and dashed lines in Figure 3 identifies the optimum associated with r_4 (\$200M), namely $d^*=0.3$. Closer inspection of the solid line in Figure 3 reveals that the optimum is $d^*=0$ up to $c=\$106M$, and that d^* increases almost linearly with c thereafter. In other words, a decision maker who is concerned with high cost thresholds should spend more resources on retrofit according to the risk measure $r_4(c)$.

Another risk measure that can be evaluated by direct inspection of the EP curve is $r_3(p)$, which is essentially the inverse of $r_4(c)$ with respect to the EP curve. In the same way as it was necessary to select the value of c to evaluate r_4 , it is necessary to select the probability level p to evaluate r_3 . A natural choice of p is 2% in 50 years, because this is the probability level, or “risk tolerance level,” specified by the National Building Code of Canada for the seismic hazard (IRC 2010). Coincidentally, the risk measure $r_3(0.02\text{-in-50-years})$ is easily evaluated here because the presented EP curves show probabilities for a 50-year time period. In fact, the contour lines of the EP surface in Figure 3, visible as borderlines between the different shades of gray, trace d^* for fixed probability values, again exhibiting the characteristic bath-tub variation. Such plots have revealed that the optimum level of retrofit increases from $d=0$ once small probability values are considered. As an example, $d^*\approx 0.12$ when the cost is minimized at the probability level 2%-in-50-years. The corresponding minimum cost is \$162M, i.e. $r_3(0.02\text{-in-50-years})=\$162M$. This suggests that the buildings should be strengthened by almost 12% according to a cost-benefit analysis at the risk tolerance level set forth by the code. However, it is stressed that the selection of this risk tolerance level must be scrutinized before making final recommendations.

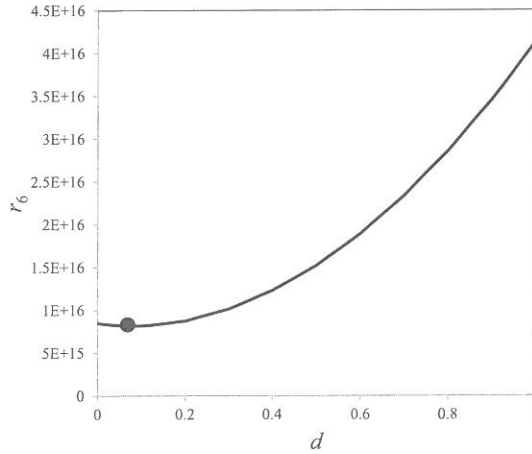


Figure 4: Variation of r_6 with d .

While the risk measures r_3 and r_4 can be evaluated by inspection of the EP curves, attention is now turned to expectation-based risk measures, which require the evaluation of an integral. In particular, it was mentioned earlier that the mean square, r_6 , appears to have appealing properties. Figure 4 shows the variation of r_6 with d , evaluated with the same 100,000 samples as previously used. Again, the bath-tub variation of the risk measure as d is varied is observed. Examination of Figure 4 reveals that $d^*=0.08$ for r_6 . This result has the advantage that it is invariant to the subjective selection of values for c and p in r_3 and r_4 . However, it may be argued that, statistical moments of higher order than r_6 , i.e. higher penalization of high costs, merit consideration. Although such results are omitted here, preliminary studies suggest that the consideration of higher statistical moments yields higher values of d^* . In short, the optimum design depends quite strongly on the selection of risk measure, in addition to the quality of the probabilistic models that form the basis for all the presented results.

7 CONCLUSIONS

The premise for the developments in this paper is a comprehensive seismic risk analysis of a region that comprises 622 buildings. A new computer program, Rt, is tailored to carry out this type of analysis, which entails a large number of probabilistic models. This particular analysis included 14 model types, 4,389 model instances, 8,097 model responses, and 281 random variables. In the context of classical structural reliability software, Rt is unique in several aspects. Most importantly, Rt is a growing library of probabilistic models. The object-oriented parameterization of random variables, decision variables, and response in Rt is also unique, and facilitates the interaction between models at run-time. It is also noted that Rt computes model response sensitivities both by the direct differentiation method and the finite difference method. In fact, the response objects have a “smart” feature, which means that finite difference analysis requires re-run only of models that are affected by the parameter that is perturbed. Rt also has an interactive graphical user interface, which allows modification of analysis parameters at run-time. All these features were utilized in the analyses in this paper, where cost exceedance probability curves were produced. Based on these results, risk measures were extracted and subjected to minimization. In doing so, less focus was placed on coherency of the risk measures and more focus was placed on how a risk measure reflects the decision-maker’s preference. It was observed that several risk measures are available, and it was demonstrated that those risk measures exhibit behavior that make them suitable as basis for minimization of the uncertain cost of earthquakes.

8 ACKNOWLEDGEMENTS

The financial support from the Natural Science and Engineering Research Council of Canada through the Strategic Project Grant 336498-06 is gratefully acknowledged. Mojtaba Mahsuli thanks the Killam Trusts for support in the form of a Killam Doctoral Fellowship. The authors also thank Mr. Aprizal Kristijanto, who surveyed buildings at the campus of the University of British Columbia in Vancouver during a summer internship in the undergraduate program.

9 REFERENCES

- Artzner, P., Delbaen, F., and Eber, J. M. (1999). “Coherent measures of risk.” *Mathematical Finance*, 9(3), 203–228.
- Aven, T. (2012). “The risk concept—historical and recent development trends.” *Reliability Engineering & System Safety*, Elsevier, 99, 33–44.
- Baker, J. W., and Cornell, C. A. (2008). “Uncertainty propagation in probabilistic seismic loss estimation.” *Structural Safety*, 30(3), 236–252.
- Bernstein, P. L. (1998). *Against the Gods: The remarkable story of risk*. Wiley.
- Cornell, C. A., and Krawinkler, H. (2000). “Progress and challenges in seismic performance assessment.” *PEER Center News*, Vol. 3 No. 2, <<http://peer.berkeley.edu/news/2000spring/>>.
- Haukaas, T. (2008). “Unified reliability and design optimization for earthquake engineering.” *Probabilistic Engineering Mechanics*, 23(4), 471–481.
- IRC. (2010). “National Building Code of Canada.” Institute for Research in Construction.
- Mahsuli, M., and Haukaas, T. (2012). “A computer program for multi-model reliability and optimization analysis.” *Journal of Computing in Civil Engineering*, In press.
- Pellissetti, M. F., and Schuëller, G. I. (2006). “On general purpose software in structural reliability – An overview.” *Structural Safety*, 28(1-2), 3–16.
- Rockafellar, R. T. (2007). “Coherent approaches to risk in optimization under uncertainty.” *Tutorials in Operations Research*, T. Klastorin and P. Gray, eds., Institute for Operations Research and the Management Sciences, INFORMS, 38–61.
- Rockafellar, R. T., and Royset, J. O. (2010). “On buffered failure probability in design and optimization of structures.” *Reliability Engineering & System Safety*, Elsevier, 95(5), 499–510.
- Wen, Y. K. (1990). *Structural load modeling and combination for performance and safety evaluation*. Elsevier.

Sequential selection of an optimal operating window

M.A. Maes

University of Calgary, Canada

A. Naess

Norwegian University of Science and Technology, Trondheim, Norway

ABSTRACT: An important issue in construction, repair, maintenance and testing is the ability to select an optimal window of opportunity within a short-term period of time. This optimal window is typically governed by external variables, such as weather, or affected by operational conditions. A decision maker faces therefore sequential decisions to “start”, or to wait for “better” conditions. We examine how this problem is best formulated, which optimization criteria make sense from an engineering point of view, which kind of “stopping” rules can be used, and which stochastic solutions or solution methods are known and/or available. We also discuss how discounting affects the decision making and its outcome, as in many practical situations “waiting” comes with an expensive price tag. The effect on the outcome of the selection process of assuming a simple dependence structure between the opportunities is also assessed. To illustrate the various formulations of this problem, we contrast different criteria and decision rules, assuming different scenarios.

1 INTRODUCTION

Consider an engineering decision maker (DM) facing a finite sequence of opportunities and needs to decide, at each step in this sequence, whether to continue and wait for a better opportunity, or else to stop in the hope that this particular opportunity is the “best”. This setting has six fundamental aspects:

- (1) the decisions are made sequentially
- (2) the decisions at each step are binary: to turn down the opportunity, or to commit to it
- (3) the decisions are made online in real time
- (4) the decisions are irrevocable
- (5) the opportunities have a finite horizon
- (6) opportunities can be assessed fairly and ranked in a unique way

Examples include:

- waiting for favourable environmental conditions or for a suitable sea state window to perform a short-term operation; this situation is fairly typical in offshore, arctic, or harsh environments.
- scheduling testing, repair, and inspection activities that depend on favourable combinations of accessibility and down-time.
- contracting, hiring, and other sequential selection problems.
- selling large assets, with “offers” being the opportunities.

Notwithstanding the above commonalities, the problem can be formulated in many ways depending on:

- the criterion for optimality and the type of “valuation” of the opportunity
- the type of decision rule used
- the probabilistic structure of the sequence of opportunities

Accordingly, different selection schemes are to be expected depending on the problem formulation. The objective of this paper is to review the results and the techniques, and the optimal decision strategies for given model assumptions.

2 OBJECTIVES AND STRATEGIES

Assume a finite set of n opportunities that can be ranked in a unique way from best to poorest. A DM inspects each opportunity sequentially without “replacement”. Ranking presumes that it is possible to value each opportunity. This valuation depends on the objective of the sequential search which could be one of the following:

- Objective α -- searching for the (single) best opportunity; this requires us to assign a payoff of +1 for the best opportunity and 0 for all others. The objective is to maximize the expected return associated with the selection strategy, which is equivalent to selecting the top opportunity with the highest probability.
- Objective β -- to minimize the rank of the selected opportunity with 1 being the best, 2 the second-best, and so on.
- Objective γ -- to maximize the “value” of the selected opportunity. Objective α being rather strict, it is reasonable to consider that one would rather select a higher-valued than a lower-valued opportunity. There may after all be some benefit to an opportunity that is not necessarily the very best. This scheme assigns a scale of values x_1, x_2, \dots, x_n to each opportunity with (only) one permutation being the (unique) best-to-poorest ranking. The goal is then to maximize the expected value $E(X_\gamma)$ where X_γ is the one opportunity chosen online, and where the expectation is over all random orders as well as any random aspects of the selection algorithm.

To tackle such problems, we can use a variety of decision rules (DR), such as:

- DR1 -- Aspiration Strategy. In a first “exploratory” phase, opportunities are observed. Subsequently, the first opportunity that outranks all previous ones up to that point in time is selected. The length q of the exploratory phase needs to be optimized.
- DR2 -- q -th Exceedance Strategy. Select the q -th opportunity that exceeds all previous ones.
- DR3 -- Lousy Run Strategy. Select the first opportunity that outranks all previous ones after having observed q non-qualifying opportunities.
- DR4 -- Variable Acceptance Thresholds. Identify optimal value thresholds for each of the n “steps” in the selection process above which an opportunity is to be accepted, below which the search continues. This DR requires some prior information about the possible value structure.
- DR5 -- Constant Thresholds. Select the first or q -th opportunity that exceeds a predetermined threshold. Unlike DR4 this implies that there is a nonzero probability that no opportunity is actually selected.

3 OPPORTUNITIES WITH UNCERTAIN VALUE STRUCTURE

If, a priori, nothing is known about the structure of the search sequence, or about the “values” to be expected (other than there being exactly n opportunities), then a reasonable objective is to aim at selecting the (very) best opportunity in the sequence (Objective α in Section 2). This problem was originally considered by Johannes Kepler and is known as the secretary problem (Ferguson 1989). A large number of scientific publications exist in statistical literature of this emblematic problem where the goal is to hire the best secretary, by making an offer immediately after interviewing a candidate. The optimal strategy as shown by Ferguson (1989) is the “aspiration” strategy DR1. It consists in first observing exactly q opportunities in what we can treat as an exploration phase, and after that, to select the first opportunity that exceeds the aspiration level set during the exploration.

For large n , the optimal learning length q/n approaches $1/e = 0.368$ of the total number of opportunities. The probability of actually selecting the (very) best opportunity is a meagre $1/e \cong 36.8\%$ but no strategy can do better than this.

If however, the objective is, instead, to minimize the expected rank of the opportunity (Objective β in Section 2), then it can be shown (Chow et al., 1991) that the best expected rank one can achieve given a best strategy of the type DR1 is 3.86.

In both cases, it is important to realize that nothing is known about the opportunities X and that the only thing we can do is rank them, i.e. we can compare them vis-à-vis each other. The secretary type of strategy DR1 requires quite a long learning phase; 36.8% of opportunities must essentially be wasted. One might suspect this is caused by the fact that there is no cost for waiting but this is not the case (Mahdian et al., 2008). It is simply due to the fact that we consider no prior information about the opportunities, resulting in the equivalent of a worst-case distribution.

Another way of appreciating the DR1 aspiration strategy, is to note that Ferguson (1989) shows that the basic “secretary” formulation is in fact equivalent with the following game: let the “opponent” first select a cumulative probability distribution (cdf) $F(x)$ from which the opportunities X_i will be “drawn” independently. Any kind of $F(x)$ will do. The objective is to maximize the probability that the opportunity selected has the maximum value, or, equivalently, to maximize the expected value of the ratio of this value and the maximum value observed during the initial exploration phase.

Now assume that the opportunities have values X_i which form an random sample with an unknown pdf f and a cdf F . but make the “engineering” assumption that the hazard function $f(x)/(1-F(x))$ does not decrease with x , i.e. that the tail is at most exponential or light/bounded. In other words, given that an opportunity exceeds x , the likelihood that it is equal to x increases as x increases. This information alone considerably shortens the exploration phase of the aspiration optimal procedure used to select the best opportunity (Mahdian et al., 2008). Its duration is now only $n/\ln n$ which is considerably less than the n/e in the case of the “secretary” problem. Solutions corresponding to other objectives such as rank minimization are not available for this assumed problem set.

4 INDEPENDENT OPPORTUNITIES WITH KNOWN VALUE CDF

Prior knowledge of the distribution $F(x)$ and the pdf $f(x)$ of a random iid sequence of the opportunities X_i ($i = 1, \dots, n$) opens the door for an even more optimal selection procedure. Not surprisingly, the wait and pick procedure DR1 of the above two scenarios may no longer be optimal (Chow et al., 1991), but this depends on the assumed $F(x)$.

Consider instead the selection strategy shown in Figure 1. It is based on a type DR4 decision rule. Assume an acceptance threshold c_i is set at each time step t_i ($i = 1, \dots, n$). The decision rule is as follows: opportunity i is accepted at time t_i only if its value X_i exceeds c_i – else, the DM waits for the next opportunity in the sequence (see Figure 1).

In order to set up an optimal strategy, we assume that our objective is to achieve the greatest possible return in terms of the expected value of the selected opportunity. This is the γ -type objective discussed in Section 2.

We can achieve this using backward induction as follows. Clearly c_n must be zero since, or if we do reach $t = t_n$, then any offer is better than nothing. Under the optimal strategy s defined in terms of a set of optimal acceptance levels $\{c_1, c_2, \dots, c_n\}$ the expected return v_i of the selected X_γ if the selection process reaches t_i can be related to the expected return at time t_{i+1} as follows:

$$\begin{aligned} v_i &= E(X_i | X_i > c_i)P(X_i > c_i) + v_{i+1}P(X_i < c_i) = \\ &= \int_{c_i}^{\infty} x f(x)dx + v_{i+1} \int_0^{c_i} f(x)dx \quad (i = 1, \dots, n-1) \end{aligned} \quad (1)$$

where as shown in Figure 1 the first and the second term represent the expected values when opportunity i is accepted and declined, respectively. Thus the optimal acceptance level c_i at each time t_i is the one which maximizes each v_i and is based on:

$$\frac{dv_i}{dc_i} = 0 \quad \text{or} \quad -c_i f(c_i) + v_{i+1}f(c_i) = 0 \quad (i = 1, \dots, n-1) \quad (2)$$

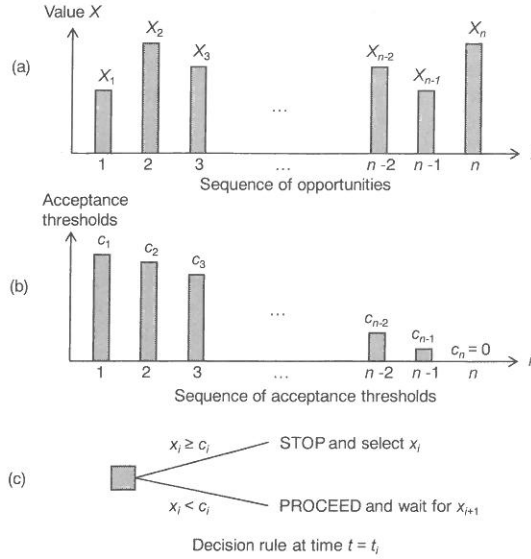


Figure 1: Sequential decision strategy DR4

from which we find the recursive relation:

$$c_i = v_{i+1} \quad (3)$$

For $i = n$, when the very last opportunity gets to be selected, the expected return v_n is simply the expected value $E(X)$ because the threshold $c_n = 0$. Therefore the optimal levels c_i can all be determined using Equation 3 starting from c_n and going backwards toward c_1 . The expected return at time t_i is of course a decreasing function of time which can be seen by plugging Equation 3 into Equation 1:

$$\begin{aligned} v_i &= \int_{v_{i+1}}^{\infty} x f(x) dx + v_{i+1} F(v_{i+1}) = \\ &= v_{i+1} + \int_{v_{i+1}}^{\infty} (1 - F(x)) dx = c_i + \int_{c_i}^{\infty} (1 - F(x)) dx \end{aligned} \quad (4)$$

Therefore, the consecutive optimal acceptance levels c_i also form a decreasing sequence. When increasing the number of opportunities n , only the front end values and acceptance thresholds will change, since they depend recursively on future values.

As an example, consider the values of the opportunities to be exponentially distributed with mean x_m , then the optimal selection strategy s consists of n acceptance levels and expected returns as shown in Table 1 where for instance $c_{n-2} = x_m + \int_{x_m}^{\infty} \exp\left(-\frac{x}{x_m}\right) dx = x_m(1 + e^{-1}) = 1.368 x_m$.

For given n , the "overall" expected return $E(X_Y | s)$ associated with strategy s is simply equal to its value v_1 at the very start of the sequence. Table 1 shows this expected payoff as a function of the number of opportunities n .

We can also compare the expected return with the expected largest value in a random sample of n opportunities:

$$E(x_{\max, n}) = \int_0^{\infty} n x F(x)^{n-1} f(x) dx \quad (5)$$

This would be the average value of the best possible opportunity if the entire sequence of n opportunities were to be fully exposed. Ideally this would be the opportunity we wish to pick. The

efficiency $\text{eff}(s)$ of the selection process s would therefore be measured in terms of how close $E(X_Y)$ can approach $E(X_{\max}|n)$:

$$\text{eff}(s) = \frac{E(X_Y|s=\{c_1, \dots, c_n\})}{E(x_{\max, n})} \quad (6)$$

For instance, in the case of the exponential distribution the expected largest return Equation 5 is equal to $\sum_{j=1}^n \frac{1}{j}$ which approaches $\ln n + 0.5772$ as n increases (Gumbel, 1958, p. 117) The corresponding efficiencies are shown in the fourth column of Table 1 for various horizons n .

However, another example is a uniformly distributed random sample. In that case, the DR4 strategy is in fact inferior to a secretary-type DR1 approach. The optimal length of the experimental phase is now either $\lfloor \sqrt{n} \rfloor$ or $\lceil \sqrt{n} \rceil$ which is much smaller than the n/e learning phase required for the a -distributional selection process.

Table 1. Optimal DR4 acceptance thresholds for exponentially distributed opportunities with mean x_m .

Horizon	First acceptance threshold c_1	Overall expected return v_1	Efficiency $\text{eff}(s)$ of strategy s (6)
$n = 5$	1.820 x_m	1.982 x_m	86.8 %
$n = 20$	3.083 x_m	3.129 x_m	87.0 %
$n = 50$	3.956 x_m	3.975 x_m	88.4 %
$n = 100$	4.631 x_m	4.641 x_m	89.5 %
$n = 500$	6.221 x_m	6.223 x_m	91.6 %

5 ACCOUNTING FOR THE COST OF WAITING

It is common knowledge in behavioural operations research and experimental economics that people in general tend to stop searching too soon. This may be explained in part by impatience, by distrust of a rule that tells them to wait longer, or by the cost inherent in waiting and evaluating opportunities.

In engineering, “waiting” does usually involve a cost run-up. Crews or equipment on standby can cost lots of money. Evaluating opportunities is also expensive. Therefore one reasonable extension of the decision rules discussed above is to account for the cost associated with waiting, or, equivalently the decrease of the intrinsic value as time goes on.

A discounted version of the non-distributional DR1-type strategies was studied, without significant success, by a series of authors (Babaioff et al., 2009). The problem is hard as it is quite sensitive to the assumed discounting model and to any assumptions about the value structure.

However, the “variable acceptance thresholds” approach DR4 is amenable to discounting, and it often – but not always – turns out to be an optimal strategy. The latter actually depends on the distribution of opportunity values $F(x)$ and on the severity of the discounting function. For instance, consider a decreasing discounting function $\eta(t)$ with $\eta(t_1) = 1$ such that the effective value of an opportunity at time t_i becomes:

$$X_i^* = X_i \eta(t_i) \quad (7)$$

If now $\eta(t)$ decreases very rapidly, then it is clear that the trivial strategy that always picks the first opportunity $X_Y = X_1$ will outperform all other strategies since it has an (undiscounted) expected return equal to $x_m \eta(t_1)$. Thus the DR4 decision algorithm may not be optimal if the cost of waiting is too expensive, and its applicability should always be verified.

The various acceptance thresholds using DR4 can now be found from the following recursive relationship replacing Equation 1:

$$v_i^* = \eta(t_i) \int_{c_i}^{\infty} x f(x) dx + F(c_i) v_{i+1}^* \quad (i = 1, \dots, n - 1) \quad (8)$$

Differentiation results in the optimal threshold c_i at time t_i :

$$c_i = \frac{v_{i+1}^*}{\eta(t_i)} \quad (9)$$

Note that at the very last time step t_n , the threshold c_n must be zero like before and the expected return is equal to $E(X) \eta(t_n) = x_m \eta(t_n)$.

Since, based on (9) the $(n-1)^{\text{th}}$ threshold c_{n-1} is equal to this pay off divided by $\eta(t_{n-1})$, it follows that $c_{n-1} = x_m \left[\frac{\eta(t_n)}{\eta(t_{n-1})} \right]$ compared to x_m in the no-cost-for-waiting case, such that this and all other thresholds are smaller than in the undiscounted case. This means that we will be inclined sooner to select and stop at a given opportunity that satisfies the criterion.

The recursive expected return at time t_i given previously by Equation 4 now becomes:

$$v_i^* = v_{i+1}^* + \eta(t_i) \int_{v_{i+1}^*}^{\infty} (1 - F(x)) dx \quad (i = 1, \dots, n-1) \quad (10)$$

6 CONDITIONALLY DEPENDENT OPPORTUNITIES

In some cases the assumption that the opportunities are iid may not be realistic. To simplify a situation having sequential dependence, let us assume that for each i the distribution of X_i depends on the previous observation x_{i-1} . We write $F_i(x|x_{i-1})$ and $f_i(x|x_{i-1})$ to reflect this.

Under the same formulation and assumptions as those given in Section 5, the expected return v_i in Equation 1 is now replaced by:

$$\begin{aligned} v_i &= E(X_i | X_i > c_i) P(X_i > c_i) + v_{i+1} P(X_i < c_i) = \\ &= \int_{c_i}^{\infty} x f_i(x|x_{i-1}) dx + v_{i+1} \int_0^{c_i} f_i(x|x_{i-1}) dx \quad (i = 1, \dots, n-1) \end{aligned} \quad (11)$$

Thus the optimal acceptance level c_i at each time t_i is found from:

$$-c_i f_i(c_i|x_{i-1}) + v_{i+1} f_i(c_i|x_{i-1}) = 0, \quad (i = 1, \dots, n-1) \quad (12)$$

from which we find the same recursive relation as in Equation 3.

Therefore the optimal levels c_i can all be determined using Equation 3 starting from c_n and going backwards toward c_1 . However, it is imperative to realize that these levels now depend on the sequence of observed values $\{x_i, \dots, x_{n-1}\}$. The expected return at time t_i is now:

$$\begin{aligned} v_i &= \int_{v_{i+1}}^{\infty} x f_i(x|x_{i-1}) dx + v_{i+1} F_i(v_{i+1}|x_{i-1}) = \\ &= v_{i+1} + \int_{v_{i+1}}^{\infty} (1 - F_i(x|x_{i-1})) dx = c_i + \int_{c_i}^{\infty} (1 - F_i(x|x_{i-1})) dx \end{aligned} \quad (13)$$

To get an idea about the behaviour of the sequence of optimal levels (Equation 3) and returns (Equation 13), a simulation study would be required.

7 EXAMPLE

Subsea manifold installation for a 2,000 m deep water oil and gas field development involves a large number of specialized tasks most of which are performed remotely by ROVs. In many designs, manifolds are now spatially dispersed into a set of 20-50 Flowline Termination Assemblies (FTAs) which are small self-contained units of about 15 ... 20 tonnes that house valving and flowline connections.

The present example focuses on ROV operations for various clamping and connection tasks performed on FTAs. They typically last between 16 and 24 hours without lead and lag times which add about 50 % to the duration of a task. The key variable affecting the efficiency of such operations is the mean near bottom current speed. In general, the larger the mean current speed the lower, the more difficult, and the less effective the ROV operations. A pretty well standard quadratic relation between total cost (direct + indirect costs due to slowdown, repeats, delays) and 3-day current speed is assumed to apply. At the site considered energetic bursts and quiet regimes persist typically for about 3 days. This is due to the preponderance of topographic deep waves at the edge of loop oceanic currents. One of the FTAs is equipped with a current meter package that transmits deep current data on demand every few days. On this basis the DMs

make an online decision to launch, load and operate the ROV, or they decide to wait for a better opportunity that would occur in the planned window of duration T .

Consider $T = 1$ month which contains $n = 10$ "opportunities" of 3 day-slots. The cost of waiting is considered to be negligible as personnel and equipment can be mobilized for other parallel tasks. The 3d-current U at the deepwater site has a mean of 0.20 m/s and is assumed to persist during each 3 day-slot. Its cdf is a Weibull distribution:

$$F_U(u) = 1 - \exp\left(-\left(\frac{u}{a}\right)^b\right) \quad u > 0 \quad (14)$$

with exponent $b = 2$ and scale $a = 0.226$ m/s.

The operating conditions are as follows: ideal operation conditions occur at mean currents less than 0.05 m/s but they are still acceptable up to 0.10 m/s which is often used as a criterion above which routine non-emerging deployment is avoided. Conditions between 0.10 m/s and 0.25 m/s are termed "difficult" whereas they become virtually impossible during high energy bursts. The value of each "opportunity" X is taken as the negative of the generic cost which, as discussed above is proportional to the square of current speed. Since this amounts to a one-to-one transformation of $U \rightarrow X$, we can express all the results in terms of U with, of course, lower values being more preferable.

We contrast the seven strategies listed in Table 2. In scenario (S4), the cost of waiting is assumed to increase linearly in time such that if the final opportunity were to be reached and selected, the total cost would be double of that when no penalty is assigned to inactivity.

The expected minimum cost for $n = 10$ iid opportunities, based on Equation 5 corresponds to a current speed of 0.0632 m/s. This is used as the denominator in Equation 6 to evaluate the efficiencies of each strategy in terms of its expected pay off. Table 3 shows the value $\text{eff}(s)$ for each strategy. Strategy (S3) is the overall "winner" closely followed by the fixed threshold criterion (S6) having $u \leq 0.10$ m/s. Note that the fixed criteria are ineffective if the threshold is either too low or too high as shown in Table 2 for (S5) and (S7), it needs to be "just right". However, while (S6) comes close to the optimal (S3) in terms of pay off, there is a nonzero probability that no activity takes place if none of the n opportunities meets the fixed criterion. This contrasts with the variable acceptance threshold strategy (S3) which is heavily influenced by the fact that any choice, at the end of the selection process, would be better than none.

Table 3 also shows the probability that, based on each strategy, no single opportunity would be "good enough". Hence, no selection would be made and this would result in inactivity. Table 3 also includes the expected duration of the selection process. For processes with a nonzero probability of non-termination, the duration is assumed to be $n + 1 = 11$ time steps. The cost of waiting strategy (S4) shortens the waiting time but it increases the overall expected cost. The higher the current threshold, the shorter the waiting process (S7) but the deep sea installation process will likely be poor and comes at high cost and low efficiency. Table 4 summarizes and contrasts the optimal decisions at each of the 10 decision points.

8 CONCLUSIONS

Several formulations, valuations, and objectives can be considered for real-time sequential decision making problems involving irrevocable choices in a finite set of opportunities. Various decision making strategies are reviewed including aspiration strategies for low-information conditions and fixed/variable threshold acceptance strategies, for situations where the probabilistic structure of opportunities is known.

In the latter case a recursive algorithm can, at least partially, be used to optimize thresholds with or without discounting due to waiting. It is shown that in sequential online decision making, irrevocable decisions tend to be made too early. In other words, it often pays to wait for a better opportunity down the line. The variable threshold decision rule is valid for (1) independent sequences, (2) dependent sequences, and (3) the consideration of waiting cost. However, the valuation recursive algorithm as well as the optimal thresholds are different for all three cases. An example shows the superiority of the variable acceptance threshold approach in a specific application, where it has the best overall expected valuation, a reasonable expected duration, and a very low probability of making an unsatisfactory selection.

The above models may need to be generalized before using them for specific engineering problems. Ones such extensions would include portfolio selection, where instead of just one opportunity, a portfolio $m < n$ of opportunities is to be selected with the objective of maximizing its collective return.

REFERENCES

Babaioff, M., Dinitz, M., Gupta, A., Immorlica, N. & Talwar, K., 2009. Secretary problems: Weights and discounts. *Proc. 20th annual ACM-SIAM Symposium on Discrete Algorithms SODA 2009*. pp. 1245-1254, Society for Industrial and Applied Mathematics, Philadelphia.
 Bearden, J.N. & Murphy, R.O., 2004. On generalized secretary problems. *Uncertainty and Risk – Mental, Formal, and Experimental Representations*. Abdellaoui et al. (Eds.), Springer, NY.
 Chow, Y.S., Robbins, H. & Sigmund, D., 1991. *Great Expectations: The Theory of Optimal Stopping*. Dover publications.
 Ferguson, T.S., 1989. Who solved the secretary problem? *Statistical Science*, Vol. 4, No. 3: pp. 282-289.
 Finch, S.R., 2003. Optimal Stopping Constants. *Mathematical Constants*, Vol. 94: pp. 361-363. Cambridge University Press.
 Gumbel, E.J., 1958. *Statistics of Extremes*. Columbia University Press, New York and London.
 Mhdian, M., McAfee, R.P. & Pennock, D., 2008. The Secretary Problem with a Hazard Rate Condition. *Proc. 4th International Workshop on Internet and Network Economics*.

Table 2. Subsea FTA operations: opportunity selection strategies.

Selection Strategy	
S1	The optimal (non-informative) aspiration strategy (Section 3)
S2	The optimal aspiration strategy based on known regular tail behaviour (Section 4)
S3	The optimal (variable) acceptance threshold strategy (Section 5)
S4	The optimal (variable) acceptance threshold strategy including a cost for waiting/delaying (Section 6)
S5	The fixed threshold strategy allowing “ideal”, $u \leq 0.05$ m/s
S6	The fixed threshold strategy allowing “ideal” or “acceptable”, $u \leq 0.10$ m/s
S7	The fixed threshold strategy allowing “ideal”, “acceptable”, or “difficult”, $u \leq 0.25$ m/s

Table 3. Efficiency of the optimal strategy, probability of inactivity, and expected duration (Subsea FTA)

	eff (s) as per (5) and (6)	probability (%)	expected duration
S1	0.60	30.8%	8.19 out of 10
S2	0.67	4.4%	5.00 out of 10
S3	0.78	0	4.83 out of 10
S4	0.52	0	3.58 out of 10
S5	0.47	61.2%	8.71 out of 10
S6	0.74	14.0%	4.96 out of 10
S7	0.43	0	1.41 out of 10

Table 4. Details of the optimal strategies for $n=10$ consecutive time steps (Subsea FTA operations).

Values denote current thresholds (m/sec) below which operations are to go ahead.
 WO: wait and observe
 SFM: select the first opportunity that has a current reading smaller than all previous ones.

Time step:	1	2	3	4	5	6	7	8	9	10
S1	WO	WO	WO	WO	SFM	SFM	SFM	SFM	SFM	SFM
S2	WO	WO	SFM	SFM	SFM	SFM	SFM	SFM	SFM	SFM
S3	0.085	0.090	0.095	0.102	0.110	0.121	0.135	0.158	0.200	any
S4	0.121	0.122	0.123	0.127	0.132	0.140	0.152	0.172	0.211	any
S5	0.005	0.005	0.005	0.005	0.005	0.005	0.005	0.005	0.005	0.005
S6	0.010	0.010	0.010	0.010	0.010	0.010	0.010	0.010	0.010	0.010
S7	0.025	0.025	0.025	0.025	0.025	0.025	0.025	0.025	0.025	0.025

Life-cycle cost based optimal design of fluid viscous dampers

Alexandros A. Taflanidis & Ioannis Gidaris

University of Notre Dame, Department of Civil and Environmental Engineering and Earth Sciences

ABSTRACT: A simulation-based, probabilistic framework is discussed in this paper for design of viscous dampers based on life-cycle cost criteria. This framework allows for explicit consideration in the design process of all important nonlinearities for both the dampers and the structural behavior, as well as of all sources of uncertainty related to the seismic hazard. It is based on an assembly-based vulnerability approach for estimating earthquake losses, and on description of the earthquake hazard through stochastic ground motion models, along with predictive relationships that relate their parameters to regional seismicity characteristics. In this setting, the life-cycle cost is quantified by its expected value over the space of the uncertain parameters for the structural and excitation models, and is estimated through stochastic simulation. For the design-optimization an algorithm appropriate for costly global optimization problems is adopted. An illustrative example is presented that considers the optimal life-cycle based design of fluid viscous dampers for retrofitting a three-story concrete structure.

1 INTRODUCTION

Probabilistic approaches for comprehensive cost-effective design of viscous dampers for seismic hazard mitigation are gaining increasing attention within the structural engineering community, especially in the context of retrofitting strategies (Taflanidis and Beck, 2009). A realistic treatment of such a design requires proper integration of (i) methodologies for addressing the uncertainties related to the seismic hazard over the entire life-cycle of the building, (ii) tools for evaluating the performance using socioeconomic criteria, as well as (iii) algorithms appropriate for stochastic analysis and optimization. This work uses a simulation-based framework that addresses all important challenges associated with these steps for the design of fluid viscous dampers for retrofitting of building structures. A probabilistic foundation is used to address the various sources of uncertainty and quantify the expected life-cycle cost which is comprised by the lifetime repair cost of the structure due to expected future seismic losses and the upfront cost of the damper devices. An assembly based vulnerability approach is used to estimate the repair cost. This approach uses the nonlinear time-history response of the structure under a given excitation to estimate the damage in a detailed, component level. A probabilistic excitation model is then presented for describing the ground motion time history for future earthquake excitations. This is established by adopting a stochastic ground motion model as well as predictive relationships that relate the properties of the excitation to characteristics of the seismic hazard. In this setting, the life-cycle cost is quantified by its expected value over the space of the uncertain parameters for the structural and excitation models. Because of the complexity of these models, calculation of this expected value is performed using stochastic simulation techniques. This approach, though, involves an unavoidable estimation error and significant computational cost, features which make efficient design optimization challenging. To alleviate this burden, an efficient algorithm belonging in the greater family of Costly Global Optimization (CGO) search techniques is adopted here.

2 QUANTIFICATION OF LIFE-CYCLE COST

For evaluation of seismic cost adoption of appropriate models is needed for the structural system, the earthquake excitation and the loss evaluation (Figure 1). The combination of the first two models provides the structural response and in the approach adopted here this is established in terms of nonlinear time-history analysis. The loss evaluation model quantifies, then, earthquake performance in economic terms based on that response. The characteristics, though, of these models are not known with absolute certainty. Uncertainties may pertain, for example, to (i) the properties of the structural system, to (ii) the variability of future seismic events (moment magnitude or the epicentral distance), or to (iii) the predictive relationships about the characteristics of the excitation given a specific seismic event. A probabilistic approach provides a rational framework for quantifying these uncertainties through the entire life-cycle.

To formalize this idea, let $\varphi = [\varphi_1, \varphi_2, \dots, \varphi_{n_\varphi}] \in \Phi \subset \mathbb{R}^{n_\varphi}$ denote the vector of controllable parameters that define the system design, referred to herein as design variables, where Φ denotes admissible design space. For the application discussed here, φ consists of the design characteristics of the fluid viscous dampers. Let $\theta \in \Theta \subset \mathbb{R}^{n_\theta}$, denote the augmented vector of model parameters where Θ represents the space of possible model parameter values. Vector θ is composed of all the model parameters for the individual structural system, excitation, and performance evaluation models indicated in Figure 1. For addressing the uncertainty in θ a probability density function (PDF) $p(\theta)$, is assigned to it, quantifying the relative likelihood of different model parameter values. The favorability of the system response, given the values of the model parameters, is evaluated by the risk consequence measure $h(\varphi, \theta): \mathbb{R}^{n_\varphi \times n_\theta} \rightarrow \mathbb{R}^+$, $h(\varphi, \theta) = C_{in}(\varphi, \theta) + C_{lif}(\varphi, \theta)$, where $C_{in}(\varphi, \theta): \mathbb{R}^{n_\varphi \times n_\theta} \rightarrow \mathbb{R}^+$ corresponds to the initial cost and $C_{lif}(\varphi, \theta): \mathbb{R}^{n_\varphi \times n_\theta} \rightarrow \mathbb{R}^+$ to the additional cost over the lifetime of the structure. The expected life-cycle cost $C(\varphi)$ is then simply given by the expected value:

$$C(\varphi) = \int_{\Theta} h(\varphi, \theta) p(\theta) d\theta \quad (1)$$

which leads to the following optimal design problem

$$\varphi^* = \arg \min_{\varphi \in \Phi} C(\varphi) \quad (2)$$

Note that in this formulation, all performance requirements against future natural hazards are directly incorporated in the objective function. Also, all associated constraints, for example related to spacing of dampers, are directly incorporated into the definition of admissible design space Φ . For evaluation of the objective function in (1) and for the associated design optimization problem (2), an approach based on stochastic simulation will be discussed later in Section 6 that can seemingly integrate recent high-performance computing advances to provide a powerful framework that allows adoption of complex sub-models for describing the overall system in Figure 1. First these models are reviewed.

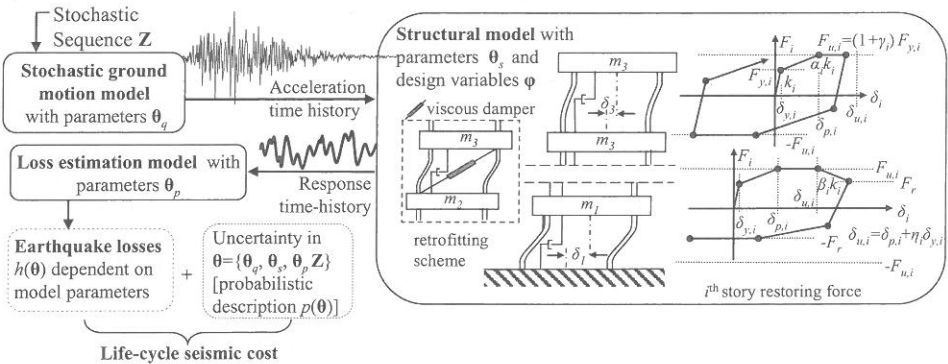


Figure 1: Augmented system model for life-cycle cost estimation

3 CHARACTERISTICS AND INITIAL COST OF DAMPERS

The force of (nonlinear) fluid dampers can be expressed in form $F_D=C_D\text{sgn}(\dot{x}_D)|\dot{x}_D|^\alpha$ (Taflanidis, 2011), where C_D is the damper coefficient, \dot{x}_D is the damper velocity and α is the velocity exponent. For a structure equipped with n dampers (at different stories and/or locations), the design variables for the optimization problem include the damper coefficients $C_{D,i}$ and the velocity exponents α_i for each of the dampers, $i = 1, \dots, n$. The cost of each damper is estimated based on its corresponding maximum force capacity $F_{ud,i}$, defined as the maximum force the damper is expected to develop under the maximum credible earthquake (Taylor Devices, 2012). Therefore, for a given configuration of $C_{D,i}$ and α_i , the maximum force capacity $F_{ud,i}$ can be calculated by selecting an appropriate reference velocity. Under the probabilistic description established for the seismic hazard later, this reference velocity is easy to quantify; it simply corresponds to the velocity with certain probability of exceedance. After the damper capacity F_{ud} has been determined the evaluation of its cost is relatively straight-forward; it can be performed using data for existing commercial devices (Taflanidis and Beck, 2009).

4 LOSS ESTIMATION METHODOLOGY

For estimating direct earthquake losses an assembly-based vulnerability approach is adopted. According to this methodology, the components of the structure are grouped into n_{as} damageable assemblies. Each assembly consists of components of the structural system that have common characteristics with respect to their vulnerability and repair cost. Such assemblies may include, for example, beams, columns, wall partitions, contents of the building, and so forth. For each assembly $j=1, \dots, n_{as}$, $n_{d,j}$ different damage states are designated and a fragility function is established for each damage state $d_{k,j}$, $k=1, \dots, n_{d,j}$. These functions quantify the probability $P_e[d_{k,j}|EDP_j, \boldsymbol{\varphi}, \boldsymbol{\theta}]$ that the component has reached or exceeded its k th damage state, conditional on some engineering demand parameter (EDP_{*j*}) which is related to the time-history response of the structure under a given excitation (for example, peak transient drift, peak acceleration, etc.). Damage state 0 is used to denote an undamaged condition. A repair cost $C_{k,j}$ is then assigned to each damage state, which corresponds to the cost needed to repair the component back to the undamaged condition. The expected losses in the event of the earthquake are:

$$L(\boldsymbol{\varphi}, \boldsymbol{\theta}) = \sum_{j=1}^{n_{as}} \sum_{k=1}^{n_{d,j}} P[d_{k,j} | \boldsymbol{\varphi}, \boldsymbol{\theta}] C_{k,j} \quad (3)$$

where $P[d_{k,j}|\boldsymbol{\varphi}, \boldsymbol{\theta}]$ is the probability that the assembly j will be in its k^{th} damage state and the explicit dependence on EDP_{*j*} has been dropped (since knowledge of the design and model parameter assumed to leads to estimation of EDP_{*j*}). The probability $P[d_{k,j}|\boldsymbol{\varphi}, \boldsymbol{\theta}]$ may be readily obtained from the information from the fragility curves; it is equal to the probability of exceeding state $d_{k,j}$ minus the probability that it has exceeded the subsequent state $d_{k+1,j}$:

$$P[d_{k,j} | \boldsymbol{\varphi}, \boldsymbol{\theta}] = P_e[d_{k,j} | \boldsymbol{\varphi}, \boldsymbol{\theta}] - P_e[d_{k+1,j} | \boldsymbol{\varphi}, \boldsymbol{\theta}] \quad P[d_{n_{d,j},j} | \boldsymbol{\varphi}, \boldsymbol{\theta}] = P_e[d_{n_{d,j},j} | \boldsymbol{\varphi}, \boldsymbol{\theta}] \quad (4)$$

5 EXCITATION MODEL

This loss-estimation approach requires development of a probabilistic model of the entire ground motion time history that will adequately describe the uncertainty in future earthquake events. This model needs to describe moderate (in range of 5-6.5 moment magnitude) and strong (in range of 6.5-8 moment magnitude) seismic events as both contribute to the overall damages and repair cost over the life-cycle of a building (Taflanidis and Beck, 2009), the former creating primarily damages in the non-structural components and the latter impacting additionally the structural components. Moreover, for comprehensive characterization of the seismic hazard in regions close to active faults, consideration of the probability of occurrence of a forward-directivity pulse is required, as such type of excitations, can cause severe damage in structural systems. In this study this taken into account, through introduction of the probability for velocity pulse existence for specified earthquake and site characteristics (Shahi and Baker, 2011).

A stochastic ground motion model that can address pulse like excitations is briefly discussed next: according to it, the high-frequency and long period components of the motion are independently modeled and then combined to form the acceleration time history.

High Frequency Component: For modeling the higher-frequency ($>0.1-0.2$ Hz) component of ground motions, a point source stochastic model is chosen here. This approach is based on a parametric description of the ground motion's radiation spectrum $A(f;M,r)$, which is expressed as a function of the frequency, f , for specific values of the earthquake magnitude, M , and the closest distance to the rupture surface r . This spectrum consists of many factors which account for the spectral effects from the source (source spectrum) as well as propagation through the earth's crust up to the structural site. The temporal characteristics of the ground motion are addressed through an envelope function $e(t;M,r)$, which again depends on M and r . These frequency and time domain functions, $A(f;M,r)$ and $e(t;M,r)$, completely describe the model, and their characteristics are provided by predictive relationships that relate them directly to the seismic hazard, i.e. to M and r . More details about them are provided in (Boore, 2003; Taflanidis and Beck, 2009). In particular, the two-corner point-source model by Atkinson and Silva (Atkinson and Silva, 2000) can be selected for the source spectrum because of its equivalence to finite fault models. The time history (output) for a specific event magnitude, M , and source distance, r , is obtained according to this model by modulating a white-noise sequence $\mathbf{Z} = [Z(i\Delta t):i=1,2,\dots,N_T]$, where Δt the chosen discretization interval, by $e(t;M,r)$ (in the time domain) and subsequently by $A(f;M,r)$ (in the frequency domain).

Long-period pulse: For describing the pulse characteristics of near-fault ground motions, the simple analytical model developed by Mavroeidis and Papageorgiou (2003) is selected. According to it, the pulse component of near-fault motions is described through the following expression for the ground motion velocity pulse:

$$V(t) = A_p / 2[1 + \cos(2\pi f_p / \gamma_p (t - t_o))] \cos[2\pi f_p (t - t_o) + \nu_p] \\ \text{if } t \in [t_o - \gamma_p / (2f_p), t_o + \gamma_p / (2f_p)] \quad (5) \\ = 0 \text{ otherwise}$$

where A_p , f_p , ν_p , γ_p and t_o describe the signal amplitude, prevailing frequency, phase angle, oscillatory character (i.e. number of half cycles), and time shift to specify the envelope's peak, respectively. These pulse characteristics can be estimated by predictive relationships that connect them to the seismic hazard of a site. In this study the predictive equations proposed by Dabaghi et al. (2011) are used. These empirical equations link the pulse parameters to the following earthquake and site characteristics: the type of faulting (strike-slip or non strike-slip), the moment magnitude, M , the shear wave velocity in the top 30m of soil at the site, V_{s30} , the epicentral distance R_{epi} , the closest distance to fault rupture, r , the length of rupture between the fault and the site, s , and the angle between the strike of the fault and the line joining epicenter and the site, θ . Figure 2 illustrates the source-to-site parameters r , R_{epi} , θ , s and the rupture length L , for the case that the site is located before (left) and after (right) of the end of the rupture length for a strike-slip fault. Note that due to geometric relationships only four of these parameters are independent. The rupture length is estimated here by the predictive equation proposed by Wells and Coppersmith (1994) $\log_{10}(L) = -3.55 + 0.74M + e_L$, where e_L is a prediction error following Gaussian distribution with zero mean and a specified standard deviation. Additionally, since not all the near-fault ground motions exhibit this long period pulse, the probability of occurrence of the velocity pulse is calculated using the predictive equation for strike-slip faults proposed by (Shahi and Baker, 2011), $P(\text{pulse}|r,s) = 1/[1 + e^{(0.642 + 0.167r - 0.075s)}]$.

Near-fault ground motion: The stochastic model for near-fault motions is finally established by combining the above two components (Taflanidis, 2011) and ultimately provides a complete probabilistic description for the seismic hazard based on the seismicity characteristics M , r , R_{epi} and θ , the various predictive relationships (for $A(f;M,r)$, $e(t;M,r)$, L and the pulse characteristics) and \mathbf{Z} . Establishing probability models for M , r , R_{epi} and θ (primary model parameters) and addressing in a similar way the uncertainty in the predictive relationships (secondary model parameters) and in the stochastic sequence \mathbf{Z} , leads then to the desired probabilistic seismic hazard characterization, that can be used for quantifying the life-cycle cost in Equation (1) as well as for defining the reference velocity for estimating the cost of the dampers.

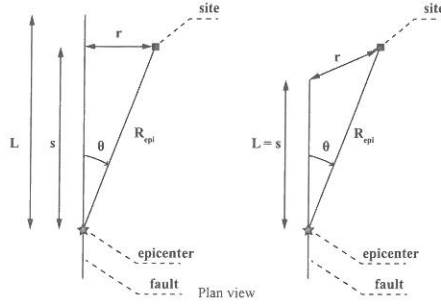


Figure 2: Source to site geometry for strike-slip faults

6 LIFE-CYCLE COST OPTIMAL DESIGN

The system, excitation and performance evaluation models described earlier lead to quantification of the loss function $h(\boldsymbol{\varphi}, \boldsymbol{\theta})$. The optimization in (2) requires, additionally, the evaluation of the integral corresponding to the objective function. Since the nonlinear models considered are complex and include a large number of uncertain model parameters an efficient approach for this task is to use stochastic simulation (Taflanidis and Beck, 2008). Using a finite number, N , of samples of $\boldsymbol{\theta}$ drawn from some proposal density $p_{is}(\boldsymbol{\theta})$, an estimate for (1) is:

$$\hat{C}(\boldsymbol{\varphi}) = 1/N \sum_{i=1}^N h(\boldsymbol{\varphi}, \boldsymbol{\theta}^i) p(\boldsymbol{\theta}^i) / p_{is}(\boldsymbol{\theta}^i) \quad (6)$$

where $\boldsymbol{\theta}^i$ denotes the sample of the uncertain parameters used in the i^{th} simulation. As $N \rightarrow \infty$, then $\hat{C} \rightarrow C$ but even for finite, large enough N , (6) gives a good approximation for (1). The importance sampling density $p_{is}(\boldsymbol{\theta})$ may be used to improve the efficiency of this estimation, by focusing the computational effort on regions of the $\boldsymbol{\theta}$ space that contribute more to integrand of (1). For problems with a large number of model parameters, such as the application discussed here, choosing efficient importance sampling densities for all components of $\boldsymbol{\theta}$ is challenging; thus it is preferable to formulate importance sampling densities only for the important components of $\boldsymbol{\theta}$, i.e. the ones that have biggest influence on the seismic risk, and use $p_{is}(\cdot) = p(\cdot)$ for the rest (Taflanidis and Beck, 2008). For seismic risk applications the characteristics of the hazard, especially the moment magnitude is generally expected to have the strongest impact on the calculated risk (Taflanidis and Beck, 2009), so selection of importance sampling densities may preliminary focus on it. Note that formulation (6) allows to seemingly integrate recent advanced in high performance computing (parallel/distributed computing) to perform the required N evaluation of the system performance independently in parallel mode. This significantly reduces the computational barriers that have been traditionally associated with stochastic simulation techniques, and along with adaptive techniques for formulation of importance sampling densities (Taflanidis and Beck, 2009) can significantly improve efficiency.

Finally, optimization (2) may be performed using estimate (6). For this optimization problem, an exterior sampling approximation (ESA) is adopted in this study (Taflanidis and Beck, 2008). ESA adopts the same stream of (a sufficiently large number of) random numbers throughout all iterations in the optimization process, thus transforming the optimization into a deterministic system design problem, which can be solved by any appropriate deterministic optimization algorithm. Still, the estimate of the objective function for this optimization involves significant computational cost since N evaluations of the (nonlinear) model response are needed for each analysis. This feature make the optimization problem challenging. An efficient search technique, belonging in the greater family of costly global optimization, CGO, algorithms (Holmstrom, et al., 2009), is adopted here, utilizing a response surface approximation for the objective function. Based on a small number of evaluations of the objective function a response surface is built in the design variable space, and used to adaptively select the candidate location of the global minimum. Evaluation of the objective function at that point provides then additional information for updating the response surface and convergence towards the final design solution.

7 ILLUSTRATIVE EXAMPLE

For the illustrative example, a three-story reinforced concrete office building with nonlinear fluid viscous dampers is considered. The dimension of the building is 32 x 36 m and the height of each story is 4.0 m. The shear wave velocity in the top 30m of the soil at the site, V_{s30} , is assumed to be 310 m/sec, which corresponds to generic soil conditions, while the type of the fault is assumed to be strike –slip. The design variables in this problem correspond to the damper coefficients in each story $C_{D,i}$, $i = 1,2,3$. The damper capacities $F_{ud,i}$ are calculated by assuming that the velocity exponents for each α_i is equal to 0.5, and that the reference velocity discussed in Section 3 is equal to the one that has 1% probability of exceedance.

7.1 Structural and excitation models

A planar frame model (illustrated in Figure 1 earlier) with peak oriented hysteretic behavior and deteriorating stiffness and strength is assumed. The median value for the lumped masses of all the stories are $[m_i] = [976, 932, 887]$ metric tons, $i=1,2,3$. All three masses are assumed uncertain, following a log-normal distribution with coefficient of variation (c.o.v.) 10%. The initial inter-story stiffnesses k_i of all the stories are parameterized by $k_i = \bar{k}_i \theta_{k,i}$, $i=1,2,3$, where $[\bar{k}_i] = 789.02[1.00, 0.85, 0.70]$ MN/m are the most probable values and $\theta_{k,i}$ are nondimensional uncertain parameters, assumed to be correlated Gaussian variables with mean value one and covariance matrix with variances 0.10 for all the floors and correlation coefficients 0.5 between adjacent floors and 0.2 between first and third floor. For each story, the post-yield stiffness coefficients a_i , stiffness deterioration coefficient β_i , over-strength factor γ_i , ductility coefficient μ_i , and yield displacement $\delta_{y,i}$ have median values 0.1, 0.2, 4 and 0.5% of story height, respectively (see Figure 1 for proper definition of some of these parameters). All these parameters are treated as independent log-normal variables with c.o.v. 10%. Additionally, a residual strength is assumed equal to 10% of the maximum strength. The structure is assumed to be modally damped. The damping ratios for all modes are treated as log-normal variables with median values 5% and c.o.v. 30%.

Seismic events are assumed to occur following a Poisson distribution and so are independent of previous occurrences. The uncertainty in moment magnitude M is modeled by the Gutenberg-Richter relationship truncated on the interval $[M_{min}, M_{max}] = [5.0, 8.0]$, leading to the PDF and expected number of events per year given, respectively, by:

$$p(M) = \frac{b_M \exp(-b_M M)}{\exp(-b_M M_{min}) - \exp(-b_M M_{max})} \quad \nu = \exp(a - b M_{min}) - \exp(a - b M_{max}) \quad (7)$$

Only events with magnitude greater than $M > 5.0$ are considered since earthquakes with smaller magnitude are not expected to lead to significant damage to the structure. After each earthquake the structure is assumed to be restored quickly to its original, undamaged, condition. The regional seismicity factors are selected as $b = 0.9 \log_e(10)$ and $a = 4.35 \log_e(10)$, leading to $\nu = 0.25$. Following discussion of Section 6 importance sampling density was used only for M ; it was used a truncated on the interval $[M_{min}, M_{max}]$ Gaussian PDF with mean value 6.8 and standard deviation 1. For the uncertainty in the event location and orientation with respect to the fault, the epicentral distance R_{epi} , for the earthquake events is assumed to follow a log-normal distribution with median 22 km and c.o.v. 0.4, whereas the angle between the strike of the fault and the line joining epicenter and the site, θ , is assumed to follow a Beta distribution with parameters $a_{beta} = 1.73$ and $b_{beta} = 4.07$. The prediction error e_L for the rupture length is treated as a Gaussian variable with zero mean and standard deviation 0.23. Parameters r and s can be derived from the source to site geometry as depicted in Figure 2.

7.2 Expected life-cycle cost

The damper cost and it is estimated based on their maximum force capacity $F_{ud,i}$, as $C_{mit,i} = \$(0.77(F_{ud,i})^{1.207} + 2806)$. This approximate cost equation has been derived by fitting to a curve of some commercially-available dampers (Taylor Devices, 2012). The constant term in

the above equation corresponds to installation cost of the dampers. The lifetime cost corresponds to the present value of the losses from future seismic events which is calculated by $C_{lif}(\boldsymbol{\varphi}, \boldsymbol{\theta}) = L(\boldsymbol{\varphi}, \boldsymbol{\theta}) [vt_{life}(1 - e^{-r \cdot d_{life}}) / r \cdot d_{life}]$, where r_d is the discount rate (assumed here 2.5%), t_{life} is the lifetime of the structure (taken here as 60 years) and $L(\boldsymbol{\varphi}, \boldsymbol{\theta})$ is the expected cost given the occurrence of an earthquake event. For estimating this repair cost $L(\boldsymbol{\varphi}, \boldsymbol{\theta})$ each fragility function is a conditional cumulative log-normal distribution with median x_m and standard deviation b_m , as described Table 1, which also presents the expected cost per element $\$/n_{el}$, where n_{el} corresponds to the number of elements that belong to each damageable assembly for each floor. For structural components, partitions and paint the maximum interstory drift is used as the EDP, while for the rest the maximum story absolute acceleration is used as the EDP. The fragility curves used are similar to the ones selected in (Goulet et al., 2007) for all damageable subassemblies except for the structural components. For the latter the fragility curves are chosen with respect to the characteristics of the backbone curve for the restoring force in each story.

Table 1: Characteristics of fragility functions and expected repair cost for each story

$d_{k,i}$	x_m	b_m	n_{el}	$\$/n_{el}$	$d_{k,i}$	x_m	b_m	n_{el}	$\$/n_{el}$
<i>Structural components</i>					<i>Partitions</i>				
1 (light)	$1.2\delta_{y,i}$	0.20	42	2000	1 (small)	0.25%	0.70	640 m ²	3.14
2 (moder.)	$(\delta_{y,i} + \delta_{p,i})/2$	0.35	42	9625	2 (extens.)	0.60%	0.50	640 m ²	48.44
3 (signif.)	$\delta_{p,i}$	0.40	42	18200	3 (severe)	1.40%	0.40	640 m ²	107.64
4 (severe)	$\delta_{u,i}$	0.40	42	21600	<i>Acoustical ceiling</i>				
5 (collapse)	5%	0.50	42	34300	1 (small)	0.55g	0.40	500 m ²	5.38
<i>Contents</i>					2 (extens.)	1.00g	0.40	500 m ²	25.79
1 (damage)	0.70g	0.30	50	500	<i>Paint</i>				
					1 (damage)	0.33%	0.20	640 m ²	21.53

Table 2: Optimization results (when appropriate, the coefficient of variation is reported in parenthesis)

Case	φ^* [kN/(m/sec) ^{0.5}]	F_{udi} (kN)	$C(\varphi^*)$ (\$)	$C_{init}(\varphi^*)$ (\$)	$C_{lif}(\varphi^*, \boldsymbol{\theta})$ (\$)
Dampers	$C_{D,1}$	18,407.72	7,123	115,710	79,588
	$C_{D,2}$	12,189.28	4,380		
	$C_{D,3}$	6,528.64	2,014		
No dampers	-	-	522,030	0	522,030 (3.3%)

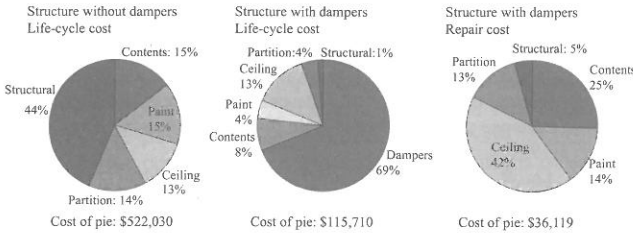


Figure 3: Details about life-cycle cost

7.3 Results and discussion

The number of evaluations, N , of the model response for each damper configuration is selected to be $N=2000$. All simulations are performed exploiting the multi-core capabilities of the Persephone high-performance computing cluster in the HIPAD Laboratory (<http://hipad.nd.edu>) at the University of Notre Dame. It is noted that approximately only 22% of the generated sample excitation time-histories exhibit the long period velocity pulse, as a consequence of the incorporation in the excitation model of the probability of occurrence of a pulse (as described earlier), given the earthquake and site characteristics. The damper coefficients in each floor are the three design variables $\boldsymbol{\varphi} = [C_{D,i}; i = 1,2,3]$. The initial design space for each variable is set to $[12 \ 20] \text{ MN}/(\text{m}/\text{sec})^{0.5}$ for $C_{D,1}$, $[8.4 \ 14] \text{ MN}/(\text{m}/\text{sec})^{0.5}$ for $C_{D,2}$ and $[6 \ 10] \text{ MN}/(\text{m}/\text{sec})^{0.5}$ for $C_{D,3}$. Table 2 presents cumulative results from the optimization, which includes the optimal

design configuration Φ^* , the maximum force capacities of the dampers for this configuration, the total life cycle cost $C(\Phi^*)$, the upfront cost of the dampers $C_{init}(\Phi^*)$ and the repair cost for the lifetime of the structure $C_{li}(\Phi^*, \theta)$, as well as the total life cycle cost for the structure without retrofitting ($C_{D,i} = 0$). The results illustrate the fact that retrofitting of the structure with fluid viscous dampers leads to a significant reduction of the total life-cycle cost ($\approx 22\%$ of the cost of the structure without dampers). Figure 3 then reports the distribution of the life-cycle cost and the lifetime repair cost for both the structure with and without the fluid viscous dampers. It can be observed that the retrofitting of the structure changes significantly the distribution of the lifetime repair cost over the different components, since the addition of the dampers increases considerably the relative importance of the acceleration sensitive components, while it reduces the importance of the drift sensitive components. The important thing to remember is that the design optimization in Table 2 and assessment of Figure 3 has been established using comprehensive models to describe the system performance and the seismic hazard.

8 CONCLUSIONS

The optimal life-cycle cost based design of fluid viscous dampers was discussed in this study. The basis of the suggested approach is a probabilistic, simulation-based framework that (a) explicitly addresses all sources of uncertainty related either to future excitations or to the structural configuration (b) facilitates a direct integration of advances in parallel/distributed computing to significantly reduce the computational burden for estimating life-cycle cost and thus (c) allows for adoption of comprehensive models for describing the structural system and the regional seismic hazard. A versatile stochastic ground motion modeling approach was discussed here for the latter. In the illustrative example considered the addition of the dampers was shown to significantly improve the structure's performance by reducing its life-cycle cost.

9 REFERENCES

- Atkinson, G. M., & Silva, W., 2000. Stochastic modeling of California ground motions. *Bulletin of the Seismological Society of America*, 90(2), 255-274.
- Boore, D. M., 2003. Simulation of ground motion using the stochastic method. *Pure and Applied Geophysics*, 160, 635-676.
- Dabaghi, M., Rezaeian, S., & Der Kiureghian, A., 2011. *Stochastic simulation of near-fault ground motions for specified earthquake and site characteristics*. Paper presented at the 11th International Conference on Applications of Statistics and Probability in Civil Engineering. Retrieved 2011,
- Goulet, C. A., Haselton, C. B., Mitrani-Reiser, J., Beck, J. L., Deierlein, G., Porter, K. A., Stewart, J.P., 2007. Evaluation of the seismic performance of code-conforming reinforced-concrete frame building-From seismic hazard to collapse safety and economic losses. *Earthquake Engineering and Structural Dynamics*, 36(13), 1973-1997.
- Holmstrom, K., Goran, A. O., & Edvall, M. M., 2009. *User's guide for TOMLAB 7*. San Diego, CA: Tomlab Optimization Inc.
- Mavroeidis, G. P., & Papageorgiou, A. P., 2003. A mathematical representation of near-fault ground motions. *Bulletin of the Seismological Society of America*, 93(3), 1099-1131.
- Shahi, S. K., & Baker, J. W., 2011. An Empirically Calibrated Framework for Including the Effects of Near-Fault Directivity in Probabilistic Seismic Hazard Analysis. *Bulletin of the Seismological Society of America*, 101(2), 742-755.
- Taflanidis, A. A., 2011. Optimal probabilistic design of seismic dampers for the protection of isolated bridges against near-fault seismic excitations. *Engineering Structures*, 33(12), 3496-3508.
- Taflanidis, A. A., & Beck, J. L., 2008. An efficient framework for optimal robust stochastic system design using stochastic simulation. *Computer Methods in Applied Mechanics and Engineering*, 198(1), 88-101.
- Taflanidis, A. A., & Beck, J. L., 2009. Life-cycle cost optimal design of passive dissipative devices *Structural Safety*, 31(6), 508-522.
- Taylor Devices., 2012. Personal communication.
- Wells, D. L., & Coppersmith, K. J., 1994. New empirical relationships among magnitude, rupture length, rupture width, rupture area, and surface displacement. *Bulletin of the Seismological Society of America*, 84(4), 974-1002.

Optimization of sequential decisions by least squares Monte Carlo method

K. Nishijima & A. Anders

Department of Civil Engineering, Technical University of Denmark, Denmark

ABSTRACT: The present paper considers the sequential decision optimization problem. This is an important class of decision problems in engineering. Important examples include decision problems on the quality control of manufactured products and engineering components, timing of the implementation of climate change adaptation measures, and evacuation of people and assets in the face of an emerging natural hazard event. Focusing on the last example, an efficient solution scheme is proposed by Anders and Nishijima (2011). The proposed solution scheme takes basis in the least squares Monte Carlo method, which is proposed by Longstaff and Schwartz (2001) for pricing of American options. The present paper formulates the decision problem in a more general manner and explains how the solution scheme proposed by Anders and Nishijima (2011) is implemented for the optimization of the formulated decision problem. For the purpose to demonstrate the use and advantages two numerical examples are provided, which is on the quality control of manufactured products.

1 INTRODUCTION

Pre-posterior/sequential¹ decision analysis has been proven to be a useful theoretical decision framework for different applications in engineering. Classical successful examples include quality control of manufactured products, e.g. De Groot (1970), and risk-based inspection planning and maintenance, see e.g. Corotis et al. (2005) and Straub and Faber (2005). Furthermore, recently the concept of the pre-posterior/sequential decision analysis has been applied to real-time decision optimizations in the context of early warning and operations of engineering facilities in the face of emerging natural hazard events by Nishijima et al. (2008) and Nishijima et al. (2009). Other important examples include the optimal timing of implementation of climate change adaptation measures. In spite of these successful applications, there still is a general challenge.

The challenge lies in that rigorous formulations of the decision problems often require exceedingly demanding computations to obtain the solutions. This is the case where a sequence of decisions are allowed at multiple times in response to random phenomena. In such cases, the original decision problems are often simplified and the solutions are obtained for the simplified

¹ The term "sequential" decision problem is utilized in Section 2 and later also for pre-posterior analysis, appreciating the characteristics of the decision problem considered in the present paper; i.e., test and action decisions are allowed sequentially. Such sequential decisions are, however, pre-posterior by nature. Furthermore, although the length of the sequence may be finite or infinite in theory, only finite length of the sequential decision problems are considered, which may be justified as approximation in practice.

problems; however, the ways to simplify the problems are case-by-case, and justifications for the simplifications require careful investigations.

The present paper presents an efficient solution scheme, which is proposed by Anders and Nishijima (2011), and demonstrates the applicability of the solution scheme to a broader class of sequential decision problems, with remarks regarding the application of the scheme.

2 FORMULATION OF SEQUENTIAL DECISION PROBLEMS

The sequential decision problems can be generally formulated as to find the optimal decisions at the decision times based on the decisions made earlier and the information available up to the decision times, considering the future states of the underlying random phenomena and the future decision opportunities. An important constraint of the sequential decision problems assumed in the present paper is that the random phenomena of relevance underlying the decision problems are not affected by the decisions in the course of sequential decisions. For example, in quality control of manufactured products a decision maker undertakes decisions on whether inspections are to be continued or to be terminated in an inspection campaign; however, the decisions do not change the probabilistic characteristics of the manufactured products; these only change the decision maker's degree of belief. For another example, in the decision situation on the evacuation of people and assets in an emerging natural hazard event, decisions have to be undertaken whether the evacuation should be initiated or to be postponed in response to the information that becomes available in real time. In this case, too, the decisions do not change the probabilistic characteristics of the emerging natural hazard event. In contrast, for example, in the context of risk-based inspection and maintenance optimization problems decisions to execute repair works change the probabilistic characteristics of the realization of the structure.

Denote by A_t the decision space consisting of possible decision alternatives at time t . Here, time t is discretized. It is further assumed that the decisions must be terminated before or at time n ; hence, $t \in \{0, 1, 2, \dots, n\}$. Time t is in some cases technical; i.e. indexing the number of decision time. In general, the decision space A_t depends not only on time t but also on the decisions made before time t . Especially, if the decision maker decides to terminate the sequential decisions, no decision alternative is available at later decision times. It is thus convenient to divide the decision space into two subsets; i.e. $A_t = A_t^{(c)} \cup A_t^{(s)}$, $A_t^{(c)} \cap A_t^{(s)} = \emptyset$ where $A_t^{(c)}$ is the set consisting of "continuing" decision alternatives and $A_t^{(s)}$ is the set consisting of "stopping" decision alternatives. Let the information space E_t consisting of the states of observable information at time t , which depends on the decisions made up to time t .

The optimal decision a_t^* at time t is identified as the one that maximizes the conditional expected utility at time t given the set of information up to time t and decisions up to time $t-1$ as:

$$E[U_t(\mathbf{Z}, a_t^*) | \underline{a}_{t-1}, \underline{e}_t] = \begin{cases} \max_{a_t \in A_t} E[U_t(\mathbf{Z}, a_t) | \underline{a}_{t-1}, \underline{e}_t], & \text{for } t = 0, 1, \dots, n-1 \\ \max_{a_t \in A_t^{(s)}} E[U_t(\mathbf{Z}, a_t) | \underline{a}_{t-1}, \underline{e}_t], & \text{for } t = n. \end{cases} \quad (1)$$

where, for $a_t^{(c)} \in A_t^{(c)}$ and $t = 0, 1, \dots, n-1$,

$$E[U_t(\mathbf{Z}, a_t^{(c)}) | \underline{e}_t] = \int E[U_{t+1}(\mathbf{Z}, a_{t+1}^*) | \underline{a}_{t-1}, a_t^{(c)}, \underline{e}_{t+1}] f(e_{t+1} | \underline{a}_{t-1}, a_t^{(c)}, \underline{e}_t) de_{t+1} \quad (2)$$

Note in Equations 1 and 2 a_{-1} should be regarded as null. $U_t(\mathbf{z}, a_t)$ is the utility, which is a function of the realization of the index \mathbf{Z} relevant for the decision problem as well as the decision alternative a_t . The index \mathbf{Z} is defined through the underlying random sequence $\{\mathbf{Y}_t\}_{t=0}^n$. $\underline{e}_t = (e_0, e_1, \dots, e_t)$ is the set of information available up to time t . $\underline{a}_{t-1} = (a_0, a_1, \dots, a_{t-1})$ is a set of decisions made up to time $t-1$. $f(\cdot | \cdot)$ is the conditional probability density/mass function of E_{t+1} given $\underline{a}_{t-1}, a_t^{(c)}, \underline{e}_t$. The information e_t may be observable with or without uncertainty. Namely, $e_t = y_t$ or a deterministic function of y_t ; or the information e_t may be probabilistically related to y_t , i.e. the probability distribution of e_t is defined conditional on y_t . For example, in the quality control of manufactured product, the index \mathbf{Z} may be the failure probability of a product, the underlying random process Y_t may be a sequence of inspection outcomes (e.g. good quality or bad quality) and $e_t = y_t$ (i.e., the outcome of the inspection is de-

terministically know to the decision maker). Note from Equation 2 it is seen that the optimization of the decision a_t^* at time t requires one to determine all the optimal decisions at future times, $t+1, t+2, \dots, n$; hence, backward induction.

Equation 1 can be rewritten as follows:

$$q_t(\underline{a}_{t-1}, \underline{e}_t) = \begin{cases} \max \{h_t(\underline{a}_{t-1}, \underline{e}_t), c_t((\underline{a}_{t-1}, \underline{e}_t))\} & \text{for } t = 0, 1, \dots, n-1 \\ h_t(\underline{a}_{t-1}, \underline{e}_t), & \text{for } t = n. \end{cases} \quad (3)$$

Here,

$$q_t(\underline{a}_{t-1}, \underline{e}_t) = E[U_t(\mathbf{Z}, a_t^*) | \underline{a}_{t-1}, \underline{e}_t] \quad (4)$$

$$h_t(\underline{a}_{t-1}, \underline{e}_t) = \max_{a_t \in A_t^{(s)}} l_t(\underline{a}_{t-1}, a_t, \underline{e}_t), \quad (5)$$

$$c_t(\underline{a}_{t-1}, \underline{e}_t) = \max_{a_t \in A_t^{(c)}} d_t(a_t, \underline{a}_{t-1}, \underline{e}_t), \quad (6)$$

$$l_t(\underline{a}_{t-1}, a_t, \underline{e}_t) = E[U_t(\mathbf{Z}, a_t) | \underline{a}_{t-1}, \underline{e}_t], \quad a_t \in A_t^{(s)} \quad (7)$$

$$d_t(\underline{a}_{t-1}, a_t, \underline{e}_t) = E[q_{t+1}((\underline{a}_{t-1}, a_t), (\underline{e}_t, E_{t+1})) | \underline{a}_{t-1}, \underline{e}_t], \quad a_t \in A_t^{(c)}. \quad (8)$$

The evaluations of the functions $h_t(\underline{a}_{t-1}, \underline{e}_t)$, $t = 0, 1, 2, \dots, n$, are straightforward in a sense that these do not require backward induction. On the other hand, the evaluations of the functions $c_t(a_t, \underline{a}_{t-1}, \underline{e}_t)$ require backward induction. However, it should be emphasized that no matter how complex the structure of the decision optimization problem may seem, $d_t(a_t, \underline{a}_{t-1}, \underline{e}_t)$ is only a function of \underline{e}_t for any given \underline{a}_{t-1} , a_t ($a_t \in A_t^{(c)}$); this observation plays a vital role in the proposed solution scheme.

3 METHODOLOGY

3.1 Fundamental idea behind Least-squares Monte Carlo method

The Least Squares Monte Carlo method (LSM) is originally proposed by Longstaff and Schwartz (2001) for the pricing of American options. The similarity of the structure between the American option pricing and the sequential decision problems in the context of shut-down decisions of engineering facilities in the face of evolving natural hazard event is pointed out by Anders and Nishijima (2011). Based on this observation and focusing on the shut-down decision problem, they propose an efficient solution scheme for the sequential decision optimizations, based on the original LSM and relaxing several assumptions made specifically for American option pricing. In the following, the fundamental idea behind the LSM is explained. In the subsequent section, the optimization scheme for the above formulated sequential decision problem is presented.

Consider the estimation of the expected values of $q(X, e)$ for different values of parameter $e \in E$ by means of Monte Carlo simulations (MCS). Here, X is a random variable and $q(\cdot, \cdot)$ is assumed to be a slowly-varying function with respect to both x and e . One way to estimate $E[q(X, e)]$ by MCS for different values of e is to estimate them individually. This way is illustrated in Figure 1 (left). A more sensible way is to estimate $E[q(X, e)]$ for different values of e simultaneously by "sharing" MCS realizations simulated for different values of e , see Figure 1 (right). This is performed as follows: (1) Simulate MCS realizations of $q(X, e)$ for different values of e . The values of e can be chosen deterministically but also chosen randomly; (2) Assume a functional form for the approximation of $E[q(X, e)]$; (3) Estimate the parameters of the assumed function by the least squares method using the MCS realizations. Here, it should be emphasized that a single MCS realization for each value of e can be enough as long as the sufficient numbers of MCS realizations are available at neighbors of the respective values of e .

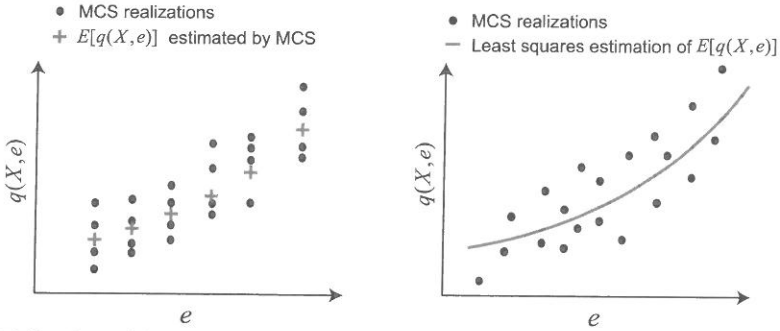


Figure 1. Estimations of the expected values by MCS: Individual estimations (left); simultaneous estimation by sharing information (right).

3.2 Proposed optimization scheme to sequential decision problems

In the following, the steps to identify the optimal decisions by the proposed scheme are presented.

Step 1: The proposed optimization scheme starts by simulating MCS realizations, $\mathbf{y}_n^i = (y_0^i, y_1^i, \dots, y_n^i)$, $i = 1, 2, \dots, b$, of the underlying random sequences $\{\mathbf{Y}_t\}_{t=0}^n$.

Step 2: Having simulated the realizations, for any given set of decisions a_{n-1} up to $t = n - 1$ and for each realization of \mathbf{y}_n^i , the sequence of information e_n^i is: (1) computed in case the information e_t is deterministically related to y_t ; or (2) simulated by the conditional probability distribution of e_t given y_t (only one realization is simulated for each y_t^i). Note e_n^i depends on a_{n-1} ; therefore, it should be denoted as $e_n^i(a_{n-1})$. However, for simplicity unless confused it is denoted as e_n^i .

Step 3: Since at time $t = n$ the decision must be undertaken out of the set $a_n \in A_n^{(s)}$ consisting of stopping decision alternatives, the identification of the optimal decision at time $t = n$ does not require backward induction. Therefore, the optimal decision at time $t = n$ is obtained straightforwardly for each e_n^i and a_{n-1} . Equivalently, the maximized expected utility $q_n(a_{n-1}, e_n^i)$ at time n is obtained.

Step 4: Using the maximized expected utility $q_n(a_{n-1}, e_n^i)$ at time $t = n$, $d_t((a_{n-1}, a_t), e_t)$ at time $t = n - 1$ is obtained, employing the idea of LSM as follows: first, realize $q_n((a_{n-2}, a_{n-1}), (e_{n-1}, e_n^i) | a_{n-2}, e_{n-1} = q_n(a_{n-1}, e_n^i)$; second, generate the pairs of $(e_{n-1}, q_n((a_{n-2}, a_{n-1}), (e_{n-1}, e_n^i) | a_{n-2}, e_{n-1}))$, see the black dots in Figure 2; third, assuming a functional form and applying the least squares method, $E[q_n((a_{n-2}, a_{n-1}), (e_{n-1}, E_n)) | a_{n-2}, e_{n-1}]$, $a_{n-1} \in A_{n-1}^{(c)}$ is estimated. $d_{n-1}((a_{n-2}, a_{n-1}), e_{n-1})$, $a_{n-1} \in A_{n-1}^{(c)}$ is obtained from Equation 8.

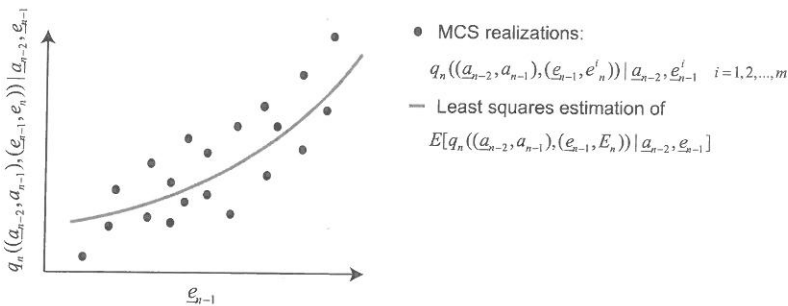


Figure 2. Least squares estimation of $E[q_n((a_{n-2}, a_{n-1}), (e_{n-1}, E_n)) | a_{n-2}, e_{n-1}]$ for each combination of a_{n-2} and $a_{n-1} \in A_{n-1}^{(c)}$.

Step 5: $c_{n-1}(\underline{a}_{n-2}, \underline{e}_{n-1})$ is obtained using Equation 6. Since $h_{n-1}(\underline{a}_{n-2}, \underline{e}_{n-1})$ is obtained straightforwardly, $q_{n-1}(\underline{a}_{n-2}, \underline{e}_{n-1})$ at time $t = n - 1$ is obtained using Equation 3.

Step 6: Repeating Steps 4 and 5 backward for $t = n - 2, n - 3, \dots, 1$, the optimal decision at time $t = 0$ is identified.

3.3 Remarks on the proposed optimization scheme

3.3.1 Efficiency

The realizations of the underlying random sequence $\{\mathbf{Y}_t\}_{t=0}^n$ are simulated once at the first step. In the remaining part of the optimization, these realizations are repeatedly referenced. It may appear that, in some cases, additional MCS is required to estimate the expected utilities corresponding to stopping decision alternatives at each decision time, if the values of these expected utilities are not analytically obtained; however, these additional MCS can be avoided as presented in Anders and Nishijima (2012), by applying the idea introduced in Section 3.1 also for calculating $l_t(\underline{a}_{t-1}, a_t, \underline{e}_t)$.

The realizations of information E_t ($t = 0, 1, 2, \dots, n$) are simulated along with each realization of the underlying random sequence $\{\mathbf{Y}_t\}_{t=0}^n$. Assuming that the number of possible decision alternatives is k at each decision time, the total number of the realization for E_t is $k \times b \times n$. The computational effort required for Steps 3 - 6 is proportional to n . Therefore, the total computational effort for the optimization increases only proportional to n .

3.3.2 Choice of functional form for least squares estimation

Any regular function $g(\mathbf{x})$ can be approximated as a superposition of basis functions (e.g. power series, Hermite series, etc.) as:

$$g(\mathbf{x}) \approx \sum_{k=1}^K r_k L_k(\mathbf{x}). \quad (9)$$

In principle, this can be utilized as a functional form for the least squares estimations in Step 4 in the previous section, and r_k ($k = 1, 2, \dots, K$) are to be estimated, where the argument $\mathbf{x} = (x_1, x_2, \dots)$ in Equation 9 corresponds to (e_1, e_2, \dots) . However, more economical functional forms can be often constructed as follows.

Consider a least squares estimation of $E[q_{t+1}((\underline{a}_{t-1}, a_t), (\underline{e}_t, E_{t+1})) | \underline{a}_{t-1}, \underline{e}_t]$ for a given set of \underline{a}_{t-1} and $a_t \in A_t^{(c)}$. This is a function of e_1, e_2, \dots, e_t , which seems to require t -dimensional basis functions. However, for example, if the information E_t follows or can be assumed to approximately follow the s^{th} -order Markov sequence ($s < t$), only the last s information, $e_{t-s+1}, e_{t-s+2}, \dots, e_t$, is the active arguments of the function; hence, the dimension can be reduced. As another example, if the information E_t is binary (e.g. 0 or 1), representing good quality or bad quality in the inspection, only the sum n_t of e_1, e_2, \dots, e_t is sufficient to characterize $E[q_{t+1}((\underline{a}_{t-1}, a_t), (\underline{e}_t, E_{t+1})) | \underline{a}_{t-1}, \underline{e}_t]$; hence, the dimension can be reduced to one. Such reductions of the dimension of the functional form increase the stability of the approximation of $E[q_{t+1}((\underline{a}_{t-1}, a_t), (\underline{e}_t, E_{t+1})) | \underline{a}_{t-1}, \underline{e}_t]$ with a functional form by the least squares method.

4 EXAMPLES

For the purpose to illustrate how the proposed scheme can be applied and to investigate the performance, the decision problems examined in De Groot (1970) are employed (Examples 1 and 4 of Chapter 12). These examples are selected here, since the analytical solution (Example 1) and the boundary of the solution (Example 4) are obtained.

4.1 Example 1: Sequential sampling from the Bernoulli distribution

4.1.1 Decision problem

A manufactured product is designed, and the performance of the product line is to be controlled. For simplicity, the probability p that a product is good quality is assumed to be either $1/3$ or $2/3$. If $p=2/3$, the product line is satisfactory; otherwise unsatisfactory. It is to be judged whether the product line is satisfactory. The decision maker has the option to perform inspections before her judgment. The maximum number of inspections is assumed to be n . The outcomes of the inspections are the sequence of random samples Y_1, Y_2, \dots, Y_n , which independently follow an identical Bernoulli distribution with a given parameter $p = \Pr[Y_i=0] = 1 - \Pr[Y_i=1]$ (0: good quality, 1: not good quality). The cost for inspecting one sample is assumed to be $c=1$. Given that the design was made and the product line was built, the penalty is imposed if and only if the judgment is incorrect, which is assumed to be $c_p = 20$. The prior distribution of p is assumed to be $\xi = \Pr[p=1/3] = 1 - \Pr[p=2/3]$ ($0 \leq \xi \leq 1$). The decision shall be made for a given value of ξ whether the first inspection should be performed, or make the judgment without any inspection. In the following the case of $n=2$ is considered, the analytical solution to which is available in De Groot (1970).

4.1.2 Application of the proposed scheme and result

The underlying random sequence Y_i in this decision problem is the outcomes from the inspections, each of which follows the Bernoulli distributions of the parameter p , which in turn is uncertain and is characterized by $\xi = \Pr[p=1/3] = 1 - \Pr[p=2/3]$. The information E_i is equal to Y_i ; i.e. the state of the underlying random sequence is deterministically known to the decision maker without uncertainty. The decision alternatives are $a^{(0)}$ (continue sampling), $a^{(1)}$ (terminate sampling and judge $p=1/3$) and $a^{(2)}$ (terminate sampling and judge $p=2/3$) at each decision time; hence, $A_i^{(c)} = \{a^{(0)}\}$, $A_i^{(s)} = \{a^{(1)}, a^{(2)}\}$. Decisions at a decision time are possible only if $a^{(0)}$ is chosen at all the earlier decision times.

The steps to apply the proposed scheme are explained for one value of ξ . These steps are repeated in order to obtain the set of the solutions for different values of ξ , which are shown in Figure 3. Note, however, such repetitions are not necessary in practice, since in a practical situation a single value of ξ is assigned based on the decision maker's degree of belief, for which the optimal decision is to be identified.

The first step is to simulate the realizations of p , i.e. $p^i, i=1, 2, \dots, b$. For each p^i , the realizations of the underlying random sequence (Y_1, Y_2) are simulated, i.e. $(y_1^i, y_2^i), i=1, 2, \dots, b$ (Step 1). In this example, $e_t^i = y_t^i, i=1, 2, \dots, b, t=1, 2$ (Step 2). The expected cost for $a^{(1)}$ at time $t=2$ is calculated for each realization (e_1^i, e_2^i) . For this, first the probability of $\Pr[p=1/3]$ is updated with the realization (e_1^i, e_2^i) by the Bayes' theorem. Based on the updated probability the expected cost for $a^{(1)}$ is calculated. The expected cost for $a^{(2)}$ is calculated in the same manner. By comparing these two values, the optimal decision at time t is obtained for each $e_2^i = (e_1^i, e_2^i)$. The maximized expected utilities, which are defined as the negative of the expected costs, $q_2(a_1, e_2^i)$, are obtained for each realization i (Step 3). The expected cost for $a^{(0)}$ (continuing sampling) at time $t=1$ is assumed to be approximated by $r_{1,0} + r_{1,1}e_1$. The coefficients $r_{1,0}, r_{1,1}$ are estimated with the set of points $(e_1^i, q_2(a_1, e_2^i))$ by the least square method. Then, the expected cost for $a^{(0)}$ at time $t=1$ is obtained for each realization i . Note in this example, the functional form $r_{1,0} + r_{1,1}e_1$ can precisely represent the expected cost for $a^{(0)}$, since e_1 takes only two values; therefore, a function with two coefficients is flexible enough (Step 4). The expected costs for $a^{(1)}$ and $a^{(2)}$ at $t=1$ are calculated in the same manner as $t=2$ for each realization i . The minimum of the expected costs for $a^{(0)}, a^{(1)}$ and $a^{(2)}$ is calculated for each realization i , whose negative values are the maximized expected utilities at time $t=1$ (Step 5). The average of these minimum expected costs for all the realizations i is the estimate of the expected cost for $a^{(0)}$ at time $t=0$. By comparing this with the expected costs for $a^{(1)}$ and $a^{(2)}$, the optimal decision at time $t=0$ is obtained. The optimal decisions for different values of ξ are shown in Figure 3. It is seen that the proposed scheme performs satisfactorily.

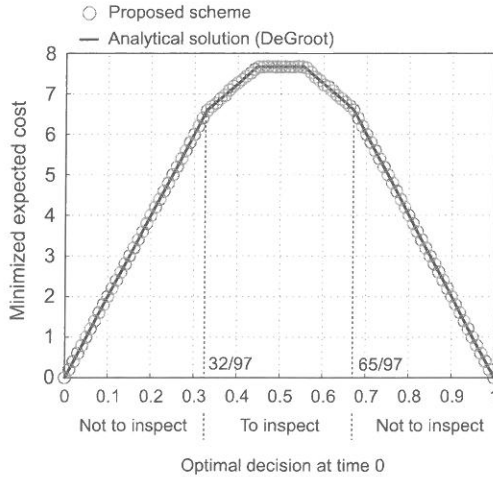


Figure 3. Optimal decisions in Example 1.

4.2 Example 2: Sequential sampling from the normal distribution

4.2.1 Decision problem

A manufactured product is designed, and the performance of the product line is to be controlled. The quality of the product is measured through an indicator Y and the indicator follows the normal distribution with unknown mean W and known precision r (= inverse of variance). The decision maker has the option to perform inspections before her judgment. The maximum number of inspections is assumed to be n . The outcomes of the inspections are the sequence of random samples Y_1, Y_2, \dots, Y_n , which follows the identical distributions as Y . The random samples are observable without uncertainty to the decision maker; hence, the information $E_t = Y_t$. The decision maker has to judge whether the mean of Y is above w_0 or not. The penalty of misjudgment is proportional to the difference between the true mean value w and w_0 ; i.e. $L = |w - w_0|$. The cost for one inspection is c .

4.2.2 Application of the proposed scheme and result

The decision alternatives are $a^{(0)}$ (continue sampling), $a^{(1)}$ (terminate sampling and judge $w \leq w_0$) and $a^{(2)}$ (terminate sampling and judge $w > w_0$) at each decision time; $A_t^{(c)} = \{a^{(0)}\}$, $A_t^{(s)} = \{a^{(1)}, a^{(2)}\}$. Decisions at a decision time are possible only if $a^{(0)}$ is chosen at all the earlier decision times. In this example, the expected cost for continuing sampling at time t is found to be a function only of the average m_t of the realizations of $e_t = (e_1, e_2, \dots, e_t)$. Here, a functional form $r_{t,0} + r_{t,1}m_t + r_{t,2}m_t^2 + r_{t,3}m_t^3$ is assumed for the least squares estimation, where $m_t = \sum_{j=1}^t e_j / t$. Note that other functional forms are tested and the results are found to be insensitive to the choice of functional forms.

The optimal decisions are computed and shown for different values of the mean μ and precision τ (inverse of variance) of the unknown mean W , for the case where $n=10$, $w_0=1$ and $c=0.2$, see Figure 4. The optimal decisions obtained by the proposed scheme are indicated with the symbols. The optimal decision bounds for the case where n is infinite are analytically obtained by De Groot (1970) for a subset of μ and τ : At the left side of the left line in the figure the optimal decision is $a^{(0)}$, at the right side of the right line the optimal decision is $a^{(1)}$ for $\mu \leq 1$ and $a^{(2)}$ for $\mu > 1$, and between the two lines, optimal decisions are not obtained. Given that $n=10$ is sufficient large, these two results are comparable. As can be seen in Figure 4, the optimal decisions obtained by the proposed scheme corresponds to the optimal decisions obtained by De Groot (1970); furthermore, the proposed scheme can identify the optimal decisions in the domain where the optimal decisions are not obtained by De Groot (1970).

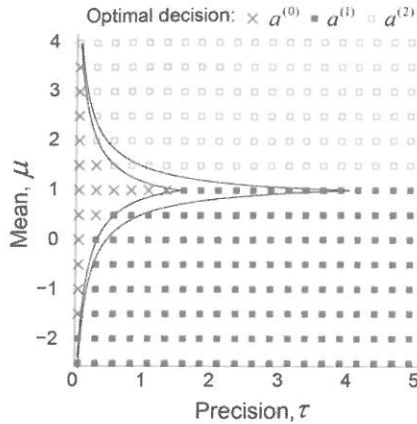


Figure 4. Optimal decisions in Example 2.

5 CONCLUSION AND FUTURE WORK

An optimization scheme for a class of the sequential decision problem is proposed. The class of the decision problem is characterized as: the random phenomena of relevance underlying the decision problems are not affected by the decisions in the course of sequential decisions. The efficiency and advantages of the proposed optimization scheme are demonstrated with two numerical examples on the sequential sampling in the context of quality control of manufactured product. Note however that under this framework variable decision rules or competing decision rules are possible.

In the examples, the updated probability distributions given the information \underline{e}_i can be obtained analytically. However, in general this is not the case. In such cases, Markov Chain Monte Carlo simulations to simulate a realization(s) from the updated probably distributions may be useful; the implementation of which is addressed as a future task.

An engineering application example of the presented scheme is provided in an accompanying paper by Anders and Nishijima (2012) in the context of early warning for avalanche.

REFERENCES

- Anders A, Nishijima K. 2011. Adaption of option pricing algorithm to real time decision optimization in the face of emerging natural hazards. 11th International Conference on Application of Statistics and Probability in Civil Engineering, ICASP11, Faber MH, Kohler J, Nishijima K, eds., Zurich, Switzerland.
- Anders A, Nishijima K. 2012. Enhanced least squares Monte Carlo method for real-time decision optimizations. IFIP WG 7.5, Armenia.
- Corotis R, Ellis JH, Jiang M. 2005. Modeling of risk-based inspection, maintenance and life-cycle cost with partially observable Markov decision processes. *Structure and Infrastructure Engineering* 1 (1): 75-84.
- De Groot H. 1970. *Optimal Statistical Decisions*, John Wiley&Sons, Inc.
- Longstaff FA, Schwartz ES. 2001. Valuing American Options by Simulation: A Simple Least-Squares Approach. *The Review of Financial Studies* 14 (1): 113-147.
- Nishijima K, Graf M, Faber MH. 2008. From Near-real-time Information Processing to Near-real-time Decision Making in Risk Management of Natural Hazards. *Inaugural International Conference of the Engineering Mechanics Institute, EM08*, University of Minnesota, Minneapolis, Minnesota.
- Nishijima K, Graf M, Faber MH. 2009. Optimal evacuation and shut-down decisions in the face of emerging natural hazards. *Proceedings of the tenth international conference on structural safety and reliability, ICOSSAR2009*, Osaka, Japan.
- Straub D, Faber MH. 2005. Risk Based Inspection Planning for Structural Systems. *Structural Safety* 27 (4): 335-355.

Enhanced least squares Monte Carlo method for real-time decision optimizations for evolving natural hazards

A. Anders & K. Nishijima

Department of Civil Engineering, Technical University of Denmark, Denmark

ABSTRACT: The present paper aims at enhancing a solution approach proposed by Anders & Nishijima (2011) to real-time decision problems in civil engineering. The approach takes basis in the Least Squares Monte Carlo method (LSM) originally proposed by Longstaff & Schwartz (2001) for computing American option prices. In Anders & Nishijima (2011) the LSM is adapted for a real-time operational decision problem; however it is found that further improvement is required in regard to the computational efficiency, in order to facilitate it for practice. This is the focus in the present paper. The idea behind the improvement of the computational efficiency is to “best utilize” the least squares method; i.e. least squares method is applied for estimating the expected utility for terminal decisions, conditional on realizations of underlying random phenomena at respective times in a parametric way. The implementation and efficiency of the enhancement is shown with an example on evacuation in an avalanche risk situation.

1 INTRODUCTION

Real-time decision optimization has become an interesting and challenging topic with the progress of real-time information processing technology. Relevant applications in civil engineering include situations where operational decisions have to be made in response to real-time information on evolving natural hazard events. In these situations, all real-time information available can and should be best utilized to find the optimal decisions at respective times; taking into account not only possible future outcomes, but also opportunities to make decisions in future times. This type of decision problem is generally described within the framework of the pre-posterior/sequential decision analysis, see Nishijima et al. (2009); however, the development of efficient solution schemes to the formulated decision problems has remained a technical challenge.

An efficient solution scheme is proposed by Anders & Nishijima (2011), taking basis in the Least Squares Monte Carlo method (hereafter, abbreviated as LSM), which is developed originally by Longstaff & Schwartz (2001) for American option pricing. In Anders & Nishijima (2011) the original LSM is extended and applied to an example for a real-time operational decision problem for shut-down of the operation of a technical facility in the face of an approaching typhoon. However, due to multiple evaluations of the expected consequences for different possible future states of the typhoon by means of Monte Carlo simulation (MCS), the solution scheme becomes less efficient, if the computational time required for MCS becomes dominant. The present paper proposes an enhanced solution scheme, which overcomes this drawback.

The present paper is organized as follows. Section 2 formulates the real-time decision problems in consideration within the framework presented in Nishijima & Anders (2012). Section 3 provides a brief introduction to the extensions of the LSM. Thereafter, the proposed enhancement to the extended LSM is introduced. Section 4 presents an application example, which illustrates the performance of the enhanced LSM (eLSM). Section 5 concludes the presented work.

2 REAL-TIME DECISION FRAMEWORK

2.1 Problem setting

The decision situation considered in the present work is characterized by the following characteristics, see Nishijima et al. (2009): (a) The hazard process evolves relatively slowly and allows for reactive decision making; (b) information relevant to predict the severity of the evolving hazard event can be obtained prior to its impact; (c) the decision making is subject to uncertainties, part of which might be reduced at a cost; (d) decision makers have options for risk reducing activities which may be commenced at any time, supported by the information available up to the time. Here, "waiting" to commence the risk reducing measures implies the reduction of uncertainty but might also reduce available time to complete the risk reducing activities; (e) and on top of all, the decisions must be made fast, in near-real time. The decision makers are then required to make decisions whether they commence one of the risk reducing activities which at the same time terminates the decision process (hence, hereafter these are called terminal decisions) or they postpone making a terminal decision.

2.2 Formulation of decision problem

The decision problem characterized above can be formulated in accordance with Nishijima & Anders (2012). Denote by A_t the decision set consisting of possible decision alternatives at time t . Here, time is discretized. It is assumed that the decisions must be terminated before or at time n ; hence, $t = \{0, 1, 2, \dots, n\}$. The decision set A_t generally depends on the decisions made before time t . If a decision maker decides to terminate the decision process, no decision alternative is available at later decision times. It is thus convenient to divide the decision set into two mutually exclusive subsets; i.e. $A_t = A_t^{(c)} \cup A_t^{(s)}$, $A_t^{(c)} \cap A_t^{(s)} = \emptyset$ where $A_t^{(c)}$ consists of one decision alternative $a_t^{(c)}$ "waiting" (i.e. $A_t^{(c)} = \{a_t^{(c)}\}$) and $A_t^{(s)}$ is the set consisting of risk reducing decisions available. Let \mathbf{E}_t be a set of variables representing possible information available at time t on the states of the evolving natural hazard event in consideration.

Given that no terminal decision is made up to time t , the optimal decision a_t^* at time t is identified as the one that maximizes the expected utility at time t conditional on the collection of the information up to time t :

$$E[U_t(\mathbf{Z}, a_t^*) | \mathbf{e}_t] = \begin{cases} \max_{a_t \in A_t} E[U_t(\mathbf{Z}, a_t) | \mathbf{e}_t], & \text{for } t = 0, 1, \dots, n-1 \\ \max_{a_t \in A_t^{(s)}} E[U_t(\mathbf{Z}, a_t) | \mathbf{e}_t], & \text{for } t = n \end{cases} \quad (1)$$

where, for $t = 0, 1, \dots, n-1$ and $a_t^{(c)}$,

$$E[U_t(\mathbf{Z}, a_t^{(c)}) | \mathbf{e}_t] = \int E[U_{t+1}(\mathbf{Z}, a_{t+1}^*) | a_t^{(c)}, \mathbf{e}_{t+1}] f(\mathbf{e}_{t+1} | \mathbf{e}_t) d\mathbf{e}_{t+1}. \quad (2)$$

Here, $U_t(\mathbf{z}, a_t)$ is the utility, which is a function of the decision alternative a_t and the realization \mathbf{z} of the hazard index \mathbf{Z} relevant for the decision problem. The hazard index \mathbf{Z} is defined through the underlying random sequence $\{\mathbf{Y}_t\}_{t=0}^n$, representing the evolution of the natural hazard event. $\mathbf{e}_t = (\mathbf{e}_0, \mathbf{e}_1, \dots, \mathbf{e}_t)$ is the collection of the information available up to time t . Here, it is assumed that $\mathbf{y}_t = \mathbf{e}_t$, ($t = 0, 1, \dots, n$); namely, the state of the event relevant to the decision problem is known to the decision maker without uncertainty. Thus, the symbols \mathbf{y}_t and \mathbf{e}_t are utilized interchangeably in the following. $f_t(\cdot | \mathbf{e}_t)$ is the conditional probability density/mass function of information \mathbf{E}_{t+1} given $\mathbf{E}_t = \mathbf{e}_t$. From Equation 2 it is seen that for the decision $a_t^{(c)}$ at time t the optimization requires to know all optimal decisions at future times, $t+1, t+2, \dots, n$; hence, backward induction is required. Equation 1 can be rewritten as:

$$q_t(\mathbf{e}_t) = \begin{cases} \max\{h_t(\mathbf{e}_t), c_t(\mathbf{e}_t)\}, & \text{for } t = 0, 1, \dots, n-1 \\ h_t(\mathbf{e}_t), & \text{for } t = n. \end{cases} \quad (3)$$

Here,

$$q_t(\mathbf{e}_t) = E[U_t(\mathbf{Z}, a_t^*) | \mathbf{e}_t] \quad (4)$$

$$h_t(\underline{\mathbf{e}}_t) = \max_{a_t \in A_t^{(s)}} l_t(a_t, \underline{\mathbf{e}}_t) \quad (5)$$

$$l_t(a_t, \underline{\mathbf{e}}_t) = E[U_t(\mathbf{Z}, a_t) | \underline{\mathbf{e}}_t], \quad a_t \in A_t^{(s)} \quad (6)$$

$$c_t(\underline{\mathbf{e}}_t) = E[q_{t+1}(\underline{\mathbf{e}}_t, \mathbf{E}_{t+1}) | \underline{\mathbf{e}}_t]. \quad (7)$$

The function $q_t(\underline{\mathbf{e}}_t)$, $t=0,1,\dots,n$, is the maximized expected utility, hereafter abbreviated as MEU. The functions $h_t(\underline{\mathbf{e}}_t)$ and $c_t(\underline{\mathbf{e}}_t)$ are named stopping value function (SVF) and continuing value function (CVF), respectively. Note that, whereas the evaluation of the SVF is straightforward in the sense that it does not require backward induction, the evaluation of CVF requires backward induction. However, no matter how complex the structure of the decision optimization problem may seem, $c_t(\underline{\mathbf{e}}_t)$ is only a function of $\underline{\mathbf{e}}_t$. Furthermore, if the underlying random sequence $\{\mathbf{Y}_t\}_{t=0}^n$ follows s^{th} -order Markov sequence, $c_t(\underline{\mathbf{e}}_t)$ is a function effectively of the last s information, $\mathbf{e}_{t-s+1}, \mathbf{e}_{t-s+2}, \dots, \mathbf{e}_t$.

3 ENHANCEMENT OF THE EXTENDED LSM

3.1 Extended LSM

The main technical challenge of the optimization problem formulated in Section 2.2 is the evaluation of the CVF. The CVF can in principle be evaluated by calculating the expected utility for each combination of all possible discretized future states and possible decision opportunities. However, in practice this is not computationally feasible, since the total number of the possible combinations increases exponentially as a function of the number n . The LSM circumvents this by employing the least squares method. The idea behind the LSM is that any regular function can be represented by a linear combination of an appropriate set of basis functions; therefore, the CVF is approximated as such, for details see Longstaff & Schwartz (2001). In the context of American option pricing, this means that if the price of a stock follows a first order Markov sequence, the price of its American option is a function only of the current stock price. Consequently the CVF is approximated as a superposition of basis functions whose argument is only the current stock price. The way on how this idea is implemented in the optimization is explained along with the extended version of the LSM (called extended LSM) in the following.

In Anders & Nishijima (2011), it is demonstrated that the idea behind the LSM can be applied for the case where the underlying random sequence follows an inhomogeneous higher-order Markov sequence. Therein, two extensions are made: (1) the assumptions on the underlying random sequence is relaxed from stationary first-order Markov sequence to non-stationary higher-order Markov sequence, and (2) the SVF is evaluated by MCS. Note that in many engineering applications the SVF cannot be evaluated analytically, unlike the case when executing American options. Moreover, the MCS in the second extension is computationally expensive and the computational effort increases proportional to n . In the following, the steps of the extended LSM are presented:

Step 1: A set of b independent realizations (paths) of the random sequence \mathbf{Y}_t is generated by MCS according to the Markov transition density $f_t(\mathbf{y}_{t+1} | \mathbf{y}_t)$, $t=0,1,\dots,n-1$ with the initial condition $\mathbf{Y}_0 = \mathbf{y}_0$, where $\mathbf{y}_t = (\mathbf{y}_{t0}, \mathbf{y}_{t1}, \dots, \mathbf{y}_{ts})$. These paths are denoted by $\mathbf{y}^i = (\mathbf{y}_0^i, \mathbf{y}_1^i, \dots, \mathbf{y}_n^i)$, $i=1,2,\dots,b$, where $\mathbf{y}_0^i = \mathbf{y}_0$ for all paths, see Figure 1 (a).

Step 2: The SVF for all realizations $\{q_n^i(\mathbf{y}_{n-1}^i)\}$, $i=1,2,\dots,b$, are estimated by additional MCS.

Step 3: Starting at the time horizon n as illustrated in Figure 1 (a), for each path i the value of the MEU $q_n(\underline{\mathbf{y}}_{n-1}, \mathbf{Y}_n)$ is identified by equating $q_n(\mathbf{y}_{n-1}^i) = h_n(\mathbf{y}_{n-1}^i)$ according to Equation 3.

Step 4: Moving to time $n-1$ the CVF is approximated. This begins by relating each MEU $q_n(\mathbf{y}_{n-1}^i)$ to \mathbf{y}_{n-1}^i , to obtain the dataset $(\mathbf{y}_{n-1}^i, q_n(\mathbf{y}_{n-1}^i))$, $i=1,2,\dots,b$, see the dots in Figure 1 (b). This dataset is utilized to approximate the CVF $c_{n-1}(\underline{\mathbf{y}}_{n-1})$ with the least squares method. The

approximated CVF is illustrated by the curve in Figure 1 (b). See Nishijima & Anders (2012) for details. The approximated CVF is denoted by $\hat{c}_{n-1}(\underline{y}_{n-1})$.

Step 5: Having obtained $\hat{c}_{n-1}(\underline{y}_{n-1})$ for time $t = n-1$, the realizations of $q_{n-1}(\underline{y}_{n-1}, \mathbf{Y}_{n-1})$, i.e. $q_{n-1}(\underline{y}_{n-1}^i)$, $i = 1, 2, \dots, b$, are determined as follows:

$$q_{n-1}(\underline{y}_{n-1}^i) = \begin{cases} h_{n-1}(\underline{y}_{n-1}^i), & \text{if } h_{n-1}(\underline{y}_{n-1}^i) > \hat{c}_{n-1}(\underline{y}_{n-1}^i) \\ q_n(\underline{y}_n^i), & \text{otherwise.} \end{cases} \quad (8)$$

The procedure is repeated backwards in time until $t=1$, hence $q_1(\underline{y}_1^i)$ is obtained for all paths.

Step 6: At $t=0$ the estimate $\hat{c}_0 = \hat{c}_0(\mathbf{y}_0)$ is defined as the average of the realizations $q_1(\underline{y}_1^i)$, $i = 1, 2, \dots, b$. Finally $q_0(\mathbf{y}_0)$ is obtained as the maximum of $\hat{c}_0(\mathbf{y}_0)$ and $h_0(\mathbf{y}_0)$. The optimal decision is the one that corresponds to the maximum.

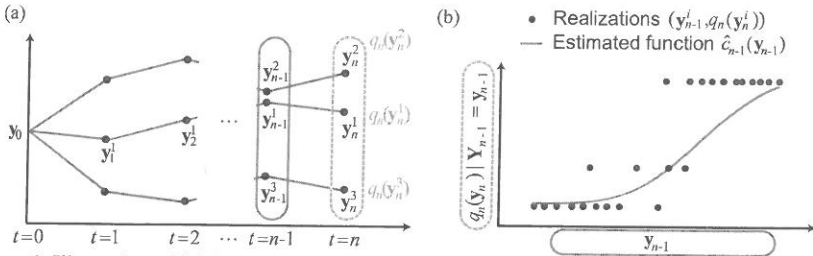


Figure 1. Illustration of (a) three paths of a underlying random sequence with corresponding values $q_n(\underline{y}_n^i)$ ($i = 1, 2, 3$) at time n and (b) the estimation of the CVF using the sets $(\underline{y}_{n-1}^i, q_n(\underline{y}_n^i))$.

3.2 Enhancement of the extended LSM

As seen in Section 3.1, additional MCS are required in Step 2 to estimate the SVF in the extended LSM. The enhanced LSM (eLSM) circumvents this by applying the least squares method for the estimation of the SVF. The general idea is explained in the following.

Analogous to Equation 5 the SVF $h_{t,\text{eLSM}}(\underline{y}_t)$ of the eLSM is defined as maximum of the conditional expected utilities $l_{t,\text{eLSM}}(a_t^{(j)}, \underline{y}_t)$ with respect to the terminal decisions $a_t^{(j)} \in A_t^{(s)}$. Here, the functions $l_{t,\text{eLSM}}(a_t^{(j)}, \underline{y}_t)$ are estimated with the least squares method using the realizations $\{\underline{y}_t^i\}_{i=1}^b$, similar to the estimation of the CVF described in Section 3.1; i.e. by linear combination of basis functions $\{L_{t,k}(\cdot)\}_{k=1}^K$ with unknown coefficients $r_{t,k}^{(j)}$

$$l_{t,\text{eLSM}}(a_t^{(j)}, \underline{y}_t) \cong \sum_{k=1}^K L_{t,k}(\underline{y}_t) r_{t,k}^{(j)}. \quad (9)$$

Therein the least squares method is utilized to estimate the coefficients $\mathbf{r}_t^{(j)} = (r_{t,1}^{(j)}, r_{t,2}^{(j)}, \dots, r_{t,K}^{(j)})^T$ by minimizing the sum of the squared distances between the observed realizations of the dependent variable $l_{t,\text{eLSM}}(a_t^{(j)}, \underline{y}_t)$ in the dataset and their fitted values; in the matrix form this is expressed by

$$\mathbf{r}_t^{(j)} = \arg \min_{\mathbf{r}} \|\mathbf{u}_t^{(j)} - \mathbf{L}_t \mathbf{r}\|_2^2 \quad (10)$$

where $\|\cdot\|_2$ denotes the Euclidian norm, \mathbf{L}_t is a $b \times K$ matrix consisting of values of basis functions $\{L_{t,k}(\cdot)\}_{k=1}^K$ which are functions of realizations of \underline{y}_t and $\mathbf{u}_t^{(j)}$ the $b \times 1$ vector of observed future utilities $u_t(\mathbf{z}^i, a_t^{(j)})$, $i = 1, 2, \dots, b$, given the realization \mathbf{z}^i of the hazard index related to the path \underline{y}_t^i and decision $a_t^{(j)}$ is made at time t . Note that $u_t(\mathbf{z}^i, a_t^{(j)})$ is a realization of $l_{t,\text{eLSM}}(a_t^{(j)}, \underline{y}_t^i)$. Furthermore, to avoid a bias introduced by the least squares estimation within the determination of the MEU, Equation 8 is changed to:

$$q_{t,\text{eLSM}}(\underline{y}_t^i) = \begin{cases} u_t^*(\mathbf{z}^i, a_t^*), & \text{if } \hat{h}_{t,\text{eLSM}}(\underline{y}_t^i) > \hat{c}_{t,\text{eLSM}}(\underline{y}_t^i) \\ q_{t+1,\text{eLSM}}(\underline{y}_{t+1}^i), & \text{otherwise} \end{cases} \quad (11)$$

where $u_t^*(\mathbf{z}^i, a_t^*)$ is the observed future utility of path i for the optimal terminal decision a_t^* .

4 EXAMPLE

The aim of this section is to demonstrate how the eLSM can be applied to an engineering decision problem and to compare its performance to that of the extended LSM. For this purpose, a decision situation of the evacuation of people in the face of an avalanche event is considered.

4.1 Problem setting

Consider a village located nearby a mountain slope having a critical angle for snow avalanches. Given prevailing winter conditions and critical snow heights, a decision has to be made whether to evacuate people from the village. Assume that the occurrence of a severe avalanche, causing significant damages to the village, depends only on the additional snow height S_t ; i.e. S_t is the hazard index. Further, if S_t exceeds the threshold \tilde{s} ($=800$ [mm]) a severe avalanche occurs. Weather forecast by a meteorological agency predicts that snowfall can occur within the next hours, which increases the likelihood of the occurrence of the avalanche. However, the duration and the intensity of the snowfall are uncertain. New information becomes available every 8 hours from the meteorological agency; i.e. the time interval between the subsequent decision phases is set to 8 hours ($dt=8$). At each decision phase a decision is made according to information available. Three decision alternatives are assumed; i.e. to evacuate the people $a^{(1)}$, not to evacuate $a^{(2)}$, and to wait $a^{(c)}$. It is assumed that the evacuation takes 16 hours to complete.

4.2 Consequence model

The consequences are postulated as follows, see also Table 1: The consequence is equal to $C_{Ev}=1$ in two cases: (1) when the evacuation has been initiated but the avalanche does not occur, and (2) when the evacuation is completed before the avalanche occurs. A consequence of $C_D=10$ is incurred if the avalanche occurs and the people are not evacuated or the evacuation was initiated but not completed. No consequence is incurred only in the case when no evacuation is initiated and no avalanche occurs.

Table 1. Conditions and associated consequences postulated in the consequence model.

People	Additional snow height in the time period $[0, t]$	
	$S_t > \tilde{s} = 800$ [mm]	$S_t \leq \tilde{s} = 800$ [mm]
Not evacuated	$C_D = 10$	0
Evacuated	$C_{Ev} = 1$	$C_{Ev} = 1$

4.3 Probabilistic snowfall model

A hypothetical probabilistic snowfall model is assumed, which is adapted from a rainfall model developed by Hyndman & Grunwald (2000). Let X_t denote the random sequence representing the amount of snowfall in the time period $(t-dt, t]$. Hereafter, this time period is denoted by $(t-1, t]$ (i.e. the time unit is $dt=8$) and thus $\{X_t\}_{t=0}^n$ for simplicity. The distribution of X_t is a mixture comprising a discrete component concentrated at $x_t=0$ and a continuous component for $x_t>0$. The discrete component of X_t represents the non-occurrence of snowfall and is characterized by the Bernoulli sequence J_t , whose conditional probability function is:

$$\pi_t(\mathbf{y}_{t-1}, \mathbf{y}_{t-2}) = P(J_t = 1 | \mathbf{Y}_{t-1} = \mathbf{y}_{t-1}, \mathbf{Y}_{t-2} = \mathbf{y}_{t-2}) = l(\mu_t(\mathbf{y}_{t-1}, \mathbf{y}_{t-2})) \quad (12)$$

where $\mathbf{Y}_t = (J_t, X_t)$ and $l(\cdot)$ denotes the logit function which is defined as $l(\mu) = \exp(\mu) / (1 + \exp(\mu))$ if $\mu > 0$ and $l(\mu) = 0$ otherwise, and

$$\mu_t(\mathbf{y}_{t-1}, \mathbf{y}_{t-2}) = \alpha_0 + \alpha_1 j_{t-1} + \alpha_2 j_{t-2} + \alpha_3 \log(x_{t-1} + c_1) + \alpha_4 \log(x_{t-2} + c_2) + \alpha_5 t^2. \quad (13)$$

The continuous component of X_t is strictly positive and characterizes the intensity of the snowfall. If $J_t = 1$, X_t is described by the continuous conditional density $g_t(x | \mathbf{y}_{t-1})$, $x > 0$. $g_t(\cdot | \cdot)$ follows the Gamma distribution with shape parameter κ and mean $v_t(\mathbf{y}_{t-1})$, where

$$\log(v_t(\mathbf{y}_{t-1})) = \beta_0 + \beta_1 j_{t-1} + \beta_2 \log(x_{t-1} + c_3) + \beta_3 t^2. \quad (14)$$

Then the transition probability density function of X_t is defined as (see Figure 2):

$$f_t(x_t | \mathbf{y}_{t-1}, \mathbf{y}_{t-2}) = (1 - \pi_t(\mathbf{y}_{t-1}, \mathbf{y}_{t-2}))\delta_0(x_t) + \pi_t(\mathbf{y}_{t-1}, \mathbf{y}_{t-2})g_t(x_t | \mathbf{y}_{t-1}) \quad (15)$$

where δ_0 is the Dirac delta function. The additional snow height is obtained by multiplying the snow intensity by the factor F_s , which accounts for the density of the snow; i.e.

$$S_t = S_t(\mathbf{y}_t) = \sum_{s=0}^t F_s x_s 1_{\{j_s=i\}} = S_{t-1} + F_t x_t 1_{\{j_t=i\}}. \quad (16)$$

Hence, S_t (the hazard index) at time t is characterized by the index S_{t-1} at time $t-1$ and a stochastic process composed of a second- and a first-order Markov process (the second term in the rightmost equation). The values of the parameters of the model are summarized in Table 2. The time frame is set to three days; i.e. $n=9$.

Table 2. Parameters of the probabilistic snowfall model.

Parameter	Value	Parameter	Value
j_{-1}, j_0, S_0	0, 0, 0	$\mathbf{c} = (c_1, c_2, c_3)$	(0.15, 0.3, 0.5)
$\boldsymbol{\alpha} = (\alpha_0, \alpha_1, \dots, \alpha_5)$	(4.5, 0.26, 0.1, 0.5, 0.05, -0.2)	κ	1.5
$\boldsymbol{\beta} = (\beta_0, \beta_1, \beta_2, \beta_3)$	(1.95, -0.2, 0.25, -0.04)	F_s	10

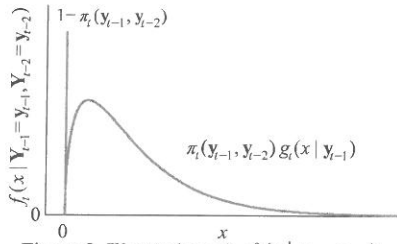


Figure 2. Illustration of $f_t(x | \mathbf{y}_{t-1}, \mathbf{y}_{t-2})$.

4.4 Solution with the eLSM

Here, the MEU in Equation 3 is defined by the expected consequence; i.e. the minimum operator is used and the inequality sign of Equation 8 is turned. The steps in Section 3.1 are executed with the extended LSM and the eLSM to obtain the optimal decision.

Step 1: By MCS, generate b independent realizations of $\{\mathbf{Y}_t\}_{t=1}^n$ and $\mathbf{S}^i = (S_0^i, S_1^i, \dots, S_n^i)$, $i=1, 2, \dots, b$, where $S_t^i = S_t^i(\mathbf{y}_t^i)$ and $\mathbf{y}_t^i = (j_t^i, x_t^i)$. The realizations $\mathbf{y}_1^i, \mathbf{y}_2^i, \dots, \mathbf{y}_n^i$ are simulated according to the probability density functions in Equations 12 and 15; the paths are denoted by $\mathbf{y}^i = (\mathbf{y}_{-1}^i, \mathbf{y}_0^i, \dots, \mathbf{y}_n^i)$, where $\mathbf{y}_{-1}^i = \mathbf{y}_{-1}$, $\mathbf{y}_0^i = \mathbf{y}_0$ and $i=1, 2, \dots, b$.

Step 2: For each \mathbf{y}_t^i the value $h_t^i = h_t(\mathbf{y}_t^i, \mathbf{y}_{t-1}^i)$ of the SVF is estimated. At time $n=9$ the consequence related to each realization and decision is assumed to be known; i.e. either s_n^i exceeds the threshold \tilde{s} or not, thus $h_{n,MC}^i = h_{n,eLSM}^i$ for all i . Further, for $t=1, 2, \dots, n-1$

(1) with the extended LSM: Simulation of additional M paths $\mathbf{y}_n^{i,m} = (\mathbf{y}_{-1}^i, \dots, \mathbf{y}_t^i, \mathbf{y}_{t+1}^{i,m}, \dots, \mathbf{y}_n^{i,m})$, $m=1, 2, \dots, M$, for which the observed consequences $u_t(\mathbf{s}^m, a_t^{(j)})$, $j=1, 2$, are determined. Here \mathbf{s}^m is the realization of the additional snow height related to the path realization $\mathbf{y}_n^{i,m}$. Define $\hat{l}_{t,MC}(a_t^{(j)}, \mathbf{y}_t^i, \mathbf{y}_{t-1}^i) = \sum_{m=1}^M u_t(\mathbf{s}^m, a_t^{(j)}) / M$, then

$$\hat{h}_{t,MC}^i = \min\{\hat{l}_{t,MC}(a_t^{(1)}, \mathbf{y}_t^i, \mathbf{y}_{t-1}^i), \hat{l}_{t,MC}(a_t^{(2)}, \mathbf{y}_t^i, \mathbf{y}_{t-1}^i)\} \quad (17)$$

(2) with the eLSM as explained in Section 3.2: Define

$$\hat{h}_{t,eLSM}^i = \min\{\hat{l}_{t,eLSM}(a_t^{(1)}, \mathbf{y}_t^i, \mathbf{y}_{t-1}^i), \hat{l}_{t,eLSM}(a_t^{(2)}, \mathbf{y}_t^i, \mathbf{y}_{t-1}^i)\} \quad (18)$$

where $\hat{l}_{t,eLSM}(a_t^{(j)}, \mathbf{y}_t^i, \mathbf{y}_{t-1}^i) = \mathbf{L}_t^i \cdot \mathbf{r}_t^{(j)}$, $j=1, 2$. The vector $\mathbf{r}_t^{(j)}$ of the coefficients related to $a_t^{(j)}$ is computed by Equation 10. \mathbf{L}_t^i denotes the i^{th} row of matrix \mathbf{L}_t ; \mathbf{L}_t consists of values of basis functions with arguments \mathbf{y}_t , \mathbf{y}_{t-1} and S_t ; e.g. for 1st order linear basis functions

$$\mathbf{L}_t = \begin{bmatrix} 1 & x_t^1 & x_{t-1}^1 & s_t^1 \\ 1 & x_t^2 & x_{t-1}^2 & s_t^2 \\ \vdots & \vdots & \vdots & \vdots \\ 1 & x_t^b & x_{t-1}^b & s_t^b \end{bmatrix} \quad (19)$$

For $t=0$ set $\hat{l}_0^{(j)} = \hat{l}_{0,MC}^{(j)}(a_0^{(j)}, \mathbf{y}_0, \mathbf{y}_{-1}) = \hat{l}_{0,eLSM}^{(j)}(a_0^{(j)}, \mathbf{y}_0, \mathbf{y}_{-1}) = \sum_{i=1}^b u_0(s^i, a_0^{(j)}) / b$, $j=1,2$.

Step 3: Starting at time n , for both LSM approaches, the values of $q_{n,MC}^i = q_{n,MC}(\mathbf{y}_n, \mathbf{y}_{n-1})$ and $q_{n,eLSM}^i$ are set equal to $\hat{h}_{n,MC}^i$ and $\hat{h}_{n,eLSM}^i$ respectively, for all i .

Step 4: Moving to time $n-1$ the values of $c_{n-1}(\mathbf{y}_{n-1}, \mathbf{y}_{n-2})$ are similarly estimated for both approaches using the least squares method as described in Section 3.1.

Step 5: Then, for each path i determine the values of $q_{n-1}(\mathbf{y}_{n-1}, \mathbf{y}_{n-2})$:
(1) for the extended LSM with the estimate $\hat{h}_{i,MC}^i$ obtained by means of MCS:

$$q_{n-1,MC}^i = \begin{cases} \hat{h}_{n-1,MC}^i, & \text{if } \hat{h}_{n-1,MC}^i < \hat{c}_{n-1,MC}^i \\ q_{n,MC}^i, & \text{otherwise} \end{cases} \quad (20)$$

(2) for eLSM with the estimate $\hat{h}_{i,eLSM}^i$ obtained by means of the least squares method:

$$q_{n-1,eLSM}^i = \begin{cases} u_{n-1}^{*,i}, & \text{if } \hat{h}_{n-1,eLSM}^i < \hat{c}_{n-1,eLSM}^i \\ q_{n,eLSM}^i, & \text{otherwise} \end{cases} \quad (21)$$

where $u_{n-1}^{*,i}$ denotes the observed future consequence in path i for the optimal terminal decision a_{n-1}^* . As in Section 3.1, moving another time step back the same procedure is repeated. This is continued until time $t=1$ and for each path $q_{1,MC}^i$ and $q_{1,eLSM}^i$ are determined.

Step 6: Execute Step 6 of Section 3.1.

4.5 Results

To evaluate the performance of the eLSM compared to the extended LSM, both methods are applied to solve the decision problem of the example. The optimal decision at the initial time is obtained by estimating the expected consequences for the three decisions alternatives. Various types and degrees of basis functions are implemented; e.g. linear, Legendre and Chebyshev polynomials. Applying these basis functions, it is found that the results do not significantly differ. Thus, only the results obtained with linear basis functions are presented.

Figure 3 illustrates the findings for different parameter settings of the LSM. Therein, Figure 3 (a) shows for increasing number b of paths, $b = \{10^2, 3 \cdot 10^2, 10^3, 3 \cdot 10^3, 10^4, 3 \cdot 10^4, 10^5\}$, the convergence of the consequence estimates for the three decisions. For each b the estimates are calculated by the average of 100 computations of the indicated method. To be able to compare the results 100 different yet fixed sets of random numbers are used to generate the paths in Step 1. Hence, the estimates for the terminal decisions are identical for all methods; they are presented by solid lines with circles. The following results are obtained for $b=10^5$: $\hat{l}_0^{(1)} = 1.0192$, $\hat{l}_0^{(2)} = 0.8969$ and e.g. $\hat{c}_{0,eLSM} = 0.8055$ with the eLSM. The optimal decision is $a_0^{(c)}$ which is independent of the type of LSM; see Figure 3 (a). Further, the figure shows that the estimate \hat{c}_0 obtained by the extended LSM with $M=10$ is biased. Therefore it is not considered in Figure 3 (b) which illustrates the convergence rate in terms of the coefficient of variation (COV) of the estimates \hat{c}_0 as a function of the computational time [sec]. The figure shows a significant improvement with the eLSM in terms of computational time; a reduction by the factor of 100.

An application of the proposed approach in practice is presented in Figure 4. Figure 4 (a) illustrates a hypothetical time series of the additional snow height $\{S_t\}_{t=0}^6$ where the threshold \bar{s} is exceeded within the time interval (3,4]. Applying the eLSM subsequently for each time step it is found that the optimal decision at time $t=0$ is $a^{(c)}$ whereas at time $t=1$ it is found to be $a^{(1)}$ given that the snow height at time $t=1$ in the figure is realized.

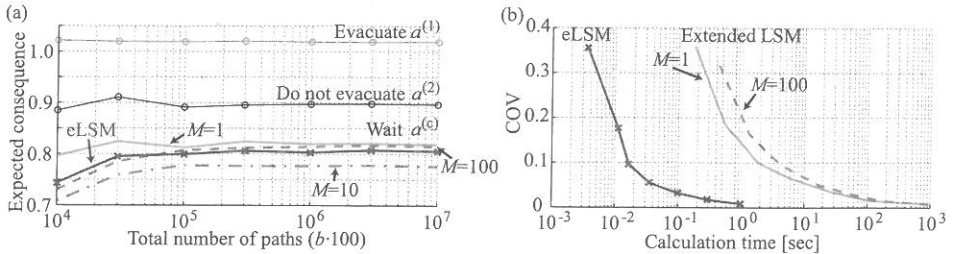


Figure 3. Comparison of the results of the extended LSM (with various numbers M of additional MCS) and eLSM. (a) Convergence of the average expected consequences with increasing total number of paths. (b) Illustration of the decreasing COV of \hat{c}_0 related to the increasing calculation time for one LSM computation as the number b of paths increases.

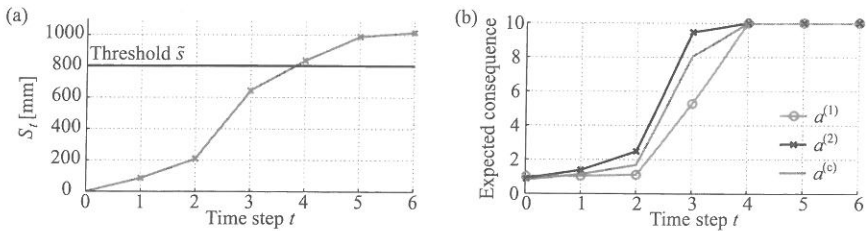


Figure 4. Illustration of (a) a hypothetical time series of S_t and (b) the corresponding time series of the estimated expected consequence of the three decision alternatives calculated with the eLSM and $b = 10^5$.

5 CONCLUSION

The present paper proposes an enhancement of the extended LSM in the context of real-time operational decision problems for evacuation in the face of emerging natural hazards. The proposed approach (eLSM) is applied to an example and it is found that the eLSM significantly improves the computational efficiency; by the factor up to 100.

6 ACKNOWLEDGEMENT

This research was partly supported by the Swiss National Science Foundation (Project number: 200021-125263).

REFERENCES

- Anders, A. & Nishijima, K., 2011. Adaption of option pricing algorithm to real time decision optimization in the face of emerging natural hazards. *Proceedings of 11th International Conference on Applications of Statistics and Probability in Civil Engineering* M. H. Faber, J. Köhler and K. Nishijima, Zurich, Switzerland.
- Hyndman, R. J. & Grunwald, G. K., 2000. Generalized additive modelling of mixed distribution Markov models with application to Melbourne's rainfall. *Australian & New Zealand Journal of Statistics*, 42 (2): pp. 145-158.
- Longstaff, F. A. & Schwartz, E. S., 2001. Valuing American Options by Simulation: A Simple Least-Squares Approach. *The Review of Financial Studies*, 14 (1): pp. 113-147.
- Nishijima, K. & Anders, A., 2012. Optimization of sequential decisions by least squares Monte Carlo method. *Proceedings of 16th IFIP WG 7.5 Working Conference*, Armenia, Yerevan.
- Nishijima, K., Graf, M. & Faber, M. H., 2009. Optimal evacuation and shut-down decisions in the face of emerging natural hazards. *Proceedings of ICOSSAR2009*, H. Furuta, D. M. Frangopol and M. Shinozuka, Osaka, Japan.

Sensitivity analysis methods for reliability problems

K.W. Breitung
Technical University of Munich, Germany

ABSTRACT: In reliability problems an important aspect is the study of the influence of parameter changes on the target reliability which is often more an operational value. Since in complex problems such quantities have to be computed often, efficient methods for doing this are desirable. Here some methods for sensitivity analysis are outlined. For a FORM/SORM analysis it is possible to get sensitivity measures from the Lagrange multiplier at the beta point. This allows simple estimates for the sensitivities with respect to parameters without additional computations. In the general case the partial derivatives and sensitivities of the failure probability with respect to parameters are given by surface integrals over the limit state surface. Such integrals can be transformed into domain integrals over the safe domain using the divergence theorem (Gauss-Ostrogradsky theorem). By modifying the integrands in a suitable way, it is possible to modify the integration domains such that the integrals can be estimated in a more efficient way.

1 INTRODUCTION

In many reliability problems one has parameters which can be varied or are not exactly known. Therefore the influence of changes in these parameters is an important information in studying such problems.

The basic reliability problem is in the form

$$P = \int_{g(\mathbf{x}) \leq 0} f(\mathbf{x}) \, d\mathbf{x} \quad (1)$$

where P is the failure probability, $f(\mathbf{x})$ is the probability density function and $g(\mathbf{x})$ the limit state function. If we consider the existence of parameters, the more general form of this problem can be written as:

$$P(\boldsymbol{\theta}_1, \boldsymbol{\theta}_2) = \int_{g(\mathbf{x}, \boldsymbol{\theta}_1) \leq 0} f(\mathbf{x}, \boldsymbol{\theta}_2) \, d\mathbf{x} \quad (2)$$

Here the first parameter vector $\boldsymbol{\theta}_1$ includes the parameters of the limit state function and the second vector $\boldsymbol{\theta}_2$ includes the parameters of the probability density function.

For sake of simplicity we will study here only the case that the limit state function depends on a single parameter τ , i.e. integrals of the form:

$$P(\tau) = \int_{g(\mathbf{x}, \tau) \leq 0} f(\mathbf{x}) \, d\mathbf{x} \quad (3)$$

These results can be generalized for the more complex cases.

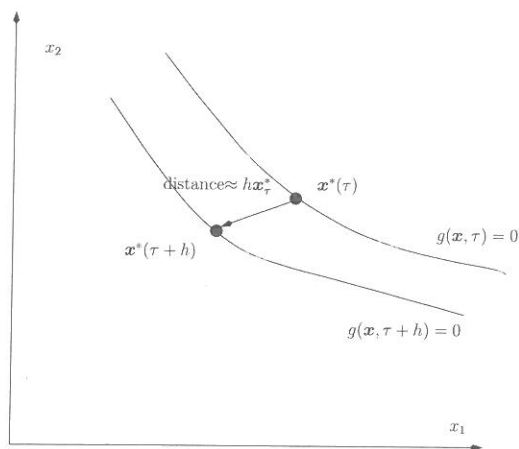


Figure 1: The movement of the PML-point as function of τ

2 PARAMETER DEPENDENCE OF THE PML-POINT

For the functions f and $g: \mathbb{R}^n \rightarrow \mathbb{R}$ in eq. (3) let the gradients of these functions be denoted by $\nabla_{\mathbf{x}} f$ (resp. $\nabla_{\mathbf{x}} g$) and the partial derivative with respect to τ by g_{τ} . The Hessian of f is written as \mathbf{H}_f and the Hessian of the function $g(\mathbf{x}, \tau)$ with respect to the first n variables is written as \mathbf{H}_g . We assume that for a fixed value of τ there is a unique PML (Point of maximum likelihood) $\mathbf{x}^*(\tau)$ and we write in a shorthand notation \mathbf{x}^* . The vector of the first derivatives of \mathbf{x}^* with respect to τ is written as \mathbf{x}_{τ}^* .

In the case of a standard normal distribution the PML is the beta point. This point \mathbf{x}^* is a stationary point of the Lagrangian function $L(\mathbf{x}, \lambda, \tau)$ defined by

$$L = f - \lambda g \quad (4)$$

Therefore for the point \mathbf{x}^* the following equation system must be fulfilled for arbitrary τ :

$$\begin{aligned} \nabla_{\mathbf{x}} f - \lambda \nabla_{\mathbf{x}} g &= \mathbf{o}_n, \\ g &= 0 \end{aligned} \quad (5)$$

with \mathbf{o}_n the n -dimensional zero row vector.

To find now the derivatives of the coordinates of the PML with respect to changes in the parameter τ , we differentiate this system with respect to τ and set all derivatives equal to zero. Differentiating the term in the i -th row ($1 \leq i \leq n$) gives

$$\begin{aligned} & \frac{d}{d\tau} \left[\frac{\partial f(x_1^*(\tau), \dots, x_n^*(\tau))}{\partial x_i} - \lambda \frac{\partial g(x_1^*(\tau), \dots, x_n^*(\tau), \tau)}{\partial x_i} \right] \\ &= \sum_{j=1}^n \left[\frac{\partial^2 f(x_1^*(\tau), \dots, x_n^*(\tau))}{\partial x_i \partial x_j} - \lambda \frac{\partial^2 g(x_1^*(\tau), \dots, x_n^*(\tau), \tau)}{\partial x_i \partial x_j} \right] \frac{dx_j^*(\tau)}{d\tau} \\ & - \lambda_{\tau} \frac{\partial g(x_1^*(\tau), \dots, x_n^*(\tau), \tau)}{\partial x_i} - \lambda \frac{\partial g(x_1^*(\tau), \dots, x_n^*(\tau), \tau)}{\partial x_i \partial \tau} = 0 \end{aligned} \quad (6)$$

and for the last line we get:

$$\sum_{i=1}^n \frac{\partial g(x_1^*(\tau), \dots, x_n^*(\tau), \tau)}{\partial x_i} \frac{dx_i^*(\tau)}{d\tau} + \frac{\partial g(x_1^*(\tau), \dots, x_n^*(\tau), \tau)}{\partial \tau} = 0 \quad (7)$$

This yields written in vector notation:

$$\begin{aligned} \mathbf{H}_f \mathbf{x}_\tau^* - \lambda \mathbf{H}_g \mathbf{x}_\tau^* - \lambda_\tau \nabla \mathbf{x} g - \lambda \nabla \mathbf{x} g_\tau &= \mathbf{o}_n, \\ (\nabla \mathbf{x} g)^T \mathbf{x}_\tau^* + g_\tau &= 0 \end{aligned} \quad (8)$$

Rearranging the terms we get:

$$\begin{aligned} (\mathbf{H}_f - \lambda \mathbf{H}_g) \mathbf{x}_\tau^* - \lambda \nabla \mathbf{x} g_\tau - \lambda_\tau \nabla \mathbf{x} g &= \mathbf{o}_n \\ (\nabla \mathbf{x} g)^T \mathbf{x}_\tau^* + g_\tau &= 0 \end{aligned} \quad (9)$$

This is a linear equation system with the $n + 1$ unknowns \mathbf{x}_τ^* and λ_τ

$$\begin{aligned} (\mathbf{H}_f - \lambda \mathbf{H}_g) \mathbf{x}_\tau^* - \lambda_\tau \nabla \mathbf{x} g &= \lambda \nabla \mathbf{x} g_\tau \\ -(\nabla \mathbf{x} g)^T \mathbf{x}_\tau^* + \lambda_\tau \cdot 0 &= g_\tau \end{aligned} \quad (10)$$

The solution is then:

$$\begin{pmatrix} \mathbf{x}_\tau^* \\ \lambda_\tau \end{pmatrix} = \begin{pmatrix} \mathbf{H}_f - \lambda \mathbf{H}_g & -\nabla \mathbf{x} g \\ -\nabla \mathbf{x} g^T & 0 \end{pmatrix}^{-1} \begin{pmatrix} \lambda \nabla \mathbf{x} g_\tau \\ g_\tau \end{pmatrix}$$

The result for standard normal densities was derived by Enevoldsen (1994). This can be generalized for the case of several equality and inequality constraints.

3 SURFACE INTEGRALS OVER BOUNDARIES OF STAR-SHAPED DOMAINS

For some special cases it is easy to calculate surface integrals, i.e. convex and star-shaped domains. For a given star-shaped domain D (i.e. for every point in the domain D all points on the straight line between the origin and this point are in D) we consider a surface integral over the boundary of the domain given by limit state function $g(\mathbf{x})$

$$I = \int_{g(\mathbf{x})=0} h(\mathbf{x}) \, ds(\mathbf{x}) \quad (11)$$

with $ds(\mathbf{x})$ denoting surface integration. This integral can be computed using directional sampling. Let \mathbf{u}_i , $i = 1, \dots, k$ be independent random unit vectors each with a uniform distribution over the n -dimensional sphere. Then an estimate of the integral is given by

$$\hat{I} = k^{-1} \sum_{i=1}^k F(\mathbf{u}_i) \quad (12)$$

with

$$F(\mathbf{u}_i) = \left(\frac{2\pi^{n/2}}{\Gamma(n/2)} \right) h(\mathbf{x}_i) \frac{|\mathbf{x}_i|^{n-1}}{|\mathbf{u}_i^T \cdot \mathbf{n}(\mathbf{x}_i)|} \quad (13)$$

where \mathbf{x}_i is the point where the ray from the origin in the direction of the normal \mathbf{u}_i hits the surface and $\mathbf{n}(\mathbf{x}_i) = |\nabla g(\mathbf{x})|^{-1} \nabla g(\mathbf{x})$ is the surface normal of the surface $\{g(\mathbf{x}) = 0\}$ at this point. The term in the round brackets is the surface of the unit sphere in the n -dimensional Euclidean space. The term in the second denominator is the cosine between the directions of \mathbf{u}_i and $\mathbf{n}(\mathbf{x}_i)$. The denominator adjusts the weight of the sample point to take into account the projection onto the unit sphere (see for example Thomas and Finney (1988), p. 1040).

4 THE SENSITIVITY OF INTEGRALS OVER THE FAILURE DOMAIN

For the general case Straub (2011) proposed a method based on replacing the surface integral by a domain integral using an auxiliary variable. Here we describe an alternative which allows also to calculate such surface integrals with holes in the safe or unsafe domain. Given is a limit state function $g(\mathbf{x}, \tau)$ depending on a parameter τ . To find the derivative of the integral with respect to the parameter τ , we write the difference

$$P(\tau + h) - P(\tau) = \int_{g(\mathbf{x}, \tau+h) \leq 0} f(\mathbf{x}) d\mathbf{x} - \int_{g(\mathbf{x}, \tau) \leq 0} f(\mathbf{x}) d\mathbf{x} \quad (14)$$

This can be written making a coordinate transformation (see figure 2) as

$$\int_{g(\mathbf{x}, \tau)=0}^{\delta(\mathbf{x})} f(\mathbf{x} + \delta(\mathbf{x})\mathbf{n}(\mathbf{x})) J(\mathbf{x} + \delta(\mathbf{x})\mathbf{n}(\mathbf{x})) ds_{\tau}(\mathbf{x}) \quad (15)$$

$J(\mathbf{x} + \delta(\mathbf{x})\mathbf{n}(\mathbf{x}))$ is the Jacobian of the coordinate transformation and the outward point-

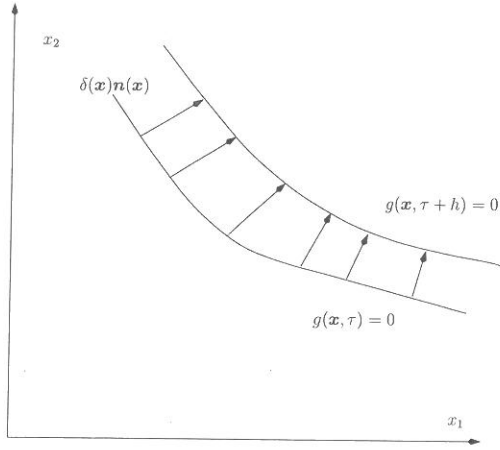


Figure 2: The difference $P(\tau + h) - P(\tau)$

ing surface normal is $\mathbf{n}(\mathbf{x}) = \nabla_{\mathbf{x}}g(\mathbf{x}, \tau) / |\nabla_{\mathbf{x}}g(\mathbf{x}, \tau)|^{-1}$. Further $ds_{\tau}(\mathbf{y})$ denotes surface integration over the surface $\{g(\mathbf{x}, \tau) = 0\}$. Due to the choice of the coordinate transformation we have that $J(\mathbf{x}) = 1$. The value of δ is implicitly defined by

$$g(\mathbf{x} + \delta(\mathbf{x})\mathbf{n}(\mathbf{x}), \tau + h) = 0 \quad (16)$$

To find an explicit formula for $\delta(\mathbf{x})$, we make a first order Taylor expansion of $g(\mathbf{x}, \tau)$.

$$g(\mathbf{x} + \delta(\mathbf{x})\mathbf{n}(\mathbf{x}), \tau + h) \approx \underbrace{g(\mathbf{x}, \tau)}_{=0} + \delta(\mathbf{x})\mathbf{n}(\mathbf{x})^T \nabla_{\mathbf{x}}g(\mathbf{x}, \tau) + hg_{\tau}(\mathbf{x}, \tau) \quad (17)$$

Setting the lefthand side equal to zero yields then

$$\delta(\mathbf{x}) \approx h \cdot \frac{-g_{\tau}(\mathbf{x}, \tau)}{|\nabla_{\mathbf{x}}g(\mathbf{x}, \tau)|} \quad (18)$$

This derivation is outlined in more detail in Breitung (1994), p. 23-5.

For an integral in the form as in eq. (3) the partial derivative with respect to τ is given by:

$$P'(\tau) = \int_{g(\mathbf{y}, \tau)=0} f(\mathbf{y}) \frac{-g_{\tau}(\mathbf{y}, \tau)}{|\nabla_{\mathbf{y}}g(\mathbf{y}, \tau)|} ds_{\tau}(\mathbf{y}) \quad (19)$$

Now we will try using the divergence theorem (also called Gauss-theorem or Gauss-Ostrogradsky-theorem) for transforming this surface integral into a domain integral. For a domain $\{g(\mathbf{x}, \tau) > 0\}$ and a vector function $\Phi(\mathbf{x})$ defined on this domain, this theorem says that:

$$\int_{g(\mathbf{y}, \tau)=0} \Phi(\mathbf{y})^T \mathbf{n}(\mathbf{y}) ds_\tau(\mathbf{y}) = \int_{g(\mathbf{x}, \tau) > 0} \text{div}(\Phi(\mathbf{x})) d\mathbf{x} \quad (20)$$

where \mathbf{n} is the outward pointing normal as defined before.

This result can be understood easily if the vector function $\Phi(\mathbf{x})$ is interpreted as the flow velocity of a fluid. The surface integral gives the total flow out of the domain $\{g(\mathbf{x}, \tau) \geq 0\}$, the domain integral the local changes in the flow. This result is valid even if there are holes in the domain as shown in figure 3. The integral of the divergence over the domain by the horizontal stripes gives the flows over the two dashed curves. If the integral of the divergence of the function is known over the domain with the horizontal stripes and the flow over one of the curves also we can calculate the flow over the other curve. By

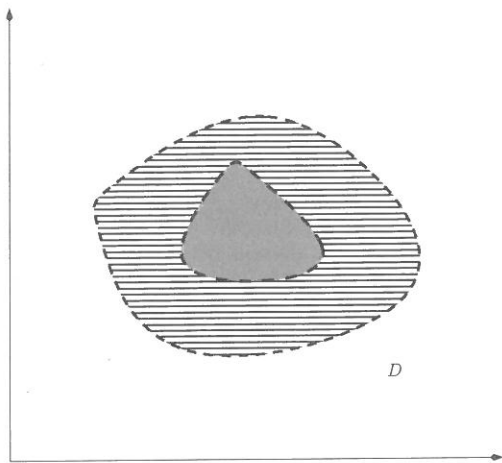


Figure 3: The divergence theorem for domains with holes

choosing an appropriate form for the vector function Φ we can ensure that the scalar product of it with the surface normal on the limit state surface is equal to the function $f(\mathbf{y})g_\tau(\mathbf{y}, \tau)|\nabla g(\mathbf{y}, \tau)|^{-1}$ there. This is the case if we set

$$\Phi(\mathbf{x}) = -f(\mathbf{x}) \frac{g_\tau(\mathbf{x}, \tau) \nabla_{\mathbf{x}} g(\mathbf{x}, \tau)}{|\nabla_{\mathbf{x}} g(\mathbf{x}, \tau)|^2} = -f(\mathbf{x}) \frac{g_\tau(\mathbf{x}, \tau)}{|\nabla_{\mathbf{x}} g(\mathbf{x}, \tau)|} \mathbf{n}(\mathbf{x}) \quad (21)$$

If we now try to apply the divergence theorem by calculating the divergence of the vector function $\Phi(\mathbf{x})$, we see that the integrand is not defined in the whole integration domain. The domain is the set where $g(\mathbf{x}, \tau) \geq 0$ and therefore the function will have at least one maximum there which means that the gradient $\nabla_{\mathbf{x}} g(\mathbf{x}, \tau)$ vanishes there. The integrand will be undefined at this maximum point and also at all other points where $\nabla_{\mathbf{x}} g(\mathbf{x}, \tau) = \mathbf{o}_n$, see figure 4. To resolve this problem, first we can try to exclude small neighborhoods of these points from the integration domain. In Breitung (1994) some results, theorem 22 and corollary 23 are proven for solving this difficulty, but these results are valid only if the Hessians \mathbf{H}_g at the points where the gradient vanishes are **definite**, not as erroneously stated there if they are regular. One way now would be to exclude all these points where the gradient is vanishing by introducing small spheres around them which are excluded from the integration domain.

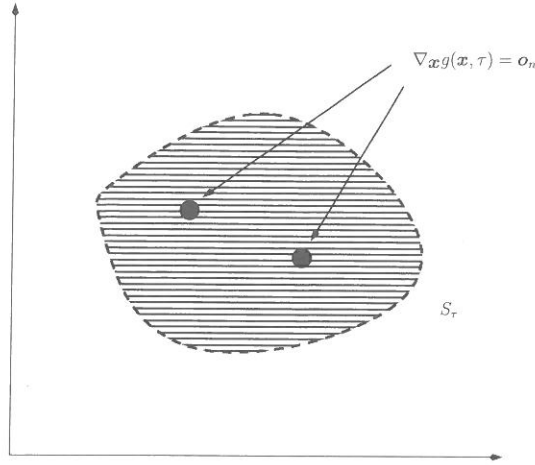


Figure 4: Points to be excluded

Another remedy for the problem of the zero gradients is to change the limit state function so that such zeros can be avoided. Let be given an upper bound for the norm of the gradient $\nabla_{\mathbf{x}}g(\mathbf{x}, \tau)$, i.e.

$$M = \max_{\mathbf{x} \in S} |\nabla_{\mathbf{x}}g(\mathbf{x}, \tau)| \quad (22)$$

We define a domain

$$S_{\epsilon, \beta_0} = \{|\mathbf{x}| > \beta_0, g(\mathbf{x}, \tau) > \epsilon\} \quad (23)$$

Such a domain is shown in figure 5. This is a subset of the safe domain if β_0 is chosen not

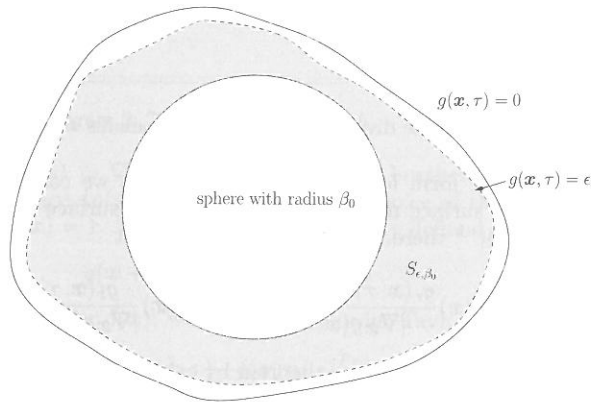


Figure 5: The domain S_{ϵ, β_0}

too large. Now a new limit state function g^* is defined by

$$g^*(\mathbf{x}, \tau) = g(\mathbf{x}, \tau) \exp\left(\mu|\mathbf{x}|^2/2\right) \quad (24)$$

where $\mu > 0$ is a parameter. This function defines the same limit state surface as the original limit state function g . The gradient of this new limit state function is:

$$\begin{aligned} \nabla_{\mathbf{x}}g^*(\mathbf{x}, \tau) &= \exp(\mu|\mathbf{x}|^2/2)\nabla_{\mathbf{x}}g(\mathbf{x}, \tau) + \mu g(\mathbf{x}, \tau) \exp(\mu|\mathbf{x}|^2/2)\mathbf{x} \\ &= \exp(\mu|\mathbf{x}|^2/2) (\nabla_{\mathbf{x}}g(\mathbf{x}, \tau) + \mu g(\mathbf{x}, \tau)\mathbf{x}) \end{aligned} \quad (25)$$

Under which conditions does the gradient $\nabla \mathbf{x}g^*$ vanish in the domain S_{ϵ, β_0} ? It will be equal to the zero vector if

$$\nabla \mathbf{x}g(\mathbf{x}, \tau) + \mu g(\mathbf{x}, \tau)\mathbf{x} = \mathbf{o}_n. \quad (26)$$

A necessary condition for this is:

$$|\nabla \mathbf{x}g(\mathbf{x}, \tau)| = \mu |g(\mathbf{x}, \tau)| |\mathbf{x}| \quad (27)$$

Since we assumed that $|\mathbf{x}| > \beta_0$ this condition says:

$$|\nabla \mathbf{x}g(\mathbf{x}, \tau)| \geq \mu |g(\mathbf{x}, \tau)| \beta_0 \quad (28)$$

Now, further in the domain of integration we have that $|g(\mathbf{x}, \tau)| > \epsilon$; this yields then

$$|\nabla \mathbf{x}g(\mathbf{x}, \tau)| \geq \mu \epsilon \beta_0 \quad (29)$$

Now, since M is an upper bound for the norm of the gradient in S , we find that the inequality

$$M \geq \mu \epsilon \beta_0 \quad (30)$$

$$\mu \leq \frac{M}{\epsilon \beta_0} \quad (31)$$

has to be fulfilled if there is a point in $S_{\beta_0, \epsilon}$ where the gradient is zero. If μ is chosen larger than $M/(\beta_0 \epsilon)$ there are no zeros of the gradient in the domain and the divergence theorem can be applied to calculate the integral of the divergence over S_{ϵ, β_0} .

For arbitrary ϵ we can integrate over the domain S_{ϵ, β_0} if the parameter μ is chosen large enough in dependence from ϵ . This allows to approximate the integral over the whole domain $\{|\mathbf{x}| > \beta_0, g(\mathbf{x}, \tau) > 0\}$ by extrapolating from these results for $\epsilon \rightarrow 0$.

The divergence can now be written in a simpler form using the result of Gradshteyn and Ryzhik (1980), p. 1116, equation 4'. If ϕ is a function and Ψ a vector function $\mathbb{R}^n \rightarrow \mathbb{R}^n$ then

$$\text{div}(\phi \cdot \Psi) = (\nabla \phi)^T \Psi + \phi \cdot \text{div}(\Psi) \quad (32)$$

This gives with the definition $h(\mathbf{x}) = -f(\mathbf{x})g_\tau(\mathbf{x}, \tau)|\nabla \mathbf{x}g(\mathbf{x}, \tau)|^{-1}$ the following form for the integrand in eq.(21)

$$\text{div}(h\mathbf{n}) = (\nabla h)^T \mathbf{n} + h \cdot \text{div}(\mathbf{n}) \quad (33)$$

Now, the divergence of the normal vector is related to the mean curvature $H(\mathbf{x})$ of the surface at this point by (see for example, exercise 12.18, p. 94 in Thorpe (1979)):

$$\text{div}(\mathbf{n}) = -(n-1)H(\mathbf{x}) \quad (34)$$

Therefore:

$$\text{div}(h\mathbf{n}) = (\nabla h)^T \mathbf{n} - h \cdot (n-1)H(\mathbf{x}) \quad (35)$$

For the case that the safe domain is unbounded, we can get a solution by considering a second sphere so far outside that the integral over this sphere of the integrand is negligible. Then we can estimate the integral over the limit state surface between the larger sphere and a smaller sphere inside using the divergence theorem.

5 CONCLUSIONS

Several methods for computing surface integrals were outlined. The method based on the divergence theorem allows to compute such integrals for arbitrary shapes by transforming them to domain integrals.

REFERENCES

- Breitung, K. (1994). *Asymptotic Approximations for Probability Integrals*. Berlin: Springer. Lecture Notes in Mathematics, Nr. 1592.
- Enevoldsen, I. (1994). Sensitivity Analysis of Reliability-Based Optimal Solution. *Journal of the Engineering Mechanics Division ASCE* 120(1), 198–205.
- Gradshteyn, I. and I. Ryzhik (1980). *Table of Integrals, Series and Products*. New York: Academic Press.
- Straub, D. (2011). Reliability updating with equality information. *Probabilistic Engineering Mechanics* 26(2), 254–258.
- Thomas, G. and R. Finney (1988). *Calculus and Analytic Geometry* (7th ed.). Reading, Mass.: Addison-Wesley.
- Thorpe, J. (1979). *Elementary Topics in Differential Geometry*. New York: Springer.

slangTNG - Scriptable software for stochastic structural analysis

C. Bucher
Vienna University of Technology, Vienna, Austria

S. Wolff
DYNARDO Austria GmbH, Vienna, Austria; formerly: Vienna University of Technology

ABSTRACT: Most engineering problems are so complex that the solution requires the application of computer-based numerical algorithms. For research purposes, particularly for algorithmic developments, interpreted scripting languages are chosen as the primary tools. While this enables rapid prototyping of the algorithms, it typically leads to substantial loss of computational performance as compared to solutions based on compiled languages. Hence, the final versions of the algorithms are frequently re-coded in a compilable language. This process, however, may involve quite substantial re-organization of the flow of execution, and possibly introduces unwanted errors. This paper presents an innovative approach to bringing interpreted and compiled languages close together. Applications to simple structural reliability analysis demonstrate the applicability and potential of this new approach.

1 INTRODUCTION

1.1 *Scripting for engineering application*

In many engineering application there is an increasing demand on the availability of tools to incorporate unavoidable random variability of loads and system properties into the workflow of structural analysis. This requires a close relation between the data structures as required for traditional Finite Element analyses and the stochastics tool required to obtain a suitable statistical description of the relevant responses. This is readily achievable by using established software development environments such as e.g. C++. Due to the required compilation process and the possibly code optimization associated with it, the computational performance can be quite impressive. On the other hand, the compile-link-cycles do not allow for quick checks how minor algorithmic modifications or extensions affect the quality of the desired results. This is particularly annoying when developing larger software projects in a distributed work environment, since each compile-link must check for potential changes in dependent modules which may lead to substantial delays.

It turns out that such algorithmic modifications or checking steps can be much faster performed using an interpreted scripting language, albeit at some loss of algorithmic performance. Typically this is not a real problem because test examples are usually chosen small enough not run into performance problems. A fairly thorough discussion on the use of scripting languages in computational science is given e.g. in (Langtangen 2008).

This paper focuses on the development of a C++ module library for structural, mathematical, and statistical analysis including graphics named slangTNG which can be driven through a scripting language as well. For performance reasons, the scripting language lua (Jerusalimschy 2006) was chosen. Since the flow control of lua is not too far from the flow of C++, it is fairly straightforward

to convert pieces of lua-Code to C++-code carrying out the same task. This is quite useful once the algorithm is fixed and computational performance must be enhanced.

A previous software project in which the authors were involved (SLang - the Structural Language) has been presented in (Bucher, Schorling, and Wall 1995). For a current commercial software project (*optiSLang* 2012), the reliability analysis module was developed exactly in this way, i.e. by implementing and testing the algorithms in `sLangTNG`. During this test phase, time-consuming compile-link-cycles could be eliminated. After finalizing the algorithms in script form, they were subsequently transferred into fast-running C++.

1.2 Motivating example

Suppose you want to generate random samples of a log-normally distributed random variable with a mean value of 1 and a standard deviation of 0.1. For checking purposes, you want to estimate mean and standard deviation from the samples. The easy way to answer the question is to fire up octave (or a commercial equivalent) and run the following script:

```
1 % Monte Carlo simulation of log-normal random variable
2 % Define mean value and standard deviation
3     x_bar = 1
4     sigma_x = 0.5
5
6 % Compute distribution parameters
7     mu = log(x_bar^2/sqrt(x_bar^2+sigma_x^2))
8     s = sqrt(log(sigma_x^2/x_bar^2+1))
9
10 % Produce samples
11 samples = lognrnd(mu, s, 1, 100);
12
13 % Check statistics
14     mm = mean(samples)
15     ss = std(samples)
```

While this procedural code is simple to read and understand, larger program structures in this style may have unfavorable consequences for C++ developers aiming at high levels of numerical performance:

- Not compatible with object-oriented paradigm
- Transition from script code to underlying C++ code not straightforward
- Quite difficult to support complex data structures
- Dependence on commercial development
- Portability cannot be controlled

Within `sLangTNG`, the procedure to carry out Monte Carlo simulation is based on random variable C++ objects. These objects carry information such as mean value and standard deviation, and they provide their own methods to generate samples. In addition, free functions are utilized to carry out tasks which are independent of the particular type of random variables such as estimation of mean values or standard deviations. Details are shown in the following section.

2 CONNECTING COMPILED VERSIONS AND SCRIPT VERSIONS

2.1 Making C++ objects available in lua

Any scripting language requires some “glue”-code which connects the data structures of the script interpreter to the data structures of the compiled object library. Establishing and maintaining this glue code can be substantial effort, particularly if parts of the class interfaces are changing over time. It is therefore helpful to utilize an automatic binding process. For the software package

sLangTNG, this binding of the C++ code to lua is performed automatically using swig (SWIG Documentation 2012). Several tests showed that the wrapper code generated is fast and efficient for virtually all practical cases. A further advantage of swig is the fact that bindings to other scripting languages such as python can be generated without additional effort.

For a class defining random variables, the following code contains sufficient information for swig to generate wrapper code and place it into a small library accessible from lua through the module name `stoch`. Although the module name can be chosen freely, for convenience it is helpful to use the name of the C++ namespace in which the class `Ranvar` resides.

```

1 %module stoch
2 %{ /* The includes required for the wrapper code: */
3 #include "stoch/simulate/ranvar.hpp"
4 %}
5
6 /* Our classes and methods to be wrapped: */
7 #include "stoch/simulate/ranvar.hpp"

```

Whenever the definition of the class `Ranvar` changes, the above listed code is passed through swig thus updating the class for the lua interpreter.

2.2 Compare C++ code to lua code

As a very simple case, consider again the Monte Carlo simulation of random variables. Within a C++ program structure, an object defining the random variable is constructed. The object's class must have methods to assign distribution parameters or statistical data, and a method to generate random samples. The procedure to simulate samples of a log-normally distributed random variable is shown below for the C++ version:

```

1 // Create and simulate a log-normally distributed random variable
2
3 // Instantiate an object rv of class RanvarLognormal
4 stoch::RanvarNormal rv();
5
6 // Instantiate an object s of class Matrix
7 tmath::Matrix s(2);
8
9 // Assign values to the matrix elements
10 s[0] = 1; s[1] = 0.5;
11
12 /* Use a method of the object rv (the class RanvarLognormal) to
13    assign statistics */
14 rv.SetStats(s);
15
16 /* Use a method of the object rv (the class RanvarLognormal) to
17    generate samples */
18 tmath::Matrix r = rv.Simulate(100);
19
20 // Access values in a loop
21 for (int i=0; i<100; ++i) {
22     printf("i: %d, r %g\n", i, r[i]);
23 }
24
25 // Estimate mean value
26 tmath::Matrix mean = stoch::statistics::Mean(r);
27
28 // Estimate standard deviation
29 tmath::Matrix std = stoch::statistics::Sigma(r);

```

This procedure utilizes several object-oriented features of C++. In the implementation of the classes such as `RanvarLognormal`, features such as inheritance and overloading are used. Note that the properties of the random variable can conveniently be defined in terms of mean and standard deviations (rather than in terms of distribution parameters).

The same procedure is shown below for the script version as implemented in sLangTNG:

```

1  -- Create and simulate random variables
2  -- Instantiate an object rv of class RanvarLognormal
3    rv = stoch.RanvarLognormal()
4
5  -- Instantiate an object s of class Matrix
6    s = tmath.Matrix(2)
7
8  -- Assign values to the matrix elements
9    s[0] = 1; s[1] = 0.5;
10
11 -- Use a method of the object rv (the class RanvarLognormal) to
12   assign statistics
13   rv:SetStats(s)
14
15 -- Use a method of the object rv (the class RanvarLognormal) to
16   generate samples
17   r = rv:Simulate(100)
18
19 -- Access values in a loop
20   for i=0,99 do
21     print("i", i, "r", r[i])
22   end
23
24 -- Estimate mean value
25   mean = stoch.Mean(r)
26
27 -- Estimate standard deviation
28   std = stoch.Sigma(r)

```

3 RELIABILITY ANALYSIS

3.1 FORM algorithm

As a further example, consider the implementation of the First-Order Reliability Method (FORM). This method can be cast into the form of an optimization algorithm in which the objective function is the distance from the origin β (or its squared value) in standard Gaussian space, and one single constraint that the value of the limit state function must be zero (i.e. the solution belongs to the failure domain and it is located on the boundary). However, for computational reasons (depending on the optimization algorithm) it might be more suitable to formulate the constraint as an inequality (i.e. the value of the limit state function must be non-positive). This is appropriate whenever the origin in standard Gaussian space does not belong to the failure domain. In most applications this will be true. The algorithm then realizes the following steps:

- Transformation to standard Gaussian space (Rosenblatt transform, implemented specifically for Nataf-model, Nataf 1962; Liu and DerKiureghian 1986). The first step involves a transformation to zero mean, unit variance correlated Gaussian variables Y_i by marginal transformations:

$$Y_i = \Phi^{-1}[F_{X_i}(X_i)]; \quad i = 1 \dots n \quad (1)$$

and the second step a transformation to standardized uncorrelated variables U_i :

$$\mathbf{U} = \mathbf{L}^{-1}\mathbf{Y}; \quad \mathbf{C}_{\mathbf{Y}\mathbf{Y}} = \mathbf{L}\mathbf{L}^T \quad (2)$$

- The inverse transformation is then given by:

$$X_i = F_{X_i}^{-1} \left[\Phi \left(\sum_{k=1}^n L_{ik} U_k \right) \right] \quad (3)$$

- Computation of "design point" \mathbf{u}^* by solving the constrained optimization problem

$$\mathbf{u}^* : \mathbf{u}^T \mathbf{u} \rightarrow \text{Min.}; \quad \text{subject to: } g(\mathbf{x}(\mathbf{u})) = 0 \quad (4)$$

- Linearization of the limit state function at the design point in standard Gaussian space. In general, any linear function $g(\cdot)$ in dimension n can be expressed as

$$\bar{g} : - \sum_{i=1}^n \frac{u_i}{s_i} + 1 = 0 \quad (5)$$

The quantities s_i can be interpreted geometrically as the intersection distances of the zero hyperplane $g(\mathbf{u}) = 0$ with the coordinate axis u_i (cf. Fig. 1). The minimum distance β of this hyperplane from the origin can easily be computed by

$$\sum_{i=1}^n \frac{1}{s_i^2} = \frac{1}{\beta^2} \quad (6)$$

By rotating the coordinate system with one axis into the direction from the origin to \mathbf{u}^* we immediately obtain

$$\text{Prob}(F) = \Phi(-\beta) \quad (7)$$

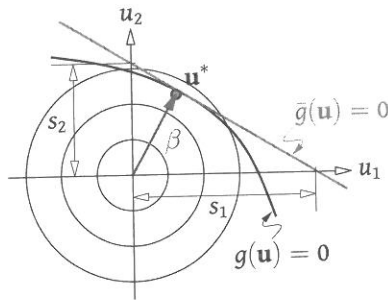


Figure 1: Linearization as utilized in FORM algorithm

The following listing shows a complete implementation of the FORM algorithm in `slangTNG`. It uses the gradient-based optimizer CONMIN (Method of feasible directions, Vanderplaats and Moses 1973; Vanderplaats 1973).

```

1 function form()
2   ops=optimize.Conmin(nvar, 1)
3   start = tmath.Matrix(nvar)
4   start:SetZero()
5   ops:SetDesign(start)
6   done = false
7   while (not done) do
8     done=(ops:Compute()==0)
9     x = ops:GetDesign()
10
11     obj = tmath.Norm(x)^2
12     ops:SetObjective(obj)
13
14     g = limitState(x)
15     ops:SetConstraints(tmath.Matrix({{g}}))
16   end
17   despo_u = ops:GetDesign()
18   beta = tmath.Norm(despo_u)
19   despo = rcev:FromStandardGauss(despo_u)
20 end

```

The algorithm is constructed such that the optimizer runs in *reverse communication* mode, i.e. the optimizer at each step immediately returns to the caller with a new set of design variables and asks for the value of objective function and constraints for this design. As such, the optimization is constructed as an infinite loop which is terminated at the optimizer's direct request for termination.

The same FORM algorithm has then been transferred into C++. The resulting code is shown in the following listing.

```

1 void stochTUL::doFORM() {
2     Conmin ops(nvar, 1);
3     tmath::Matrix start(nvar,1);
4     start.SetZero();
5     ops.SetDesign(start);
6     bool done = false;
7     while (!done) {
8         done = (ops.Compute()==0);
9         tmath::Matrix x = ops.GetDesign();
10
11         double obj = x.squaredNorm();
12         ops.SetObjective(obj);
13
14         double g = doLimit(x);
15         tmath::Matrix gg(1);
16         gg[0] = g;
17         ops.SetConstraints(gg);
18     }
19     despo_u = ops.GetDesign();
20     double beta = despo_u.norm();
21     despo = rvec->FromStandardGauss(start);
22 }

```

It is quite apparent that the structure of the algorithm is essentially identical in both languages. While the basic flow of the algorithm is *procedural*, it still makes use of *object-oriented* features.

The C++ code as shown calls the limit state function "doLimit" with the current design as supplied by the optimizer. This call can be used to feed results from a lua-script back into C++. This is particularly interesting for software which should be user-configurable in essential parts. For the FORM code as shown, the typical user-configurations are located in

- The set of random variables (distribution types, parameters, correlations)
- The limit state function defining the failure condition

Using the C++-interface of the lua interpreter, this can be achieved as shown in the following code (sanity checks have been removed for clarity)

```

1 double stochTUL::doLimit(const tmath::Matrix &X) {
2     tmath::Matrix Y = rvec->FromStandardGauss(X);
3     // Get access to limit state function
4     lua_getglobal(L, limit.c_str());
5     if (!lua_isfunction(L, -1)) return 0;
6     // Push random variables as lua table
7     lua_newtable(L);
8     for (unsigned int i=0; i<nvar; i++) {
9         lua_pushnumber(L, i); /* Push the table index */
10        lua_pushnumber(L, Y[i]); /* Push the cell value */
11        lua_rawset(L, -3); /* Stores the pair in the table */
12    }
13    int s=lua_pcall(L, 1, 1, 0);
14    // Convert result on the stack to number (g<0 means failure)
15    double g = lua_tonumber(L, -1);
16    return g;
17 }

```

3.2 SORM algorithm

A second-order correction can be readily obtained using a simple formula developed by Breitung 1992; Breitung 2012. With the aid of this formula, the SORM approximation of the probability of failure can be expressed as

$$P_{F,SORM} = \sqrt{\det \mathbf{H}^*} \cdot P_{F,FORM} \quad (8)$$

in which the matrix \mathbf{H}^* is defined in terms of the Hessian matrix \mathbf{H} and the gradient \mathbf{g} of the limit state function at the design point:

$$\mathbf{H}^* = \mathbf{P}^T \mathbf{H} \mathbf{P} + \mathbf{N} \mathbf{N}^T; \quad \mathbf{P} = \mathbf{I} - \mathbf{N}; \quad \mathbf{N} = \mathbf{n} \mathbf{n}^T; \quad \mathbf{n} = \frac{\mathbf{g}}{\|\mathbf{g}\|}; \quad \mathbf{H}' = \mathbf{I} - \frac{\mathbf{H}}{\|\mathbf{g}\|^2} \quad (9)$$

Note that this formulation requires neither a rotation of the coordinate system nor an eigenvalue analysis. The implementation in `slangTNG` code is shown below.

```

1 — Breitung's formula
2 function breitung(H, g)
3   local dim = H:Rows()
4   local n = g/tmath.Norm(g)
5   local eye = tmath.Identity(dim)
6   local Hp = eye-H/norm_g^2
7   local N = n*n:Transpose()
8   local P = eye - N
9   local Hstar = P:Transpose()*Hp*P + N:Transpose()*N
10  local fac = tmath.Det(Hstar)
11  return math.sqrt(fac)
12 end

```

As a numerical example, consider the problem of a simple linear limit state function $g(X_1, X_2) = X_1 - X_2$ containing two random variables X_1 and X_2 . Here X_1 is assumed to be lognormal with a mean value of 1.5 and a standard deviation of 0.3, and X_2 is exponential with a mean value of 0.2. The iteration progress (totally 113 evaluations of the limit state function) is shown in Fig. 2. The reliability index is $\beta = 2.99$, the first order approximation to the failure probability is 0.00138 and the second order approximation is 0.00136. The design point in original space is $\mathbf{x}^* = [1.191, 1.191]^T$ and in standard Gaussian space it is $\mathbf{u}^* = [-1.066, 2.795]^T$.

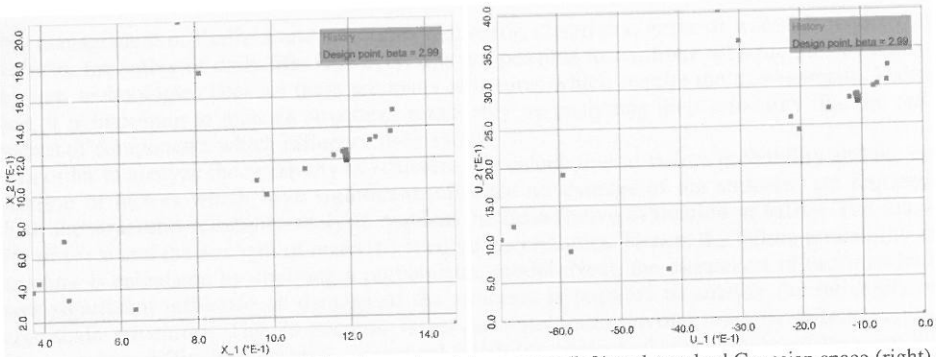


Figure 2: Iteration progress of FORM shown in original space (left) and standard Gaussian space (right)

4 CONCLUDING REMARKS

The software project `slangTNG` demonstrates that it is fairly easy to establish and maintain a stable connection between code written in a compiled language (C++) and an interpreted language (lua). This enables fast development cycles regarding the implementation of new or modified algorithms

for stochastic structural analysis using scripting and yet allows for a smooth transition to compiled versions of these algorithms.

The software is in the public domain (BSD-style license) and can be downloaded from <http://tng.tuxfamily.org>. Ready-made binaries for Mac OSX and Windows are available from the first author's homepage at Vienna University of Technology <http://info.tuwien.ac.at/bucher/Private/slangTNG.html>. An iOS version is available on the Apple App Store.

5 ACKNOWLEDGMENT

The authors would like acknowledge financial support from the Austrian Science Funds (FWF) as part of the Vienna Doctoral Programme on Water Resource Systems (DK-plus W1219-N22).

REFERENCES

- Langtangen, H. P. (2008). *Python Scripting for Computational Science*. Springer.
- Bucher, C., Y. Schorling, and W. A. Wall (1995). "SLang—the Structural Language, a tool for computational stochastic structural analysis". In: *Engineering Mechanics, Proceedings of the 10th Conference*. Ed. by S. Sture. ASCE, pp. 1123–1126.
- optiSLang*. URL: <http://www.dynardo.de/en/software/optislang.html> (visited on 10/10/2012).
- Ierusalimsky, R. (2006). *Programming in Lua*. 2nd. Rio de Janeiro: lua.org.
- SWIG Documentation*. URL: <http://www.swig.org/Doc2.0/SWIGDocumentation.html> (visited on 06/21/2012).
- Nataf, A. (1962). "Détermination des distributions de probabilités dont les marges sont données". In: *Comptes rendus de l'Académie des sciences* 225, pp. 42–43.
- Liu, P.-L. and A. DerKiureghian (1986). "Multivariate distribution models with prescribed marginals and covariances". In: *Probabilistic Engineering Mechanics* 1(2), pp. 105–112.
- Vanderplaats, G. N. and F. Moses (1973). "Structural optimization by methods of feasible directions". In: *Computers and Structures* 3, pp. 739–755.
- Vanderplaats, G. N. (Aug. 1973). *CONMIN: A FORTRAN program for constrained function minimization: User's manual*. Tech. rep. NASA-TM-X-62282. NASA Ames Research Center.
- Breitung, K. (1992). "Laplace Integrals and Structural Reliability". In: *Proceedings of the Second Canadian Conference on Computing in Civil Engineering*. Ed. by A. Razaqpur and M. Cheung. Society for Civil Engineering, pp. 437–447.
- Breitung, K. (2012). Personal communication at IFIP WG7.5 Working Conference on Reliability and Optimization of Structural Systems, Yerevan.

Reliability analysis of structure using metaheuristic method

K. Nakatsu, H. Furuta, K. Takahashi, K. Ishibashi & K. Ando
Kansai University, Japan

ABSTRACT: The purpose of this paper is the development of a new method to analyze the reliability of large-scale structures. The structural reliability analysis requires the quantitative evaluation of safety and the estimation of factors which have significant influence on damage of the structure. However, it is difficult to perform the practical reliability analysis of large-scale structures due to the trade-off between the accuracy and efficiency of calculation. The proposed method of this paper attempts to obtain samples which involve various failure modes by applying metaheuristics to the estimation of probabilistic space. In the propose method, global and local searches with a metaheuristic can perform the efficient sampling based on the occurrence probability of failure sample. Furthermore, it is expected that the obtained samples are useful for the calculation of the failure probability of structures. Numerical examples are presented to demonstrate the applicability of the proposed method to the structural reliability analysis.

1 INTRODUCTION

The management of lifelines and structures like roads, electricity, gases or waters is required to maintain the safety of daily life. However, it is not possible to reinforce all structures by applying new technologies because there are many structures which require the management. Therefore, it is important to manage structures reasonably by analyzing their reliability like the estimation of components which influence their safety.

In order to analyze the reliability of structure, the calculation of failure probability and the estimation of factors which have significant influence on damage of the structure are required. First, the structural reliability analysis requires the quantitative evaluation of safety. The intensity of force and the strength of materials involve uncertainties. Hence, the failure probability of structure is calculated by applying a probabilistic model. Next, the estimation of factors which have significant influence on damage of the structure is required to analyze the reliability of large-scale structures. This is because large-scale structures involve various failure modes. However, it is difficult to perform a practical reliability analysis due to a trade-off between the accuracy and efficiency of calculation (Cho 1993, Watanabe 1999, Matsubara 2008 and Tsuda 1997).

The purpose of this paper is to develop an efficient method to analyze the system reliability of large-scale structures. Importance Sampling or Subset Method has been used as a powerful tool to calculate the failure probability of structures with low failure probability. These methods previously need to estimate components which have large influence on damage of the structure. Authors have proposed a method to calculate the failure probability by using Markov Chain Monte Carlo (MCMC) (Gilks et al. 1996, Omori 2001, Iba 2003 and Garnerman 2006). However, it has been difficult to calculate the failure probability considering various failure modes in large-scale and complicated structures (Furuta et al. 2010). This is because there are large dif-

ferences among sampling probabilities of failure modes; if excluding failure modes with a high sampling probability, the calculated failure probability can not be accurate. In this paper, an attempt is made to propose a new method which can obtain samples which involve various failure modes by applying metaheuristics to the estimation of probabilistic space. In the propose method, global and local searches with a metaheuristic can perform the efficient sampling based on the occurrence probability of failure samples. Furthermore, it is expected that obtained samples are useful for the calculation of the failure probability of structures. Numerical examples are presented to demonstrate the applicability of the proposed method to the structural reliability analysis.

2 SEARCH OF FAILURE SAMPLES USING METAHEURISTICS

2.1 Application of Metaheuristics

In order to analyze the reliability of large-scale structures, it is necessary to evaluate the safety quantitatively by considering various failure modes. Then, the calculation of failure probability needs to resolve a trade-off between the efficiency and accuracy of calculation. It is considered that it becomes easier to overcome this problem if the probabilistic space of problem is clear. Therefore, in order to estimate the probabilistic space, this study attempts to search for samples of various failure modes by using Multi-Agent Optimization (MAO) (Nakatsu et al. 2011). Recently, many researchers focus on the application of metaheuristics to optimization problems. This is because many metaheuristic methods can perform the collective search to local optimum and global search to various solutions appropriately. In MAO which is one of metaheuristic methods, an agent which is a solution candidate searches for the optimum solution autonomously. In the search, an agent refers neighbor agent and decides the transition action based on the relation between them. In this paper, an agent selects an appropriate action from three transition actions, "approach", "repulsion" and "restraint". For example, an agent approaches better ones by "approach" in order to improve its state. Furthermore, the local change of each agent causes a big change in a design space; an agent can indirectly use information of design space obtained by others. Therefore, it is expected that MAO is effective to search for various failure samples efficiently and accurately.

2.2 Resampling Multi Agent Optimization

In order to estimate the probabilistic space efficiently and accurately, it is effective to search samples in descending order of occurrence probability. In this paper, re-sampling MAO is proposed in order to perform this search. Procedures of the proposed method are as follows:

- Step 1: Initialization of each agent's state
- Step 2: Action of agents
- Step 3: Re-sampling
- Step 4: If the search has not satisfied a termination conditions yet, go to Step2. Otherwise, the search has completed.

The proposed method uses the re-sampling operator and the search history in Steps 2 and 3. In Step2, an agent is compared to another based on its state. The comparison is performed using the following evaluation criteria.

Criterion 1: value of limit state function

An agent which does not satisfy any failure criteria is compared by the value of limit state function calculated by Equation 1.

$$lsf(x) = \sum_{j=1}^m f_j(x) \quad (1)$$

Here, x represents a random variable decided by agent. And, if a problem has m failure criteria, $f_j(x)$ represents the j -th failure criterion. If the failure of structure occurs when $f_j(x)$ is less than 0, $lsf(x)$ is minimized.

Criterion 2: occurrence probability

An agent which satisfies failure criteria is compared by the occurrence probability of sample calculated by Equation 2.

$$p(x) = \prod_{i=1}^d X(x_i) \quad (2)$$

Here, $X(x_i)$ represents the probabilistic distribution function of x_i . Failure agents are separated into several groups based on their failure modes or factors. Then, the indexes of agents for comparison are decided by their groups. In this paper, the number of search history of group is applied to the decision. For example, if the number of history of group A is less than group B, an agent of group A uses the occurrence probability of sample which is the highest among group A, and another of group B uses the occurrence probability of sample which is the lowest among group B. Moreover, if two groups have the same number of history, each agent uses the average of occurrence probability of its group. The high occurrence probability is superior to low in order to search failure samples which have high occurrence probabilities.

The proposed method can search for failure sample by using the evaluation criteria corresponding to a state of each agent respectively with the search history and the re-sampling. The re-sampling means the initialization of agent's state. The search history and re-sampling become useful by combining them. The search history is recorded by separating to groups and an agent which has the highest occurrence probability is recorded. In the proposed method, the re-sampling is applied to an agent which referred better search history. Moreover, an agent applying the re-sampling is added to the search history before its state is initialized. Through these processes, the evaluation criteria of agents change according to circumstances and then agents repeat the search and initialization. Agents intensively search around the sample which has the highest occurrence probability at first. This search increases the number of search history of certain groups. Hence, failure samples of other groups are better than the group which involves the highest occurrence probability with running the search. Therefore, it is expected that the proposed method can obtain various failure samples efficiently and accurately by increasing the number of executing generations.

3 NUMERICAL EXAMPLES

3.1 Application to one-bay and one-story rigid-frame structure

A one-bay and one-story rigid-frame structure shown in Figure 1 is used to demonstrate the applicability of the proposed method to the search of samples which involve various failure modes. The failure mechanism of this structure was given in Furuta (1993). The failure of the structure can be defined by four variables; vertical load P , horizontal load H , full plastic moment capacity of beam M_B and full plastic moment capacity of column M_C . In the numerical example, these factors are dealt with as random variables with the probabilistic distributions given in Table 1. The structure has 8 failure modes shown in Figure 2. Failure criteria of these modes are expressed in Equation 3.

$$\left. \begin{aligned}
 Z_1 &= 4M_B - 2PL \\
 Z_2 &= 2M_B + 2M_C - 2PL \\
 Z_3 &= 3M_B + M_C - 2PL \\
 Z_4 &= 4M_C - HL \\
 Z_5 &= 2M_B + 2M_C - HL \\
 Z_6 &= M_B + 3M_C - HL \\
 Z_7 &= 2M_B + 4M_C - 2PL - HL \\
 Z_8 &= 4M_B + 2M_C - 2PL - HL
 \end{aligned} \right\} \quad (3)$$

Here, L represents the length of column. In this numerical example, L is set to 100. The proposed method uses the failure criteria Z_i ($i=1\sim 8$) as the value of limit state function. In the applications of the proposed method, the number of agents is set to 100, the number of executing generations is set to 2,000 and the rate of accepting worse state is set to 20%. Furthermore, the proposed method is compared to the result of by Monte Carlo simulation with 100 million samples. The result obtained by Monte Carlo simulation can be considered as the exact solution because the probabilistic space of the structure in this example is small.

Table 1. Probability density function

Random variable	Basic probability distribution
P	$N(50, 10^2)$
H	$N(50, 10^2)$
M_B	$N(0.5, 0.1^2)$
M_C	$N(1.0, 0.2^2)$

Failure samples obtained by the proposed method and the result by Monte Carlo simulation are shown in Table 2. The column "Failure Modes" represents failure modes involved in the corresponding sample. For example if Z_7 and Z_8 in Equation 3 are lower than 0 in a sample, the content of "Failure Modes" is represented as "7, 8". In Table 2, samples were separated into groups based on their satisfied failure criteria shown in Equation 1. Then, samples which have the highest occurrence probability among each group were ranked based on the value of their occurrence probability. Therefore, samples of top 15 groups are shown in Table 2. The result of comparison demonstrated that the proposed method had the sampling accuracy equivalent to the exact solution. This is because there was no much difference among samples obtained by the proposed method and Monte Carlo simulation. In addition, in this study, it was verified that the number of groups of failure samples increases with the increase of the number of executing generations. In the proposed method, agents intensively search for samples with high occurrence probabilities at first. Then, each agent changes search areas based on the search history. In these processes, agents repeat intensive and global searches by using the re-sampling operator. Therefore, the proposed method could obtain various failure samples based on their occurrence probabilities.

Furthermore, the proposed method could obtain samples of top 15 groups equivalent to the results shown in Table 2 with 60 thousand samples (the number of agents was set to 40 and the number of executing generation was set to 1,500). On the other hand, Monte Carlo simulation required 1.5 million samples in order to obtain the equivalent accuracy. This is because the proposed method can search for various samples efficiently with the re-sampling operator and the search history. Through the numerical example, the applicability of the proposed method to the structural reliability analysis was confirmed.

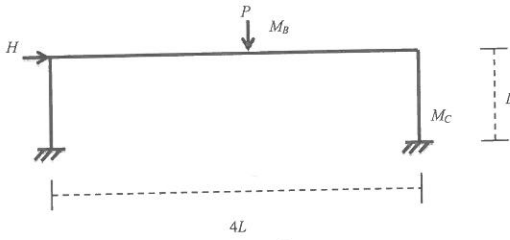


Figure 1: One-bay and one-story rigid-frame structure

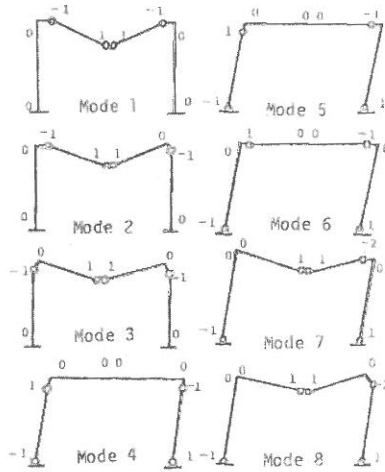


Figure 2: Basic failure modes

Table 2. Comparison to Monte Carlo method

Rank	Monte Carlo method	Rank	Proposed method	Failure modes
1	2.117.E-03	1	2.047E-03	8
2	2.113.E-03	2	1.860E-03	7
3	1.836.E-03	3	1.756E-03	7, 8
4	1.036.E-03	4	9.845E-04	4, 7
5	1.034.E-03	6	9.539E-04	1, 8
6	1.033.E-03	7	9.486E-04	1
7	1.028.E-03	5	9.750E-04	4
8	6.931.E-04	8	6.450E-04	4, 7, 8
9	6.876.E-04	9	5.752E-04	1, 7, 8
10	3.541.E-04	13	3.158E-04	4, 6, 7, 8
11	3.539.E-04	10	3.446E-04	1, 3, 7, 8
12	3.524.E-04	12	3.401E-04	4, 6, 7
13	3.512.E-04	11	3.438E-04	1, 3, 8
14	1.950.E-04	14	1.896E-04	1, 2, 3, 7, 8
15	1.948.E-04	15	1.881E-04	2, 7, 8

3.2 Application to lifeline network

In order to verify the effectiveness to the reliability analysis of large-scale structures, the proposed method is applied to a network model with 17 components (8 nodes and 9 links) shown in Figure 3. In this paper, the reliability analysis of the network model is performed according to Furuta et al. (2010). In the model of Figure 3, water distribution capacity of each component is given in Table 3. Here the external force F is a random variable distributed according to $N(3.0, 0.3^2)$. And, there is no correlation among components and random variables of all components are independently distributed. In the application of the proposed method, the number of agents is set to 200, the number of executing generations is set to 3,000 and the rate of accepting worse state is set to 20%.

First, the effectiveness of the search of failure samples is demonstrated, in which the results obtained by the proposed method and Monte Carlo simulation are compared as shown in Table 4. In this example, Monte Carlo simulation used 100 million samples. In Table 4, "Failure mode" represents failure components involved in the mode. In these results, the obtained samples were separated into groups according to their failure modes. Monte Carlo method could obtain only 8 failure modes. On the other hand, the proposed method could obtain more various failure modes and more samples with higher occurrence probabilities than Monte Carlo method. Therefore, it is expected that the proposed method is effective for the search of failure samples in the reliability analysis of large-scale structures.

Next, the availability of samples obtained by the proposed method in the reliability analysis is examined, in which the obtained samples were applied to the calculation of failure probability of the network model shown in Figure 3. The exact solution of failure probability is $2.00E-4$. In this paper, the failure probability was calculated by applying Importance Sampling, and samples obtained by the proposed method were used as the design points. Moreover, the proposed method was compared to MCMC Importance Sampling and Monte Carlo method with one million samples. The results obtained by 10 trials of each method are shown in Figures 4 and 5. In Figure 4, it was seen that the proposed method and MCMC Importance Sampling could calculate more accurate failure probabilities than Monte Carlo method. Figure 5 showed that the accuracy of MCMC Importance Sampling was superior to the proposed method. However, the study by Furuta et al. (2010) demonstrated that it was difficult for MCMC Importance Sampling to obtain samples which involved various failure modes. On the other hand, the application result shown in Table 3 demonstrated that the proposed method could obtain various failure modes in the network model. Therefore, the applicability and effectiveness of the proposed method to the reliability analysis of large-scale structure was confirmed.

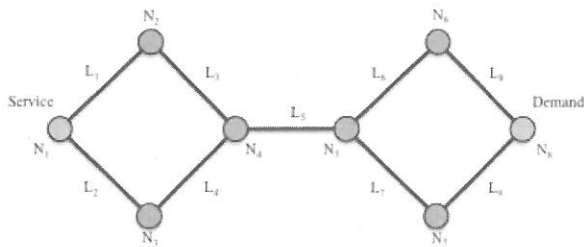


Figure 3: Network model with 17 components

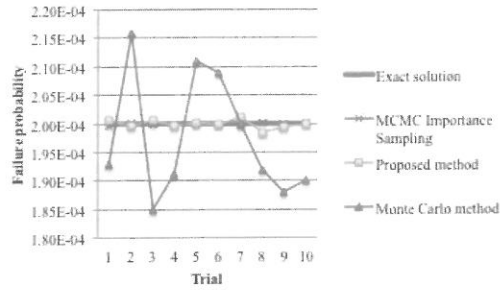


Figure 4: Calculation of failure probability (first trial case)

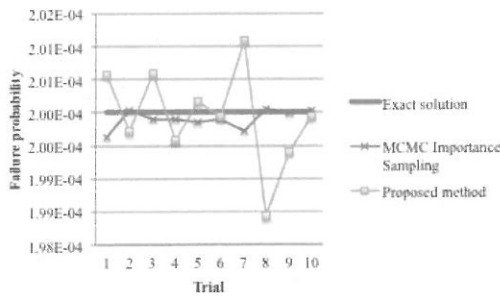


Figure 5: Calculation of failure probability (second trial case)

Table 3. Distribution capacities of components

Node		Link	
Component	Capacity	Component	Capacity
N_1	$N(6.8, 0.8^2)$	L_1	$N(7.0, 1.0^2)$
N_2	$N(6.8, 0.8^2)$	L_2	$N(6.5, 0.7^2)$
N_3	$N(6.8, 0.8^2)$	L_3	$N(6.5, 0.7^2)$
N_4	$N(6.8, 0.8^2)$	L_4	$N(7.0, 1.0^2)$
N_5	$N(7.0, 1.0^2)$	L_5	$N(7.0, 1.0^2)$
N_6	$N(7.0, 1.0^2)$	L_6	$N(7.0, 1.0^2)$
N_7	$N(6.9, 0.9^2)$	L_7	$N(8.0, 1.5^2)$
N_8	$N(7.0, 1.0^2)$	L_8	$N(6.0, 0.5^2)$
		L_9	$N(7.0, 1.0^2)$

Table 4. Failure probabilities of failure modes

Failure mode	Monte Carlo method		Proposed method	
	Rank	Probability	Rank	Probability
N5	1	7.63E-11	1	2.22E-10
N8	2	6.32 E-11	3	2.20E-13
L5	3	6.26 E-11	2	1.40E-10
N4	4	1.39 E-12	4	4.46 E-12
N1	5	1.20 E-12	5	60.9 E-12
N6,L7	6	7.73 E-15	7	8.12 E-15
N6,L7	7	3.32E-16	16	2.54 E-13
L6,L9	8	1.10E-19	13	1.02 E-16

4 CONCLUSIONS

In order to analyze the reliability of large-scale structure accurately and efficiently, in this paper, an attempt was made to propose a new method which can obtain samples which involve various failure modes by applying metaheuristics to the estimation of probabilistic space of problem. Through numerical examples, the applicability and effectiveness of the proposed method were demonstrated.

In order to estimate the probabilistic space, the proposed method attempted to search for samples of various failure modes based on their occurrence probabilities. In the proposed method, MAO which is one of metaheuristics uses the re-sampling operator and search history. Hence, agents repeat the search of failure samples and the initialization of their state. Moreover, the evaluation criteria change based on the search history. These additions enable MAO to obtain samples of various failure samples with multiple modes.

In numerical examples using simple and large-scale structures, the proposed method could obtain samples of various failure modes. The obtained samples had high occurrence probabilities in the probabilistic space of problem. In additions, the comparison to Monte Carlo simulation demonstrated that the proposed method could obtain various failure samples efficiently and accurately. Furthermore, samples obtained by the proposed method were useful to calculate the failure probability.

In order to sustain and improve the safety of structures, the reasonable structural management is required. Hence, a method of structural reliability analysis which can perform the quantitative evaluation of safety and the estimation of factors which have significant influence on damage of the structure is important. Therefore, it is expected that the proposed method is effective for the realization of reasonable structural management.

As the future works of this study, the proposed method requires additional verifications of the effectiveness to more larger or complicated structures.

REFERENCES

- Cho, T., 1993, *Structural Reliability Design as fundamental knowledge*, Sankaido (in Japanese).
- Garnerman, D., 2006, *Markov Chain Monte Carlo: Stochastic Simulation for Bayesian Inference*, CHAPMAN & HALL/CRC.
- Furuta, H., 1993, Evaluation of structural reliability based on fuzzy set theory, *Journal of japan society for fuzzy theory and systems*, 5(5): 1014-1022.
- Furuta, H., Nakatsu, K., Ishibashi, K., Motomura, N. and Shimizu, S., 2010, Efficient Calculation of Low Failure Probability by Using MCMC Importance Sampling, *Proceedings of the 25th Symposium on Reliability*, 86-91 (in Japanese).
- Gilks, W. R., Richardson, S. and Spiegelhalter, D. J., 1996, *MARKOV CHAIN MONTE CARLO IN PRACTICE*, CHAPMAN & HALL/CRC.
- Iba, Y., 2003, *Bayesian Statistics and Statistical Physics*, Iwanami Shoten (in Japanese).
- Matsubara, N., 2008, *Institution of Bayesian Statistics – Theory and Development*, Tokyo Tosho (in Japanese).
- Nakatsu, K., Furuta, H., Takahashi, K., Ishibashi, K. and Ando, K., 2011, Multi-Agent Optimization Method Focused on Individual Evolution, *9th World Congress on Structural and Multidisciplinary Optimization (WCSMO-9)*, CD-ROM.
- Omori, H., 2001, Recent Developments in Markov Chain Monte Carlo Method, *Journal of Japan Statistical Society*, 31(3): 305-344 (in Japanese).
- Tsuda, T., 1997, *Monte Carlo Method and Simulation – Stochastic Application of Computer –*, Baifukan (in Japanese).
- Watanabe, H., 1999, *Institution of Bayesian Statistics*, Fukumura Shuppan (in Japanese).

Designing for wind actions based on time-domain analysis: Accounting for statistical uncertainty

Daniel Straub, Iason Papaioannou

Engineering Risk Analysis Group, Technische Universität München
straub@tum.de, iason.papaioannou@tum.de

Alexander Michalski

SL-Rasch GmbH, Stuttgart, alex.michalski@sl-rasch.de

ABSTRACT: Engineers designing structures must work with incomplete and imperfect models. In standard design situations, safety provisions in codes implicitly account for these uncertainties. However, for more advanced design procedures that are not covered by the code, e.g. when dealing with non-linear dynamic problems, the engineer must explicitly address this uncertainty. A special case of uncertainty arises when time domain analysis is applied for determining the extreme response under wind loading: The statistical uncertainty due to a limited duration of the dynamic simulation. In this paper, we discuss this uncertainty and propose a reliability-based approach to account for this uncertainty in a semi-probabilistic design format. A quantitative relation between the computational efforts made in design and the additional safety required is established. Numerical investigations are performed for large membrane structures analyzed by means of Fluid Structure Interaction (FSI) simulation.

1 INTRODUCTION

Engineers designing structures must work with incomplete and imperfect models (Ditlevsen and Madsen 1996; Der Kiureghian and Ditlevsen 2009). In standard design situations, safety provisions in codes (e.g. Eurocode 0) implicitly account for these uncertainties. However, for more advanced design procedures that are not covered by the code, e.g. when dealing with non-linear dynamic problems, the engineer must explicitly address this uncertainty. A special case of model uncertainty arises when time domain analysis is applied for determining the extreme response under wind loading: The statistical uncertainty due to a limited duration of the dynamic simulation. As will be shown in this paper, this uncertainty can be considerable for realistic design situations.

In Eurocode 0, reference to this type of uncertainty is made in paragraph 5.2, which deals with design assisted by testing: “The statistical uncertainty due to a limited number of test results shall be taken into account.” The informative annex D of Eurocode 0 provides some additional guidance on how to deal with the uncertainty, but specific recommendations are made only for the case of resistance variables that have the Normal or Lognormal distribution. (The recommendations are based on, among others, work by Rackwitz (1983).) No detailed guidance is provided for the case where design values for load actions or load effects are determined based on limited samples, e.g. from a time series that is obtained either by numerical simulation or experiments (e.g. wind tunnel testing). To propose a criterion and a procedure for dealing with the statistical uncertainty in these cases is the goal of the present paper.

We discuss the uncertainty and propose a reliability-based approach to account for it in a semi-probabilistic design format. A quantitative relation between the computational efforts made in design and the additional safety required is established. Numerical investigations are performed for large membrane structures analyzed by means of Fluid Structure Interaction (FSI) simulation (Michalski et al. 2011).

2 DETERMINING THE EXTREME RESPONSE OF MEMBRANE STRUCTURES SUBJECT TO WIND LOADS

2.1 Structural analysis

The reliability of membrane structures (e.g. Figure 1) is commonly determined by extreme wind loads due to their large surface-to-mass ratio and their flexibility. Particularly transient wind load combined with wide spans and low pre-stress levels of the membrane can lead to dynamic amplifications of the structural response. The assessment of dynamic response of membrane structures is highly complex due to their special load carrying behavior, their material properties and their distinct structural interaction with flow induced effects.

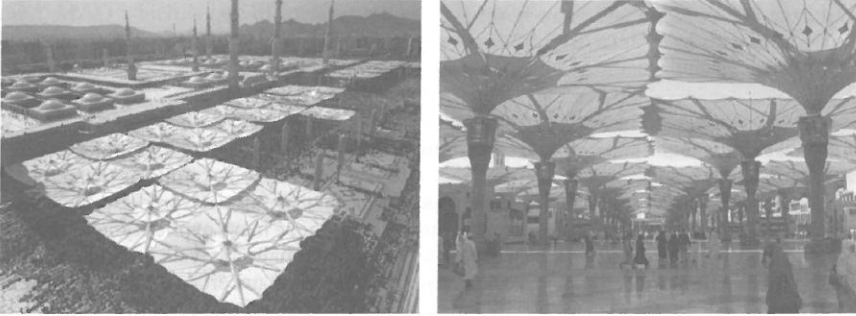


Figure 1. Medina Piazza Shading Project, 26m Umbrellas, Medina, Saudi Arabia, SL-Rasch GmbH.

Common methods in wind engineering practice, such as small scale wind tunnel experiments, do not fully cover non-linear structural behavior, contact interaction between membrane and structural elements and the interaction of the flow field with the structural response. Therefore, numerical tools – developed and validated during several scientific and applied engineering studies (Michalski 2010, Michalski et al. 2011) – are proposed to overcome limitations of existing structural analysis approaches and are used for structural engineering.

2.2 Computational wind engineering methodology

The complete simulation methodology, consisting of the numerical wind flow simulation and the fluid–structure coupling simulation, is summarized in Fig. 2. With this simulation approach it is possible to examine all aspects of wind-loaded membrane structures. The applied fluid structure interaction (FSI) simulation methodology allows the realistic description of the nonlinear structural behavior at the real scale, which is especially important in the case of textile structures, and of the stochastic wind excitation. The analysis is performed in time-domain.

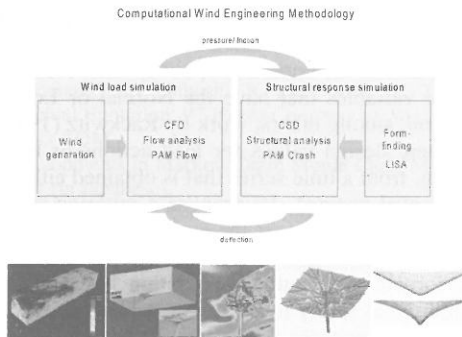


Figure 2. Computational Wind Engineering Methodology using a fully partitioned FSI approach.

The unknown parameters of the flow (velocity and pressure) as well as the structure (forces and deformations) are calculated including the fluid–structure coupling conditions. It should be noted that for wind load assessments by applying CFD techniques, an accurate time dependent analysis is required. Therefore turbulent flow is modeled by large eddy simulation (LES) based on the Smagorinsky subgrid scale (SGS) model. It is used because it enables the prediction of peak pressures and maximum/minimum structural response in the FSI context.

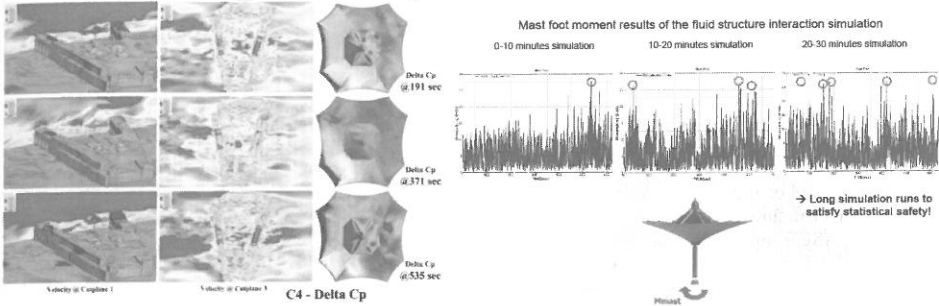


Figure 3. Time domain FSI analysis of large umbrella structures (left: CFD/LES pressure contour results, right: structural response results)

2.3 Design requirement

The load-and-resistance-factor-design (LRFD) principle implemented in Eurocode 0 requires that structural elements comply with the following design requirement:

$$\frac{R_k}{\gamma_R} \geq E_d \tag{1}$$

Wherein:

- R_k : characteristic value of the capacity R ;
- γ_R : partial safety factor for the capacity R ; and
- E_d : design value of the load effect.

In the standard Eurocode approach, the design load effect E_d is determined as a function of the design wind action on the structure $Q_d = Q_k \gamma_Q$, with Q_k being the characteristic wind action and γ_Q the partial safety factor for wind loads. However, due to the coupling of the actions to the structural response (deformations), such an approach is not meaningful for the considered structures. Instead, the non-linear coupled structural analysis is performed for a characteristic wind field \mathbf{V}_k and characteristic weight G_k , resulting in a characteristic load effect E_k . The design load effect is then determined as

$$E_d = E_k \gamma_Q \tag{2}$$

The characteristic wind field \mathbf{V}_k is defined based on the 50 year wind speed (corresponding to a 98% quantile in of the annual maximum wind speed). The characteristic load effect E_k is defined as the expected value of the maximum response during a 10 min time period in which the structure is subjected to \mathbf{V}_k .

Note that for the considered application (Sec. 2.1) this approach is on the conservative side when compared to the standard Eurocode procedure of determining the response as a function of the design action Q_d . In the static or quasi-static analysis of Eurocode 0, the characteristic action Q_k acting on the structure is proportional to the square of the wind velocity v^2 . If the load effect was a linear function of v^2 , it would be irrelevant whether the safety factor γ_Q were introduced at the level of the load action or the level of the load effect. For the considered application, it was found by numerical checks that the load effects increase under-proportional to v^2 . Introducing the safety factor γ_Q at the level of the load effect thus leads to larger design loads and is conservative.

2.4 Extreme value analysis to determine the characteristic load effect

For a given characteristic wind field V_k , the FSI analysis results in a time series of the relevant load effect with length T , an example of which is provided in Fig. 4. This time series $x(t)$ represents one realization of the stochastic process $X(t)$ of the load effect resulting from the considered wind field V_k .

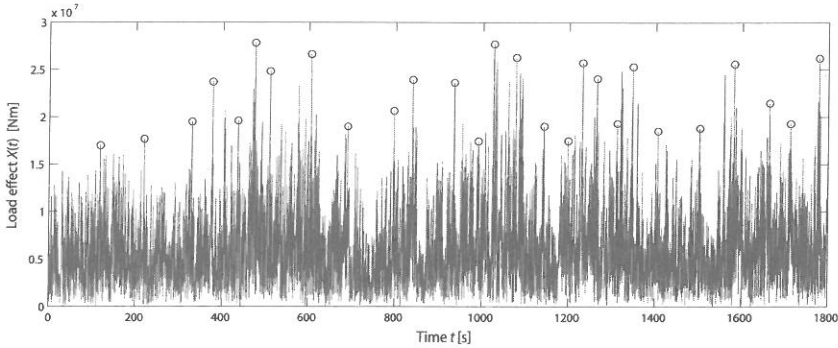


Figure 4. Time series of a load effect (resulting moment) obtained from the FSI analysis, with peaks identified using the declustering algorithm of Tawn (1988).

Through a series of tests, it is found that $X(t)$ can be considered a stationary process. In addition, it is assumed to be ergodic and have limited long-range dependence at extremal levels.

Let Y denote the maximum of $X(t)$ during a 10 min period:

$$Y = \max X(0:10\text{min}) \quad (3)$$

The distribution of Y can be estimated from a time series $x(t)$ as in Fig. 4 using extreme value theory (Coles 2007). Both the Peak-over-threshold (POT) and the block-maxima approach are implemented and results are compared. For brevity, only the latter is reported here. With the block-maxima approach, the data $x(t)$ is separated in blocks of length b . A value $b = 60$ s is used. The set of maximum observed values in each block $x_{m,1}, \dots, x_{m,n}$ is identified and a Generalized Extreme Value (GEV) distribution is fitted to this data using a Maximum Likelihood Estimator (MLE). The GEV distribution is:

$$F_{X_m}(x; \theta) = \exp \left\{ - \left[1 + \frac{\beta(x - \epsilon)}{\alpha} \right]^{\frac{1}{\beta}} \right\}, \quad x \geq \epsilon - \frac{\alpha}{\beta} \quad (4)$$

where $\theta = [\alpha; \beta; \epsilon]$ are the parameters of the distribution (scale, shape and location parameter, respectively). This is the distribution of X_m , the maxima in each block of duration b . The distribution of Y , the maxima in 10 min, is

$$\begin{aligned} F_Y(y; \theta) &= [F_{X_m}(y; \theta)]^{\left(\frac{10\text{min}}{b}\right)} \\ &= \exp \left\{ - \left(\frac{10\text{min}}{b}\right) \left[1 + \frac{\beta(y - \epsilon)}{\alpha} \right]^{\frac{1}{\beta}} \right\} \\ &= \exp \left\{ - \left[1 + \frac{\beta \left(y - \left(\epsilon - \frac{\alpha}{\beta} + \frac{\alpha}{\beta} \left(\frac{10\text{min}}{b}\right)^\beta \right) \right)}{\alpha \left(\frac{10\text{min}}{b}\right)^\beta} \right]^{\frac{1}{\beta}} \right\}, \quad y \geq \epsilon - \frac{\alpha}{\beta}. \end{aligned} \quad (5)$$

This corresponds to a GEV distribution with parameters $\alpha_{10} = \alpha \left(\frac{10\text{min}}{b}\right)^\beta$, $\beta_{10} = \beta$ and $\epsilon_{10} = \epsilon - \frac{\alpha}{\beta} + \frac{\alpha}{\beta} \left(\frac{10\text{min}}{b}\right)^\beta$.

For given parameter values θ , the characteristic value of the load effect E_k is defined as the expected value of the maximum of $X(t)$ in a 10 min period, i.e. the expected value of Y :

$$\begin{aligned} E_k(\theta) &= E(Y|\theta) \\ &= \int_{\epsilon - \frac{\alpha}{\beta}}^{\infty} [1 - F_Y(y; \theta)] dy \\ &= \epsilon_{10} + \frac{\alpha_{10}}{\beta_{10}} [\Gamma(1 - \beta_b) - 1] \\ &= \epsilon + \frac{\alpha}{\beta} \left[\left(\frac{10\text{min}}{b}\right)^\beta \Gamma(1 - \beta) - 1 \right]. \end{aligned} \tag{6}$$

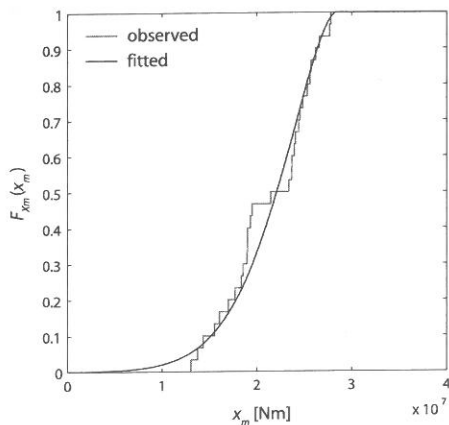
The third identity follows from the fact that E_k has the GEV distribution with parameters α_{10} , β_{10} and ϵ_{10} .

The MLE of θ is computed from the observed block maxima $x_{m,1}, \dots, x_{m,n}$ by:

$$\theta_{\text{MLE}} = \max_{\theta} l(\theta) = \max_{\theta} \sum_{i=1}^n \ln f_{X_m}(x_i; \theta) \tag{7}$$

Figure 5a shows the empirical and the fitted probability distribution of X_m for the extremes of the time series shown in Fig. 4. The probability distribution of Y with the fitted parameters θ_{MLE} is shown in Fig. 5b.

a) Block maxima X_m



b) Maxima in 10 min time period Y

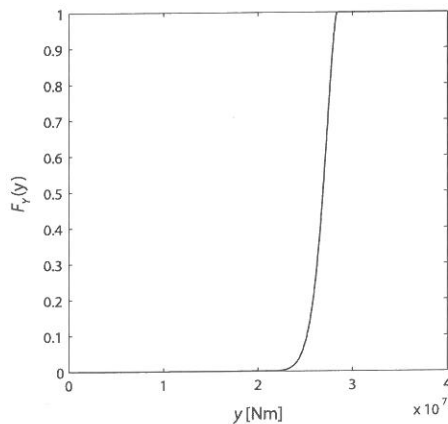


Figure 5. (a) Empirical and fitted probability distribution of block maxima X_m obtained from the time series in Fig. 4; (b) corresponding probability distribution of Y , the maximum load effect in a 10 min period.

2.5 Statistical uncertainty

A Bayesian estimate of θ is applied for representing the statistical uncertainty associated with the limited sample size. We use the asymptotic Normal approximation of the likelihood. Using a non-information prior distribution, this leads to a multivariate Normal posterior distribution of θ given the data $x_{m,1}, \dots, x_{m,n}$:

$$\boldsymbol{\theta} | x_{m,1}, \dots, x_{m,n} \sim \text{MVN}(\boldsymbol{\theta}_{\text{MLE}}, \mathbf{C}_{\boldsymbol{\theta}\boldsymbol{\theta}}). \quad (8)$$

where the covariance matrix $\mathbf{C}_{\boldsymbol{\theta}\boldsymbol{\theta}}$ is the inverse of the observed Fisher information matrix \mathbf{I}_O evaluated at the MLE (Coles 2007):

$$\mathbf{C}_{\boldsymbol{\theta}\boldsymbol{\theta}} = \mathbf{I}_O(\boldsymbol{\theta}_{\text{MLE}})^{-1} \quad (9)$$

The observed Fisher information matrix $\mathbf{I}_O(\boldsymbol{\theta})$ is equal to the Hessian of the log-likelihood $l(\boldsymbol{\theta})$ with respect to the parameters $\boldsymbol{\theta}$.

For the limiting case of an infinite time series, $\mathbf{C}_{\boldsymbol{\theta}\boldsymbol{\theta}}$ is zero and $\boldsymbol{\theta}$ is deterministically equal to $\boldsymbol{\theta}_{\text{MLE}}$.

Based on the posterior distribution of $\boldsymbol{\theta}$, the posterior probability density function of the characteristic value E_k , f_{E_k}'' , can be determined. Due to the non-linearity of the function $E_k(\boldsymbol{\theta})$, Eq. (6), the distribution f_{E_k}'' can only be determined numerically. Here, Monte Carlo Simulation (MCS) is used for this purpose. Alternatively, numerical integration or a first-order approximation can be applied. The first-order approximation results in a Normal distribution with mean and variance as follows:

$$\hat{\mu}_{E_k} = E_k(\boldsymbol{\theta}_{\text{MLE}}), \quad (10)$$

$$\hat{\sigma}_{E_k}^2 = \nabla E_k^T \mathbf{C}_{\boldsymbol{\theta}\boldsymbol{\theta}} \nabla E_k, \quad (11)$$

with

$$\nabla E_k = \left[\frac{\partial E_k(\boldsymbol{\theta})}{\partial \alpha}, \frac{\partial E_k(\boldsymbol{\theta})}{\partial \beta}, \frac{\partial E_k(\boldsymbol{\theta})}{\partial \epsilon} \right]^T, \quad (12)$$

evaluated at $\boldsymbol{\theta} = \boldsymbol{\theta}_{\text{MLE}}$.

For illustrative purposes, in Fig. 6 the resulting posterior distribution of E_k is shown for different lengths T of the simulated time series $x(t)$. This distribution is obtained with the data of Fig. 4. This illustrates the effect of T on the statistical uncertainty in the design parameter. As expected, the posterior variance of E_k is decreasing with increasing length of the time series. Furthermore, it is observed that the first-order approximation is underestimating the true variability of E_k , in particular for shorter time series.

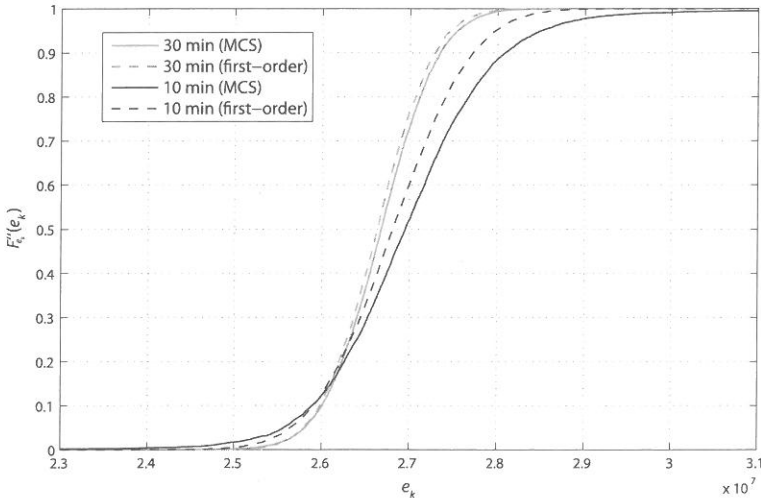


Figure 6. Example of F_{E_k}'' , the posterior distribution of the characteristic load effect E_k , for different lengths T of the simulated time series $X(t)$. Results as obtained with MCS and with a first-order approximation are shown.

What is the interpretation of f''_{E_k} , and what is its relevance in the design? For the given wind scenario, there is one true value of E_k , which – under the assumption of ergodicity – could be determined if a time series $x(t)$ of infinite duration $T = \infty$ were available. In practice, due to a limited duration T , it is only possible to determine a distribution of E_k as shown above. If the MLE estimate $E_k(\boldsymbol{\theta}_{\text{MLE}})$ were employed, there is a large probability (in the order of 50%) that the true value of E_k is underestimated, leading to a non-conservative design. For this reason, instead of $E_k(\boldsymbol{\theta}_{\text{MLE}})$ an upper quantile value of the distribution f''_{E_k} should be used in design. Let E_{kq} denote this upper quantile. But which is the appropriate quantile level q to be applied? This question will be addressed in the next section.

3 RELIABILITY-BASED DETERMINATION OF QUANTILES FOR DESIGN

3.1 Quantile value of E_k

To account for the statistical uncertainty described in Section 2.5, upper quantile values of f''_{E_k} must be used in the design. However, no guidance on the appropriate quantile level q is found in Eurocode or other literature. Therefore, the following criterion is proposed to determine the appropriate quantile level:

The level of the upper quantile is selected so that the reliability of a design based on a limited time series $x(t)$ of duration T is equal to the reliability of a design based on an infinite time series (when no statistical uncertainty is present).

Because structural analyses are only performed for a characteristic wind field \mathbf{V}_k , it is not possible to actually compute the reliability. Instead, the reliability conditional on the characteristic wind field \mathbf{V}_k is computed and the above criterion is applied to this conditional reliability. (Note that we make no assessment of the appropriateness of the characteristic wind field.) Let β_k denote this conditional reliability index. To make explicit the dependence on the computation, let $\beta_k^{(T,q)}$ denote the conditional reliability index obtained from a design based on a limited time series of length T and using an upper quantile level q . The goal is thus to find a value of q that fulfills the following condition:

$$\beta_k^{(T,q)} = \beta_k^{(\infty)} \quad (13)$$

$\beta_k^{(\infty)}$ is the conditional reliability index obtained from a design based on infinite time series. In the following, the probabilistic model and the computation of $\beta_k^{(T,q)}$ and $\beta_k^{(\infty)}$ are presented.

3.2 Probabilistic model

E is the maximum value of the load effect occurring during the 10min duration of the representative wind scenario. It is modeled as:

$$E = Y \cdot Z_m, \quad (14)$$

with Z_m being the model error of the structural (FSI) analysis. The distribution of Z_m is estimated from previous experimental validations of the FSI, as reported in Michalski et al. (2011), as the Lognormal distribution with mean value 1 and standard deviation 0.25. To assess the sensitivity of the final results with respect to this parameter, alternative choices were investigated, which are not reported here.

For given parameters $\boldsymbol{\theta}$, Y has the probability distribution $F_Y(y; \boldsymbol{\theta})$ according to Eq. (5). Because $\boldsymbol{\theta}$ itself is a random variable with posterior distribution $f''_{\boldsymbol{\theta}}(\boldsymbol{\theta})$ according to Eq. (8), Y is described by its predictive distribution, defined as

$$\tilde{F}_Y(y) = \int_{\boldsymbol{\theta}} F_Y(y; \boldsymbol{\theta}) f''_{\boldsymbol{\theta}}(\boldsymbol{\theta}) d\boldsymbol{\theta}. \quad (15)$$

This integral is evaluated numerically by means of MCS. For the reference case (with $T = \infty$), $\theta = \theta_{MLE}$ deterministically, and the predictive distribution reduces to

$$\tilde{F}_Y(y) = F_Y(y; \theta_{MLE}). \quad (16)$$

The capacity R is modeled by a Lognormal distribution with coefficient of variation 0.1. The mean value of R is determined through the design criterion as follows.

3.3 Design criterion

The design criterion is given by Eqs. (1) and (2) as

$$\frac{R_k}{Y_R} \geq E_k Y_Q. \quad (17)$$

Replacing E_k by its quantile value E_{kq} and assuming a design at the limit of the admissible domain, we obtain

$$R_k = E_{kq} Y_Q Y_R. \quad (18)$$

Since the characteristic value of the capacity R_k is defined as the 5% quantile, the mean value of R is obtained from the condition

$$F_R^{-1}(0.05) = E_{kq} Y_Q Y_R. \quad (19)$$

Here, F_R^{-1} is the inverse CDF of R . As evident from Eqs. (18) and (19), the characteristic value of R , and consequently its mean value, are a function of the selected quantile q .

3.4 Reliability assessment

The reliability associated with a given quantile value q can be determined by means of the classical structural reliability methods. The load effect E is given by Eq. (14) and it follows that the limit state function describing failure is

$$g(R, Y, Z_m) = R - Y Z_m. \quad (20)$$

Here, MCS is applied for determining the probability of failure

$$\Pr(F) = \Pr[g(R, Y, Z_m) \leq 0] \quad (21)$$

and the corresponding reliability index

$$\beta_k^{(T,q)} = \Phi^{-1}[\Pr(F)], \quad (22)$$

with Φ^{-1} being the inverse of the standard Normal cumulative probability function.

4 NUMERICAL INVESTIGATIONS

Numerical investigations are carried out for 18 load effects and different lengths of simulation T . Because only one simulation of total length $T = 30$ min is available for each load effect, the shorter time series are obtained by taking parts of these simulations.

The results for the reference solutions $\beta_k^{(\infty)}$ are obtained by applying the MLE and hypothetically assuming that the covariance of the estimator is zero. For the time series shown in Fig. 2, the resulting values of the characteristic load effect E_{kq} and the corresponding reliability indexes are presented in Fig. 5. The reference reliability index $\beta_k^{(\infty)}$ is also presented. For this case, the necessary quantile to achieve the reference reliability $\beta_k^{(\infty)} = 2.6$ is 0.9.

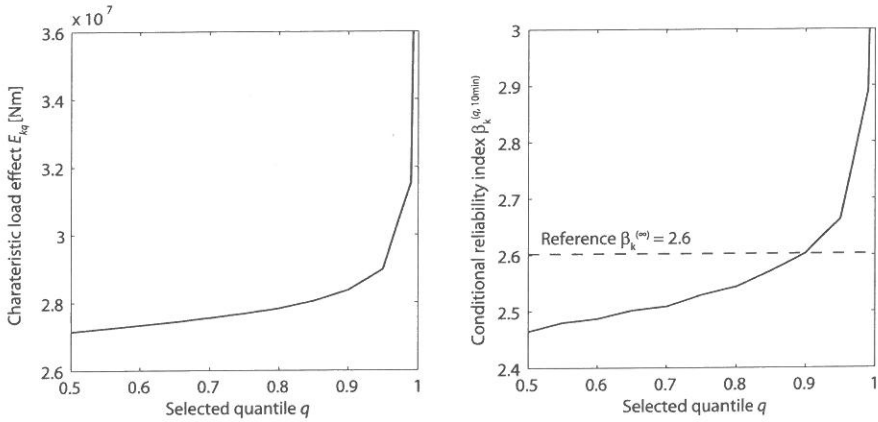


Figure 7. Characteristic value of the load effect and corresponding conditional reliability index $\beta_k^{(q, 10\text{min})}$ as a function of the selected quantile value q , for a 10 min time series taken from the one in Fig. 2. The reference reliability index $\beta_k^{(\infty)} = 2.6$ is the value that would be obtained with an infinite time series. The required minimum quantile for this case is 0.9.

A summary of the resulting required quantiles as calculated for the 18 load effects and different durations of the FSI simulation is presented in Fig. 6. The computations show that the necessary quantile q is a function of the length of the simulation: the necessary q decreases with increasing length of the time series.

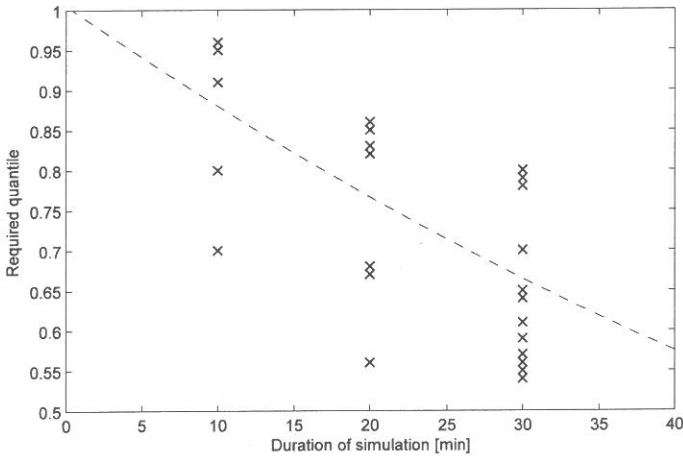


Figure 8. Required quantile values calculated for different load effects and different durations of FSI simulation. The dashed line shows the trend.

The resulting conditional reliability index is in the range 2.4 – 2.7. It is noted that this value is low. However, the reliability of structures subject to predominantly wind load designed according to Eurocode is known to be lower than for structures subject to other loads (JCSS 1996).

Based on the results of this study, it was decided to apply a quantile value of 0.95 and 30 min time series for the design, which is on the conservative side.

5 SUMMARY AND CONCLUSION

Due to computational limitations, the length of time-domain FSI simulations is limited. When estimating the maximum load effect, the uncertainty arising from the limited duration of the load effect should be taken into account. In this paper, we present an engineering approach to dealing with this problem: The statistical uncertainty arising from the limited data is estimated and quantified using a Bayesian approach. It is then proposed to use a quantile value with respect to this uncertainty in the design. The necessary quantile value of the maximum load effect is determined by requiring that the reliability achieved with this quantile value is equal to the reliability that would be achieved when complete information was available (corresponding to an infinite time series). This quantile value must be applied on top of other safety factors and characteristic values; in particular, it does not address the uncertainty in determining the characteristic wind field. The approach is applicable to other problems involving the estimation of extreme actions and load effects on structures based on limited time series, whether they arise from numerical computations or from observations.

REFERENCES

- Coles, S. (2007): *An introduction to statistical modeling of extreme values*. 4th printing. London: Springer (Springer Series in Statistics).
- Der Kiureghian, A; Ditlevsen, Ove (2009): Aleatory or epistemic? Does it matter? *Structural Safety* 31 (2): 105–112.
- Ditlevsen, O.; Madsen, H.O. (1996): *Structural Reliability Methods*: John Wiley & Sons.
- Joint Committee on Structural Safety JCSS (1996). *Background documentation – Eurocode 1 (ENV 1991) – Part 1: Basis of Design*. Working document, JCSS report #94.
- Leadbetter, M.R. (1983): *Extremes and Related Properties of Random Sequences and Processes*. Springer.
- Michalski, A. (2010). *Numerische Simulation leichter Flächentragwerke in einer numerisch generierten atmosphärischen Grenzschicht*, Ph.D. thesis, Chair of Structural Analysis, TU München [in German].
- Michalski, A., P. D. Kermel, et al. (2011). Validation of the computational fluid-structure interaction simulation at real-scale tests of a flexible 29 m umbrella in natural wind flow. *Journal of Wind Engineering and Industrial Aerodynamics* 99(4): 400-413.
- Rackwitz, R. (1983): Predictive Distribution of Strength under Control. *Materials & Structures*, 16(4): 259–267.
- Tawn J.A. (1988). An extreme value theory model for dependent observations. *Journal of Hydrology*, 101: 251-262.

Adaptive importance sampling using nonparametric density function

N. Kurtz & J. Song

University of Illinois at Urbana-Champaign, Urbana, USA

ABSTRACT: This paper presents a new adaptive importance sampling method that finds a near-optimal sampling density by minimizing Kullback-Leibler cross entropy, i.e. a measure of the difference between the absolute best sampling density and the importance sampling density. In particular, the proposed method employs a nonparametric multimodal probability density model called Gaussian mixture as the importance sampling density in order to fit the complex shape of the best sampling density through very few rounds of pre-sampling. The final importance sampling using the near-optimal density requires far less samples than crude Monte Carlo simulation or cross-entropy-based importance sampling employing a unimodal density function requires for achieving the desired level of convergence. The proposed method is applicable to various component and system reliability problems that have complex limit-state surfaces including those with multiple important regions. The parameters of the converged Gaussian mixture can be used to identify important regions and quantify their relative importance.

1 INTRODUCTION

The most commonly used sampling method, due to its straightforward application, is crude Monte Carlo Simulation. Given enough time, this method finds the “exact” failure probability; however, the computational cost may be exceedingly large, especially for low-probability events or those described by computationally expensive limit state functions. To remedy this issue, an importance sampling (IS) approach is often used. For a successful implementation of IS, one must specify an alternative sampling density that reduces the variability of the sampling estimate. One of the simplest of such densities is a multivariate Gaussian density whose mean is located near the “design point” (Fujita & Rackwitz 1988, Melchers 1989) found from a structural reliability analysis by the first-order reliability method (FORM). However, due to the complexity of the failure surface in the search space, multiple or competing design points, or various other issues, IS employing the design point found in FORM analysis may not converge to accurate failure probabilities. Moreover, there have been attempts to determine IS density functions for specific types of system reliability problems, but there exist no general procedure that is applicable to a variety of system reliability problems.

To address some of these issues, several adaptive IS procedures have been suggested in past research. Bucher (1988) proposed an adaptive IS approach in which the sampling density is updated based on statistical moments estimated by pre-samples. Ang et al. (1991) used an IS density found by constructing kernel models based on samples generated in the failure domain. Some have sought to model the limit state function using various approximations. Ching and Hsieh (2005) used subset simulations coupled with a maximum entropy optimization to find a local approximation of a limit state for given design values. The maximum entropy approach selects a probability density function (PDF) that maximizes its entropy subject to moment constraints from sample data. Dubourg et al. (2011) used a variance minimizing IS with a surrogate meta-model based on a Kriging procedure. Grooteman (2011) used an adaptive directional IS

approach to improve efficiency on previous directional IS approaches by finding the most important directions and sampling the rest using a response surface. Several other methods have been suggested, but most of these fall within similar veins of those described earlier.

One possible adaptive IS approach is to minimize the Kullback-Leibler cross entropy (CE) (Rubinstein & Kroese 2004). In this methodology, CE measures the “distance” between the best sampling density and the current adaptive IS density. This CE approach is largely absent from general use in the field of structural reliability. This paper presents a new adaptive IS approach recently developed by the authors, which improves the existing CE approach by fitting the complex shape of the best sampling density more effectively by use of a nonparametric multimodal density model. As an example of a nonparametric distribution, the Gaussian mixture is used. The developed method updates the IS density described by a Gaussian mixture model through a few rounds of pre-sampling so that the CE with respect to the best IS density is minimized. This paper first summarizes the existing CE-based adaptive importance sampling approach. Then, the proposed adaptive IS procedure using Gaussian mixture will be explained. Several numerical examples of component and system reliability problems will be presented to demonstrate the performance of the proposed method.

2 CROSS ENTROPY BASED ADAPTIVE IMPORTANCE SAMPLING

Suppose one aims to perform a numerical integration

$$I_t = \int H(\mathbf{x})f(\mathbf{x}; \mathbf{u})d\mathbf{x} \quad (1)$$

where $H(\mathbf{x})$ is a function to be integrated in the space of the random variables \mathbf{x} , which follows the joint PDF with parameter \mathbf{u} , i.e. $f(\mathbf{x}; \mathbf{u})$. For example, when the probability of the event $g(\mathbf{x}) \leq 0$ is of concern for structural reliability analysis, $H(\mathbf{x})$ becomes $I_{\{g(\mathbf{x}) \leq 0\}}$ where I is the indicator function with binary outcomes, i.e. “1” for the occurrence of the event, and “0” otherwise. Polynomial functions of \mathbf{x} can be used as $H(\mathbf{x})$ for computing statistical moments. The integral in Equation 1 can be evaluated more efficiently by introducing an alternative sampling density $h(\mathbf{x})$ with the parameter \mathbf{v} , that is,

$$I_t = \int \left[\frac{H(\mathbf{x})f(\mathbf{x}; \mathbf{u})}{h(\mathbf{x}; \mathbf{v})} \right] h(\mathbf{x}; \mathbf{v})d\mathbf{x} = E_{\mathbf{v}} \left[\frac{H(\mathbf{x})f(\mathbf{x}; \mathbf{u})}{h(\mathbf{x}; \mathbf{v})} \right] \cong \frac{1}{N} \sum_{i=1}^N \frac{H(\mathbf{x}_i)f(\mathbf{x}_i; \mathbf{u})}{h(\mathbf{x}_i; \mathbf{v})} \quad (2)$$

where $E_{\mathbf{v}}[\cdot]$ is the mathematical expectation with respect to the density $h(\mathbf{x}; \mathbf{v})$, and $\mathbf{x}_i, i = 1, \dots, N$ are pre-samples generated from $h(\mathbf{x}; \mathbf{v})$. The performance of IS is optimal when the variance of the estimate is minimized. The optimal IS density $p^*(\mathbf{x})$ is derived as (Rubinstein 1981).

$$p^*(\mathbf{x}) = \frac{|H(\mathbf{x})|f(\mathbf{x}; \mathbf{u})}{\int |H(\mathbf{x})|f(\mathbf{x}; \mathbf{u})d\mathbf{x}} \quad (3)$$

This optimal sampling density cannot be used as the IS density because the denominator in Equation 3 is practically equivalent to computing I_t in Equation 1, and exactly the same if $H(\mathbf{x})$ has non-negative sign everywhere. However, one can still improve the efficiency by finding a “near-optimal” IS density whose shape is similar to that of $p^*(\mathbf{x})$ in Equation 3.

One can find a near-optimal IS density by minimizing a measure of the difference between the best IS density $p^*(\mathbf{x})$ and the current IS density $h(\mathbf{x}; \mathbf{v})$, such as the Kullback-Leibler CE

$$D(p^*(\mathbf{x}), h(\mathbf{x}; \mathbf{v})) = \int p^*(\mathbf{x}) \ln p^*(\mathbf{x})d\mathbf{x} - \int p^*(\mathbf{x}) \ln h(\mathbf{x}; \mathbf{v})d\mathbf{x} \quad (4)$$

Rubinstein & Kroese (2004) proposed to identify an IS density function whose shape is similar to $p^*(\mathbf{x})$ in Equation 3 by finding the values of the parameter \mathbf{v} that minimizes the CE in Equation 4. Since the IS density parameter \mathbf{v} appears in the second term only, one can find a near-optimal IS density $h(\mathbf{x}; \mathbf{v})$ by maximizing the second integral in Equation 4. For structural reliability analysis, it is noted that $H(\mathbf{x})$ is non-negative, and thus from Equation 3, $p^*(\mathbf{x})$ is proportional to $H(\mathbf{x})/f(\mathbf{x}; \mathbf{u})$. Therefore, substituting this to Equation 4, one finds

$$\arg \min_{\mathbf{v}} D(p^*(\mathbf{x}), h(\mathbf{x}; \mathbf{v})) = \arg \max_{\mathbf{v}} \int H(\mathbf{x}) \ln h(\mathbf{x}; \mathbf{v}) f(\mathbf{x}; \mathbf{u}) d\mathbf{x} \quad (5)$$

For purposes of evaluating the expectation in Equation 5 as a function of the parameter \mathbf{v} , another sampling density $h(\mathbf{x}; \mathbf{w})$ is introduced, i.e.

$$\begin{aligned} \arg \min_{\mathbf{v}} D(p^*(\mathbf{x}), h(\mathbf{x}; \mathbf{v})) &= \arg \max_{\mathbf{v}} \int H(\mathbf{x}) \ln h(\mathbf{x}; \mathbf{v}) \frac{f(\mathbf{x}; \mathbf{u})}{h(\mathbf{x}; \mathbf{w})} h(\mathbf{x}; \mathbf{w}) d\mathbf{x} \\ &= \arg \max_{\mathbf{v}} E_{\mathbf{w}}[H(\mathbf{x}) \ln h(\mathbf{x}; \mathbf{v}) W(\mathbf{x}; \mathbf{u}, \mathbf{w})] \end{aligned} \quad (6)$$

where $E_{\mathbf{w}}[\cdot]$ denotes the mathematical expectation with respect to the density function $h(\mathbf{x}; \mathbf{w})$, and $W(\mathbf{x}; \mathbf{u}, \mathbf{w})$ is the likelihood ratio $f(\mathbf{x}; \mathbf{u})/h(\mathbf{x}; \mathbf{w})$. Estimating the expectation in Equation 6 by the IS density $h(\mathbf{x}; \mathbf{w})$, one can obtain a near-optimal density approximately by

$$\arg \min_{\mathbf{v}} D(p^*(\mathbf{x}), h(\mathbf{x}; \mathbf{v})) \cong \arg \max_{\mathbf{v}} \frac{1}{N} \sum_{i=1}^N H(\mathbf{x}_i) \ln h(\mathbf{x}_i; \mathbf{v}) W(\mathbf{x}_i; \mathbf{u}, \mathbf{w}) \quad (7)$$

where \mathbf{x}_i is the i th sample generated using the density $h(\mathbf{x}; \mathbf{w})$, $i=1, \dots, N$. In most applications, the function in Equation 7 is concave and differentiable with respect to \mathbf{v} (Rubinstein & Kroese, 2004); therefore, the values of the parameters \mathbf{v} that make $h(\mathbf{x}; \mathbf{v})$ a near-optimal density can be obtained by setting the gradient of Equation 7 to be zero, i.e.

$$\frac{1}{N} \sum_{i=1}^N H(\mathbf{x}_i) W(\mathbf{x}_i; \mathbf{u}, \mathbf{w}) \nabla_{\mathbf{v}} \ln h(\mathbf{x}_i; \mathbf{v}) = 0 \quad (8)$$

It is noted that if a member of the exponential family of distributions is used for $h(\mathbf{x}; \mathbf{v})$, the applied logarithm ensures that each parameter has an explicit updating rule. Rubinstein & Kroese (2004) derived such explicit updating rules for selected distribution models so that one can find a near-optimal density function by a few rounds of pre-sampling, and then perform the final IS until the target level of convergence is achieved.

3 CE-BASED ADAPTIVE IMPORTANCE SAMPLING USING GAUSSIAN MIXTURE

The aforementioned cross-entropy-based adaptive importance sampling (CE-AIS) by Rubinstein & Kroese (2004) uses parametric uni-modal distribution models for the IS density $h(\mathbf{x}; \mathbf{v})$, and assumes statistical independence between random variables so that the parameters of the marginal PDFs in $h(\mathbf{x}; \mathbf{v})$ can be updated individually. When a structural reliability problem has multiple design points or complex failure domains, such IS density models may not be flexible enough to fit the complex shape and orientation of the best IS density in Equation 3. Therefore, in this paper, a nonparametric multi-modal density model called the Gaussian mixture is implemented into the CE-AIS approach, and updating rules are derived to obtain optimal parameters of the Gaussian mixture through a few rounds of pre-sampling.

3.1 Gaussian mixture distribution model

Suppose the outcome of a random vector \mathbf{x} is determined by one of the K multivariate Gaussian distributions selected each time according to their pre-specified relative likelihoods. This random selection of a Gaussian density can be described by use of a "latent variable" $\mathbf{z} = \{z_1, z_2, \dots, z_K\}$, which is a K -dimensional binary random variable array where only one entry z_k can be 1 at a given time to describe the event that the k th density is selected. Let π_k denote the probability that the k th density is selected at a given time, that is, $P(z_k=1) = \pi_k$ where $\pi_1 + \dots + \pi_K = 1$, and $0 \leq \pi_k \leq 1$. Then, the joint PDF of \mathbf{x} is derived as (Bishop 2006)

$$p(\mathbf{x}) = h(\mathbf{x}; \mathbf{v}) = \sum_{k=1}^K \pi_k N(\mathbf{x} | \boldsymbol{\mu}_k, \boldsymbol{\Sigma}_k) \quad (9)$$

where $N(\mathbf{x} | \boldsymbol{\mu}_k, \boldsymbol{\Sigma}_k)$ is the joint PDF of the Gaussian distribution with mean vector $\boldsymbol{\mu}_k$ and cova-

riance matrix Σ_k , $k=1, \dots, K$. In the proposed AIS method, the joint PDF in Equation 9 is used as the IS density $h(\mathbf{x}; \mathbf{v})$ in the aforementioned CE-AIS approach.

3.2 Updating rules to minimize CE for Gaussian mixture

Substituting the IS density in Equation 9 into Equation 8, the CE minimization problem for a given round of pre-sampling becomes

$$\frac{1}{N} \sum_{i=1}^N H(\mathbf{x}_i) W(\mathbf{x}_i; \mathbf{u}, \mathbf{w}) \nabla_{\mathbf{v}} \ln \left\{ \sum_{k=1}^K \pi_k N(\mathbf{x}_i | \boldsymbol{\mu}_k, \boldsymbol{\Sigma}_k) \right\} = 0 \quad (10)$$

where \mathbf{x}_i is the i th sample generated using the density $h(\mathbf{x}; \mathbf{w})$, $i=1, \dots, N$. Based on a similar procedure developed for maximum likelihood estimation (Bishop 2006), updating rules to find the parameter values $\mathbf{v} = \{\pi_1, \dots, \pi_K, \boldsymbol{\mu}_1, \dots, \boldsymbol{\mu}_K, \boldsymbol{\Sigma}_1, \dots, \boldsymbol{\Sigma}_K\}$ satisfying Equation 10 are developed as

$$\boldsymbol{\mu}_j = \frac{\sum_{i=1}^N H(\mathbf{x}_i) W(\mathbf{x}_i; \mathbf{u}, \mathbf{w}) \gamma_i(z_j) \mathbf{x}_i}{\sum_{i=1}^N H(\mathbf{x}_i) W(\mathbf{x}_i; \mathbf{u}, \mathbf{w}) \gamma_i(z_j)} \quad (11)$$

$$\boldsymbol{\Sigma}_j = \frac{\sum_{i=1}^N H(\mathbf{x}_i) W(\mathbf{x}_i; \mathbf{u}, \mathbf{w}) \gamma_i(z_j) (\mathbf{x}_i - \boldsymbol{\mu}_j) (\mathbf{x}_i - \boldsymbol{\mu}_j)^T}{\sum_{i=1}^N H(\mathbf{x}_i) W(\mathbf{x}_i; \mathbf{u}, \mathbf{w}) \gamma_i(z_j)} \quad (12)$$

$$\pi_j = \frac{\sum_{i=1}^N H(\mathbf{x}_i) W(\mathbf{x}_i; \mathbf{u}, \mathbf{w}) \gamma_i(z_j) \mathbf{x}_i}{\sum_{i=1}^N H(\mathbf{x}_i) W(\mathbf{x}_i; \mathbf{u}, \mathbf{w})} \quad (13)$$

where $\gamma_i(z_j) = P(z_j=1 | \mathbf{x}_i) = \pi_j N(\mathbf{x}_i | \boldsymbol{\mu}_j, \boldsymbol{\Sigma}_j) / \sum_{k=1}^K \pi_k N(\mathbf{x}_i | \boldsymbol{\mu}_k, \boldsymbol{\Sigma}_k)$ is the ‘‘responsibility’’ z_j takes for describing observation \mathbf{x}_i . This responsibility indicates from which region of importance the samples may come from. When converged, the mean vector $\boldsymbol{\mu}_j$, $\boldsymbol{\Sigma}_j$ and π_j in Equations 11-13 respectively indicate the location, the size and orientation of spread, and relative importance of the important region represented by the j th Gaussian density in the mixture. It is also noted that at times some densities may cluster together to fit the complex shape of one important region.

3.3 Algorithm for CE-based AIS using Gaussian mixture

Using the updating rules in Equations 11-13, an algorithm is developed as follows to find a near-optimal (i.e. minimum CE) Gaussian mixture model:

- [Step 1] Initialize: Choose initial values of parameters $\pi_k^{(0)}$, $\boldsymbol{\mu}_k^{(0)}$ and $\boldsymbol{\Sigma}_k^{(0)}$, $k=1, \dots, K$. For example, uniform weights (i.e. $\pi_1^{(0)} = \pi_2^{(0)} = \dots = \pi_K^{(0)} = 1/K$), and covariance matrices with unit-standard deviations and zero correlations (i.e. the identity matrix for all $\boldsymbol{\Sigma}_k$'s) will suffice. For $\boldsymbol{\mu}_k^{(0)}$, the authors propose that the CE-based IS method be run using a single Gaussian density (Rubinstein and Kroese, 2004), and K points be sampled uniformly on the surface of the hypersphere with the radius being the half of $\boldsymbol{\mu}$ obtained from the AIS by a single Gaussian density. These sampled points can be used as $\boldsymbol{\mu}_k^{(0)}$, $k=1, \dots, K$.
- [Step 2] Sample: Generate N random samples $\mathbf{x}_1, \dots, \mathbf{x}_N$, using $h(\mathbf{x}; \mathbf{w})$ with \mathbf{w} being the initial parameters from Step 1 (for the first pre-sampling round) or the updated parameters \mathbf{v} from the previous round (for the other pre-sampling rounds). Since $h(\mathbf{x}; \mathbf{w})$ is following a Gaussian mixture, each sample is generated by ‘‘ancestral’’ sampling: First, a latent variable \mathbf{z} is sampled according to a multinomial distribution with parameters π_1, \dots, π_K in \mathbf{w} to determine which Gaussian density will be used to generate samples; and \mathbf{x} is then sampled from the selected Gaussian density with the corresponding mean and covariance in \mathbf{w} . Calculate the ρ -

quantile of the limit-state function $g(\mathbf{x})$ from the samples $\{g(\mathbf{x}_1), \dots, g(\mathbf{x}_N)\}$, denoted by g_p . If $g_p < 0$, set $g_p = 0$, indicating that the adaptive scheme has converged. This corresponds to the instance in which at least $\rho \times N$ of the samples are within the failure domain, i.e. $g(\mathbf{x}) < 0$.

- [Step 3] Update: Find the parameters \mathbf{v} satisfying Equation 10 using the samples from Step 2. Use the updating rules in (11)-(13).
- [Step 4] Check convergence: If $g_p > 0$, update the iteration step t to $(t+1)$ and return to Step 2. Otherwise, proceed to Step 5.
- [Step 5] Final importance sampling: Estimate the probability of the event $\{g(\mathbf{x}) \leq 0\}$ using the Gaussian mixture with the updated parameters $\mathbf{v}^{(t)}$ as a near-optimal IS density, i.e.

$$\hat{I}_t = \frac{1}{N_f} \sum_{i=1}^{N_f} I_{\{g(\mathbf{x}_i) \leq 0\}} W(\mathbf{x}_i; \mathbf{u}, \mathbf{v}^{(t)}) \quad (14)$$

where N_f denotes the number of samples for the final importance sampling, $\mathbf{v}^{(t)}$ denotes the parameters in the Gaussian mixture optimized by the previous steps, \mathbf{u} corresponds to the parameters of the nominal density, e.g., uncorrelated standard normal distribution, and \mathbf{x}_i , $i=1, \dots, N_f$ are samples generated from the Gaussian mixture PDF in Equation 9 with the updated parameters $\mathbf{v}^{(t)}$.

From the authors' experience, the quantile percentage in Step 2, ρ , is typically on the order of 10%. A good rule of thumb for K is " $K \geq N_{RV}$ and $K \geq N_{comp}$ " where N_{RV} is the number of random variables in \mathbf{x} , and N_{comp} is the number of components (for a system reliability problem).

4 NUMERICAL EXAMPLES

The breadth of applications and improved performance of the adaptive IS procedure are tested by several numerical examples. First, to demonstrate the performance of the method for component problems with multiple design points, parabolic limit state functions are explored. Then, the method is applied to a series, parallel and cut-set system problem to show its applicability to a wide range of system problems. All limit-state functions in the examples are described in the standard normal space, i.e. $f(\mathbf{x}; \mathbf{u}) = N(\mathbf{x} | \mathbf{0}, \mathbf{I})$ where $\mathbf{0}$ and \mathbf{I} respectively denote the vector of zero's and the identity matrix.

4.1 Component reliability analysis for parabolic limit-state functions

The first example comes from Der Kiureghian & Dakessian (1998) focusing on FORM and SORM for situations in which multiple design points occur. The limit-state function is

$$g(\mathbf{x}) = b - x_2 - \kappa(x_1 - e)^2 \quad (15)$$

where b , κ and e are deterministic parameters (5, 0.5 and 0.1, respectively for the example), and x_1 and x_2 are uncorrelated standard normal random variables. Figure 1 shows the limit-state surface, the two design points and the contour plots of a function proportional to the best IS density in Equation 3.

The Gaussian mixture IS density at each round of the pre-sampling is shown in Figure 2 ($N=10^2$, $K=2$ for each round). The Gaussian mixture density quickly converges to the optimal distribution parameters after only two rounds. The optimal IS density ("Step 2" in Figure 2) clearly identifies the most important regions associated with the failure probability, and matches the best IS density in Figure 1 fairly well. Table 1 summarizes the final results in which the proposed method (CE-AIS-GM) shows superior efficiency to crude Monte Carlo simulations (MCS) and CE-AIS with a single Gaussian density (CE-AIS-SG). The columns named "Number of Samples" in the tables of this paper give the sum of the samples for finding the optimal density ($N \times K$) and those for the final importance sampling (N_f) to achieve a given level of coefficient of variation (c.o.v.). For example, "400+3,000" means 400 samples for the pre-sampling and 3,000 for the final IS. The results demonstrate that the proposed method significantly reduces the number of function evaluations required to achieve a reliable estimate on the failure probability, while also identifying the most important regions of interest from the mean vectors of the optimal Gaussian mixture.

In further investigation by Kurtz and Song (2012), the proposed method performed well even when the limit-state function is modified such that the top of the limit-state surface becomes as important as the areas around the two design points; and the number of Gaussian mixture was increased, e.g. $K = 10, 25, 50,$ and 100 .

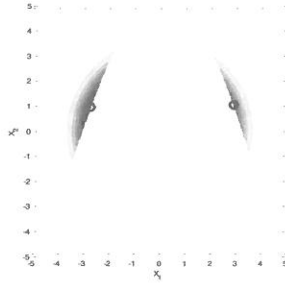


Figure 1. Limit-state surface, design points and contours of the best importance sampling density

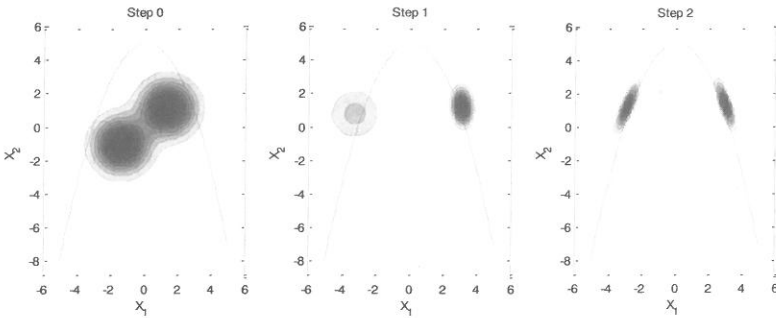


Figure 2. Convergence of Gaussian mixture for parabolic limit-state surface

Table 1. Comparison for parabolic limit-state surface with two design points.

c.o.v. (%)	Number of Samples			Failure Probability		
	MCS	CE-AIS-SG	CE-AIS-GM	MCS	CE-AIS-SG	CE-AIS-GM
10	32,000	400+3,000	400+403	3.16×10^{-3}	2.85×10^{-3}	2.61×10^{-3}
5	1.28×10^5	400+8,000	400+434	3.12×10^{-3}	2.98×10^{-3}	2.49×10^{-3}
3	3.64×10^5	400+23,000	400+1,390	3.06×10^{-3}	2.98×10^{-3}	2.85×10^{-3}

4.2 System reliability problems

To demonstrate the performance of the proposed method in a wide range of system reliability problems, Kurtz and Song (2011) applied the method to a series system with the complex limit-state surface (Waarts 2000), a parallel system with a “joint design point” (Melchers and Ahammed 2001), and a cut-set system problem (Song and Der Kiureghian 2003).

For the series system example (Waarts 2000), a near-optimal Gaussian mixture density was found through very few rounds of pre-samplings as shown in Figure 3 ($N=10^3$ and $K=4$). It is noted that the proposed method immediately identifies important regions without performing preliminary component reliability analysis for each limit-state. The effect of Σ_k at each important region can easily be seen, as this effectively ensures that samples adhere to the slope of the limit-state surface. The proposed method converged two orders of magnitude quicker than crude-MCS. Also note that the single search adaptive IS converges to a wrong value, since the single Gaussian density converged to only one of the four important regions spaced far away from one another. The c.o.v. behavior for the single point search exhibits a very jagged behavior and can lead to false confidence at small amounts of samples.

Next, the method was applied to the parallel system example (Melchers & Ahammed 2001) using $N=10^2$ and $K=2$. Figure 4 shows how the two Gaussian densities converge to one located

near the “joint” design point. It is noteworthy that, for limit-state surfaces with only one region of importance, multiple Gaussian densities in the mixture model can merge to one density without causing numerical issues.

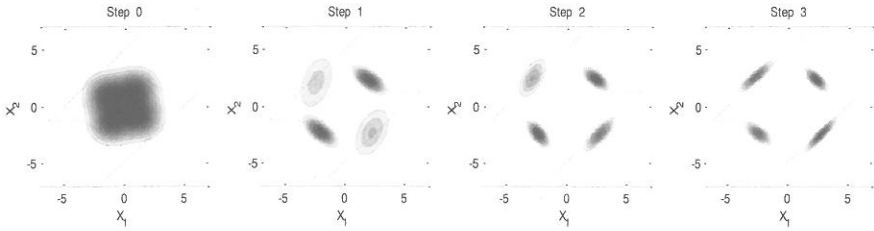


Figure 3. Convergence of Gaussian mixture for series system problem

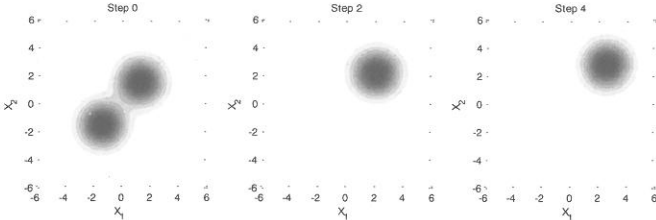


Figure 4. Convergence of Gaussian mixture for parallel system problem

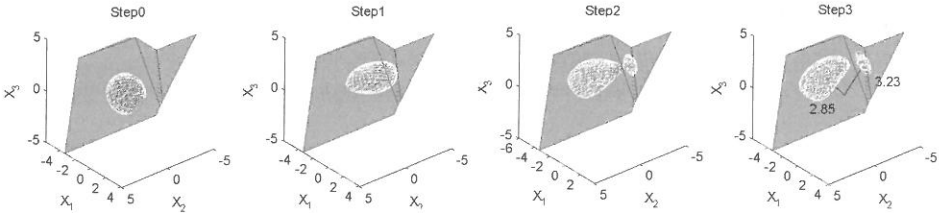


Figure 5. Convergence of Gaussian mixture for cut-set system problem

Finally, the proposed method was applied to a general (i.e. neither series nor parallel) system example in Song and Der Kiureghian (2003). The cut-set system event in the paper has three cut-sets consisting of a total of five components. The results obtained using $N=10^3$ and $K=10$ confirmed that even for a general system event, the proposed method requires much fewer samples than MCS to achieve the same level of c.o.v. They also indicate that the single point search results in a density that displays both jagged convergence and a possibility of false early convergence. The limit state and a contour of each Gaussian mixture during the updating process are shown in Figure 5. One can see that there are two important regions and that the method managed to identify both of them, even in a domain that is difficult to visualize. The surface of the density contour is strongly non-spherical, which implies that having more than two densities in the mixture helped fit the complex shape in this example. This example demonstrates that the proposed method can be used for general system events with complex limit-state surfaces.

5 SUMMARY AND CONCLUSIONS

To address issues associated with structural reliability problems having complex limit-state surfaces and to further enrich the field of importance sampling methods, a new adaptive importance sampling method using Kullback-Leibler cross entropy coupled with a Gaussian mixture has been developed. The method searches for a near-optimal importance sampling density by minimizing the difference between a Gaussian mixture model and the best importance sampling

density, measured by the cross entropy. This new method obtains a near-optimal sampling density in very few rounds of pre-sampling by use of closed-form updating rules, which greatly improve the efficiency and accuracy of the final importance sampling. The breadth of applications of this method was demonstrated through several component problems, a series system problem, a parallel system problem, and a general system problem. For every situation, the proposed method required significantly less samples than crude Monte Carlo simulations and adaptive importance sampling using a single Gaussian density. One also finds that the proposed method avoids false convergence that may manifest for importance sampling approaches using a unimodal density model. It is also noted that the mean values and the weights of the converged sampling densities in the Gaussian mixture can respectively identify important regions and quantify the relative importance in a variety of component and system reliability problems.

ACKNOWLEDGEMENT

The authors would like to thank the U.S. National Science Foundation for funding under grant number CMMI 1031318. Any opinions, findings and conclusions or recommendations expressed in this material are those of the authors and do not necessarily reflect the views of the National Science Foundation.

REFERENCES

- Ang, G.L., Ang, A.H.-S, & Tang, W.H., 1991. Multidimensional kernel method in importance sampling. *Proceedings, 6th International Conference on Applications of Statistics and Probability in Civil Engineering*, L. Esteva & S.E. Ruiz Ed., 1:289-296, Mexico.
- Bishop, C., 2006. *Pattern recognition and machine learning*, New York (NY), Springer.
- Bucher, C.G., 1988. Adaptive sampling – an iterative fast Monte Carlo procedure. *Structural Safety*, 5: 119-126.
- Ching, J., & Hsieh, Y., 2006. Local estimation of failure probability function and its confidence interval with maximum entropy principle. *Probabilistic Engineering Mechanics*, 22(1): 39-49.
- Der Kiureghian, A. & Dakessian, T., 1998. Multiple design points in first and second-order reliability. *Structural Safety*, 20(1): 37-49.
- Dubourg, V., Deheeger, F., & Sudret, B., 2011. Metamodel-based importance sampling for the simulation of rare events. *Proceedings, 11th International Conference on Applications of Statistics and Probability in Civil Engineering*, M.H. Faber, J. Kohler & K. Nishima Ed., 661-668, Zurich, Switzerland.
- Fujita, M., & Rackwitz, R., 1988. First- and second-order reliability estimates by importance sampling. *Structural Engineering/Earthquake Engineering*, 5: 53-59.
- Grooteman, F., 2011. An adaptive importance sampling method for structural reliability. *Probabilistic Engineering Mechanics*, 26(2):134-141.
- Kurtz, N., & Song, J., 2012, Adaptive nonparametric importance sampling for structural reliability analysis. *Proceedings, 11th ASCE Joint Specialty Conference on Probabilistic Mechanics and Structural Reliability*, A. Kareem, T. Kijewski-Correa & A. Taflanidis Ed., Notre Dame, USA.
- Melchers, R.E., & Ahammed, M., 2001. Estimation of failure probabilities for intersections of non-linear limit states. *Structural Safety*, 23(2): 123-135.
- Melchers, R.E., 1989. Importance sampling in structural systems. *Structural Safety*, 6: 3-10.
- Rubinstein, R., & Kroese, D., 2004. *The cross entropy method: a unified approach to combinatorial optimization, Monte-Carlo Simulation, and machine learning*, New York (NY), Springer.
- Rubinstein, R., 1981. *Simulation and the Monte Carlo methods*, Hoboken (NJ), John Wiley and Sons.
- Song, J., & Der Kiureghian, A., 2003. Bounds on system reliability by linear programming. *Journal of Engineering Mechanics*, 129(6):627-636.
- Waarts, P.H., 2000. *Structural reliability using finite element an appraisal of DARS: Directional Adaptive Response Surface Sampling*, Ph.D. thesis of Delft, the Netherlands.

Enhancing meta-model-based importance sampling by subset simulation

B. Sudret

Université Paris-Est – Laboratoire Navier (Ecole des Ponts ParisTech, IFSSTAR, CNRS)
Marne-la-Vallée, FRANCE

V. Dubourg

Phimeca Engineering, Centre d’Affaires du Zénith, Courmon d’Auvergne, FRANCE

J.-M. Bourinet

Clermont Université, IFMA, Institut Pascal, Aubière, FRANCE

ABSTRACT: Meta-models are commonly used in structural reliability analysis in order to surrogate limit state functions that depend on the output of a computationally-expensive simulation model such as a finite element model. In this paper we present a way of using a Kriging surrogate of the limit state function as a means to derive a quasi-optimal importance sampling density, which leads to an unbiased estimator of the probability of failure. For computational efficiency a splitting technique similar to that introduced in subset simulation is used. The method is illustrated on a two-component series system and a truss reliability problem. It appears remarkably accurate also for cases with very small probabilities of failure (e.g. $10^{-6/-7}$).

1 INTRODUCTION

Structural reliability methods aims at quantifying the probability of failure of mechanical systems subject to uncertainty in their design parameters (e.g. geometry), constitutive laws (material properties) and loading. In the context of modern engineering, the performance of the system is assessed through the use of time-consuming numerical models such as finite element models.

Let us denote by \mathcal{M} such a computational model, *i.e.* a function whose input vector $\mathbf{x} \in \mathcal{D} \subset \mathbb{R}^M$ gathers all the parameters describing the geometry, the material properties and the loading. The response quantities of interest, *e.g.* displacements, stress and strain components are gathered into a vector $\mathbf{y} = \mathcal{M}(\mathbf{x})$. This notation means that for any value of the input vector, the model is run (whatever its complexity, may it be an analytical model or a complex computational workflow) to compute the relevant quantities in \mathbf{y} .

Due to uncertainty, a probabilistic model of the input parameters is built from the available information and data, leading to representing the latter by a random vector \mathbf{X} with prescribed probability density function $f_{\mathbf{X}}$. In the context of structural reliability, the performance of the structure is assessed using a *limit state function* g that depends on the structural response $\mathcal{M}(\mathbf{x})$ and additional parameters \mathbf{d} or random variables \mathbf{X}' describing the capacity (*e.g.* strength parameters). This limit state function is conventionally defined as follows:

- The set of parameters $\{\mathbf{x}, \mathbf{x}', \mathbf{d}\}$ such that $g(\mathcal{M}(\mathbf{x}), \mathbf{x}', \mathbf{d}) > 0$ defines the *safe domain* \mathcal{D}_s .
- The set of parameters $\{\mathbf{x}, \mathbf{x}', \mathbf{d}\}$ such that $g(\mathcal{M}(\mathbf{x}), \mathbf{x}', \mathbf{d}) \leq 0$ defines the *failure domain* \mathcal{D}_f .
- The *limit state surface* corresponds to the zero-level of the g -function.

Gathering all the parameters into a single notation $\mathbf{x} \in \mathcal{D}_{\mathbf{X}}$ for the sake of simplicity, the probability of failure of the system is defined by:

$$P_f = \mathbb{P}[g(\mathbf{X}) \leq 0] = \int_{\mathcal{D}_f = \{\mathbf{x}: g(\mathbf{x}) \leq 0\}} f_{\mathbf{X}}(\mathbf{x}) d\mathbf{x} \quad (1)$$

The classical methods for evaluating a probability of failure may be gathered into three main groups:

- methods based on Monte Carlo simulation (MCS): apart from the crude approach which is computationally unaffordable for typical probabilities of failure in the range $10^{-3} - 10^{-6}$, importance sampling (Au and Beck 1999) and subset simulation (Au and Beck 2001) have proven their efficiency in many applications. However the number of calls to the limit state function remains large, typically in the range 10^{4-5} .
- classical approximation methods such as FORM/SORM are far more efficient but do not guarantee any accuracy in the result.
- response surface methods rely upon the construction of a *surrogate model* (e.g. a polynomial function) which may then be used for intensive Monte Carlo sampling.

Reliability methods based on surrogate models have gained much attention in the last few years due to the development of high-fidelity surrogate such as polynomial chaos expansions (Sudret and Der Kiureghian 2002, Berveiller et al. 2004, 2006), Kriging (Bichon et al. 2008, Echard et al. 2011) and support vector machines (Hurtado 2004, Bourinet et al. 2011) which outperform the well known second order polynomial approximations. A review of the use of surrogates in structural reliability may be found in Sudret (2012).

In all these approaches, the surrogate model \tilde{g} of the limit state function is built first (possibly in an adaptive manner) using some criterion that allows the iterative refinement of the model. Then it is *substituted* for the original limit state function in order to evaluate the probability of failure, denoted by \tilde{P}_f :

$$P_f \approx \tilde{P}_f \stackrel{\text{def}}{=} \mathbb{P}[\tilde{g}(\mathbf{X}) \leq 0] = \int_{\tilde{\mathcal{D}}_f = \{\mathbf{x}: \tilde{g}(\mathbf{x}) \leq 0\}} f_{\mathbf{X}}(\mathbf{x}) d\mathbf{x} \quad (2)$$

However there is usually no indication about the closeness between the true probability of failure P_f and its surrogate-based approximation \tilde{P}_f . Recently, Dubourg et al. (2011, 2012) proposed to use a *Kriging* surrogate model to devise a "smart" importance sampling density: the method remains within the scope of importance sampling (no substitution) while the sampling density derived from $\tilde{g}(\mathbf{x})$ is quasi-optimal, thus reducing the number of samples required for a target accuracy. The goal of the present paper is to extend the idea of *meta-model based importance sampling* as originally introduced in Dubourg et al. (2012) by coupling it with subset simulation. The paper is organized as follows. First the basics of Kriging, a technique for building meta-models is recalled. Then it is shown how a Kriging surrogate model may be used as a quasi-optimal importance sampling density, leading to an unbiased estimator of the probability of failure. Finally the approach is used for two application examples, namely a two-dimensional analytical limit state function and a 10-dimensional truss reliability problem.

2 THE KRIGING SURROGATE

The origin of Kriging is to be found in the field of geostatistics, where engineers try to model the spatial variability of some quantity based on measurements at specific points in space. It has been introduced in the domain of *computer experiments* by Sacks et al. (1989) in the late 80's. The modern formulation of this approach is also known as *Gaussian process modelling* (Santner et al. 2003). Indeed, it is assumed that the function to approximate, say $\mathbf{x} \in \mathcal{D}_{\mathbf{X}} \subset \mathbb{R}^M \mapsto g(\mathbf{x})$ is a particular *realization* of a Gaussian process $Y(\mathbf{x}, \omega)$:

$$Y(\mathbf{x}, \omega) = \mathbf{f}(\mathbf{x})^T \mathbf{a} + Z(\mathbf{x}, \omega), \quad \mathbf{x} \in \mathcal{D}_{\mathbf{X}} \quad (3)$$

In this equation $\mathbf{f}(\mathbf{x})^\top \mathbf{a}$ is the mean of the process, which is represented by a set of basis functions $\{f_i, i = 1, \dots, P\}$ (e.g. polynomial functions) and $Z(\mathbf{x}, \omega)$ is a stationary zero mean Gaussian process with variance σ_Y^2 and autocorrelation function:

$$C_{YY}(\mathbf{x}, \mathbf{x}') = \sigma_Y^2 R(\mathbf{x} - \mathbf{x}', \boldsymbol{\theta}), \quad (\mathbf{x}, \mathbf{x}') \in \mathcal{D}_X \times \mathcal{D}_X \quad (4)$$

In the above equation $\boldsymbol{\theta}$ gathers all the parameters defining C_{YY} . Note that for the sake of brevity the notation ω that recalls the randomness of the various quantities is abandoned in the sequel. In practice, square exponential models are generally postulated:

$$R(\mathbf{x} - \mathbf{x}', \boldsymbol{\theta}) = \exp\left(\sum_{k=1}^M -\left(\frac{x_k - x'_k}{\theta_k}\right)^2\right) \quad (5)$$

In order to obtain the Kriging surrogate a set of computer experiments is run. An *experimental design*, i.e. a finite set of points $\mathfrak{X} = \{\mathbf{x}^{(i)} \in \mathcal{D}_X, i = 1, \dots, N\}$ is selected. The computational model is run and the limit state function is evaluated. The obtained values are gathered in a vector $\boldsymbol{\Gamma} = (g(\mathbf{x}^{(1)}), \dots, g(\mathbf{x}^{(N)}))^\top$. This procedure is similar to Monte Carlo simulation since the points in \mathfrak{X} may be drawn e.g. by Latin Hypercube sampling.

The Kriging estimator at a given point $\mathbf{x} \in \mathcal{D}_X$ is by definition a Gaussian random variate $\hat{Y}(\mathbf{x}) \sim \mathcal{N}(\mu_{\hat{Y}}(\mathbf{x}), \sigma_{\hat{Y}}^2(\mathbf{x}))$ obtained by requiring that it is the *best linear unbiased estimator* (BLUE) of $g(\mathbf{x})$ conditioned to the observations gathered in \mathfrak{X} . After some algebra the Kriging estimator reads as follows (Santner et al. 2003):

$$\mu_{\hat{Y}}(\mathbf{x}) = \mathbf{f}(\mathbf{x})^\top \hat{\mathbf{a}} + \mathbf{r}(\mathbf{x})^\top \mathbf{R}^{-1}(\boldsymbol{\Gamma} - \mathbf{F}\hat{\mathbf{a}}) \quad (6)$$

In this equation the following notation \mathbf{r} , \mathbf{R} et \mathbf{F} is used:

$$r_i(\mathbf{x}) = R(\mathbf{x} - \mathbf{x}^{(i)}, \boldsymbol{\theta}), \quad i = 1, \dots, N \quad (7)$$

$$\mathbf{R}_{ij} = R(\mathbf{x}^{(i)} - \mathbf{x}^{(j)}, \boldsymbol{\theta}), \quad i = 1, \dots, N, \quad j = 1, \dots, N \quad (8)$$

$$\mathbf{F}_{ij} = f_j(\mathbf{x}^{(i)}), \quad i = 1, \dots, p, \quad j = 1, \dots, N \quad (9)$$

Eq.(6) reads whatever the value of the (still) unknown parameters, namely the regression coefficients \mathbf{a} , the variance of the process σ_Y^2 and the parameters $\boldsymbol{\theta}$ defining the correlation function (5). In order to best fit these unknown parameters to the available data, a likelihood function is defined for the "observations", i.e. the pairs $\{(\mathbf{x}^{(i)}, g(\mathbf{x}^{(i)})), i = 1, \dots, N\}$. The maximum likelihood problem yields analytical expressions for \mathbf{a}, σ_Y^2 as a function of $\boldsymbol{\theta}$:

$$\hat{\mathbf{a}} = (\mathbf{F}^\top \mathbf{R}(\boldsymbol{\theta})^{-1} \mathbf{F})^{-1} \mathbf{F}^\top \mathbf{R}(\boldsymbol{\theta})^{-1} \boldsymbol{\Gamma} \quad \hat{\sigma}_Y^2 = \frac{1}{N} (\boldsymbol{\Gamma} - \mathbf{F}\hat{\mathbf{a}})^\top \mathbf{R}(\boldsymbol{\theta})^{-1} (\boldsymbol{\Gamma} - \mathbf{F}\hat{\mathbf{a}}) \quad (10)$$

The best values for the correlations lengths gathered in $\boldsymbol{\theta}$ are obtained by a numerical optimization.

Apart from the *mean prediction* given in Eq.(6), Kriging yields the so-called *Kriging variance* $\sigma_{\hat{Y}}^2(\mathbf{x})$ which corresponds to an *epistemic uncertainty* of prediction that is related to the finite size of the available observation data gathered in \mathfrak{X} :

$$\sigma_{\hat{Y}}^2(\mathbf{x}) = \sigma_Y^2 \left(1 - \langle \mathbf{f}(\mathbf{x})^\top \mathbf{r}(\mathbf{x})^\top \rangle \left[\begin{array}{cc} \mathbf{0} & \mathbf{F}^\top \\ \mathbf{F} & \mathbf{R} \end{array} \right]^{-1} \left[\begin{array}{c} \mathbf{f}(\mathbf{x}) \\ \mathbf{r}(\mathbf{x}) \end{array} \right] \right) \quad (11)$$

It is important to notice that the mean Kriging estimator given in Eq.(6) is *interpolating* the data (meaning that $\mu_{\hat{Y}}(\mathbf{x}^{(i)}) = g(\mathbf{x}^{(i)})$, $i = 1, \dots, N$) and that the Kriging variance is zero in these points ($\sigma_{\hat{Y}}^2(\mathbf{x}^{(i)}) = 0$, $i = 1, \dots, N$).

These features are shown graphically in Figure 1, in which a univariate function $x \mapsto x \sin x$ is approximated using 6 points in the experimental design. The dashed area corresponds to the mean prediction ± 2 Kriging standard deviations (Eq.(11)). Improving the Kriging meta-model will be possible if new points are added in the experimental design that are drawn in regions where the dashed area is wide.

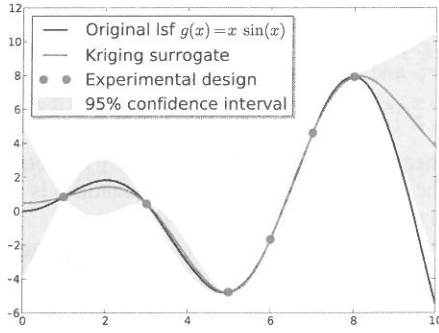


Figure 1: Kriging surrogate of a univariate function $x \mapsto x \sin x$ using 6 observations. The dashed area corresponds to the mean prediction ± 2 Kriging standard deviations (confidence interval).

NB: The Kriging variance $\sigma_{\hat{Y}}^2(\mathbf{x})$ is interpreted as a measure of the epistemic uncertainty of prediction in each point \mathbf{x} . It shall not to be confused with the aleatoric uncertainty represented through random vector \mathbf{X} that is related to the probability measure $\mathbb{P}[d\mathbf{x}] = f_{\mathbf{X}}(\mathbf{x}) d\mathbf{x}$. Thus $\sigma_{\hat{Y}}^2(\mathbf{x})$ may be used as an indicator for adaptively enrich the experimental design and refine the meta-model.

3 META-MODEL-BASED IMPORTANCE SAMPLING

3.1 Principle

As already mentioned in the introduction, meta-models are usually used as a substitute for the *true* limit state function in reliability analysis. As a consequence it is hardly possible to master the accuracy of the obtained results. The idea of using the surrogate as a means to derive an optimal importance sampling density has emerged in Dubourg et al. (2011, 2012). The principle is now recalled. Introducing an *importance sampling density* $h(\mathbf{x})$, Eq.(2) may be recast as:

$$P_f = \int_{\mathbb{R}^M} \mathbf{1}_{\mathcal{D}_f}(\mathbf{x}) \frac{f_{\mathbf{X}}(\mathbf{x})}{h(\mathbf{x})} h(\mathbf{x}) d\mathbf{x} = \mathbb{E}_h \left[\mathbf{1}_{\mathcal{D}_f}(\mathbf{X}) \frac{f_{\mathbf{X}}(\mathbf{X})}{h(\mathbf{X})} \right] \quad (12)$$

The optimal density, *i.e.* the one that leads to a minimal variance in the context of Monte Carlo simulation is proven to be (Rubinstein & Kroese 2008) :

$$h^*(\mathbf{x}) = \frac{\mathbf{1}_{\mathcal{D}_f}(\mathbf{x}) f_{\mathbf{X}}(\mathbf{x})}{\int_{\mathcal{D}_X} \mathbf{1}_{\mathcal{D}_f}(\mathbf{x}) f_{\mathbf{X}}(\mathbf{x}) d\mathbf{x}} = \frac{\mathbf{1}_{\mathcal{D}_f}(\mathbf{x}) f_{\mathbf{X}}(\mathbf{x})}{P_f} \quad (13)$$

It is nothing but the original density of the input parameters $f_{\mathbf{X}}$ which is truncated to the failure domain. It is of no direct use since it includes the unknown quantity P_f in its definition. Starting from a Kriging surrogate of the g function as described in Section 2, Dubourg et al. (2012) propose to use the following *probabilistic classification function* π as a surrogate of the indicator function $\mathbf{1}_{\mathcal{D}_f}(\mathbf{x})$ of the failure domain:

$$\pi(\mathbf{x}) = \mathcal{P} \left[\hat{Y}(\mathbf{x}) \leq 0 \right] = \Phi \left(\frac{0 - \mu_{\hat{Y}}(\mathbf{x})}{\sigma_{\hat{Y}}(\mathbf{x})} \right) \quad (14)$$

where Φ is the standard normal cumulative distribution function. In this equation $\mathcal{P}[\cdot]$ is the Gaussian probability measure associated to Kriging, not to be confused with $\mathbb{P}(\cdot)$. Consequently the proposed quasi-optimal importance sampling (also called *instrumental*) density reads:

$$\tilde{h}(\mathbf{x}) \stackrel{\text{def}}{=} \frac{\pi(\mathbf{x}) f_{\mathbf{X}}(\mathbf{x})}{P_{f\varepsilon}} = \frac{\Phi(-\mu_{\hat{Y}}(\mathbf{x})/\sigma_{\hat{Y}}(\mathbf{x})) f_{\mathbf{X}}(\mathbf{x})}{P_{f\varepsilon}} \quad (15)$$

where the normalization constant P_{f_ϵ} reads:

$$P_{f_\epsilon} \stackrel{\text{def}}{=} \mathbb{E}[\pi(\mathbf{X})] = \int_{\mathcal{D}_X} \Phi(-\mu_{\hat{Y}}(\mathbf{x})/\sigma_{\hat{Y}}(\mathbf{x})) f_X(\mathbf{x}) d\mathbf{x} \quad (16)$$

P_{f_ϵ} is called the *augmented probability of failure* as it takes into account both the aleatory uncertainty in the input parameters (modelled by \mathbf{X}) and the epistemic uncertainty in the Kriging prediction. Using this notation, Dubourg et al. (2012) prove that:

$$P_f = \alpha_{corr} P_{f_\epsilon} \quad \alpha_{corr} = \mathbb{E}_{\hat{h}} \left[\frac{\mathbf{1}_{\mathcal{D}_f}(\mathbf{X})}{\pi(\mathbf{X})} \right] \quad (17)$$

where α_{corr} is a correction factor obtained by taking an expectation w.r.t. the instrumental PDF in Eq.(15). The augmented probability of failure P_{f_ϵ} and the correction terms are given Monte Carlo estimates, see details in the above reference.

3.2 Enhancing meta-IS through subset simulation

According to Eq.(16) the augmented probability of failure may be computed by Monte Carlo simulation using samples drawn with respect to the input PDF $f_X(\mathbf{x})$:

$$\widehat{P}_{f_\epsilon} = \frac{1}{N_\epsilon} \sum_{l=1}^{N_\epsilon} \pi(\mathbf{x}^{(l)}) = \frac{1}{N_\epsilon} \sum_{l=1}^{N_\epsilon} \Phi(-\mu_{\hat{Y}}(\mathbf{x}^{(l)})/\sigma_{\hat{Y}}(\mathbf{x}^{(l)})) \quad (18)$$

As each evaluation only requires computing the Kriging mean and standard deviation in Eqs.(6), (11), it is computationally inexpensive in usual cases. However, when small probabilities of failure are sought, millions or tens of millions evaluations of the latter equations become intractable. For this purpose, it is proposed to compute P_{f_ϵ} by introducing a *splitting technique* similar to the one used in subset simulation.

Let us define a decreasing sequence of real numbers $q_0 = +\infty > q_1 > \dots > q_s = 0$ and the associated probabilistic classification functions $\{\pi_i(\mathbf{x}), i = 1, \dots, s\}$ and probabilities of failure $p_{i\epsilon}$:

$$\pi_i(\mathbf{x}) = \mathcal{P}[\hat{Y}(\mathbf{x}) \leq q_i] = \Phi\left(\frac{q_i - \mu_{\hat{Y}}(\mathbf{x})}{\sigma_{\hat{Y}}(\mathbf{x})}\right) \quad p_{i\epsilon} = \mathbb{E}[\pi_i(\mathbf{X})] \quad (19)$$

The augmented probability of failure is recast as:

$$P_{f_\epsilon} = \int_{\mathcal{D}_X} \pi_s(\mathbf{x}) f_X(\mathbf{x}) d\mathbf{x} = \int_{\mathcal{D}_X} \frac{\pi_s(\mathbf{x})}{\pi_{s-1}(\mathbf{x})} \pi_{s-1}(\mathbf{x}) f_X d\mathbf{x} = p_{s-1\epsilon} \times p_{s|s-1\epsilon} \quad (20)$$

where:

$$p_{s-1\epsilon} = \mathbb{E}_X[\pi_{s-1}(\mathbf{X})] \quad (21)$$

$$p_{s|s-1\epsilon} = \mathbb{E}_{h_{s\epsilon}^*} \left[\frac{\pi_s(\mathbf{X})}{\pi_{s-1}(\mathbf{X})} \right] = \int_{\mathcal{D}_X} \frac{\pi_s(\mathbf{x})}{\pi_{s-1}(\mathbf{x})} h_{s\epsilon}^*(\mathbf{x}) d\mathbf{x}$$

In the latter equation the quasi-optimal intermediate instrumental PDF reads:

$$h_{s\epsilon}^*(\mathbf{x}) = \frac{\pi_{s-1}(\mathbf{x}) f_X(\mathbf{x})}{\int_{\mathcal{D}_X} \pi_{s-1}(\mathbf{x}) f_X(\mathbf{x}) d\mathbf{x}} \quad (22)$$

By applying the splitting technique ($s - 2$) times one eventually gets $P_{f_\epsilon} = p_{1\epsilon} \prod_{i=2}^s p_{i|i-1\epsilon}$.

As in classical subset simulation, the generation of samples that follow the instrumental density $h_{i\epsilon}^*(\mathbf{x}) \propto \pi_{s-1}(\mathbf{x}) f_X$ is carried out using a modified Metropolis-Hastings algorithm and the intermediate thresholds $\{q_1, \dots, q_{s-1}\}$ are determined on-the-fly so that the intermediate probabilities of failure are around 10%. The coefficient of variation of the simulation which rely upon Markov chain Monte Carlo sampling and associated issues with correlated samples is discussed in Dubourg (2011).

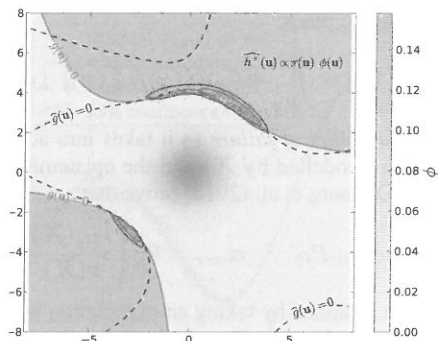


Figure 2: Example 1: limit state surface (Eq.(23)) and quasi-optimal, bimodal importance sampling density obtained from Kriging (contours)

4 APPLICATION EXAMPLES

4.1 A 2D series system

Let us consider a two-component series system where the limit state function is defined by Au & Beck (1999) as follows:

$$g(x_1, x_2) = \min \left\{ c - 1 - x_2 + e^{-x_1^2/10} + \left(\frac{x_1}{5} \right)^4, \frac{c^2}{2} - x_1 x_2 \right\} \quad (23)$$

where c is set equal to 3, 4 or 5 respectively. The results obtained by Meta-IS are reported in Table 1 together with reference values obtained by crude Monte Carlo simulation, subset simulation (as implemented in FERUM 4.1 (Bourinet et al. 2009)) and the original results by Au & Beck (1999).

It is observed that the approach by Au & Beck (1999) leads to a relative error up to 29% in P_f (4% in β), as does subset simulation for $c = 5$ (29% in P_f , 1.5% in β). In contrast the proposed approach is always more accurate with less than 4% error in P_f (less than 0.2 % in β) whatever the threshold.

Table 1: 2D series system – reliability results

Method	Monte Carlo (ref)	Subset	Au & Beck (1999) ¹	Meta-IS ²	
$c = 3$	N	10^7	300,000	100 + 500	44 + 600
	p_f	3.48×10^{-3}	3.48×10^{-3}	2.47×10^{-3}	3.54×10^{-3}
	C.o.V.	0.5%	<3%	11%	<5%
$c = 4$	N	10^8	500,000	100 + 500	64 + 600
	p_f	8.94×10^{-5}	8.34×10^{-5}	6.30×10^{-5}	8.60×10^{-5}
	C.o.V.	3.3%	<4%	8%	<5%
$c = 5$	N	10^9	700,000	100 + 500	40 + 2,900
	p_f	9.28×10^{-7}	6.55×10^{-7}	6.54×10^{-7}	9.17×10^{-7}
	C.o.V.	3.3%	<5%	12%	<5%

The total computational cost $N_{tot} = N + N_{IS}$ is reported in Column #5, where N is the size of the experimental design for the Kriging surrogate and N_{IS} is the number of samples used for evaluating the correction factor. It is equal to a few hundreds for $c = 3$ and $c = 4$. It amounts to almost 3000 for $c = 5$: this is due to the fact that the optimal sampling density is multimodal (as shown in Figure 2), where the two modes are far away from each other when $c = 5$, which leads to some difficulties in applying the Metropolis-Hastings algorithm in this case.

4.2 A truss structure

Let us consider the truss structure sketched in Figure 3. The structure made of 23 members, namely 11 horizontal bars and 12 oblique bars is modelled by truss elements. The upper part is subject to

vertical loads. Ten parameters are modelled by independent input random variables, namely the Young's moduli and the cross-section areas of the horizontal and the oblique bars (respectively denoted by E_1, A_1 and E_2, A_2) and the applied loads (denoted by $P_i, i = 1, \dots, 6$), whose mean and coefficient of variation are reported in Table 2. Thus the input random vector is defined by:

$$\mathbf{X}^{phys} = \{E_1, E_2, A_1, A_2, P_1, \dots, P_6\}^T \quad (24)$$

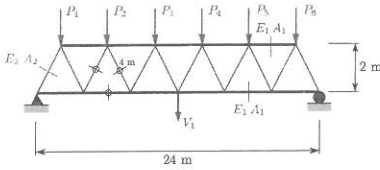


Figure 3: Example #2 – Truss structure with 23 members

Table 2: Example #2 – Input random variables

Variable	Distribution	Mean	C.V
E_1, E_2 (Pa)	Lognormal	2.10×10^{11}	10%
A_1 (m ²)	Lognormal	2.0×10^{-3}	10%
A_2 (m ²)	Lognormal	1.0×10^{-3}	10%
P_1 - P_6	Gumbel	5.0×10^4	15%

The limit state function is related to the serviceability of the truss with respect to its midspan deflection:

$$g(\mathbf{X}) = u_{\max} - FEM(\mathbf{X}) \quad (25)$$

Two values of the threshold are selected, namely $u_{\max} = 10$ cm and $u_{\max} = 14$ cm. The associated probabilities of failure are reported in Table 3 together with reference results obtained by Blatman (2009)

Table 3: Truss structure – reliability results

Threshold (cm)		Importance sampling (Blatman, 2009)	FORM	Meta-IS ³
10	N_{tot}	500,000	121	160 +31
	P_f	4.00×10^{-2}	2.81×10^{-2}	4.35×10^{-2} (C.o.V.=1.2%)
	β	1.75	1.91	1.71
14	N_{tot}	500,000	121	160 +31
	P_f	3.45×10^{-5}	1.28×10^{-5}	3.47×10^{-5} (C.o.V.=3.7%)
	β	3.98	4.21	3.98

In this example again, the accuracy of the proposed method is remarkable, with only a few percent of error on the probability of failure for both cases $u_{\max} = 10$ and 14 cm (with respect to a reference solution obtained by a design-point-based importance sampling approach, see Blatman (2009) for details) at a computational cost which is in the same order of magnitude as FORM.

5 CONCLUSION

A meta-model-based importance sampling method has been proposed in order to compute unbiased estimates of the probability of failure appearing in structural reliability analysis. A Kriging surrogate model of the limit state function is built first using a set of computer experiments. It then helps to define quasi-optimal instrumental densities that are used in the context of importance sampling. The probability of failure is cast as the product of a) an augmented probability of failure which takes into account both the aleatory uncertainty on the model parameters and the epistemic uncertainty related to Kriging, and b) a correction factor. Only the latter requires running the “true” limit state function.

In a basic setting the augmented probability of failure could be evaluated by crude Monte Carlo simulation since it does only use calls to the surrogate limit state function (more specifically, the Kriging mean and standard deviation). For small probabilities of failure though, this becomes intractable. Thus a procedure is proposed to decrease the associated computational cost using splitting, as in the original subset simulation method.

Two application examples are shown, namely a two-dimensional series system and a finite element reliability analysis of an elastic truss. In both cases the proposed approach enables the computation of small probabilities of failure (up to 10^{-7}) with a remarkable accuracy, i.e. than 5% error on P_f and a two-digit accuracy on the associated generalized reliability index.

REFERENCES

- Au, S. & J. Beck (1999). A new adaptive importance sampling scheme for reliability calculations. *Structural Safety*, 21(2): 135–158.
- Au, S. & J. Beck (2001). Estimation of small failure probabilities in high dimensions by subset simulation. *Prob. Eng. Mech.*, 16(4): 263–277.
- Berveiller, M., B. Sudret, & M. Lemaire (2004). Presentation of two methods for computing the response coefficients in stochastic finite element analysis. Proceedings, 9th ASCE Specialty Conference on Probabilistic Mechanics & Structural Reliability, Albuquerque, USA.
- Berveiller, M., B. Sudret, & M. Lemaire (2006). Stochastic finite elements: a non intrusive approach by regression. *Eur. J. Comput. Mech.*, 15(1-3): 81–92.
- Bichon, B., M. Eldred, L. Swiler, S. Mahadevan, & J. McFarland (2008). Efficient global reliability analysis for nonlinear implicit performance functions. *AIAA Journal*, 46(10): 2459–2468.
- Blatman, G. (2009). *Adaptive sparse polynomial chaos expansions for uncertainty propagation & sensitivity analysis*. Ph. D. thesis, Université Blaise Pascal, Clermont-Ferrand.
- Bourinet, J.-M., F. Deheeger, & M. Lemaire (2011). Assessing small failure probabilities by combined subset simulation & support vector machines. *Structural Safety*, 33(6): 343–353.
- Bourinet, J.-M., C. Mattrand, & V. Dubourg (2009). A review of recent features & improvements added to the FERUM software. In H. Furuta, D. Frangopol, & M. Shinozuka (Eds.), *Proceedings, 10th Int. Conf. Struct. Safety & Reliability (ICOSSAR'2009), Osaka, Japan*.
- Dubourg, V. (2011). *Adaptive surrogate models for reliability analysis and reliability-based design optimization*. Ph. D. thesis, Université Blaise Pascal, Clermont-Ferrand, France.
- Dubourg, V., F. Deheeger, & B. Sudret (2011). An alternative to substitution for metamodel-based reliability analysis. In M. Faber (Ed.), *Proceedings, 11th Int. Conf. on Applications of Stat. & Prob. in Civil Engineering (ICASP11), Zurich, Switzerland*.
- Dubourg, V., F. Deheeger, & B. Sudret. Metamodel-based importance sampling for structural reliability analysis. *Prob. Eng. Mech.*. In press.
- Echard, B., N. Gayton, & M. Lemaire (2011). AK-MCS: an active learning reliability method combining kriging and monte carlo simulation. *Structural Safety*, 33(2): 145–154.
- Hurtado, J. (2004). An examination of methods for approximating implicit limit state functions from the viewpoint of statistical learning theory. *Structural Safety*, 26: 271–293.
- Rubinstein, R. & D. Kroese (2008). *Simulation & the Monte Carlo method*. Wiley Series in Probability & Statistics. Wiley.
- Sacks, J., W. Welch, T. Mitchell, & H. Wynn (1989). Design & analysis of computer experiments. *Stat. Sci.*, 4: 409–435.
- Santner, T., B. Williams, & W. Notz (2003). *The Design & Analysis of Computer Experiments*. Springer, New York.
- Sudret, B. (2012). Meta-models for structural reliability & uncertainty quantification. In K. Phoon, M. Beer, S. Quek, & S. Pang (Eds.), *Proceedings, 5th Asian-Pacific Symp. Struct. Reliab. (APSSRA'2012), Singapore*, pp. 53–76. Keynote lecture.
- Sudret, B. & A. Der Kiureghian (2002). Comparison of finite element reliability methods. *Prob. Eng. Mech.*, 17: 337–348.

Assessment of MCMC algorithms for subset simulation

I. Papaioannou, K. Zwirgmaier & D. Straub

Engineering Risk Analysis Group, Technische Universität München, Germany
iason.papaioannou@tum.de

ABSTRACT: The subset simulation is an adaptive simulation method that efficiently solves structural reliability problems with a large number of random variables. The method includes sampling from conditional distributions, which is achieved through Markov Chain Monte Carlo (MCMC) algorithms. This paper investigates the performance of different MCMC algorithms for subset simulation. It is found that most of the MCMC algorithms proposed in the literature, based on the Metropolis-Hastings (M-H) sampler, do not present significant improvements over the component-wise M-H algorithm originally proposed for subset simulation in [Au & Beck, Prob Eng Mech, 16(4): 263-277, 2001]. Based on these findings, a novel approach for MCMC sampling in the standard normal space is introduced, which has the benefit of simplicity. Moreover, it is shown that an optimal scaling of either this new approach or the component-wise M-H algorithm can improve the accuracy of the original algorithm, without the need for additional model evaluations.

1 INTRODUCTION

Let \mathbf{X} denote the basic random variable space of dimension n , which models the system variables that are expected to present an uncertain behavior. Assuming the usual case, where the probabilistic description of \mathbf{X} comes in terms of marginal distributions and correlations, we can adopt the Nataf model (Gaussian copula) for the joint distribution of \mathbf{X} and then define a mapping $\mathbf{U} = \mathbf{T}(\mathbf{X})$ to a transformed space \mathbf{U} consisting of n independent standard normal random variables (Der Kiureghian & Liu 1986). In the case where the joint distribution of \mathbf{X} is known, then the transformation $\mathbf{U} = \mathbf{T}(\mathbf{X})$ can be performed in a straightforward fashion (Hohenbichler & Rackwitz 1981). Let $F \subset \mathbb{R}^n$ be the failure domain in the \mathbf{U} -space, such that $\mathbf{u} \in F$ defines the event of unsatisfactory performance of the system. The probability of failure can then be expressed as follows:

$$P_f = P(F) = \int_{\mathbf{u} \in F} \varphi_n(\mathbf{u}) d\mathbf{u} = \int_{\mathbf{u} \in \mathbb{R}^n} I_F(\mathbf{u}) \varphi_n(\mathbf{u}) d\mathbf{u} \quad (1)$$

where $\varphi_n(\mathbf{u}) = \prod_{i=1}^n \varphi(u_i)$ and $\varphi(\cdot)$ is the standard normal PDF. The function $I_F(\mathbf{u})$ is the indicator function: $I_F(\mathbf{u}) = 1$ if $\mathbf{u} \in F$ and $I_F(\mathbf{u}) = 0$ otherwise.

The evaluation of the probability of failure is not a trivial task, especially when the performance of the system for a realization of the random variables is obtained through a computationally demanding model evaluation. The Monte Carlo method is a robust technique that is able to handle any model, independent of its complexity. In this method, the probability of failure is estimated by the sample mean of the indicator function:

$$P_f \approx \hat{P}_f = \frac{1}{N} \sum_{k=1}^N I_F(\mathbf{u}_k) \quad (2)$$

where $\{\mathbf{u}_k: k = 1, \dots, N\}$ are independent and identically distributed samples of the joint PDF $\varphi_n(\mathbf{u})$. Equation 2 gives an unbiased estimate of P_f . The coefficient of variation of the estimate reads:

$$\delta_{\hat{P}_f} = \sqrt{\frac{1 - P_f}{NP_f}} \quad (3)$$

As shown in Equation 3, the coefficient of variation, which serves as a measure of accuracy of the estimate, does not depend on the dimension n . Hence, the efficiency of the Monte Carlo method does not depend on the number of random variables. However, for small values of P_f , a large number of samples N is required to achieve a sufficiently small $\delta_{\hat{P}_f}$.

In order to overcome the inefficiency of the Monte Carlo method in estimating small failure probabilities, while maintaining its independency on the number of random variables n , a number of advanced simulation methods have been developed, including the subset simulation (Au & Beck 2001), the spherical subset simulation (Katafygiotis & Cheung 2007) and the asymptotic sampling method (Bucher 2009). Here, we focus on the subset simulation. This method expresses P_f as a product of conditional probabilities that are significantly larger than P_f . These conditional probabilities are then estimated by application of Markov Chain Monte Carlo (MCMC) sampling.

This paper discusses different MCMC algorithms that have been proposed for subset simulation. Moreover, a new approach is presented for MCMC in the \mathbf{U} -space. In Section 2, the subset simulation is described. Section 3 reviews the considered MCMC methods and evaluates their performance.

2 SUBSET SIMULATION

The subset simulation is an adaptive Monte Carlo method proposed by Au & Beck (2001) for the estimation of small failure probabilities in high dimensional problems. The idea behind subset simulation is to express the failure domain F as the intersection of M larger intermediate failure domains:

$$F = \bigcap_{j=1}^M F_j \quad (4)$$

where $F_1 \supset F_2 \supset \dots \supset F_M = F$, hence the name ‘‘subset simulation’’. The probability of failure is then estimated as a product of conditional probabilities:

$$P_f = P(F) = P\left(\bigcap_{j=1}^M F_j\right) = P(F_1) \prod_{j=2}^M P(F_j|F_{j-1}) \quad (5)$$

An appropriate selection of the intermediate failure domains can lead to large conditional probabilities. That is, the original problem of evaluating a small failure probability reduces to a sequence of M intermediate problems that correspond to the estimation of larger probabilities.

The probability $P(F_1)$ can be computed by application of crude Monte Carlo simulation through sampling of $\varphi_n(\mathbf{u})$. For estimating the probabilities $\{P(F_j|F_{j-1}): j = 2, \dots, M\}$, we need to generate samples of the conditional PDFs $\{\varphi_n(\mathbf{u}|F_{j-1}): j = 2, \dots, M\}$, where:

$$\varphi_n(\mathbf{u}|F_{j-1}) = \frac{\varphi_n(\mathbf{u})I_{F_{j-1}}(\mathbf{u})}{P(F_{j-1})} \quad (6)$$

A direct sampling of $\varphi_n(\mathbf{u}|F_{j-1})$ by application of the acceptance-rejection method is inefficient, especially as the domain F_{j-1} approaches the actual failure domain. However, MCMC techniques can be applied for sampling $\varphi_n(\mathbf{u}|F_{j-1})$. MCMC methods produce samples of a target distribution, by constructing a Markov chain that has the target distribution as its stationary distribution (Rubinstein & Kroese 2007). The derived samples will be distributed according to $\varphi_n(\mathbf{u}|F_{j-1})$, however they will not be independent.

We now need to specify the intermediate failure domains $\{F_j: j = 1, \dots, M - 1\}$. Let $G(\mathbf{u})$ denote a limit-state function with negative values defining the failure event, i.e. $F = \{\mathbf{u} \in \mathbb{R}^n: G(\mathbf{u}) \leq 0\}$. Without loss of generality, we assume that the function $G(\mathbf{u})$ can express any type of system failure in the \mathbf{U} -space. The intermediate failure domain F_j can then be defined as $F_j = \{\mathbf{u} \in \mathbb{R}^n: G(\mathbf{u}) \leq c_j\}$, where $c_1 > c_2 > \dots > c_M = 0$. The values of $\{c_j: j = 1, \dots, M - 1\}$ can be chosen adaptively, so that the estimates of the conditional probabilities correspond to a chosen value p_0 , e.g. $p_0 = 0.1$. This is achieved by successively sampling each conditional PDF $\varphi_n(\mathbf{u}|F_{j-1})$ and setting c_i equal to the $[(1 - p_0)N + 1]$ -th largest value among the samples $\{G(\mathbf{u}_k): k = 1, \dots, N\}$. This procedure is repeated until the actual failure domain F_M is reached, for which the threshold $c_M = 0$ is given. We can then obtain an estimate of the failure probability as follows:

$$P_f \approx \hat{P}_f = p_0^{M-1} \hat{P}(F_M|F_{M-1}) \quad (7)$$

The estimate $\hat{P}(F_M|F_{M-1})$ of the conditional probability is as follows:

$$\hat{P}(F_M|F_{M-1}) = \frac{1}{N} \sum_{k=1}^N I_F(\mathbf{u}_k) \quad (8)$$

where $\{\mathbf{u}_k: k = 1, \dots, N\}$ are samples of $\varphi_n(\mathbf{u}|F_{M-1})$. It should be noted that the estimator \hat{P}_f in Equation 7 is biased for a finite N , due to the correlation between the estimates of the conditional probabilities, but it is asymptotically unbiased (Au & Beck 2001).

3 MCMC ALGORITHMS FOR SUBSET SIMULATION

As discussed in Section 2, the subset simulation applies MCMC sampling to simulate each conditional PDF $\varphi_n(\mathbf{u}|F_{j-1})$. In this section, first the general principle of MCMC sampling for subset simulation is summarized, followed by a review of different proposed and new methods.

Let us define a stationary discrete-time vector random process $\{\mathbf{U}_t, t \in \mathbb{N}\}$ with marginal PDF $\varphi_n(\mathbf{u}|F_{j-1})$, which possesses the Markov property. That is, the random vector at position t is distributed according to a conditional PDF given the outcome of the random vector at position $t - 1$. This conditional PDF is termed transition PDF and is denoted by $p(\mathbf{u}_1|\mathbf{u}_0)$, where $\mathbf{u}_0, \mathbf{u}_1$ are subsequent states of the chain. The transition PDF satisfies the following condition:

$$p(\mathbf{u}_1|\mathbf{u}_0)\varphi_n(\mathbf{u}_0|F_{j-1}) = p(\mathbf{u}_0|\mathbf{u}_1)\varphi_n(\mathbf{u}_1|F_{j-1}) \quad (9)$$

The above is termed reversibility condition and it is an essential property of the Markov process \mathbf{U}_t , since it ensures that the stationary PDF of the process is $\varphi_n(\mathbf{u}|F_{j-1})$.

MCMC methods produce samples of a distribution by simulating states of a stationary Markov process whose marginal distribution is the desired distribution. This can be achieved by simulating every new state of the process from a transition PDF $p(\mathbf{u}_1|\mathbf{u}_0)$ that satisfies the reversibility condition. Starting from a state that may or may not be distributed according to the target distribution, the Markov chain will asymptotically converge to the target (stationary) distribution (Rubinstein & Kroese 2007). The transient period that is required until the Markov chain reaches its stationary state is termed burn-in period. Moreover, the generated samples will be correlated according to the correlation of the Markov process which will depend on the particular choice of $p(\mathbf{u}_1|\mathbf{u}_0)$.

In the context of subset simulation, MCMC sampling is applied at subset j to sample $\varphi_n(\cdot|F_{j-1})$ through simulating states of a Markov chain using as starting point (or 'seed') each sample $\{\mathbf{u}_k: k = 1, \dots, N_f\}$ that fell in F_{j-1} at subset $j - 1$. Since all the samples \mathbf{u}_k are distributed according to $\varphi_n(\cdot|F_{j-1})$, all states of the Markov chains will be distributed according to the target distribution $\varphi_n(\cdot|F_{j-1})$. Hence, the Markov chains do not require a burn-in period to reach their stationary states. The coefficient of variation of the estimate of each conditional probability $\hat{P}_j = \hat{P}(F_j|F_{j-1})$ can be estimated in terms of the sample variance of the stationary process $I_{F_j}(\mathbf{U}_t)$ (Au & Beck 2001):

$$\delta_{\hat{p}_j} = \sqrt{\frac{1 - P_j}{NP_j}} (1 + \gamma_j) \quad (10)$$

where

$$\gamma_j = 2 \sum_{k=1}^{N/N_f-1} \left(1 - \frac{kN_f}{N}\right) \rho_j(k) \quad (11)$$

where N_f is the number of seeds, N/N_f is the length of each chain and $\rho_j(k)$ is the autocorrelation coefficient of the sequence $\{I_{F_j}(\mathbf{u}_t), t = 1, \dots, N/N_f\}$. $\rho_j(k)$ can be estimated from the samples. The estimator of Equation 10 assumes that the different chains are uncorrelated through the indicator function, i.e. possible dependence between the different seeds is neglected. Equation 10 indicates that the efficiency of the subset simulation decreases if the chain correlation increases. A decreased chain correlation implies that the chain explores its state space faster. This motivates the introduction of a new measure of the efficiency of the estimator \hat{P}_j , based on the expected Euclidean distance between two successive samples, say \mathbf{u}_0 and \mathbf{u}_1 :

$$\lambda_j = \frac{1}{\sqrt{n}} \text{E} \left[\sqrt{\sum_{i=1}^n (u_{0i} - u_{1i})^2} \right] \quad (12)$$

where u_{0i} is the i -th coordinate of \mathbf{u}_0 . λ_j can be viewed as the average velocity of the different chains. A maximum λ_j will give a minimum chain dependence and hence a minimum coefficient of variation $\delta_{\hat{p}_j}$.

In the following, we assess the efficiency of different MCMC algorithms for subset simulation.

3.1 Metropolis-Hastings algorithm

The Metropolis-Hastings (M-H) algorithm (Metropolis et al. 1953, Hastings 1970) is the most widely used MCMC method for sampling from distributions that are difficult to sample from directly. Consider a n -dimensional proposal PDF $q(\cdot | \mathbf{u}_0)$ that depends on the current state of the chain. The transition from the state \mathbf{u}_0 to the next state \mathbf{u}_1 is described by the following steps:

1. Generate a candidate \mathbf{v} .
 - 1.a. Generate a pre-candidate ξ by sampling from from the PDF $q(\cdot | \mathbf{u}_0)$
 - 1.b. Accept or reject ξ

$$\mathbf{v} = \begin{cases} \xi, & \text{with prob. } a(\mathbf{u}_0, \xi) \\ \mathbf{u}_0, & \text{with prob. } 1 - a(\mathbf{u}_0, \xi) \end{cases} \quad (13)$$

where

$$a(\mathbf{u}_0, \xi) = \min \left\{ 1, \frac{\varphi_n(\xi) q(\mathbf{u}_0 | \xi)}{\varphi_n(\mathbf{u}_0) q(\xi | \mathbf{u}_0)} \right\} \quad (14)$$

2. If ξ was rejected set $\mathbf{u}_1 = \mathbf{u}_0$. Else, accept or reject \mathbf{v}

$$\mathbf{u}_1 = \begin{cases} \mathbf{v}, & \mathbf{v} \in F_{j-1} \\ \mathbf{u}_0, & \mathbf{v} \notin F_{j-1} \end{cases} \quad (15)$$

It can be shown that the transition PDF that results from the above procedure will satisfy Equation 9 independent of the choice of the proposal PDF $q(\cdot | \mathbf{u}_0)$ (Hastings 1970). If the proposal PDF has the symmetry property, i.e. $q(\mathbf{v} | \mathbf{u}) = q(\mathbf{u} | \mathbf{v})$, the algorithm reduces to the original Metropolis sampler (Metropolis et al. 1953).

As discussed in (Au & Beck 2001), the M-H algorithm becomes inefficient for high dimensional problems. This is due to the fact that the probability that the pre-candidate is rejected in step 1 increases rapidly with increasing number of dimensions n . This will lead to many repeated samples and hence to an increased correlation of the Markov chain. This is illustrated in Fig-

ure 1, where the acceptance rate of the pre-candidate state of the M-H algorithm is plotted against the random dimension n .

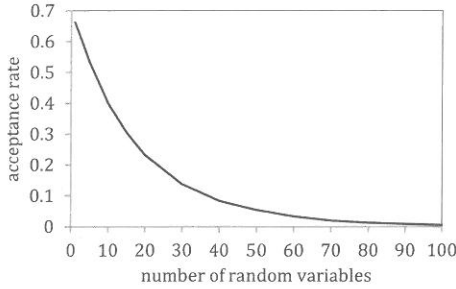


Figure 1: Acceptance rate of the original M-H algorithm applied to sampling from the independent standard normal distribution, as a function of the number of random variables n .

3.2 Component-wise M-H

The component-wise M-H algorithm was proposed by Au & Beck (2001) for sampling from high dimensional conditional distributions. The method requires that the random variable space be independent, however independence is achieved by the transformation of the original random variable space to the \mathbf{U} -space. The method differs from the original M-H algorithm in the generation of the candidate state. That is, instead of using a n -dimensional proposal PDF, each coordinate v_i of the candidate state is generated from a one-dimensional proposal PDF $q(\cdot | u_{0i})$ that depends on the i -th coordinate u_{0i} of the current state. The algorithm is summarized as follows:

1. Generate a candidate $\mathbf{v} = (v_1, \dots, v_n)$. For each $i = 1, \dots, n$
 - 1.a. Generate a pre-candidate ξ_i from the PDF $q(\cdot | u_{0i})$
 - 1.b. Accept or reject ξ_i

$$v_i = \begin{cases} \xi_i, & \text{with prob. } a(u_{0i}, \xi_i) \\ u_{0i}, & \text{with prob. } 1 - a(u_{0i}, \xi_i) \end{cases} \quad (16)$$

where

$$a(u_{0i}, \xi_i) = \min \left\{ 1, \frac{\varphi(\xi_i) q(u_{0i} | \xi_i)}{\varphi(u_{0i}) q(\xi_i | u_{0i})} \right\} \quad (17)$$

2. Accept or reject \mathbf{v} : apply Equation 15.

Due to the independence of the random vector \mathbf{U} , the component-wise M-H algorithm satisfies the reversibility condition independent of the choice of the one-dimensional proposal PDF. Au & Beck (2001) suggest to choose $q(\cdot | u_{0i})$ as the uniform PDF centered at u_{0i} with width of 2, i.e. twice the standard deviation at the \mathbf{U} -space – the optimal choice of the spread of the proposal PDF is discussed in Section 3.7. Moreover, due to the component-wise generation of the candidate state, the probability of repeated candidates decreases fast with increasing number of random variables n . Hence, the method is suitable for application to high-dimensional problems.

3.3 M-H with repeated generation of pre-candidate states

A different approach for reducing the correlation of the samples was proposed by Santoso et al. (2011). In this method, the candidate state is generated through a repeated generation of pre-candidate samples until acceptance of the pre-candidate is achieved. Hence, the algorithm avoids the generation of repeated candidates, thus reducing the chain correlation, as compared to the original M-H algorithm. The update of the Markov chain is as follows:

1. Generate a candidate \mathbf{v} .
 - 1.a. Generate a pre-candidate ξ from the PDF $q(\cdot | \mathbf{u}_0)$
 - 1.b. Accept or reject ξ

$$\mathbf{v} = \begin{cases} \xi, & \text{with prob. } \alpha(\mathbf{u}_0, \xi) \\ \mathbf{u}_0, & \text{with prob. } 1 - \alpha(\mathbf{u}_0, \xi) \end{cases} \quad (18)$$

where

$$\alpha(\mathbf{u}_0, \xi) = \min \left\{ 1, \frac{\varphi_n(\xi) q(\mathbf{u}_0 | \xi)}{\varphi_n(\mathbf{u}_0) q(\xi | \mathbf{u}_0)} \right\} \quad (19)$$

- 1.c. If ξ is rejected go to 1.a.
2. Accept or reject \mathbf{v} : apply Equation 15.

This approach is based on the M-H with delayed rejection (Tierney & Mira 1999), however in the latter method the acceptance probability of the pre-candidate sample is updated in each regeneration in order to ensure the satisfaction of the reversibility condition.

The method does not allow for an analytical expression of the transition PDF. Santoso et al. (2011) evaluated the transition PDF numerically for a one-dimensional truncated normal distribution using a uniform proposal PDF and showed that the reversibility condition is approximately satisfied. However, it turns out that the stationary distribution of the chain will differ from the target distribution. This is illustrated in Figure 2, where the CDF of the one-dimensional truncated normal distribution with different normalizing constants is compared to the empirical CDF from 10^4 samples.

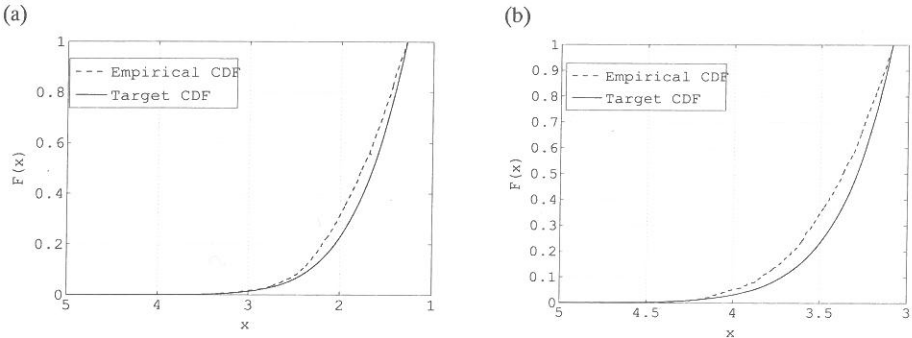


Figure 2: Empirical CDF of the M-H with repeated generation of pre-candidate states against target CDF of the Markov chain for the one-dimensional truncated normal distribution with probability normalizing constant (a) 10^{-1} and (b) 10^{-3} .

The fact that the target distribution is different from the stationary distribution of the chain may lead to biased probability estimates. Consider a reliability problem modeled by the following linear limit-state function at the \mathbf{U} -space:

$$G(\mathbf{U}) = -\frac{1}{\sqrt{n}} \sum_{i=1}^n U_i + \beta \quad (20)$$

The probability of failure for this function is $\Phi(-\beta)$, where $\Phi(\cdot)$ is the standard normal CDF. For a chosen conditional probability p_0 , the failure probability at each subset level j is p_0^j . Hence, the threshold c_j at the corresponding subset level is $c_j = \beta + \Phi^{-1}(p_0^j)$. Figure 3 shows the relative bias for subset levels $j = 2$ and $j = 4$, i.e. the difference between the true probability P_f and the estimate \hat{P}_f averaged over 500 independent subset simulation runs and divided by P_f , for $p_0 = 0.1$ and 500 samples per subset level. It is shown that the probability estimate is slightly biased and the bias tends to increase with increasing subset level, corresponding to a decreasing failure probability. On the other hand, the component-wise M-H gives a nearly unbiased estimate, since the produced samples follow the target distribution of the Markov chain.

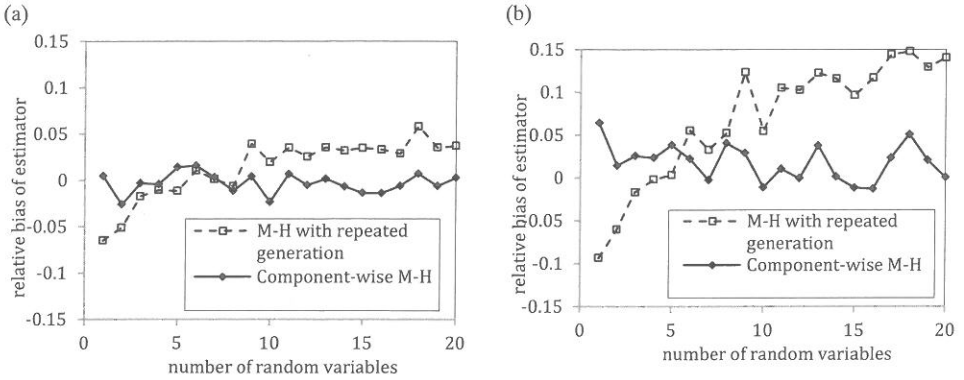


Figure 3: Relative bias of the estimator \hat{P}_f from 500 independent simulation runs with the M-H with repeated generation of pre-candidate states and the component-wise M-H at subset level (a) $j = 2$ and (b) $j = 4$.

3.4 Component-wise M-H with delayed rejection at the first acceptance level

As discussed in Section 3.3, a repeated generation of pre-candidate states requires that the acceptance probability is adapted to account for the fact that the sample was rejected, in order to model the target distribution exactly. This procedure is called delayed rejection and was developed by Tierney & Mira (1999) for application to Bayesian statistics. Miao & Ghosn (2011) applied this approach in combination with the component-wise M-H algorithm leading to the following updating procedure:

1. Generate a candidate $\mathbf{v} = (v_1, \dots, v_n)$. For each $i = 1, \dots, n$
 - 1.a. Generate a pre-candidate ξ_{1i} from the PDF $q_1(\cdot | u_{0i})$
 - 1.b. Accept or reject ξ_{1i}

$$v_i = \begin{cases} \xi_{1i}, & \text{with prob. } a_1(u_{0i}, \xi_{1i}) \\ u_{0i}, & \text{with prob. } 1 - a_1(u_{0i}, \xi_{1i}) \end{cases} \quad (21)$$

where

$$a_1(u_{0i}, \xi_{1i}) = \min \left\{ 1, \frac{\varphi(\xi_{1i}) q_1(u_{0i} | \xi_{1i})}{\varphi(u_{0i}) q_1(\xi_{1i} | u_{0i})} \right\} \quad (22)$$

- 1.c. If ξ_{1i} was rejected, generate ξ_{2i} from $q_2(\cdot | u_{0i}, \xi_{1i})$
- 1.d. Accept or reject ξ_{2i}

$$v_i = \begin{cases} \xi_{2i}, & \text{with prob. } a_2(u_{0i}, \xi_{1i}, \xi_{2i}) \\ u_{0i}, & \text{with prob. } 1 - a_2(u_{0i}, \xi_{1i}, \xi_{2i}) \end{cases} \quad (23)$$

where

$$a_2(u_{0i}, \xi_{1i}, \xi_{2i}) = \min \left\{ 1, \frac{\varphi(\xi_{2i}) q_1(\xi_{1i} | \xi_{2i}) q_2(u_{0i} | \xi_{2i}, \xi_{1i}) [1 - a_1(\xi_{2i}, \xi_{1i})]}{\varphi(u_{0i}) q_1(\xi_{1i} | u_{0i}) q_2(\xi_{2i} | u_{0i}, \xi_{1i}) [1 - a_1(u_{0i}, \xi_{1i})]} \right\} \quad (24)$$

2. Accept or reject \mathbf{v} : apply Equation 15.

The algorithm allows for the second proposal PDF to depend not only on the current state of the chain but also on the rejected pre-candidate. It can be shown that the method satisfies the reversibility condition independent of the choices of the two proposal PDFs. The method will reduce the chain correlation, since fewer repeated pre-candidates will occur, however its benefit is limited to low-dimensional problems. For high-dimensional problems, the acceptance rate is high already for the first pre-candidate.

3.5 Simulation of conditional samples in \mathbf{U} -Space

In the first step of the M-H algorithm for subset simulation, one is sampling a candidate \mathbf{v} from the joint Gaussian PDF $\varphi_n(\cdot)$, conditional on the previous sample \mathbf{u}_0 . One is free to assume that \mathbf{v} and \mathbf{u}_0 are jointly Gaussian with correlation coefficient ρ . Hence, the PDF of \mathbf{v} will be the conditional normal distribution with mean value $\rho\mathbf{u}_0$ and covariance matrix $(1 - \rho^2)\mathbf{I}$, where \mathbf{I} is the unit diagonal matrix. It is possible to directly sample from this distribution, thus avoiding the generation of repeated candidates through rejection of pre-candidate states. This leads to the following updating scheme:

1. Generate a candidate $\mathbf{v} = (v_1, \dots, v_n)$. For each $i = 1, \dots, n$
 Generate v_i from the normal distribution with mean ρu_{0i} and standard deviation $\sqrt{1 - \rho^2}$
2. Accept or reject \mathbf{v} : apply Equation 15.

It is trivial to see that the transition PDF between \mathbf{u}_0 and \mathbf{u}_1 satisfies the reversibility condition. Since we eventually sample from the conditional normal distribution $\varphi_n(\cdot | F_{j-1})$, a small correlation between the actual and the candidate state does not imply a small correlation of the final samples. This is due to the fact that a very small ρ will lead to many rejected samples. On the other hand, a large ρ will increase the acceptance rate but will lead to a larger correlation of the resulting samples. Section 3.7 comments on the optimal choice of ρ .

Besides its simplicity, the advantage of this approach lies with the fact that the candidate state is always accepted, without compromising the stationary distribution of the chain. Figure 4 compares the coefficient of variation of the probability estimate obtained by the algorithms described in Sections 3.2-3.5 for the limit-state function of Equation 20 in terms of the number of random variables n . For the component-wise M-H and the M-H with repeated generation of pre-candidates, the proposal PDF is chosen as the uniform PDF with width 2. The same PDF is chosen for both proposal PDFs for the component-wise M-H with delayed rejection. For the conditional sampling method, the correlation was chosen as 0.8. It is shown that the methods have similar performance for $n > 10$, while the conditional sampling algorithm performs better than the other methods in low dimensional problems. However, it should be noted that the algorithms with lower acceptance rate of the pre-candidate have the advantage that fewer limit-state function evaluations are required.

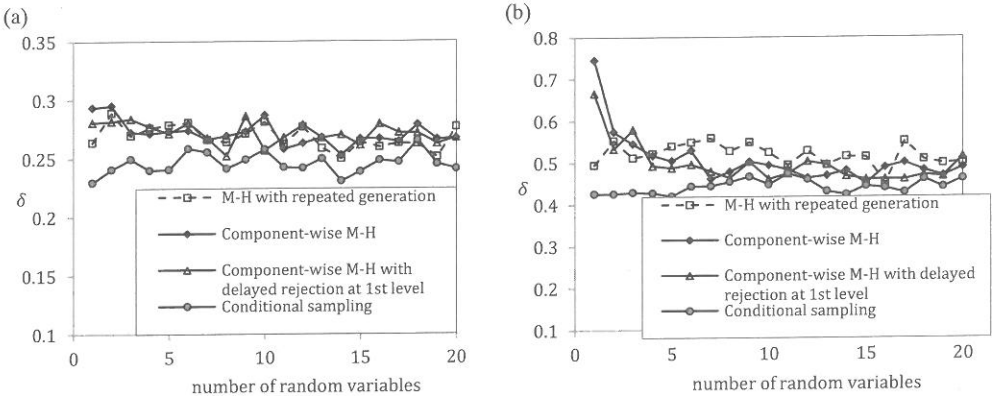


Figure 4: Coefficient of variation δ of the probability estimates evaluated from 500 independent subset simulation runs by the algorithms presented in Sections 3.2-3.5 at subset level (a) $j = 2$ and (b) $j = 4$.

3.6 Component-wise M-H with delayed rejection at the second acceptance level

The algorithms considered until now focus on the generation of the candidate state, i.e. they share the same second acceptance step. Therefore, they do not involve additional limit-state function evaluations. Zuev & Katafygiotis (2011) applied the delayed rejection concept at the second acceptance level, i.e. after the limit-state function has been evaluated to check whether the candidate state lies in F_{j-1} . If the candidate state is rejected, the accepted coordinates of the

pre-candidate state are re-sampled from a different one-dimensional proposal PDF and accepted or rejected with a suitably computed probability. The updating procedure reads:

1. Generate a candidate $\mathbf{v} = (v_1, \dots, v_n)$. For each $i = 1, \dots, n$
 - 1.a. Generate a pre-candidate ξ_{1i} from the PDF $q_1(\cdot | u_{0i})$
 - 1.b. Accept or reject ξ_{1i}

$$v_i = \begin{cases} \xi_{1i}, & \text{with prob. } a_1(u_{0i}, \xi_{1i}) \\ u_{0i}, & \text{with prob. } 1 - a_1(u_{0i}, \xi_{1i}) \end{cases} \quad (25)$$

where

$$a_1(u_{0i}, \xi_{1i}) = \min \left\{ 1, \frac{\varphi(\xi_{1i}) q_1(u_{0i} | \xi_{1i})}{\varphi(u_{0i}) q_1(\xi_{1i} | u_{0i})} \right\} \quad (26)$$

2. Accept or reject \mathbf{v} : apply Equation 15.
3. If \mathbf{v} was rejected. For each $i = 1, \dots, n$, if ξ_{1i} was accepted
 - 3.a. Generate a new pre-candidate ξ_{2i} from the PDF $q_2(\cdot | u_{0i}, \xi_{1i})$
 - 3.b. Accept or reject ξ_{2i}

$$v_i = \begin{cases} \xi_{2i}, & \text{with prob. } a_2(u_{0i}, \xi_{1i}, \xi_{2i}) \\ u_{0i}, & \text{with prob. } 1 - a_2(u_{0i}, \xi_{1i}, \xi_{2i}) \end{cases} \quad (27)$$

where

$$a_2(u_{0i}, \xi_{1i}, \xi_{2i}) = \min \left\{ 1, \frac{\varphi(\xi_{2i}) q_1(\xi_{1i} | \xi_{2i}) q_2(u_{0i} | \xi_{2i}, \xi_{1i}) a_1(\xi_{2i}, \xi_{1i})}{\varphi(u_{0i}) q_1(\xi_{1i} | u_{0i}) q_2(\xi_{2i} | u_{0i}, \xi_{1i}) a_1(u_{0i}, \xi_{1i})} \right\} \quad (28)$$

4. Accept or reject \mathbf{v} : apply Equation 15.

Zuev & Katafygiotis (2011) showed that the algorithm satisfies the reversibility condition. The method reduces the chain correlation, since the acceptance probability of the candidate state increases. Moreover, its efficiency is independent of the random dimension. However, the method requires additional limit-state function evaluations, as compared to all the previous approaches.

In Figure 5, the performance of the algorithm for the limit-state function of Equation 20 with $n = 100$ is compared to the one of the component-wise M-H. The proposal PDF is chosen as the uniform PDF with width of 2 for both levels. The conditional probability is chosen as $p_0 = 0.1$, while the number of samples N at each level for the component-wise M-H is chosen such that the two algorithms result in the same limit-state function evaluations, starting with $N = 500$ for the algorithm with delayed rejection. The coefficient of variation of the probability estimates is evaluated from 500 independent simulation runs. It is shown that the gain in efficiency is rather small, which agrees with the findings in (Zuev & Katafygiotis 2011). However, the authors show that a larger gain in efficiency might be achieved by choosing a different proposal PDF in the second level.

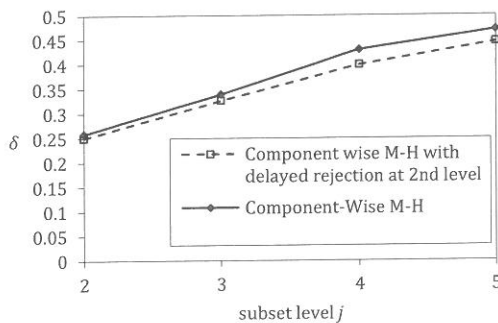


Figure 5: Coefficient of variation of the probability estimates by the component-wise M-H and the component wise M-H with delayed rejection at second acceptance level with the same LSF evaluations.

3.7 Adaptive MCMC with optimal scaling

It is shown above that the component-wise M-H and the conditional sampling method have similar performance in high dimensions. Also, it is discussed that the performance of the conditional sampling method depends on the choice of the correlation ρ between the actual and the candidate state. Similarly, the performance of the component-wise M-H depends on the variance of the proposal PDF. A large variance (resp. small ρ) will lead to many rejected candidates and a small variance (resp. large ρ) to a high correlation between states. Zuev et al. (2011) conjectured that an optimal variance of the proposal PDF at each subset level will give the minimum γ_j in Equation 11 and hence the minimum coefficient of variation of the conditional probability estimates. In their study, they varied the variance of the proposal PDF and evaluated γ_j and the second level acceptance rate of the algorithm. This led to the observation that γ_j is rather flat at the optimal acceptance rate, which lies in the interval $[0.3, 0.5]$.

Here, we perform a similar study by varying the variance of the proposal PDF of the component-wise M-H algorithm and the parameter ρ of the conditional sampling method. Moreover, we measure the performance of the methods in terms of the average velocity of the chains λ_j , defined in Equation 12. The curves obtained for the limit-state of Equation 20 at the subset levels $j = 2$ and $j = 4$ are shown in Figure 6. The results for the two algorithms agree with the ones in (Zuev et al. 2011). That is, the performance of the two algorithms can be optimized if the acceptance rate is kept between 0.3 and 0.5. This can be achieved by a scaling of the parameter of each algorithm after the simulation of each chain. If the acceptance rate of the chain is smaller than 0.3 then the variance of the proposal PDF is decreased (resp. the correlation parameter ρ is increased) and if it is larger than 0.5 the variance is increased (resp. ρ is decreased). Figure 7 shows the coefficient of variation of the probability estimates obtained from this adaptive procedure with the two considered algorithms for the limit-state function of Equation 20 with $n = 100$. The results are compared with the original version of the algorithms with a uniform proposal PDF with width 2 for the component-wise M-H algorithm and a correlation parameter $\rho = 0.9$ for the conditional sampling method. It is shown that the adaptive approaches give a smaller coefficient of variation at all subset levels.

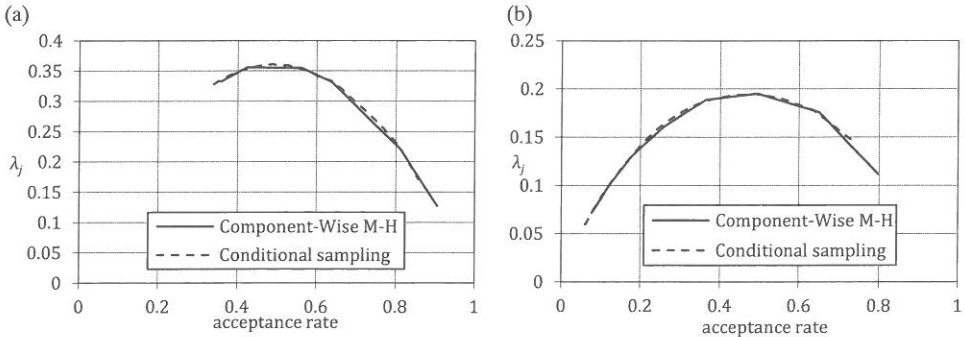


Figure 6: Chain velocity in terms of the second level acceptance rate for the component-wise M-H and the conditional sampling method at subset level (a) $j = 2$ and (b) $j = 4$.

4 CONCLUSION

This paper reviewed existing MCMC methods for subset simulation and proposed a new method that is based on sampling from a conditional normal distribution. The new approach is simpler and performs better than the other methods in low dimensional problems, since it accepts all candidate states of the Markov chain, without compromising the target distribution of the chain. In high-dimensional problems, the new method, together with all other algorithms that increase the first level acceptance rate, has a similar performance as the component-wise M-H algorithm, which was originally proposed for subset simulation. The component-wise M-H with delayed rejection at the second acceptance level provides better estimates at the expense of addi-

tional limit-state function evaluations. Finally, an adaptive procedure that adjusts the parameter of either the component-wise M-H or the conditional sampling method based on the chain acceptance rate provides better estimates without the need for further limit-state function evaluations.

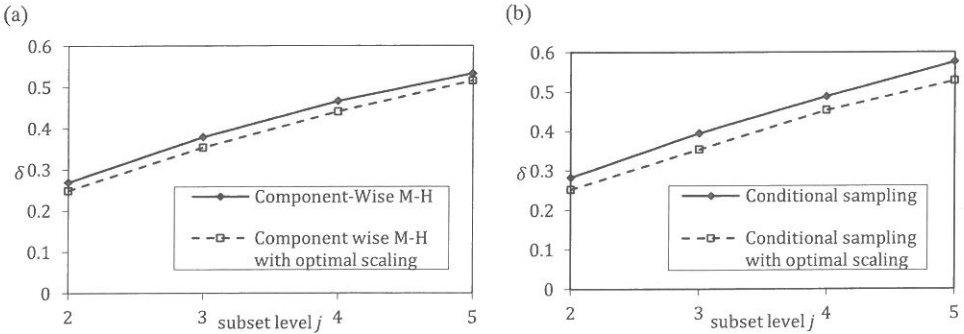


Figure 7: Coefficient of variation of the probability estimates by the (a) component-wise M-H and the (b) conditional sampling method and their optimal scaling variants.

REFERENCES

- Au, S.K. & Beck, J.L. 2001. Estimation of small failure probabilities in high dimensions by subset simulation. *Probabilistic Engineering Mechanics*, 16(4): 263-277.
- Bucher, C. 2009. Asymptotic sampling for high-dimensional reliability analysis. *Probabilistic Engineering Mechanics*, 24: 504-510.
- Der Kiureghian, A. & Liu, P.-L. 1986. Structural reliability under incomplete probability information. *Journal of Engineering Mechanics*, 112(1): 85-104.
- Hastings, W.K. 1970. Monte Carlo sampling methods using Markov chains and their applications. *Biometrika*, 57(1): 97-109.
- Hohenbichler, M. & Rackwitz, R. 1981. Non-normal dependent vectors in structural safety. *Journal of Engineering Mechanics*, 107: 1227-1238.
- Katafygiotis, L.S. & Cheung S.H. 2007. Application of the spherical subset simulation method and auxiliary domain method on a benchmark reliability study. *Structural Safety*, 29: 194-207.
- Metropolis, N., Rosenbluth, A.W., Rosenbluth, M.N., Teller, A.H. & Teller, E. 1953. Equation of state calculations by fast computing machines. *Journal of Chemical Physics*, 21(6): 1087-1092.
- Miao, F. & Ghosn M. 2011. Modified subset simulation method for reliability analysis of structural systems. *Structural Safety*, 33: 251-260.
- Rubinstein, R.Y. & Kroese, D.P. 2007. *Simulation and the Monte Carlo Method*, 2nd ed., Hoboken, John Wiley & Sons.
- Santoso, A.M., Phoon, K.K. & Quek, S.T. 2011. Modified Metropolis-Hastings algorithm with reduced chain correlation for efficient subset simulation. *Probabilistic Engineering Mechanics*, 26: 331-341.
- Tierney, L., & Mira, A. 1999. Some adaptive Monte Carlo methods for Bayesian inference. *Statistics in Medicine*, 18: 2507-2515.
- Zuev, K.M., Beck, J.L. & Katafygiotis, L.S. 2011. On the optimal scaling of the modified Metropolis-Hastings algorithm. *Proceedings, 11th International Conference on Applications of Statistics and Probability in Civil Engineering, ICASP 11*, Faber, Köhler & Nishijima (eds), Zurich, Switzerland.
- Zuev, K.M. & Katafygiotis, L.S. 2011. Modified Metropolis-Hastings algorithm with delayed rejection. *Probabilistic Engineering Mechanics*, 26: 405-412.

Identification and reliability of reinforced concrete structural systems for model updating purposes

S. Sessa,
Politecnico di Milano, Italy

F. Marmo
Universita' di Napoli "Federico II", Italy

N. Valoroso
Universita' di Napoli "Parthenope", Italy

ABSTRACT: A new strategy for in-situ testing of reinforced concrete structures is presented. Its ultimate goal is to provide real-time information about the structural behavior during the test. Statistical results of structural tests are employed in order to get general information about model statistics so that parameters uncertainties will be represented by a set of mutually consistent probability distributions. The proposed procedure relies upon a probabilistic formulation and takes advantage of the Bayesian Network theory to account for structural and design uncertainties.

1 INTRODUCTION

The structural characterization of existing buildings cannot neglect an accurate experimental test schedule in order to get statistical information about geometrical and constitutive features. Many reliable techniques of identification and updating are able to properly define a structural model, however, their employment in common practice usually deals with procedural drawbacks. This work aims to summarize an identification procedure which will be employed in a large structural test campaign in southern Italy focused on the characterization of more than 50 school buildings and on the evaluation of their structural reliability. It is important to emphasize that the structural problem is strictly interconnected with bureaucratic issues so that the test choice and scheduling must consider several commitments. The structures to be identified have been built between '70 and '80; thus original plans and material tests are not available and the buildings have never been validated; moreover neither building code nor seismic rules were enforced at the construction time-. Moreover, the public purchaser and current rules also fix some requirements about the test campaign: i) it has to be as cheap as possible; ii) it should mainly consist in "traditional" tests (static load tests among all); iii) it has to ensure the complete structural functionality while the tests are carried out. In this sense, the proposed strategy aims to be a fair compromise between usual technical practice and law requirements.

The employment of Bayesian Networks is very profitable in order to relate different kinds of structural tests and to properly consider the knowledge confidence. An effective idealization of the structural model consists in defining a domain containing geometrical and mechanical properties, a set of external loads and a set of responses. Each parameter should be characterized in a probabilistic way through *a priori* probability distributions; note that some of the parameter distributions will try to describe design choices based on historical common practice. Then, a non-linear finite element analysis is run in order to simulate the tests and to get the structural responses probability distributions. It is well known how the Bayesian Network links *parental* random variables (i.e. the model parameters) with *child* ones (i.e. the structural responses). Thus, while the tests are carried out, Bayesian inference updates the structural model probabilistic description using the structural responses as evidences.

This leads to interesting results. The updating of structural parameters provides a probabilistic model whose distributions take into account for the real knowledge provided by the experi-

mental data. In this sense, the procedure is more accurate than the ones suggested by European and Italian codes. Furthermore, while the Bayesian Network will pay a great computational demand before the test execution, it also provides results in real time during the test. This is a very important feature since structural safety could be compromised by high test loads; the Bayesian Network is able to highlight potential induced disorders before that the structure will be fatally damaged.

More considerations about the strategy will be made in the closure section of this work. Beforehand, the structural model description is explained in chapter 2; thereafter, chapter 3 gives a brief description of the employed algorithm for non-linear analysis. Then, chapter 4 summarizes the Bayesian Network definitions for two structural applications whose results are also provided and commented.

2 STRUCTURAL MODEL RANDOMNESS

As written before, a simple though effective idealization of a structure consists in defining a domain containing geometrical and mechanical properties, a set of external loads and a set of responses. Accordingly to the Bayesian Network theory, each parameter is defined by a marginal or conditional probability density function (PDF); while the parent distributions are defined by random models, the mutual relationship between parents and children is get by a Monte Carlo simulation laying on a non-linear FEM analysis. Several models are available for constitutive and geometrical properties so that their selection depends on the required accuracy and the available information. So far, a limited set of parameters has been chosen. The most obvious parameters are the steel and concrete yield stresses and stiffness, whereas the parameter that is expected to have high influence is the reinforcement bars quantity. A Gaussian noise with 5% c.o.v. has been included in order to consider the discrepancy between measurements and numerical prediction. In order to test the procedure effectiveness, no more geometrical randomness is considered since those parameters provide a sufficiently accurate description.

2.1 Concrete parameters

The concrete constitutive model has been defined by the ultimate strength accordingly to Kent and Park (1971). Its probabilistic definition is based on a statistic study about Italian buildings, Cristofaro (2009), where a wide test campaign is presented. The tested buildings have been split in four classes depending on the building age. Each class provides the mean and the standard deviation of a normally distributed variable which defines the concrete yield stress of a standard concrete specimen.

Table 1. Concrete yield stress parameters.

Building year	mean MPa	coefficient of variation
'50	11.2	32%
'60	15.3	40%
'70	19.7	51%
'80	24.1	28%

The reason of this choice is to avoid the dependence of usual probabilistic models on the concrete class, since it is usually unknown. On the contrary, the ratio F_2 between the specimen and structural strength has been defined as a normal variable with mean 1.06 and c.o.v. 14%, accordingly to Melchers (2001).

2.2 Steel parameters

While the concrete class is usually concealed, the reinforcement bars specifications are usually available through waybills. This makes possible to employ the definition provided by Melchers (2001) where the steel Young modulus is assumed to be lognormal with mean 201GPa and c.o.v. 3.3% and the yield stress is beta distributed with parameters summarized in Table 2 and

PDF defined in Equation 1. The steel constitutive model is assumed to be an ideal elasto-plastic uniaxial relationship without hardening.

$$f_{F_y}(F_y) = A \left(\frac{F_y - a}{c} \right)^B \cdot \left(\frac{b - F_y}{c} \right)^C \quad (1)$$

Table 2. Concrete yield stress parameters.

Class	mean	cov	A	B	C	a	b	c
	MPa							
300	310	35%	4.106	2.21	3.82	228	428	200
410	461	38%	7.587	2.02	6.95	372	703	331

At element level, the geometry of reinforcement bars is described in a conventional way. First, the element’s cross-section is assumed to be approximately rectangular. Then, the reinforcement bars are described by areal percentages rather than by diameters and position. This latter is defined as the ratio between the area of bars belonging to the same section side and the total cross-section area. The percentage should be defined for the top, the bottom and the lateral side of the section. This convention is undoubtedly approximate, but it permits a statistical analysis of reinforcement geometries by a reasonably limited number of parameters.

This is due the fact that no structural plans are available and also there were no rules enforced about structural and seismic analysis when the structures of interest were built. Structural models, load hypothesis and safety criteria were up to the experience and the “design style” of structural analyzer. Thus, any simulated design could be grossly inaccurate if it does not even try to guess “design habits and standards” usually employed in common practice.

The percentage convention is directed to make a catalogue and a statistical analysis of a large enough set of available structural plans. Specifically, each plan provides global information such as the ones shown in Figure 1(a). Also, each element is characterized by geometrical parameters: length and type (beam or column), cross-section height and width, story, reinforcement percentages and spans, see Figure 1(b).

REINFORCEMENT BARS DETECTION FORM										
Building	SA 01_445		PGA	0.15		n. deck	2			
Latitude	40.682208		Wind zone	C		h deck	3			
Longitude	14.769925									
Mean deck area	550	m ²	Steel type	FeB44k		Build. Year	1978			
First deck height	4	m	Load type	House						
Element	Type	L	h	b	% top	% bott.	% side	Story	Span	h-span
		[m]	[m]	[m]					[m]	[m]
1	col	4.00	0.60	0.40	3.50%	3.50%	2.10%	2	2.25	2.70
4	bea	5.50	0.60	0.40	3.20%	3.50%	0.00%	2	2.70	

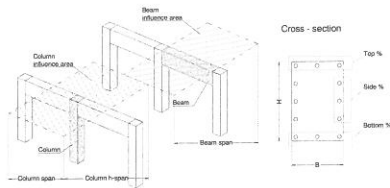


Figure 1: (a) Structure geometrical information; (b) Elements’ geometrical characterization

A statistical analysis of the collected data, based on analogous parameters, provides probability distributions of reinforcements’ percentages for the identifying structure. These PDFs constitute the basic knowledge of the probabilistic model; far away to be exhaustive, they provide a widespread trend about the expected design in order to perform a consistent updating. A rough data-fitting provides generalized extreme value distributions employed afterwards in the numerical examples. It must be emphasized that designers are prone to cluster congruent cross sections in a few typologies; the reinforcements’ design is then ruled by the most stressed section so that the steel bars configuration is the same for the entire cluster. On the basis of this assumption, the extreme value distribution makes sense. The bars configuration comes out from the most conservative design among a set referred to the same cross section subjected to several different loads.

3 STRUCTURAL ANALYSIS: FIBER-FREE INTEGRATION

After that the parameter distributions have been defined, it is necessary to get the conditional probability distributions of the structural response. This duty has been carried out by a Monte Carlo simulation and a non linear finite element analysis. Both procedures do not require any deeper elucidation since ordinary algorithm have been employed. However, an essential description is required for the integration algorithm at element level.

In order to speed up the structural analysis, a fiber-free algorithm (Marmo and Rosati, 2008) has been employed in carrying out the integration of the RC constitutive relationship and for the evaluation of the stiffness matrix of frame cross sections owing to its superior performances with respect to the fiber integration (Zupan and Saje, 2005).

The geometry of the frame sections is defined by one or more polygonal domains; cross sections are assumed to obey the Euler-Bernoulli hypothesis whereby the axial strain at a generic point $\mathbf{r} = [x \ y]^T$ of the section can be evaluated as $\varepsilon = \varepsilon + \mathbf{g} \cdot \mathbf{r}$, i.e. as sum of the strain at the origin of the coordinate system (ε) the curvature (\mathbf{g}) and coordinate vectors (\mathbf{r}). The material constitution in the direction of the beam axis associated with each polygonal domain is described by means of a uniaxial inelastic stress-strain relationship. The normal stress at point \mathbf{r} is expressed as a function of the strain current value X and of the maximum compressive strain X ever reached at \mathbf{r} . Such assumption is common to most of the stress-strain laws for concrete, and it can be expressed symbolically as:

$$\sigma(\varepsilon, \varepsilon_m) = \begin{cases} 0 & \text{if } \varepsilon \leq \varepsilon_p \\ \frac{\sigma_e(\varepsilon_m)(\varepsilon - \varepsilon_p(\varepsilon_m))}{\varepsilon_m - \varepsilon_p(\varepsilon_m)} & \text{if } \varepsilon_p \leq \varepsilon \leq \varepsilon_m \\ \sigma_e(\varepsilon_m) & \text{if } \varepsilon \geq \varepsilon_m \end{cases} \quad (2)$$

The function σ_e is the envelope curve while ε_p is the residual strain which is generally expressed solely as a function of the maximum compressive strain. The characteristic vectors of the normal stress distribution over the beam cross section are the axial force and the bending moments:

$$N = \int_{\Omega} \sigma(\varepsilon, \varepsilon_m) d\Omega; \quad \mathbf{M}^{\perp} = [-M_y \ M_x]^T = \int_{\Omega} \sigma(\varepsilon, \varepsilon_m) \mathbf{r} d\Omega \quad (3)$$

Equation (2) shows how different expressions of the stress have to be considered over the cross section; this naturally suggests to split it into partitions Ω_i characterized by values of ε_m so that both the current and the maximum compressive strain are expressed by means of a single equation of the kind of Equation (2). A suitable manipulation of the constitutive function and the continuous updating of the partitions lead to the integration of stress resultants section stiffness matrix. Specifically, this latter can be expressed only in terms of integrals at the partitions vertices. It is important to emphasize that the integrals in Equation 3 can be evaluated in closed form as long as the employed constitutive laws are furnished with their primitives. It provides the exact solution for the Euler-Bernoulli beam ensuring a high computational speed.

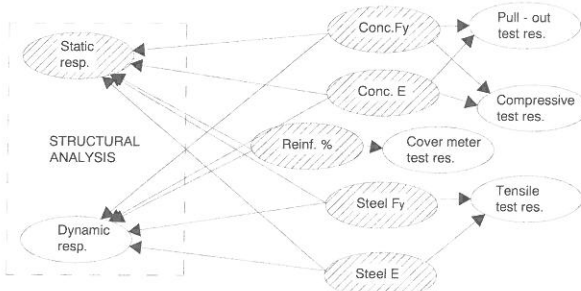


Figure 2: General-purpose Bayesian Network

4 THE BAYESIAN NETWORKS

The reason of the Bayesian Network employment relies in its skill to relate several random variables of different natures. A general-purpose Bayesian scheme is provided in Figure 2; it aims to link together all the possible data get by tests. In this sense, each experimental result properly contributes to the general knowledge of the structure. This work focuses on the highlighted nodes since a general purpose test campaign is in progress and a first updating will provide information about the static load test effectiveness; furthermore, it is possible to choose further tests on the base of the updated knowledge.

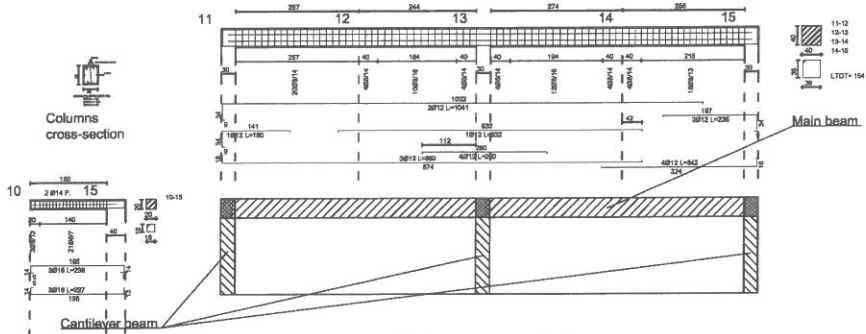


Figure 3: Shelter structural plan

Two different structures have been analyzed. The first one is a just built reinforced concrete shelter consisting of a plane shell deck supported by three cantilever beams wedged to a single-floor three columns frame. The structural plan is shown in Figure 3. The shelter has been tested by loading the deck using an inflatable water tank set on the deck floor, whose load area is shown in Figure 4(a). Static load has been linearly increased to the maximum design load (i.e. 4000 N/m^2) and vertical displacements at selected locations ($U_1 \dots U_5$ shown in Figure 4(a)) have been recorded by dial gauges.

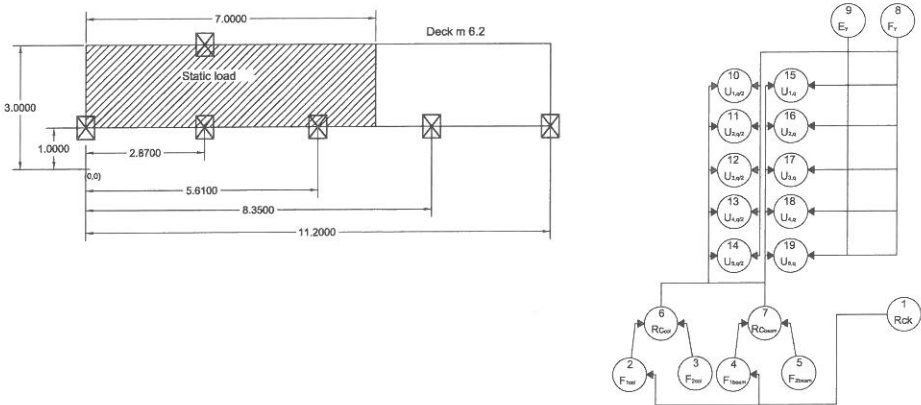


Figure 4: (a) Shelter load scheme; (b) Bayesian Network

The mechanical parameters have been conveniently defined on the basis of the previously shown *a priori* distributions. Mechanical parameters of steel and concrete should be defined as random field since their values are usually heterogeneous. However, it seems reasonable that concrete uncertainties are negligible over each single casting. In this sense, the construction sequence defines individual groups of structural elements where the mechanical parameters are likely to be constant. In this case, the first casted region includes the columns only whereby the

second one includes the beams and the shells. Similarly, the steel properties are assumed to be constant for the bars coming from the same batch. Because the steel reinforcement geometry is fixed, the purpose is to update the probability distributions of material parameters. The employed network is schematized in Figure 4(b).

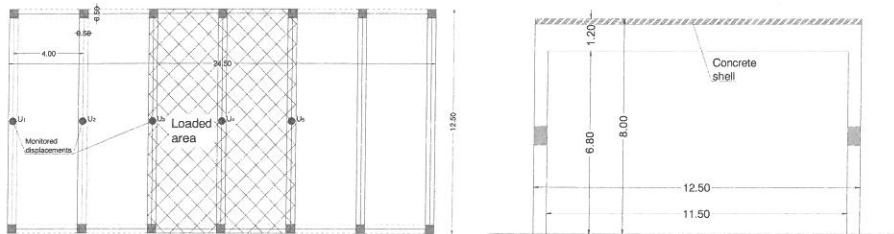


Figure 5: Shed structural plan (dimensions in meters)

The second monitored structure is a one story reinforced concrete shed whose plans are shown in figure 5. It is made by seven symmetric frames, each one made by a high beam wedged to two columns. The top deck is made by a reinforced concrete shell. Static load has been applied on the highlighted area up to 5000 N/m^2 . The test purpose, this time, is to identify the reinforcement percentages since no plans are available. It is still possible to make some hypothesis about the reinforcement geometry. Because of the structural scheme, it looks believable that the columns are symmetrically reinforced with the same bars geometry. For this reason, two random variables are employed in order to define the beam and the column reinforcement percentages and five random variables are required for the material properties, i.e. strengths and stiffness of concrete and steel, and the structure-specimen concrete strength ratio F_2 .

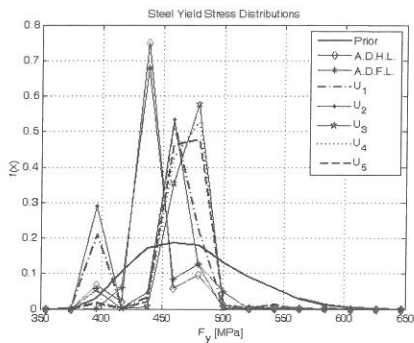
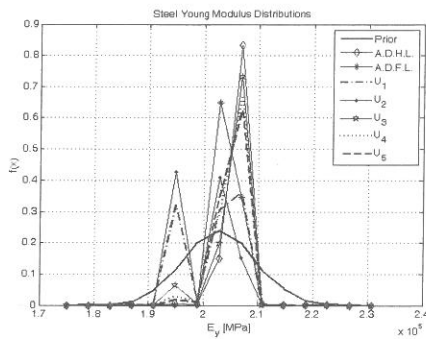


Figure 6: (a) Shelter steel yield stress PDFs;



(b) Shelter steel stiffness PDFs

In order to get the *a posteriori* probability distributions of the random variables of interest, the recorded displacements have been set as evidences of the network. The network is updated as the test goes along and the displacements are recorded. Shelter steel and concrete parameter distributions are presented respectively in figure 6 and 7. Specifically, the figures show the posterior distributions corresponding to: i) all the displacement records at half load (A.D.H.L. curves), ii) all the displacement records at full load (A.D.F.L. curves), iii) only the *i*-th dis-

placement at full load set as evidences (U_i curves). This last case can be useful if we cannot evaluate the accuracy of the record procedure.

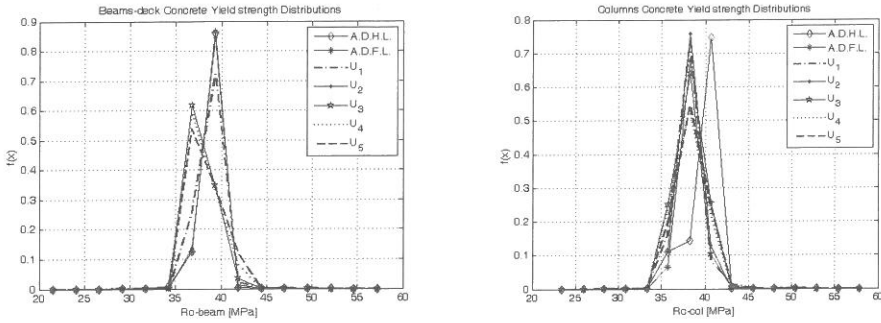


Figure 7: (a) Shelter beam concrete strength;

(b) Shelter column concrete strength PDFs

A first consideration can be drawn for the steel parameters (Figure 6): the updated strength distribution seems to be independent by the load value while the elastic modulus' one looks more sensitive. This makes sense since column steel always remains in the linear range while the deck reinforcements attain the yield stress even at half load because of the small thickness. In case of single displacement set, distributions appear to be bi-modal, in particular for U_1 or U_2 : this suggests a possible anomalous measurement of the structural response. This consideration is consistent with the test history because the U_1 and U_2 dial gauges went several times from the shadow to the sunlight before the test was ended.

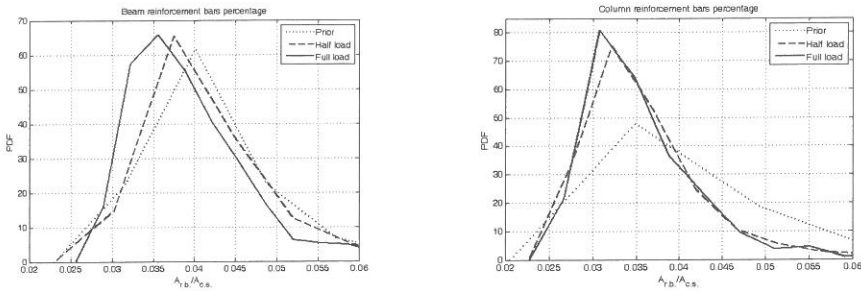


Figure 8: (a) Shed beam reinforcement percentage;

(b) Shed column reinforcement percentage PDFs

Even more interesting are the posterior distributions of column concrete limit stress (Figure 7). In this case, the ADHL distribution differs from the other ones. In this case, the concrete limit stress affects the nonlinear behavior of the frames which does not occur for small loads. The beam concrete distribution, on the other hand, is affected by geometrical variability. Displacements U_3 , U_4 and U_5 seem to be inaccurate. This is due the spatial position of the dial gauges: because the deck and the cantilever beams are quite thin, the farther the dial is from the loaded area, the less the displacement will be sensitive to the loads and the mechanical parameters.

The Shed structure provides information of both material parameters and reinforcement percentage. Figure 8 shows beam and column updated distributions. The mode looks to translate while the test is carried out trending to 3%. Even if the difference between the modes looks to be negligible, note that a 0.5% of difference corresponds to almost four 20mm bars. In this sense, this updating provides useful information in order to guess the reinforcement geometry.

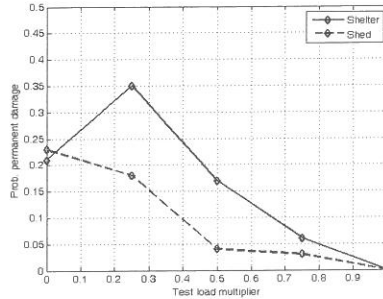


Figure 9: Probability of permanent damage

Even more interesting is the evolution of the permanent damage probability which is shown in Figure 9. Before the test was started, a safety threshold had been set. Its purpose is to avoid permanent damages in the structure due to the static load test. The Shelter structure presents a peak at $\frac{1}{4}$ of the maximum load applied. This can be due to the initial sliding between steel bars and the concrete core. In this case, the recorded displacements at the beginning of the test results higher than the simulated ones which, on the contrary, increase smoothly. The Shed does not show the same behavior. The reason could be related to the greater dimensions and to the fact that its deck has been subjected to high loads so that the steel bars already toothed the concrete.

5 CONCLUSIONS AND FURTHER WORK

A strategy for the probabilistic characterization of reinforced concrete structures during experimental tests is presented. Focusing on the employment of static load tests, the procedure provides probability distributions of mechanical and geometrical parameters, trying to overcome the lack of knowledge about the specific structural design. Not less important, the fact that a probabilistic formulations properly considers the contribution of each single test to the global knowledge. The particular formulation is specific for in-field applications so that preliminary results can be obtained while the test is carried out. This makes possible to make changes to the test schedule and, above all, to get a preliminary evaluation of the structural reliability so that damage induced by the load test can be avoided. Research developments can be oriented to the interaction in a larger Bayesian network with other kinds of structural tests and to properly consider the presence of non-structural elements.

REFERENCES

- Cristofaro M.T., 2009. Metodi di valutazione della resistenza a compressione del calcestruzzo di strutture in c.a. esistenti, *PhD dissertation, University of Florence*.
- Kent D.C., Park R., 1971. Flexural members with confined concrete, *Journal of the Structural Division, ASCE*, 97(ST7): 1969-1990.
- Marmo F., 2008. A fiber-free approach to the inelastic analysis of reinforced concrete structures, *PhD dissertation, University of Naples "Federico II"*.
- Melchers R.E., 2001. *Structural Reliability Analysis and Prediction*, West Sussex, Wiley.

Reliability analysis for adhesive bonded composite stepped lap joints loaded in fatigue

A. Kimiaefar, J. D. Sørensen, E. Lund, O. T. Thomsen

Aalborg University, Aalborg East, Denmark.

ABSTRACT: This paper describes a probabilistic approach to calculate the reliability of adhesive bonded composite stepped lap joints loaded in fatigue using three-dimensional finite element analysis (FEA). A method for progressive damage modelling is used to assess fatigue damage accumulation and residual strength under fully reversed cyclic loading based on stiffness/strength degradation. The FEA simulations are conducted using the commercial FEA code ANSYS 12.1. A design equation for fatigue failure of wind turbine blades is chosen based on recommendations given in the wind turbine standard IEC 61400-1, where partial safety factors are introduced together with characteristic values. Asymptotic sampling is used to estimate the reliability with support points generated by randomized Sobol sequences. The predicted reliability level is compared with the implicitly required target reliability level defined by the wind turbine standard IEC 61400-1. Finally, an approach for the assessment of the reliability of adhesive bonded composite stepped lap joints loaded in fatigue is presented. The introduced methodology can be applied in the same way to calculate the reliability level of wind turbine blade components loaded in fatigue.

1 INTRODUCTION

Adhesive bonded joints are being extensively and increasingly used for a large variety of applications in the automotive, aerospace, civil engineering, marine and wind turbine industries to mention a few [1]. Adhesive bonded joints are gaining preference over mechanical fastening techniques because of their almost negligible weight penalty [2]. In the design of stepped lap adhesive joints, scattering and physical as well as subjective uncertainties including neglect, mistakes, incorrect modelling and manufacturing errors must be considered when designing for materials, stacking sequence, dimensions, etc.

There is a lack of reliable methodologies for assessing the fatigue life and residual strength of composite structures. To predict residual strength/stiffness degradation of a composite laminate, a number of models have been suggested [3, 4]. So far, fundamental damage mechanisms that occur in composites during fatigue, such as matrix cracking, delamination, fiber failure, etc., have not been completely taken into account. Several researchers have studied the reliability assessment of wind turbine blades in the fatigue limit state using a linear SN-curve in combination with fatigue life diagrams accounting for the mean load effects [5] and uncertainties related to the fatigue loading [6]. To perform a detailed reliability analysis of the blade and its components such as adhesive joints and various substructures, three-dimensional finite element modelling is necessary.

In the present article, the method of progressive damage modelling [3] is used to assess the reliability level of stepped lap composite joint loaded in fatigue under T-C fatigue ($R = -1$). A set of seven 3-D polynomial stress-based failure criteria is used to detect seven failure modes. Specifically, for detecting matrix tensile and compressive cracking, fiber compressive failure

and fiber-matrix shear-out, a set of 3-D Hashin-type failure criteria are used. The FEA simulations are conducted using the commercial FEA code ANSYS 12.1. A design equation for fatigue failure of wind turbine blades exposed to out of plane bending moments is chosen, where partial safety factors are introduced together with characteristic values. Asymptotic sampling is used to estimate the reliability with support points generated by randomized Sobol sequences.

2 STEPPED LAP COMPOSITE JOINT

Fig. 1 shows a generic model of the stepped lap composite joint, which is considered in this study. The considered stepped lap joint includes only two steps, representative for typical joint configurations used for e.g. wind turbine blade main laminates with respect to geometry, joint overlap steps, adhesive layer thicknesses and material composition. The constituent materials assumed are epoxy adhesive, Fibredux-HTA/6376 plies/layers as shown in Tables 1 and 2 based on [3, 7]. Table 3 shows a stochastic model for the geometrical properties. The loading condition imposed is a prescribed horizontal displacement applied at the right side (the loading is further described in section 4), and a simple support boundary condition is imposed for the left side of the joint.

Table 1. Stochastic variables for the epoxy adhesive [3, 7].

Parameter	Mean	COV	Distribution	Characteristic value
Young's modulus, E_A (GPa)	2.21	10.0%	Lognormal	2.21
Poisson's ratio, ν_A	0.3	18.0%	Lognormal	0.3
Tensile strength, S_A (MPa)	80	10.6%	Weibull	37 (5% quantile)

Table 2. Stochastic variables: Elastic coefficients and strengths for graphite/epoxy[3, 7].

Parameter	Mean	COV	Distribution	Characteristic value(quantile)
E_1 (GPa)	39	10.6%	Lognormal	39
E_2 (GPa)	14.5	13.6%	Lognormal	14.5
E_3 (GPa)	9.8	13.6%	Lognormal	9.8
ν_{12}	0.29	18.0%	Lognormal	0.29
ν_{13}	0.07	18.0%	Lognormal	0.07
ν_{23}	0.29	18.0%	Lognormal	0.29
G_{12} (GPa)	4.2	10.7%	Lognormal	4.2
G_{13} (GPa)	4.2	10.7%	Lognormal	4.2
G_{23} (GPa)	2.7	10.7%	Lognormal	2.7
S_{11T} (MPa)	779	13.8%	Normal	602 (5%)
S_{22T} (MPa)	54	10.4%	Weibull	44 (5%)
S_{33T} (MPa)	54	10.4%	Weibull	44 (5%)
S_{11C} (MPa)	526	14.3%	Normal	402 (5%)
S_{22C} (MPa)	165	11.2%	Weibull	131 (5%)
S_{33C} (MPa)	165	11.2%	Weibull	131 (5%)
t_{12} (MPa)	56	10.6%	Weibull	45 (5%)
t_{13} (MPa)	56	10.6%	Weibull	45 (5%)
t_{23} (MPa)	56	10.6%	Weibull	45 (5%)

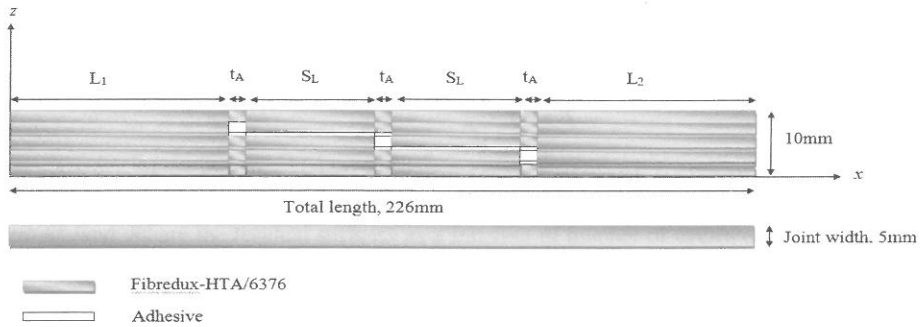


Fig. 1. Geometry of adhesive stepped lap joint, the thickness of the adhesive is exaggerated for illustration purposes.

Fig. 2 shows the FEA model and the adopted meshing. A macro is used to generate a parametric model. All the above geometry parameters are obtained based on realisations of the stochastic variables in Table 1. The commercial FE code ANSYS version 12.1 has been used for all the FE calculations. Solid shell elements (SOLSH190) are used for the composite part, and solid elements with Enhanced Assumed Strain formulation (SOLID185) are used for the adhesive layers with three displacement DOFs per node.

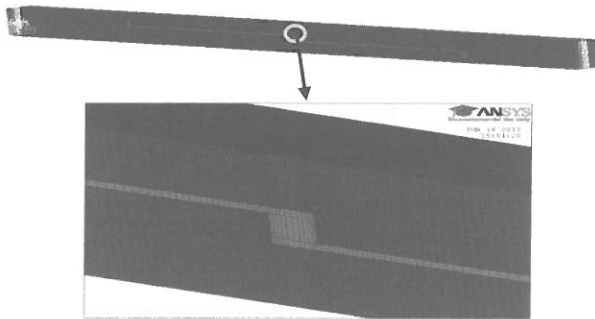


Fig. 2. Element distribution of the joint.

Table 3. Stochastic variables for the stepped lap joint geometry.

Parameter	Mean	COV	Distribution	Characteristic value
Lamina thickness, t_l (mm)	0.125	10%	Normal	0.125
Joint width (mm)	5.00	10%	Normal	5.00
Adhesive thickness, t_a (mm)	0.125	10%	Normal	0.125
Adhesive bondline length, t_A (mm)	2.00	10%	Normal	2.00
Step length, S_L (mm)	40.0	10%	Normal	40.0
Initial length, L_I (mm)	70.0	10%	Normal	70.0
Lateral length L_2 (mm)	70.0	10%	Normal	70.0
Fibre angles	-	10%	Normal	-

3 ASYMPTOTIC SAMPLING

The basic idea of the Asymptotic Sampling technique proposed by Bucher [8] is to utilize the asymptotic behaviour of the reliability index β and the probability of failure in Gaussian space as the standard deviation of the variables and therefore the failure probability approaches zero [19].

$$\beta = Af + \frac{B}{f} \quad (1)$$

The parameters A and B are determined by curve fitting based on reliability indices β determined using an appropriate number of supporting points, f .

4 FATIGUE FAILURE ANALYSIS

A set of seven 3-D polynomial stress-based failure criteria is used to detect seven failure modes. Specifically, for detecting matrix tensile and compressive cracking, fiber compressive failure and fiber-matrix shear-out, a set of 3-D Hashin-type, Max-Stress criterion for fiber failure, and for delamination (equations 7 and 8) the Ye-delamination criterion is used as shown in Table 4. It should be noted that the condition in equation (6) is always dominant and will be fulfilled before equation (5) except for the case of zero shear stress when the two conditions will result in identical failure load estimates.

Table 4. Fatigue failure criteria

Failure mode	Failure Criterion	
Matrix tensile cracking, for $\sigma_{yy} > 0$	$\left(\frac{\sigma_{yy}}{Y_T^F}\right)^2 + \left(\frac{\sigma_{xy}}{S_{xy}^F}\right)^2 + \left(\frac{\sigma_{zy}}{S_{zy}^F}\right)^2 \geq 1$	(2)
Matrix compressive cracking, for $\sigma_{yy} < 0$	$\left(\frac{\sigma_{yy}}{Y_C^F}\right)^2 + \left(\frac{\sigma_{xy}}{S_{xy}^F}\right)^2 + \left(\frac{\sigma_{zy}}{S_{zy}^F}\right)^2 \geq 1$	(3)
Fiber tensile failure $\sigma_{xx} > 0$	$\left(\frac{\sigma_{xx}}{X_T^F}\right) \geq 1$	(4)
Fiber compressive failure $\sigma_{xx} < 0$	$\left(\frac{\sigma_{xx}}{X_C^F}\right) \geq 1$	(5)
Fiber-matrix shear out, for $\sigma_{xx} < 0$	$\left(\frac{\sigma_{xx}}{X_C^F}\right)^2 + \left(\frac{\sigma_{xy}}{S_{xy}^F}\right)^2 + \left(\frac{\sigma_{zy}}{S_{zy}^F}\right)^2 \geq 1$	(6)
Delamination in tension $\sigma_{zz} > 0$	$\left(\frac{\sigma_{zz}}{Z_T^F}\right)^2 + \left(\frac{\sigma_{xy}}{S_{xy}^F}\right)^2 + \left(\frac{\sigma_{zy}}{S_{zy}^F}\right)^2 \geq 1$	(7)
Delamination in compression $\sigma_{zz} < 0$	$\left(\frac{\sigma_{zz}}{Z_C^F}\right)^2 + \left(\frac{\sigma_{xy}}{S_{xy}^F}\right)^2 + \left(\frac{\sigma_{zy}}{S_{zy}^F}\right)^2 \geq 1$	(8)

5 GRADUAL MATERIAL PROPERTY DEGRADATION ON ALL PLIES

Gradual degradation of the composite material is due to cyclic loading and it is applied on the basis of material stiffness and strength [3]. A linear equation was proposed [4] for modelling the stiffness degradation for each stress level as follows:

$$E_{ij}^F(n) = \left[G \frac{n}{N_{fij}} + 1 \right] E_{ij}^S$$

Here E_{ij}^F and E_{ij}^S are the residual stiffness as a function of number of cycles and the static stiffness, respectively, n is the number of cycles, N_{fij} is the number of cycles to failure, and G is an experimental fitting parameter.

The general form of the polynomials in terms of normalized residual strength and normalized number of cycles (n/N_f) is [4]:

$$T_{ij}^F(n) = \left[B \left(\frac{n}{N_{fij}} \right)^2 + C \left(\frac{n}{N_{fij}} \right) + 1 \right] T_{ij}^S$$

where T_{ij}^F and T_{ij}^S are the residual and static strengths, respectively; and B , C experimental fitting parameters. It should be noted that, adhesive properties remain constants during calculations. Moreover, the model uncertainties can be estimated on basis of test results and corresponding model predictions with deterministic realizations of the stochastic variables in the model according to the test plan using a procedure as described in e.g. Eurocode EN 1990 [10]. Due to lack of available test results, it is not possible to estimate the model uncertainty in this paper.

6 SUDDEN DEGRADATION

The failure approach is based on element failure. When failure is predicted in a composite layer by the failure criteria indicated in part 4, its elastic properties and strengths are degraded by implementing an appropriate sudden degradation rule [3].

Table 5. Sudden material properties degradation rules [3].

Failure mode	Failure Criterion	
Matrix tensile cracking	$E_{yy}^d = 0.2 * E_{yy}, E_{xy}^d = 0.2 * E_{xy}, E_{yz}^d = 0.2 * E_{yz}$	(9)
Matrix compressive cracking	$E_{yy}^d = 0.4 * E_{yy}, E_{xy}^d = 0.4 * E_{xy}, E_{yz}^d = 0.4 * E_{yz}$	(10)
Fiber tensile failure	$E_{xx}^d = 0.07 * E_{xx}$	(11)
Fiber compressive failure	$E_{xx}^d = 0.14 * E_{yy}$	(12)
Delamination in tension or compression	$E_{zz}^d, E_{yz}^d, E_{xz}^d = 0$	(13)

7 LOAD

A fully reversed cyclic loading ($R=-1$) is applied to the model and in each cycle, only the σ_{max} tensile load is applied in the joint, the stresses are calculated by the FE model and a check for possible failure modes is performed. Then, based on the elastic solution the compressive stresses can be obtained:

$$\sigma_{min} = R \cdot \sigma_{max} = -\sigma_{max} \quad (14)$$

A design equation is formulated for the situation where it is assumed that the wind turbine is operational. The design equation is written as:

$$G = \frac{1}{\gamma_n \gamma_m} \frac{S_c}{\gamma_f} - \gamma_f S_e(L_c) = 0 \quad (15)$$

where γ_n , γ_m and γ_f are partial safety factors, see Table (6). S_e is the equivalent stress which is obtained from the failure criteria, and S_c is characteristic load carrying capacity.

Table (6). Partial safety factors according to IEC 61400-1 [9].

Partial Safety Factor	Ultimate
γ_n – Consequences of failure	1.00
γ_m – Material properties	1.30
γ_f – Load	1.00

To obtain the characteristic load, first the 5% quantile of the composite layers strength and adhesive is calculated based on the characteristic strength parameters in Table 2 and 3. The maximum allowable characteristic load is then obtained through FEA by calculating $S_e(L_c)$. When L_c is obtained, it is used that it is a mean value in the distribution for the equivalent fatigue load, and L_s is assumed to be modelled by a Weibull distribution with COV = 15% [28]. Further, a load model relevant for wind turbine blades is applied. The load is described in terms of a number of stochastic variables:

$$L = L_s X_{dyn} X_{exp} X_{st} X_{aero} \quad (16)$$

The limit state equation corresponding to the design equation Eq. (15) is:

$$g(n) = X_R S(N_f) - S_e(L, n) \quad (17)$$

Table (7). Stochastic variables for the model and physical uncertainty related to the loading [7].

Variable	Description	Distribution	Mean	COV	Characteristic value
X_R	Load carrying capacity	Lognormal	1	5%	X_R
X_{st}	Limited wind data	Lognormal	1	10%	X_{st}
X_{dyn}	Dynamic response	Lognormal	1	5%	X_{dyn}
X_{exp}	Exposure	Lognormal	1	10%	X_{exp}
X_{aero}	Lift/Drag coefficients	Gumbel	1	10%	X_{aero}

8 METHODOLOGY AND APPROACH

The FEA code ANSYS 12.1 is run in batch mode from Matlab using geometric parameters, material properties and loads simulated from the distribution functions describing the stochastic variables. Each simulated parameter is read by ANSYS using a macro file, the number of cycles is increased and after the numerical processing a post processing is carried out. The stresses and strains are selected and imported to Matlab. A failure analysis is done using Hashin failure criterion, and finally the number of failures is calculated. This procedure is conducted for 1280 simulations using the Asymptotic Sampling technique, and finally the probability of failure (P_f) is obtained. The reliability index, β is obtained from:

$$\beta = -\Phi^{-1}(P_f) \quad (18)$$

where Φ is the standard Normal distribution function. The following flowchart explains the methodology and approach.

9 RESULTS AND DISCUSSIONS

IEC-61400-1 [9] standard requires a minimum annual reliability index for structural wind turbine component equal to 3.1. To reduce the computational time and present a more efficient technique

with respect to FEA based evaluation of the limit state equations, Asymptotic Sampling was used. In conducting this, 5 support points were chosen for different values of the scaling factor f , and 256 iterations were carried out for each support point. This means that 1280 simulations were performed to obtain the results. For the curve fitting, a set of supporting points and reliability indices associated with the supporting points is constructed, and using Eq. (2) the constants A and B are determined (see Fig. 4). The results are presented in Table 9 which show the reliability level of the joint loaded in fatigue is satisfactory.

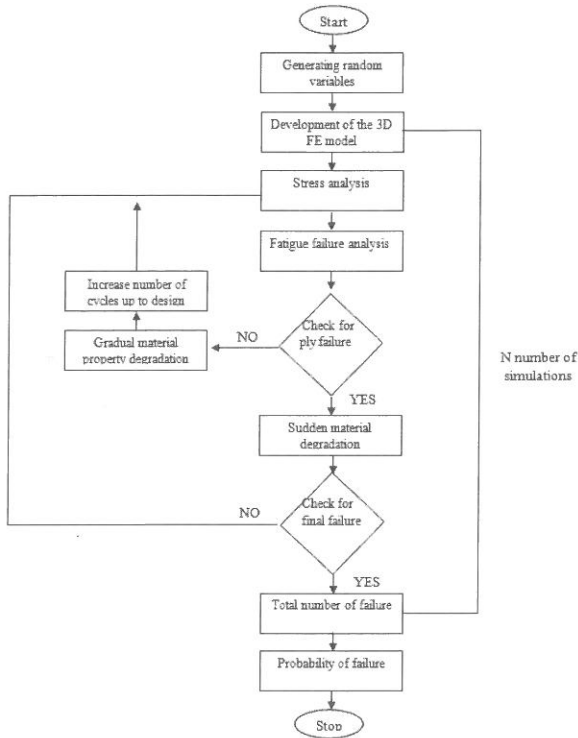


Fig.3. Methodology flowchart

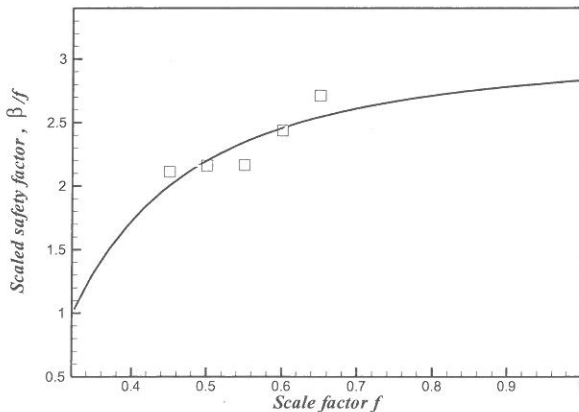


Fig.4. Asymptotic Sampling results obtained using the Hashin criterion based on 5 supporting points.

Table 9. Predicted probability of failure based on 1280 simulations (Asymptotic Sampling method).

Method	Probability of failure	Reliability index	Computational time
Asymptotic Sampling	0.0023	2.83	~2 days

10 CONCLUSIONS

A probabilistic model for the reliability analysis of adhesive bonded composite stepped lap joints loaded in fatigue has been proposed, in which the influence of variations in the geometrical, physical, strength parameters and external loading over the joint have been included. A reliability assessment for composite adhesive stepped lap joints was presented using stochastic models for the uncertain parameters, and Asymptotic Sampling techniques based on the use of a 3D FEA model were used to estimate the probability of failure. In summary, a simple and novel approach for the assessment of the reliability and probability of failure for adhesive bonded composite stepped lap joints has been presented, and it was illustrated how partial safety factors for semi-probabilistic design can be calibrated.

ACKNOWLEDGEMENT

The work presented in this paper is part of the project "Reliability-based analysis applied for reduction of cost of energy for offshore wind turbines" supported by the Danish Council for Strategic Research, grant no. 09-065195. The financial support is greatly appreciated.

REFERENCES

- [1] Dan H, Sawa T, Iwamoto T, Hirayama Y, Stress analysis and strength evaluation of scarf adhesive joints subjected to static tensile loadings, *International Journal of Adhesion & Adhesives* 30 (2010) 387–392.
- [2] Kumar S.B, Sivashanker S, Bag A, Sridhar I, Failure of aerospace composite scarf-joints subjected to uniaxial compression, *Materials Science and Engineering A* 412 (2005) 117–122.
- [3] Tserpes KI, Papanikos P, Kermanidis Th. A three-dimensional progressive damage model for bolted joints in composite laminates subjected to tensile loading. *Fatigue Fract Eng Mater Struct* 2001; 24 (10) 673–86.
- [4] Papanikos P, Tserpes KI, Pantelakis Sp. Modelling of fatigue damage progression and life in CFRP laminates. *Fatigue Fract Eng Mater Struct* 2003; 26: 37–47.
- [5] Ronold KO, Wedel-Heinen J, Christensen CJ. Reliability-based fatigue design of wind-turbine rotor blades. *Engineering Structures*, 21(1999) 1101–14.
- [6] Tarp-Johansen NJ. Examples of fatigue lifetime and reliability evaluation of larger wind turbine components. Roskilde, Denmark: *Risø National Laboratory*; 2003. Report No.: Risø-R-1418(EN).
- [7] Kimiaçifar A, Toft H, Lund E, Thomsen O. T, Sørensen J. D, Reliability Analysis of Adhesive Bonded Scarf Joints, *Engineering Structures*, 35 (2012) 281–287.
- [8] Bucher C, Asymptotic Sampling for high-dimensional reliability analysis, *Probabilistic Engineering Mechanics* 24 (2009) 504-510.
- [9] IEC 61400-1. Wind turbines-part1: design requirements. 3rd edition, 2005.
- [10] EN 1990. Basis of structural design. *CEN* 2002.

Multi-dimensional risk interdependence analysis for buildings and building users

G. Ginda

University of Bielsko-Biala, Bielsko-Biala, Poland

M. Maślak

Cracow University of Technology, Cracow, Poland

ABSTRACT: Contemporary buildings must be technically complex due to a need for assuring a proper level of safety. There are numerous risks that buildings and building users are subject to. Building regulations require the application of appropriate countermeasures to mitigate the possible effects of risks. The countermeasures are delivered by material, structural and maintenance solutions utilised in a building. Space limitations and limited financial resources force decision makers to search for cost-effective solutions which are capable of mitigating the effects of different risks concurrently. Different risks can interrelate with each other. These interactions can thus influence risk-aware effectiveness of solutions applied in buildings. The paper deals with an approach which facilitates the identification of interrelations between risks. It delivers both qualitative and quantitative information about these interrelations. Such information can be incorporated into effective building solution alternative selection procedures.

1 INTRODUCTION

1.1 *Risks for buildings and building users*

Fire risk for buildings and building users involves various safety measures. Fire safety risk is not, however, the only one kind of risk buildings and building users are subject to. A concise definition of considered risks is included in the building regulations together with a description of appropriate countermeasures. There are a lot of competitive fire risk countermeasures available. The same measures can be applied for addressing different risks. Conscious selection of technological, material and maintenance building solutions can therefore result in efficient addressing of several risks at once. Such selection will deliver benefits with regard to the simplification of design, construction and maintenance of buildings.

Detailed knowledge about the interdependence of risks facilitates therefore a selection of risk countermeasures. Such knowledge cannot be acquired successfully without including a realistic, multi-dimensional nature of potential solutions and an imprecise nature of available information. A suitable approach for knowledge acquisition is presented in the paper.

1.2 *Applied approach*

The proposed approach is devoted to the identification of cause-effect chain structure which expresses interdependence of general risks a building and occupants are subject to. DEMATEL (DECISION MAKING TRIAL and EVALUATION LABORATORY) proposed by Gabus & Fontela (1972) is utilised with this regard. DEMATEL maturity and flexibility facilitates computational implementation and automation of the approach. A concept of multi-dimensional overall influence map is applied for modelling interrelation between risks. Feedback-aware digraph structures are utilised for the expression of map components.

2 DEMATEL

2.1 Origin and applications

DEMATEL is a decision analysis method which is capable of identification of a cause-effect chain structure of considered problems. It was founded to facilitate the identification of inter-relations between contemporary economic, social and environmental world problems possible (Fontela & Gabus 1976). It was hoped that the identification of the inter-relations would help in an effective solution of the problems. The method became soon popular in the world community of researchers.

DEMATEL is rather old. It gained nevertheless even more popularity at the turn of the centuries. Advantages offered by the method favoured its rapid dissemination. Several improvements were also introduced into the method to adapt it to diverse applications and utilisation areas.

2.2 DEMATEL basics

A direct influence comprises the main concept of the method. The concept is applied for the expression of a cause-effect relation between two objects. The intensity of direct influence is expressed by a dedicated evaluation scale. An order scale is usually applied with this regard. The lowest scale level is 0 and means a lack of direct influence. The highest level N expresses the extreme direct influence. Intermediate levels from 1 to $N-1$ correspond to stepwise increase in direct influence. A number of applied scale levels depends on a specific need. For example, the original DEMATEL scale consists of 5 levels ($N=4$). Its intermediate levels express:

- 1 - a slight influence of the first object on the second object,
- 2 - a noticeable influence of the first object on the second one,
- 3 - a big influence of the first object on the second one.

It is worth mentioning that feedback i.e. the influence of both compared objects on each other can be included. And no influence of a particular object on itself is assumed.

A complete set of relation evaluations for a group of n objects therefore consists of $(n-1) \cdot n$ judgments. An influence map is applied for the expression of direct influence. A digraph called a direct influence graph $X(V, E_X)$ is applied for map implementation. Graph vertices V denote objects and graph arcs E_X express the influence between objects. The digraph is represented by an $n \times n$ quadratic matrix \mathbf{X} called a matrix of direct influence. A matrix component located in the i -th row and the j -th column expresses the effect of the i -th object on the j -th object ($i, j = 1, 2 \dots n$).

The overall influence of objects comes from both explicit - direct and implicit - indirect effects of objects. The structure of overall influence is described by a digraph called a total influence graph $T(V, E_T)$. It is represented by an $n \times n$ quadratic matrix called a matrix of total influence \mathbf{T} :

$$\mathbf{T} = \bar{\mathbf{X}} \cdot (\mathbf{I} - \bar{\mathbf{X}})^{-1}, \quad (1)$$

where $\bar{\mathbf{X}}$ = a normalised matrix of direct influence:

$$\bar{\mathbf{X}} = \frac{1}{\lambda} \cdot \mathbf{X}, \quad (2)$$

where λ = the maximal row-wise and column-wise sum of matrix \mathbf{X} components:

$$\lambda = \max \left\{ \max_i \sum_{j=1}^n x_{ij}, \max_j \sum_{i=1}^n x_{ij} \right\}. \quad (3)$$

Matrix $\bar{\mathbf{X}}$ consists therefore of components which are equal to 0 at least and equal to 1 at most. Row-wise or/and column-wise sums of matrix components are at most equal to 1.

DEMATEL analysis results can be presented in several ways. Total influence graph $T(V, E_T)$ provides the primary means for the presentation of DEMATEL outcomes. Two indices, namely the prominence s^+ and the relation s^- are applied to express the overall nature of objects. The prominence expresses the overall importance of an object during the identification of the nature of considered objects. The relation indicates causal or effect nature of considered objects.

Values of both indices come from the sum of \mathbf{T} components from the i -th row (R_i) and from the i -th column (C_i):

$$s_i^+ = R_i + C_i, \quad s_i^- = R_i - C_i, \quad R_i = \sum_{j=1}^n t_{ij}, \quad C_i = \sum_{j=1}^n t_{ji}. \quad (4)$$

A positive s_i^- value confirms the causal nature of the object and a negative value - the effect nature of the object. Zero and close to zero value denotes a rather neutral object role.

A Resultant net overall influence structure can be also presented. Net overall influence is obtained for each pair of objects using the following formula:

$$\Delta n_{ij} = \begin{cases} t_{ij} - t_{ji} & \text{for } t_{ij} > t_{ji}, \\ 0 & \text{otherwise.} \end{cases} \quad (5)$$

A net total influence map is expressed by a net total influence digraph $N(V, E_N)$. Arcs E_N indicate the direction and resultant intensity of the overall influence between two objects.

A total influence map can be too complex. An influence threshold δ is introduced to facilitate the presentation of DEMATEL analysis outcomes. The application of the threshold leans the total influence map. Arcs which correspond to the total influence intensity lower than the threshold are removed from a total influence digraph. A reduced influence map is thus obtained. It is expressed by a reduced total influence matrix $\bar{\mathbf{T}}$:

$$\bar{t}_{ij} = \begin{cases} t_{ij} & \text{for } t_{ij} \geq \delta, \\ 0 & \text{otherwise} \end{cases} \quad (6)$$

DEMATEL is based on expert opinions. It is capable of including group opinions. Direct influence matrices delivered by m independent experts are utilised for opinion aggregation. A simple arithmetic average formula is applied to obtain an average direct influence matrix \mathbf{X} :

$$\mathbf{X} = \frac{1}{m} \cdot \sum_{i=1}^m \mathbf{X}^{(i)} \quad (7)$$

where $\mathbf{X}^{(i)}$ = a direct influence matrix derived by the i -th expert.

Several useful extensions have been incorporated into original DEMATEL methodology. The most interesting improvements address imprecise and vague data e.g. linguistic variables are applied for expression of the fuzzy evaluation scale levels (Lin & Wu 2004). The levels are usually expressed by Triangular Fuzzy Numbers, TFNs (Fig.1).

A sample 4-level linguistic scale is presented in Figure 1 (N means no influence scale level, L - low influence, H - high influence, S - strong influence, α - a TFN membership value, \tilde{x}_{ij} - TFN evaluation of i -th object influence on the j -th object influence).

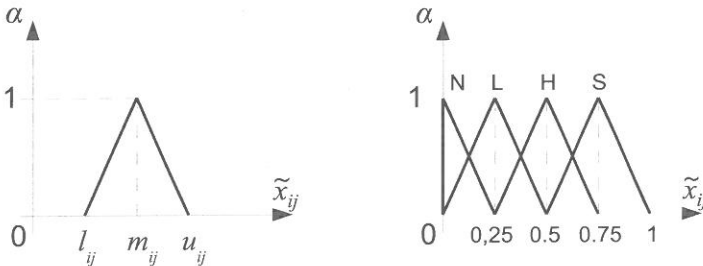


Figure 1: A triangle fuzzy number concept and a sample linguistic DEMATEL evaluation scale

The application of TFNs requires the appropriate accommodation of DEMATEL calculation

formulae. A fuzzy direct relation matrix $\tilde{\mathbf{X}}$ is usually normalised by means of a maximal row-wise sum of upper TFN limit parameters ($i = 1, 2, \dots, n$):

$$\tilde{\mathbf{X}} = \frac{1}{\lambda} \otimes \tilde{\mathbf{X}}, \quad \lambda = \max_i \sum_{j=1}^n u_{ij}. \quad (8)$$

The components of fuzzy average direct influence matrix are defined as follows ($i, j = 1, 2, \dots, n$):

$$\tilde{x}_{ij} = \left(\frac{l_{ij}}{\lambda}, \frac{m_{ij}}{\lambda}, \frac{u_{ij}}{\lambda} \right). \quad (9)$$

A fuzzy direct influence is usually expressed using 3 crisp matrices $\bar{\mathbf{X}}_l$, $\bar{\mathbf{X}}_m$ and $\bar{\mathbf{X}}_u$ which correspond to the lower limit, medium value and upper limit TFN parameters respectively. Such expression of influence facilitates the derivation of fuzzy total influence map. Separate processing of crisp matrices due to Equation 7 is utilised for obtaining crisp parameters of TFN outcomes:

$$\mathbf{T}_l = \bar{\mathbf{X}}_l \cdot (\mathbf{I} - \bar{\mathbf{X}}_l)^{-1}, \quad \mathbf{T}_m = \bar{\mathbf{X}}_m \cdot (\mathbf{I} - \bar{\mathbf{X}}_m)^{-1}, \quad \mathbf{T}_u = \bar{\mathbf{X}}_u \cdot (\mathbf{I} - \bar{\mathbf{X}}_u)^{-1}. \quad (10)$$

Fuzzy total influence matrix components $\tilde{\mathbf{T}}$ are defined as follows ($i, j = 1, 2, \dots, n$):

$$\tilde{t}_{ij} = (t_{lij}, t_{mij}, t_{uij}) \quad (11)$$

TFN values for both the prominence and the relation are described by the formulae:

$$\tilde{s}_i^+ = \tilde{R}_i \oplus \tilde{C}_i, \quad \tilde{s}_i^- = \tilde{R}_i - \tilde{C}_i, \quad (12)$$

where \tilde{R}_i = row-wise and \tilde{C}_i = column-wise sum of $\tilde{\mathbf{T}}$ matrix components: ($i = 1, 2, \dots, n$):

$$\tilde{R}_i = \tilde{t}_{i1} \oplus \tilde{t}_{i2} \oplus \dots \oplus \tilde{t}_{in}, \quad \tilde{C}_i = \tilde{t}_{1i} \oplus \tilde{t}_{2i} \oplus \dots \oplus \tilde{t}_{ni}. \quad (13)$$

Defuzzification of fuzzy outcomes is necessary to enable the presentation of DEMATEL outcomes. The center of gravity technique is applied to obtain crisp values corresponding to TFN values. Let's assume the following general representation for TFN:

$$\tilde{z} = (l, m, u), \quad (14)$$

The following formula therefore expresses an equivalent crisp value z :

$$z = m + \frac{u^2 + 2 \cdot m \cdot (l - u) - l^2}{3 \cdot (u - l)}. \quad (15)$$

3 SAMPLE ANALYSIS

3.1 Tentative assumptions

Current Polish building regulations require buildings to be erected, equipped and operated in the ways which ensure proper reduction of unfavorable influence of different factors. The regulations also provide information about critical measures which assure an appropriate level of safety to a building and occupants. The following safety dimensions are included:

- general structural safety (SS),
- fire safety (FS),
- occupational safety (OS),
- hygienic and health safety (HH).

The dimensions correspond to different risks a building and building users are subject to. They can be also further divided into subcategories. For example, a successful implementation of fire safety measures satisfies the requirements of structural capacity, limits smoke and fire spread and provides proper evacuation means for occupants.

A proper level of safety should be ensured by building design (D), construction (C), occupation and building maintenance (U) activities. These activities are of a man controllable nature. Effects of these activities influence safety level for a building and occupants. The resulting risks for example pertain to imperfect or defective design and constructional solutions, the application of improper building occupation or maintenance modes etc. There are also essential accidental factors which are considered independent on decisions of parties involved in building design, erection and occupation. It seems that accidental factors should be further divided into 2 separate groups due to their origins:

- inherent accidental factors I,
- external accidental factors E.

Inherent factors can relate to the risks of possible defects of building components. External factors correspond to the risks of unfavorable influence of the surrounding environment which can result from fire, flood, hurricane, air and water pollution, transportation means impact etc.

A compound nature of building design, constructional and maintenance solutions, corresponding building regulations' requirements and a commonly recognised paradigm of sustainable development inevitably leads to inter-relations between general risks. The identification of such relations is therefore worth a thorough investigation.

A direct influence is applied for the expression of cause-effect relations between general risks and their effects. A 4-level linguistic fuzzy judgement scale is applied to address the intensity of the direct influence of general risk factors on other risk factors (Fig.1).

Reliable investigation requires including multi-dimensionality of safety measures induced by building regulations. All mentioned safety dimensions are therefore considered during the identification of a risk influence map. The opinions of 4 experts are applied for the evaluation of the influence of general risks on each other. Each expert is responsible for addressing a single safety dimension he or she is the best accustomed to. The evaluations provided by separate experts $\tilde{X}^{(SS)}$, $\tilde{X}^{(FS)}$, $\tilde{X}^{(OS)}$, $\tilde{X}^{(HH)}$ are then combined:

$$\tilde{X} = \frac{1}{4} \otimes (\tilde{X}^{(SS)} \oplus \tilde{X}^{(FS)} \oplus \tilde{X}^{(OS)} \oplus \tilde{X}^{(HH)}) \quad (16)$$

Aggregated judgements are processed due to Equations 8-15. Data processing results in the structure of overall influence.

3.2 Structural Safety Dimension

The opinions of the expert appointed to the evaluation of a direct influence with regard to structural safety merits are applied for the presentation of data acquirement principles. The expert decides that:

- design-related risks D influence construction workmanship-related risks C at low level L and occupational risks U at high level H, internal and external accidental risks I and E, are not influenced at all (N evaluation scale level) by D risks,
- construction workmanship-related risks influence design-related risks at high level H, occupational risks at the highest possible level S, inherent accidental risks at high level H and external accidental risks at low level L,
- occupational risks influence design-related and construction workmanship-related risks at high level H, inherent and external accidental risks at low level L,
- inherent accidental risks influence design-related risks and construction workmanship-related risks at low level L, occupational risks and external accidental risks aren't influenced (N level),
- external accidental risks influence design-related risks at low level L and construction workmanship-related risks at high level H, occupational risks at low level L and inherent accidental risks aren't influenced (N).

Structural safety-related evaluations are presented in Table 1. A complete set of evaluations makes up a direct influence matrix $\tilde{X}^{(SS)}$ given in Equation 17. It is worth noticing that due to general DEMATEL rule general risks do not influence themselves at all. A zero TFN value $\tilde{0} = (0, 0, 0)$ is therefore utilised for the expression of the risk influence in this case.

Table 1. A complete set of general risk influence evaluations (the structural safety case)

Risk	D	C	U	I	E
D	-	L	H	N	N
C	H	-	S	H	L
U	H	H	-	L	L
I	L	L	N	-	N
E	L	H	L	N	-

$$\tilde{\mathbf{X}}^{(SS)} = \begin{bmatrix} \tilde{0} & L & H & N & N \\ H & \tilde{0} & S & H & L \\ H & H & \tilde{0} & L & L \\ L & L & N & \tilde{0} & N \\ L & H & L & N & \tilde{0} \end{bmatrix} \quad (17)$$

The TFN direct influence matrix looks therefore as follows:

$$\tilde{\mathbf{X}}^{(SS)} = \begin{bmatrix} (0,0,0) & (0, \frac{1}{4}, \frac{1}{2}) & (\frac{1}{4}, \frac{1}{2}, \frac{3}{4}) & (0,0, \frac{1}{4}) & (0,0, \frac{1}{4}) \\ (\frac{1}{4}, \frac{1}{2}, \frac{3}{4}) & (0,0,0) & (\frac{1}{2}, \frac{3}{4}, 1) & (\frac{1}{4}, \frac{1}{2}, \frac{3}{4}) & (0, \frac{1}{4}, \frac{1}{2}) \\ (\frac{1}{4}, \frac{1}{2}, \frac{3}{4}) & (\frac{1}{4}, \frac{1}{2}, \frac{3}{4}) & (0,0,0) & (0, \frac{1}{4}, \frac{1}{2}) & (0, \frac{1}{4}, \frac{1}{2}) \\ (0, \frac{1}{4}, \frac{1}{2}) & (0, \frac{1}{4}, \frac{1}{2}) & (0,0, \frac{1}{4}) & (0,0,0) & (0,0, \frac{1}{4}) \\ (0, \frac{1}{4}, \frac{1}{2}) & (\frac{1}{4}, \frac{1}{2}, \frac{3}{4}) & (0, \frac{1}{4}, \frac{1}{2}) & (0,0, \frac{1}{4}) & (0,0,0) \end{bmatrix} \quad (18)$$

The matrix corresponds to a direct influence map. Direct influence maps based on the opinions of all appointed experts are presented in Figure 2. Different line styles are applied to express diversified direct influence intensity. N level of direct influence is denoted by a dotted line, L level - by a dashed line, H level - by a solid line and S level - by a bold line.

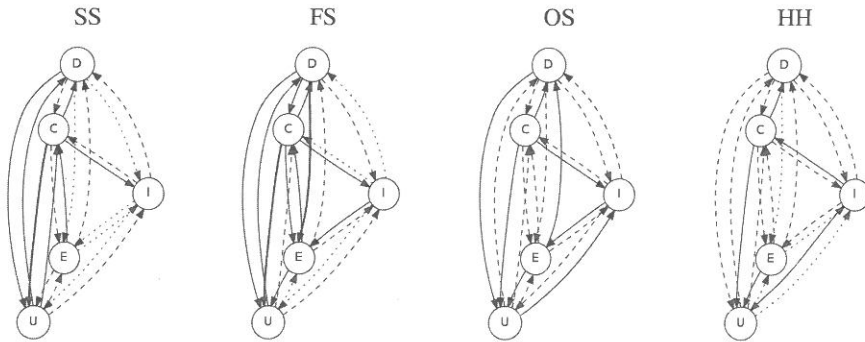


Figure 2: Assumed direct influence maps for general risks obtained for different dimensions

The application of the formula given in Equation 16 makes obtaining an aggregated matrix of a direct influence $\tilde{\mathbf{X}}$ possible. The application of formulae given in Equations 8-15 results in fuzzy $(\tilde{s}^+, \tilde{s}^-)$ and crisp values (s^+, s^-) of the indices and a total influence matrix \mathbf{T} . An average value of crisp total influence matrix \mathbf{T} components is applied for total influence map leaning:

$$\delta = \frac{1}{n \cdot n} \cdot \sum_{i=1}^n \sum_{j=1}^n t_{ij} \quad (19)$$

The overall influence structure is finally presented in Figure 3. A reduced total influence map, a net total influence map and the prominence vs. the relation graph facilitate the expression of the structure. Line patterns correspond to the strength of overall influence and net overall influence. A bold line, a solid line, a dashed line and a dotted line address the intensity of the overall and net overall influence in a descending order.

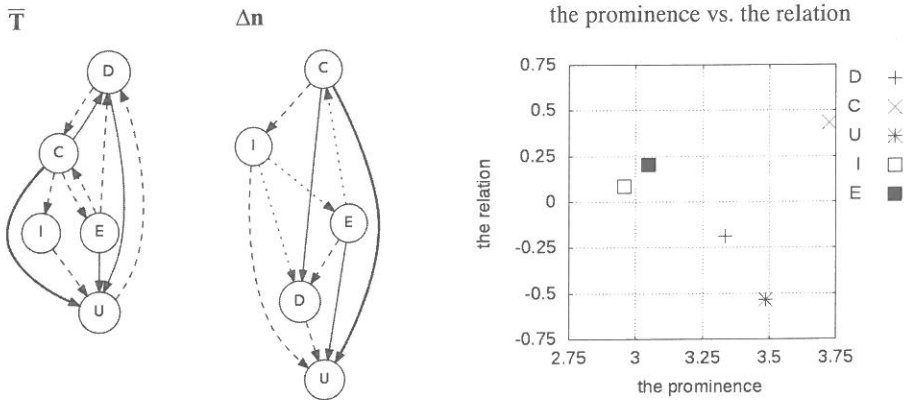


Figure 3: Overall structure of total influence

The obtained results confirm that construction workmanship-related risks C comprise the primary causes. They influence other risks apart from external accidental risks. Occupational risks are influenced at most. External accidental risks E are the secondary causes. They influence design-related risks, occupational risks and even construction workmanship-related risks. Occupational risks are influenced at most.

Inherent risks I comprise causes rather than effects. They influence occupational risks at most. A net total influence map reveals a resulting influence of inherent accidental risks on external accidental and design-related risks.

The remaining risks are effects. Occupational risks are the most evident effects. They influence design risks only and are influenced by other risks. Design-related risks influence construction workmanship-related risks only and are influenced by other risks besides inherent accidental risks.

There exists a considerable overall influence feedback between:

- construction workmanship-related risks C and external accidental risks E,
- construction workmanship-related risks and design-related risks,
- design-related risks and occupational risks.

A net total influence map confirms also the presence of an indirect overall influence feedback between construction workmanship-related risks, inherent and external accidental risks.

The obtained results confirm that construction workmanship-related risks C influence other risks. They correspond to man-controllable risks. Their influence should be therefore limited to minimise the influence on and of other risks. The proper preparation and control of building erection activities thus comprise the most successful factor with regard to the safety of a building and its occupants. Other influencing risks i.e. accidental risks I and E are of uncontrollable nature. Their unfavourable influence is therefore unlikely to be successfully limited.

Revealed feedback between construction workmanship risks and design risks indicates the possibility of improvement in safety thanks to the appropriate co-ordination of design and construction activities and their effects. Revealed feedback between construction workmanship risks and inherent accidental risks suggests the additional improvement in the safety for a building and its occupants. For example, such improvements can be introduced by extremely cautious selection of contractors, technical means, building components and suppliers.

4 CONCLUSIONS

DEMATEL is a well established yet not widely recognised method which facilitates a reliable identification of cause-effect chains. Included results confirm the usability of DEMATEL-based approach for the clarification of multi-dimensional relations between general risks which influence the safety of a building and its occupants. The availability of such information facilitates both the coordination of different safety-oriented efforts and proper trade-offs during a building design, construction and operation.

The identified structure of overall influence can be also utilised for deriving quantitative evaluation of risks influence on the overall safety of a building and the occupants. The application of a method which is capable of including an identified feedback between general risks is however required with this regard. For example, recent developments suggest coupling DEMATEL with Analytic Hierarchy/Network Process (AHP/ANP) - see: Ou Yang et al. (2011) for details.

There are also other recent DEMATEL enhancements which facilitate a multi-dimensional identification of cause-effect chain elements. For example, a concept of multi-thematic DEMATEL (Wu et al. 2011) can be utilised with this regard. More details about useful DEMATEL enhancements will be soon available in a work (Dytczak & Ginda, in prep.).

Inherent DEMATEL advantages, existing and approaching enhancements and extendibility make its application worth considering in the case of the analysis of other safety-related problems. There are also other works which confirm it (Ginda & Maślak 2012). We, therefore, strongly advise DEMATEL application as we are sure that it is really capable to deliver the information which not only facilitates the decision making process but is also otherwise hard to obtain.

5 ACKNOWLEDGEMENTS

This paper was elaborated with the financial support of the project granted by Polish Ministry of Science and Higher Education (N N506 243938).

6 REFERENCES

- Dytczak, M., Ginda G., in prep. DEMATEL. Theory and Applications. Polish Academy of Sciences, Warsaw, Poland.
- Gabus, A., Fontela, E., 1976, *The DEMATEL observer. DEMATEL 1976 Report*. Batelle Institute, Geneva Research Center, Geneva, Switzerland.
- Gabus, A., Fontela, E., 1972. *World Problems, An invitation to Further Thought Within the Framework of DEMATEL*. Batelle Institute, Geneva Research Centre, Geneva, Switzerland.
- Ginda, G., Maślak, M., 2012. Application of FDM-based Approach For Assessment of Influence of Fire Safety Factors. *Proceedings of the 1st International Conference in Safety and Crisis Management in the Construction, Tourism and SME Sectors (1st CoSaCM), European University Cyprus Cultural Center, Nicosia, Cyprus, 24-28 June 2011*, G. Boustras & N. Boukas Eds. BrownWalker Press, Boca Raton, Florida, USA:570-579.
- Lin, C., Wu, W., 2004. A Fuzzy Extension of the DEMATEL Method for Group Decision-Making. *Journal of Operational Research Society of Taiwan*,
- Ou Yang, Y.P., Shieh, H.M., Leu, J.D., Tzeng, G.H., 2008. A novel hybrid MCDM model combined with DEMATEL and ANP with applications. *International Journal of Operational Research*, 5(3):160-168.
- Tamura, H., Akazawa, K., (2005), Stochastic DEMATEL for structural modeling of a complex problematic for realizing safe, secure and reliable society. *Journal of Telecommunications and Information Technology*, 4:139-146.
- Wu, W.-W., Lan, L.W., Chen, Y.-M., Lee, Y.-T., 2011. Kansei Product Design for New Product Development - Duo-theme DEMATEL Approach. *International Journal of Kansei Information*, 2:61-70.

Truck load modeling for reliability based code calibration

G.Fu

Illinois Institute of Technology, USA

P.Yen

Federal Highway Administration, USA

J.You and L.Liu

Tongji University, China

ABSTRACT: A number of civil engineering practice specifications have been advanced to be reliability based. They include the LRFD Bridge Design Specifications and the Manual for Bridge Evaluation in the US issued by the American Association of State Highway and Transportation Officials (AASHTO). An important feature substantiating the reliability concept in these codes is the accordingly calibrated truck load models and live load factors. On the other hand, the reliability based calibration process then used very limited truck weight data gathered in Canada. It has been three decades or so from then and a much larger amount of truck weight data has been made available since then. Research work is reported here using much more statistically significant truck weight data from many weigh-in-motion stations in the US collected in recent years. More rigorous statistical analysis and projection are thereby made possible and are applied on these data to examine the assumptions used in the calibration process of the AASHTO codes. It was found that many of these assumptions are actually not valid. Application cases of code calibration are also reported in this paper.

1 INTRODUCTION

In developing structural design specifications critical for safety of the structures thereby governed, a critical step is to project future maximum loads and/or load effects to cover the expected life span of the structures. This has been performed by extrapolation, namely using load data collected over a short period of time to project to the future. For example, the American Association of State Highway Transportation Officials (AASHTO) LRFD Bridge Design Specifications (2012) mandated in the US is supposed to cover the expected bridge life span of 75 years. The truck load data used to project to the 75-year maximum level were collected over a short time period of about 2 weeks (Nowak 1999, Kulicki *et al.* 2007).

In general, engineering prediction may be performed using extrapolation or interpolation. The former is however far less reliable than the latter where prediction is done using data that cover the entire application range. Extrapolation is instead based on data out of the range of application. For structural design code development, this extrapolation is more questionable due to the very remote future being predicted to. Using two weeks of data to project to the future of 75 years is an example of such practice - 75 years being 1,950 times longer than 2 weeks ($52 \text{ weeks / year} \times 75 \text{ years} = 3,900 \text{ weeks}$). Owing to costly data collection for long duration, it has been impossible to investigate this important issue for the safety of the structures thereby designed. Recently, in the area of highway bridge design for vehicular load, such investigations have become possible due to the availability of more and higher quality vehicular live load data. This paper has a focus on the application, also with an intention to provide a starting point for other applications relevant to structural safety.

The application of extrapolation may be formulated as follows. Let $F_I(x)$ denote the cumulative probability function (CPF) of one event load level x , which is estimated based on measurement data over a short period of time. For example, about 10,000 trucks were weighed and their load effects were used to develop $F_I(x)$ shown in (Nowak 1999) for the AASHTO LRFD design code calibration. For the design life of 75 years, N such load events are expected, and $F_N(x)$ is used to denote the CPF of the maximum values of x for N load events over 75 years. According to the definitions, the two CPFs have the following relation:

$$F_N(x) = F_I^N(x) \quad (1)$$

$F_I(x)$ was further assumed to be normally distributed in Sivakumar *et al.* (2008) for NCHRP Project 12-76, which brings an advantage of analytical expressions of the mean μ_N and variance σ_N^2 for the asymptotic distribution $F_N(x)$ for the future maximum value. The probability density functions (PDFs) for one event and N events are respectively denoted as $f_I(x)$ and $f_N(x)$ below to conceptually define the statistics of the random variables. Note that one event may also be interpreted as the maximum value event for one time period and N events are then understood as the maximum value event over N time periods in the future.

$$f_N(x) = N F_I^{N-1}(x) f_I(x) \quad (2)$$

$$\mu_N = \int_{-\infty}^{\infty} x f_N(x) dx \quad (3)$$

$$\sigma_N^2 = \int_{-\infty}^{\infty} (x - \mu_N)^2 f_N(x) dx \quad (4)$$

For practical applications with large N values, its accuracy can become low and even questionable. For example, for an average daily truck traffic (ADTT) of 3,000 events/day, N will be 3000/day*365days/year*75years = 82,125,000 (evens). As seen in Eq.2, $f_N(x)$ can be very close to zero for a wide range of x values, because the corresponding smaller-than-1 $F_I(x)$ values raised to a large N th power will be practically zero. Beyond this range of x , $F_I(x)$ will suddenly change from almost 0 to almost 1 with increase of x . This behavior then requires an extremely accurate estimation in the high tail part (*i.e.*, large x values), which is often difficult to provide if not impossible because it means that a very large amount of data needs to be used.

Another approach to extrapolation is the Monte Carlo simulation using many computer generated realizations according to $f_I(x)$. After N realizations are made available, their maximum value is found and saved. After repeating this process for, say, L times being statistically significant, the resulting L maximum values will be used to estimate the mean μ_N and variance σ_N^2 for the maximum value. This approach also requires an accurate and reliable estimation of $f_I(x)$, since any deviation of this function from the real one will cause unwanted bias in the final result. In addition, the requirement for computation time can be high due to the large N value. Furthermore, the quality of random number generator deserves attention for verification. For example, one should have the period of the random number generator not to be exceeded by the required N , and the random samples need to be independent of one another to satisfy the basic assumption for them (Fu 1994). The latter is much more difficult to have, particularly when multiple random variables are involved.

2 A NEW APPROACH FOR EXTRAPOLATION

Based on significantly more truck load data available today, a new extrapolation approach is proposed here to address the issue related to large N or extrapolation to very remote future. Many state departments of transportation in the US and transportation agencies in other countries have gathered such load data using the weigh-in-motion (WIM) technique continuously for some years, with the longest history more than 10 years. For the specification-required design life of 75 years, several to more than 10 years of load data can provide a much better foundation for extrapolation, compared with only several days of data in the past. On the other hand, it is critical to have a validated and efficient method to perform

extrapolation for its reliability and thus the structural safety assured by thereon based code provisions.

The concept of extrapolation has been formulated in Eqs.1 through 4. As discussed, the number of recursive periods N is an important parameter. More data are advantageous and smaller N values are equivalently desired because that means fewer recursive periods or a not very remote future to be predicted.

Accordingly, it is proposed here to have n data records each covering an approximately equal length of M months as the basic time period. Then the maximum values of the n M -week records will be used to perform extrapolation. Since each maximum value is for an M -week period, N can be then significantly reduced to enhance the reliability of extrapolation based prediction. For example, for $M=3$ (months) and extrapolation to 75 years, N will be $75\text{years} \times 12\text{months/year} / 3\text{months} = 300$ (events). Compared with the example above for the site of $ADTT=3,000$ with an $N=82,125,000$ events, 300 is certainly much smaller, significantly reducing the accuracy requirement for the high tail.

As shown, N can be found simply as $75 \times 12 / M$. If the projection is to be done for a site with an $ADTT$ different from the site where data were collected, N can be accordingly adjusted for projection computation. For example, if the data are from a site with an $ADTT=1,000/\text{day}$ and the extrapolation needs to be performed for the calibration purpose for sites with $ADTT=750/\text{day}$. Then $N = 75 \times 12 / M \times (750 / 1,000)$. Namely the projection length can be reduced or increase by the ratio of the $ADTT$ values.

The distributions and statistical parameters in Eqs.1 to 4 can be used to determine the needed statistics μ_N and σ_N . Again, $f_i(x)$ in Eq.2 is for a generalized one load event, namely the maximum load in the M -week period. Accordingly, $f_N(x)$ in Eq.2 is the PDF for N such M -week periods. Since the extrapolation now starts from this maximum value distribution, it is accordingly modeled as an Extreme I distribution for that period. As a result, the PDF for the future maximum value $f_N(x)$ is also an Extreme I variable (e.g., Gumbel 1958). Its mean and standard deviation defined in Eqs.3 and 4 are found analytically as follows, related to $f_i(x)$'s mean μ_i and standard deviation σ_i :

$$\mu_N = \mu_i + \frac{\ln N}{\pi} \sqrt{6} \sigma_i \quad (5)$$

$$\sigma_N = \sigma_i \quad (6)$$

3 EVALUATION FOR PROPOSED EXTRPOLATION APPROACH

It has been observed that extrapolation to future maximum load statistics has suffered from lack of evaluation, mainly due to lack of long term data needed for such evaluation. This subject is investigated and an evaluation method for the proposed approach is presented here, using two error indices as follows.

$$COV_{\mu_N} = V^{1/2}(\mu_N) / E \quad (7)$$

$$COV_{\sigma_N} = V^{1/2}(\sigma_N) / E(\sigma_N) \quad (8)$$

where COV stands for coefficient of variation, V for variance, and E for expectation or mean. Eqs.7 and 8 treat μ_N and σ_N defined in Eqs.3 and 4 as estimators (Fu 1994). Their realizations, i.e., the extrapolation results, depend on the random variation of data sample. In other words, given a data sample, μ_N and σ_N in Eqs.3 and 4 produce a respective sample of estimates.

These estimates are subject to random variation, which is described using their COV values in Eqs.7 and 8. The mean value and variance of μ_N and σ_N are generally defined as follows.

$$E(\mu_N) = \int_{-\infty}^{+\infty} \mu_N(x_i) f_i(x) dx \quad (9)$$

$$V(\mu_N) = \int_{-\infty}^{+\infty} [\mu_N(x_i) - E(\mu_N)]^2 f_1(x) dx \quad (10)$$

where x_i ($i=1,2,\dots,n$) are data samples of x , namely data collected over the short time period. For better quality in the high tail, not all the collected data are used, but only those in the high tail. For example, for the proposed method, only n maximum values over respective M -week periods are used. For the method in NCHRP project 12-76 reported in (Sivakumar, *et al.* 2008) only a top percentage of the entire data set is used to form the n -data-point set.

For the proposed approach using the Extreme I distribution assumption for $f_1(x)$, the mean and variance can be more explicitly written as

$$E(\mu_N) = \int_{-\infty}^{+\infty} (\mu_1 + \frac{\ln N}{\alpha_1}) f_1(x) dx \quad (11)$$

$$V(\mu_N) = \int_{-\infty}^{+\infty} [\mu_1 + \frac{\ln N}{\alpha_1} - E(\mu_N)]^2 f_1(x) dx \quad (12)$$

$$E(\sigma_N^2) = \int_{-\infty}^{+\infty} (\frac{\pi}{\sqrt{6\alpha_1}})^2 f_1(x) dx \quad (13)$$

$$V(\sigma_N^2) = \int_{-\infty}^{+\infty} [(\frac{\pi}{\sqrt{6\alpha_1}})^2 - E(\sigma_N^2)]^2 f_1(x) dx \quad (14)$$

where

$$\alpha_1 = \frac{n \sum_{i=1}^{i=n} x_i y_i - \sum_{i=1}^{i=n} x_i \sum_{i=1}^{i=n} y_i}{n \sum_{i=1}^{i=n} x_i^2 - (\sum_{i=1}^{i=n} x_i)^2} \quad (15)$$

$$\mu_1 = \frac{\sum_{i=1}^{i=n} y_i - \alpha_1 \sum_{i=1}^{i=n} x_i}{n\alpha_1} \quad (16)$$

$$y_i = -\ln(-\ln(\frac{i}{n+1})) \quad (17)$$

Here the quantities with a subscript I are for $f_I(x)$ or $F_I(x)$ for the basic time period of M months, and those with a subscript N are for $f_N(x)$ or $F_N(x)$ for the future, or $N \times M$ months away. Eqs.15 to 17 are based on a linear regression for estimating the parameters of $f_1(x)$ and $F_I(x)$ in the space of Extreme I distribution probability paper.

It is difficult to analytically perform the integrations in Eqs.11 to 17. A numerical approach using Monte Carlo simulation can be used to obtain these results. In order to include scatter variation of the original data in projection, samples x_i in Eqs.11 to 17 are generated according to $f_1(x)$ and with the standard deviation σ_I increased by $(\mu_N/\mu_I)\sigma_{\eta X}$ where $\sigma_{\eta X}$ is the conditional standard deviation of the data used for fitting to $f_1(x)$ in the space of Extreme I distribution probability paper. It describes the goodness of fitting and thus indicates the random deviation of the data from the fitted function $f_1(x)$.

4 APPLICATION CASES OF EXTRAPOLATION AND THEIR EVALUATION

4.1 California Data

The WIM data used here were provided by California Department of Transportation in US at Site LA710 with three lanes simultaneously recorded. Only the most heavily traveled lane is focused here. However, if multiple trucks are on the span simultaneously their load effects are superimposed to find the total load effect. Both transverse and longitudinal multiple presence are included. They are referred to as "side by side" and "front and back" multiple presence, respectively. Two years of data for 2006 and 2007 and a total of about 1.44 million trucks are used in this application case.

Table 1 Error (%) of Proposed Approach for Simply Supported Spans

span length	15m	30m	67m	76m	85m	94m	Average
Midspan moment:							
4 week μ_N ; N=4	0.05	0.58	1.31	1.18	0.91	0.59	0.77
20 week μ_N ; N=20	0.96	0.06	0.53	1.52	2.13	1.86	1.18
48 week μ_N ; N=48	0.17	0.31	1.73	1.55	1.07	0.77	0.93
4 week σ_N ; N=4	3.94	7.71	8.61	12.78	14.43	15.07	10.42
20 week σ_N ; N=20	4.37	4.19	2.54	7.40	8.63	10.17	6.22
Support shear:							
4 week μ_N ; N=4	0.79	0.95	1.39	0.68	1.18	0.58	0.93
20 week μ_N ; N=20	1.56	1.94	2.22	1.95	1.11	1.68	1.74
48 week μ_N ; N=48	2.20	2.04	2.47	3.12	1.75	2.65	2.37
4 week σ_N ; N=4	14.62	11.50	8.75	9.67	11.48	13.40	11.57
20 week σ_N ; N=20	9.85	4.49	11.55	10.19	3.83	20.00	9.98

Table 2 Errors (%) of Two Extrapolation Methods for Midspan Moment

span length		15m	30m	67m	76m	85m	94m	Average
4 week μ_N ; N=4	Proposed Method	0.05	0.58	1.31	1.18	0.91	0.59	0.77
	N=32368 NCHRP 12-76 Method	20.02	17.32	17.43	18.13	18.77	19.33	18.50
4 week σ_N ; N=4	Proposed Method	3.94	7.71	8.61	12.78	14.43	15.07	10.42
	N=32368 NCHRP 12-76 Method	63.65	55.21	57.19	57.59	58.45	59.32	58.57
20 week μ_N ; N=20	Proposed Method	0.96	0.06	0.53	1.52	2.13	1.86	1.18
	N=161840 NCHRP 12-76 Method	24.31	21.86	22.48	22.62	22.82	23.51	22.93
20 week σ_N ; N=20	Proposed Method	4.37	4.19	2.54	7.40	8.63	10.17	6.22
	N=161840 NCHRP 12-76 Method	68.88	62.93	62.39	62.43	63.30	63.76	63.95
48 week μ_N ; N=48	Proposed Method	0.17	0.31	1.73	1.55	1.07	0.77	0.93
	N=388416 NCHRP 12-76 Method	27.31	23.56	23.73	24.90	26.00	26.78	25.38

Using the proposed approach, one week is selected to be the basic period for $f_i(x)$. Several N values (4, 20, and 48) are used for extrapolation, constrained by the amount of available long term data for validation. For example for $N=4$ (weeks), the 2-year data set can provide up to 26 maximum values to produce estimates of the mean and standard deviation for comparison with the projected μ_N and σ_N . For a larger N value, the available long term data limit such evaluation. For example for $N=48$ (weeks), the 2-year data set can provide only two maximum values to barely produce an estimate for the mean but not the standard deviation. Table 1 displays the error of extrapolation using the proposed method, compared with the observed results using the long term data. For the case of $N=48$, the error for σ_N extrapolation cannot be given due to limited long term data. These results show that the proposed me-

thod is able to produce reliable results, with error for μ_N between 0.05% and 3.12% and σ_N within 2.54% and 20.00%. In general, the error in σ_N is larger than that in μ_N , since the former depends on the latter.

Table 3 Errors (%) of Extrapolation Methods for Support Shear

span length		15m	30m	67m	76m	85m	94m	Average
4 week μ_N ; N=4	Proposed Method	0.79	0.95	1.39	0.68	1.18	0.58	0.93
	N=32368 NCHRP 12-76 Method	19.10	16.78	17.37	18.61	18.84	19.94	18.44
4 week σ_N ; N=4	Proposed Method	14.62	11.50	8.75	9.67	11.48	13.40	11.57
	N=32368 NCHRP 12-76 Method	58.51	57.01	62.38	63.37	63.80	63.96	61.50
20 week μ_N ; N=20	Proposed Method	1.56	1.94	2.22	1.95	1.11	1.68	1.74
	N=161840 NCHRP 12-76 Method	23.51	20.81	22.43	23.52	24.95	25.25	23.41
20 week σ_N ; N=20	Proposed Method	9.85	4.49	11.55	10.19	3.83	20.00	9.98
	N=161840 NCHRP 12-76 Method	62.88	65.62	63.98	65.64	70.84	64.40	65.56
48 week μ_N ; N=48	Proposed Method	2.20	2.04	2.47	3.12	1.75	2.65	2.37
	N=388416 NCHRP 12-76 Method	25.36	22.99	24.86	25.37	27.22	27.33	25.52

Table 4 % Error and Estimated Error of Proposed Approach for Midspan Moment

Span length		15m	30m	67m	76m	85m	94m	Average
4 week μ_N ; N=4	Error	0.05	0.58	1.31	1.18	0.91	0.59	0.77
	Estimated Error	3.53	2.61	2.99	2.90	3.24	2.88	3.02
4 week σ_N ; N=4	Error	3.94	7.71	8.61	12.78	14.43	15.07	10.42
	Estimated Error	15.72	13.33	13.21	13.59	12.19	11.90	13.32
20 week μ_N ; N=20	Error	0.96	0.06	0.53	1.52	2.13	1.86	1.18
	Estimated Error	5.28	4.24	3.78	4.78	4.37	4.36	4.47
20 week σ_N ; N=20	Error	4.37	4.19	2.54	7.40	8.63	10.17	6.22
	Estimated Error	15.91	15.68	12.26	16.31	12.86	12.46	14.25
48 week μ_N ; N=48	Error	0.17	0.31	1.73	1.55	1.07	0.77	0.93
	Estimated Error	3.46	4.74	3.92	5.35	4.77	5.24	4.58

Tables 2 and 3 display the errors of the NCHRP 12-76 method for comparison with the proposed method, respectively for the midspan moment and support shear. Note that although the N values for these two methods are different but they represent the same time lengths for projection and thus the extrapolation results are comparable. Comparison of these results shows that the proposed method is more reliable with smaller and sometimes much smaller errors. The error of the NCHRP 12-76 method is often 10 times larger or more than the proposed method. To simultaneously see the reliability of the estimates of μ_N and σ_N , Fig.1 plots the PDF $f_N(x)$ based on the real data, compared with the proposed method and the NCHRP 12-76 method. The latter is seen to always underestimate μ_N and σ_N . It appears that the process of extrapolation from the Normal PDF $f_I(x)$ to the asymptotic Extreme I PDF $f_N(x)$ may bear significant error.

This comparison also exhibits the effect of N in the computation. As discussed earlier, larger N values require higher quality data that is difficult to achieve, which leads to a lower reliability indicated by larger errors in these results. Tables 4 and 5 exhibit the estimated error defined in Eqs.7 and 8 compared with the observed error using the WIM data. It is seen that the former is in a reasonable agreement with the latter, being offered as a practical evaluation tool for the extrapolation method. For example, using 26 weeks as the basic period for $f_I(x)$, extrapolating to 75 year means $N=150$. With this relatively smaller N value, possible error can be so estimated for a quantitative evaluation.

Table 5 Error and Estimated Error of Proposed Method for Support Shear

Span length		15m	30m	67m	76m	85m	94m	Average
4 week $\mu_N, N=4$	Error	0.79	0.95	1.39	0.68	1.18	0.58	0.93
	Estimated Error	3.78	2.37	2.97	2.95	3.02	2.88	2.99
4 week $\sigma_N, N=4$	Error	14.62	11.50	8.75	9.67	11.48	13.40	11.57
	Estimated Error	15.24	12.40	15.82	11.03	11.08	13.93	13.25
20 week $\mu_N, N=20$	Error	1.56	1.94	2.22	1.95	1.11	1.68	1.74
	Estimated Error	4.35	3.64	3.51	4.67	3.66	3.75	3.93
20 week $\sigma_N, N=20$	Error	9.85	4.49	11.55	10.19	3.83	20.00	9.98
	Estimated Error	13.70	12.87	11.79	13.59	12.20	12.44	12.77
48 week $\mu_N, N=48$	Error	2.20	2.04	2.47	3.12	1.75	2.65	2.37
	Estimated Error	4.16	4.70	4.93	4.84	5.33	5.10	4.84

Figure 1 graphically exhibits the differences between the future PDF based on the WIM data and the predicted PDFs respectively using the proposed approach and the NCHRP 12-76 method for the midspan moment in two simply supported spans of highway bridge. They show that the NCHRP 12-76 method under-predicts the mean value and standard deviation of future maximum values, which can lead to un-conservative design.

4.2 New York Data, Henan Data, and Jiangxi Data

The New York data set is provided by New York State Department of Transportation from Site 8280 with two lanes simultaneously recorded. It includes a total of about 0.33 million trucks over a period of more than 4 years between 2003 and 2008. The mostly loaded driving lane is used for projection, with multiple presence of trucks covered in the same way as for the California data. Similar results were observed as in Tables 1 through 5, also with comparisons of the proposed and NCHRP 12-76 methods, again indicating higher reliability of the former. Due to limit on space, more details are not shown here. The observed agreement between the proposed approach and real data also supports the estimated error as a good index for practical evaluation of extrapolation using the proposed method.

The Henan data set was collected over about 25 months in 2005 to 2007, including about 2.42 million trucks and obtained from Henan Province Department of Transportation in China. The WIM station records three lanes simultaneously, including a shoulder lane that had much fewer trucks recorded. The driving lane that is most intensively traveled is focused here, and multiple presence of trucks is also included. This data set, along with the next one, provides an application opportunity of the proposed method for different data sources. The proposed method performed more reliably as seen similarly in the previous data sets, while more details are not tabulated here due to space limit. Again, it often has 10 times smaller errors compared with the NCHRP 12-76 method.

The Jiangxi data set was obtained from Ganding Highway Bureau in Jiangxi Province, China, recorded over a period of about 30 months in 2005 to 2007. The data set includes about 2.02 million trucks on all available three lanes simultaneously recorded. The driving lane was most heavily loaded and is used here for application, with both “side by side” and “front and back” multiple presences also covered in the same way as for the Henan data. The estimated error also exhibits the observed trend of error increasing with N and being smaller for μ_N than for σ_N . Therefore, it can serve as an index for extrapolation evaluation. Due to space limit, further details are not exhibited here.

5 APPLICATIONS FOR CODE CALIBRATION

The proposed approach has also been applied in calibrating load factors for evaluating existing highway bridges in China consistent with their design requirement and in developing multiple presence factors for the AASHTO design specifications improved using measured truck weights. More details of the former are presented in (Fu and You 2009) and the latter in (Fu *et al.* 2011).

6 ACKNOWLEDGMENTS

The work reported here was funded by the US National Cooperative Highway Research Program, Michigan Department of Transportation, the CCCC Highway Consultants Co., Ltd in China, and the Transportation Construction and Science Program of the Western Regions of China— (2008 318 494 04's research task). This support is gratefully appreciated. We also would like to express our gratitude to the following agencies that provided WIM data used in the work: California Department of Transportation in US, Ganding Highway Bureau in Jiangxi Province in China, Henan Province Department of Transportation in China, and New York State Department of Transportation in US.

7 REFERENCES

- AASHTO *LRFD Bridge Design Specifications*, 6th Edition, Washington, D.C., 2012
 AASHTO *Manual for Bridge Evaluation*, 2nd Ed, Washington, D.C., 2011
 Fu,G. "Variance Reduction by Truncated Multimodal Importance Sampling", *Structural Safety*, Vol.13, 1994, pp.267-283
 G.Fu and J.You "Truck Loads and Bridge Safe Capacity Evaluation in China" *ASCE Journal of Bridge Engineering*, Vol.14, No.5, p.327-336, Sept. 2009
 Fu,G., Liu,L., and Bowman,M "Multiple Presence Factor for Truck Load on Highway Bridges", (in press) *ASCE Journal of Bridge Engineering*, 2012, online published October 24, 2011
 Gumbel, E.J. *Statistics of Extreme*, Columbia University Press, New York, 1958
 Kulicki,J., Prucz,Z., Clancy,C.M. D.R.Mertz, and Nowak, A.S. "Updating the Calibration Report for AASHTO LRFD Code" Final Report for NCHRP 20-7/186, Jan. 2007
 Nowak,A.S. *Calibration of LRFD Bridge Design Code, NCHRP Report 368*, Transportation Research Board, National Academy Press, Washington D.C. 1999
 Sivakumar,B., Ghosn,M., and Moses,F. "Protocols for Collecting and Using Traffic Data in Bridge Design", Draft Final Report for NCHRP Project 12-76, 2008

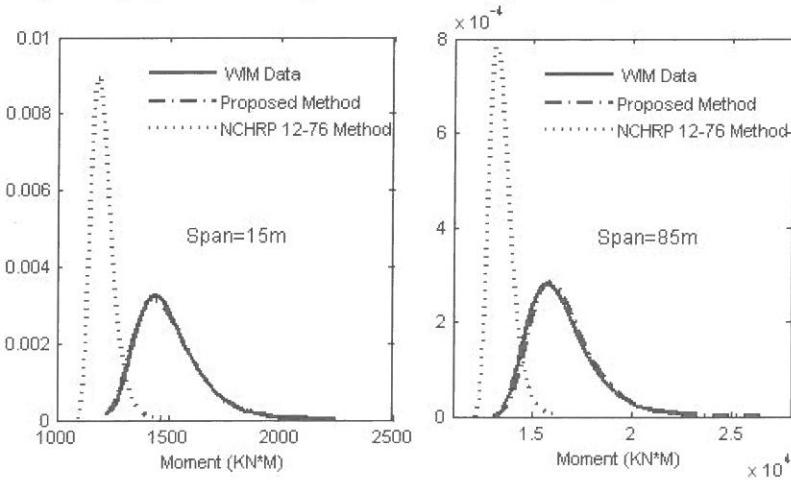


Figure 1 Comparison of Extrapolated PDF by Two Methods for Midspan Moment of Two Spans (California Data)

Structural reliability methods for wind power converter system component reliability assessment

E.E. Kostandyan & J.D. Sørensen
Aalborg University, Aalborg, Denmark

ABSTRACT: Wind power converter systems are essential subsystems in both off-shore and on-shore wind turbines. It is the main interface between generator and grid connection. This system is affected by numerous stresses where the main contributors might be defined as vibration and temperature loadings. The temperature variations induce time-varying stresses and thereby fatigue loads. A probabilistic model is used to model fatigue failure for an electrical component in the power converter system. This model is based on a linear damage accumulation and physics of failure approaches, where a failure criterion is defined by the threshold model. The attention is focused on crack propagation in solder joints of electrical components due to the temperature loadings. Structural Reliability approaches are used to incorporate model, physical and statistical uncertainties. Reliability estimation by means of structural reliability methods and simulation are implemented for the power converter system and results are compared. Based on an illustrative example, it is shown that structural reliability methods are appropriate techniques to use for further convertor system reliability estimation studies.

1 INTRODUCTION

Structural reliability methods are powerful tools for reliability levels estimation. These approaches are based on limit state equations, where parameters and models uncertainties are taken into the account. In this paper, a time dependent limit state equation is used and First Order Reliability Method (FORM) is employed for reliability level estimation. The results are compared with simulation results using the same limit state equation.

Section 2 details the preliminaries of the study with detailing on convertor system, components structure, physics of failure model as well as deterministic and probabilistic approaches. Section 3 outlines the FORM approach, details its application for the particular example, reveals the results and compares the FORM results with simulation results.

2 PRELIMINARIES

2.1 *Wind turbine convertor system*

Wind Turbine (WT) power convertor systems are a 'bridge' between the generator and the power grid. The convertor system is an interface for variable voltage amplitudes and frequencies at generator side to adapt for the stable levels of voltage amplitudes and frequencies at the grid side. Therefore, convertor system is considered to have two parts: generator side and grid side. Multilevel convertor systems are used in practice, which consists of Insulated Gate Bipolar Transistors (IGBT) modulus. An IGBT module is a three-terminal power semiconductor device (PSD), which consists of diodes and silicon chips. These components are mainly comprised from semiconductors, aluminum, copper and ceramics (see Bailey et al. 2007, Ciappa 2002).

Converter system designs and IGBT modules differ depending on grid outputs and WT rated power. In this paper, based on Kostandyan & Ma (2012) a two level converter topology, see Figure 1, is used. It is based on the 2.3 MW Siemens WT with 3 m/s cut in and 25 m/s cut out wind speeds.

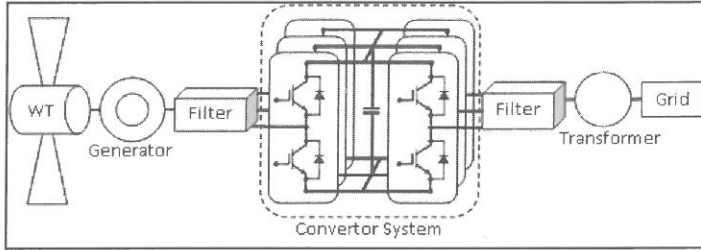


Figure 1: Two level converter topology in wind generating system

The selected IGBT module was FZ3600R17HP4_B2, see Figure 2a. The FZ3600R17HP4_B2 IGBT module consists of 24 parallel connected chips. In Kostandyan & Ma (2012) it was assumed that these chips were Infineon Technologies SIGC186T170R3 chips with dimensions of 13.63 mm in length and 13.63 mm in width. The assumption was justified because selected chip parameters satisfy the selected IGBT module parameters, so it will satisfy converter system requirements. Also in Kostandyan & Ma (2012), IGBT's junction temperature is considered for grid side converter system, and minimum, maximum, mean junction temperatures depending on wind speeds were presented for an ambient temperature of 28°C, see Figure 2b.

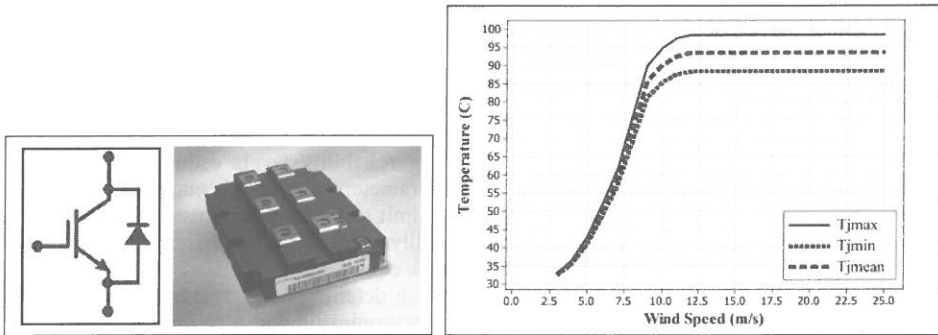


Figure 2: (a) FZ3600R17HP4 IGBT module; (b) Grid side IGBT's junction temperature vs. wind speed, ambient temperature 28°C

2.2 Physics of failure in solder cracking under silicon die

In Ciappa (2002) the selected IGBT chip failure mechanisms as well as the architecture were presented. Bond wire lift off, bond wire heel cracking, solder joint cracking (solder fatigue) between silicon chip and DCB upper layer copper as well as between DCB lower layer copper and mounting plate were the four most common failure modes. In Kostandyan & Sorensen (2012a) the model was developed for solder joint cracking (solder fatigue) between silicon chip and DCB upper layer copper failure mode.

This model has a mixed Coffin-Manson and Arrhenius form model and estimates the average accumulated plastic strain based on temperature loading by the following form:

$$\Delta \varepsilon_p = A(\Delta T)^B (\alpha_{Cu} - \alpha_{Si}) e^{\left(-\frac{Q}{RT_m}\right)} \quad (1)$$

where A, B are constants, Q is activation energy, R is the universal gas constant, α_{Cu} and α_{Si} are CTE at 20° C for copper and silicon, ΔT and T_m are the temperature range and temperature mean.

Based on finite element analysis data in Yin et al. (2008), the constants in (1) were estimated (see Kostandyan & Sorensen 2012a and Table 1) for SnAg solder. In this paper, it is assumed that estimated parameters have values as shown in Table 1. However, it is noted that more accurate parameters are reported in Kostandyan & Ma (2012) and it is possible to estimate the parameters experimentally. As far as this research is concentrated on structural reliability methods illustration, parameters precisions have secondary importance.

Table 1: Estimated parameters for the model described in (1), temperature in Kelvin

Model Parameters	Estimates
$\log(A(\alpha_{Cu} - \alpha_{Si}))$	-416.16
B	74.122
Q/R	4,610.0

The required number of cycles for a crack to reach the length L in solder interconnect can be expressed by:

$$N_L(\Delta \varepsilon_p) = \frac{L}{a(\Delta \varepsilon_p)^b} \quad (2)$$

where L is the solder interconnect length in millimeters, a, b are constants, N_L is the required number of cycles to failure or number of cycles for the crack to reach L and $\Delta \varepsilon_p$ is the average accumulated plastic strain per cycle.

In Lu et al. (2007) the constants a, b were estimated ($a=0.00562, b=1.023$) for SnAg solder interconnect between baseplate and ceramic for the defined failure criteria as 20% reduction of the total interconnect area. In Bailey et al. (2007), Lu et al. (2009) and Yin et al. (2008) the same constants were used for further research.

This paper is focused on crack propagation in solder joints under silicon die. It is assumed that solder thicknesses either between die and ceramic or ceramic and baseplate are almost the same. This assumption will allow using estimated constants a, b from Lu et al. (2007).

2.3 Deterministic damage model for reliability estimation

A deterministic damage model was presented in Kostandyan & Sorensen (2012a) and applied to the estimate reliability level for each temperature profile based on Palmgren-Miner rule, see Madsen & Krenk (1986). Component stresses were expressed by temperature fluctuations. Pair of $\Delta T_i, T_{m,i}$ were defined as the temperature range and temperature mean at level i , such that the damage level at time t could be expressed as:

$$D(t) = \sum_{all\ i \leq t} \frac{n_i(\Delta T_i, T_{m,i})}{N_i(\Delta T_i, T_{m,i})} \quad (3)$$

and the deterministic time to failure would be defined by $t = t_f$, where $D(t_f) = 1$.

Combining (1), (2) and (3) deterministic damages were estimated based on IGBT's junction temperature profiles. Failure was defined by crack length to reach to the predetermined length associated with 20% reduction of the total interconnect area.

Based on wind speed profile and junction temperature estimates for each wind speed defined in Kostandyan & Ma (2012), the IGBT's junction temperature for grid side convertor system

was estimated. Next, a rainflow counting algorithm was applied to the IGBT junction temperature profile in order to estimate the pairs of $\Delta T_i, T_{m,i}$. It was assumed in Kostandyan & Ma (2012) that there was enough time for an ambient temperature to propagate into the IGBT module. This means that an ambient temperature affects linearly on IGBT-operational junction temperature. The operational wind profile contains wind speeds that are between cut-in and cut-out speeds. Data for wind speeds and ambient temperatures were available for 3-hour averages at 10 meter height, which were selected for a 5MW power WT located near Thyborøn, Denmark with latitude 56.71° and longitude 8.20°. The wind profile power law was used to estimate the operational wind speeds at 100 m height with a wind shear exponent of 0.1. Also, it was assumed that the SIGC186T170R3 chip has dimensions of 13.63 mm in length and 13.63 mm in width, so 20% shrinkage of the total solder interconnected area under the chip would be defined by crack length of 0.72 mm.

2.4 Probabilistic damage model for reliability estimation

Kostandyan & Sorensen (2012b) and Kostandyan & Sorensen (2011) described the parameters in the damage accumulation model to be estimated. Uncertainty and variability that were emerged from parameters estimation should be accounted for in the reliability assessment as well as model uncertainties.

(1) and (2) are reformulated in order to include randomness by considering uncertainties and be written:

$$\Delta \varepsilon_p' = \Delta \varepsilon_p \varepsilon_m = A(\Delta T)^B (\alpha_{Cu} - \alpha_{Si}) e^{\left(-\frac{Q}{RT_m}\right)} \varepsilon_m \quad (4)$$

$$N_L'(\Delta \varepsilon_p') = \frac{L}{a \varepsilon_a (\Delta \varepsilon_p')^b} \quad (5)$$

where ε_a models estimation uncertainty associated to the constant "a" and ε_m is the model uncertainty associated with eq (1).

Reliability estimation by structural reliability methods incorporates estimated parameters variabilities through limit state equation(s). The limit state equation is written:

$$g(t, \Delta m, \varepsilon_a, \varepsilon_m) = \Delta m - \sum_{i=1}^n \frac{n_i(\Delta T_i, T_{m,i})}{N_L'(\Delta T_i, T_{m,i}, \varepsilon_a, \varepsilon_m)} \quad (6)$$

where Δm models the uncertainty associated to Miner's rule (linear damage model uncertainty). Mean values, standard deviations and distributions are summarized in Table 2, where the assumptions are defined by (*).

Table 2. Parameters for stochastic variables

Stochastic Variable	Distribution	Mean	Standard deviation
Δm	Normal*	1	0.1*
ε_a	LogNormal*	1	0.5*
$Ln(\varepsilon_m)$	Normal	0	0.36

(*) represents the assumption regarding the parameter

3 FIRST ORDER RELIABILITY METHOD

The reliability index (β) as function of time, t , is determined by FORM, see e.g. Madsen & Krenk (1986). Using the limit state equation defined in (6), the cumulative distribution, probability density and hazard functions are obtained by:

$$F_f(t) = P(g(t, \Delta m, \varepsilon_a, \varepsilon_m) \leq 0) = \Phi(-\beta(t)) \quad (7)$$

$$f(t) = \frac{d}{dt} F_f(t) \quad (8)$$

$$h(t) = \frac{f(t)}{1 - F_f(t)} \quad (9)$$

FORM allows estimating measures of the relative importance of the stochastic variables used in the stochastic modeling. The limit state equation in (6) was employed for reliability estimation by FORM. The same operational wind speed data as in Kostandyan & Ma (2012) and junction temperature relationship with wind speeds, see Figure 2b, were used to estimate junction temperature profiles by taking into the account ambient temperature linear effect, see Figure 3a.

Based on these profiles the rainflow counting algorithm was applied and pairs of $\Delta T_i, T_{m,i}$ were estimated for the given time period, e.g. see Figure 3b for maximum junction temperature profile until 240 hrs).

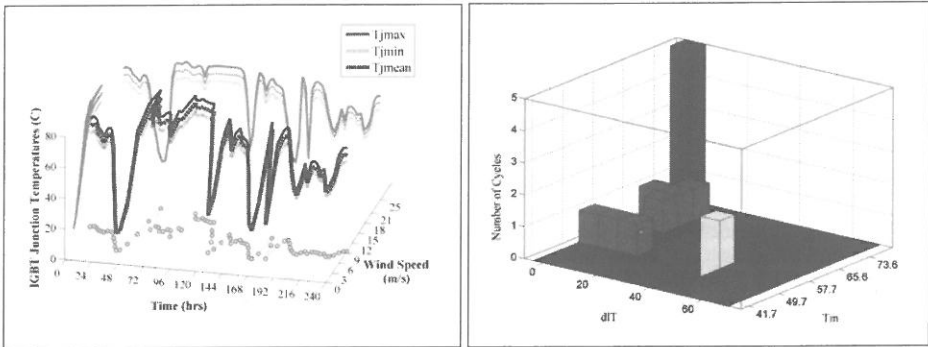


Figure 3: (a) Wind speeds vs. junction temperatures vs. time; (b) Rain flow counting for Tjmax profile until 240 hrs of operation

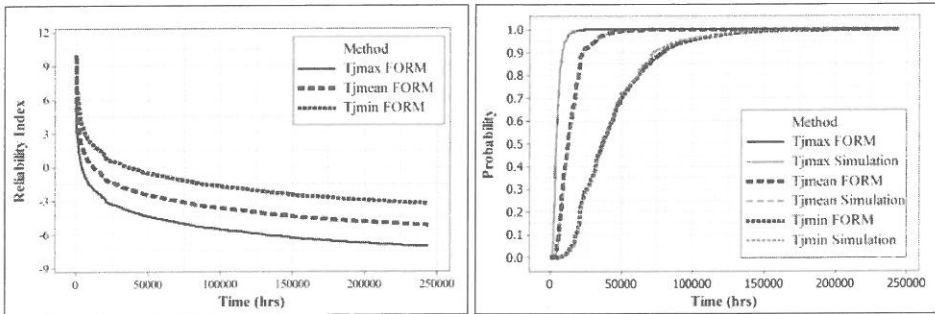


Figure 4: (a) Reliability indexes based on all operational junction temperatures; (b) Cumulative probability of failures based on FORM and simulation results

The limit state equation in (6) was defined in time domain based on the beginning of wind speed profile to the end of each time interval, with 240 hours increment. MATLAB functions were created that handle transformation, time dependent limit state equations, numerical differentiation and reliability index estimation. The difference quotient in numerical differentiation was set to 10^{-8} and error for reliability index estimation was set to 10^{-3} . Reliability indices based on each operational junction temperature profile during the time were found and depicted in Figure 4a.

The reliability indices decrease in time for all exposed profiles, indicating an increase in probability of failures during the time. The rates of decrease between exposed profiles are different due to the severity of them.

The simulation techniques are used to estimate reliability levels for each IGBT-operational junction temperature profiles based on 1000 simulation runs. These results are compared with results from FORM in this paper. Comparisons of the results have been performed and exactness has been observed. Estimated reliability indices from each junction temperature profile are converted by standard normal distribution function to their corresponding probability values. Plots of cumulative distribution functions are depicted in Figure 4b. It is seen that FORM estimates reliability levels with high accuracy.

The non-parametric Kaplan–Meier estimation method was used to estimate empirical cumulative distribution functions. Based on this method B10 (or L10, 90% reliability level) fatigue lives were estimated from simulation results and linear interpolation was used to find B10 fatigue lives based on FORM, see Table 3.

Table 3: Probabilistic fatigue failure times comparison

IGBT-operational junction temperature profile	Simulation based B10 fatigue failure times (hrs)	FORM based B10 fatigue failure times (hrs)
Tjmax	2273	2253
Tjmin	18613	17642
Tjmean	6075	5843

A damage caused from the highest temperature (Tjmax) profile will shorten useful life much more than the damage caused by the mild temperature (Tjmin) profile. Such a consequence will influence on B10 fatigue life depending on the exposed temperature profile.

In this paper, based on the same wind speed profile the junction temperature profiles were estimated. A different wind speed profile will result in different junctions temperatures and thus different fatigue lives would be estimated. However, two key points are:

- the shortest (longest) fatigue life will always be observed under the Tjmax (Tjmin) temperature profile irrespective of wind profile
- the wind speed profile for the particular location will have established autocorrelation factor and aleatory variability, assuming steady environment (e.g. no climate change effect, no new constructed high buildings close to the turbines that might change wind speeds, etc.)

Based on the applied FORM, the omission sensitivity factors are estimated for the stochastic variables (see Table 2). The temperature profile did not have effect on sensitivity factors and estimated values in time were presented in Table 4.

Table 4: Omission sensitivity factors

Stochastic Variable	Mean
Δm	1.012
ε_n	1.600
ε_m	1.257

It is seen that the uncertainty related to the constant “a” in (2) is important. A 60% of error will be accrued in the reliability index estimation if constant “a” in (2) is assumed deterministic. Therefore, it is desirable to allocate resources for estimating especially the constant “a” in (2) as accurately as possible.

4 CONCLUSION

The paper demonstrates application of structural reliability techniques for reliability assessment of electrical component. FORM was used to evaluate the reliability of the grid side IGBT chip, used in two level wind generating converter systems. Failure was defined by the fatigue crack length of 0.72 mm, which corresponds to 20% shrinkage of the total solder interconnected area under the chip. A time dependent limit state equations was formulated based on physics of failure model and the linear damage accumulation rule. Three temperature-loading profiles were constructed via wind profile and reliability levels were estimated under the exposure of each profile.

Traditionally reliability analyses of electrical components are made based on classical reliability methods that do not allow for a more detailed modeling of aleatory and epistemic uncertainties. This is possible using structural reliability techniques which further allows sensitivity studies to be made without much extra effort.

Close estimates of reliability levels are achieved by FORM in comparison with simulation results. This indicates that for the further research, based on the described updated limit state equation, FORM is the appropriate technique to use. Advantages of the FORM vs. simulation are short computational time, possibility for parameters sensitivity analysis and ability for factors calibration. One of the disadvantages of the FORM in the particular application is achieving result without ability to visualize damage behavior and degradation paths. However, for a probabilistic operation and maintenance strategy application these visualizations are not necessary and a software module might be integrated into WTs that might do calculations based on actual / observed loads.

This research is conducted in order to illustrate the application of structural reliability methods and it should be noted that the determined failure times / rates not necessary represent the real-life operating lifetimes, this is due to the fact that the some parameters distributions and COVs were assumptions.

ACKNOWLEDGEMENTS

This work has been (partially) funded by Norwegian Centre for Offshore Wind Energy (NOR-COWE) under grant 193821/S60 from Research Council of Norway (RCN). NORCOWE is a consortium with partners from industry and science, hosted by Christian Michelsen Research.

REFERENCES

- Bailey, C., Lu, H., & Tilford, T., 2007. Predicting the Reliability of Power Electronic Modules. *Proceedings, 8th International Conference on Electronics Packaging Technology*, Shanghai, China.
- Ciappa, M., 2002. Selected failure mechanisms of modern power modules. *Microelectronics Reliability*, 42: 653-667.
- Kostandyan, E., & Ma, K., 2012. Reliability estimation with uncertainties consideration for high power IGBTs in 2.3 MW wind turbine converter system. *Microelectronics Reliability*, (in press).
- Siemens wind turbine parameters, March 2012, http://www.energy.siemens.com/mx/pool/hq/power-generation/wind-power/SWT-2.3-113-product-brochure_EN.pdf
- Kostandyan, E. & Sørensen, J.D., 2012a. Reliability of wind turbine components — solder elements fatigue failure. *Proceedings, 17th Reliability and Maintainability Symposium*, Reno, Nevada, USA.
- Lu, H., Tilford, T., Bailey, C., & Newcombe, D., 2007. Lifetime prediction for power electronics module substrate mount-down solder interconnect. *Proceedings, High Density Packaging and Microsystem Integration*.
- Lu, H., Bailey, C., & Yin, C., 2009. Design for reliability of power electronics modules. *Microelectronics Reliability*, 49: 1250-1255.

- Yin, C.Y., Lu, H. , Musallam, M. , Bailey, C. , & Johnson, C.M., 2008. A physics-of-failure based prognostic method for power modules. *Proceedings, 10th Electronics Packaging Technology Conference*, Singapore.
- Madsen, H.O., Krenk, S., & Lind, N.C., 1986. *Methods of Structural Safety*. London, Prentice-Hall.
- Kostandyan, E.E., & Sørensen, J.D., 2012b. Weibull parameters estimation based on physics of failure model. *Proceedings, IIE Industrial and Systems Engineering Research Conference*, Orlando, Florida, USA.
- Kostandyan, E.E., & Sørensen, J.D., 2011. Reliability assessment of solder joints in power electronic modules by crack damage model for wind turbine applications. *Energies*, 4: 2236-2248.
- Hasofer, A.M. & N.C. Lind, 1974. An exact and invariant first order reliability format. *Journal of the Engineering Mechanics Division*, 100: 111-121.

Reliability of offshore wind turbines subject to seismic loading

M. Mardfekri

Texas A&M University, College Station, Texas, USA

P. Gardoni

University of Illinois at Urbana-Champaign, Illinois, USA

ABSTRACT: Probabilistic models are developed to predict shear and moment demands on wind turbine support structures subject to seismic excitations, and environmental (wind, wave, and current) and operational loadings. The probabilistic models are formulated starting from existing deterministic models and developing correction terms that capture the inherent bias. The correction terms and a model error are assessed using data obtained from detailed three dimensional nonlinear finite element analyses of a set of wind turbine systems that consider different design parameters. The finite element analyses account for the aerodynamic damping of operating wind turbines and the dynamic soil-structure interaction. The proposed probabilistic seismic demand models provide unbiased predictions of the seismic demand on support structures and properly account for the underlying uncertainties. The developed demand models are used to compute fragility estimates of an example support structure defined as the conditional probability of not meeting specified capacity levels.

1 INTRODUCTION

Extensive installation of offshore wind farms for electricity production in moderate to high seismic regions in the United States and other countries has raised a new concern about the safety of wind turbine support structures subject to seismic loads (Prowell & Veers 2009). The demands on the support structure of wind turbines are typically determined using computational models. Several aeroelastic simulation codes such as FAST (Jonkman & Buhl Jr. 2005) and ADAMS (Laino & Hansen 2001) are used in the industry to simulate fatigue, aerodynamics, structural dynamic response, and turbulence. The main limitation of these simulators is that they are not capable of modeling the nonlinear foundation behavior and the soil-structure interaction.

Mono-piles are common foundations for offshore wind turbine support structures installed in water depths less than 30 meters, which is the focus of this paper. Typical methods for the analysis of laterally loaded single piles in general are based on Winkler (elastic) foundation models, or continuous models accounting for the coupling of forces and displacements in the soil along the pile. For nonlinear analyses, the p-y method (Matlock 1970), is the most commonly used foundation model. However, depending on the pile diameter and soil type, the p-y method may result in inaccurate responses. This is true in particular for the pile sizes typical of foundations of offshore wind turbines (Mardfekri et al. 2012).

Mardfekri & Gardoni (2012) developed probabilistic model for the deformation, shear and moment demands on the support structure of offshore wind turbines subject to wind, wave, current and turbine operational loadings properly accounting for the nonlinear soil-structure interaction. However, with the extensive installation of wind farms in seismic regions, it is important to consider also seismic loading. Witcher (2005) showed a significant difference in the response of wind turbine support structures in different load cases including continuous operation throughout the earthquake, emergency shutdown initiated during the earthquake and parked

throughout the earthquake. He concluded that this difference is due to the absence of aerodynamic damping in the parked condition and after the emergency shutdown. This paper develops shear and moment demand models for the support structure of offshore wind turbines subject to seismic loading in addition to environmental (wind, wave, and current) and operational loadings. The wind turbine is considered to be operating throughout the earthquake and the aerodynamic damping due to the operation of the turbine is included in the dynamic response analyses of wind turbine support structures. The proposed demand models are then used to assess the seismic fragility of an example offshore wind turbine support structure for given values of the intensity measure of the loading (i.e., the mean wind speed, significant wave height and spectral acceleration.)

2 PROBABILISTIC DEMAND MODELS

Ideally a model should incorporate all available sources of information including the rules of physics and mechanics, and experimental and field data. To incorporate the rules of physics and mechanics and facilitate the acceptance of the proposed models, following Gardoni et al. (2002, 2003), we develop probabilistic demand models by adding a correction term to a selected existing deterministic demand model. A probabilistic demand model for a system having K different demands is formulated as

$$D_k(\mathbf{x}, \mathbf{w}, \Theta_k) = \hat{d}_k(\mathbf{x}, \mathbf{w}) + \gamma_k(\mathbf{x}, \mathbf{w}, \theta_k) + \sigma_k \varepsilon_k \quad k = 1, \dots, K \quad (1)$$

where $D_k(\mathbf{x}, \mathbf{w}, \Theta_k) = k^{th}$ probabilistic demand model, \mathbf{x} = vector of material properties, structural dimensions and boundary conditions, $\mathbf{w} = (W_s, H_s, S_a) =$ vector of measures of external loading, including the mean wind speed (W_s), significant wave height (H_s), and spectral acceleration (S_a), $\Theta_k = (\theta_k, \sigma_k)$, in which $\theta_k =$ vector of unknown model parameters, $\hat{d}_k(\mathbf{x}, \mathbf{w}) =$ selected deterministic demand model, $\gamma_k(\mathbf{x}, \mathbf{w}, \theta_k) =$ correction term, and $\sigma_k \varepsilon_k =$ model error, in which $\varepsilon_k =$ random variable with zero mean and unit variance and $\sigma_k =$ standard deviation of the model error. In this paper, $k = v$ or m , for the shear or moment demand, respectively. In formulating the model in Eq. (1), we employ a logarithmic transformation of the data to satisfy the homoskedasticity assumption (i.e., σ_k is constant), the normality assumption (ε_k follows the standard normal distribution), and the additive form used in the equation. The correction term, $\gamma_k(\mathbf{x}, \mathbf{w}, \theta_k)$, is added to incorporate the missing or correct for the misrepresented terms in $\hat{d}_k(\mathbf{x}, \mathbf{w})$. It is written as

$$\gamma_k(\mathbf{x}, \mathbf{w}, \theta_k) = \sum_{i=1}^p \theta_{ki} h_{ki}(\mathbf{x}, \mathbf{w}) \quad (2)$$

where $\theta_k = [\theta_{ki}]$, $h_{ki}(\mathbf{x}, \mathbf{w}) =$ normalized explanatory functions that might be significant in correcting $\hat{d}_k(\mathbf{x}, \mathbf{w})$, and $p =$ the number of unknown model parameters. The vector of model parameters, Θ_k , can be estimated following a Bayesian approach using available data.

In this section, we develop probabilistic shear and moment demand models for horizontal axis offshore wind turbines rated between 0.5 and 5 megawatts (medium to large wind turbines). The wind turbines of interest in this paper are supported by a tubular steel tower, which is seated on a steel mono-pile foundation at the base and installed in water depths less than 30 meters. We predict shear and moment demands on the support structures subject to seismic excitation, in addition to wind, wave, current and turbine operational loadings.

2.1 Deterministic demand model

An ideal deterministic model should be simple and yet accurate, and commonly accepted in practice. Because of these reasons, Mardfekri & Gardoni (2012) used the program FAST to compute deterministic predictions of the demands on the support structure of wind turbines subject to environmental and operational loadings. FAST employs a combined modal and multibody dynamics formulation to simulate the aerodynamics and structural response of wind turbines. For given values of the mean wind speed and turbulence intensity, a time history of wind speed is generated internally to FAST by TurbSim and used as an input for the dynamic analysis in FAST. TurbSim uses a statistical model to numerically simulate time series of three-component wind-speed vectors (Jonkman 2009). TurbSim supports the IEC Kaimal model (Kelley & Jonkman

2007) that is used in this study. More details on the Kaimal model can be found in Mardfekri & Gardoni (2012). In addition, FAST supports the JONSWAP/Pierson-Moskowitz spectrum (Dean & Dalrymple 1991) to model linear irregular waves for given significant wave height and wave peak period. It then uses the Morison's equation to determine the hydrodynamic forces on the tower. Current loading is also incorporated in the Morison's Equation. Additional details on the modeling of the wave and current loading can be found in Mardfekri & Gardoni (2012).

Following a consistent approach to the one that Mardfekri & Gardoni (2012) used to generate environmental loadings, for given intensity and duration parameters and frequency content of the ground motion, we generate synthetic ground motions using a stochastic model proposed by Rezaeian & Der Kiureghian (2010). Generated ground motions are then used as input for dynamic analyses also carried out using FAST.

2.2 Model correction

To construct $\gamma_k(\mathbf{x}, \mathbf{w}, \theta_k)$, we select $h_{k1}(\mathbf{x}, \mathbf{w})=1$ to capture potential constant bias in the model, and $h_{k2}(\mathbf{x}, \mathbf{w})=d_k(\mathbf{x}, \mathbf{w})$ to capture any possible under- or over-estimation of the deterministic model. To capture possible dependences of the residuals on foundation, environment and earthquake parameters, additional explanatory functions are also considered as shown in Table 1.

Table 1. Explanatory functions for demand models

Explanatory function	Formula	Parameters
h_{k1}	1	$k = v$ or m
h_{k2}	\hat{d}_k	\hat{d}_k = Deterministic shear or moment demand
h_{k3}	$\ln(W_s \cdot T_n / H_H)$	W_s = Mean wind speed; H_H = Hub height T_n = Natural period of the support structure
h_{k4}	$\ln(IT_w)$	IT_w = Wind turbulence intensity
h_{k5}	$\ln(H_s / H_H)$	H_s = Significant wave height
h_{k6}	$\ln(T_n / T_n)$	T_n = Wave peak period
h_{k7}	$\ln(S_a / g)$	S_a = Spectral acceleration; g = Ground acceleration
h_{k8}	$\ln(S_d / H_H)$	S_d = Spectral displacement
h_{k9}	$\ln(PGA / g)$	PGA = Peak ground acceleration
h_{k10}	$\ln(PGV \cdot T_n / H_H)$	PGV = Peak ground velocity
h_{k11}	$\ln(PGD / H_H)$	PGD = Peak ground displacement
h_{k12}	$\ln[2\pi PGV / (PGA \cdot T_n)]$	
h_{k13}	$\ln[2\pi PGD / (PGV \cdot T_n)]$	
h_{k14}	$\ln(RD / H_H)$	RD = Rotor diameter
h_{k15}	$\ln(C_s / C_{smax})$	C_s = Soil shear wave velocity; $C_{smax} = 194.594$ m/s
h_{k16}	$\ln(C_{soil} / E_{soil})$	C_{soil} = Soil cohesion; E_{soil} = Soil modulus of elasticity
h_{k17}	$\ln[\tan(\phi_{soil})]$	ϕ_{soil} = Soil friction angle
h_{k18}	$\ln(K_t / K_f)$	K_t = Tower stiffness; K_f = Foundation stiffness

To develop parsimonious probabilistic demand models, we desire to keep only the explanatory functions that are strictly needed. Therefore, a step-wise deletion process is used to identify the important functions among the candidate ones listed in Table 1. In this process the model is reduced by the deletion of unimportant explanatory functions based on the posterior statistics of model parameters θ_k and σ_k . More details on step-wise deletion process are presented in Gardoni et al. (2002). Due to the lack of available data needed to conduct the statistical analysis required to estimate the model parameters, we generate a database of virtual experiments using accurate non-linear dynamic analyses of offshore wind turbine support structures as explained next.

2.3 Virtual experiment data

A set of representative configurations is selected to generate the virtual experiments. The representative configurations are selected by using a "space filling" experimental design technique to ensure that the configurations have a good coverage of the design space. For this purpose we use a Latin hypercube sampling technique (McKay et al. 1979). A total of 100 configurations are gener-

ated. Table 2 presents the variables considered to characterize each wind turbine configuration and their ranges.

Table 2. Geometrical, mechanical and loading parameters used in experimental design

Property	Ranges	Property	Ranges
Rotor diameter, RD (m)	40 - 126	Soil elasticity modulus, E_{soil} (MPa)	13 - 200
Tower height, H_t (m)	40 - 80	Friction between pile and soil, μ	0.2 - 0.3
Tower top diameter, D_1 (m)	1.9 - 4.0	Soil type	Clay Sand
Tower base diameter, D_2 (m)	3.0 - 6.0	Soil cohesion, C_{soil} (kPa)	10 - 200 0 - 80
Tower diameter to thickness ratio	100 - 200	Soil friction angle, ϕ_{soil} ($^\circ$)	10 - 25 35 - 45
Water depth, WD (m)	20 - 30	Mean wind speed, W_s (m/s)	3.0 - 30
Marin segment height, H_2 (m)	WD+(2.5 - 10)	Turbulence intensity, IT_w	0 - 0.16
Steel type	S235, S275, S355	Significant wave height, H_s (m)	1.0 - 10
Tower vibration period, T_n (s)	0.9 - 11.9	Significant wave period, T_p (s)	$3.6\sqrt{H_s} - 5.0\sqrt{H_s}$
Pile penetration, H_3	10 - 50	Rated wind speed, $W_{s,rated}$ (m/s)	10.3 - 11.7
Pile diameter to thickness ratio	50 - 100		

2.3.1 Analytical modeling

Finite element models are developed in ABAQUS (2007) to simulate the dynamic response of the support structure of typical offshore wind turbines, subject to environmental and operational loading as well as earthquake excitations. The finite element model of the support structure accounts for the aerodynamic damping by considering a 5% structural damping for the steel tower. The value for the damping is based on Witcher (2005). The tubular steel tower, marine segment and pile foundation are modeled using linear elastic 3D shell elements. Foundation nonlinearities are considered explicitly in defining soil behavior and soil-pile interactions. The Mohr-Coulomb plasticity model is used to define the nonlinear behavior of the soil. The nonlinear behavior of the soil-pile contact is modeled using "contact pair," a formulation in ABAQUS to define interaction between two bodies. An elastic-plastic Coulomb model is used to describe the nonlinear behavior of the soil-pile contact. The aerodynamics of the turbine is simulated using FAST. The time history of the forces at the top of the tower due to the wind and the operation of the turbine, resulted from the simulation in FAST, is then used in the finite element model of the support structure as an external loading in addition to wave, current and earthquake. We select ground motion records from the PEER NGA database (1999). Following Shome and Cornell (1999), the selected ground motions are subdivided into five bins based on moment magnitude (M) and the closest distance between the record location and the rupture zone (R). Each bin represents specific combinations of the earthquake characteristics and the collection of all bins captures all possible characteristics. The major horizontal ground motion component is used in the analyses.

2.3.2 Equality and lower bound data

Finite element analyses for large deformations are sensitive to how the solution method handles large displacements and second order effects. As a result, the outcomes might not always be accurate. Following Gardoni et al. (2002) and Ramamoorthy et al. (2006), the data from the virtual experiments are divided into equality and lower bound data. We consider a threshold for drift of 5%, such that if the maximum drift during one time history analysis is less than 5%, then the shear and moment data are considered as equality data. If an analysis produces a drift that exceeds 5%, then we consider the maximum shear and moment that occurred prior to reaching the 5% drift as lower bound data.

2.4 Bayesian updating

The unknown model parameters Θ_k are estimated using the Bayesian rule (Box & Tiao 1992)

$$f(\Theta_k) = \kappa L(\Theta_k) p(\Theta_k) \quad (3)$$

where $f(\Theta_k)$ = the posterior distribution of Θ_k that represents the updated state of knowledge; $L(\Theta_k)$ = the likelihood function that represents the objective information on Θ_k that comes from

the results of virtual experiments; $p(\Theta_k)$ = the prior distribution of Θ_k that reflects the state of knowledge about Θ_k prior to conducting the virtual experiments; and κ = a normalizing factor. In this paper, due to the lack of prior information, we use a non-informative prior in assessing the posterior statistics of Θ_k . The likelihood is a function proportional to the conditional probability of observing the results from the virtual experiments for a given value of Θ_k . Under the assumption of statistically independent observations and given that ε_k follows a normal distribution, $L(\Theta_k)$ is written as (Gardoni et al. 2002)

$$L(\Theta_k) \propto \prod_{\text{Equality data}} \left\{ \frac{1}{\sigma_k} \varphi \left[\frac{r_{ik}(\theta_k)}{\sigma_k} \right] \right\} \times \prod_{\text{Lower bound data}} \Phi \left[-\frac{r_{ik}(\theta_k)}{\sigma_k} \right] \quad (4)$$

where $r_{ik}(\theta_k) = D_{ik} - \hat{d}_k(\mathbf{x}_i, \mathbf{w}_i) - \dot{\gamma}_k(\mathbf{x}_i, \mathbf{w}_i, \theta_k)$ and D_{ik} = observed value for the k^{th} demand for given \mathbf{x}_i and \mathbf{w}_i .

2.5 Shear demand model

The probabilistic shear demand model is formulated as the natural logarithm of the shear demand at the base of the tower normalized by the mean value of the yield shear force, defined as $\hat{V}_y = \hat{f}_y A (3/4)(R^2 + r^2) / (R^2 + Rr + r^2)$, where \hat{f}_y = expected yield stress of steel, A = tower base cross section area, and R and r = outer and inner diameter of the tower section, respectively. The model selection results in the following probabilistic shear demand model:

$$D_v(\mathbf{x}, \mathbf{w}, \Theta_v) = \hat{d}_v(\mathbf{x}, \mathbf{w}) + \theta_{v1} + \theta_{v2} \hat{d}_v(\mathbf{x}, \mathbf{w}) + \theta_{v9} \ln \left(\frac{PGA}{g} \right) + \theta_{v18} \ln \left(\frac{K_t}{K_f} \right) + \sigma_v \varepsilon_v \quad (5)$$

Table 3 gives the posterior statistics of $\Theta_v = (\theta_{v1}, \sigma_v)$. Figure 1 shows a comparison between measured and predicted shear demands. The dashed lines in Figure 1b delimit the region within one standard deviation of the model. The figure clearly shows an improvement in predicting the demand when using the proposed probabilistic demand model.

2.6 Moment demand model

The probabilistic moment demand model is formulated as the natural logarithm of the moment demand at the tower base normalized by $\hat{M}_y = \hat{f}_y S$, where S = elastic section modulus at tower base. The model selection leads to the following model form:

$$D_m(\mathbf{x}, \mathbf{w}, \Theta_m) = \hat{d}_m(\mathbf{x}, \mathbf{w}) + \theta_{m1} + \theta_{m2} \hat{d}_m(\mathbf{x}, \mathbf{w}) + \theta_{m11} \ln \left(\frac{PGD}{H_H} \right) + \theta_{m13} \ln \left(2\pi \frac{PGD}{PGV.T_n} \right) + \theta_{m15} \ln \left(\frac{C_s}{C_{s\max}} \right) + \theta_{m18} \ln \left(\frac{K_t}{K_f} \right) + \sigma_m \varepsilon_m \quad (6)$$

Table 4 gives the posterior statistics of $\Theta_m = (\theta_{m1}, \sigma_m)$, and Figure 2 shows a comparison between measured and predicted moment demands. Comments analogous to those made on Figure 1 can also be made for the results shown in Figure 2.

Table 3. Posterior statistics of the parameters in the shear demand model

Parameter	Mean	Standard Deviation	Correlation coefficient				
			θ_{v1}	θ_{v2}	θ_{v9}	θ_{v18}	σ_v
θ_{v1}	-3.12	0.428	1				
θ_{v2}	-0.76	0.061	0.74	1			
θ_{v9}	0.30	0.040	-0.11	-0.39	1		
θ_{v18}	-0.24	0.041	0.71	0.12	-0.09	1	
σ_v	0.42	0.033	0.02	0.09	-0.17	-0.03	1

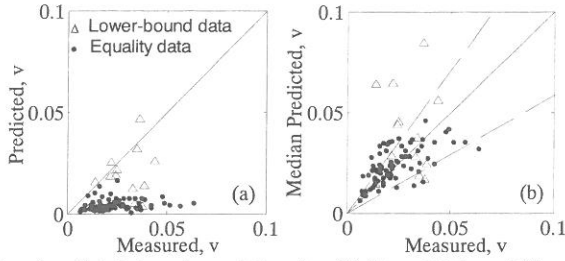


Figure 1: Measured and predicted shear demands based on (a) deterministic and (b) probabilistic models

Table 4. Posterior statistics of the parameters in the moment demand model

Parameter	Mean	Standard Deviation	Correlation coefficient						
			θ_{m1}	θ_{m2}	θ_{m11}	θ_{m13}	θ_{m15}	θ_{m18}	σ_m
θ_{m1}	-0.32	0.640	1						
θ_{m2}	-0.70	0.066	0.25	1					
θ_{m11}	0.20	0.044	0.35	-0.36	1				
θ_{m13}	-0.24	0.080	-0.49	0.46	-0.62	1			
θ_{m15}	-0.38	0.181	0.61	0.37	-0.14	0.07	1		
θ_{m18}	-0.24	0.066	0.87	0.39	-0.06	-0.10	0.68	1	
σ_m	0.45	0.033	-0.02	0.13	-0.04	0.04	-0.05	-0.03	1

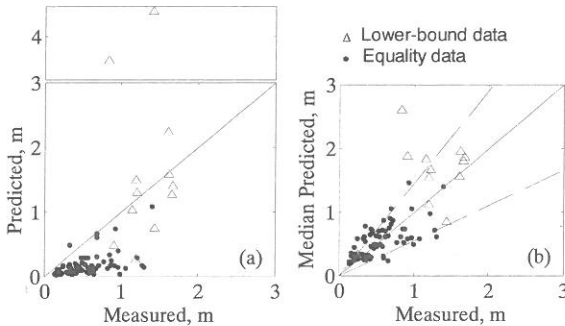


Figure 2: Measured and predicted moment demands based on (a) deterministic and (b) probabilistic models

3 PROBABILITY OF FAILURE

We now use the developed demand models to assess the fragility of an example offshore wind turbine support structure. For this purpose we consider the configuration of a typical 5-MW offshore wind turbine supported by a mono-pile installed in a 20 m water depth. The structure of interest is called NREL offshore 5-MW baseline wind turbine and its specifications are documented by Jonkman et al. (2009).

Fragility is defined as the conditional probability of attaining or exceeding a specified performance level for a given value of the vector \mathbf{w} . Following Gardoni et al. (2002), a predictive estimate of the fragility is formulated as

$$\bar{F}_j(\mathbf{w}) = P \left[\bigcup_k \{g_{kj}(\mathbf{x}, \mathbf{w}, \Theta_k) \leq 0\} \mid \mathbf{w} \right] \quad (7)$$

where $g_{kj}(\mathbf{x}, \mathbf{w}, \Theta_k)$ is the k^{th} limit state function defined as

$$g_{kj}(\mathbf{x}, \mathbf{w}, \Theta_k) = C_{kj}(\mathbf{x}) - D_k(\mathbf{x}, \mathbf{w}, \Theta_k) \quad (8)$$

in which $C_{kj}(\mathbf{x})$ represents the capacity corresponding to $D_k(\mathbf{x}, \mathbf{w}, \Theta_k)$ and $j = y$ or u stands for yield and ultimate performance level, respectively.

Table 5 illustrates the proposed damage states and the corresponding performance levels. The shear capacity is defined as the shear force in the hollow cross section of the steel tower $C_{sj} = f_y A (3/4)(R^2 + r^2) / (R^2 + Rr + r^2)$ where, f_y is equal to the steel yield stress, f_y , for the yield limit, and to the ultimate steel stress f_u , for the ultimate limit. The yield and ultimate stresses, f_y and f_u , are considered to be lognormal random variables with a mean 300 and 410 MPa (for a structural steel of grade S235 according to EN 10 025 (2004) standard), respectively, and a coefficient of variation of 10%. In addition, $C_{mj} = \hat{f}_y S$ is used to calculate the yield bending moment capacity in which S = elastic section modulus. Finally, the ultimate bending moment capacity, C_{mu} , is considered to be a lognormal random variable with a mean of 390.6 MN-m and a standard deviation of 39.57 MN-m. The statistics of C_{mu} are obtained using moment-curvature diagrams constructed for the tubular cross section of the tower base, considering the stress-strain curve of structural steel of grade S235. Monte Carlo simulations are used to estimate the fragility for each failure mode, where all the model parameters and error terms in the developed demand models are considered as random variables, in addition to f_y and f_u as already described.

Figure 3a shows the predictive fragility estimates for the example offshore wind turbine for $H_s = 1\text{m}$ and plotted as a function of the spectral acceleration S_a in units of g, at the natural period of the support structure ($T_n = 2.5\text{ s}$) within its linear elastic range, for both the yield and ultimate limit states. The dotted, solid and dashed lines in the figure show the fragilities for cut-in, rated and cut-out wind speeds, respectively. Cut-in and cut-out wind speeds are the lower and upper limits of the range of wind speeds in which a turbine is operating and producing power. The rated wind speed is the wind speed at which a control system is activated to limit the aerodynamic forces on the blades of the wind turbine and keep the power generated constant by changing the blade pitch angle. As shown in the figure, the fragility at the rated wind speed is higher than the fragilities at the other two wind speeds due to the higher wind speed than the cut-in wind speed and higher operational loading than at the cut-out wind speed. However, the contribution of the wind loading is not significant compared to the seismic excitation even for small earthquakes. In addition, the fragility in shear failure mode is found to be negligible compared to the bending failure mode, as expected for slender elements like wind turbines towers.

Predictive fragility estimates due to ultimate limit state are also plotted as a function of the wind speed, for different values of spectral accelerations (Figure 3b) and $H_s = 1\text{m}$. The figure again shows that changes in wind speed do not affect noticeably the probability of failure, especially for large earthquakes. It is also found that the effect of changes in H_s on the probability of failure is negligible.

Table 5. Proposed damage states

Damage state	Description	Performance level
No significant damage (ND)	No structural damage.	Tower base shear or moment exceeds yield limit
Permanently out-of-service (PO)	Support structure yields. Permanent excessive deformations.	Tower base shear or moment exceeds ultimate limit
Complete (C)	Support structure is unable to carry additional loads	

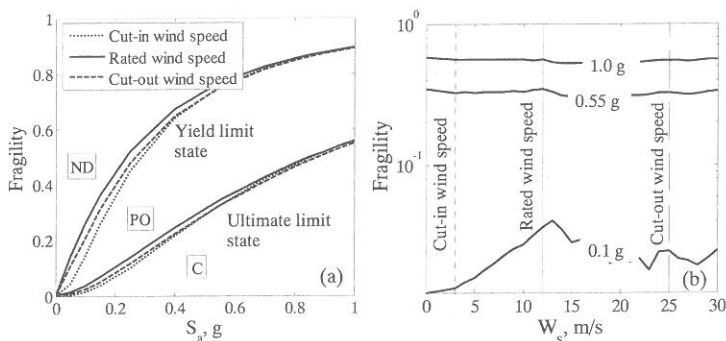


Figure 3: Fragility estimates for a typical 5-MW offshore wind turbine

4 CONCLUSIONS

This paper developed probabilistic models for shear and moment demands on the support structure of offshore wind turbines subject to seismic, environmental and operational loads. Employing an experimental design, 100 wind turbine configurations were generated to produce a virtual experiment database used to calibrate the probabilistic models. Detailed finite element analyses were conducted on the generated configurations accounting for the aerodynamic damping due to the operation of wind turbines, the nonlinearities in the soil behavior and soil-structure interaction. A Bayesian approach was used to assess unknown model parameters.

As an illustration, the developed demand models were used to estimate the fragility of a typical offshore wind turbine support structure. The fragility estimates show that bending failure controls the failure of the support structure. Also the fragility estimates show that wind speeds within the operational range do not noticeably affect the probability of failure in case of a seismic excitation, especially for large earthquakes.

5 REFERENCES

- ABAQUS (2007). Version 6.7-2, Hibbit, Karlsson and Sorensen, Inc.
- Box, G.E.P., and Tiao, G.C. (1992). *Bayesian inference in statistical analysis*, Wiley, New York.
- CEN (2004). EN 10025. *Hot rolled products of structural steels*, Brussels, Belgium.
- Dean, R.G., and Dalrymple, R.A. (1991). *Water wave mechanics for engineers and scientists*, World Scientific.
- Gardoni, P., Der Kiureghian, A., and Mosalam, K.M. (2002). "Probabilistic capacity models and fragility estimates for RC columns based on experimental observations." *J. Eng. Mech.* 128(10), pp. 1024-1038.
- Gardoni, P., Mosalam, K.M., and Der Kiureghian, A. (2003). "Probabilistic seismic demand models and fragility estimates for RC bridges." *J. Earthquake Eng.* 7(1), pp. 79-106.
- Jonkman, J.M., and Buhl Jr., M.L. (2005). "FAST user's guide." *Technical Report NREL/EL-500-38230*, National Renewable Energy Laboratory, Golden, CO.
- Jonkman, B.J. (2009). "TurbSim user's guide." Revised August 26, 2009 for Version 1.50. *Technical Report NREL/TP-500-46198*, National Renewable Energy Laboratory, Golden, CO.
- Jonkman, J., Butterfield, S., Musial, W., and Scott, G. (2009). "Definition of a 5-MW reference wind turbine for offshore system development." *Technical Report NREL/TP-500-38060*, National Renewable Energy Laboratory, Golden, CO.
- Kelley, N.D., and Jonkman, J.M. (2007). "Overview of the TurbSim stochastic inflow turbulence simulator." *Technical Report NREL/TP-500-41137*, National Renewable Energy Laboratory, Golden, CO.
- Laino, D. J., and Hansen, A. C. (2001). "User's guide to the computer software routines AeroDyn interface for ADAMS®", Salt Lake City, UT: *Windward Engineering LLC*, Prepared for the National Renewable Energy Laboratory under Subcontract No. TCX-9-29209-01.
- Mardfekri, M., and Gardoni, P. (2012). "Probabilistic demand models and fragility estimates for offshore wind turbine support structures." Submitted to *Engineering Structures*.
- Mardfekri, M., Gardoni, P., and Roesset, J.M. (2012). "Modeling laterally loaded single piles accounting for nonlinear soil-pile interactions." Submitted to *Journal of Engineering*.
- Matlock, H. (1970). "Correlations for design of laterally loaded piles in soft clay." *Proc., 2nd Annu. Offshore Technol. Conf.*, Paper 1204, 1, 577-588.
- McKay, M.D., Conover, W.J., and Beckman, R.J. (1979). "A comparison of three methods for selecting values of input variables in the analysis of output from a computer code." *Technometrics*, 22(2), 239-245.
- Pacific Earthquake Engineering Research Center. (1999). "Pacific Earthquake Engineering Research Center: NGA Database." (<http://peer.berkeley.edu/nga>), Accessed in Sep. 2011.
- Prowell, I., and Veers, P., (2009). "Assessment of wind turbine seismic risk: Existing literature and simple study of tower moment demand." *SAND2009-1100*, Sandia National Laboratories, Albuquerque, NM.
- Ramamoorthy, K.S., Gardoni, P., and Bracci, M.J., (2006). "Probabilistic demand models and fragility curves for reinforced concrete frames." *ASCE Journal of Structural Engineering*, 132(10), 1563-1572.
- Rezaeian, S., and Der Kiureghian, A. (2010). "Stochastic modeling and simulation of ground motions for performance-based earthquake engineering." *PEER 2010/02*, University of California, Berkeley, CA.
- Shome, N., and Cornell, C. A. (1999). "Probabilistic seismic demand analysis of nonlinear structures." Reliability of Marine Structures Rep. No. RMS-35, Dept. of Civil and Envir. Engineering, Stanford Univ., Palo Alto, CA.
- Morgan, E.C., Lackner, M., Vogel, R.M., Baise, L.G. (2011). "Probability distribution for offshore wind speeds." *Energy Conversion and Management*, 52, 15-26.
- Witcher, D. (2005). "Seismic analysis of wind turbines in the time domain." *Wind Energy*, 8(1), 81-91.

Reduction of the random variables of the turbulent wind field

Mahdi T. Sichani & Søren R.K. Nielsen

Department of Civil Engineering, Aalborg University, 9000 Aalborg, Denmark

ABSTRACT: Applicability of the Probability Density Evolution Method (PDEM) for realizing evolution of the probability density for the wind turbines has rather strict bounds on the basic number of the random variables involved in the model. The efficiency of most of the Advanced Monte Carlo (AMC) methods, i.e. Importance Sampling (IS) or Subset Simulation (SS), will be deteriorated on problems with many random variables. The problem with PDEM is that a multi-dimensional integral has to be carried out over the space defined by the random variables of the system. The numerical procedure requires discretization of the integral domain; this becomes increasingly difficult as the dimensions of the integral domain increase. On the other hand efficiency of the AMC methods is closely dependent on the design points of the problem. Presence of many random variables may increase the number of the design points, hence affects the efficiency of the AMC methods. The idea of the paper is to propose new schemes which allow reduction of the basic random variables of the turbulence such that PDEM and Advanced Monte Carlo (AMC) methods, i.e. subset simulation, are applicable on it.

1 INTRODUCTION

Realizing the evolution of the Probability Density Function (PDF) of a stochastic processes provides sufficient tools for solution of many problems related to stochastic processes i.e. reliability analysis. One important problem, of especial importance for design of the wind turbines, that fits into this category is the failure probability estimation. However realizing evolution of the PDF of a process is a challenging task elaborated by many scientists. One of the most recent discovery in this direction may be the introduction of the PDEM (Li and Chen 2009) which represents the hyperbolic differential equation that governs the evolution of the PDF with respect to time. An attractive feature of this method is that it provides a decoupled equation for systems which are governed by coupled partial differential equations i.e. nonlinear Multi Degree Of Freedom (MDOF) structures. Nevertheless applying PDEM on wind turbines faces difficulties due to high number of basic random variables involved in this problem.

Here we consider uncertainty of the system stems from the stochastic nature of the load e.g. turbulent wind field. A common method to generate wind field is the random phase assignment in frequency domain e.g. spectral method. Other methods are based on covariance matching of the stochastic process using finite difference equations i.e. Auto Regressive Moving Average (ARMA) models or the Markovian State Space models (Sichani 2011). However these approaches require too many random variables in order to apply in connection with the GDEM. Indeed the spectral method in this aspect is more favorable to the ARMA models since it requires less number of basic random variables. Still the number of basic random variables required by spectral methods is far beyond what the PDEM (Li and Chen 2009) can handle (Chen 2009). The number of these basic random variables increases the number of the generated grid nodes in simulation will increase in an exponential manner. However by using number theoretical methods this increase can be controlled to a reasonable extent, c.f. (Fang and Wang 1993), still the number of basic random variables on which these methods are applicable are quite limited i.e. about 20 (Li et al. 2012).

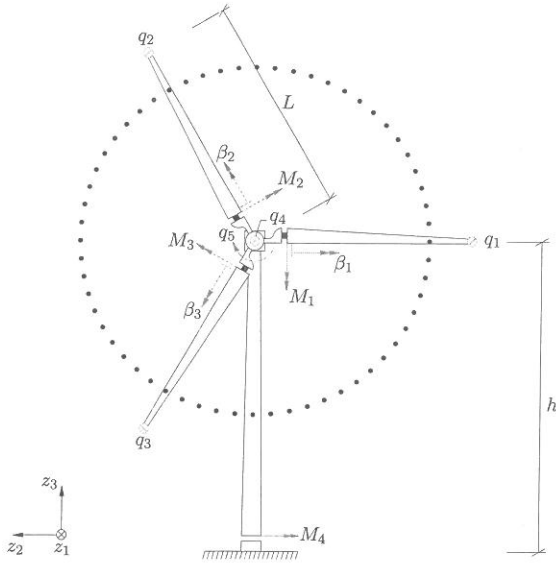


Figure 1: Degree of freedom of the wind turbine model

This study aims at reducing the number of the basic random variables of a wind field such that PDEM and AMC methods can be applied on the system. In this direction the Karhunen-Loève expansion and the turbulence simulation based on linear combination of realizations is considered. Finally the simulation results for the latter case are compared to the Standard Monte Carlo (SMC) results as a qualitative analysis.

2 STATISTICAL CHARACTERISTICS OF 3D TURBULENCE

The incoming turbulent wind field $\{v_j(\mathbf{z}; t), (\mathbf{z}; t) \in \mathbb{R}^4\}$, with components defined in the (z_1, z_2, z_3) system shown in figure 1, is modeled as a zero mean Gaussian homogeneous and stationary process with the cross covariance function

$$\kappa_{ij}(\mathbf{r}; t) = E[v_i(\mathbf{z}_1; t_1)v_j(\mathbf{z}_2; t_2)] \quad , \quad \mathbf{r} = \mathbf{z}_2 - \mathbf{z}_1 \quad , \quad \tau = t_2 - t_1 \quad (1)$$

The IEC code of practice for wind turbine design, (IEC 2005), admits the application of the Taylor hypothesis of frozen turbulence which states that the eddies are fixed to and advected by the mean flow; hence the fundamental properties of the eddies will not change as they pass through the turbine (Panofsky & Dutton 1984)

$$\tilde{v}_j(z_1, z_2, z_3, t) = \tilde{v}_j(z_1 - V_1 t, z_2, z_3) \quad (2)$$

resulting in the following cross-covariance function

$$\kappa_{ij}(\mathbf{r}, \tau) = \tilde{\kappa}_{ij}(r_1 - V_1 \tau, r_2, r_3) \quad (3)$$

where $\tilde{\kappa}_{ij}(\mathbf{r}) = E[\tilde{v}_i(\mathbf{z}_1)\tilde{v}_j(\mathbf{z}_2)]$ is the cross-covariance function of an arbitrary frozen turbulence field $\{\tilde{v}_i(\mathbf{z}), \mathbf{z} \in \mathbb{R}^3\}$. Due to the shear the frozen field is not isotropic, (IEC 2005). Especially a negative correlation is present between $\tilde{v}_1(\mathbf{z})$ and $\tilde{v}_3(\mathbf{z})$. Further, the underlying spectral tensor is determined based on rapid distortion theory (Townsend 1980). This means that the realizations fulfill the linearized Navier-Stokes equation and the continuity equation. V_1 is the mean wind

velocity in the z_1 – direction orthogonal to the rotor area, c.f. figure 1. In the following, merely homogeneous isotropic turbulence will be considered in which case, (Batchelor 1982)

$$\tilde{\kappa}_{ij}(\mathbf{r}) = \sigma_v^2 \left(\frac{f(r) - g(r)}{r^2} r_i r_j + g(r) \delta_{ij} \right) \quad , \quad i, j = 1, 2, 3 \quad , \quad r = \|\mathbf{r}\|_2 \quad (4)$$

σ_v^2 is the variance of the turbulence, and $f(r)$ and $g(r)$ denote the auto-correlation coefficient function for turbulence co-directional to \mathbf{r} and in an arbitrary direction orthogonal to \mathbf{r} . Due to incompressibility the functions $f(r)$ and $g(r)$ can not be chosen arbitrarily but are related as (Batchelor 1982)

$$g(r) = f(r) + \frac{r}{2} \frac{df(r)}{dr} \quad (5)$$

Normally, the undetermined function is given in the wave number space in terms of the 3D-spectrum function $E(k)$. For this von Kármán's semi-analytical suggestion will be applied (Kármán 1948)

$$E(k) = L\sigma_v^2 \frac{55}{9} \frac{\Gamma(\frac{5}{6})}{\Gamma(\frac{1}{2})\Gamma(\frac{1}{3})} \frac{(kL)^4}{(1 + (kL)^2)^{17/6}} \quad , \quad k = \|\mathbf{k}\|_2 \quad (6)$$

L is the integral length scale, which defines the linear range within which the velocities have considerable correlation, defined as

$$L = \int_0^\infty f(r) dr = 2 \int_0^\infty g(r) dr \quad (7)$$

Based on this the correlation coefficient function may be shown to be

$$\left. \begin{aligned} f(r) &= \frac{2^{2\nu}}{\Gamma(\nu)} (\kappa_0 r)^\nu K_\nu(\kappa_0 r) \\ g(r) &= \frac{2^{2\nu}}{\Gamma(\nu)} (\kappa_0 r)^\nu \left[K_\nu(\kappa_0 r) - \frac{\kappa_0 r}{2} K_{-2\nu}(\kappa_0 r) \right] \end{aligned} \right\} \quad (8)$$

where $\kappa_0 = 1/L$, $\nu = 1/3$, $K_\nu(\cdot)$ is the modified Bessel function of second kind and $\Gamma(\cdot)$ is the Gamma function.

3 REDUCTION SCHEMES

From the reliability point of view, obtaining information of the evolution of the Probability Density Function (PDF) of any problem is highly bounded to the basic random variables of the problem (Sichani 2011). However it is shown by the author that Asymptotic Sampling (AS) (Sichani et al. 2011) and Enhanced Monte Carlo (EMC) simulation (Sichani et al. 2012) can handle this difficulty reasonably, still most of the methods for reliability analysis, such as Importance Sampling (IS) or Subset Simulation (SS), will face difficulties in such circumstances (Hurtado 2012; Sichani and Nielsen 2012). In this view reducing the number of basic random variables will be useful by extending the range of applicable reliability methods.

We try two different reduction schemes; first we use the Karhunen-Loève transformation which approximates the process based on its eigen-functions. Second, the reduction based on random combination of base realizations. It should be noted that the aim of these reductions is to provide identical results as that of the SMC for the extreme value distributions of the responses of the wind turbines. Therefore primarily both reduction schemes are checked and the one with more attractive features is tested on a wind turbine model. In this stage we use a reduced order 5 Degrees Of Freedom (DOF) wind turbine developed in previous studies, (Sichani 2011). The model consists of three DOFs, one at the tip of each blade, one DOF for its tower at the hub level and one for the azimuth angle shown in figure 1. The rotational speed of the rotor is kept around its nominal value by a PID controller. The failure event is defined as: *the displacement of the tip of the tower within the time $T \in [0, 600]$ s of simulation exceeds the threshold level b .*

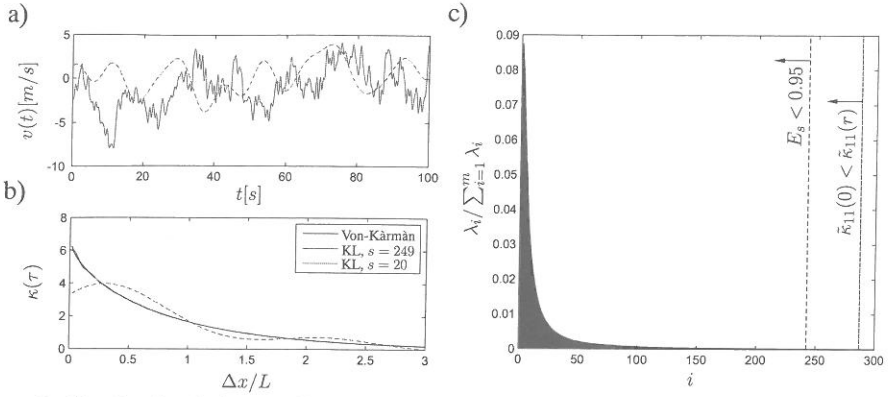


Figure 2: Simulated turbulence with truncated terms in KL expansion; a) Turbulence realizations, b) Correlations of truncated processes, c) Normalized eigenvalues of the KL expansion

3.1 Karhunen-Loève expansion

Only turbulence in the z_1 direction is considered for which reason

$$\tilde{\kappa}_{11}(r) = \sigma_v^2 f(r) \quad (9)$$

Then $\{v_1(\mathbf{z}), \mathbf{z} \in \mathbb{R}^3\}$ admits the Karhunen-Loève expansion

$$\tilde{v}_1(z_1) = \sum_{j=1}^{\infty} \xi_j \sqrt{\lambda_j} \phi_j(z_1) \quad (10)$$

where $\xi_i \sim \mathcal{N}(0, 1)$ are set of iid random variables, e.g. $E\{\xi_i \xi_j\} = \delta_{ij}$, which form the basic random variables. $(\lambda_j, \phi_j(z_1))$ are obtained as solutions to the homogeneous Fredholm integral equation of the second kind (Tricomi 1985; Press et al. 2007)

$$\sigma_v^2 \int_{-\infty}^{\infty} f(z_1 - y_1) \phi_j(y_1) dy_1 = \lambda_j \phi_j(z_1) \quad (11)$$

the eigenfunctions fulfill the orthogonality condition

$$\int_{-\infty}^{\infty} \phi_i(\zeta) \phi_j(\zeta) d\zeta = \delta_{ij} \quad (12)$$

the process may be approximated by retaining the first say s largest eigenvalues and their eigenvectors.

$$\tilde{v}_1(z_1) \approx \sum_{j=1}^s \xi_j \sqrt{\lambda_j} \phi_j(z_1) \quad (13)$$

The error in reconstruction of the autocorrelation function will therefore be $e_s = \sum_{j=s+1}^{\infty} \lambda_j \phi_j(z_1)$.

In order to check feasibility of applying this technique on a turbulent wind field with the grid of 31 nodes on each plane in the frozen field, c.f. (Sichani et al. 2012), is simulated. Two samples of the turbulence at hub level using the truncated KL expansion terms with $s = 20$ and $s = 249$ terms are shown in figure 2.a. The quality of the reconstructed correlations of the processes of this approximation are shown in figure 2.b. From this figure it is clear that the approximated autocorrelation function by only 20 terms in the truncation is not conforming well with the target correlation function which was already expected considering figure 2.a. The ratio $E_s = \sum_{i=1}^s \lambda_i / \sum_{i=1}^m \lambda_i$ is an indicator of the percentage of the energy of the true signal which is presented by the truncated

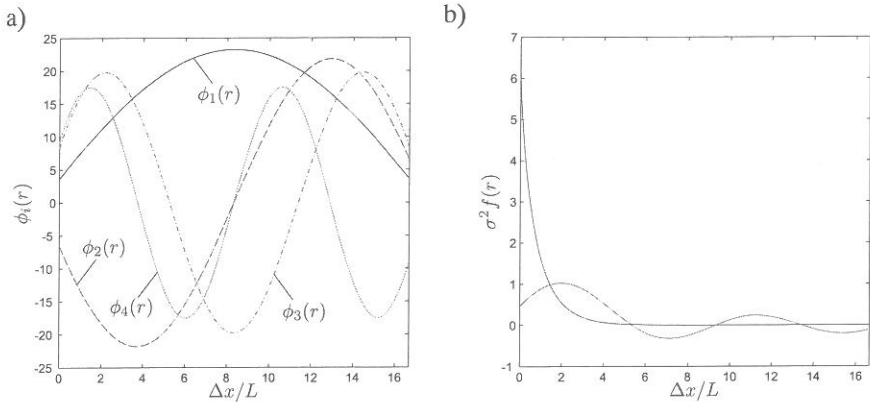


Figure 3: Simulated turbulence with truncated terms in KL expansion; a) Normalized eigenvectors of the KL expansion, b) Covariance function of the process and its approximation

approximation. Figure 2.c shows the normalized eigenvalues of the KL sorted and in descending order. This figure reveals that eigenvalues approach zero rather slowly; hence many terms are needed to be kept in truncation. In order to get a good approximation this ratio should be roughly $E_s > 0.95$. This ratio for the signal truncated with $s = 20$ is $E_{20} = 0.71$. In order to have $E_s > 0.95$, it is seen that $s = 249$ for this case. A sample of the reconstructed signal with 249 terms and its related covariance matrix are shown in figure 2.a. It can be concluded that roughly speaking less than 100 terms in the KL expansion leads to very poor estimations of the turbulence process. It is clear that as the number of processes increase, the number of terms needed to be kept in truncation of the KL expansion increases. This is still too many variables for our purpose, e.g. PDEM application, therefore this approach is not considered appropriate for reduction and is not followed in this study.

Covariance function of a homogeneous turbulence process fulfills $\tilde{\kappa}_{11}(0) \geq \tilde{\kappa}_{11}(r)$. Figure 3.a shows the eigenvectors of the turbulence covariance matrix. As can be seen, these are harmonics with different frequencies hence their linear combination, i.e. approximated covariance function, may not fulfil the homogeneity condition. The approximated curve with only four eigenvectors together with the target covariance function is plotted with green ink in figure 3.b. In this case in order for the approximated process to fulfill the homogeneity condition $s \gtrsim 280$. Hence the homogeneity requirement of the approximation results in similar though more number of eigenfunctions to be used in the approximation as that of energy criterion.

3.2 Random combination of base realizations

In the previous section it was shown that simulating turbulent wind field with less than 100 random variables by the KL expansion leads to severe lack of information about the process. Anyway this may be useful for AMC but definitely not for PDEM. In order to circumvent this problem we take another approach into consideration. Here we try combining a set of turbulence realizations, generated based on a method with correct correlation function, i.e. spectral or ARMA method, with proper random weights. The weights should be adjusted such that the second order moments of the combined process is equal to the target e.g. (14).

$$\tilde{v}_i(\mathbf{z}) = \sum_{p=1}^s \zeta_p \tilde{v}_i^{(p)}(\mathbf{z}) \quad (14)$$

where $\tilde{\mathbf{v}}(\mathbf{z})$ are bases of the expansion, we call them *base realizations* hereafter, and $\zeta_i \sim \mathcal{N}(0, s^{-1/2})$. If $\tilde{\mathbf{v}}^{(p)}(\mathbf{z})$'s fulfill the linearized Navier-Stokes and the continuity equation, so will $\tilde{\mathbf{v}}(\mathbf{z})$ for any value of ζ_p 's. Here we assume identical correlation structure for all base realizations. The correlation

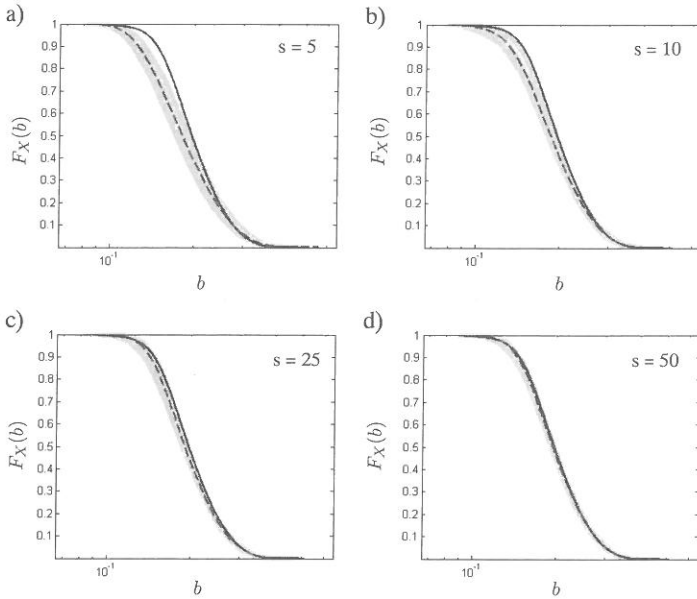


Figure 4: Exceedance probability of the response of the wind turbine; high probability region

structure of the synthesized process $\tilde{\mathbf{v}}$ on the left hand side of (14) can be computed as

$$\tilde{\kappa}_{ij}(r) = \sum_{p=1}^s \sum_{q=1}^s E\{\zeta_p \zeta_q \tilde{v}_i^{(p)}(\mathbf{z}_1) \tilde{v}_j^{(q)}(\mathbf{z}_2)\} = \sum_{p=1}^s \sum_{q=1}^s E\{\zeta_p \zeta_q\} E\{\tilde{v}_i^{(p)}(\mathbf{z}_1) \tilde{v}_j^{(q)}(\mathbf{z}_2)\} \quad (15)$$

Since ζ_p 's are independent identically distributed variables

$$\tilde{\kappa}_{ij}(r) = s\sigma_\zeta^2 \check{\kappa}_{ij}(r) = \check{\kappa}_{ij}(r) \quad (16)$$

This is a simple yet feasible to be applied on a wind turbine model. Therefore this approach is tested on the wind turbine model. Figure 4 shows the Cumulative Distribution Function (CDF) of the failure event c.f. section 3. 5 sets of Monte Carlo simulations, each one with 15000 samples have been carried out where excitation is considered as the linear random combination of s base turbulence processes according to (14). The results of simulation with $s = 5, 10, 25, 50$ are shown in figures 4.a, 4.b, 4.c and 4.d respectively. The solid line indicated the CDF of the Standard Monte Carlo (SMC) simulation of same quantity with 4×10^5 samples. It is clear that the CDF of the samples generated by linear random combination of the processes as excitation deviate from that of the SMC. Nevertheless the deviation tends to disappear as the number of base processes increase from 5 to 50. Figure 5 shows the CDF for the exceedance probability with focus on the tails of the distributions. It seems that by increasing the number of the basic random variables with this method it is possible to get qualitatively similar results as that of the SMC. However it is noted that SMC involves much higher number of basic random variables.

4 CONCLUSIONS

Conventional methods for this purpose require many random variables to be used i.e. of order 10^4 or more. However handling reliability problems which involves so many random variables is a very difficult task. Therefore any scheme which allows reduction of this number without significant

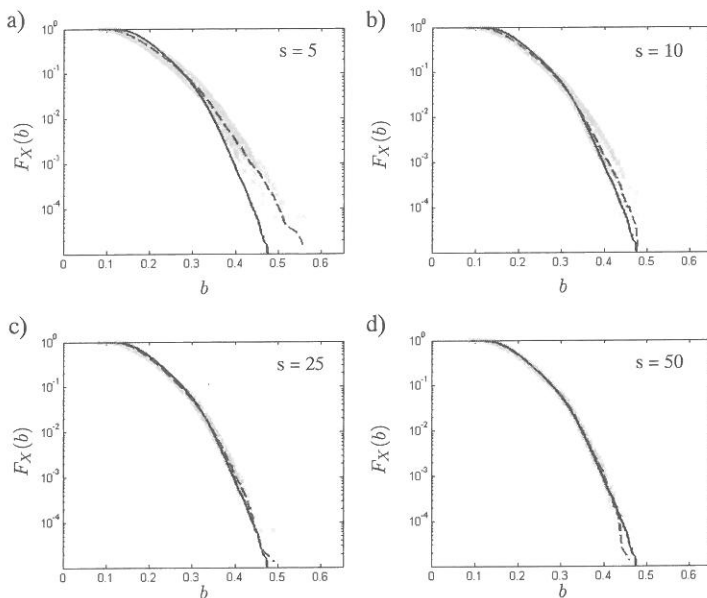


Figure 5: Exceedance probability of the response of the wind turbine; low probability region

loss of accuracy makes essential improvements in reliability analysis of these structures. This paper assesses efficiency of the Karhunen-Loève (KL) transformation as a reduction scheme when applied on a turbulent wind field. It is seen that the reduction of the random variables with this scheme is good but still ways more that the strict bounds on the newly developed methods such as the PDEM. Therefore another scheme based on the sums of the processes is proposed in the paper which is to be applied on a wind turbine model. The elaborated simulations suggest that using linear random combination of turbulence realizations has the potential to reproduce similar results as that of the SMC. Moreover fine tuning and careful selection of the base processes can improve efficiency of the method i.e. less random variables.

REFERENCES

- Batchelor, G. K. (1982). *The Theory of Homogeneous Turbulence*. Cambridge University Press.
- Chen, J.-B., G. R. L. J. (2009). Partition of the probability-assigned space in probability density evolution analysis of nonlinear stochastic structures. *Probabilistic Engineering Mechanics* 24(1), 27–42. cited By (since 1996) 4.
- Fang, K.-T. & Y. Wang (1993). *Number-Theoretic Methods in Statistics*. Chapman and Hall/CRC; 1st edition.
- Hurtado, J. E. (2012). Dimensionality reduction and visualization of structural reliability problems using polar features. *Probabilistic Engineering Mechanics* 29(0), 16 – 31.
- IEC (2005). *IEC 61400-1 (2005) International Standard, Wind turbines - Part 1: Design requirements* (3rd edition ed.). International Electrotechnical Commission.
- Kàrmàn, T. V. (1948). Progress in the statistical theory of turbulence. *Physics: proc. N.A.S.* 34, 530–539.
- Li, J. & J. Chen (2009). *Stochastic Dynamics of Structures*. Wiley.

- Li, J., J. Chen, W. Sun, & Y. Peng (2012). Advances of the probability density evolution method for nonlinear stochastic systems. *Probabilistic Engineering Mechanics* 28(0), 132 – 142. Computational Stochastic Mechanics CSM6.
- Panofsky, H. A. & J. A. Dutton (1984). *Atmospheric Turbulence: Models and Methods for Engineering Applications*. Wiley-Interscience; 1 edition.
- Press, W. H., S. A. Teukolsky, W. T. Vetterling, & B. P. Flannery (2007). *The Structure of Turbulent Shear Flow* (3rd edition ed.). Cambridge University Press.
- Sichani, M. T. (2011). *Estimation of Extreme Responses and Failure Probability of Wind Turbines under Normal Operation by Controlled Monte Carlo Simulation*. Ph. D. thesis, Department of Civil Engineering, Aalborg University, Aalborg, Denmark.
- Sichani, M. T. & S. R. Nielsen (2012). First passage probability estimation of wind turbines by markov chain monte carlo. *Structure and Infrastructure Engineering* ; doi:10.1080/15732479.2012.659739, 1–13.
- Sichani, M. T., S. R. K. Nielsen, & C. Bucher (2011). Application of asymptotic sampling on high dimensional structural dynamics problems. *Structural Safety* 33, 305–316.
- Sichani, M. T., S. R. K. Nielsen, & A. Naess (2012). Failure probability estimation of wind turbines by enhanced monte carlo method. *Journal of Engineering Mechanics* 138(4), 379–389.
- Townsend, A. (1980). *The Structure of Turbulent Shear Flow* (2nd edition ed.). Cambridge University Press.
- Tricomi, F. G. (1985). *Integral Equations*. Dover Publications.

Some observations on the subset simulation related to the wind turbine mechanics

Mahdi T. Sichani, Søren R.K. Nielsen & Palle Thoft-Christensen

Department of Civil Engineering, Aalborg University, 9000 Aalborg, Denmark

ABSTRACT: The subset simulation method is considered to be one of the most powerful methods among the variance reduction Monte Carlo techniques. Potential shortcomings of the method are the bias in its estimations and potential challenges in finding important directions in high dimensional nonlinear problems. The important directions in the n -dimensional space of the problem are those toward which the failure region extends i.e. by moving in those directions the simulation will fall into the safe domain. It is clear that finding these important directions becomes increasingly difficult as the number of the basic random variables of the problem increases. Moreover when the failure domain of the problem is not a simply connected domain, e.g. failure islands, finding the correct direction, or island, becomes even more difficult. This case occurs frequently in time variant dynamic reliability analysis of nonlinear systems. It is interesting to determine applicability of the Subset Simulation (SS) techniques, as a powerful representative of Variance Reduction Monte Carlo (VRMC) methods, on the wind turbine systems specifically with an active controller. Hence in this paper we apply and discuss these methods on a benchmark wind turbine model and analyze the results in view of their applicability.

1 INTRODUCTION

In order to estimate the return period of the wind turbines (IEC 2005a) it is necessary to estimate the first passage probability, alternatively called failure probability, of these systems. For this aim the IEC standard recommends fitting one of the extreme value distributions, i.e. reversed Weibull or the Gumbel distribution, to the peaks extracted from six epoches of 10min. duration, of the wind turbine data (IEC 2005b). Unfortunately the choice of Extreme Value Distribution (EVD) combined with the part of the data used to find EVD parameters result in considerably different extrapolated design values. Alternative to extreme value curve fitting and extrapolation, simulation techniques may be used for estimating these return periods. The natural choice for this purpose is the Standard Monte Carlo (SMC) simulation. The computation cost of this approach is however far beyond reach of the available computers' power even on a modern machine. This is since wind turbines have rather complicated dynamic models which ends up in a high dimensional nonlinear Limit State Function (LSF). The nonlinearities coupled with high dimensions of LSF is enough to make the problem very difficult to solve (Valdebenito, Pradlwarter, & Schueller 2010; Katafygiotis & Zuev 2008). Therefore a method that can handle these problems with reasonable effort could be of great interest in this area. The Variance Reduction Monte Carlo (VRMC) methods are an alternative choice which are able to produce estimations similar to SMC but with less variance. The Subset Simulation (SS), introduced by Au & Beck (Au & Beck 2001), for estimation of small probabilities of high dimensional systems is reportedly one of the most powerful techniques in the field of structural dynamics. An advantage of SS over the other VRMC methods, such as IS, is its capability in handling high dimensional and complicated problems within reasonable effort (Schueller & Pradlwarter 2007). Recently two new algorithms have been proposed to increase the efficiency of the subset simulation (Santoso, Phoon, & Quek 2011; Zuev & Katafygiotis 2011).

These algorithms tackle the problem by the way they generate the conditional samples of the problem. The first algorithm (Santoso, Phoon, & Quek 2011) aims at increasing the quality of the estimates by decreasing the correlation of the chains which are generated during simulation e.g. Markov Chains. The other algorithm (Zuev & Katafygiotis 2011) improves the performance by delaying the rejection of the generated Markov Chain in the Limit State Function evaluation. In this article a nonlinear model of a wind turbine according to (Sichani, Nielsen, & Bucher 2011; Sichani, Nielsen, & Naess 2011) is used as a benchmark for analysis of the applicability of these methods. The discussed algorithms are applied to this benchmark problem and the results in terms of their bias and capability of estimating low probabilities are studied.

2 SUBSET SIMULATION

Assume that the LSF is defined as $G(\mathbf{X})$ where \mathbf{X} consists of the random variables of the problem. The barrier level b_j which corresponds to a sample of \mathbf{X} , i.e. \mathbf{x}_j , is then given by $b_j = G(\mathbf{x}_j)$. In view of structural dynamics \mathbf{X} can be recognized as the stochastic excitation within a given time duration and b as the maximum of the magnitude of the response to the given excitation. The strategy of the SS is to obtain samples of b which have low probability of occurrence, starting by that which can be accurately estimated with low number of simulations e.g. $b^{(1)}$. Next, this barrier level will be increased gradually until the highest(required) barrier level or probability is estimated with desired accuracy. This is done by defining intermediate probability levels $p_f = p_f^{(m)} < p_f^{(m-1)} < \dots < p_f^{(1)}$ corresponding to the intermediate barrier levels $b = b^{(m)} > b^{(m-1)} > \dots > b^{(1)}$. Using this property taken from the fact that the first passage probability can not increase as the barrier level increases, the required first passage probability p_f can be written as

$$p_f(b^{(2)}|b^{(1)}) = \frac{p_f(b^{(2)} \cap b^{(1)})}{p_f(b^{(1)})} = \frac{p_f(b^{(2)})}{p_f(b^{(1)})} \quad (1)$$

$p_f(b^{(2)}|b^{(1)})$ is the conditional probability of exceeding $b^{(2)}$ on the condition that $b^{(1)}$ is exceeded. Using Equation (1) the final first passage probability, i.e. the lowest first passage probability required, may be written as the following product

$$p_f(b) = p_f(b^{(1)}) \prod_{i=1}^{m-1} p_f(b^{(i+1)}|b^{(i)}) \quad (2)$$

The SS method aims at estimating each of the m terms on the right hand side of Equation (2) by some type of Monte Carlo simulation. Therefore it is beneficial to let the barrier level be chosen after simulation of each stage is performed and fix the intermediate first passage probabilities associated with them. All the terms in the product are chosen large enough so that they can be estimated with low number of samples i.e. $p_0 = 0.1$ in conjunction with Equation (3).

$$\left. \begin{aligned} p_f(b^{(1)}) &= p_0 \\ p_f(b^{(i+1)}|b^{(i)}) &= p_0, \quad i = 1, \dots, m-1 \end{aligned} \right\} \quad (3)$$

$b^{(1)}$, with its probability $p_f(b^{(1)}) = p_0$, is determined by performing SMC with low number of samples, i.e. $N_{sim} = 500$, as the $(p_0 \times N_{sim})^{\text{th}}$ barrier level when all simulated barrier levels are sorted in descending order. The conditional probability terms on the right hand side of Equation (1) cannot be estimated by SMC and need a technique which is capable of generating samples conditioned on the previous samples. For this reason those samples of $\mathbf{X}^{(1)}$ which correspond to the barrier levels higher than $b^{(1)}$, the so-called seeds, are saved for simulating next generation of the excitation. This consists of $N_{seed} = p_0 \times N_{sim}$ seeds to be kept in memory. In the next section the original Metropolis-Hastings algorithm is described which is the basis for the conditional sampling. In the following sections the proposed modifications are explained with emphasis on their difference with the original algorithm.

2.1 Metropolis-Hastings algorithm

Let $x(k)$ denote the samples of a discrete stochastic load process $X(k)$ at the instants of time $k = 1, \dots, N$ - in the reliability analysis these refer to the basic random variables used to generate the loads -. The random variables $X(k)$ are assumed to be mutual independent and identical distributed with the Probability Density Function (PDF) $\pi(x(k))$. $X(k)$ is assembled in the random vector \mathbf{X} with the Joint Probability Density Function (JPDF) $\pi(\mathbf{x})$. Due to the iid components $\pi(\mathbf{x})$ becomes as indicated in Equation (4). It should be noted that in our context the random variables $X(k)$ refer to neither the time samples of the turbulence process nor the response of the wind turbine. These are the basic random variables which will be transformed into the turbulence process (Sichani 2011). Correspondingly the samples are stored in the vector \mathbf{x} . Let $\mathbf{X}^{(i)}$ and $\mathbf{X}^{(i+1)}$ denote stochastic vectors representing (or transformed into) the load process, when changing from barrier level $b^{(i)}$ to barrier level $b^{(i+1)}$. Both of these vectors are identical distributed, but not independent. The transition kernel, or alternatively called the *proposal distribution*, that $\mathbf{X}^{(i)} = \mathbf{x}$ moves to $\mathbf{X}^{(i+1)}$ is shown by $p(\mathbf{X}^{(i+1)}|\mathbf{X}^{(i)})$. Due to the independence and identical distribution of the components within $\mathbf{X}^{(i+1)}$ and $\mathbf{X}^{(i)}$, respectively, this may be written as

$$\left. \begin{aligned} \pi(\mathbf{x}^{(i)}) &= \prod_{k=1}^N \pi(x^{(i)}(k)) \\ p(\mathbf{x}^{(i+1)}|\mathbf{x}^{(i)}) &= \prod_{k=1}^N p(x^{(i+1)}(k)|x^{(i)}(k)) \end{aligned} \right\} \quad (4)$$

where $\pi(\cdot)$ and $p(\cdot)$ are the one dimensional PDFs of the discrete components $X(k)$. Consider " N_{sim} " samples $\{\mathbf{x}_1^{(i)}, \dots, \mathbf{x}_{N_{sim}}^{(i)}\}$ of $\mathbf{X}^{(i)}$ from the i^{th} simulation level. The transition kernel that $\mathbf{X}^{(i)} = \mathbf{x}_j^{(i)}$ moves to a state in $\mathbf{X}^{(i+1)}$, e.g. $p(\mathbf{X}^{(i+1)}|\mathbf{X}^{(i)} = \mathbf{x}_j^{(i)})$, can be chosen with the mean value $\mathbf{x}_j^{(i)}$, but can otherwise be arbitrarily chosen (Santoso, Phoon, & Quek 2011). For instance a uniform or Gaussian distribution with an arbitrary standard deviation, such as the sample standard deviation of the seeds (Au, Cao, & Wang 2010), and its mean value at the value of $x_j^{(i)}(k)$ for $k = 1, \dots, N$. Initially a candidate ξ_j for $\mathbf{x}_j^{(i+1)}$, $j = 1, \dots, N_{sim}$ is drawn from $p(\cdot|\mathbf{x}_j^{(i)})$. In order to ensure that samples of $\mathbf{X}_j^{(i+1)}$ generated by MH will also be distributed with distribution $\pi(\cdot)$, it is necessary that the so-called "reversibility condition", which states that $\pi(\xi_j)p(\mathbf{x}_j^{(i)}|\xi_j) = \pi(\mathbf{x}_j^{(i)})p(\xi_j|\mathbf{x}_j^{(i)})$, be satisfied for all samples of $\mathbf{x}_j^{(i)}$ and ξ_j (Chib & Greenberg 1995; Santoso, Phoon, & Quek 2011). For this reason Equation (5) is used as the probability of accepting candidate samples.

$$a(\mathbf{x}_j^{(i)}, \xi_j) = \min \left\{ 1, \frac{\pi(\xi_j)p(\mathbf{x}_j^{(i)}|\xi_j)}{\pi(\mathbf{x}_j^{(i)})p(\xi_j|\mathbf{x}_j^{(i)})} \right\} \quad (5)$$

Next, ξ_j is accepted as the next sample, e.g. $\mathbf{x}_j^{(i+1)} = \xi_j$, with probability

$$\mathbf{x}_j^{(i+1)} = \begin{cases} \xi_j & \text{w.p. } a(\mathbf{x}_j^{(i)}, \xi_j) \\ \mathbf{x}_j^{(i)} & \text{w.p. } 1 - a(\mathbf{x}_j^{(i)}, \xi_j) \end{cases} \quad (6)$$

where the term w.p. means "with probability". Therefore after generation of a candidate sample ξ_j a random number is drawn from a uniform distribution between 0 and 1 e.g. $\mathcal{U}(0, 1)$. If this number is less than $a(\mathbf{x}_j^{(i)}, \xi_j)$ of Equation (5), ξ_j will be accepted as the next sample; else will be rejected and replaced by the seed $\mathbf{x}_j^{(i)}$. This procedure guarantees that the distribution of the samples will not be changed as barrier levels increase (Hoff 2009). In case the proposal distribution is chosen to be symmetric, i.e. $p(\mathbf{B}|\mathbf{A}) = p(\mathbf{A}|\mathbf{B})$, it is called the *random walk Metropolis Hastings* and Equation (5) reduces to

$$a(\mathbf{x}_j^{(i)}, \xi_j) = \min \left\{ 1, \frac{\pi(\xi_j)}{\pi(\mathbf{x}_j^{(i)})} \right\} \quad (7)$$

2.2 Conditional probability estimation

The method follows the procedure described in section 2 that started by a SMC and defining the first barrier level $b^{(1)}$. In the next step(s) N_{sim} candidate samples for $\mathbf{x}_j^{(i+1)}$, $j = 1, \dots, N_{sim}$ will be generated using a conditional sampler, i.e. MH. The next generation of excitations are conditioned on a randomly chosen seed of the previous simulation. If ξ_j is accepted according to Equation(6) using either Equation (5) or Equation (7), the second accept\reject test will be performed as

$$\mathbf{x}_j^{(i+1)} = \begin{cases} \xi_j & \text{if } \xi_j \in \mathfrak{F}^{(i)} \\ \mathbf{x}_j^{(i)} & \text{if } \xi_j \notin \mathfrak{F}^{(i)} \end{cases} \quad (8)$$

where $\mathfrak{F}^{(i)}$ denotes the failure domain of the i^{th} level e.g. $\mathfrak{F}^{(i)} = \{\xi_j | G(\xi_j) > b^{(i)}\}$. Equation (8) means that ξ_j is accepted (after being accepted in the accept\reject test of the MH) only if it increases the barrier level to higher than $b^{(i)}$, else is rejected and replaced with its seed. This step provides the estimation for the conditional terms in Equation (2) and will be repeated $m - 1$ times, c.f. Equation (2). The same strategy that was described in section 2 for choosing barrier levels and seeds will be used in all $m - 1$ stages of the simulation. This results in

$$p_f^i = \frac{p_0^{i-1}}{N_{sim}} \sum_{j=1}^{N_{sim}} I_{\mathfrak{F}^{(i)}}(\mathbf{x}_j^{(i)}) \quad , \quad i = 1, \dots, m \quad (9)$$

p_f^i represents the minimum failure\first passage probability calculated in the i^{th} step of the simulation. p_0^{i-1} means p_0 raised to power " $i - 1$ ". $I_{\mathfrak{F}^{(i)}}(\mathbf{x}_j^{(i)})$ is the indicator function which will be one if the response to $\mathbf{x}_j^{(i)}$ lies in the i^{th} intermediate failure domain and is zero otherwise.

2.3 Modified Metropolis-Hastings algorithm

The MH algorithm as presented in section 2.1 breaks down in high dimensional problems. This is since the probability of moving from $\mathbf{x}_j^{(i)}$ to ξ_j , defined as Equation (5), decreases exponentially as the number of basic variables - dimension of the problem - increases (Au & Beck 2001). Therefore Markov chains do not move so frequently from their current state to the next state and get stocked where they are. This problem can be solved by taking advantage of independency between candidate coordinates(components) and breaking the N -dimensional JPDFs $\pi(\mathbf{x}_j^{(i)})$ and $p(\cdot | \mathbf{x}_j^{(i)})$ into their corresponding N independent one dimensional PDFs $\pi(x_j^{(i)}(k))$ and $p(\cdot | x_j^{(i)}(k))$ respectively. Accordingly probability of accepting the next state for each sample is defined independently as

$$a(x_j^{(i)}(k), \xi_j(k)) = \min \left\{ 1, \frac{\pi(\xi_j(k)) p(x_j^{(i)}(k) | \xi_j(k))}{\pi(x_j^{(i)}(k)) p(\xi_j(k) | x_j^{(i)}(k))} \right\} \quad (10)$$

which in case of symmetric proposal distribution $p(B|A) = p(A|B)$ reduces to

$$a(x_j^{(i)}(k), \xi_j(k)) = \min \left\{ 1, \frac{\pi(\xi_j(k))}{\pi(x_j^{(i)}(k))} \right\} \quad (11)$$

Next, the accept\reject test will be performed for each component of each realization. So for $k = 1, \dots, N$

$$x_j^{(i+1)}(k) = \begin{cases} \xi_j(k) & \text{w.p. } a(x_j^{(i)}(k), \xi_j(k)) \\ x_j^{(i)}(k) & \text{w.p. } 1 - a(x_j^{(i)}(k), \xi_j(k)) \end{cases} \quad (12)$$

This process will be repeated for $j = 1, \dots, N_{sim}$ times to generate the next set of excitations i.e. $\mathbf{X}^{(i+1)} = \{\mathbf{x}_1^{(i+1)}, \dots, \mathbf{x}_{N_{sim}}^{(i+1)}\}$. This modification is proposed in (Au & Beck 2001) and is called

the *Modified Metropolis-Hastings* (MMH). Hereafter when this sampling scheme is used for the SS, it is invoked by the term SS-MMH.

2.4 Modified Metropolis Hastings with Reduced Chain Correlation

The Modified Metropolis-Hastings with Reduced chain Correlation (MMHRC) is recently proposed by (Santoso, Phoon, & Quek 2011) which aims in reducing the correlation between the Markov chains in the MMH. In view of the sample generation MMHRC follows the original MH algorithm based on Equation (5), Equation (6) and Equation (7), i.e. the N -dimensional JPDF is used. However every time the generated ξ_j is rejected according to Equation (6), a new sample is generated conditioned on the same seed. This process is repeated as many times as needed to let the generated candidate be accepted by Equation (6). Clearly this modification takes more time for sample generation compared to MMH. SS-MMHRC shows good performance for low to medium dimensional problems i.e. $N \leq 100$ (Santoso, Phoon, & Quek 2011). However on the numerical simulation performed in this study, see section 3, the Markov chains generated by MMHRC have high tendency to stay in the initial state, i.e. $a(\mathbf{x}_j^{(i)}, \xi_j) \approx 0$. This means that the barrier level is rarely increased. This is due to the high dimensions of the problem which is the same problem that causes breaking down of the original MH algorithm in high dimensions (Au & Beck 2001).

2.5 Modified Metropolis Hastings with Delayed Rejection

Following the idea of (Tierney & Mira 1999) the so-called Modified Metropolis-Hastings with Delayed Rejection (MMHDR) is proposed by (Zuev & Katafygiotis 2011). Here the MMH approach is followed for generation of the conditional samples. Although in case a candidate sample does not belong to the failure region, i.e. $\xi_j \notin \mathcal{F}^{(i)}$ in Equation (8), it will not be rejected and will be given a second chance. In such a case the components of the candidate ξ_j , e.g. $\xi_j(k)$, are divided into two non-overlapping sets. Set $T = \{k | x_j^{(i)}(k) = \xi_j(k)\}$ which consists of the set of coordinates which have evolved to new states; and its complementary set \bar{T} which includes the rest of the components. Next, the coordinates which belong to T will be given another chance to evolve to a new state $\xi^{(2)}$. The proposal density of moving to $\xi_j^{(2)}(k)$, e.g. $q(\cdot | x_j^{(i)}(k), \xi_j(k))$, can in general be chosen different from the proposal density of moving from $x_j^{(i)}(k)$ to $\xi_j(k)$, e.g. $p(\cdot | x_j^{(i)}(k))$. It should be noted that the candidate samples for $\xi_j^{(2)}$ are again generated around the original seed $x_j^{(i)}(k)$ and not $\xi_j(k)$ i.e. $q(\cdot | x_j^{(i)}(k), \xi_j(k)) = q(\cdot | x_j^{(i)}(k))$ (Zuev & Katafygiotis 2011). The probability of accepting the new samples conditioned on the two previous samples is defined as (Tierney & Mira 1999)

$$\left. \begin{aligned}
 & a^*(x_j^{(i)}(k), \xi_j(k), \xi_j^{(2)}(k)) = \\
 & \min \left\{ 1, \frac{\pi(\xi_j^{(2)}(k)) p(\xi_j(k) | \xi_j^{(2)}(k))}{\pi(x_j^{(i)}(k)) p(\xi_j(k) | x_j^{(i)}(k))} \times \right. \\
 & \left. \frac{q(x_j^{(i)}(k) | \xi_j^{(2)}(k), \xi_j(k)) a(\xi_j^{(2)}(k), \xi_j(k))}{q(\xi_j^{(2)}(k) | x_j^{(i)}(k), \xi_j(k)) a(x_j^{(i)}(k), \xi_j(k))} \right\}
 \end{aligned} \right\} \quad (13)$$

where $a(\xi_j(k), \xi_j^{(2)}(k))$ determines the probability of moving from $\xi_j(k)$ to $\xi_j^{(2)}(k)$ in the same manner as defined in Equation (10). In case that both transition kernels are chosen symmetry

Equation (13) reduces to

$$a^*(x_j^{(i)}(k), \xi_j(k), \xi_j^{(2)}(k)) = \min \left\{ 1, \frac{p(\xi_j(k)|\xi_j^{(2)}(k)) \min \left\{ \pi(\xi_j^{(2)}(k)), \pi(\xi_j(k)) \right\}}{p(\xi_j(k)|x_j^{(i)}(k)) \min \left\{ \pi(x_j^{(i)}(k)), \pi(\xi_j(k)) \right\}} \right\} \quad (14)$$

where in Equation (14) the equality $a \times \min \{1, b/a\} = b \times \min \{1, a/b\}$ is used which is true for any positive pair $\{a, b\}$.

3 SUBSET SIMULATION ON WIND TURBINE

The time duration for simulation is chosen $800[sec]$ where the first $200s$ are discarded to take into account the effect of the transient phase of the system response. The rest simulates a 10min. interval which is prescribed in design codes for extraction of probabilistic behavior of the turbines (IEC 2005b). The resolution of the time integrator is set to $\Delta t = 0.2s$. Turbulent wind field is simulated on 31 nodes, one on the hub and others at $0.8L$ radial distance from hub on an equidistance angular grid. The mean wind is set to $V_r = 15[m/s]$ and the cut-in and cut-out speeds are set to $V_i = 5[m/s]$ and $V_o = 25[m/s]$ respectively. The limit state function is defined as the first passage of the magnitude of the tower displacement from the threshold (barrier) level b i.e. $p_f(b) = \text{Prob} \left(\max_{t \in [0, T]} |z_d(t)| \geq b \right)$ with $T = 600[s]$ of simulation. Discarding the transient simulation time, the LSF is defined as a function of 93000 stochastic variables. Failure probability of the model is estimated by SS compared to the SMC with 4.95×10^5 samples.

A practical issue is the very high number of the basic random variables, e.g. the iid Gaussian random numbers which will pass through the turbulence filter, needed to be stored in the memory for the next stage of the simulation. These consists of seeds for two consecutive simulation levels which contains $2N_{seed}$ sets of basic random variables requiring approximately 12MB of disc space for only one simulation. Therefore a simulation with 500 initial samples and $p_0 = 0.1$ requires approximately 1.2GB memory (or disc space) to save $2N_{seed} = 100$ seeds for two simulation levels. The proposal distributions are chosen uniform centered at the sample seed with spread equal to 2 times standard deviation of the seeds of the previous level. Figures 1a and 1b show estimates of the first passage probability of the fixed speed wind turbine with SS-MMH and SS-MMHDR respectively. In both figures number of samples is $N_{sim} = 500$ and probability increment is set to $p_0 = 0.1$. Each figure shows 10 estimates of the first passage probability with SS together with the SMC results. The thick solid lines the figures show the SMC simulation results. The figures show that both methods are successful in increasing barrier levels and their estimates are close to that of the SMC. However SS-MMHDR results suffer from small over estimation of the first passage probability at high barrier levels. Figures 2a and 2b show the estimates of the first passage probability of the variable speed wind turbine. The figures show that presence of the controller has considerable effect on first passage probability estimation. The controller not only changes the range of barrier levels but also makes the estimation of the first passage probability a more difficult task. As seen in figures 2a and 2b both methods have rather poor estimates of the first passage probabilities of order 10^{-7} for the variable speed wind turbine case. For the fixed speed wind turbine the value $p_0 = 0.1$ is shown to be a good choice and both methods overcome the difficulties faced by high dimensions of the model. However the variable speed model has difficulties in estimating very low probabilities.

4 CONCLUSIONS

The low first passage probability of a reduced order wind turbine model is estimated based on the Makov Chain Monte Carlo. A well-known method for this aim, e.g. SS-MMH, with two of

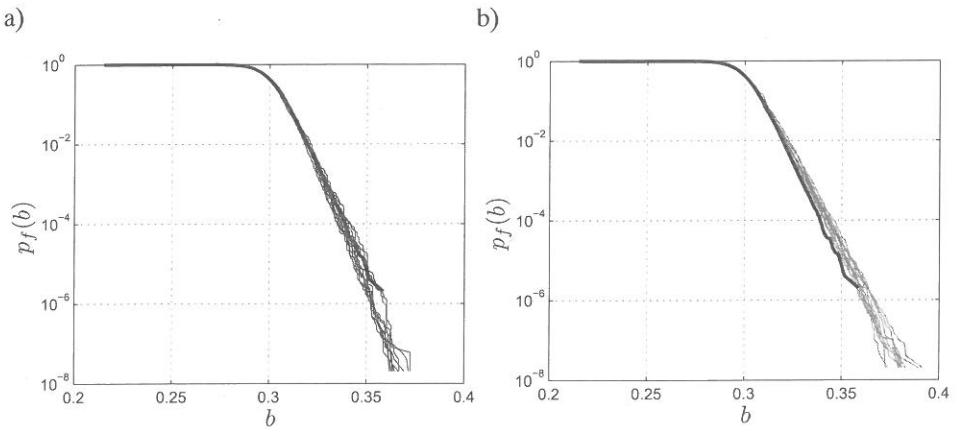


Figure 1: First passage probability estimation of the fixed speed wind turbine; 6 stages with $p_0 = 0.1$, a) Subset simulation with MMH sampling scheme b) Subset simulation with MMHDR sampling scheme

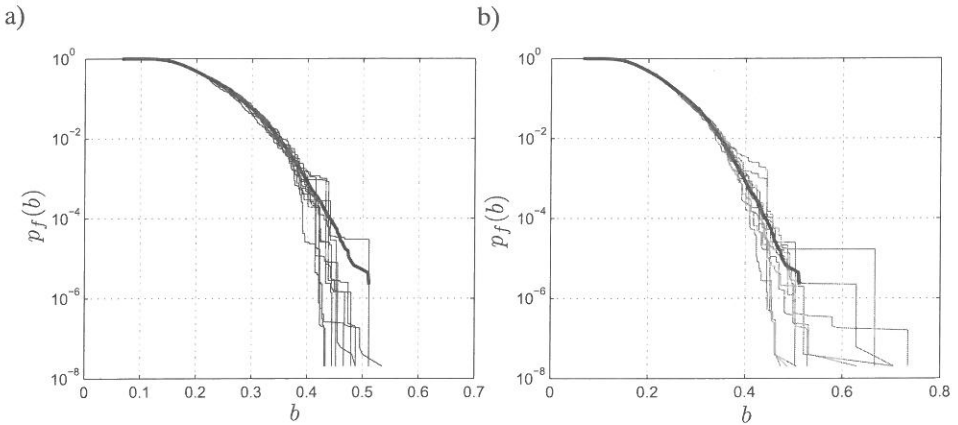


Figure 2: First passage probability estimation of the variable speed wind turbine; 6 stages with $p_0 = 0.1$, a) Subset simulation with MMH sampling scheme b) Subset simulation with MMHDR sampling scheme

the most recent modifications to the original algorithm have been implemented and compared to the original method on the wind turbine model. The estimated first passage probability of the fixed speed wind turbine with SS-MMH is in good agreement with SMC. On the other hand SS-MMHDR results have small over estimations in their predictions. Nevertheless estimations of the first passage probability of the variable speed wind turbine is more difficult. The results show that in high dimensions the chains constructed by SS algorithms do not move to the next state often, and tend to stay in their initial state.

In most nonlinear problems the failure domain of the problem is not a continuous region but a set of the so-called failure islands surrounded by the safe domain. Therefore scaling up an excitation which belongs to the failure domain, may end in the safe domain. In case these islands are not small and distant from each other, i.e. the fixed speed model, Markov chains have a fair chance to increase the barrier level as they evolve. However finding the directions toward which (the islands in which) the barrier level increases becomes increasingly difficult as the islands shrink or their

distance increases. This seems to be the case in the variable speed wind turbine model. The aforementioned reasons seem to be responsible for deterioration of the performance of the method in estimating the small failure probabilities of the variable speed model.

Results of this study show that subset simulation will suffer from presence of too many basic random variables in dynamic reliability analysis of wind turbines. Hence further research should take direction toward decreasing the number of the basic random variables to as few as possible. This is possible by using reduction schemes such as Karhunen-Loève expansion or stochastic harmonic functions. Reducing the number of basic random variables however may affect the shape of the LSF of the problem and make it more complicated. These changes may be more design points, irregularities or discontinuities. It is already suspicious that the wind turbine model has discontinuous LSF; so reduction of the number of random variables may make it worse.

REFERENCES

- Au, S., Z. Cao, & Y. Wang (2010). Implementing advanced monte carlo simulation under spreadsheet environment. *Structural Safety* 32(5), 281 – 292. Probabilistic Methods for Modeling, Simulation and Optimization of Engineering Structures under Uncertainty in honor of Jim Beck's 60th Birthday.
- Au, S.-K. & J. L. Beck (2001). Estimation of small failure probabilities in high dimensions by subset simulation. *Probabilistic Engineering Mechanics* 16(4), 263 – 277.
- Chib, S. & E. Greenberg (1995). Understanding the Metropolis-Hastings Algorithm. *The American Statistician* 49(4), 327–335.
- Hoff, P. (2009). *A First Course in Bayesian Statistical Methods* (2nd ed.). Springer.
- IEC (2005a). *Amendment to the IEC 61400-1:2005 standard*. International Electrotechnical Commission.
- IEC (2005b). *IEC 61400-1 (2005) International Standard, Wind turbines - Part 1: Design requirements* (third ed.). International Electrotechnical Commission.
- Katafygiotis, L. & K. Zuev (2008). Geometric insight into the challenges of solving high-dimensional reliability problems. *Probabilistic Engineering Mechanics* 23(2-3), 208 – 218. 5th International Conference on Computational Stochastic Mechanics.
- Santoso, A., K. Phoon, & S. Quek (2011). Modified metropolis-hastings algorithm with reduced chain correlation for efficient subset simulation. *Probabilistic Engineering Mechanics* 26(2), 331 – 341.
- Schueller, G. & H. Pradlwarter (2007). Benchmark study on reliability estimation in higher dimensions of structural systems - an overview. *Structural Safety* 29(3), 167 – 182. A Benchmark Study on Reliability in High Dimensions.
- Sichani, M., S. Nielsen, & C. Bucher (2011). Efficient estimation of first passage probability of high dimensional non-linear systems. *Probabilistic Engineering Mechanics* 26(4), 539 – 549.
- Sichani, M., S. Nielsen, & A. Naess (2011). Failure probability estimation of wind turbines by enhanced monte carlo. *Engineering Mechanics, ASCE* 138(4), 379 – 389.
- Sichani, M. T. (2011). *Estimation of Extreme Responses and Failure Probability of Wind Turbines under Normal Operation by Controlled Monte Carlo Simulation*. Ph. D. thesis, Department of Civil Engineering, Aalborg University, Aalborg, Denmark.
- Tierney, L. & A. Mira (1999). Some adaptive monte carlo methods for bayesian inference. *Statistics in Medicine* 18, 2507 – 2515.
- Valdebenito, M., H. Pradlwarter, & G. Schueller (2010). The role of the design point for calculating failure probabilities in view of dimensionality and structural nonlinearities. *Structural Safety* 32(2), 101 – 111.
- Zuev, K. & L. Katafygiotis (2011). Modified metropolis-hastings algorithm with delayed rejection. *Probabilistic Engineering Mechanics* 26(3), 405 – 412.

Fatigue reliability of offshore wind turbine systems

S. Márquez-Domínguez & J.D. Sørensen
Aalborg University, Denmark

ABSTRACT: Optimization of the design of offshore wind turbine substructures with respect to fatigue loads is an important issue in offshore wind energy. A stochastic model is developed for assessing the fatigue failure reliability. This model can be used for direct probabilistic design and for calibration of appropriate partial safety factors / fatigue design factors (FDF) for steel substructures of offshore wind turbines (OWTs). The fatigue life is modeled by the SN approach. Design and limit state equations are established based on the accumulated fatigue damage. The acceptable reliability level for optimal fatigue design of OWTs is discussed and results for reliability assessment of typical fatigue critical design of offshore steel support structures are presented.

1 INTRODUCTION

The wind turbine industry is growing fast. Offshore wind turbines (OWTs) are placed at sites with larger water depths and harsher environment far away from the coast, implying that fatigue and corrosion deterioration processes becomes very important. In order to minimize the cost of energy (CoE), it is important to optimize the design of the substructures with respect to the fatigue limit state. Wind turbines need to be analyzed and designed taking in account complex loads interacting together and highly influenced by the wind turbine control system. The wave and wind loads influence the dynamical behavior of OWTs resulting in increased fatigue damage on the substructure. Different regimens of equivalent turbulence intensity can be analyzed and modeled by aerodynamic codes such as FAST, see Jonkman & Buhl (2005). This code in this paper is used to estimate the wind fatigue load effects, see section 2.

Experience from the oil & gas industry can be used to assess the factors influencing the costs for the design, inspection, repair and failure of OWT substructures. In the oil & gas industry, probabilistic tools have been developed. Design equations and limit state equations are developed using these principles in order to optimize the design of offshore wind turbine substructures with respect to fatigue loads. The fatigue life is modeled by the SN approach, see section 3. Design and limit state equations are established based on the accumulated fatigue damage. The acceptable reliability level for optimal fatigue design of OWTs is discussed and results for reliability assessment of typical fatigue critical design of offshore steel support structures are presented in section 4.

2 WIND TURBINE MODEL

Substructures such as jacket type are difficult to simulate in conventional aeroelastic codes. Therefore, in this paper is assumed that the OWT can be simulated as a fixed-bottom monopile with rigid foundation representing an equivalent jacket OWT substructure in order to obtain rep-

representative hot spots stresses. The behavior of the representative 5MW NREL OWT model is simulated using the aeroelastic simulation code called FAST (Jonkman et al. 2009). The water depth is assumed to be 30 m and the blades are controlled with pitch active control. The wind field is simulated by different equivalent wind turbulence intensities based on the reference turbulence intensity, 'I_{ref}'. For this study, 'I_{ref}' is equal to 0.12 (low turbulence) corresponding to the 90% quantile of the characteristic value in IEC 61400-1 (2005); see table 1 where equivalent turbulence intensities are shown for different mean wind speeds 'U' and quantile values 'P_{lev}' of the turbulence intensity modeled by a LogNormal distribution (according to IEC 61400-1 (2005)). These equivalent wind turbulence intensities were the main input into Turbsim (Turbulent-wind simulator); see Jonkman (2009), to generate the turbulence field for each equivalent turbulence intensity. The Turbsim output is used as input into AeroDyn which is a set of routines used in connection with FAST to model and predict the aerodynamics of horizontal axis wind turbines (Moriarty & Hansen 2005).

Table 1. Equivalent wind turbulence intensities, I_{eqv}.

U	P _{lev} =0.10	P _{lev} =0.30	P _{lev} =0.50	P _{lev} =0.70	P _{lev} =0.90
m/s	I _{eqv} (%)	I _{eqv} (%)	I _{eqv} (%)	I _{eqv} (%)	I _{eqv} (%)
4	7.0	8.5	9.5	10.5	12.0
6	7.7	9.0	9.9	10.7	12.0
8	8.3	9.4	10.1	10.9	12.0
10	8.7	9.7	10.4	11.0	12.0
12	9.0	9.9	10.5	11.1	12.0
14	9.3	10.1	10.7	11.2	12.0
16	9.5	10.3	10.8	11.3	12.0
18	9.7	10.4	10.9	11.3	12.0
20	9.9	10.5	11.0	11.4	12.0
22	10.0	10.6	11.0	11.4	12.0
24	10.2	10.7	11.1	11.5	12.0

During the simulations an initial blade pitch angle between 0 and 9 degrees is selected suitable for the given simulation in order to keep the power and rotor speed at rated values. A time series of 70 minutes was simulated. However, the first 10 minutes were eliminated in order to obtain a wind turbine behavior similar to operational conditions without any disturbance from initial conditions.

Once the turbine response has been simulated, a point between sea water level and mudline was chosen (around 16 m of height from the mudline). This point will be considered as a representative hot spot where the bending moments and stress concentration are important. The bending moments are calculated considering normal operating conditions with the wind turbine rotor perpendicular to the wind direction. The distribution of wind directions are not taken into account. Therefore, the reliability indices calculated can be considered conservative. After modeling, the stress ranges are grouped in intervals by a rainflow counting analysis in order to calculate the frequency at each wind speed bin. For reliability assessment the OWT can be modeled by a system consisting of hot spots and their interrelations (stochastic and functional interdependencies). This paper only considers a reliability analysis in a critical hot spot.

3 PROBABILISTIC MODEL FOR FATIGUE FAILURE

3.1 Assessment of reliability

This section describes how the reliability of the fatigue critical details can be performed using the SN-approach with SN-curves in combination with the Miner's rule as generally recommended in codes and standards, see e.g. EN 1993-1-9 (2005), IEC 61400-1 (2005), DNV (2010), and GL (2005).

If a bilinear SN-curve is applied the SN relation can be written (Faber et al. 2005):

$$N = K_1 \left(\Delta s \left(\frac{T}{T_{ref}} \right)^\alpha \right)^{-m_1} \quad \text{and} \quad N = K_2 \left(\Delta s \left(\frac{T}{T_{ref}} \right)^\alpha \right)^{-m_2} \quad (1)$$

where K_1 , m_1 = material parameters for $N \leq N_C$; K_2 , m_2 = material parameters for $N > N_C$; Δs = stress range; N = number of cycles to failure; T = material thickness (50 mm); T_{ref} = reference thickness (25 mm); and α = scale exponent that depends on the detail considered, see DNV-RP-C203. Further, it is assumed that the total number of stress ranges for a given fatigue critical detail can be grouped in n_σ groups/intervals ΔQ_i such that the number of stress ranges in group i is n_i per year. $(\Delta Q_i, n_i)$ is obtained by Rainflow counting. Therefore, this procedure is applied for each simulation model with different equivalent wind turbulence intensity.

The code-based, deterministic design equation using the Miner rule is written

$$G = 1 - \sum_i \sum_k \frac{T_{FAT}^{n_{i,j=5,k}}}{K_1^c s_i^{-m_1}} \cdot P(V_i) - \sum_i \sum_k \frac{T_{FAT}^{n_{i,j=5,k}}}{K_2^c s_i^{-m_2}} \cdot P(V_i) = 0 \quad (2)$$

where $s_i = \frac{\Delta Q_{i,j=5,k}}{z} \left(\frac{T}{T_{ref}} \right)^\alpha$ = stress range 'k' given mean wind speed V_i and turbulence σ_{u_5} (90 % quantile); $n_{i,j=5,k}$ = number of stress ranges equal to $(\Delta Q_{i,j=5,k}/z)$ given mean wind speed V_i and turbulence σ_{u_5} ; $P(V_i)$ = probability of mean wind speed at bin number 'i'; ΔQ_i = range of load effect (proportional to stress range s_i in group 'i'); z = design parameter, e.g. cross sectional area; T_{FAT} = fatigue design life; K_i^c = characteristic value of K_i ($\log K_i^c$ equal to the mean of $\log K_i$ minus two standard deviations of $\log K_i$).

The probability of failure (and the corresponding reliability index) is calculated using the design value 'z' which is determined from the design equation (2) and used in the following limit state equation to estimate the reliability:

$$g = \Delta - \sum_i \sum_j \sum_k \frac{t \cdot n_{ijk}}{K_1 s_i^{-m_1}} \cdot P(\sigma_{u_j} | V_i) \cdot P(V_i) - \sum_i \sum_j \sum_k \frac{t \cdot n_{ijk}}{K_2 s_i^{-m_2}} \cdot P(\sigma_{u_j} | V_i) \cdot P(V_i) = 0 \quad (3)$$

where Δ = model uncertainty related to Miner's rule for linear damage accumulation. Δ is assumed to be Log-Normal distributed with mean value=1 and coefficient of variation COV_Δ ;

$s_i = X_w X_{SCF} \frac{\Delta Q_{ijk}}{z} \left(\frac{T}{T_{ref}} \right)^\alpha$ = stress range 'k' given V_i and σ_{u_j} ; $I = (\sigma_{u_j} / V_i)$ = turbulence intensity;

n_{ijk} = number of stress ranges equal to $(\Delta Q_{ijk} / z)$ during 60 minutes given V_i and σ_{u_j} ;

$P(\sigma_{u_j} / V_i)$ = probability of turbulence in the bin number 'j'. According with the table 1, the discretization is divided in 5 bins such that $P(\sigma_{u_j} | V_i) = 0.2$ and σ_{u_j} are the quantile values: $\sigma_{u_1} = 10\%$;

$\sigma_{u_2} = 30\%$; $\sigma_{u_3} = 50\%$; $\sigma_{u_4} = 70\%$; $\sigma_{u_5} = 90\%$.

A representative stochastic model is represented in the table 2. The COV values for X_{SCF} and X_w should be associated with specific recommendations for how detailed the estimation of stress concentration factors and wind/wave loads should be made; $\log K_i$ is modeled by a Normal distributed stochastic variable according to a specific SN-curve and follows the recommendations in DnV-C203 (2010). t = time ($0 \leq t \leq T_L$) where T_L indicates the service life. σ_{u_j} is the standard deviation of turbulence at a given mean wind speed U . σ_{u_j} is modeled as Log-Normal distributed with characteristic value $\hat{\sigma}_{u_j}$ defined as the 90% quantile and standard deviation equal to $I_{ref} \cdot 1.4$ m/s. $\hat{\sigma}_{u_j}$ is modeled based on 61400-1(2005):

$$\hat{\sigma}_u(U) = I_{ref} \cdot (0.75 \cdot U + b); \quad b = 5.6 \text{ m/s} \quad (4)$$

The cumulative (accumulated) probability of failure in the time interval $[0, t]$ is obtained by

$$P_f(t) = P(g(t) \leq 0) \quad (5)$$

The probability of failure can be estimated by FORM/SORM techniques or simulation, see Madsen et al. (1986), and Sørensen (2011). For OWT components the maximum annual probability of failures between 10^{-3} and 10^{-4} considering that usually no people are in danger in case of failure and the economic losses are limited, see also Sørensen (2012). The upper bound 10^{-4} corresponds to the reliability level often used for unmanned offshore structures for oil and gas. The lower bound 10^{-3} corresponds approximately to the annual probability of failure implicitly used for calibration of partial safety factors for onshore wind turbines. The reliability indices (with reference period one year) corresponding to 10^{-3} and 10^{-4} are 3.1 and 3.7. It is noted that the required reliability level also depends on the consequences for the structural system that fatigue failure occurs in a structural detail.

3.2 Random fatigue limit model proposed by Lassen et al. (2005).

As an alternative model for the linear and bilinear SN-curves for welded fatigue critical details normally specified in design codes, Lassen et al. (2005) proposed a non-linear model for estimating the fatigue life, called the random fatigue limit model (RFLM). In this paper it is compared with the above traditional S-N curves considering as basis an 'F'-structural detail from DNV-RP-C203 (2010). RFLM considers both the fatigue life and the fatigue limit as random variables; see Lassen et al. (2005). The advantage of RFLM is that it takes into consideration the variation in the fatigue critical stress range threshold and that run-out results can easily be included. The model gives a nonlinear S-N curve in a log-log scale in the fatigue-limit area; the fatigue life is gradually increasing and is approaching a horizontal line asymptotically instead of the abrupt knee point of the bilinear curve.

The RFLM SN-curve proposed by Lassen et al. (2005) is written:

$$\ln N = \beta_0 - \beta_1 \ln(\Delta\sigma - \gamma) + \varepsilon \quad (6)$$

where β_0, β_1 are constants and γ, ε model the threshold and random variations in fatigue life.

The deterministic parameters, β_0, β_1 and stochastic variables, γ, ε are shown in table 2 corresponding to DNV-RP-C203, class 'F' SN-curve.

The limit state equation considering a RFLM SN-curve is written:

$$g(t) = \Delta - \sum_i \sum_j \sum_k \frac{1}{N(\Delta\sigma_{ijk}, \beta_0, \beta_1, \gamma, \varepsilon)} t \cdot n_{ijk} \cdot P(\sigma_{u_j} | V_i) P(V_i) \quad (7)$$

4 EXAMPLE

A welded detail (hot spot) in an offshore wind turbine steel support structure is considered. The OWT is assumed to have an expected life $T_L = 25$ years and $T_{FAT} = 75$ years. Two different kind of fatigue critical details ('F' and 'D') are considered in combination with three different SN-curves (in air, in sea water with cathodic protection and free corrosion according to DnV-C203 (2010)). The annual and accumulated reliability indices were calculated with first order reliability method (FORM) and verified with Monte Carlo Simulation (MCS) using the stochastic model proposed in the Table 2. The alternative fatigue-life model (RFLM) is compared with traditional models based on a linear / bi-linear S-N curve approach, for this case the thickness relationship is considered, see section 3.

5 RESULTS

Tables 3 to 6 show results of different analyses considering 'D' and 'F' fatigue critical details based on DNV-RP-C203 (2010) and Lassen et al. (2005). The following cases are considered:

Table 2. Stochastic model. D: Deterministic, N: Normal, LN: LogNormal.

Variable	Distribution	Exp. value	Standard deviation	Charac. value	Comments
Δ	LN	1	0.30	1	
X_{SCF}	LN	1	0.10	1	Stresses
X_w	LN	1	0.10	1	Wind/Wave loads
'D'-STRUCTURAL DETAIL					
m_1	D	3			
$\log K_1$	N	12.564	0.20	12.164	In air
$\log K_1$	N	12.164	0.20	11.764	Cathodic protection
$\log K_1$	N	12.087	0.20	11.687	Free corrosion
m_2	D	5			
$\log K_2$	N	16.006	0.20	15.606	In air
$\log K_2$	N	16.006	0.20	15.606	Cathodic protection
'F'-STRUCTURAL DETAIL					
m_1	D	3			
$\log K_1$	N	12.255	0.20	11.855	In air
$\log K_1$	N	11.855	0.20	11.455	Cathodic protection
$\log K_1$	N	11.778	0.20	11.378	Free corrosion
m_2	D	5			
$\log K_2$	N	15.491	0.20	15.091	In air
$\log K_2$	N	15.491	0.20	15.091	Cathodic protection
logK ₁ and logK ₂ are assumed fully correlated					
RANDOM FATIGUE LIMIT MODEL (RFLM) BY T. LASSEN (F-CLASS)					
Variable	Distribution	Exp. value	Standard deviation	Comments	
β_0	D	22.48		Fatigue curve coefficient	
β_1	D	2.100		Fatigue curve coefficient	
logy	N	4.1	0.16	Fatigue Limit	
ϵ	N	0.0	0.14	Error term	

- Case A: design equation with linear SN-curve ($m=3$) and limit state equation with linear SN-curve ($m=3$)
- Case B: design equation with linear SN-curve ($m=3$) and limit state equation with bilinear SN-curve;
- Case C: design equation with bilinear SN-curve and limit state equation with linear SN-curve ($m=3$);
- Case D: design equation with bilinear SN-curve and limit state equation with bilinear SN-curve;
- Case E: Design: Bi-linear SN-curve and limit state equation with RFLM model – with and without thickness reduction.

Figures 1 and 2 show the annual and cumulative reliability indices respectively with $T_L = 25$ years and a $T_{FAT} = 75$ years with different combinations of the design equation and LSE for structural details from DNV ('F' and 'D') considering the SN-curves 'in sea water with cathodic protection'. The results include the reliability indices corresponding to the accumulated and annual probability of failure at year 25 ($=T_L$). Further, also the design value 'z' is shown normalized with respect to the design value obtained using the case 'D' combination with cathodic protection for a class 'F'. The results show that the endurance limit is quite important for reliability assessment of fatigue critical details in wind turbine support structures. This is due to the large number of cycles and that the stress ranges are distributed over a wide range. The endurance limit and the slope of the SN-curve for small stress ranges are generally quite uncertain, and more fatigue tests in this range (although costly) would be important for improving the reliability assessment.

For case 'D' which corresponds to the usual design recommendations, the results show that the annual reliability index exceeds the target level 3.1 during the whole lifetime, but the target level 3.7 is reached after 12 years. For case 'A' the reliability level 3.7 is reached after 22 years,

but it is also seen that the design parameter 'z' (e.g. the cross-sectional area) for case 'A' is increased by 74% compared to case 'D' for a class 'F' detail. If a reliability level with a minimum annual reliability index equal to 3.7 is required then it is necessary for a case 'D' design situation to increase the deterministic design fatigue life or to perform inspections during the lifetime, see below.

In table 7, results are shown using the case 'E' corresponding to a class 'F' structural detail. The results show that with the design parameter 'z' obtained using a bilinear SN-curve for design that both the annual and the cumulative reliability indices are increased significantly compared to case 'D'. However, it is noted that the RFLM model does not include a thickness reduction effect which could be expected to minimize the difference slightly.

In table 8, results are shown for case 'D' with cathodic protection SN-curves with a wide range of fatigue design lives for $T_L = 25$ years and class 'F' and 'D' details. The corresponding fatigue design factors (FDFs) are also shown and it is seen that in order to satisfy minimum annual reliability indices larger than 3.1 and 3.7 FDF values equal to 2.5 and 4.9 have to be required. Alternatively, inspections have to be required. Table 8 also shows the design parameter 'z' value need to be increased. For offshore wind turbine substructures the required FDF values and the possibility of performing inspections can be decided based on cost-benefit considerations since typically only monetary consequences will result in case of failures. Further, site-specific conditions can be accounted for.

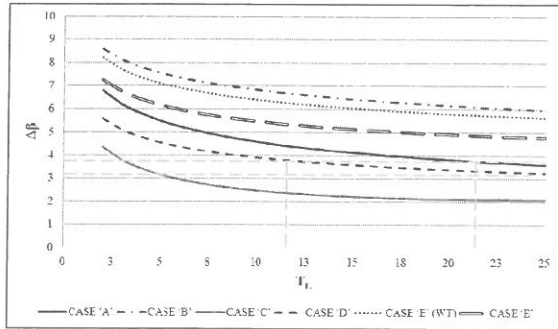


Figure 1: Annual reliability indices for structural details ('D' and 'F').

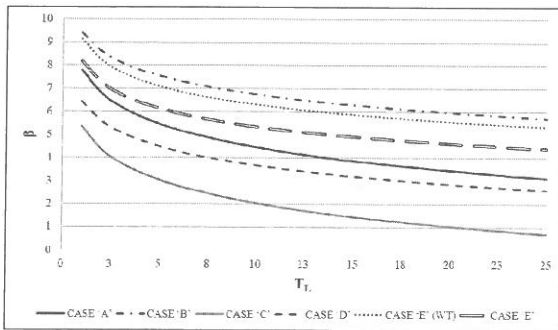


Figure 2: Cumulative reliability indices for structural details ('D' and 'F').

Table 3. Annual and accumulated reliability indices and design values for Case A ($T_L = 25$ years)

	'D'-DETAIL			'F'-DETAIL		
	In air	Cathodic protection	Free corrosion	In air	Cathodic protection	Free corrosion
β	3.13	3.13	3.13	3.13	3.13	3.13
$\Delta\beta$	3.60	3.60	3.60	3.60	3.60	3.60
z	1.01	1.37	1.45	1.28	1.74	1.85

Table 4. Annual and accumulated reliability indices and design values for Case B ($T_L = 25$ years)

	'D'-DETAIL		'F'-DETAIL	
	In air	With cathodic protection	In air	With cathodic protection
β	4.21	5.71	4.21	5.71
$\Delta\beta$	4.56	5.95	4.56	5.95
Z	1.01	1.37	1.28	1.74

Table 5. Annual and accumulated reliability indices and design values for Case C ($T_L = 25$ years)

	'D'-DETAIL		'F'-DETAIL	
	In air	With cathodic protection	In air	With cathodic protection
β	1.96	0.72	1.96	0.72
$\Delta\beta$	2.72	2.10	2.72	2.10
z	0.77	0.78	0.98	1.00

Table 6. Annual and accumulated reliability indices and design values for Case D ($T_L = 25$ years)

	'D'-DETAIL		'F'-DETAIL	
	In air	With cathodic protection	In air	With cathodic protection
β	2.81	2.61	2.81	2.61
$\Delta\beta$	3.37	3.25	3.37	3.25
z	0.77	0.78	0.98	1.00

Table 7. Annual and accumulated reliability indices and design values for the Case E (F-Detail and $T_L = 25$ years)

	with thickness relationship		without thickness relationship	
	β	4.40	5.35	
$\Delta\beta$	4.78	5.64		
z	1.00	1.00		

Table 8. Influence of 'z' parameter in the annual and cumulative reliability indices, Fatigue Design Factors (FDF) calculated for a wide range of fatigue design live (years) for 'F and D' details with cathodic protection SN-curve considering the case 'D' ($T_L = 25$ years).

T_{FAT}	25	40	60	75	100	120	140	160	180	200	250
B	1.39	1.92	2.37	2.61	2.93	3.13	3.31	3.45	3.58	3.70	3.95
$\Delta\beta$	2.46	2.76	3.07	3.25	3.50	3.66	3.80	3.92	4.03	4.13	4.35
$z(F)$	0.80	0.88	0.95	1.00	1.06	1.09	1.13	1.16	1.19	1.22	1.26
$z(D)$	0.63	0.70	0.76	0.78	0.83	0.87	0.89	0.92	0.93	0.95	1.00
FDF	1.00	1.60	2.40	3.00	4.00	4.80	5.60	6.40	7.20	8.00	10.0

6 CONCLUSIONS

A probabilistic model was formulated for fatigue failure in jacket type offshore wind turbine substructures accounting for the operational characteristics of wind turbines and deterministic design with specifications in IEC 61400. A comparative analysis between different SN-curves shows a large effect on the reliability depending on the SN-curves used. Further, an alternative non-linear SN-curve model, RFLM, was considered. The results with the RFLM model indicates that higher reliabilities can be obtained compared to the traditional bilinear SN-curves. For application within offshore wind turbine substructures more research are needed with respect to calibration of fatigue design factors for inclusion in design standards. Also it is important to account for system effects in case of fatigue failure in different fatigue critical details in one and/or many wind turbine support structures in a wind farm, Also the information from inspections and condition monitoring should be included. Furthermore, wake effects should be included to account for wind farm effects.

7 ACKNOWLEDGEMENT

The authors wish to thank to the financial support from the mexican national council of science and technology (CONACYT) and the norwegian centre for offshore wind energy (NORCOWE) under grant 193821/S60 from the research council of Norway (RCN). NORCOWE is a consortium with partners from industry and science, hosted by the Christian Michelsen research institute.

8 REFERENCES

- BS 7910:2005. *Guide to methods for assessing the acceptability of flaws in metallic structures*.
DNV-RP-C203: 2010. *Fatigue design of offshore steel structures*. DnV, April 2010.
EN 1993-1-9:2005. *Eurocode 3: Design of steel structures - Part 1-9: Fatigue*. CEN. 2005.
Faber M.H., Sørensen, J.D., Tychsen J. & Straub D., 2005. Field implementation of RBI for jacket structures. *Journal of Offshore Mechanics and Arctic Engineering*. August 2005 Vol. 127.
GL: 2005. Guideline for the certification of offshore wind turbines.
IEC 61400-1:2005. *Wind turbine generator systems – Part 1: Safety requirements*. 2005.
Jonkman, J.M., 2009. *Turbsim User's Guide*, Technical Report NREL/TP-500-46198.
Jonkman J.M., Butterfield S., Musial W. & Scott G., 2009. *Definition of a 5-MW Reference Wind Turbine for Offshore System Development*, Technical Report NREL/TP-500-38060.
Jonkman J.M. & Buhl, M.L., 2005. *FAST User's Guide*, Technical Report NREL/EL-500-38230.
Lassen, T., Darcis Ph., & Recho N., 2005. *Fatigue Behavior of Welded Joints Part 1 — Statistical Methods for Fatigue Life Prediction*. Supplement to the *welding journal*, December 2005 sponsored by the american welding society and the welding research council.
Madsen, H.O., S. Krenk & N.C. Lind, 1986: *Methods of structural reliability*. Prentice-Hall.
Moriarty, P.J. & Hansen A.C., 2005. *AeroDyn Theory Manual*, Technical Report NREL/TP-500-36881.
Sørensen, J.D., 2012. Reliability-Based Calibration of Fatigue Safety Factors for Offshore Wind Turbines. *International Journal of Offshore and Polar Engineering*. ISSN 1053-5381. Vol. 22, No. 2.
Sørensen, J.D., 2011. Notes in 'Structural Reliability Theory - and Risk Analysis'. Aalborg University.

Maintenance optimization for offshore wind turbines using POMDP

J.S. Nielsen & J.D. Sørensen
Aalborg University, Denmark

ABSTRACT: In this work, a Partially Observable Markov Decision Process (POMDP) is used for decision support for offshore wind turbines. The optimal decision policies for inspection and repair are obtained for each time step dependent on the belief state for the damage state after monitoring, and thus dynamic programming can be used. Seasonal weather variations are included through their influence on weather constrains for inspections and repairs, as well as costs to lost production, when corrective repair is not possible after failure. Application of the model is illustrated through an example, where the main bearing is considered. Optimization is initially performed for one component, and decision making for an entire wind farm is considered by using revised decision policies, when mobilization costs are already paid for another repair. The total costs are calculated for an entire wind farm using simulation and by using the identified decision policies.

1 INTRODUCTION

Maintenance decision making for offshore wind turbines is both an important and complex topic. Important because maintenance costs are high and need to be reduced to make offshore wind energy more competitive to other energy sources. Complex because decisions need to be made taking into account entire wind farms, costs to inspections, preventive repairs, corrective repairs and lost production, and weather constrains are present for maintenance actions. Furthermore, large uncertainties are present for the deterioration processes and condition monitoring information.

For many mechanical components, more failures can be observed than foreseen in the design, because the actual behavior for e.g. bearings and gears is different compared to the design assumptions. This leads to large costs for corrective and unplanned preventive maintenance. These costs can potentially be reduced if decisions on inspections and preventive maintenance are made with support from risk-based methods.

2 PRE-POSTERIOR DECISION PROBLEM

Maintenance planning for offshore wind turbines basically contains decisions regarding inspections and repairs. If the lifetime is divided into a discrete number of time steps and decisions regarding inspections and repairs are made at each time step, the associated simplified decision tree is shown in Figure 1.

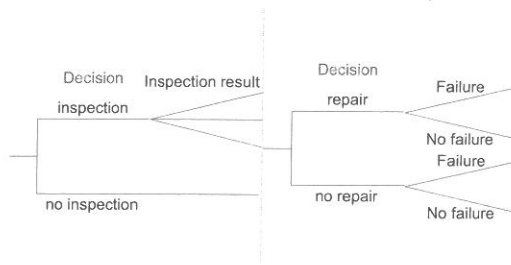


Figure 1: Simple decision tree for inspection and repair planning. Should be repeated for each time step. At the dashed vertical lines all branches continue as the showed one.

This decision problem contains two decisions at each time step, and earlier decisions influence later decisions; therefore, the problem is a pre-posterior decision problem. For pre-posterior decision problems, optimal decisions should be made such that the expected costs are minimized. When a decision is made, it is necessary to take into account the optimal decisions for all future decisions. The number of branches to evaluate in the decision tree increase exponentially with the number of time steps, and in the unreduced form it becomes intractable. Various approximations can be applied to make it possible to solve the problem. In this paper, the decision process is modeled as a Partially Observable Markov Decision Process (POMDP).

2.1 Markov decision problems

A Markov process has the property that the future is independent of the past given the present. The simplest decision problem related to the Markov process is the discrete Markov Decision Process (MDP). For this kind of problems, the state of nature is fully observed at each time step and a decision is made based on the current state of the system. The effects of the actions related to the decisions are uncertain, and costs are associated with the state of nature and decisions. The optimal decision then only depends on the current state of nature. Therefore, an optimal policy can be found for each possible state of nature by simply calculating the expected costs during the lifetime for all possible policies, and choosing those with lowest costs. (Jensen & Nielsen 2007)

Often, the deterioration state is not fully observed, but instead only observed through some indicator. This is called a Partially Observable Markov Decision Process (POMDP). This means that all past observations are relevant when the decision is made, and not only the present one. However, the past observations can be summarized by using Bayes rule to calculate the probability distribution for the present state of nature (belief state) given the observations. Then, the optimal policy can be found for a given belief state. (Jensen & Nielsen 2007)

For unbounded time horizons, the strategies are stationary. This means that the optimal policy is the same for all the time steps. For bounded time horizons, the policies will be different at different time steps. Near the end of the lifetime, it will not be cost-effective to make expensive repairs, even though it would be at the same probability belief state at earlier time steps. In this paper, only bounded time horizons are considered.

The advantage of the Markov decision models is that only the current belief state is of importance. This means that Dynamic Programming, introduced by Bellman in 1957 can be used (Dasgupta et al. 2006). When only the current belief state is of importance, the optimal decision can be found for all possible belief states for each time step, by starting from the last time steps, and using the optimal decisions found there, when earlier time steps are evaluated. Then the computational time is only linear with the number of time steps, and not exponential as for a traditional decision tree.

In reality, for discrete state spaces, the belief state is a continuous valued vector with unity magnitude. Therefore, there are infinitely many possible belief states. One way to solve this is to discretize the belief vectors, and interpolate the costs from other belief states between these states (Faddoul et al. 2011).

The classical POMDP has an uncertain inspection at the beginning of each time step, and the decision is made on whether a repair should be made. Corotis et al. (2005) extended the ap-

proach to include decisions on various types of inspection and maintenance methods for Risk-based inspection and maintenance planning for bridge girders. Faddoul et al. (2011) further extended the procedure to use submodels for more advanced inspection sequences, for example two inspections at each time step.

The general limitation with Markov models is the Markov assumption of independence between past and future given the present. Deterioration processes are generally not Markovian when epistemic time-invariant uncertainties are dominant. However, if time independent variables are included in the model, the future deterioration state is independent of the past given these time dependent variables (Straub 2009). Therefore, the policies can be found for each time step based on current belief state for the deterioration state and current belief state for the time-independent variable. This increases the number of calculations for each time step, but it is still only linear with the number of time steps.

For the case presented in this paper, a simple three state model for the component health have been applied, and therefore, time-invariant uncertainties are not included in the model. It can be relevant to use such a simple model in cases, where only limited knowledge about the deterioration processes is available. This is the case for many wind turbine components, as the observed behavior is different than the behavior expected from the theoretical models.

3 MODEL

The model presented in this section takes into account condition monitoring and inspections and optimal decision policies are found for each time step for the decision on inspections and repairs. The influence of the weather on accessibility has been included, such that it is uncertain if inspections and repairs are possible in a given time step. In each time step, the following takes place:

- Monitoring result is obtained
- Decision on inspection followed by inspection, if possible
- Decision on preventive repair followed by preventive repair, if possible
- Possible failure due to deterioration followed by corrective repair, if possible

The decision tree considered in the model is shown in Figure 2.

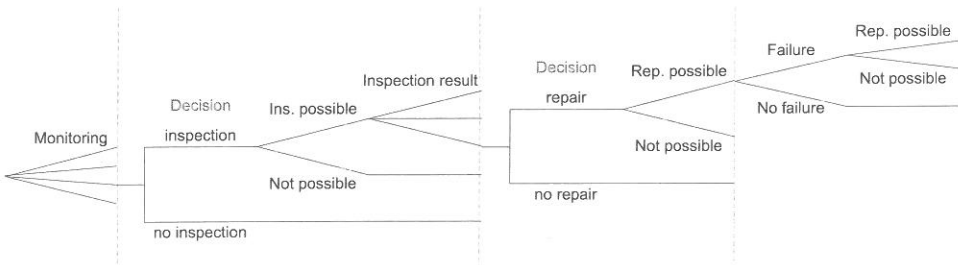


Figure 2: Decision tree. Should be repeated for each time step. At the dashed vertical lines all branches continue as the showed ones.

In this model, the health of the component can take three states; healthy, damaged, and failed. At each time step, there is a probability that the component advances to the following health state, else it remains at the current health state. If a component has failed, it is known, and only corrective repair is possible. Therefore, the belief state for the component health at the time of the decisions can be described by one continuous number, the probability of being damaged, $P(\text{dmg})$. The model can be extended to more damage states, and in that case the belief state for the component health will be a vector.

The component is assumed to be healthy at time step 1, and all repairs are perfect, and will therefore bring the component to the healthy state.

The costs included in the model are cost of inspections, preventive repairs, corrective repairs, and lost production. Lost production is incurred when failure happens, and in the following time steps, if corrective repairs are not possible.

3.1 *Weather constrains*

For offshore operations, vessels have limitations with regard to wave height and wind speed when a wind turbine needs to be accessed, and repair actions have to be made. If the duration of the operation as well as the weather limits are known and long term time series from the location are available, the probability of having an appropriate weather window in a given month of the year can be found. This probability can be found for all months and for all types of operations. Generally, the longer the weather window and the stricter the weather requirements, the larger is the probability that operations are not possible in a given time step. In the model it is assumed that repairs have stricter requirements than inspections, and corrective repairs have stricter requirements than preventive repairs. Therefore, at each time step, there should be correlation between whether inspections are possible and whether repairs are possible, such that repairs are not possible if inspections are not possible. However, if inspections are possible, repairs can still be impossible. The probabilities included in the model are therefore:

- Probability of inspection being possible
- Probability of preventive repairs being possible given that inspections are possible
- Probability of corrective repairs being possible given than preventive repairs are possible

In the model, the year has been divided in seasons, and the probabilities of operations not being possible are constant through each season. Initially these (conditional) probabilities have all been set to 0.1.

3.2 *Optimization procedure*

The principle behind the optimization calculations is dynamic programming, as explained in section 2.1. First, the state space for the component health is discretized into a finite number of belief states. For all these belief states, the optimal decision policies are found sequentially for each time step, starting at the last time step. At the final branches, at each time step, the expected costs for the remaining life time are needed in the calculations. These costs only depend on the belief state, and can be found by interpolation between the values found at the following time step. Further, each time step was divided in two, such that the interpolation was performed after the monitoring branches and after corrective repair branches. This reduces the number of branches to calculate at each time step by a factor three. At each time step, the probabilities and expected costs for all branches are calculated. This includes using Bayes rule for updating of the health state after monitoring and after inspections. The decision policies are found such that the expected costs are minimized.

4 EXAMPLE

The purpose of this example is to test that the model works as intended. The model could be used for various components, and in this example the main bearing is considered. The time step length is chosen to one month, and the lifetime of the turbine is set to 20 years.

4.1 *Deterioration model*

The deterioration model has been set such that the mean time to failure is 40 years, and the time in the damaged state is shorter than time in the healthy state. The transition probabilities are:

$$P(D_i | D_{i-1}) = \begin{bmatrix} 0.9972 & 0 & 0 \\ 0.0028 & 0.9917 & 0 \\ 0 & 0.0083 & 1 \end{bmatrix} \quad (1)$$

where there is a column for each old damage state. The belief state for the damage state is updated by multiplying this matrix by the old damage state, represented by a column vector:

$$P(D_i) = P(D_i | D_{i-1})P(D_{i-1}) \quad (1)$$

The optimal policies have been found for belief states in 0.01 discretization.

4.2 Monitoring and inspection model

A condition monitoring system based on vibration measurements is assumed to be available, and at each time step it is evaluated whether the measurements are low, medium, or high, or whether failure has occurred. This gives four outcomes for the monitoring result. The conditional probabilities for these outcomes are set to:

$$P(Mon_i | D_i) = \begin{bmatrix} 0.6 & 0.1 & 0 \\ 0.3 & 0.3 & 0 \\ 0.1 & 0.6 & 0 \\ 0 & 0 & 1 \end{bmatrix} \quad (2)$$

It is then decided, whether an inspection should be made, and if made, the inspection results in detection of damage or no detection of damage. This gives three outcomes for the inspection result, where the third one is failure:

$$P(Ins_i | D_i) = \begin{bmatrix} 0.9 & 0.2 & 0 \\ 0.1 & 0.8 & 0 \\ 0 & 0 & 1 \end{bmatrix} \quad (3)$$

Based on these probabilities, the probability for each inspection outcome can be found, and the belief state for the damage given each observation can be found using Bayes rule.

4.3 Approximation for wind farm

The optimal policies are found using the POMDP for a single turbine. When decisions are made for an entire wind farm, system effects can be considered. Here it is assumed that the mobilization cost for the repair vessel is a significant contributor to the total cost of a preventive repair, and if several repairs are made at the same time step, the mobilization costs only need to be paid once. To include this, the optimal repair policy has been found during the optimization procedure for the case, where the mobilization costs are zero at the current time step, due to another repair paying them, but everything in the future is as in the normal case. These revised policies are more cost-efficient than the policies found without taking system effects into account, but the solution is still suboptimal.

4.4 Costs

The costs are in the example set to the following relative values:

- Inspection: 1
- Preventive repair
 - Mobilization costs: 100
 - Unit repair cost: 100
- Corrective repair

- Lost production per month: 100
- Repair costs: 500

For simplicity, discounting has not been included, but this could be implemented.

4.5 Policies

The primary outcomes of the decision analysis are the decision policies. In Figure 3, the optimal decision policies are shown for inspections and preventive repairs. Furthermore, the revised policies in case of repairs of other turbines at the same time step are also shown. All decisions are shown as function of time step and the probability of a damage being present, updated using the monitoring outcome. For preventive repairs, the decision further depends on whether an inspection has been made, and the result of the inspection.

Generally, no inspections or preventive repairs should be made near the end of the life time. The scatter (the white lines) for the inspection policies in Figure 3 is due to the expected costs for the two decisions being very close. Therefore, it is almost indifferent whether inspections are made.

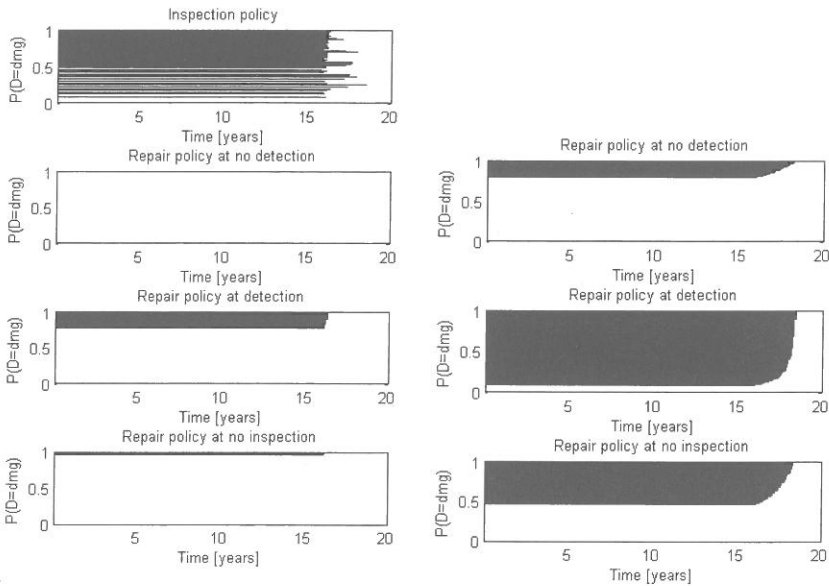


Figure 3: Policies for a wind turbine with (left) and without (right) mobilization costs. At a given time step, if the probability of a damage being present is within the black areas, inspections/repairs should be made.

4.6 Simulation for a wind farm

Simulations have been performed through the lifetime for a wind farm with 40 wind turbines. At each time step, the belief state has been updated for each wind turbine, and the optimal decision is chosen from the found decision policies. The revised decision policies with no mobilization costs are used for the remaining turbines, if any of the turbines are already being preventively or correctively repaired.

Figure 4 shows the main events of such a simulation. When repairs, but not repair decisions, are marked, the revised decision policies are the reason for the repairs.

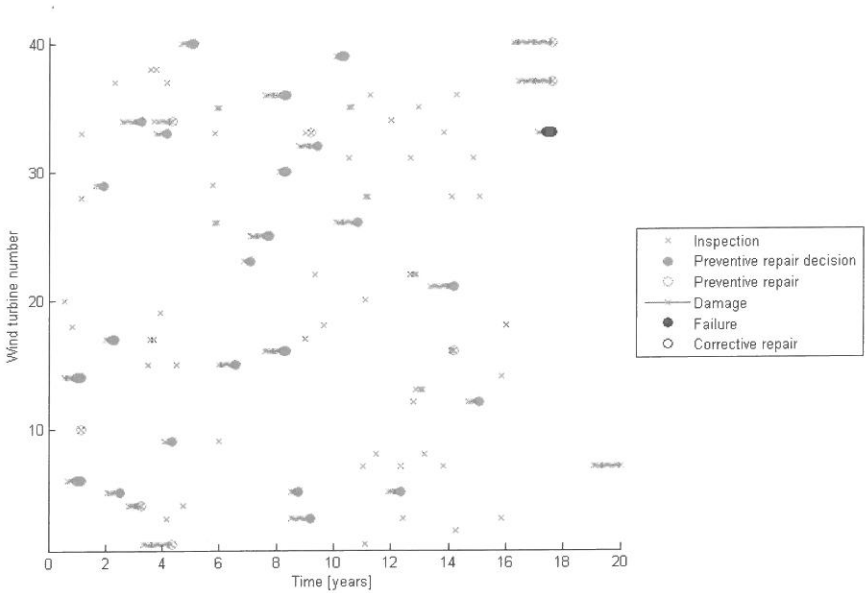


Figure 4: Simulation for a wind farm with revised policies found using POMDP.

The total expected lifetime costs have been found using only the policies with mobilizations costs included to approx 5300, and using also the revised policies to approx 5000. The costs are shown in Figure 5 divided into categories, and the 95% confidence intervals for the mean of the total costs are also shown. The total costs are 5% smaller when the revised policies are also used. Here, the mobilization costs and failure costs are smaller, while the unit repair costs are larger due to more preventive repairs.

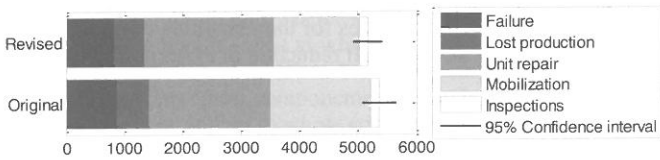


Figure 5: Comparison of costs for original policies and improved policies.

4.7 Simulation for a wind farm with harsh winter

For the simulations performed above, all conditional probabilities for repairs not being possible were 0.1 for all months. To evaluate the influence of a harsh winter, all the conditional probabilities are set to 0.9 for the first and fourth quarter of the year. The decision policies for this case is shown in Figure 6.

Here, the policies are periodic and depend on the month of year. Two months before the winter starts, repairs should be made for smaller probabilities of damage than in the beginning of the mild season. During the first part of the winter, even more repairs should be made, even though it is rarely possible. The total costs are here approx 5400 and 5200, when the original and revised policies respectively are used, which is more than the case with constant mild weather.

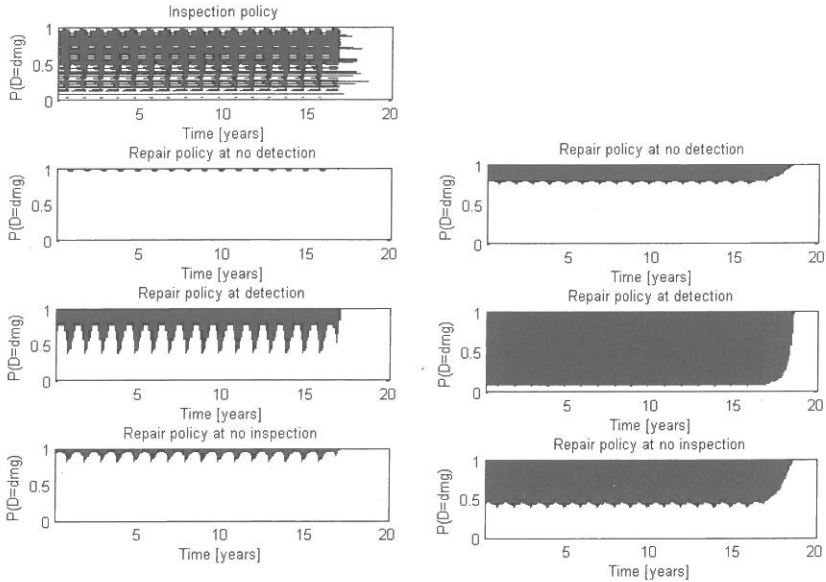


Figure 6: Policies for a wind turbine when the autumn and winter is harsh. In the black areas, inspections/repairs should be made.

5 CONCLUSIONS

A model based on POMDP was presented for decision support for inspections and repairs for offshore wind turbine components. When the weather was constant during the year, the decision policies were constant until the last few years of the lifetime, and in the case with seasonal changes in weather, the policies were periodic. Approximate decision making for a wind farm was performed by using revised decision policies for the remaining turbines, when other repairs were already being performed. This gave a small reduction in the expected costs.

6 ACKNOWLEDGEMENTS

The work presented in this paper is part of the project “Reliability-based analysis applied for reduction of cost of energy for offshore wind turbines” supported by the Danish Council for Strategic Research, grant no. 2104-08-0014. The financial support is greatly appreciated.

7 REFERENCES

- Corotis, R.B., Ellis, J.H. & Jiang, M., 2005. Modeling of risk-based inspection, maintenance and-life cycle cost with partially observable Markov decision processes. *Structure and Infrastructure Engineering*, 1(1): 75-84.
- Dasgupta, S., Papadimitriou, C.H. & Vazirani, U.V., 2006. *Algorithms*, McGraw-Hill.
- Faddoul, R., Raphael, W. & Chateauneuf, A., 2011. A generalised partially observable Markov decision process updated by decision trees for maintenance optimisation. *Structure and Infrastructure Engineering*, 7(10): 783-796.
- Jensen, F.V. & Nielsen, T.D., 2007. *Bayesian Networks and Decision Graphs*, New York, Springer.
- Straub, D., 2009. Stochastic Modeling of Deterioration Processes through Dynamic Bayesian Networks. *Journal of Engineering Mechanics*, 135(10): 1089-1099.

System reliability effects in wind turbine blades

Nikolay Dimitrov

Siemens Wind Power, Denmark

Peter Friis-Hansen

Det Norske Veritas, Norway

Christian Berggreen

Technical University of Denmark, Denmark

ABSTRACT: Laminated composite sandwich panels have a layered structure, where individual layers have randomly varying stiffness and strength properties. The presence of multiple failure modes and load redistribution following partial failures are the reason for laminated composites to exhibit system behavior from reliability point of view. The present paper discusses the specifics of system reliability behavior of laminated composite sandwich panels, and solves an example system reliability problem for a glass fiber-reinforced composite sandwich structure subjected to in-plane compression.

1 INTRODUCTION

The word “composite” originates from Latin, and literally means “made up of distinct parts”. This is indeed the most distinct feature of composite materials, which constitute of two different material phases and as a result have a number of unique properties. The combination of two material phases (fibers and matrix), arranged in multiple layers, results in a material with non-isotropic, non-homogeneous elastic strength properties, which can fail in a number of different failure modes. To the reliability engineer, the presence of distinct failure modes means that composites will exhibit system reliability behavior. This system behavior will appear on several levels, corresponding to the length scales at which the respective failure modes occur – starting from micro-scale (fibers, matrix and interface between them), through lamina (individual layers with unidirectional fibers), structural components such as laminate panels (stacks of individual laminas) and sandwich panels, and up to whole structures such as an entire wind turbine blade.

2 RELIABILITY-RELATED ASPECTS OF COMPOSITE MATERIALS

2.1 Length scales of composites

For the present paper the modeling domain is limited to three scale levels – individual lamina, laminated panels, and sandwich panels. Taking into account individual unidirectional lamina allows modeling the non-isotropic mechanical properties of composites, while avoiding the use of micromechanics. Including laminates and sandwich panels into the analysis allows modeling the reliability against failure of a given location within a structure – for example, a so-called “hot-spot” which is known or expected to be critically decisive for the overall safety of the structure.

2.2 Definition of failure events

Due to the presence of a number of layers, the failure of a laminated composite panel will often happen as a gradual event, with different layers failing in sequence. Between successive layer failures the load previously carried by the failed lamina is redistributed to the layers remaining intact. Consequently, the definition of an ultimate failure event for a composite sandwich panel

can to a high extent be a matter of subjective judgement. Probably the simplest approach to defining failure is identifying the so-called "first-ply failure" event, where failure of any of the laminate components (i.e. the first failure occurring under gradually increasing load) will be considered as a total structural failure. Such an approach can however lead to very inefficient designs, because typically the first failures are associated with matrix cracking, which does not have a significant effect on the residual stiffness and strength of the structure (see Figure 1). There is also some degree of redundancy in composite structures, meaning that the structure will often be able to withstand loads higher than the load at which the first failure has occurred.

A progressive failure analysis procedure can be used to find the maximum load which the structure can withstand while maintaining static equilibrium. This is the approach which most fully describes the failure process in the panel, however it might not be very useful for design purposes, because a large amount of irreversible damage can occur at load levels below the indicated ultimate strength. Finally, the approach adopted in this paper is to use a progressive failure analysis procedure to find the load level at which the first fiber breaching occurs. The use of progressive failure analysis means that the development of matrix-related failure events will be followed until the first fiber failure occurs. Although not describing the ultimate failure, this approach might be more realistic for design purposes as the failure event is at the point when the first significant damage occurs.

2.3 System characterization

As discussed in the preceding paragraph, progressive failure of composite laminates is characterized by redistribution of loads following each of the successive failure events. Individual lamina will have random strength, as well as random stiffness distributions, meaning that the sequence of layer failures might be different for different realizations of the stochastic quantities. This is illustrated on Figure 1, where for two different realizations of the random lamina strength properties the sequence of failure events is different.

Loading is not uniform either – a laminate can carry loads in a number of different directions, including both forces and bending moments, meaning that there will be a varying stress field inside the laminate.

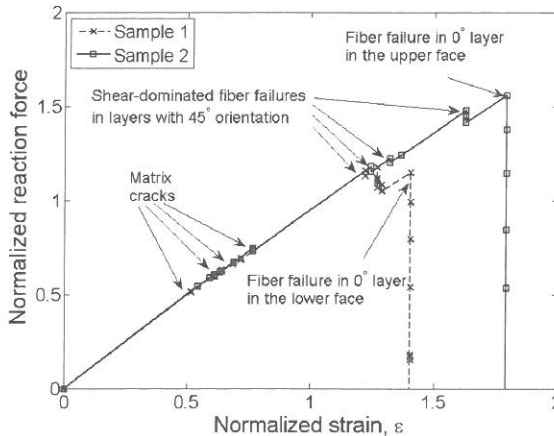


Figure 1: Path-dependent progressive failure process of a composite sandwich panel with random layer strengths

A system with the features as previously described (varying stiffness, strength, loading, and load redistribution following failures) could in principal be modeled as a parallel system, as long as the overall failure event occurred when the last system component has failed. However, according to the definitions of laminate failure given above, ultimate failure occurs when the maximum load bearing capacity of the structure has been exceeded, or significant damage has occurred. These events might happen when there are still a large number of intact layers, with

the failure event triggering a cascade failure of the remaining intact layers. This shows that a composite laminate can only be characterized as a general system.

Daniels (1945) has described the properties and derived reliability bounds for a similar type of system, consisting of equally loaded wires with random strength. The behavior of composite panels bears similarities with a Daniel's system, with failure being similarly characterized as the situation when the load exceeds the remaining bearing capacity of the structure. A difference with the classical Daniel's system is the fact that the individual components in the presently discussed problem have different stiffnesses, and are possibly loaded differently.

2.4 Solution of the system reliability problem

While a number of approaches to solving system reliability analysis problems exist, the choice of methods capable of resolving general systems is more limited. The solution methods which the authors of this paper have reviewed can in principal be divided into four groups:

- Monte Carlo simulation methods, including crude Monte Carlo, and adaptive (search-based) importance sampling (Melchers, 1990)
- Methods involving cut-set or tie-set definitions, e.g. Sequential Compounding (Kand & Song, 2010), linear programming (Song & Der Kiureghian 2003), or direct multivariate integration of the cut set / tie set when possible
- Using order statistic, transform each of the correlated component events into independent events, and compute their joint probability distributions (Friis-Hansen 1994)
- Obtaining reliability bounds by evaluation of component failure sequences leading to a point in the safe domain, thus evaluating the probability of the safe event set (Ditlevsen & Madsen 1996)

Due to the presence of multiple layers and multiple failure modes per lamina (in the example given below there are two modes per lamina) for a typical composite panel the total number of system components becomes fairly large. However, analyzing a large system in its entirety is difficult using most of the methods listed. Given the above, three most suitable approaches to solving the present reliability problem are identified:

- Use a technique not suffering from problem dimensionality (e.g., Monte Carlo);
- Simplify the problem by identifying possible critical components and focusing the analysis on those components. Consider each of the critical components as a cut-set, i.e., its failure results in an overall system failure;
- Use FORM/SORM analysis to find a possible design point, and correct the reliability estimate for any nonlinearity in the failure surface by applying importance sampling at the design point. This analysis can serve as an indicator to the degree of system behaviour present in the structure – under milder conditions this technique should be able to determine the correct probability of failure, while if there are significant system effects present with multiple design points far from each other, the reliability estimate will not be correct.

2.4.1 Representing laminated faces as single equivalent layers

In sandwich panels, the thickness of the core is typically much larger than the face thickness. This means that the variation of normal stresses in the faces will be relatively small, and under certain conditions it can be disregarded, assuming that the normal stresses are constant throughout the face (see Zenkert, 1995). Under this assumption, the sandwich model can be simplified by replacing the layer-wise description of the face laminate with equivalent, homogeneous layer, thus reducing the structural system to three components – upper face, lower face, and core. If the strength distributions of faces and core are available, it is straightforward to determine the system reliability by making a three-component series system analysis.

Although very useful in deterministic stiffness and strength analysis, it is possible that the single-layer representation of the faces will result in some deviations in the reliability estimate, because not all system effects and load redistribution effects under a progressive failure process will be accounted for. Here, the extent to which a homogeneous-layer representation of the faces can be used in reliability analysis is tested by comparing a reliability model based on homogeneous faces with the reliability estimates found from a full layer-wise model.

3 EXAMPLE RELIABILITY ANALYSIS OF A COMPOSITE SANDWICH PANEL

In the following, the discussion continues with the help of an example reliability problem, where the reliability against ultimate failure of a sandwich composite panel is considered.

3.1 Description of structure

The structure under consideration is a simply supported, unit-width sandwich beam with faces made of glass-fiber reinforced fibers, and a balsa wood core. The two faces are identical laminates, consisting of eight layers each. Individual layers have a thickness of 0.3mm, while the core thickness is 40mm, giving a total laminate thickness of 44.8mm. The layup sequence of the faces, $\theta = [-45^\circ +45^\circ 0^\circ 0^\circ 0^\circ 0^\circ +45^\circ -45^\circ]$, is simple, but in principle very similar to the layup sequences typically found on wind turbine blades, where the vast majority of layers have orientation of 0 and ± 45 degrees.

The sandwich beam is subject to a downward distributed load of $Q_z = -7\text{kN/m}$, and a compressive axial force $F_x = -1400\text{kN}$. This resembles a loading condition which can be typically found on the downwind surfaces of wind turbine blades.

In the typical composite structures loads are varying randomly, and are usually associated with a significant degree of uncertainty. This high uncertainty will be reflected in the reliability analysis and will make it more difficult to observe the influence of material properties. As the objectives of this study are related to material behavior, it is chosen that the load values will be deterministic, thus eliminating them as a source of uncertainty.

The presence of defects also has a significant influence to the strength of composites. However, taking defects into account needs the introduction of an additional set of theories and models, which will greatly enlarge the scope and complexity of the analysis. Therefore the materials used in the present study are considered defect-free. The influence of defects however remains an important field of study which should be addressed in future research.

3.2 Modeling of stochastic material properties

In order to allow for random variations in the material properties within the laminate, each layer should be represented by a separate set of stochastic variables describing the material properties. The properties of a lamina are typically characterized by 9 material constants, and for the 17-layer laminate this would mean at least 149 random variables (9 for each of the face layers, plus 5 for the core, where the transverse shear strength is the only strength property considered). Elastic properties have less variation than the strength properties, and for structures where geometric instabilities are not the dominant failure mechanism elastic properties have in general less influence on the load bearing capacity of the structure compared to the strength properties. Based on this argument, and in order to reduce the number of stochastic variables and to simplify the problem, it is decided to represent the elastic properties of materials with their mean values. This results in a total of 81 stochastic variables representing the material properties.

Table 1 lists the assumed statistical distributions of the five strength parameters for composite lamina used in the present study. The properties of the face materials are determined from material test data given in the OptiDat public database (Nijssen 2006).

Table 1. Statistical distributions of strength parameters.

Parameter	Designation	Mean	Cov	Distribution
Fiber tensile strength	X_t	780MPa	0.06	Lognormal
Fiber compressive strength	X_c	528MPa	0.19	Lognormal
Matrix tensile strength	Y_t	54MPa	0.08	Lognormal
Matrix compressive strength	Y_c	165MPa	0.14	Lognormal
Lamina shear strength	S	82MPa	0.15	Lognormal
Balsa core shear strength	S_c	2.2MPa	0.1	Lognormal

The correlation structure of the material variables has to represent both the spatial variation of a given mechanical property, as well as correlation between different properties (e.g., tensile

strength and shear strength). Thus the correlation coefficient between any two stochastic variables is taken as the product of two correlation coefficients,

$$\rho_{ij} = \rho_{L_i,L_j} \cdot \rho_{M_i,M_j} \quad (1)$$

where

- i, j refers to the variable number
- $L(i), L(j)$ are the layer numbers which variables i and j refer to
- $M(i), M(j)$ are the two material properties which the variables i and j refer to, respectively.
- ρ_{L_i,L_j} is the correlation coefficient between the same property for different layers. It is taken as a fixed value, with $0 \leq \rho_{L_i,L_j} \leq 1$ for $i \neq j$, and $\rho_{L_i,L_j} = 1$ for $i = j$.
- ρ_{M_i,M_j} is the correlation coefficient between the different material properties which variables i and j represent, regardless of layer number. The values of ρ_{M_i,M_j} are taken from a study by Toft (2010), based on micromechanics laws, and are listed in Table 2.

It is considered that the core strength properties are not correlated with face properties, and that properties in different faces are not correlated either.

The value of the correlation between the strength of different layers ρ_{L_i,L_j} is not known with certainty, as it is in principle very difficult to determine. It is nevertheless expected that a significant degree of correlation exists, because all material layers at a certain location within the structure have been subjected to similar conditions during the casting and curing process. In order to investigate the influence of inter-layer correlations, reliability analyses are carried out with a number of different correlation levels, $\rho_{L_i,L_j} = [0; 0.3; 0.7; 1]$. Correlation level of $\rho_{L_i,L_j} = 1$ will mean that all layers in a single face will have the same strength properties.

Table 2. Correlation coefficients between material strength variables.

	Xt	Xc	Yt	Yc	S
Xt	1	0.8	0	0.2	0.2
Xc	0.8	1	0	0.2	0.2
Yt	0	0	1	0.8	0.8
Yc	0.2	0.2	0.8	1	0.8
S	0.2	0.2	0.8	0.8	1

3.3 Evaluation of ultimate capacity of the sandwich model

The stress distribution within the panel is calculated using the assumption that the core is loaded primarily in shear, with negligible normal stresses, while the faces carry the normal stresses with negligible transverse shear loading (see Zenkert, 1995). The layer-wise stress distribution is calculated using Classical Lamination Theory, a method described in Jones, 1998. In order to determine the failure load, a step-by-step analysis is performed, where at each step the layer which will fail under the smallest load is identified. The mechanical properties of the failing layer are downgraded, the structure is updated, and a new analysis step is performed on the remaining layers. The procedure is interrupted when a fiber-mode failure is observed, which will typically happen after a number of matrix-mode failures have already occurred, which is also visible on Figure 1.

The load at which a lamina fails is identified using the Hashin composite failure criterion (Hashin, 1980). This failure criterion assumes that a lamina can fail in two distinct modes: fiber failure or shear-dominated matrix failure. Both matrix and fiber failures can be tensile or compressive, depending on the stresses acting on the lamina.

3.4 System reliability

The reliability of the structure described above is estimated using the three different approaches suggested in section 2.4, as well as using a model where laminate faces are represented as single

equivalent layers. A comparison of the performance of these four approaches is given in the following.

3.4.1 Crude Monte Carlo

Given that enough failure events are observed, crude Monte Carlo (MC) simulations are probably the most robust method for determining reliability, and are therefore used as a reference value here. All simulations used in the present study are run until at least 400 failure events have been observed, which according to the formula by Shooman (1968) corresponds to a 95% confidence that the error in the reliability estimate is less than 10%.

The results from the Monte Carlo simulations have identified that the layers in the face laminate oriented at 0 degrees are the most critical for the integrity of the structure (in most of the samples, indicating failure, the structure loses static equilibrium and collapses in a cascade of failures, following failure of one of the aforementioned 0-degree layers). In an attempt to simplify the problem and make use of more efficient reliability methods, this observation can be used as means to restrict the system analysis to the most critical parts of the structure.

The effects of correlation between properties of different lamina are also clearly visible from the MC simulations. As Figures 2.a) and 2.b) illustrate, in the case of uncorrelated material strengths in different lamina, the ultimate failure event is located at various layers, mostly the four layers with 0-degree orientation of the upper face. In the case of fully correlated layer strengths within the face laminates, almost all failure events are concentrated at a single layer, which is the highest-loaded layer with 0° fiber angle. Such a behavior is expected, as when all the lamina in a given laminate have the same properties, the one failing first will simply be the one subject to the highest stress.

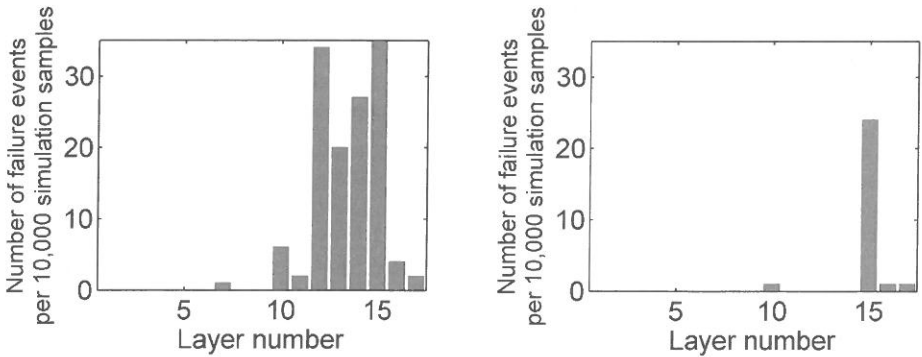


Figure 2: Location of layers where first fiber fracture is observed during a Monte Carlo simulation
 a) No correlation between lamina properties b) Full correlation between lamina properties

Results from Monte Carlo simulations, along with results from other used methods, are shown on Figure 3.

3.4.2 Series system of critical components

The results from the Monte Carlo simulations showed that some of the layers (the ones with 0-degree orientation) are the most critical to the integrity of the structure. If it is assumed that failure of any of these layers will lead to the ultimate collapse of the panel, each of the layers can be considered as a cut-set consisting of a single component. The reliability of each of these sets is equal to the component reliability, which, using single-component FORM analysis, is found to be $\beta_{component} = [2.586, 2.574, 2.562, 2.550]$ for the four 0-degree layers loaded in compression. System failure probabilities can be then estimated by $P_{f,cut-set} = 1 - \Phi_N(\beta_{components} R_{component})$, where $\Phi_N()$ denotes the N -dimensional multivariate normal distribution, and N is the number of components under consideration.

3.4.3 Equivalent layer model

The stochastic distributions of the equivalent strengths of the laminate faces used in the present problem are determined using simulation. For small failure probabilities, the tail of the strength distributions will have the greatest importance, and in order to ensure a good estimate some tail approximation technique has to be employed, as for example the ACER method by Naess (2009). For the present problem the probabilities of failure are relatively large, and a simple fit of a lognormal distribution to the data set from the MC simulation results gives excellent results too. The total probability of failure is then calculated by assuming a series system of three components (lower face, core, and upper face).

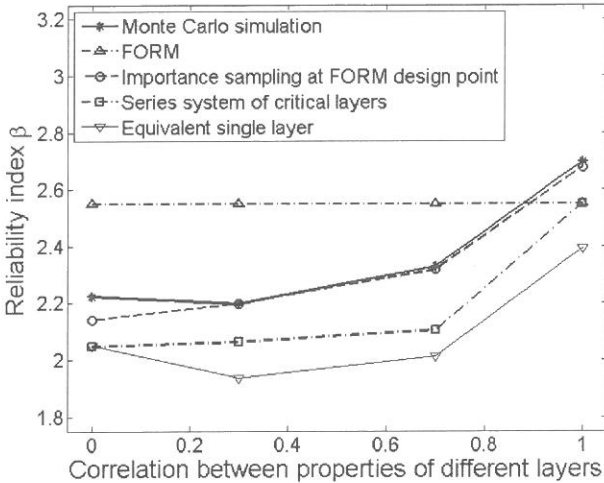


Figure 3: Results from system reliability analysis

3.4.4 Comparison of results

System reliability estimates obtained by all the methods discussed above are shown on Figure 3. The presence of system behavior is evident when looking at the performance of FORM method, which fails to predict the correct reliability index, and converges to the same design point, regardless of the degree of correlation between layers. This design point corresponds to failure of the 0-degree layer which is subjected to highest load (layer number 15, counting from the laminate bottom surface). However, due to the randomness in material properties, failure modes corresponding to layers with lower stress are also present.

Importance sampling runs, centered at the design point obtained from FORM, converge to the correct probability of failure in most of the cases considered; however the convergence is very slow, because the sampling center points correspond to a single failure mode. Other failure modes occur relatively rarely, because their probability densities are far apart from the sampling center point. As a result, the importance sampling procedure described above has efficiency similar to that of a crude MC simulation, because the importance sampling density maximizes the chances of occurrence of just one of the several failure modes present.

The two simplified approaches for solving the system problem (using a smaller part of the system, or representing the faces as homogeneous) both capture the main trends in the system behavior, however the reliability estimates are conservative, sometimes with significant difference from the reference MC simulation results. These differences are explained by the facts that with such simplified representations the redistribution of stresses between the two sandwich faces following matrix-mode failures cannot be captured. The accuracy of the homogeneous layer representation is further limited by the underlying assumption that the stresses are constant throughout the laminate face.

4 DISCUSSION AND CONCLUSIONS

The problem of estimating the reliability against ultimate failure of composite sandwich panels has been discussed. Based on the properties of composite panels, including random strength and stiffness of layers, load redistribution under successive failures, and ultimate failure load dependent on the sequence of prior failures, it is suggested that the composite structure is best represented by a general reliability system.

Reliability of the general system has been calculated using the Monte Carlo approach. It is noted that the 0-degree layers (where fibers are oriented along the load direction) are critical for the integrity of the structure, and failure of these layers often leads to overall system failure. Based on such observations, it is possible to implement reliability methods more efficient than crude simulation, by considering only the parts of the system corresponding to the most critical layers identified. In this way a crude approximate estimate of the system reliability can be obtained, with some inaccuracy caused by the lack of account for the load redistributions following failure events.

Another way for simplifying a composite sandwich model is the commonly used approach of representing the laminated faces as equivalent homogeneous layer. Using this approach allows to capture some of the characteristics of the reliability problem, however it does not account for load redistributions following partial layer failures, and it does not account for the (small) variation of stresses throughout the face thickness. As a result, representing the laminated faces as equivalent homogeneous layers results in a reliability estimate differing from the reference Monte Carlo calculation. Although being relatively inaccurate, the single homogeneous layer calculation yields an approximate, conservative estimation of the system reliability, and can be useful in some reliability calculations where model complexity will not allow the use of full layerwise representation of the sandwich faces.

5 REFERENCES

- Daniels, H. E., 1945. The statistical theory of the strength of bundles of threads. *Proc. R. Soc. London, Ser. A*, 183(995): 405-435.
- Ditlevsen, O., Madsen, H., 1996. *Structural Reliability Methods*. John Wiley & Sons, Chichester, 1996, ISBN 0 471 96086 1
- Hashin, Z., 1980. Failure Criteria for Unidirectional Fiber Composites, *Journal of Applied Mechanics*, ASME, 47: 329-334
- Jones, R., 1998. *Mechanics of Composite Materials*, Taylor & Francis, Philadelphia, PA, USA, 2nd edition
- Kang, W.H., Song, J., 2010. Evaluation of multivariate normal integrals for general systems by sequential compounding. *Journal of Structural Safety*, 32(2010): 35-41
- Nijssen, R., 2006. *Optidat Reference Document*, WMC knowledge centre, The Netherlands, <http://www.wmc.eu/>
- Song, J., Der Kiureghian, A., 2003. Bounds on system reliability by linear programming. *Journal of Engineering Mechanics*, 129(6) 627-636
- Toft, H.S., 2010 *Probabilistic Design of Wind Turbines*, PhD Thesis, Aalborg University, Department of Civil Engineering, ISSN: 1901-7294
- Zenkert, D., 1995. *An Introduction to Sandwich Constructions*. Engineering Materials Advisory Services Ltd., United Kingdom, ISBN 0 947817 77 8
- Friis-Hansen, P., 1994. *Reliability Analysis of a Midship Section*. PhD Thesis, Technical University of Denmark, Department of Naval Architecture, ISBN 87-89502-20-5
- Melchers, R.E., 1990. Search-based importance sampling. *Journal of Structural Safety*, 9(1990): 117-128
- Shoorman, M.L., 1968. *Probabilistic Reliability: An Engineering Approach*, McGraw-Hill, New York, NY, 1968, p. 508.
- Naess, A., Gaidai, O., 2009. Estimation of extreme values from sampled time series. *Journal of Structural Safety*, 31(2009): 325-334

Bayesian network with Gaussian variables for post-earthquake emergency management

M. Pozzi & A. Der Kiureghian
University of California, Berkeley, USA

Y. Yue
Xi'an Jiaotong University, China

D. Zonta
University of Trento, Italy

ABSTRACT: We propose a probabilistic methodology to assess the reliability of a network of bridges in the aftermath of an earthquake, allowing real-time updating when data collected by visual inspection or instrumented monitoring are available. The approach makes use of a Bayesian network with conditional Gaussian distributions to model the correlations in demands and capacities of the bridges. The main benefit of the approach relative to using a Bayesian network with discrete variables is that it can handle a large number of variables (in the order of a few thousand), performing exact inference. In this work, we propose a formulation to model the prior assumptions on seismic excitation and on capacity and damage state by linear relationships and conditional Gaussian distributions. We present the effectiveness of the methodology on a large bridge network, showing how the reliability of links and of the connectivity between selected locations is progressively updated as information on ground acceleration at recording sites and on observed displacement and condition state of selected bridges becomes available.

1 INTRODUCTION

In the aftermath of a major seismic event, decisions about the use and management of transportation networks are crucial to mitigate the losses induced by the earthquake. Post-event decisions include the dispatching of rescue teams, the scheduling of inspections, and selection of the operative level for each facility. In this process, managers must maintain an adequate level of safety without excessive reduction in the operation level of the network.

Knowledge about the condition state of a facility is gained from modeling the seismic intensity and structural vulnerability, and from observations collected in the field through visual inspections and sensor recordings of the ground motion and of the structural response.

The Bayesian probabilistic theory offers an ideal framework to process these data, taking into account the prior available information. Bayesian methods allow progressive updating of the probabilistic distributions describing structural condition and network performance as more and more information becomes available.

In the reliability assessment of a road network, observations collected on one bridge influence our knowledge about the conditions of other bridges. As the bridges are exposed to the same seismic event, we expect the excitations they experience to be correlated. Furthermore, one may expect that capacities of bridges with similar typologies to be positively correlated because of underlying common factors. Consequently, damage levels experienced by different bridges are expected to be positively correlated, and observing a severe damage on one bridge would suggest other bridges to be similarly damaged.

Bensi *et al.* (2010a) make use of a Bayesian Network (BN) to model the dependency among seismic demands, structure capacities and damage states. The BN is a graphical model of a set of random variables, related by conditional probability distributions. It is a statistical tool widely used in many fields of engineering, including civil engineering. The unfamiliar reader is referred to the book by Jensen & Nielsen (2007) for a general introduction. While the problem of seismic

vulnerability is properly defined by continuous variables, in the above-mentioned work by Bensi *et al.* the BN model was approximated using discrete variables in order to allow use of exact inference algorithms. Aside from the approximation involved, the drawback of discretization is that, when the number of components in the system is large, the size of the grid required in the BN to accurately describe the dependency among variables is computationally unbearable. To reduce the dimension of that grid, the work of Bensi *et al.* (2012b) proposes a method to approximate the dependency among the variables with a small number of auxiliary variables.

In this paper, we follow another path and make use of Gaussian BNs (GBNs) to address the same problem. GBNs are a special case of BNs, in which each random variable is defined by a Gaussian marginal or conditional distribution and variables are linearly related to their parents. Cowell *et al.* (1999) and Murphy (2002) provide detailed descriptions of GBNs. An application of GBNs to seismic reliability assessment is presented in Yue *et al.* (2010). We formalize the problem of seismic vulnerability using log-normally distributed random variables, related through power and product rules, so that by taking the logarithmic transformation we can map the problem into the normal space with linear relations. Using GBNs allows us to exactly include models available in the literature, notably ground motion prediction equations.

2 INFERENCE IN BAYESIAN NETWORKS WITH GAUSSIAN VARIABLES

2.1 *Updating in the canonical form*

In GBN, the joint probability of all variables is Gaussian, and each marginal or conditional is Gaussian as well. In this paper we formulate the GBN framework to directly include vectors of random variables. We arrange the quantities describing all components of the network in a single vector, so that the vector refers to the entire network. If vector \mathbf{y} is a root in the BN graph, we require the joint distribution of \mathbf{y} to be Gaussian. If it is a child, we require that its conditional distribution be of the form

$$p(\mathbf{y}|\mathbf{x}) = N(\mathbf{y}, \mathbf{T}_{\mathbf{y}\mathbf{x}}\mathbf{x} + \mathbf{c}_{\mathbf{y}}, \Sigma_{\mathbf{e}\mathbf{y}}) \quad (1)$$

where $N(\cdot, \boldsymbol{\mu}, \boldsymbol{\Sigma})$ is the multivariate Gaussian distribution with mean vector $\boldsymbol{\mu}$ and covariance matrix $\boldsymbol{\Sigma}$, vector \mathbf{x} lists all the parents of \mathbf{y} , matrix $\mathbf{T}_{\mathbf{y}\mathbf{x}}$ and vector $\mathbf{c}_{\mathbf{y}}$ define the linear relation between the parents and the conditional expectation of variables \mathbf{y} , while $\Sigma_{\mathbf{e}\mathbf{y}}$ can be seen as the covariance matrix of a zero-mean noise term added to the linear combination of \mathbf{x} .

Suppose the distribution of vector \mathbf{x} is jointly Gaussian, and we wish to update its distribution upon observing, with imperfect accuracy, the value of one of its components. It is convenient to express the normal distribution in its canonical form, which we refer to as N' :

$$p(\mathbf{x}) = N'(\mathbf{x}, \boldsymbol{\eta}, \boldsymbol{\Lambda}) \stackrel{\text{def}}{=} \exp\left[-\frac{1}{2}\mathbf{x}^T\boldsymbol{\Lambda}\mathbf{x} + \mathbf{x}^T\boldsymbol{\eta} + \alpha(\boldsymbol{\eta}, \boldsymbol{\Lambda})\right] \quad (2)$$

where $\alpha(\boldsymbol{\eta}, \boldsymbol{\Lambda})$ is a normalizing term. Precision matrix $\boldsymbol{\Lambda}$ and vector $\boldsymbol{\eta}$ are related to the covariance matrix and mean vector by the following relations:

$$\boldsymbol{\Lambda} = \boldsymbol{\Sigma}^{-1} \quad \boldsymbol{\eta} = \boldsymbol{\Lambda}\boldsymbol{\mu} \quad (3)$$

Suppose we observe the value of the i -th component in vector \mathbf{x} , assuming the value of y . Taking uncertainty into account, suppose the observation is defined by a Gaussian likelihood with mean value y and variance $\sigma_{\mathbf{e}y}^2$:

$$p(y|x_i) = N(y, x_i, \sigma_{\mathbf{e}y}^2) = N(x_i, y, \sigma_{\mathbf{e}y}^2) \quad (4)$$

Observing a single component in vector \mathbf{x} is equivalent to observing all components, if we assign infinite variance (i.e. zero precision) to the observation of all other entries. Therefore, the likelihood function can be written in the canonical form, on domain \mathbf{x} , as:

$$p(y|\mathbf{x}) = N'(\mathbf{x}, \boldsymbol{\eta}_{LH}, \boldsymbol{\Lambda}_{LH}) \quad (5)$$

where every element of precision matrix $\boldsymbol{\Lambda}_{LH}$ is zero, except the i -th entry on the diagonal, which is equal to $\sigma_{\mathbf{e}y}^{-2}$. Vector $\boldsymbol{\eta}_{LH}$ is also zero, except for the i -th entry, which according to Eq.

3 is equal to $\sigma_{\varepsilon y}^{-2} y$. Bayes formula requires multiplying the prior distribution and the likelihood function to obtain the posterior distribution of \mathbf{x} . In the canonical form, the updating reads:

$$\Lambda_U = \Lambda_{LH} + \Lambda_\pi \quad \eta_U = \eta_{LH} + \eta_\pi \quad (6)$$

where subscript π refers to the prior distribution and U to the posterior, updated one.

2.2 The junction tree

To perform inference on all variables, we use the junction tree algorithm (Murphy, 2002). The vectors of variables are arranged in cliques and separators, and potentials associated with them. The potentials are the marginal (for the roots) and conditional (for the children) distributions that define the original GBN, and they are distributed among the cliques. Marginal distributions are functions defined only on one vector variable, and they can be easily assigned to cliques. To assign conditional distributions, we need to define the expression in Eq.1 as a function on the joint domain of parent and child variables, $\mathbf{z} = [\mathbf{x}^T \quad \mathbf{y}^T]^T$. In canonical form, this function is:

$$f(\mathbf{z}) = N(\mathbf{z}, \mathbf{B}_z^T \Lambda_{\varepsilon y} \mathbf{c}_y, \mathbf{B}_z^T \Lambda_{\varepsilon y} \mathbf{B}_z) \quad (7)$$

where $\Lambda_{\varepsilon y} = \Sigma_{\varepsilon y}^{-1}$ and $\mathbf{B}_z = [-\mathbf{T}_{yx} \quad \mathbf{I}]$, in which \mathbf{I} denotes the identity matrix. Once the junction tree is initialized, we use the Hugin algorithm to find marginal distributions along all cliques and separators (Murphy, 2002). For processing each observation, we define the corresponding likelihood function, as in Eq. 5, then we update the distribution of the observed vector in a clique containing that vector and then propagate the information along the whole tree.

3 GBN FOR SEISMIC DEMAND AND NETWORK RESPONSE

3.1 Demand model

We model the demand for seismic event j at site i by the classical form

$$\log[a_{ij}(T)] = \log[\bar{a}_{ij}(T)] + \sigma_{ij}\varepsilon_{ij} + \tau_j\eta_j \quad (8)$$

where $a_{ij}(T)$ is the spectral acceleration at period T , \bar{a}_{ij} is the median prediction, and ε_{ij} and η_j are respectively the intra-event and inter-event residual terms. ε_{ij} and η_j are standard normal random variables, and coefficients σ_{ij} and τ_j define the standard deviations of the residuals.

The dependency in the seismic demand for the bridge sites is captured by the structure of the intra-event residual. Loth and Baker (2012) have recently proposed a model for the correlation between intra-event residuals, which takes into account not only the site locations but also the selected natural periods. They model the correlation matrix as:

$$\Sigma(h) = \mathbf{B}_1 \exp\left(\frac{-3h}{20\text{Km}}\right) + \mathbf{B}_2 \exp\left(\frac{-3h}{70\text{Km}}\right) + \mathbf{B}_3 \text{In}(h = 0) \quad (9)$$

where h is the distance between two sites, $\text{In}(\cdot)$ is the indicator function, and matrices $\mathbf{B}_1, \mathbf{B}_2, \mathbf{B}_3$ are calibrated for a grid of 9 by 9 periods ranging from 0.01sec to 10sec, as reported in Loth and Baker (2012).

The period T of a structure may not be known, and its value affects both the median prediction of the spectral acceleration and the correlation of the residuals. We note that the correlation is not significantly affected by small variations in the period, while the median prediction may be significantly affected. We assign a nominal period T_0 to each bridge, and assume the correlation of the residuals is that computed for nominal periods. We adopt the approximate rule:

$$\bar{a}(T) = \bar{a}(T_0) \cdot \left(\frac{T}{T_0}\right)^\beta \quad (10)$$

where β is a coefficient to be fitted to the seismic demand model. For the sake of notational simplicity, subscripts ij have not been used in the above formulas, but they apply in each case indicating the seismic event and location of the bridge.

3.2 Response model at structure level

We idealize the bridge as a single-degree-of-freedom (SDOF) system, using the classical Newmark-Hall approach as reported, for example, in Chopra (1995). The elastic natural period of the structure is $T = 2\pi\sqrt{s_y m/F_y}$, where m is the mass, s_y is the relative displacement at yield and F_y is the yield force. The acceleration that leads to yielding of the structure is $a_y = F_y/m$, while the yield-strength reduction factor is $R_y = a(T)/a_y$. Under logarithmic transformation, all previous relations are linear and preserve normality. The relation between the ductility demand, μ_d , and R_y depends on the period. For long periods, the "equal displacement" assumption holds, while the "equal energy" assumption is more appropriate for short periods:

$$\mu_d = \begin{cases} R_y & R_y \leq 1 \text{ or } R_y > 1 \text{ and } T \geq T_c \\ \frac{R_y^2 + 1}{2} & R_y > 1 \text{ and } T < T_c \end{cases} \quad (11)$$

where the period T_c , marking the transition between the two hypotheses, is a property of the spectrum. In the present study we set $T_c = 0.5\text{sec}$ for simplicity. The "equal displacement" hypothesis defines a linear relation between R_y and μ_d . Unfortunately, the "equal energy" does not, and we have to linearize it before embedding it into GBN. We fit it with relation

$$\mu_d = k_d \cdot R_y^\lambda \cdot e^{\varepsilon_d} \quad (12)$$

where parameters k_d and λ are calibrated as 1.3 and 0.25 respectively, and the standard deviation of the zero-mean, normally distributed error term ε_d is 0.24, as reported in Figure 1. The demand in terms of relative displacement is obtained as $s = \mu \cdot s_y$.

The performance of the structure under the earthquake load is described in terms of the ratio between the demand in ductility and the ultimate ductility μ_u : $r = \mu_u/\mu_d$. If r is less than unity (i.e. its logarithm is negative), the structure fails.

3.3 Network model

Variables s_y , F_y , m , μ_u and consequently T , a_y , $a(T)$, R_y , s , μ_d , and r are repeated for each bridge, and the instances of each type of variable is listed into a corresponding vector. Figure 2(a) reports the scheme of the GBN, after marginalization of some variables. Vectors \mathbf{F}_y , \mathbf{a}_0 , $\boldsymbol{\mu}$, \mathbf{s} and \mathbf{r} define the shear capacities, spectral accelerations, relative displacements and damage ratios, respectively. The prior joint distribution of vector \mathbf{a}_0 follows the model presented in Section 3.1. In the definition of the other distributions, we can accommodate arbitrary correlation structures. To model the epistemological correlation among the capacities of the bridges, we introduce a vector $\boldsymbol{\theta}$ of parameters. Each component of this vector refers to a specific structural typology, and we model the capacity of the i -th bridge, belonging to k -th typology, as

$$F_{y_i} = F_{0_i} \cdot e^{\theta_k} \cdot e^{\varepsilon_{Fi}} \quad (13)$$

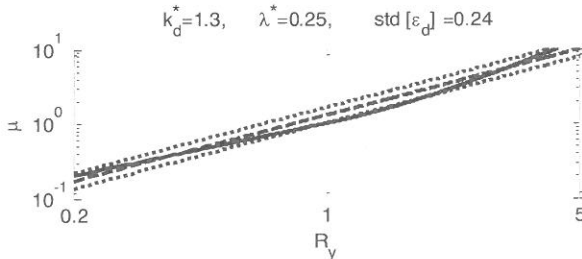


Figure 1: Yield-strength reduction factor vs ductility demand: "equal energy assumption" (continuous line) and linear approximation in the logarithm space (dashed line for mean prediction, dots lines add and subtract standard deviation).

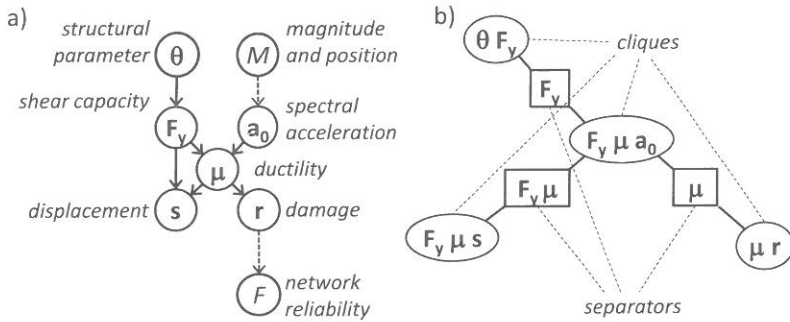


Figure 2: (a) GBN model; (b) corresponding junction tree

where F_{0i} is the nominal median capacity, obtained by a structural analysis of the component, θ_k is the parameter depending on the structural typology, and ε_{Fi} is a local error term depending on the individual structure. According to this model, capacities of structures belonging to the same typology are correlated, but those of structures belonging to different typologies are not.

The ductility demand depends on the shear capacity and spectral acceleration, the displacement depends on the shear capacity and ductility demand, and the damage depends on the ductility capacity, after marginalization of the ductility capacity. The GBN is reported in Figure 2(a). Node M represents the magnitude and epicenter location, which together define the spectral acceleration. We suppose that, shortly after the seismic event, these data are estimated with sufficient precision to be considered as deterministic quantities. In the United States, for example, the Geological Survey provides this information with high precision a few minutes after the event. Node F refers to the state of the network, and it will be illustrated in section 3.4. The junction tree for the core of the GBN is reported in Figure 2(b). In this scheme, the largest clique has the cumulative size of three vectors (F_y , a_0 , μ), each with size equal to the number of components. Therefore, the largest matrix to be stored is a square symmetric matrix of size equal to 3 times the number of components. In the Hugin algorithm, the most expensive operation is to compute the marginal on each separator. When the joint distributions are represented in the canonical form, marginalization requires inverting part of the precision matrix (Murphy, 2002). This is the main computational task in the proposed formulation. Obviously, this task could be expensive in high dimensions.

3.4 Network reliability

The performance of the road system, which is indicated by node F in the scheme reported in Figure 2, is related to the state of the components, which is described by random vector \mathbf{r} , jointly log-normally distributed at any stage of the updating procedure.

Possible reliability values of interest include the marginal probability of damage or failure of any individual component and the failure probability of any set of components arranged into a series or parallel system. For example, the failure probability of any link in the road system can be assessed by including the corresponding components in the set. The reliability assessment for any set of components requires computing the multivariate cumulative normal distribution, which can be done by efficient numerical methods, such as that in Ambartzumian *et al.* (1998).

3.5 Observations

Observation on any variable included in the GBN, i.e. any component or linear combination of components of the constituting vectors, can be processed. The observation can be "hard" when the variable is perfectly observed, or "soft" if it is observed with a Gaussian likelihood function.

However, note that the reliability node F does not fulfill the condition of GBN and, hence, we cannot accept observations collected on it. Suppose, for example, that we observe that the i -th bridge in the network has collapsed. This can be translated into a stepwise likelihood with value zero when $\ln r_i$ is negative, and one when it is positive. As this likelihood function on vector \mathbf{r} is not Gaussian, the posterior distribution is not Gaussian as well. We are currently investigating the use of a Gaussian approximation of the posterior by alternative best-fitting criteria. In the present work we restrict our attention to the observation of the GBNs variables. It is noted that once the state of a bridge is observed (for example, a bridge has collapsed), it is easy to fix the state of that bridge to the observed value in the GBN model. What the present model cannot do is propagate consistently the effect of this information onto the state of the other bridges.

4 NUMERICAL EXAMPLE

The method is applied to the reliability assessment of the road network shown in Figure 3(a). It is a network connecting 10 nodes using 17 links, on which 35 components (bridges) are located. The network is spread over a 40km×40km region, and we assume a seismic event of magnitude 7.5 occurs with the epicenter in the position marked with a cross near the upper right corner. The seismic excitation is modeled with the law calibrated by Akkar and Bommer (2010). Four bridge typologies, from T_1 to T_4 , are present in the network, as reported in Figure 3(b).

The median spectral acceleration, at the natural period of each bridge, and the shear capacity for each bridge are reported in Figures 4(a) and (b), respectively. The acceleration ranges from 5.6ms^{-2} about 5km from the epicenter, down to 0.61ms^{-2} about 40km from the epicenter. Figure 5(a) reports the corresponding failure probability for each link in the network, while Figure 6(a) reports the probability of connectivity for each pair of nodes in the network. We introduce 3 observations: The spectral acceleration at the nominal period at bridge #3 is observed to be 6.0ms^{-2} with a coefficient of variation (c.o.v.) of 20%; the relative displacement of bridge #9 is observed to be 12cm with 20% c.o.v.; the performance r_2 of bridge #2 is observed to be 2 with 10% c.o.v. The first observation is obtained from a ground motion recording, the second from recording of a sensor installed on bridge #9, the third from observation of light damage of bridge #2. Each observation affects the reliability of the bridge where the observation is collected as well as that of other bridges because of the correlation among demands and capacities. Figures 5(b) and 6(b) report the updated results after processing the three pieces of information, showing how the reliability of each link and the connectivity of each pair of nodes deteriorate.

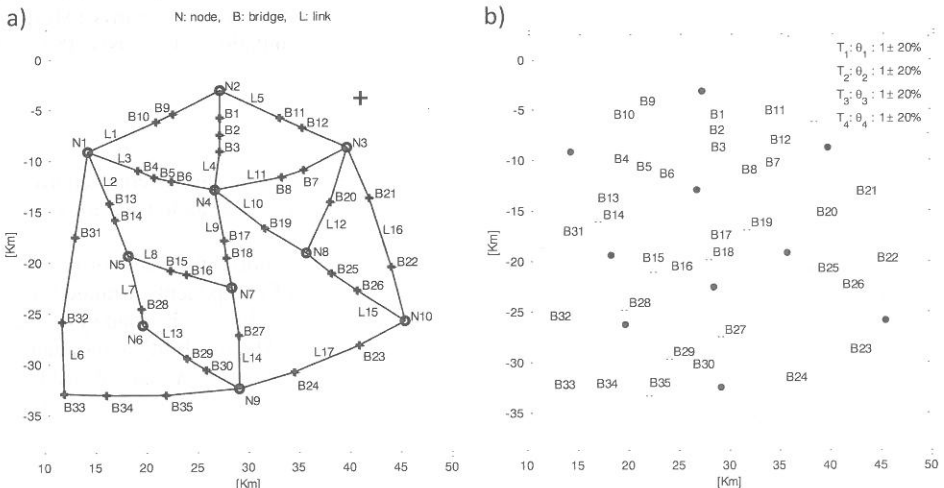


Figure 3: (a) Example of road network, (b) Structural typology of the bridges, from T_1 to T_4 .

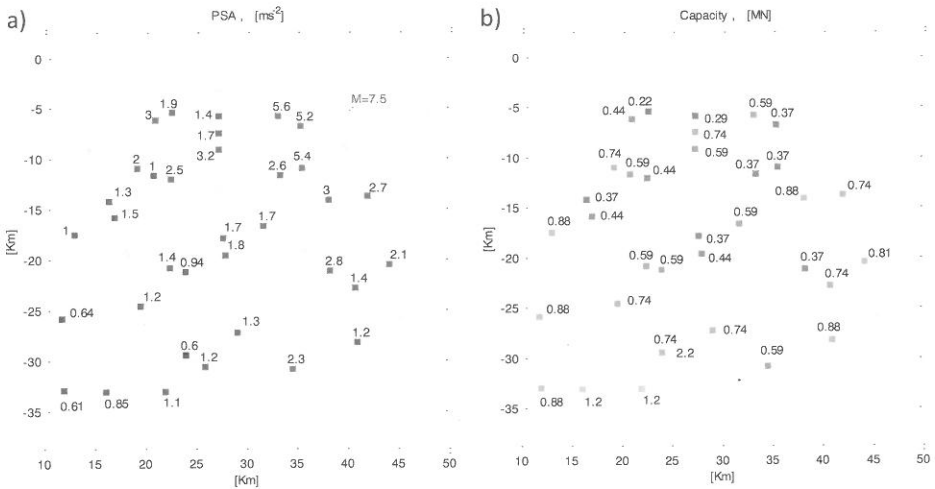


Figure 4: (a) Median Spectral Acceleration (PSA) for each bridge; (b) Capacity for each bridge.

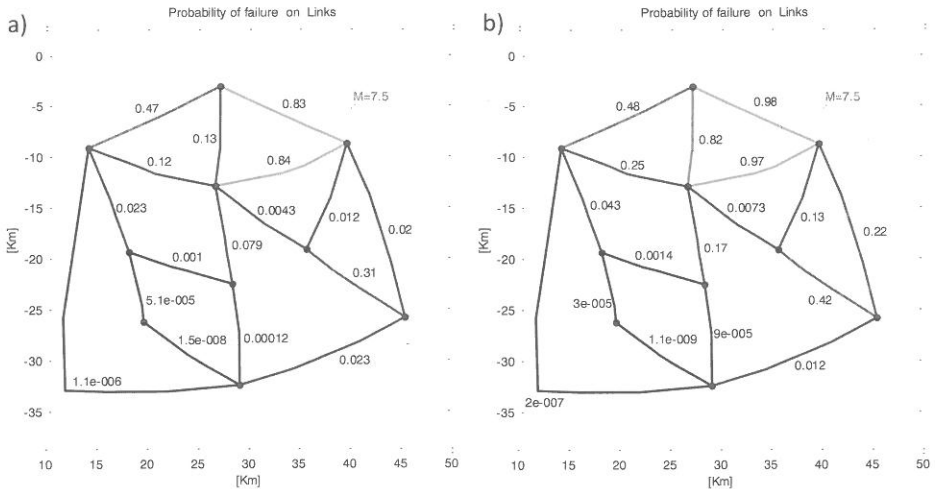


Figure 5: (a) Prior failure probability of each link; (b) Posterior failure probability of each link.

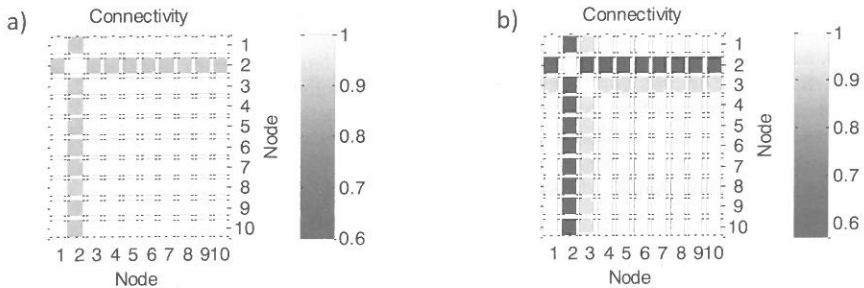


Figure 6: (a) Prior probability of connectivity for every pair of nodes; (b) Corresponding posterior connectivity.

5 CONCLUSIONS

We have presented an updating methodology based on the Gaussian Bayesian network to assess the reliability of a road network when observations on spectral acceleration, relative displacement and damage are collected. The technique allows fast computation and it can be used for the simulation of large road network, properly modeling the correlation among demands and capacities of the structures. Because of the fast numerical scheme, it can also be used for simulating many alternative seismic scenarios, with different magnitudes and epicenter locations. The Gaussian framework also allows a fast computation of the posterior uncertainty when observations are made, allowing a direct assessment of the relevance of one piece of information to the updating of the distribution of other variables.

The GBN is suitable for embedding models alternative to the Newmark-Hall approach, however only linear relations among the variables are acceptable for exact inference. The vector notation allows a simple scheme and a fast formulation of the probabilistic network.

ACKNOWLEDGEMENTS

The first author wishes to acknowledge the Fund "InfraRiskNet" supported by the Province of Trento via a grant from the European Commission within the 7th European Framework Program 2007-2013 – Specific program Persons – Actions Marie Curie.

The authors also gratefully acknowledge support from U.S. National Science Foundation Grant CMMI-1130061.

REFERENCES

- Akkar, S. & Bommer, J.J., 2010. Empirical Equations for the Prediction of PGA, PGV, and Spectral Accelerations in Europe, the Mediterranean Region, and the Middle East. *Seismological Research Letters* 81(2),195-206.
- Ambartzumian, R.V., Der Kiureghian, A., Ohanian, V.K. & Sukiasian, H.S. 1998. Multinormal probability by sequential conditioned importance sampling: theory and application. *Probabilistic Engineering Mechanics*, 13(4), 299-308.
- Bensi, M., Der Kiureghian, A. & Straub, D., 2011a. *A Bayesian Network Methodology for Infrastructure Seismic Risk Assessment and Decision Support*, PEER Report 2011/02.
- Bensi, M., Der Kiureghian, A. & Straub, D., 2011b. Bayesian network modeling of correlated random variables drawn from a Gaussian random field. *Structural Safety*, 33(6), 317-378.
- Chopra, A.K., 1995. *Dynamics of Structures: Theory and Applications to Earthquake Engineering*, Englewood Cliffs, NJ, Prentice-Hall.
- Cowell, R.G., Dawid, A.P., & Lauritzen, S.L., 1999. *Probabilistic Networks and Expert Systems*, New York, Springer.
- Jensen, F.V. & Nielsen, T.D., 2007. *Bayesian Networks and Decision Graphs*, New York, Springer.
- Loth, C., & Baker, J.W., 2012. A spatial cross-correlation model of spectral accelerations at multiple periods. *Earthquake Engng. Struct. Dyn.* doi: 10.1002/eqe.2212
- Murphy, K., 2002. *Dynamic Bayesian Networks: Representation, Inference and Learning*, PhD Thesis, UC Berkeley, Computer Science Division.
- Yue, Y., Pozzi, M., Zonta, D., Bortot, F. & Zandonini, R. 2010. Seismic Assessment using a Bayesian Network. *Proc. "International Symposium on Reliability Engineering and Risk Management (ISRERM2010)*, Shanghai, 23-26 Sep, 2010.

Probabilistic modeling of networked systems for risk assessment

J. Qin

ETH Zurich, Switzerland

M.H. Faber

Technical University of Denmark, Denmark

ABSTRACT: The present paper proposes to apply the framework for risk assessment of systems developed by the Joint Committee on Structural Safety (JCSS) to the probabilistic modeling and risk assessment of networked systems. The proposed framework which rests on the Bayesian probability theory accounts for both uncertain and given hazard events. Consequences of damages to the systems are differentiated into loss of functionality and replacement/repair costs. The uncertainty associated with the internal capacity of the systems with respect to redistribution of the internal demand is modeled probabilistically. The probabilistic analysis of damage scenarios and cascading system failure is facilitated by Monte Carlo simulations. The risk framework facilitates the assessment of both the vulnerability and the robustness of the modeled systems and thereby enhances the understanding of the system performance and risk management. The suggested framework and methodical approach is illustrated on an example considering a fictitious electrical power grid.

1 INTRODUCTION

At some level, most if not all engineered facilities may be characterized as networked systems, e.g. traffic infrastructure, offshore and onshore oil and gas distribution systems and electricity grids. Such systems are gaining increasing importance in society not least due to their growing significance for societal functionality. Constituents of such networked systems are typically geographically distributed but interconnected. Failure of one or more constituents may cause the failure of other constituents due to changes in internal flow demands, the event of which is referred to as cascading failure. However, surviving constituents may also lose their functionality due to loss of connection with the rest of the system.

Networked systems as a category is rather broad and in principle covers social networks, biological networks, infrastructure systems, etc. also referred to in the literature as complex networks. Significant theoretical and methodical achievements have been reached concerning the modeling and assessment of complex networks. Graph modeling of real-world networks is considered in e.g. Erdős & Rényi (1959), Watts & Strogatz (1998), and Barabasi & Albert (1999), the description of the internal flow distribution is considered in e.g. Motter & Lai (2002) and Dueñas-Osorio & Vemuru (2009) and the assessment of the hazards to which such networks may be exposed is treated in e.g. Mackie et al. (2011) and Poljanšek et al. (2012).

Probabilistic modeling and risk assessment of civil engineering systems is treated in Qin (2012) and there it is identified that for networked systems, integral approaches are still to be formulated which not only considers the uncertainties with respect to the resistances of the constituents to hazards acting from the outside of the systems but also with respect to the resistances of the constituents for what concerns the internal demand redistribution. Such uncertainties may affect the performance of the systems with respect to cascading failures and associated loss of functionality of the systems and should therefore be included in the risk modeling together with their associated consequences.

The aim of the present paper is to establish a framework for the probabilistic modeling of networked systems, which considers the uncertainties concerning the characteristics of the hazards and the resistance of the constituents to hazards as well as with respect to internal flow demands. To facilitate this, the approach taken here is to integrate the probabilistic system risk assessment framework proposed by JCSS (2001) into the existing performance models for complex networks. Having established this framework, a methodology is then formulated to facilitate the probabilistic analysis which is required for the system risk assessment. Finally, the proposed framework is illustrated on an example considering the risk assessment of a fictitious electrical power grid under different damage scenarios and studying the sensitivity of the risk for this system with respect to different modeling assumptions.

2 RISK MODELING OF NETWORKED SYSTEMS

The risk modeling of networked systems takes basis in the graph theory. For networked systems, the individual nodes and the connections can be treated as vertices (nodes) and edges respectively. Using graph models only, however, is not sufficient for the risk assessment of networked systems. To realize the assessment, it is necessary to establish a risk modeling accounting for the scenarios of events from the hazards to the end of cascading failures. According to the definition of risk by Faber (2009), risk of engineered systems is understood as the expected consequences associated with all the potential hazards. That is, the risk involves both the probabilities of the occurrence of all the potential hazards and the corresponding consequences. Let us assume that there are totally N nodes in an intact system. In Table 1, the categories of condition states and corresponding consequences of the nodes are summarized. To estimate the consequences accurately and to be able to represent the functionality of networked systems appropriately, the condition states of the i^{th} node are classified into three categories, 1) failure, 2) survival without functionality and 3) survival with functionality. The failure of the node might occur directly due to hazards (DF_{*i*}) or in the subsequent cascading event (CF_{*i*}). As explained before, if the node survives it might still function but can also lose its functionality due to loss of interconnection. These events are denoted availability (A_{*i*}) and unavailability (U_{*i*}), respectively. Consequences of the node are classified as either reconstruction cost C_i^R (direct consequences) or as utility losses C_i^U (indirect consequences). The reconstruction cost are due to the cost to rebuild the individual nodes and the utility losses are associated with the inconvenience to the users, fatalities, etc., in principle all the other potential losses different from the reconstruction costs. The consequences that correspond to the three different condition states are $C_i^R + C_i^U$, C_i^U , and 0 respectively.

Table 1. Categories of condition states and corresponding consequences of the nodes ($i=1,2,\dots,N$)

Phase	Cause of damages	Condition states	Consequences
I: Initial phase	Hazards	DF _{<i>i</i>}	$C_i^R + C_i^U$
		CF _{<i>i</i>}	$C_i^R + C_i^U$
II: Cascading phase	Initial damages (given that the node does not fail in the initial phase)	A _{<i>i</i>}	0
		U _{<i>i</i>}	C_i^U

In the probabilistic modeling of systems, it is of great importance to represent all relevant uncertainties in full consistency with available information (Faber (2009)). For the networked systems subject to different hazards, the uncertainties exist in:

(1) Estimation of the demands from various natural hazards NH_{ji} ($i=1,2,\dots,N$) ($j=1,2,\dots,H$), such as snow, earthquake and lightning. H is total number of indicators of demands from natural hazards. NH_{ji} is the demand on the i^{th} node from the j^{th} indicator. In the present paper, for illustrational purposes the demands on the individual nodes from different natural hazards NH_{ji} are assumed to be independent. The sub-subscript in the term represents the spatial dependency of the natural hazards.

(2) The extent of the imposed damages represented by the indicator vector $\Delta^{IA} = (\delta_1^{IA}, \delta_2^{IA}, \dots, \delta_N^{IA})^T$. δ_i^{IA} ($i=1,2,\dots,N$) indicate whether the i^{th} node is damaged or not. In the

following, it is set equal to either 1 and 0 depending on whether the node is the target or not. If it is equal to 1, it is assumed that the i^{th} node fails instantaneously.

(3) The resistances of the nodes with respect to natural hazards, $R_i^{\text{NH}_j}$ ($i=1,2,\dots,N$) ($j=1,2,\dots,H$). $R_i^{\text{NH}_j}$ represents the resistance of the i^{th} node to the j^{th} natural hazard, which here are assumed to be mutually independent for the same node. It is also reasonable to assume that $R_i^{\text{NH}_j}$ is independent of NH_j .

(4) The resistances of the nodes to internal demand changes, R_i^{IF} ($i=1,2,\dots,N$). R_i^{IF} represents the resistance of the i^{th} node to the internal change caused by damages of one or more nodes.

A model that describes the internal demands and resistances of nodes of complex networks is presented by Motter & Lai (2002). There the internal demand of a node is defined as the total number of shortest paths passing through the node. The capacity of a node is defined as the maximum demand the node can resist. It is further assumed by Motter & Lai (2002) that the resistance of a node can be described as a linear function of its initial internal demand.

$$C_i^{\text{IF}} = (1 + \alpha)L_{i|\text{G}}^{\text{IF}} \quad (1)$$

where G represents the original graph model of the networked system. C_i^{IF} is the capacity of the i^{th} ($i=1,2,\dots,N$) node, and $L_{i|\text{X}}^{\text{IF}}$ represents the internal demand on the node in the graph model X ($L_{i|\text{G}}^{\text{IF}}$ is the initial internal demand on the i^{th} node in the original graph model G). α is called as tolerance parameter.

As introduced in Section 1, the described model undertakes the analysis of the scenarios of cascading failures deterministically. However, the uncertainties associated with the resistances as well as internal flow demands must be taken into account in the risk assessment of engineered structures. A probabilistic framework to establish standardized probabilistic models for the representation of uncertainties associated with the resistances of structures is proposed by JCSS (2001). This framework can facilitate an improvement of the model of the performance of complex networks by Motter & Lai (2002). To this end, the resistances of all the nodes C_i^{IF} ($i=1,2,\dots,N$) in the system introduced by Motter & Lai (2002) can be regarded as design resistances. These are different from the actual resistances which in the subsequent are represented by R_i^{IF} ($i=1,2,\dots,N$) to avoid confusion. The resistance of a node to the internal demand is modeled by a random variable. The expected value of the resistance is defined as:

$$E(R_i^{\text{IF}}) = C_i^{\text{IF}} = (1 + \alpha)L_{i|\text{G}}^{\text{IF}} \quad (2)$$

The parameters presented above are adopted to formulate the risk modeling of networked systems. The probability distribution function and the characteristics of the parameters can be determined according to the applied design practice and available data. The detailed probabilistic analysis of the condition states of the nodes in the networked systems will be introduced in the subsequent (Section 3).

3 PROBABILISTIC ANALYSIS OF NETWORKED SYSTEMS

The probabilistic analysis of networked systems concerns the probabilistic assessment of the different scenarios of the system under all the potential hazards. As indicated in the foregoing, the probabilistic analysis can be divided into a probabilistic analysis of the nodes (constituent level) and a probabilistic analysis of the whole system (system level). Different from the probabilistic analysis of individual engineered structures, individual constituents of such systems (nodes) are associated with their own consequences (utilities and reconstruction costs), and therefore, the probabilistic analysis of the nodes is necessary for the estimation of the total risk of the whole system.

The failure of the i^{th} node due to a hazard event can be described by $\text{DF}_i = \left\{ \bigcup_{j=1}^H (R_i^{\text{NH}_j} - \text{NH}_j < 0) \right\}$. Based on the independencies among variables as introduced in the last section, the probability $P(\text{DF}_i)$ is:

$$P(\text{DF}_i) = P\left(\bigcup_{j=1}^H (R_i^{\text{NH}_j} - \text{NH}_j < 0)\right) = \iint_{\bigcup_{j=1}^H y_j - x_i < 0} \dots \prod_{j=1}^H (f_{R_i^{\text{NH}_j}}(y_j) f_{\text{NH}_j}(x_j)) dx_1 dy_1 dx_2 dy_2 \dots dx_H dy_H \quad (3)$$

where $f_z(\bullet)$ is the probability density function of the random variable Z (if the variable Z is replaced by vector \mathbf{Z} , $f_z(\bullet)$ becomes the joint probability density function of the components of the vector). Considering the deterministically imposed initial damages, the probability of the i^{th} node in the condition state DF_i becomes:

$$P(DF_i) = \delta_i^{\wedge A} \quad (4)$$

The probability that the i^{th} node fails in the cascading event $P(CF_i)$ is:

$$P(CF_i) = P(CF_i \cap \overline{DF_i}) = P(\overline{DF_i})P(CF_i | \overline{DF_i}) = (1 - P(DF_i))P(CF_i | \overline{DF_i}) \quad (5)$$

Similarly, the probability that the i^{th} node survives and is functional with availability $P(A_i)$ is:

$$\begin{aligned} P(A_i) &= P(A_i \cap (\overline{DF_i} \cap \overline{CF_i})) = P(\overline{DF_i} \cap \overline{CF_i})P(A_i | (\overline{DF_i} \cap \overline{CF_i})) \\ &= (1 - P(DF_i) - P(CF_i))P(A_i | (\overline{DF_i} \cap \overline{CF_i})) \end{aligned} \quad (6)$$

The integral in the Equation (3) may be calculated either analytically or numerically depending on the formulation of the problem. For the probabilities in the Equations (5) and (6), a simple method appropriate for this purpose is the Monte Carlo method because they cannot be expressed explicitly. To estimate the probabilities of the nodes in different condition states, we need to know the total number of the nodes in these states in the Monte Carlo simulations. In

Figure 1, the simulation procedure of cascading event with imposed deterministic failure nodes in the initial phase is illustrated, which can be also used as modulus in the simulation of the system under uncertain initial damages by natural hazards.

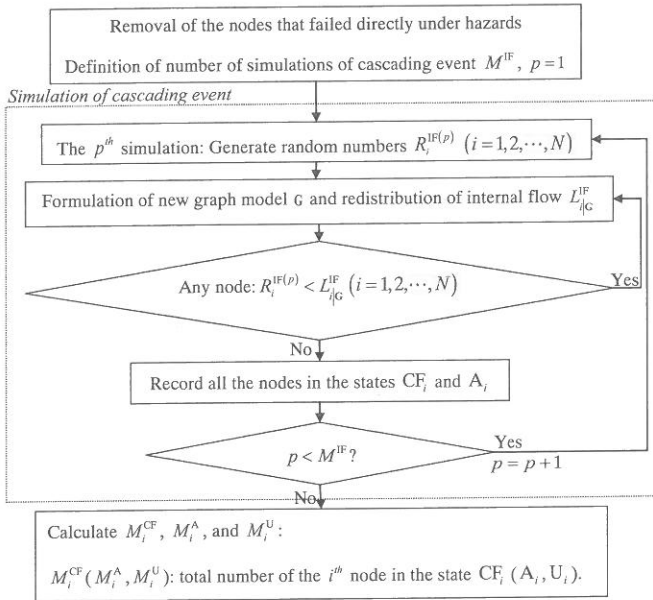


Figure 1: Flow chart of simulation of cascading event by Monte Carlo simulation

4 VULNERABILITY AND ROBUSTNESS OF NETWORKED SYSTEMS

The aim of probabilistic modeling of networked system is the risk assessment. As introduced above, the risk of one node of a networked system is the sum of the multiplication of the probabilities of the node in various condition states with the corresponding consequences (see Table 1), while the risk of the whole system is simply the sum of the risks of all the nodes of the system. However, the calculation of the total risk does not provide specific information concerning the performance of a system. To this end, the indicators vulnerability and robustness as described in Faber (2009) may enhance system understanding and thereby also facilitate the identification of more efficient risk reducing measures. The vulnerability of a system considers the measurement of the total direct consequences associated with the system, while the robustness of a system describes the contribution of the direct risks to the total system risk. In a robust system the indirect risks do not contribute significantly to the total system risk, see also Baker et al. (2008).

Indexes of vulnerability and robustness (denoted I_V and I_R here respectively) are presented in Baker et al. (2008) as means to quantify vulnerability and robustness of structural systems respectively. These indexes may be utilized for systems in general as also outlined in Faber (2009). The index of vulnerability is defined as the ratio of the direct risk to the sum of direct consequences associated with the loss of each component of the system. In the modeling of networked systems presented above, the nodes of the system are its components. Following the introduction by Baker et al. (2008), the index of vulnerability for networked systems is:

$$I_V = \frac{R_{Dir}}{\sum_{i=1}^N C_i^R} \quad (7)$$

where R_{Dir} is the direct risk from various hazards. The index of robustness measures the contribution of the direct risk to the total system risk:

$$I_R = \frac{R_{Dir}}{R_{Dir} + R_{Ind}} \quad (8)$$

where R_{Ind} represents the indirect risk from various hazards. The direct and indirect risks concern both the probabilities of various states of the nodes in the system and the corresponding consequences as shown in Table 1. Consider as an example one special type of networked system, for which all the individual nodes have the same reconstruction cost and costs of loss of functionality. The two indices introduced above will be equivalent or proportional to other existing indicators of the performance of networks, e.g. relative size G by Motter & Lai (2002) and connectivity loss C_L by Dueñas-Osorio & Vemuru (2009). However, note that the two consequences, reconstruction cost and loss of functionality, act as the weights of the individual nodes in the risk evaluation of the system performance and the uncertainties in the system presented in this paper are also integrated in the two indices.

Consider the networked systems under uncertain initial damages caused by natural hazards. It is possible to compute the risk of the i^{th} node subject to a given hazard, which is the sum of the multiplication of the consequence of each scenario with its corresponding probability of occurrence. The risk obtained here is then integrated over all the demands from natural hazards and all the nodes in the system. The direct and indirect risks of the system are:

$$R_{Dir} = \sum_{i=1}^N C_i^R \left(P(DF_i) + P(\overline{DF}_i) P(CF_i | \overline{DF}_i) \right) \quad (9)$$

$$R_{Ind} = \sum_{i=1}^N C_i^U \left(P(DF_i) + P(\overline{DF}_i) P(CF_i | \overline{DF}_i) + P(\overline{DF}_i) P(U_i | \overline{DF}_i) \right) \quad (10)$$

where all the variables in the integrations are illustrated in terms of N -component column vectors composed by their corresponding values of the N nodes in the system, e.g.

$\mathbf{C}^R = (C_1^R, C_2^R, \dots, C_N^R)^T$. The unconditional index of vulnerability and unconditional index of robustness can be obtained directly using Equations (7) and (8) respectively.

Now consider the networked systems with certain initial damages (e.g. under a specified intentional attack). The direct and indirect risks of the system are:

$$R_{Dir|\Delta^{IA}} = \sum_{i=1}^N C_i^R P(CF_i|\Delta^{IA}) \quad (11)$$

$$R_{Ind|\Delta^{IA}} = \sum_{i=1}^N C_i^U (P(CF_i|\Delta^{IA}) + P(U_i|\Delta^{IA})) \quad (12)$$

5 EXAMPLE

5.1 Introduction

In the following, the proposed probabilistic modeling is applied to a 20-node electrical power grid, whose graph model is illustrated in Figure 2. There are a total of 9 supply nodes in the graph model and the remaining 11 nodes are distribution nodes. The supply nodes represent the high voltage substations to generate the electricity. The electricity is distributed to the users by the low voltage substations represented by distribution nodes in the graph. The parameters related to the consequences, including the reconstruction costs and utilities of the two types of nodes in the network, are listed in Table 2. The risk analysis here considers two main aspects, 1) the network with imposed deterministic damage states and 2) the network with uncertain initial damages, based on the following assumptions:

- (1) Earthquake is considered as the only potential natural hazard as the cause of uncertain initial damages. The measure of the intensity of the earthquake at the nodes is expressed in terms of peak ground acceleration (PGA), which is assumed to be same for the whole network considering the small area covered by the network.
- (2) Since the demand from the natural hazard (earthquake) is defined by a single variable, PGA, the resistance of the nodes to external hazards is also expressed in terms of this variable.
- (3) The resistances of different nodes, to earthquake and to internal flow demand respectively, are statistically independent and they have same distribution with different probabilistic characteristics. The adopted probabilistic modeling of the resistances to earthquake and internal flow demands is summarized in Table 3.
- (4) The internal flow of the electrical distribution network is directed from high voltage substations (supply nodes) to low voltage substations (distribution nodes). The internal demand of one node, therefore, is defined as the number of shortest paths that pass through it when the flow is distributed from each available supply node to each distribution node.

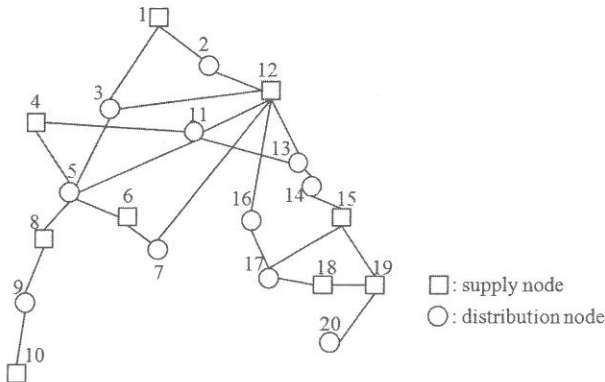


Figure 2: Graph model of the 20-node electrical distribution network

Table 2. Reconstruction costs and utilities of the nodes

	Supply node	Distribution node
Reconstruction cost	2	1
Utility	0	5

Table 3. Probability modeling of resistances of the nodes

		Prob. distr.	Mean value	COV
External-Earthquake	Supply node	Lognormal	0.1(g)	0.5
	Distribution node	Lognormal	0.15(g)	0.7
Internal	Supply node	Lognormal	$(1 + \alpha)L_{dc}^{IF}$	0.05
	Distribution node	Lognormal	$(1 + \alpha)L_{dc}^{IF}$	0.05

Table 4. Index of vulnerability and robustness of the network with imposed deterministic damage states

No. of node removal	I_V			I_R		
	$\alpha=0.1$	$\alpha=0.2$	$\alpha=0.3$	$\alpha=0.1$	$\alpha=0.2$	$\alpha=0.3$
1	0.4222	0.3655	0.3262	0.2442	0.2313	0.2202
2	0.2811	0.2161	0.1480	0.2794	0.3036	0.3280
3	0.0466	0.0050	7.95×10^{-5}	0.2947	0.2861	0.2857
4	0.0466	0.0050	7.29×10^{-5}	0.1410	0.0263	0.0004
5	0.0466	0.0050	7.20×10^{-5}	0.0690	0.0094	0.00014

5.2 Network with imposed deterministic damage states

In this part, the risk of the network is evaluated in the case that one to five supply nodes with largest internal initial demands are removed intentionally. The five supply nodes considered in the initial event are 12, 8, 15, 19, 18 in descending order of their initial demands. That is, the cases that “removal of one supply node” and “removal of two supply nodes” correspond to “removal of node 12” and “removal of node 12 and node 8” respectively. The rest can be deduced by analogy. The objective here is to assess the index of vulnerability and the index of robustness of the network with imposed deterministic damage states. The number of MC simulations in the calculation is 10^6 , and the results are shown in Table 4. From the results, it can be seen that the two indices do not always follow same trend with the change of α and the number of node removal. In the case that three or more nodes are removed at the beginning, both the two indices, especially I_V , are very small. That means the system become relatively stable, and the situation where more nodes are removed intentionally will not necessarily lead to cascading failure. The likelihood of cascading failure does not increase with the increase of the number of node removals.

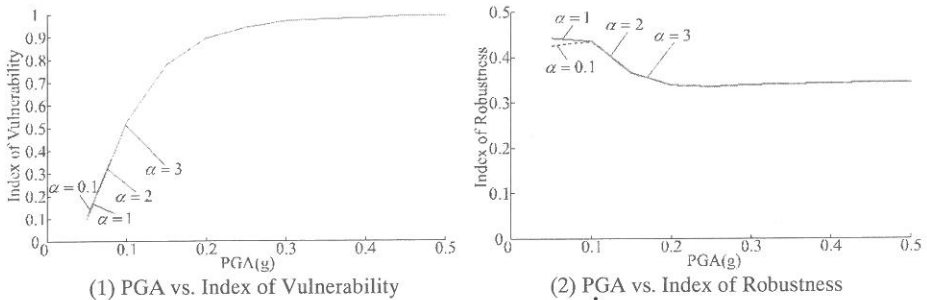


Figure 3: Risk assessment of the network subject to various intensities of earthquake (PGA)
 (Note that the curves “ $\alpha=1$ ”, “ $\alpha=2$ ”, and “ $\alpha=3$ ” are overlapped in both figures)

5.3 Network with uncertain initial damages

Now consider earthquake hazards as the cause of the uncertain initial damages. The indices of the two indicators of the risk of the network with different values of tolerance parameter α ($\alpha=0.1, 1, 2,$ and 3) are in this case investigated with the variation of the PGA.

The resultant indices differs only slightly between the network with the tolerance parameter $\alpha=0.1$ and the networks with tolerance parameters $\alpha = 1, 2$ or 3 when the PGA is small (the index I_v of the network with $\alpha=0.1$ is about 15% more than that of the network with $\alpha=1, 2$ or 3 when the PGA is $0.05(g)$, which is not clear in Figure 3). A small intensity of the earthquake will change the system a little at the beginning. However, if there is little safety margin of the nodes to resist the variation of the demand of the internal flow, the system is relatively unstable subject to small changes of the system. As long as the PGA is large, the failure probabilities of all the nodes in the initial phase are relatively high and the influence of the safety margin of the nodes can be ignored. It can also be seen from Figure 3 that the increase of the tolerance parameter, e.g. from 1 to 2, may not always improve the index of robustness and the index of vulnerability of the network. The index I_v keeps increasing with the increase of the PGA. The index I_R , however, decreases when the value of PGA changes from 0.1 to 0.2. The reason for this is that although both the direct risk and the indirect risk of the network increase with the increasing intensity of earthquake (PGA) their rate of change may be different. If the indirect risk increases more quickly than the direct risk, e.g. some nodes are surviving but not available, the index of robustness will decrease.

6 CONCLUSION

A probabilistic modeling of networked systems is proposed here to facilitate the risk assessment, which presents the uncertainties and consequences associated with the performance of networked systems subject to hazards and loss of functionalities and integrates the performance of the system in the both initial phase of node failures and the scenarios of node failures in the cascading phase into a uniform framework. The proposed modeling provides a basis for the risk assessment. To realize the risk assessment in practice, some problems such as the necessary number of MC simulations and the identification of dominant failure modes in the cascading phase are of interest and need further study.

7 REFERENCES

- Baker, J. W., Schubert, M., & Faber, M. H. 2008. On the Assessment of Robustness. *Structural Safety* 30 (3):253-267.
- Barabási, A.-L., & Albert, R. 1999. Emergence of Scaling in Random Networks. *Science* 286 (5439):509-512.
- Dueñas-Osorio, L., & Vemuru, S. M. 2009. Cascading Failures in Complex Infrastructure Systems. *Structural Safety* 31 (2):157-167.
- Erdős, P., & Rényi, A. 1959. On Random Graphs. I. *Publicationes Mathematicae* 6:290-297.
- Faber, M. H. 2009. Risk and Safety in Engineering. In *Lecture notes on risk and safety in civil engineering*. Zurich, Switzerland: ETH Zurich.
- JCSS. 2001. Probabilistic Model Code. The Joint Committee on Structural Safety.
- Mackie, K. R., Wong, J. M., & Stojadinovic, B. 2011. Bridge Damage and Loss Scenarios Calibrated by Schematic Design and Cost Estimation of Repairs. *Earthquake Spectra* 27 (4):1127-1145.
- Motter, A. E., & Lai, Y.-C. 2002. Cascade-Based Attacks on Complex Networks. *Physical Review E* 66 (065102):1-4.
- Poljanšek, K., Bono, F., & Gutiérrez, E. 2012. Seismic Risk Assessment of Interdependent Critical Infrastructure Systems: The Case of European Gas and Electricity Networks. *EARTHQUAKE ENGINEERING & STRUCTURAL DYNAMICS* 41 (1):61-79.
- Qin, J. 2012. Probabilistic Analysis of Large-Scale Engineered Systems. Doctoral and Habilitation Theses, Institute of Structural Engineering, Department of Civil, Environmental and Geomatic Engineering, ETH Zurich, Zurich.
- Watts, D. J., & Strogatz, S. H. 1998. Collective Dynamics of 'Small-World' Networks. *Nature* 393:440-442.

Fragility curves for bridges under differential support motions

K. Konakli

Technical University of Denmark

ABSTRACT: This paper employs the notion of fragility to investigate the seismic vulnerability of bridges subjected to spatially varying support motions. Fragility curves are developed for four highway bridges in California with vastly different structural characteristics. The input in this analysis consists of simulated ground motion arrays with temporal and spectral nonstationarities, and consistent with prescribed spatial variation patterns. Structural damage is quantified through displacement ductility demands obtained from nonlinear time-history analysis. The potential use of the ‘equal displacement’ rule to approximately evaluate displacement demands from analysis of the equivalent linear systems is examined.

1 INTRODUCTION

For a structural component or system of interest, seismic fragility represents the probability that the demand imposed by earthquake loading will exceed a prescribed threshold, conditioned on a measure of ground motion intensity. The notion of fragility has been used widely to convey probabilistic information on seismic related damage (e.g., Kennedy & Ravindra 1984, Singhal & Kiremidjian 1996, Straub & Der Kiureghian 2008). Empirical fragility curves are developed using actual damage information from past earthquakes, whereas analytical fragility curves are based on simulation of structural response to seismic excitation. Existing models of analytical fragility curves for bridges (e.g. Shinozuka et al. 2000, Karim & Yamazaki 2001, Gardoni et al. 2003, Nielson & DesRoches 2007) vary as to the types of bridge structures examined, the characteristics of the considered input excitations, the selected measures of structural damage and ground motion intensity and the employed analysis methods. The vast majority of these studies assume uniform support motions; however, ground motion spatial variability may have significant influence on bridge response (Konakli & Der Kiureghian 2011).

Fragility curves for bridges subjected to differential support motions have been developed by considering stationary input (Lupoi et al. 2005) or by accounting for temporal nonstationarity in ground motions simulated with the spectral representation method (Deodatis et al. 2000, Saxena et al. 2000, Kim & Feng, 2003). In the aforementioned method, iterations required to match the target response spectra may alter the coherency characteristics of the initially generated ground motion arrays that are consistent with the assumed spatial variation pattern (Saxena et al. 2000). Furthermore, with the exception of Kim & Feng (2003) who considered several measures of ground motion intensity, fragility curves incorporating effects of spatial variability have been developed as functions of Peak Ground Acceleration (PGA), which may be a poor measure of the ground motion damage potential, as demonstrated subsequently in this paper.

In the current study, spatially varying support motions with temporal and spectral nonstationarities are simulated with the method developed by Konakli & Der Kiureghian (2012). This method extends earlier works by Vanmarcke & Fenton (1991) and Liao & Zerva (2006), and generates ground motion arrays that incorporate effects of *wave passage*, representing the time delay in the arrival of seismic waves at separate locations; *incoherence*, represent-

ing random differences in the amplitudes and phases of seismic waves at separate locations, caused by reflections and refractions and/or by the differential superpositioning of waves originating from an extended source; and differential *site response*, representing variations in the amplitudes and frequency contents of the surface motions, caused by propagation of the bedrock motions through varying soil profiles. Comparisons between coherency estimates from simulated arrays with the respective target coherency models demonstrate excellent agreement (Konakli & Der Kiureghian 2012). Preliminary investigations indicate higher correlation of structural damage with Spectral Acceleration (SA) than with PGA; thus, SA is used to characterize ground motion intensity. Pier displacement demands are evaluated with nonlinear time-history analysis. The potential use of the 'equal displacement' rule to approximately evaluate inelastic demands from analyses of the corresponding elastic systems is also examined.

2 BRIDGE MODELS

Fragility curves are developed for four highway bridges designed by the California Department of Transportation (Caltrans). These are prestressed concrete box-girder bridges that vary as to the number and length of spans, the configuration of the bents and the overall stiffness.

Idealized models of the bridges are shown in Figure 1. The Penstock Bridge is a four-span bridge with a single pier per bent. The deck has a vertical grade, varying from 0.3% to 2.1%, and a constant horizontal curvature of radius $R = 458\text{m}$. The columns are rigidly connected to the deck at the top and fixed in all directions at the bottom. The South Ingram Slough Bridge is a two-span bridge with two piers per bent. The deck has a vertical grade, varying from -0.52% to -0.85% , and a constant horizontal curvature of radius $R = 1542.3\text{m}$. The columns are rigidly connected to the deck at the top and fixed in all directions at the bottom. The Big Rock Wash Bridge is a three-span bridge with three piers per bent. The longitudinal axis of the bridge is a straight line. The deck is characterized by a constant profile grade of 0.5%. The piers are rigidly connected to the deck at the top, whereas the bottom supports are fixed in all translational directions and free in all rotational directions. The Auburn Ravine Bridge is a six-span bridge with two piers per bent. The deck has a vertical grade of 0.3% and a horizontal curvature of radius $R = 1616\text{m}$. The piers are rigidly connected to the deck at the top, whereas the bottom supports are fixed in all translational directions and free in all rotational directions. The ends of all four bridges are supported on seat abutments. The abutment response is modeled through two horizontal translational springs, whereas vertical translations are fully constrained.

Following Caltrans recommendations, 3 elements per pier are used in the finite element models. The number of elements in each span varies according to the span length. Condensing out rotational degrees of freedom (DOF), the resulting number of translational unconstrained DOF is 103 for the Penstock Bridge, 55 for the South Ingram Slough Bridge, 89 for the Big Rock Wash Bridge and 163 for the Auburn Ravine Bridge.

In linear elastic analysis, the flexural stiffness of the pier elements is the effective stiffness obtained from moment-curvature analysis. No stiffness reduction is required for the deck elements. The fundamental periods of the corresponding bridge models are 2.38s for the Penstock Bridge, 1.24s for the South Ingram Slough Bridge, 0.61s for the Big Rock Wash Bridge and 0.59s for the Auburn Ravine Bridge.

The nonlinear models differ from the corresponding elastic models only in the representation of the piers. These are modeled with force-based nonlinear elements with distributed plasticity. For the piers of the Penstock Bridge and the South Ingram Slough Bridge, 5 integration points along each element are defined, whereas for the shorter piers of the Big Rock Wash Bridge and the Auburn Ravine Bridge, the number of integration points per element is 3. For all four bridges, the cross-sections of the pier elements are modeled as fiber sections with 12 subdivisions in the circumferential direction and 8 and 4 subdivisions in the radial direction for the core and the cover, respectively. The reinforcing steel bars are specified as additional layers. The properties of the unconfined concrete and the reinforcing steel are the expected material properties defined by Caltrans specifications, whereas the properties of the confined concrete are determined according to Mander's model. The fiber model of the pier section accounts for interaction between axial force and bending moment. The shear and torsional behaviors are described by aggregated

uniaxial models with the shear yield force determined from Caltrans recommendations and the torsional yield force evaluated from theory of strength of materials.

Rayleigh damping is considered with the parameters adjusted so that the damping ratios of the lower modes are close to 5%.

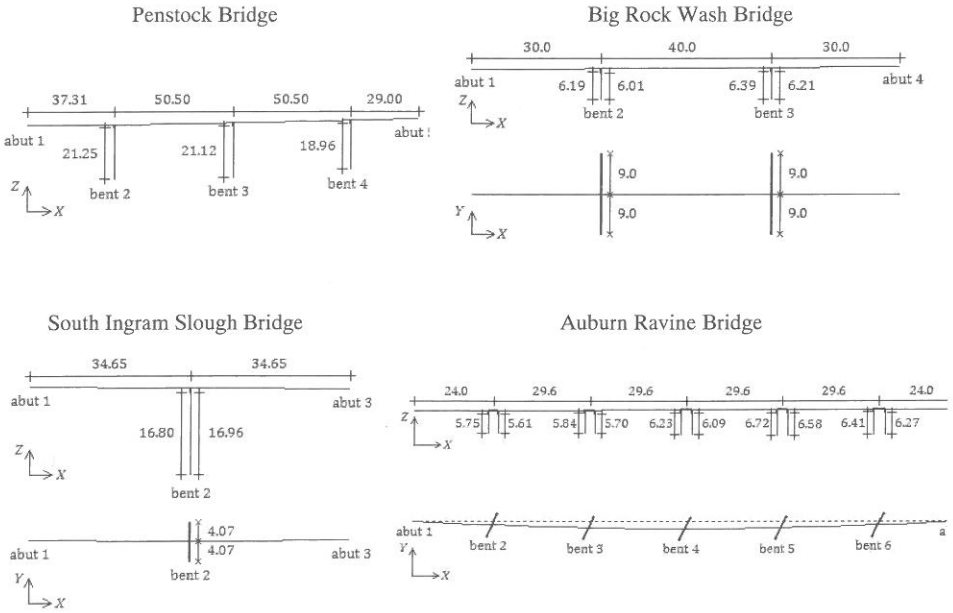


Figure 1. Bridge models.

3 INPUT EXCITATIONS

Synthetic ground motion arrays are generated with the method developed in Konakli & Der Kiureghian (2012). This method requires specification of a seed accelerogram at a reference location, a coherency function that describes the spatial variability of the ground motion random field in the frequency domain, and the Frequency Response Functions (FRF) of the soil columns underneath the bridge supports. The unconditional approach of this method, employed herein, simulates arrays of motions with uniform variability at all support points.

Two seed accelerograms are considered in this study; the fault-normal (FN) components of the Hollister South & Pine (HSP) record from the 1989 Loma Prieta earthquake and of the Pacoima Dam (PUL) record from the 1971 San Fernando earthquake. By using recorded accelerograms as seeds, the simulated motions inherit temporal and spectral characteristics of real earthquake motions. To achieve nonlinear bridge response, the HSP record is scaled with a factor of 1.5. (No scaling is applied to the stronger PUL record.) The corresponding acceleration time histories are shown in Figure 2.

The coherency between the ground acceleration processes at two sites, k and l , as a function of frequency, ω , is given by (Der Kiureghian 1996)

$$\gamma_{kl}(\omega) = |\gamma_{kl}(\omega)|^{incoherence} \exp\left\{i\left[\theta_{kl}(\omega)^{wave\ passage} + \theta_{kl}(\omega)^{site\ response}\right]\right\} \quad (1)$$

in which $|\gamma_{kl}(\omega)|^{incoherence} = \exp[-(\alpha d_{kl} \omega / v_s)^2]$ describes the incoherence component (Luco & Wong 1986), $\theta_{kl}(\omega)^{wave\ passage} = -\omega d_{kl}^L / v_{app}$ is the phase shift due to the wave-passage effect, and $\theta_{kl}(\omega)^{site\ response} = \tan^{-1} \{ \text{Im}[h_k(\omega)h_l(-\omega)] / \text{Re}[h_k(\omega)h_l(-\omega)] \}$ is the phase shift due to the

site-response effect. In these expressions, α is an incoherence parameter, d_{kl} is the distance between supports k and l , v_s is the shear wave velocity of the ground medium, d_{kl}^L is the projected horizontal distance in the longitudinal direction of wave propagation, v_{app} is the surface apparent wave velocity, and $h_s(\omega)$, $s = k, l$, is the FRF for the absolute acceleration response of the site associated with the s th support DOF. In the current example, $h_s(\omega)$ is described by the FRF of the single-degree-of-freedom oscillator.

For all bridges, it is assumed that waves propagate in the direction from abutment 1 to the abutment at the other end of the bridge. Four cases of spatial variability are considered: case 1 is uniform support excitations; cases 2 and 3 incorporate effects of incoherence and wave passage, and represent two different levels of incoherence, $a = 0.2$ and $a = 0.4$, respectively; case 4 is case 2 plus site-response effects. For each bridge, the excitation in case 1 is the motion at a reference support from the corresponding array in case 2. The reference supports are bent 3 for the Penstock Bridge, bent 2 for the South Ingram Slough Bridge, bent 2 for the Big Rock Wash Bridge and bent 4 for the Auburn Ravine Bridge. In cases 2-4, the parameter values $v_s = 600\text{m/s}$ and $v_{app} = 400\text{m/s}$ are adopted. In case 4, the assumed variation of firm (F), medium (M) and soft (S) soil types at the supports from left to right is FMSMF for the Penstock Bridge, FSF for the South Ingram Slough Bridge, FMSF for the Big Rock Wash Bridge and FMSMSMF for the Auburn Ravine Bridge. For each of the cases 1-4 with the HSP record as seed, and 1-2 with the PUL record as seed, 20 support motion arrays are generated. These motions are applied as transverse excitations.

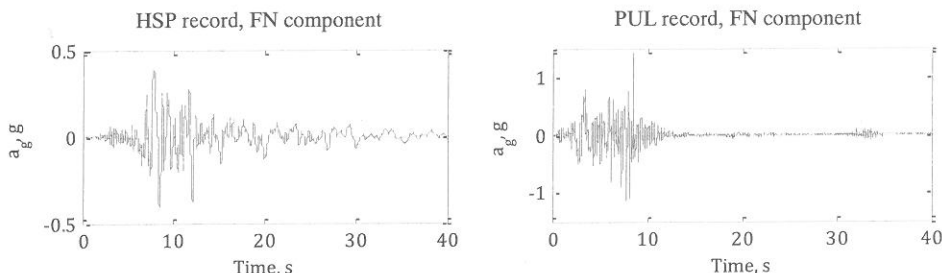


Figure 2. Acceleration time histories of seed records.

4 FRAGILITY ANALYSIS

Using a common convention, fragility curves are described by lognormal cumulative distribution functions (CDF). The parameters of the lognormal distribution are evaluated with the maximum likelihood method: Let I_k and D_k denote the values of the ground motion intensity and demand measures, respectively, in the k th simulation. Let D_{ref} denote the threshold value of the demand measure that defines 'failure'. Adopting the approach by Shinozuka et al. (2000), the k th simulation is considered a realization of a Bernoulli experiment with possible outcomes '1' or '0' depending on whether D_k exceeds D_{ref} or not. The probability of the outcome '1' at the k th trial is given by $F(I_k) = \Phi[\ln(I_k/c)/\zeta]$, in which F denotes the fragility function, Φ is the standard normal CDF, and c and ζ are the parameters of the lognormal distribution (median and log-standard deviation, respectively) to be estimated.

In the following analysis, damage is quantified through the displacement ductility factors of the piers, denoted μ . These factors are defined as the ratios of the maximum pier drifts evaluated from nonlinear time-history analysis to the corresponding yield drifts. The yield drifts are obtained from double integration of the curvature along the pier height, assuming that the section with the largest curvature has just yielded. The yield curvature is determined from moment-curvature analysis at section level. Each of the four bridges examined herein has piers with identical cross-sections and thus, identical yield curvatures.

A preliminary analysis is performed to select the ground motion intensity measure between the typically used PGA and SA. For each bridge and for all simulations in case 2, Figure 3 shows the maximum ductility factor among all piers, μ , versus PGA in the left graphs, and ver-

sus SA in the right graphs. Since PGA and SA vary among the bridge supports, the mean values over all support points are plotted. This figure clearly indicates a higher correlation of damage with SA, which is adopted as the ground motion intensity measure in the following analysis. (Similar observations were made for the other cases of spatial variability examined in this study.) In Gardoni et al. (2003), the appropriateness of SA to characterize ground motion intensity has been demonstrated as a result of a step-wise deletion process.

Accounting for the ranges of ductility factors obtained in the simulations, the threshold values that define failure are selected as $\mu_{ref} = 2$ for the Penstock Bridge, $\mu_{ref} = 2$ for the South Ingram Slough Bridge, $\mu_{ref} = 3$ for the Big Rock Wash Bridge and $\mu_{ref} = 2$ for the Auburn Ravine Bridge. Each bridge is considered a series system, i.e., failure occurs when μ_{ref} is exceeded for at least one pier. The estimated medians and log-standard deviations of the fragility functions are listed in Table 1. The corresponding curves are shown in Figure 4: The graphs on the left show fragility curves for cases 1-4 with the HSP record as seed, and thus, demonstrate effects of different spatial variation patterns. The graphs on the right show fragility curves for cases 1-2 for both HSP and PUL, and thus, demonstrate sensitivities with respect to the characteristics of the seed record. For both seeds, effects of spatial variability are mild on the Penstock Bridge and the South Ingram Slough Bridge, i.e., on the two more flexible bridges, and are more pronounced on the stiffest Auburn Ravine Bridge. The latter is less vulnerable to spatially varying support motions than to uniform motions. The opposite trend, i.e. increased seismic vulnerability due to spatial variability of the support motions, has been reported in other studies (Deodatis et al. 2000, Saxena et al. 2000, Kim & Feng, 2003, Lupoi et al. 2005). Differences in the approaches of those studies versus the approach employed herein are mentioned in the Introduction.

Computational cost as well as convergence and stability problems are main drawbacks in the nonlinear time-history analysis approach. Consideration of spatial variations in the input poses additional challenges by further complicating the system of nonlinear equations to be solved. Therefore, approximate simplified analysis methods are of major interest. On the basis of the 'equal displacement' rule (Veletsos and Newmark, 1960), displacement demands computed for the linear structure can be used to approximate the inelastic displacement demands as long as the fundamental period of the structure is larger than the predominant period of the site. In Caltrans design practice, the 'equal displacement' rule is adopted for bridges with fundamental periods within the range 0.7s and 3s. Table 2 lists the medians of the lognormal distributions describing the fragility curves estimated with the same approach as before, but with the displacement demands computed from linear time-history analysis. The numbers in the parentheses are the ratios of these approximate median estimates to the medians listed in Table 1. These ratios demonstrate trends consistent with results from analyses under uniform excitations: Approximations of the 'equal displacement' rule tend to be slightly conservative for 'sufficiently flexible' structures (Gupta and Krawinkler 2000) and depend on ductility factors for structures with lower fundamental periods (Vidic et al. 1994).

Table 1. Medians (in units of g) of fragility curves. (The numbers in parentheses are the corresponding log-standard deviations.)

Bridge name	HSP case 1	HSP case 2	HSP case 3	HSP case 4	PUL case 1	PUL case 2
Penstock	0.36 (0.17)	0.34 (0.18)	0.38 (0.03)	0.38 (0.12)	0.33 (0.11)	0.33 (0.11)
S. Ingram Slough	0.87 (0.00)	0.91 (0.13)	0.85 (0.07)	0.85 (0.09)	0.85 (0.00)	0.89 (0.00)
Big Rock Wash	0.37 (0.30)	0.44 (0.11)	0.44 (0.13)	0.44 (0.19)	0.73 (0.25)	0.83 (0.21)
Auburn Ravine	1.01 (0.11)	1.65 (0.32)	1.26 (0.11)	2.76 (0.94)	0.86 (0.20)	1.13 (0.43)

Table 2. Medians (in units of g) of fragility curves obtained with the 'equal displacement' rule. (The numbers in parentheses are the ratios of the medians in Table 2 to the medians in Table 1.)

Bridge name	HSP case 1	HSP case 2	HSP case 3	HSP case 4	PUL case 1	PUL case 2
Penstock	0.32 (0.89)	0.28 (0.82)	0.30 (0.79)	0.31 (0.82)	0.35 (1.06)	0.29 (0.88)
S. Ingram Slough	0.70 (0.80)	0.80 (0.88)	0.80 (0.94)	0.77 (0.91)	0.75 (0.88)	0.75 (0.84)
Big Rock Wash	0.41 (1.11)	0.45 (1.02)	0.40 (0.91)	0.41 (0.93)	0.79 (1.08)	0.76 (0.92)
Auburn Ravine	0.87 (0.86)	1.07 (0.65)	1.19 (0.94)	1.30 (0.47)	0.78 (0.91)	0.75 (0.66)

5 CONCLUSIONS

Effects of ground motion spatial variability on seismic fragilities were investigated for four highway bridges in California. Arrays of ground motions with temporal and spectral nonstationarities, and consistent with prescribed spatial variation patterns, were used as input. Damage was quantified through pier displacement ductility factors, evaluated from nonlinear time-history analyses. Effects of spatial variability were more pronounced for the stiffest among the bridges; for this bridge, spatial variations decreased seismic vulnerability. Approximations of the 'equal displacement' rule demonstrated trends similar to those reported in literature for the case of uniform excitations.

6 REFERENCES

- Deodatis, G., Saxena, V., & Shinozuka, M., 2000. Effect of spatial variability of ground motion on bridge fragility curves. *Proceedings of the 8th ASCE Specialty Conference on Probabilistic Mechanics and Structural Reliability*, University of Notre Dame.
- Der Kiureghian, A., 1996. A coherency model for spatially varying ground motions. *Earthquake Engineering and Structural Dynamics* 25: 99-111.
- Gardoni, P., Mosalam, K.M., & Der Kiureghian, A., 2003. Probabilistic seismic demand models and fragility estimates for RC bridges. *Journal of Earthquake Engineering* 7 (Special Issue 1): 79-106.
- Gupta, A., & Krawinkler, H., 2000. Estimation of seismic drift demands for frame structures. *Earthquake Engineering and Structural Dynamics* 29: 1287-1306.
- Karim, K.R., & Yamazaki, F., 2001. Effect of earthquake ground motions on fragility curves of highway bridge piers based on numerical simulation. *Earthquake Engineering and Structural Dynamics* 30:1839-1856.
- Kennedy, R.P., & Ravindra, M.K., 1984. Seismic fragilities for nuclear power plant risk studies. *Nuclear Engineering and Design* 79: 47-68.
- Kim, S., & Feng, M.Q. 2003. Fragility analysis of bridges under ground motion with spatial variation. *International Journal of Non-Linear Mechanics* 38: 705-721.
- Konakli, K., & Der Kiureghian, A., 2011. Stochastic dynamic analysis of bridges subjected to spatially varying ground motions. *Report No. 2011/105*, Pacific Earthquake Engineering Research Center, University of California, Berkeley.
- Konakli, K., & Der Kiureghian, A., 2012. Simulation of spatially varying ground motions including incoherence, wave-passage and site-response effects. *Earthquake Engineering and Structural Dynamics* 41: 495-513.
- Liao, S., & Zerva, A., 2006. Physically compliant, conditionally simulated spatially variable seismic ground motions for performance-based design. *Earthquake Engineering and Structural Dynamics* 35: 891-919.
- Luco, J.E., & Wong, H.L., 1986. Response of a rigid foundation to a spatially random ground motion. *Earthquake Engineering and Structural Dynamics* 14: 891-908.
- Lupoi, A., Franchin, P., Pinto, P.E., & Monti, G. Seismic design of bridges accounting for spatial variability of ground motion, 2005. *Earthquake Engineering and Structural Dynamics* 34: 327-348.
- Nielson, B.G., & DesRoches, R., 2007. Seismic fragility methodology for highway bridges using a component level approach. *Earthquake Engineering and Structural Dynamics* 36: 823-839.
- Saxena, V., Deodatis, G., Shinozuka, M., & Feng, M.Q., 2000. Development of fragility curves for multi-span reinforced concrete bridges. *Proceedings of the International Conference on Monte Carlo Simulation*, Principality of Monaco.
- Shinozuka, M., Feng, M.Q., Lee, J., & Naganuma, T., 2000. Statistical analysis of fragility curves. *Journal of Engineering Mechanics* 126(12): 1224-1231.
- Singhal, A., & Kiremidjian, A.S., 1996. Method for probabilistic evaluation of seismic structural damage. *Journal of Structural Engineering* 122(12): 1459-1467.
- Straub, D., & Der Kiureghian, A., 2008. Improved seismic fragility modeling from empirical data. *Structural Safety* 30: 320-336.
- Vanmarcke E.H., & Fenton G.A., 1991. Conditioned simulation of local fields of earthquake ground motion. *Structural Safety* 10: 247-264.
- Veletsos, A.S., & Newmark, N.M., 1960. Effect of inelastic behavior on the response of simple systems to earthquake motions. *Proceedings of the 2nd World Conference on Earthquake Engineering*, Japan, 2:895-912.
- Vidic, T., Fajfar, P., & Fischinger, M., 1994. Consistent inelastic design spectra: strength and displacement. *Earthquake Engineering and Structural Dynamics* 23: 502-521.

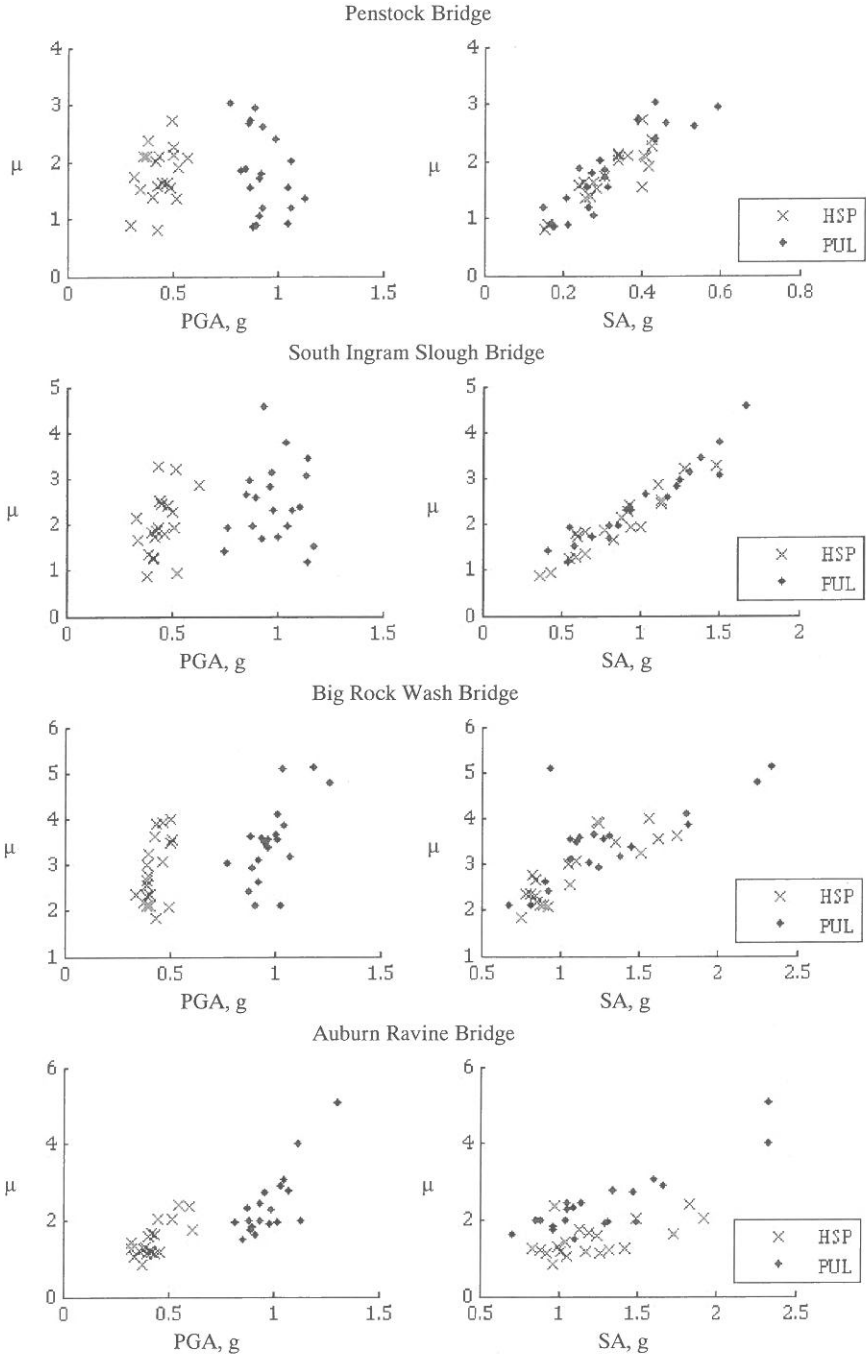


Figure 3. Maximum displacement ductility factors versus PGA (left graphs) and versus SA (right graphs).

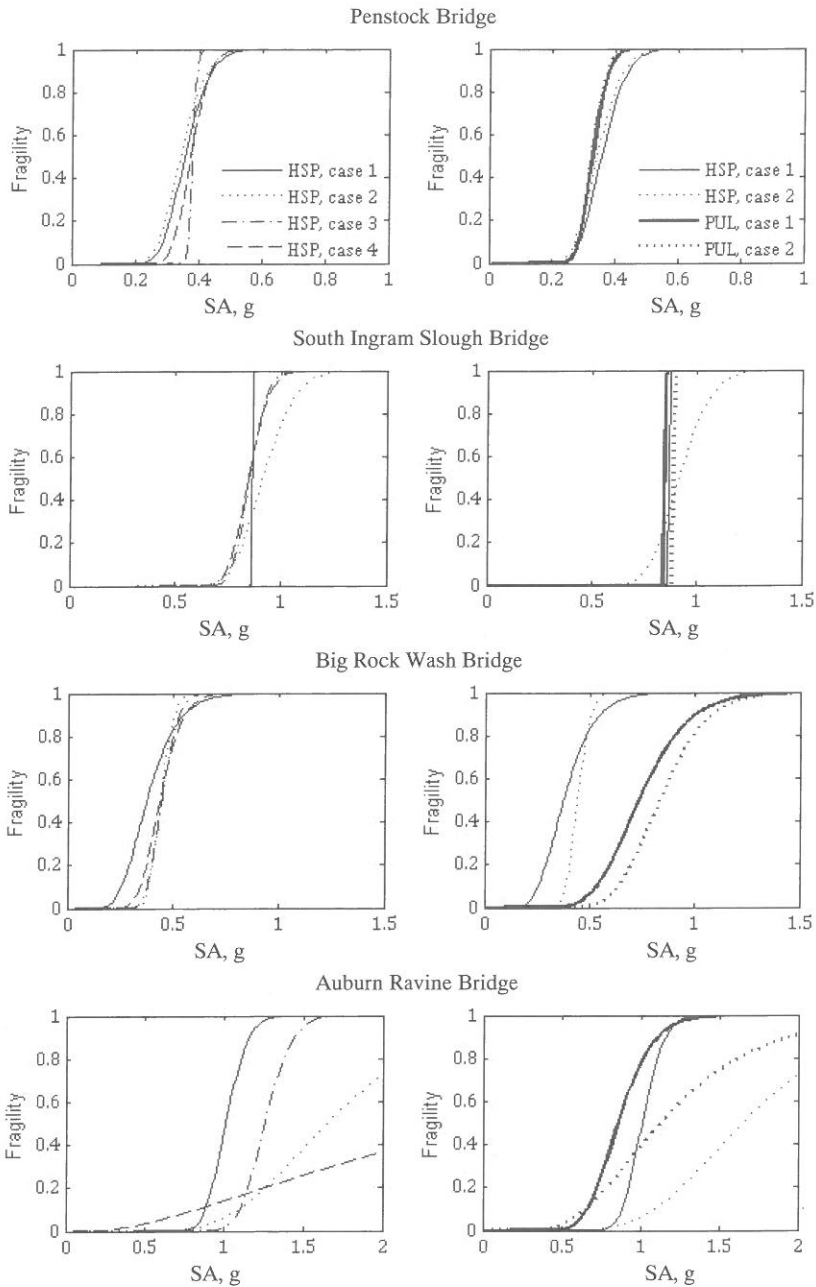


Figure 4. Fragility curves.

Bridge management system of a large number of bridges using genetic algorithms

K. Nakatsu & H. Furuta

Faculty of Informatics, Kansai University, Takatsuki, Osaka, Japan

K. Takahashi, K. Ishibashi & T. Umekage

Graduate school of Informatics, Kansai University, Takatsuki, Osaka, Japan

ABSTRACT: Recently, the bridge management in Japan has become very important and urgent, because the number of existing bridges requiring repair or replacement has increased drastically. The long term planning for bridge management has been attempted to improve the safety and serviceability by reducing Life Cycle Cost (LCC) for maintenance. In the previous study, a bridge maintenance plan minimizing LCC is searched by Improved Genetic Algorithm (IGA), which can provide flexible periods for some maintenance actions. Using the numerical simulation, it is confirmed that the plan is more robust against various uncertainties without increasing LCC by introducing the flexible period. However, a lot of computation time is needed for the long term planning of a large number of bridges due to the enormous combinations. Therefore, it is desirable to improve the convergence and to reduce the computation time. In this study, an attempt is made to propose a maintenance planning method that can produce more accurate solution for a large number of bridges. At first, in the proposed method, a maintenance plan for each bridge is searched by minimizing its LCC. Next, the overall solution is derived by modifying the solutions obtained for each bridge with the aid of the possible flexible periods that can postpone some maintenance works. Performing simultaneous maintenance works within some flexible periods, it is possible to obtain a reasonable maintenance plan for a large number of bridges, based on the plans obtained for each bridge. Numerical examples are presented to demonstrate the applicability and efficiency of the proposed method.

1 INTRODUCTION

Recently, the bridge management in Japan has become very important and urgent, because the number of existing bridges requiring repair or replacement has increased drastically. However, it is difficult to sustain the management in the future due to the shortage of engineers and budget. In the circumstances, the long term planning for bridge management has been attempted to improve the safety and serviceability by reducing Life Cycle Cost (LCC) for maintenance (Furuta et al. 2006; Ito et al. 2002). In the previous study, a bridge maintenance plan minimizing LCC is searched by Improved Genetic Algorithm (IGA) (Nakatsu et al. 2011), which can provide flexible periods for some maintenance actions. Using the numerical simulation, it is confirmed that the plan is more robust against various uncertainties without increasing LCC by introducing the flexible period. However, a lot of computation time is needed for the long term planning of a large number of bridges due to the enormous combinations. Therefore, it is desirable to improve the convergence and to reduce the computation time. Although it is possible to obtain an approximate solution by combining the solution for each bridge minimizing LCC, it may give a large difference due to the cost such as general and administrative costs between the approximate solution and the optimum solution searched for a large number of bridges at the same time.

In this study, an attempt is made to propose a maintenance planning method that can produce more accurate solution for a large number of bridges. At first, in the proposed method, a maintenance plan for each bridge is searched by minimizing its LCC. The proposed method estab-

lishes a plan considering preventive maintenance by applying Genetic Algorithm (GA) (Goldberg 1989). Next, the overall solution is derived by modifying the solutions obtained for each bridge with the aid of the possible flexible periods that can postpone some maintenance works. Performing simultaneous maintenance works within some flexible periods, it is possible to obtain a reasonable maintenance plan for a large number of bridges, based on the plans obtained for each bridge. Numerical examples are presented to demonstrate the applicability and efficiency of the proposed method.

2 OPTIMAL PLANNING OF LONG-TERM BRIDGE MANAGEMENT

The purpose of bridge management is to prolong the life of bridges by repair and reinforcement against the degradation. In order to sustain the safety of bridge, it is common to keep the intact state by regular detailed inspection, high-quality repair, reinforcement and renovation. However, it is actually difficult to perform the above maintenance. This is because these require a lot of cost and manpower. Therefore, it is important to establish a long-term bridge management plan. A long-term plan is useful to reduce the maintenance cost with sustaining the safety based on the deterioration prediction. In addition, this plan is useful to estimate for long-term budget; it is possible to improve the accountability to citizens by visualizing the purpose of budget.

2.1 *Application problem*

In this study, the proposed method is applied to the planning of management for 100 years. The application problem is same as the existing research (Furuta et al. 2009; Nakatsu et al. 2011).

In maintenance planning, it is required to sustain the safety of all components during their service period. In this study, the service period is set to be 100 years. Therefore, the purpose of planning is to minimize the maintenance cost under the circumstances. The performance of component to sustain the safety is more than 0.8 as well as the previous research (Furuta et al. 2009; Nakatsu et al. 2011). This is because the purpose of this paper is to verify the applicability of planning method through numerical examples. This value should be determined on the basis of safety required in the maintenance management in the real-world problem.

2.2 *Problems involved in maintenance planning*

In the long-term planning, maintenance cost may change due to the change of plan. The change of circumstances due to uncertainties is considered as causes of change of plan.

2.2.1 *Change of plan due to uncertainties*

In the bridge maintenance, a change of plan can happen due to uncertainties like an error of deterioration prediction. It is difficult to accurately predict deterioration because the appropriate method has not been developed yet. If the development of deterioration is faster than that predicted, the lack of safety performance and the change of cost due to moving up a maintenance work occur. On the other hand, if the development of deterioration is slower than the predicted one, the maintenance work spends extra cost because works unnecessary to acquire the safety are performed. Thus, in the long-term planning, it is important to establish a plan that can be changed by minimal increase cost with robustness against uncertainty involved in the deterioration.

2.2.2 *Planning for a large number of bridges*

Local governments in Japan are managing the several hundred numbers of bridges. The previous method (Furuta et al. 2009; Nakatsu et al. 2011) cannot search the optimal solution due to enormous combinations of a large number of bridges. Therefore, a maintenance planning method is needed that can produce more accurate solution for a large number of bridges.

Although it is possible to obtain an approximate solution by combining the solution for each bridge minimizing LCC, it may give a large difference due to the cost such as general and administrative costs between the approximate solution and the optimum solution searched for a large number of bridges at the same time. Therefore, in this study, the overall solution is derived by modifying the solutions obtained for each bridge with the aid of the possible flexible periods

that can postpone some maintenance works. Performing simultaneous maintenance works within some flexible periods, it is possible to obtain a reasonable maintenance plan for a large number of bridges, based on the plans obtained for each bridge.

3 DEALING WITH UNCERTAINTY IN LONG-TERM PLANNING

The costs exist be reduced doing many works in same year, such as general administration cost. Therefore, it is considered that the bridge management plan is necessary to formulate multiple bridges at the same time. But the method using GA in the previous study (Furuta et al. 2009; Nakatsu et al. 2011) cannot calculate the optimal solution due to enormous combinations of a large number of bridges.

- 1) Plans for each bridges and searches the flexible period.
- 2) Searched plans of multiple bridges to combines those flexible terms.

Because the flexible period shown in previous study (Furuta et al. 2009; Nakatsu et al. 2011) satisfies preventive maintenance with minimizing the LCC, it covers the suboptimal solution obtained by GA. Therefore, by considering the planning of other bridges in the flexible period for each bridge, it is possible to obtain an optimal plan considering a large number of bridges without planning at the same time.

3.1 Uncertainty Treatment

The purpose of a long-term planning is not only to minimize the maintenance cost during their service period but also to estimate a long-term budget. The re-scheduling (Yamada et al. 1998; Hirai 2008; Ishibuchi et al. 1998; Tamaki et al. 1999) is generally useful to deal with uncertainty. However, the re-scheduling is not useful for a long-term planning because it required a lot of changes of plan even if the maintenance cost was reduced and the safety was sustained. In addition, early repair and reinforcement plans cannot reduce the maintenance cost because they have tendency to perform the maintenance inappropriately.

! The proposed method is applied to a plan obtained with the preventive maintenance to estimate the flexible period. In a long-term planning, preventive and corrective maintenances are considered due to the relationship between the construction year and the performance of component. Figure 1 shows the concept of transition of performance due to corrective maintenance and preventive maintenance. In the corrective maintenance, repair and reinforcement are performed when the performance is close to the limitation of safety as shown in Figure 1. In this case, the performance would be lower than the safety level if the deterioration begins earlier than the predicted. Furthermore, if repair effect is lost faster than that expected, the performance would immediately become lower than the safety level. On the other hand, the repair and reinforcement are performed when the performance begins to deteriorate in the preventive maintenance. Thus, even if the development of deterioration is earlier than that predicted, there is also a margin to the safety limitation. There is a margin to the safety limitation as well even if the repair effect is lost faster than the expected. Therefore, a plan considering the preventive maintenance is expected to have the robustness against uncertainties; an established plan has a few possibilities to perform exclusive front-loaded re-scheduling. Focusing on these features, the proposed method estimates the flexible period of a preventive maintenance plan. Therefore, a plan established by the proposed method can satisfy both of the safety level and the cost minimization.

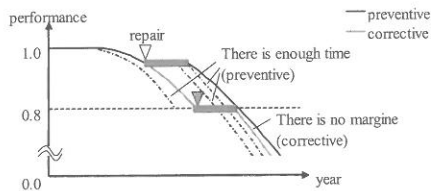


Figure 1: Deteriorations of preventive and corrective maintenance

3.2 Preventive maintenance planning by GA

3.2.1 Coding rule

In this study, the coding of gene is defined as shown in Figure 2. In this coding, a gene of individual is separated to the repair method and the interval part. The genetic array of each part has the same length. And, the length is determined so as to deal with the service period by using the number of years calculated from the interval part. In this study, the length of gene is set 50 years in order to establish the 100 years maintenance plan as described in Section 2.1. It is not realistic that 50 times of repairs or reinforcements are performed to a component of bridge in 100 years. Thus the length described above is enough to deal with this problem. Here, unnecessary genes to establish a 100 years plan are not used to optimize.

The information of gene in the repair method part represents the identification number of repair method. In this study, the identification number of each repair method is set as follows; the surface painting is 1, the surface covering is 2, the section restoring is 3, the desalting and re-alkalization is 4, the cathodic protection is 5, the section restoring with surface covering is 6 and the reconstruction is 7. The genotype described above is converted to the phenotype shown in Figure 8 in order to use as an annual plan. Here, a part containing 0 in the phenotype represents a year when a repair and reinforcement are not performed. In the crossover section, the two parts of gene is performed respectively. The uniform crossover is adopted as the crossover method in this study. In the mutation section, the two parts of gene are performed respectively as well as the crossover section. A value of gene is replaced to a randomly generated number in the repair method part. On the other hand, the operation of mutation in the interval part is performed as shown in Figure 2. Through this operation, the schedule following to a mutated gene does not change; the mutation is performed without changing the property of solution candidate.

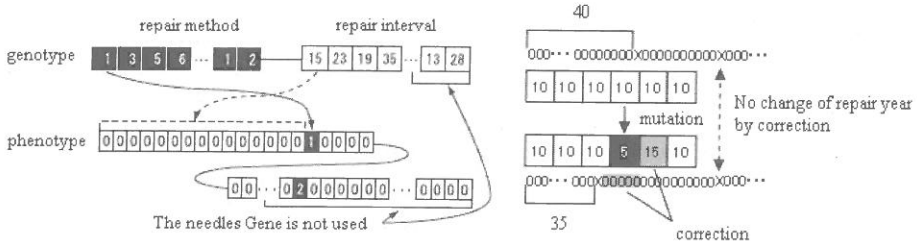


Figure 2: (a)Coding rule, (b)Mutation of interval part

3.2.2 Consideration of selection and constraints

In this study, a fitness of individual per generation is decided along the ranking followed the sorting rule as well as the previous research (Furuta et al. 2009; Nakatsu et al. 2011). In order to establish a plan considering the preventive maintenance described in Section 3.1.

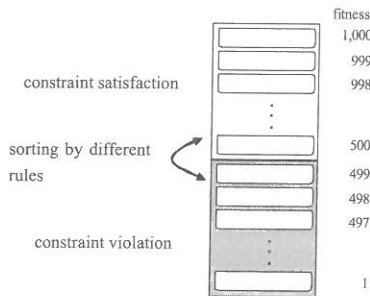


Figure 3: Determination of fitness

Figure 3 shows the image of the sorting. As shown in Figure 3, individuals are separated to two groups based on their state. In this figure, a group that satisfies the constraints is superior to another which violates the constraints. And, individuals are sorted in each group by using each evaluation. In this study, the evaluation function is defined as in Equation (1). $MC_{b,p}$ represents the maintenance cost required for component p of bridge b . The development of performance of component is defined as in Equation (2). $PI_{b,p,y}$ represents the performance of component p of bridge b in year y . In the service period, the performance of component is required to satisfy the safety level ($PI_{target} = 0.8$) as described in Section 2.1 Equations (1) and (2) are determined by the repair method for each year.

$$\sum_b \sum_p MC_{b,p} \quad (1)$$

$$PI_{b,p,y} \geq PI_{target} \quad (2)$$

! Under these constraints, the fitness of individual is determined by the following groups and sorting rule:

- Group 1: Individuals satisfying constraint: Individuals are sorted in ascending-order of maintenance cost calculated by Equation (1). If they are the same cost, they are sorted in descending-order of total of performance in the service period.
- Group 2: Individuals that violate either performance or reconstruction constraint: Individuals that violate the performance constraint are sorted in ascending-order of total of lacked performance. Individuals that violate reconstruction constraint are sorted in ascending-order of total of reconstruction violation year.
- Group 3: Individuals that violate both constraints: Individuals are sorted by the rule described in Group 2.

In Group 1, a plan performing a repair and reinforcement in the early stage of deterioration is superior to others by this sorting if plans spend the same maintenance cost each other. This plan is considered as a preventive maintenance plan.

3.3 Estimation of flexible period by numerical simulation

An attempt is made to estimate the flexible period which can sustain the safety of bridge in the preventive maintenance plan established by GA as described in Section 3.2. Estimation procedure is as follows:

- Step 1: The number of constructing works of each component is $m_{b,p} (\geq 0)$ when the bridge number is b and component number is p . If $m_{b,p}$ is more than 0, the work number k is set 0, then works are estimated in order. If $m_{b,p}$ is not more than 0, go to Step 4.
- Step 2: The flexible term of each component is estimated by forwarding the constructing year of work $w_{b,p,k}$ to the year of the next work $w_{b,p,k+1}$ in steps of one year. If a performance of component is lower than the safety level due to the forwarding, a year of work is forwarded until the year which can satisfy the safety level.
- Step 3: The work number k is incremented. Then, if k is smaller than $m_{b,p}$, go to Step 2. Otherwise, go to Step 4.
- Step 4: The flexible period of next component is estimated by following the above procedure in order from Step 1. If all components of all bridges were estimated, this procedure is completed.

3.4 Planning for a large number of bridges

It plans every few bridges considering the uncertainty by using methods described Section 3.1 and 3.2. Then, the overall long-term bridge management plan is established by combining those plans.

The proposed method doesn't cause explosion of the number of combinations and increase the computation time. Furthermore, it is possible to optimize the cost such as general and administrative costs in the flexible period.

4 FEATURES OF THREE METHODS

This section describes the same time planning, the combination planning and the proposed method.

4.1 *Same time planning*

The same time planning is the method planning of all bridges at the same time by using the previous method (Nakatsu et al. 2011). In this method, it is possible to reduce the LCC including administrative cost. This is because this method can plan considering administrative cost. However, because GA is a stochastic search, it is difficult to search the optimal solution as the search space is huge. Therefore, this method cannot search the optimal solution for a large number of bridges. For this reason, this method is considered is not practical.

4.2 *Combination planning*

The combination planning is the method combining plans established every bridge or few bridges. This method is able to minimize the LCC in planning every few bridges. In addition, it can be expected an efficient optimization and shorten the computation time sharply because this method plans every few bridges let search space narrow. However, when managing multiple bridges, it exists the cost decreases if many maintenance works are done in the same year. Therefore, it is difficult to minimize the LCC in this method. Therefore, it is necessary to consider an appropriate method for a large number of bridges comparing other method like the same time planning method.

4.3 *Proposed method*

In the proposed method, it is used that the flexible term can be changed of the maintenance year determined in previous study (Nakatsu et al. 2011). This flexible term are made by two steps. First, it plans to minimize maintenance costs as described in 3.3.3. Second, applying to numerical simulation for these plans to search the term does not lose safety and cause significant variation of cost. It is considered the reduction of LCC as well as the same time planning method by combining maintenance works in the term. Therefore, it is said that the proposed method is effective, if it is valid that considering the planning of multiple bridges in a large number of bridges.

5 MAINTENANCE PLANNING OF A LARGE NUMBER OF BRIDGES

5.1 *Numerical example*

The applicability of the proposed method is verified by applying it to the maintenance planning of multiple bridges described in Section 2.1 as a numerical example. In the first experiment, it is presented to demonstrate the effectiveness of reducing the cost of same time planning. In the second experiment, it is presented to demonstrate the planning of a large number of bridges. In this study, parameters of GA are set as follows: in the same time planning method, the population size is 1,000, the number of generations is 10,000, crossover rate is 60% and mutation rate is 0.5%. In the combination planning method and proposed method, the population size is 1,000 and the number of generations is 1,000 per one bridge. Experiment is performed five times for each planning.

5.2 *Effect of reducing the cost of same time planning*

Table 1 shows the result obtained by the experiments for 10 bridges. In Table 1, the same time planning method reduces maintenance cost 5% to 10% rather than the combination method. The construction price obtained when calculating the total cost is included in general and administrative costs which can be reduced the more construction costs during the year. The general admin-

istration cost is reduced to optimize those construction years considering multiple bridges at the same time. Therefore, it is important to plan considering multiple bridges for reduction of the LCC even in a large number of bridges.

Next, it is discussed that the plan established by proposed method optimizes the simultaneous construction of multiple bridges within in the flexible periods.

The total cost established by proposed method is 4,112,714 thousand Japanese yen. However, in terms of minimizing LCC, combining the simultaneous construction of multiple bridges within flexible periods, the total cost is 3,957,574 thousand Japanese yen. If the appropriate year to conduct simultaneous construction is selected, it is possible to reduce LCC about 3.8%. The plan that considers the construction of simultaneous by the proposed method, many constructions has been performed at the same time. For example, 21 bridges is repaired in 52 years, 21 bridges is repaired in 77 years. The results of the proposed method shown in Table 1 is higher than the same time planning method, but the cost is lower than the combination planning method about 4.2%. Therefore, it is considered the proposed method can develop the practical plan a similar cost reduction to the same time planning method.

Table 1. Results of 10 bridges (Unit: JPY1,000)

method	best	average	standard deviation
same time planning	3,667E+6	3,796E+6	7,511E+4
combination planning	3,944E+6	4,084E+6	1,744E+5
proposed	3,827E+6	3,915E+6	6,544E+4

5.3 Planning of a large number of bridges

Table 2 shows the result obtained by the experiments for 50 bridges. In the same time planning method with 50 bridges, parameters of GA are set as follows: the population size is 1,000 and the number of generations is 10,000. The computation time took about 20 hours in the computer used in experiment (Intel(R) Core(TM) i7 CPU Q740@1.73GHz, Memory 4GB, Windows 7 64bit). However, the same time planning method could not obtain optimum solution. Even if the population size increased to 5,000 and the computation time took over 100 hours, it could not obtain optimum solution which is sustained the safety. As GA search space is huge, the search for the optimal solution falls into a local solution. This is because the search space has become too huge because the number of combination has become enormous by increasing the number of bridges. Combinations for planning of 100 years in the bridge 50 is as up to $8^{50 \text{repairs}} \times 8,000^{\text{individuals}}$ $\times 50 \text{bridges}$; the repair per bridge is 50, the population size is 8,000 that combined current generations 5,000 individuals and next generations 3,000 individuals, and the repair method is 8. For this vast number of combinations, GA falls into a local solution. Therefore, it could not obtain optimum solution. In the result, it is effective to search the optimum solution for a large number of bridges at the same time. However, with an increase in the number of bridges, it is difficult to search the solution at the same time. In practical problem, since it is assumed that the planning to target more than 50 bridges, the difficulty of planning is far increased.

! The proposed method reduces maintenance costs 3% shown in Table 2 rather than the combination method. The proposed method could not obtain optimum solution in about 2 hours. In contrast to the same time planning method, the proposed method could plan in a short time. In the number of combinations, the proposed method is not to be a large design space as the same time planning method because of planning to make every each bridge's. From the number of possible combinations for the planning, it is difficult to determine whether the obtained solution is optimum solution. However, performing simultaneous maintenance works within some flexible periods, the proposed method is possible to obtain a reasonable maintenance plan for a large number of bridges, based on the plans obtained for each bridge. Therefore, the obtained solution can be estimated and close to the optimum solution, it is considered for the planning of a large number of bridges, the proposed method is useful.

Table 2. Results of 50 bridges (Unit: JPY1,000)

method	best	average	standard deviation
same time planning			
combination planning	1.827E+7	1.869E+7	2.688E+5
proposed	1.806E+7	1.804E+7	7.146E+3

6 CONCLUSIONS

In this study, an attempt was made to propose a new method that can establish a practical maintenance plan for a large number of bridges. Numerical examples demonstrated that the proposed method can deal with a large number of bridges. The proposed method could obtain optimum solution in an example with 50 bridges. Furthermore, the proposed method overcame the problem of computation time and the number of combinations in the previous method by combining flexible periods of bridges.

However, this study only demonstrated the applicability of the proposed method because the applied model of repair method adopted only the typical ones; the flexible period was not realistic. Hence, in the future, it is necessary to demonstrate the usefulness of flexible period by applying more realistic model of repair methods.

7 REFERENCES

- Furuta, H., Kameda, T. and Nakahara, K., 2006. Practical Use of Bridge Management System by Improved Genetic Algorithm. *Journal of JSCE, Division A*, 62(3): 656-668.
- Furuta, H., Nakatsu, K. and Nomura, Y., 2008. Optimal Restoration Scheduling of Damaged Networks in Uncertain Environment, *Journal of JSCE, Division A*, 64(2): 434-445.
- Goldberg, D.E., 1989. *Genetic Algorithm in Search*, Addison-Wesley Professional.
- Japan Society of Civil Engineers, 2001. *Standard Specification for Design and Construction of Concrete in Japan*, JSCE.
- Hirai, C., 2008. Re-scheduling Algorithm of Disturbed Train Schedules, *The Operations Research Society of Japan*, 53(8): 446-452.
- Ima, H. and Sannomiya, N., 1997. Genetic Algorithm Approach to a Rescheduling Problem, *Autonomous Distributed System Symposium*, 9: 313-318.
- Ishibuchi, H., Murata, T. and Lee, K. H., 1998. Flowshop Scheduling Problems with interval Processing Time, *Japan Industrial Management Association*, 49(2): 59-70.
- Ito, H., Takahashi, Y., Furuta H. and Kameda, T., 2002. An Optimal Maintenance Planning for Many Concrete Bridge on Life-Cycle-Cost, *Proc. of the 1st International Conference on Bridge Maintenance, safety and Management, IAMAS02*, Barcelona, Spain.
- Nakatu, K., Furuta, H., Nomura, Y., Takahashi, K., Ishibashi, K. and Miyoshi, N., 2011. Practical Application of Long-term Bridge Management System Using Genetic Algorithm, *Japan Society for Fuzzy Theory and Intelligent Informatics*, 23(4): 469-479.
- Tamaki, H., Arai, T. and Abe, S., 1999. A Genetic Algorithm Approach to Optimization Problems with Uncertainties, *Transactions of the Institute of Systems*, 12(5): 297-303.
- Yamada, K., Nakata, T. and Nagata, M., 1998. A Cooperative Distributed Approach to Flight Scheduling Problems, *Knowledge-Based Software Engineering*, 98(238): 9-16.

Short-term instability in stochastic systems

M.F. Dimentberg

Mechanical Engineering Department, Worcester Polytechnic Institute, Worcester, MA, USA

C. Bucher

Center of Mechanics and Structural Dynamics, Vienna University of Technology, Vienna, Austria

A. Hera

Information Technology Division, Worcester Polytechnic Institute, Worcester, MA, USA

A. Naess

Centre for Ships and Ocean Structures and Department of Mathematical Sciences, Norwegian University of Science and Technology, Trondheim, Norway

ABSTRACT: Dynamic systems are considered with lumped parameters which experience random temporal variations with potential short-term excursions out of the “classical” stability domain. The resulting system’s response is of an intermittent nature with alternating periods of (almost) zero response and rare short outbreaks. As long as it may be impractical to discard such a system its response should be analyzed to evaluate reliability. Using parabolic approximation for parameter variations during excursions the asymptotic solution can be obtained for probability density of the response and for the first-passage problem. The analysis is used also to derive on-line identification procedure for the system from observed intermittent response. Influence of nonlinearity in stiffness and damping is studied. Specific examples include galloping of elastically suspended rigid bodies in cross-flow of fluid; two-degrees-of-freedom flutter; bundles of heat exchanger tubes with potential flutter-type instability; rotordynamics.

1 INTRODUCTION

Classical definitions of stability and instability deal with long-term behavior of dynamic systems, that is, behavior as time $t \rightarrow \infty$. However these definitions are known to be not perfectly appropriate for applications with limited service life (such as missiles, projectiles, etc.) which may sometimes be qualified as acceptable in spite of being unstable in the classical sense. Design of such marginally unstable systems may be based on analysis of their transient response within limited service life.

The classical definitions of stability and instability may also prove to be not perfectly adequate for another class of dynamic systems – those that may be intended for long-term operation. Such systems are designed, as a rule, to operate within their stability domain in the classical sense as long as their “nominal” design parameters are considered. However, if the system’s parameters may experience random temporal variations around their “nominal” or expected values, the system may become “marginally unstable” within the “smeared” stability boundary. Whenever complete elimination of this kind of response may lead to impossible or impractical design, the corresponding short-time outbreaks in response should be analyzed to evaluate the system’s reliability. Thus, problems of first-passage failure and/or of low-cycle fatigue may be of concern for a system operating within the transitional state. Relevant dynamic studies may also be of importance for interpretation of test results for a machine or structure where intermittent behaviour of the response is observed.

Results of such analyses are presented for the case of slow parameter variations. Linear models of the systems are studied using parabolic approximation (PA) for the variations in the vicinity of their peaks together with Krylov-Bogoliubov (KB) averaging over the period for the transient response. This results in a solution for the probability density function (PDF) of the response in terms of that of the bifurcation parameter. The response is of an intermittent nature indeed due to the specific algorithm of its generation, with rare excursions of a bifurcation parameter into the instability domain. The procedure is also extended to nonlinear single-

degree-of-freedom systems, which implies use of quasiconservative version of averaging over the period. The analysis is also used to derive on-line identification procedure for the system from its observed response with set of rare outbreaks (nicknamed "puffs").

2 LINEAR SYSTEMS WITH SLOW VARIATIONS OF PARAMETERS

Linear systems with slow stationary random temporal variations of parameter(s) compared to the system's natural frequency(ies) are considered in this section. They operate *within classical stability domain* for the mean or "nominal" system. But any brief excursion beyond the instability threshold would lead to growth of the system's response. The growth is assumed to be limited as long as the system quickly returns back into the stability domain. The response would be seen then as a set of spontaneous brief outbreaks alternating with intervals of zero response. Basically the response is transient during each outbreak. The method for analysis is based on parabolic approximation (PA) (Stratonovich 1967) or Slepian model (Leadbetter et al. 1983) for temporal variation(s) of parameter(s) during its (their) brief excursions into instability domain. Thus the problem of random vibration is reduced to a deterministic transient problem with *random initial conditions*.

The Slepian model (Leadbetter et al. 1983) of a stationary zero-mean random process $g(t)$ with unit standard deviation implies PA in the vicinity of its peak which exceeds a given level u – that is during upcrossing level u that starts at time instant $t = 0$ namely

$$g(t/u) \cong u + (1/u) \left(\zeta t - \lambda^2 t^2 / 2 \right) \text{ so that } g(t) \cong u + \zeta t - (u/2) (\lambda t)^2 \quad (1)$$

for $t \in [0, 2\zeta/\lambda^2 u]$ and $\max_t g(t) = g(\zeta/\lambda^2 u) = g_p = u + \zeta^2 / 2\lambda^2 u$

Hereafter subscript "p" will be used for peak values of random processes, ζ is random slope of

$g(t)$ at the instant of upcrossing and $\lambda^2 = \sigma_g^2 = \int_{-\infty}^{\infty} \omega^2 \Phi_{gg}(\omega) d\omega$ where $\Phi_{gg}(\omega)$ is power spectral density (PSD) of $g(t)$ so that λ is a mean frequency of $g(t)$. Thus, according to the Equation (1) random process $g(t)$ is regarded as deterministic within the high-level excursion of duration $\tau_f = \lambda \tau_f = 2\zeta/\lambda u$ above level u , depending just on its initial slope ζ at the instant of upcrossing. This slope is regarded as a random *variable* for the excursion; in particular, it has the Rayleigh PDF in case of a Gaussian $g(t)$ (Stratonovich 1967). This probabilistic description is used together with the solution for the transient response within the instability domain.

The first example is a SDOF system with randomly varying damping – say, Den-Hartog model of 1D galloping (Den Hartog 1985) under variable wind speed

$$\ddot{X} + 2(\alpha - q(t))\dot{X} + \Omega^2 X = 0 \text{ so that } q(t) = \sigma_q \cdot g(t) \text{ and } u = \alpha/\sigma_q \quad (2)$$

Substituting approximation (1) into Equation (2) reduces the latter to an ordinary differential equation (ODE) with a single random parameter ζ . This ODE for a certain representative crossing should be integrated starting from the instant of upcrossing t_u until instant of peak of $X(t)$ for a given outbreak. Here it can be done analytically using the asymptotic Krylov-Bogoliubov (KB) method of averaging over the response period for the quite common case of a lightly damped system (1) with slow temporal variations of the damping coefficient: $|\alpha - q(t)| \ll \Omega$, $\lambda \ll \Omega$ (Bogoliubov & Mitropol'skii 1961). The method leads to first-order

ODE for slowly varying amplitude $A(t) = \sqrt{X^2 + \dot{X}^2/\Omega^2}$ which has the solution $A(\tau) = A_0 \exp f(\tau)$; $f(\tau) = (\sigma_q/\lambda) \left[(\zeta/\lambda) (\tau^2/2) - u\tau^3/6 \right]$, $\tau = \lambda(t - t_u)$, $A_0 = A(0)$ (3)

The peak amplitude of the response as attained at $\tau_f = 2\zeta/\lambda u$ is

$$A_p = A(\tau_f) = A_0 \exp(2\delta) \text{ where } \delta = \left(\sigma_g/3\lambda u^2\right)(\zeta/\lambda)^3. \quad (4)$$

This solution together with Equation (1) define in parametric form relation between $\bar{A}_p = A_p/A_0$ and g_p - that is between peak values of the amplitude ratio and of $g(t)$ - as long as both these peak values are obtained as functions of the random nondimensional slope ζ/λ of $g(t)$ at the instant of the upcrossing. The explicit relation can be simply derived by excluding ζ/λ . Let $\bar{A}_p = h(g_p)$ for $g_p \geq u$. Then the function inverse to h (denoted by superscript “-1”) can be obtained as

$$g_p = u + (\zeta/\lambda)^2 (1/2u) = h^{-1}(\bar{A}_p) = u + (1/2u) \left[(3\lambda u^2/2\sigma_g) \ln \bar{A}_p \right]^{2/3} \quad (5)$$

These relations open way to predicting reliability for the system (1) based on relevant statistics of $g(t)$. Thus, the first-passage problem for $A(t)$ with barrier A_* is reduced to that for $g(t)$ with barrier $g_* = h^{-1}(\bar{A}_*)$ as evaluated by Equation (5). Furthermore, the PDF of $g(t)$ can be used to obtain the PDF of \bar{A}_p and thus of the local peaks of $X(t)$ within the cluster of response cycles with peak amplitude A_p ; this may be of importance for evaluating low-cycle fatigue life for a system subject to the short-term dynamic instability. The derivation includes two steps. First the PDF $p_g(g_p)$ of peaks of $g(t)$ is obtained from that of the $g(t)$ itself as described in (Leadbetter 1983, Lin & Cai 1995, Stratonovich 1967); then the basic relation for the PDF of a nonlinear function of a random variable is applied:

$$p(\bar{A}_p) = p_g\left(h^{-1}(\bar{A}_p)\right) \cdot \left| dh^{-1}/d\bar{A}_p \right| \quad (6)$$

Note that this PDF is non-zero for $\bar{A}_p \geq 1$ rather than for $\bar{A}_p \geq 0$ as long as the subcritical response amplitude A_0 has been introduced. Furthermore, according to the Equations (5) and (6), this PDF has a singularity at $\bar{A}_p = 1$. It goes without saying that the *unconditional* PDF $p(\bar{A}_p)$ is normalized not to unity but to $\text{Pr ob}\{g_p > u\}$. Its direct use for predicting reliability in engineering applications is possible as long as some information on the most probable actual subcritical response amplitude A_0 is available.

Figure 1 illustrates response sample of the system (1) with $\alpha = 0.16, \Omega = 2$ which contains one excursion of the apparent damping into negative domain (see dash-dot curve of $q(t)$) with the corresponding response outbreak. To guarantee nonzero response during the short-term instability a small zero-mean stationary broadband random process had been added to the RHS of the Equation (1); one can see that the corresponding subcritical response is really very small. Figure 2 illustrates the PDF $p(\bar{A}_p)$ where solution (5), (6) for the case of Gaussian $g(t)$ is compared with result of direct Monte-Carlo simulation (where values of A_0 were measured for each upcrossing). The corresponding prediction of the PDF of the actual (nonscaled) response amplitude and/or its peaks may be improved if PDF $p(A_0)$ of the random variable A_0 is known. Thus, assuming random variables A_0 and ζ to be independent one can write

$$p(A_p) = \int_0^{\infty} p(A_p/A_0) p(A_0) dA_0.$$

The Equation (4) is convenient for evaluating the system's properties from its measured (on-line!) intermittent response with outbreaks as one shown in Figure 1. To this end one can use peak amplitudes A_p , as attained at instants $\tau_f = 2\zeta/\lambda u$ in the local time frames and corresponding amplitudes A_i at inflexion points of the curve $\ln A(\tau)$. From the Equation (4) $A_i = A(\tau_i) = A_0 \exp \delta$, so that $A_p/A_i = \exp \delta$; also $A_0 = A_i^2/A_p$.

Thus, for each one of the observed response outbreaks one can identify in a global time frame the instants $t_f = t_u + \tau_f/\lambda$ and $t_i = t_u + \tau_i/\lambda$ which correspond to peak and inflexion-point amplitudes A_p and A_i respectively; the instants of upcrossings can also be identified as $t_u = t_f - 2(t_f - t_i) = 2t_i - t_f$. The frequency λ may now be obtained by averaging time difference $t_f - t_i$ over all observed outbreaks of response. The identification procedure as described in details in (Dimentberg & Naess 2006) relies upon averaging $\ln(A_p/A_i) = \exp \delta$ over all observed outbreaks. It provides on-line estimates both for the mean apparent damping coefficient – which may be regarded as a nominal stability margin – and for standard deviation and mean frequency of its random temporal variations.

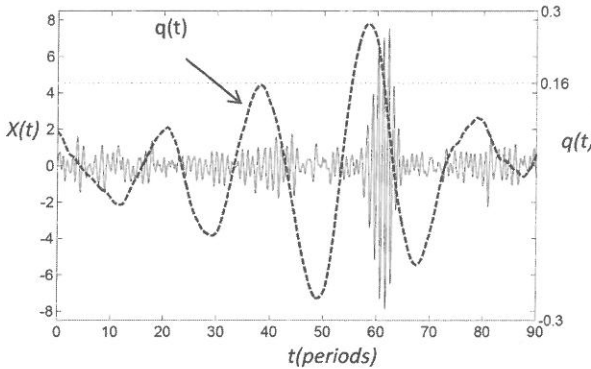


Figure 1: Response sample with “outbreak” (solid line) of a SDOF system with apparent linear viscous damping $(0.16 - q(t))$; sample of random process $q(t)$ is shown by dash-dot line.

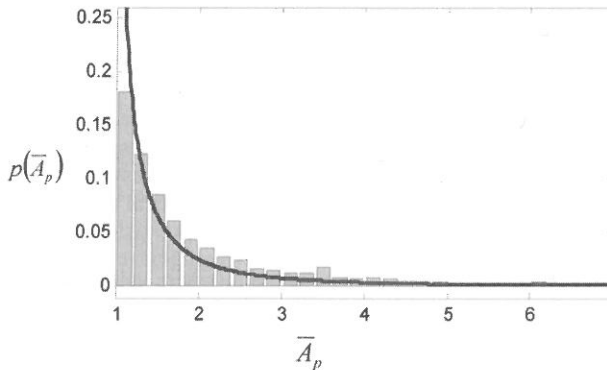


Figure 2: Theoretical PDF of scaled amplitude $\bar{A}_p = A_p/A_0$ and corresponding histogram as obtained from sample of $X(t)$

The described analytical solutions can be extended to certain TDOF systems with certain “symmetry” which permit to “wrap up” two equations of motion into a single complex equation (Dimentberg 1988, Dimentberg et al. 2008). Specifically, translational and tilting oscillations of the Jeffcott rotor had been considered in (Dimentberg 1988) and (Dimentberg et al. 2008) respectively. Thus, for the latter case equations of motion for rotating (tilting) angles ϕ_x, ϕ_y may be written as

$$\begin{aligned} \ddot{\phi}_x + 2\kappa\dot{\phi}_x + \Omega^2\phi_x + \rho\nu\dot{\phi}_y + 2\beta\nu\phi_y &= 0 \\ \ddot{\phi}_y + 2\kappa\dot{\phi}_y + \Omega^2\phi_y - \rho\nu\dot{\phi}_x - 2\beta\nu\phi_x &= 0 \end{aligned} \quad (7)$$

Here ν is rotation speed whereas $\Omega = \sqrt{K/J}$ and $\rho = J_p/J$ where J and J_p are mass moments of inertia of the rotor about anyone of transverse axes and about rotation axis respectively (K is shaft’s stiffness).

Furthermore, $\kappa = \alpha + \beta$ where $\alpha = c_n/2J, \beta = c_i/2J$ and c_n, c_r are respectively coefficients of external, or “nonrotating” and internal or “rotating” linear viscous damping; the latter may account for fluid flow in seals and/or journal bearings and thus may be subject to random temporal variations. It should be noted that except for the “gyroscopic” term, i.e. one with polar moment of inertia, the Equations (7) possess complete similarity with the equations of translational lateral displacements x, y . Namely the latter may be written in the form (7) with $\rho = 0$ and ϕ_x, ϕ_y replaced by x, y respectively, whereas the disk’s mass m should be substituted for its moment of inertia J (and it goes without saying that relevant damping coefficients c for translational rather than tilting motions should be used).

Introducing complex rotation angle $\phi = \phi_x + i\phi_y$, where $i = \sqrt{-1}$ one can replace two ODEs (7) by an equivalent single equation

$$\ddot{\phi} + 2\kappa\dot{\phi} + \Omega^2\phi - i\rho\nu\dot{\phi} - 2i\beta\nu\phi = 0 \quad \text{where it is assumed that } \beta(t) = \langle\beta\rangle + q(t) \quad (8)$$

Applying the KB-averaging to the Equation (8) yields approximate first-order ODE for $\Phi = \sqrt{|\phi^2|} = \phi_x^2 + \phi_y^2$ - amplitude of dominant forward-whirl component of the response. Solution to this ODE is

$$\Phi(\tau) = \Phi_0 \exp(\mu f(\tau)) \quad \text{where } \mu = \nu(1 - \rho/2) / \sqrt{\Omega^2 + (\rho\nu/2)^2} - 1 \quad (9)$$

with the same $f(\tau)$ as in Equation (3). (The solution (9) is valid only provided that $\mu > 0$ otherwise upcrossing the instability threshold by $\beta(t)$ wouldn’t be possible at all). In the limiting case of diminishing gyroscopic effect $\rho \rightarrow 0$ we have $\mu = \nu/\Omega - 1$, and the Equation (7) is reduced to similar solution for the rms radius of whirl in translational vibrations $R = \sqrt{x^2 + y^2}$. The solution (9) may be used to obtain the PDFs of peaks of $\Phi(t)$ or $R(t)$ in terms of that of peaks of $g(t)$; first-passage problems for response may also be reduced to those for $g(t)$.

In the general case of marginally unstable TDOF system, the equations of transient motion during short-term instability cannot be reduced to a single state variable. Thus two coupled response amplitudes remain after KB-averaging for the case of lightly damped system thereby requiring numerical integration for the two ODEs of slow motion from starting point of the response outbreak till the instant when both response variables pass their peaks. Then, as long as relation is established (numerically) between peak value(s) of response(s) and that of scaled zero-mean part $g(t)$ of the bifurcation parameter the basic procedure can be applied for

predicting response PDF. Several examples of such analysis as presented in (Dimentberg et al. 2008) are:

- Rotating shaft with anisotropy in support stiffness in translational vibrations;
- Two-dimensional galloping of a rigid body in a fluid flow (case of full 2×2 damping matrix);
- TDOF flutter of a tube row in heat exchanger subject to cross-flow of fluid.

3 NONLINEAR SDOF SYSTEMS

3.1 *System with odd nonlinear restoring force*: same procedure as for the linear case is applied with the only adjustment being quasiconservative version of the KB-averaging.

$$\ddot{X} + 2(\alpha - q(t))\dot{X} + \partial U / \partial X = 0 \quad (10)$$

The potential energy function is assumed to be even with only two roots of the equation $U(X) = H$ for any given H . The PA is applied then and a first-order ODE is obtained for the function

$$S(A) = 4 \int_0^A [2U(A) - 2U(X)]^{1/2} dX$$

where $U(A) = H$ and $S(A) = \pi \Omega A^2$ if $U(X) = \frac{1}{2} \Omega^2 X^2$.

This ODE is integrated starting from the instant of upcrossing t_u until instant t_f of peak of $X(t)$ for a given outbreak resulting in the explicit analytical solution for the response $S(\tau)$ during outbreak. Thus, complete extension of the previous results for peak response amplitude – the Equations (3) and (4) – is obtained through calculation of the single-valued function $S(A)$; formulae for $S(\tau)$ and S_p certainly match formulae (3) and (4) respectively for the limiting linear case $U(X) = \frac{1}{2} \Omega^2 X^2$.

3.2 *Cubic nonlinearity in the damping term*.

Equation of motion is now

$$\ddot{X} + 2[\alpha + \beta \dot{X}^2 - q(t)]\dot{X} + \Omega^2 X = 0 \quad (11)$$

For cases with $\alpha < 0$ and $\beta > 0$ this system without noise (i.e. with $q(t) > 0$) has a limit cycle, while for both α and β positive such a limit cycle does not exist. Using standard KB-averaging a first-order ODE for the amplitude A can be derived

$$\dot{A} = -\alpha A - \frac{3\beta}{4} A^3 + q(t)A \quad (12)$$

For the special case $q(t) = \text{const.}$, the equation can be solved by separation of variables. This can be exploited by approximating $q(t)$ by a sequence of constant values q_k within a (small) time interval. Separation yields

$$dt = \frac{dA}{(-\alpha + q_k)A - \frac{3\beta}{4} A^3} = \frac{dA}{xA + yA^3} \quad \text{and} \quad t - t_0 = \log \left(\frac{A^2}{yA^2 + x} \frac{yA_0^2 + x}{A_0^2} \right)$$

Here t_0 is the value of time at the beginning of the time interval, and $A_0 = A(t_0)$. Based on this representation, a numerical solution for the peak amplitude during an outbreak can be computed. The following numerical results are based on the parameter values $\alpha = 0.16$, $\Omega = 2$, $\lambda = 0.1$, $u = \alpha$ and an initial amplitude $A_0 = 0.0001$. The parameters ζ and β are varied. Figure 3 shows the amplitude $A(t)$ as a function of time on a logarithmic scale for a fixed value of $\zeta = 0.1$ and different values of β .

For comparison with the linear system, the functional relationship between ζ and A_p is given in terms of ζ vs. $\log A_p$ which is a linear function for the case of linear damping. This relation is shown in Figure 4 for selected values of β . Note that for the case of $\beta = 0$ there is a perfectly linear relation.

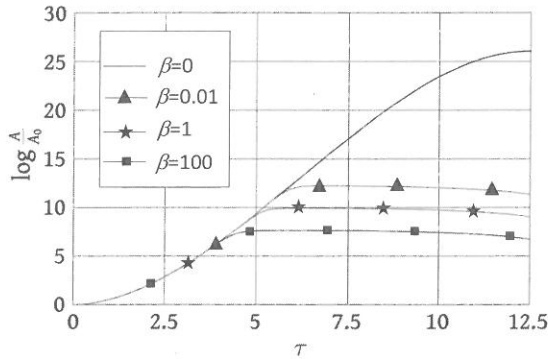


Figure 3: Logarithm of amplitude vs. non-dimensional time ($\zeta = 0.1$)

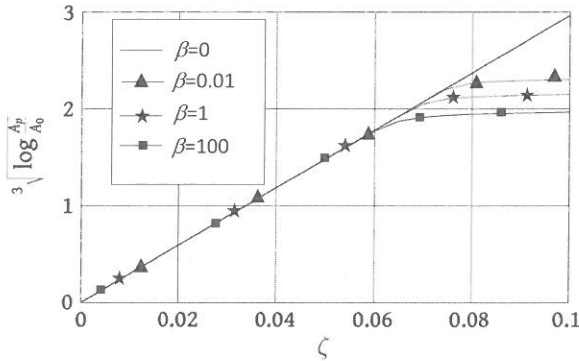


Figure 4: Maximum amplitude during outbreak depending on ζ and β

4 CONCLUSIONS

Temporal random variations of parameters in dynamic systems with potential dynamic instability may "smear" classical neutral stability boundary. The system's response within such

a “twilight zone” of marginal instability is found to be of an intermittent nature, with alternating periods of zero (or almost zero) response and rare short outbreaks. As long as it may be impractical to preclude completely such outbreaks for a designed system its response should be analyzed to evaluate reliability; in particular, prediction of response PDF and solution to first-passage problem may be of importance.

Results of such analyses are presented for the case of slow parameter variations using PA for the variations together with averaging over the response period. Subsequent analytical or numerical solution to deterministic problem for transient response amplitude or its certain special nonlinear function yields its PDF which may be important for predicting low-cycle fatigue life; the first-passage problem for the response is also reduced to that for the bifurcation parameter. The analysis is also used to derive on-line identification procedure for the system from its observed response with set of rare outbreaks. Potential examples of applications include 1D and 2D short- galloping of elastically suspended rigid bodies in cross-flow of fluid with random temporal variations of flow speed, bundles of heat exchanger tubes in cross-flow with potential for flutter-type instability, and rotating shafts.

5 REFERENCES

- Bogoliubov, N.N., Mitropol'skii Yu.A., 1961. *Asymptotic Methods in the Theory of Nonlinear Oscillations*, New York, Gordon&Breach.
- Den Hartog, J.P., 1985. *Mechanical Vibrations*, New York, Dover.
- Dimentberg M.F., 1988. *Statistical Dynamics of Nonlinear and Time-Varying Systems*, Taunton, UK Research Studies Press.
- Dimentberg, M., 2005. Vibration of a Rotating Shaft with Randomly Varying Internal Damping. *Journal of Sound and Vibration*, 285, pp. 759 – 765.
- Dimentberg, M. & Naess, A., 2006. Short-term dynamic instability of a system with randomly varying damping. *Journal of Vibration and Control*, 12, # 5, pp. 527 – 536.
- Dimentberg, M., Hera, A. & Naess, A., 2008. Marginal Instability and Intermittency in Stochastic Systems. Part I – Systems with Slow Random Variations of Parameters. *Journal of Applied Mechanics*, 75, # 4, pp. 041002-1 – 041002-8.
- Leadbetter M.R, Lindgren G. & Rootzén H., 1983. *Extremes and Related Properties of Random Sequences and Processes*, New York, Springer-Verlag.
- Lin, Y.K. & Cai, G.Q., 1995. *Probabilistic Structural Dynamics*, New York, McGraw Hill.
- Stratonovich, R.L., 1967. *Topics in the Theory of Random Noise*, vol. II, New York, Gordon&Breach.

Tolling contracts

H. Kechejian

Freepoint Commodities, Greenwich, CT, USA

V. K. Ohanyan

American University of Armenia, Yerevan

ABSTRACT: The power plant tolling contract is one of most complicated derivative instruments among energy derivatives. The buyer of the contract has the right (but not the obligation) to run the plant to receive the generated power during the contractual period by providing the fuel necessary to run the plant. The simplest way to view a tolling agreement is by representing it as a spread option between power and fuel. Let $X_t = (P_t, G_t)$ be \mathbf{R}^k -valued driving process (\mathbf{R} is the real axis), G_t is the fuel process and the P_t is $(k - 1)$ -dimensional power process. For a driving process X_t we take a k -dimensional jump-diffusion $\{X_t\}$ whose dynamic are given by a standard stochastic differential equation. Each power block peak, off-peak, weekend peak, etc., is represented by a separate driving process. We propose an approach based on stochastic impulse control framework. Our approach is to reduce the tolling contract problem to simpler problems for which we have the existence and regularity results. Some particular cases are considered in which solutions have explicit forms.

1 INTRODUCTION

A power plant tolling contract is one of most complicated derivative instruments among energy derivatives. Tolling agreements are written on fossil fuel fired power plants. A fossil-fuel plant converts a generating fuel into electricity at certain conversion rate known as heat rate.

In brief, heat rate measures the units of the fuel needed for producing one unit of electricity. The lower is the heat rate, the more efficient is the power plant. The buyer of the contract has the right to run the plant to receive the generated power during the contractual period by providing the fuel necessary to run the plant. The simplest way to view a tolling agreement is by representing it as a spread option between power and fuel. The spread between the electricity price and the heat rate adjusted fuel cost is called spark spread.

Let $X_t = (P_t, G_t)$ is \mathbf{R}^k -valued driving process (\mathbf{R} is the real axis), G_t is the fuel process and the P_t is $(k - 1)$ -dimensional power process. Each power block peak, off-peak, weekend peak, etc. is represented by a separate driving process. We assume duration of the contract is T years, where the time interval $[0, T]$ is divided into finite number of subintervals. Let us assume that for each block at moment t we have M states: $0, 1, 2, \dots, M-1$: the zeros = off, the first = C_{min} - a power plant run at minimal capacity; ...the last $C_{M-1} = C_{max}$ - a power plant run at maximal capacity. We can introduce also a control process $\gamma = \gamma(t)$ which describes the plant scheduling as a function of time. We should think of γ as an F_t^X - adapted piecewise-constant process. Let $\Gamma(t)$ is the set of all allowed scheduling policies on the interval $[t, T]$. The operational flexibility problem we investigate is reduced to finding the value function given by

$$\sup_{\gamma \in \Gamma(t)} \mathbf{E} H(x, i, [t, T]; \gamma) | X_t = x, \gamma(t) = i,$$

where \mathbf{E} stands for conditional expectation of H given $X_t = x, \gamma(t) = i$, while H is the total reward up to fixed final time T for such control γ . For a driving process X_t we take a k -dimensional jump-diffusion process whose dynamic are given by a stochastic differential equation. We make the standard assumptions that (Ω, F, P) is a fixed probability space on which is defined a Wiener process $W = (W_t)_{0 \leq t \leq T}$, $W_0 = 0$ almost surely, whose natural filtration is

$$F_0^t = \sigma\{W_s, s \leq t\}_{0 \leq t \leq T}.$$

Let $F = (F_t)_{0 \leq t \leq T}$ be the completed filtration of $(F_0^t)_{0 \leq t \leq T}$ with the P-null sets of F .

We consider the following Stochastic Differential Equation (SDE):

$$dX_t = \mu(t, X_t) dt + \sigma(t, X_t) dW_t + J(t, X_t) [dN_t - \lambda(t, X_t) dt], \quad (1.1)$$

where $(N_t)_{0 \leq t \leq T}$ is a Poisson process with intensity $\lambda(t, X_t)$, see [1]. Note that instead of a Poisson process N_t we can consider in (1.1) any semi-martingale. A jump-diffusion process is composed of a diffusion component and a jump component. The diffusion part usually takes the standard form $\mu(t, X_t) dt + \sigma(t, X_t) dW_t$, while the jump part is expressed by Poisson process. Although many other processes can be used to represent discontinuous jumps, the Poisson process is chosen more frequently.

As with deterministic ordinary and partial differential equations, it is important to know whether a given SDE has a solution, and whether or not it is unique. The following is a typical existence and uniqueness theorem for Ito- SDEs. Let x be a random variable with finite second moment, and let μ and σ be measurable functions that satisfy the Lipschitz condition.

Moreover, x_0 is independent of the σ -algebra generated by $W_s, s \geq 0$. Then initial value problem, i.e. SDE with initial condition $X_t = x_0$ has a P-almost surely unique t-continuous solution $X_t(\omega)$ such that X_t is adapted to the filtration F_t^X generated by X_0 and $W_s, s \leq t$, see [2].

2 THE BASIC MODEL

We have the following three price blocks:

- I) From 24:00 till 8:00 ;
- II) From 8:00 till 24:00 (Monday- Friday);
- III) From 0:00 till 24:00 (Saturday and Sunday).

Let $X_t = (P_t, G_t) = (P_t(I), P_t(II), P_t(III), G_t)$ be a stochastic \mathbf{R}^4 -valued driving process. Therefore, if we lease a power station for the period of 5 years, $t=1, 2, \dots, T (= 2 \times 5 \times 365) = 3,650$ (so-called a finite horizon), where each day is divided into two blocks. Let us assume that for each block at moment t we have $M \geq 3$ states: $0, 1, 2, \dots, M-1$. In General, if the capacity of the power station varies between C_{\min} and C_{\max} , we divide this interval on the $M-2$ equal subintervals of length $(C_{\max} - C_{\min}) / (M - 2)$ and obtain the following M states:

The zeros = off,

The first = C_{\min} - a power plant run at minimal capacity;

The second = $C_{\min} + \frac{C_{\max} - C_{\min}}{M-2}$

...

The m -th = $C_m = C_{\min} + (m-1) \times \frac{C_{\max} - C_{\min}}{M-2}$, where $m = 1, 2, \dots, M-1$.

The last $C_{M-1} = C_{\max}$ - a power plant run at maximal capacity.

We consider the payoff rate $\Psi(P_t(l), G_t, i)$ in state i for block l . We have $\Psi(P_t(l), G_t, 0) = 0$ and

$$\Psi(P_t(l), G_t, i) = C_i \times [P_t(l) - v_i \times G_t - K_i] = \left[C_{\min} + (m-1) \times \frac{C_{\max} - C_{\min}}{M-2} \right] \times [P_t(l) - v_i \times G_t - K_i],$$

where K_i is the operating expenses for state i , v_i is the heat rate for the state $i=1, \dots, M-1$, $P_t(l)$ is the price of electricity in block l , and C_i is the capacity of the power plant for state i , the possible values of C_i is

$$0, C_1 = C_{\min}, C_2 = C_{\min} + \frac{C_{\max} - C_{\min}}{M-2} \dots C_{\max}.$$

It is obvious that the heat rate is monotone increasing as a function depending on capacity, that is $0 = v_0 < v_1 < \dots < v_{M-1}$.

The expression $P_t(l) - v_i \times G_t - K_i$ is the profit of 1 Meg./hour for state i and block l . The operating state m can affect the dynamics of X_t through price impact. We make the simplifying assumption that this effect can be described as changing some parameters of the equation (1.1). Changing an output level is costly, requiring extra fuel and various overhead costs. We have to consider the switching costs from state i to state j :

$$a_{ij}(t, X_t), \quad a_{ii} \equiv 0$$

with potential dependence on time and current state, we have the following switching costs:

$$a_{ij}, \quad i, j = 0, 1, 2, \dots, M-1.$$

Cost of startup is

$$a_{01} = a_{02} = a_{0, M-1} = ST,$$

and all remaining a_{ij} are nonnegative. Moreover, it is obvious that a_{ij} satisfies the triangle inequality $a_{ij} \leq a_{ik} + a_{kj}$ for any i, j and k states.

We can introduce also a control process $\gamma = \gamma(t)$ which describes the plant scheduling as a function of time. The control $\gamma(t)$ is dynamically chosen and adapted to the information filtration

$$F_t^X = \text{the minimal } \sigma\text{-sigma algebra containing } \{X_s : 0 \leq s \leq t\}.$$

Because the management decisions are obviously discrete, we can represent the control function as

$$\gamma = ((\xi_1, \tau_1), (\xi_2, \tau_2), \dots, (\xi_T, \tau_T)),$$

where ξ_k taking on the values from the M-element set $\{Off, C_{\min}, \dots, C_{\max}\}$ of all possible states, and

$$0 \leq \tau_1 \leq \tau_2 \leq \dots \leq \tau_{k-1} \leq \tau_k \leq \dots \leq T$$

are the $(F_t^X$ -stopping) switching times (i.e. the time moments at which we change the state). We should think of γ as an F_t^X -adapted piecewise-constant process, where

$$\gamma(t) = \sum_{\eta_k < T} \xi_k I_{[\tau_k, \tau_{k+1})}(t).$$

denotes the operating state at t .

The total reward up to fixed final time T for such control γ and scenario $\omega \in \Omega$ (the outcome) is then

$$H(x, i, [0, T]; \gamma)(\omega) = \int_0^T \Psi(X_s, \gamma(s)) ds - \sum_{\tau_k < T} a_{\gamma(\tau_k - 0), \gamma(\tau_k)}.$$

where $X_0 = x$ and $\gamma(0) = i$.

The first term in the right hand side describes the cumulative profit corresponding to γ and the second term counts the associated switching costs at each switching time τ_k . Note that

$$\Psi(X_s, \gamma(s)) = \Psi(P_s(l), G_s, i),$$

if $\gamma(s) = i$ and s belongs to the l price block.

Let $\Gamma(t)$ is the set of all allowed scheduling policies on the interval $[t, T]$. The operational flexibility problem we investigate may now be stated as finding the value function

$$J(t, x, i) = \sup_{\gamma \in \Gamma(t)} J(t, x, i; \gamma),$$

where

$$J(t, x, i; \gamma) = \mathbf{E} H(x, i, [t, T]; \gamma) | X_t = x, \gamma(t) = i].$$

Here \mathbf{E} stands for expectation (in this formula, conditional expectation of H given $X_t = x, \gamma(t) = i$) with respect to a risk-neutral measure P . Maybe we can consider a discrete process, if we assume that the derived process in the corresponding intervals $[\tau_k, \tau_{k+1})$ are constant, i.e. the set of changing the gas price G_t is a subset of stopping moments (or the moments of changing the states).

A basic price to the operational flexibility associated with the plant by definition is

$$J(t, x, i) - \max_{m=1,2,3} J(t, x, i) \mathbf{E} \left[\int_t^T \Psi_m(X_s, \gamma(s)) ds / X_t = x \right],$$

which is the difference between expected profit with the flexibility built-in and expected profit in the best, but fixed, operating state m .

3 PARTICULAR CASES

I) A Geometric Brownian Motion or Generalized Wiener Process is a continuous-time stochastic process in which the logarithm of the randomly varying quantity follows a Brownian motion.

This example we obtain from (1.1) if we assume that $J(t, X_t) = 0$, $\mu(t, X_t) = \mu \cdot X_t$, and $\sigma(t, X_t) = \sigma \cdot X_t$, for certain constants $\mu > 0$ and σ called respectively the drift and volatility of the stock. In other words,

$$\begin{cases} \frac{dX_t}{X_t} = \mu \cdot dt + \sigma \cdot dW_t, \\ X_0 = x_0, \end{cases}$$

where X_0 is the starting price. Using Ito's formula, we obtain

$$X_t(\omega) = x_0 \exp\{\sigma W_t + (\mu - \sigma^2 / 2) \cdot t\}$$

i.e. X_t has a log-normal distribution.

The first time the authors of [5] have considered this particular case of SDE using stochastic control for tolling agreements.

II) The second particular case is the mean-reverting model which we obtain if we assume that there is not the Poisson component of the SDE equation, and $\mu(X_t) = \alpha \cdot (\mu - \ln X_t) X_t$, $\sigma(X_t) = \sigma \cdot X_t$, where α is the mean reverting intensity.

Defining $S_t = \ln X_t$ and applying Ito's lemma, the natural logarithm of the X_t can be characterized by an Ornstein-Uhlenbeck stochastic process:

$$dS_t = \alpha(m - S_t)dt + \sigma dW_t,$$

where $m = \mu - \sigma^2 / (2\alpha)$.

Integrating the previous equation and using fundamental results from stochastic calculus, we get that the conditional distribution of S_t is normal. For this type of SDE see, for example, [6].

III) Jump-diffusion processes are capable of modeling sudden discontinuous in the price evolution, but once the jumps occur and the prices move to a new level, the price tends to stay in that level until a new jump arrives. The corresponding model is called mean-reversion jump diffusion model (see [7]). We substitute in (1.1) $\mu(X_t) = \alpha \cdot (\mu - \kappa - \ln X_t) X_t$, $\sigma(X_t) = \sigma \cdot X_t$, $J(t, X_t) = 1$, κ is the market price of risk and $J(t, X_t) = \lambda$ is a constant. Defining $S_t = \ln X_t$ and applying Ito's lemma, the natural logarithm of the X_t can be characterized by the following SDE:

$$dS_t = \alpha(m - \kappa - S_t)dt + \sigma dW_t + \beta_t dN_t,$$

where $m = \mu - \sigma^2 / (2\alpha)$, while $\beta_t = \ln(1 + k_t)$, and $k_t = k(t, \omega)$ is the jump amplitude. The jump amplitude is the double stochastic parameter. In this model we have 6 parameters if we consider risk-neutral model. The inclusion of jumps into models leads to the loss of the simple analytical solutions.

IV) Much of the existing finance literature is based on jump-diffusion models, and exploits the connections between such models and partial differential equations (see for example [3]). For $M = 2$ there exists an explicit regular solution of the switching problem (see [3] and [4]).

4 REFERENCES

1. Carmona, R., and Ludkovski, M., "Pricing asset scheduling flexibility using optimal switching", *Econometrica*, vol. 15(6), pp. 405--447, 2008.
2. Oksendal, B., *Stochastic Differential Equations: An introduction with applications*, 5th Edition, Berlin, Springer, 2003.
3. Arnarson, T., Djehiche, B., Poghosyan, M., and Shahgholian, H., "A PDE approach to regularity of solutions to finite horizon optimal switching problems", *J. Nonlinear Analysis*, Elsevier, vol. 71, pp. 6054-6067, 2009.
4. Deng Shi-Jie, and Xia Zh., "Pricing and Hedging electricity supply contracts: a case with tolling agreements", Atlanta, Georgia, 2005.
5. Brennan, M., and Schwartz, E., "Evaluating natural resource investments", *J. Business*, vol. 58, pp. 135-157, 1985.
6. Lucia, J., and Schwartz, E., "Electricity prices and power derivatives: Evidence from the Nordic power exchange", vol. 5, (1), pp. 5-50, 2002.
7. Clewlow L., Strickland C. and Kaminski V., "Extending mean-reversion jump diffusion energy power risk management", Risk Waters Group, February 2001.

An alternative linear response surface method for stochastic dynamic analysis

U. Alibrandi

University of Messina, Messina, Italy

ABSTRACT: An alternative Linear Response Surface strategy is presented for the evaluation of the response statistics of dynamic systems subjected to stochastic excitation. At first the geometry of very high-dimensional reliability spaces is discussed, where it is shown that the sample points fall far away from the origin of the standard normal space, in a very narrow region of probabilistic interest. It is also seen because FORM may work well for applications of Stochastic Dynamic Analysis in high-dimensional spaces. However, it does not give any information about the obtained level of accuracy and moreover in some cases its approximation is not very close to the exact one. To this aim, in this paper we introduce a novel Linear Response Surface based on the Support Vector Method, which allows to overcome the shortcomings of FORM, starting from the knowledge of the design point direction.

1 INTRODUCTION

The aim of the stochastic dynamic analysis is the evaluation of the response of dynamic systems subjected to stochastic input. If the stochastic excitation follows a Gaussian distribution and the dynamic system is non linear, the response is Non-Gaussian and it is very difficult to be evaluated.

In the past decades, a lot of methods have been proposed to this aim, usually they are however hardly applicable to general nonlinear systems, and so they are difficult to apply in practice. These drawbacks are not shared by the Equivalent Linearization Method, but unfortunately it gives accurate results for weakly non-linear systems only (Roberts & Spanos 1991, Lutes & Sarkani 2004); moreover, it generally cannot approximate adequately the distribution probability of the response, especially in the tail region. Therefore some response statistics as crossing rates and first passage probability will be inaccurate at high thresholds.

The most robust procedure is given by the Monte Carlo Simulation (MCS), which is however strongly demanding in its crude form. For this reason, recently some smart simulation techniques have been proposed, among the other we recall the subset simulation (Au & Beck 2001), line sampling (Pradlwarter et al. 2007), asymptotic sampling (Bucher 2009).

Promising results are given from the application to the nonlinear stochastic dynamic analysis of the analytical methods of structural reliability, particularly the First-Order Reliability Method (FORM) (Der Kiureghian & Li 1996, Der Kiureghian 2000). At first, the stochastic input is discretized into a large number of standard normal random variables. The tail probability is defined as the probability that the response of the dynamic system is greater than a chosen threshold x at fixed time instant t . In this way, for given x and t the dynamic problem may be solved by using the tools of the structural reliability theory. In particular, it is seen that the design point corresponds to the realization of the stochastic input that gives rise to the tail exceedance event, and therefore it defines a critical excitation for the system. Moreover it allows the application of the recently developed Tail Equivalent Linearization Method (Fujimura & Der Kiureghian 2007, Der Kiureghian & Fujimura 2009, Garrè & Der Kiureghian 2010). Finally, it gives the FORM solution, which has been shown to give good approximations of the tail probability in many cases of practical interest (Koo & Der Kiureghian 2005, Alibrandi & Der Kiureghian 2010, 2012, Alibrandi submitted).

In this paper at first it is seen because FORM may work well in very high-dimensional reliability problems, as the one here analyzed. This task is accomplished through a close insight to

the geometry of the very high-dimensional spaces. Indeed, it is seen that the samples drawn from a multivariate normal standard distribution fall over a n -dimensional sphere, and therefore the knowledge of its geometry is a very important topic. In particular, it is seen that the samples fall far away from the origin of the standard normal space, more exactly in a very narrow region $\Xi \equiv \Xi_1 \cup \Xi_2$ given as the intersection between: (i) a very thin shell Ξ_1 whose average radius is proportional to the square root of the number of variables, and (ii) an equatorial slab Ξ_2 (containing the origin of the space) whose orientation and width depend on the particular Limit State Surface (LSS). The first region Ξ_1 allows to state that a Linear Response Surface can give very good approximations of the target LSS, while the second region Ξ_2 allows to state that this hyperplane is close to the origin of the space; note that both the properties are owned by FORM.

However, FORM has some known computational complexities and shortcomings: (i) the evaluation of the design point in high-dimensional spaces may require a great computational effort, (ii) FORM in some cases is not able to obtain a very good approximation of the target LSS, (iii) FORM does not give any information about the level of accuracy obtained. The first drawback can be solved by using a DDM-enabled software, like OpenSees (McKenna et al. 2003), or adopting a recently proposed Response Surface strategy (Alibrandi & Der Kiureghian 2010, 2012, Alibrandi submitted), and based on the Model Correction Factor Method (Ditlevsen & Arnbjerg-Nielsen 1994, Ditlevsen & Madsen 1999).

To overcome the remaining shortcomings of FORM in this paper we present an alternative Linear Response Surface method, based on the Support Vector Method (SVM), and that fully takes account of the geometry of the high-dimensional spaces.

The paper is organized as follows: in section 2 the geometry of n -dimensional spheres is presented, together with discussions about the FORM solution in this kind of spaces, in section 3 and 4 we present the nonlinear stochastic dynamic problem by using the FORM solution and its improvement through the proposed approach, respectively, and finally in section 5 the method is applied to a simple hysteretic system.

2 FORM IN HIGH-DIMENSIONAL SPACES

In structural reliability analysis the space of the basic variables \mathbf{x} may be subdivided into two distinct domains, the safe set Ω_s and the failure set Ω_f , which are separated by the Limit State Surface (LSS).

Let $g(\mathbf{x})$ the Limit State Function (LSF) so that the safe set and the failure set are defined as $\Omega_{s,x} = \{\mathbf{x}: g(\mathbf{x}) > 0\}$ and $\Omega_{f,x} = \{\mathbf{x}: g(\mathbf{x}) \leq 0\}$, respectively. Under these hypotheses and after the probabilistic transformation toward the standard normal space \mathbf{u} , the failure probability with respect to the chosen limit state is

$$P_f = \int_{g(\mathbf{u}) \leq 0} f_U(\mathbf{u}) d\mathbf{u} \quad (1)$$

where $\Omega_f = \{\mathbf{u}: g(\mathbf{u}) \leq 0\}$ is the failure set in the standard space and $f_U(\mathbf{u})$ is the multivariate normal standard probability density function. The evaluation of the failure probability P_f according to (1) requires the computation of a usually complicated multidimensional integral, whose value depends upon the failure set. Consequently, a satisfactory approximation of (1) necessarily implies a good modeling of the LSS $g(\mathbf{u}) = 0$.

Recall that the design point \mathbf{u}^* is the point belonging to the limit state closest to the origin of the standard normal space while its distance from the origin is the reliability index $\beta = \pm \mathbf{u}^* \pm$

It is well known that in low-dimensional spaces, most of samples generated by $f_U(\mathbf{u})$ fall around the design point. This property is not held in high-dimensional spaces, however in both low- and high-dimensional spaces the design point usually gives an *important direction* for the evaluation of P_f , except for particular systems, whose behavior is chaotic.

By using the FORM solution, a linearization of the LSS around the design point is done, and the first-order approximation of the failure probability is $P_{f, FORM} = \Phi(-\beta)$, where $\Phi(\bullet)$ is the cumulative distribution function of the standard normal random variable.

In high-dimensional spaces the samples fall far away from the design point, however FORM usually works well, as we show below. In the following, we will describe the geometry of the n -dimensional sphere, since the samples drawn from $f_U(\mathbf{u})$ belong to it.

2.1 The high-dimensional sphere

Let us consider an n -dimensional ball $B_n(R)$ of radius R and centered at the origin of the space, whose equation is $\sum_i u_i^2 \leq R^2$. It is the generalization of the 3-dimensional sphere to higher dimensions, so that for $n = 2$ and $n = 3$ we have the circle and the sphere, respectively. The surface of the ball, known in mathematical literature as hypersphere $S_n(R)$ and of equation $\sum_i u_i^2 = R^2$, has dimension $n-1$; for clarity's sake, for $n = 2$ and $n = 3$ we have the circumference and the circle, respectively.

The geometry of n -dimensional spheres has some very counterintuitive issues; in the following we will underline the most significant ones, with respect to the implications that they have in the context of the high dimensional reliability analysis.

Property 1: *An n -dimensional sphere has non-zero volume if $R > \text{constant} \times \sqrt{n}$*

The volume of the n -dimensional ball $B_n(R)$ and sphere $S_n(R)$ are identical, since the volume measures the total "content" of the object, including all the internal space. The volume of the 1-, 2- and 3-dimensional sphere is $\text{Vol}[S_1(R)] = 2\pi R$, $\text{Vol}[S_2(R)] = \pi R^2$ and $\text{Vol}[S_3(R)] = (4/3)\pi R^3$; a generalization of these relationships to higher dimensions gives $\text{Vol}[S_n(R)] = K_n R^n$, where K_n is a constant depending on the dimensionality n , defined as

$$K_n = \text{Vol}[S_n(1)] = \frac{\pi^{\frac{n}{2}}}{\Gamma\left(\frac{n}{2} + 1\right)} \cong \left(\sqrt{\frac{2\pi e}{n}}\right)^n \quad (2)$$

being $\Gamma(\bullet)$ the Gamma function and where the last relationship holds for $n \rightarrow \infty$. As particular cases, for $n = 2$ and $n = 3$ we obtain $K_2 = \pi$ and $K_3 = (4/3)\pi$, as expected. Noting from (2) that $K_n = \text{Vol}[S_n(1)]$ and that $K_n \rightarrow 0$ as n tends to infinity it can be stated that the unit hypersphere has zero volume in high dimensions. Moreover, from (2) it is easy to find that the radius of the hypersphere of unit volume is $R_{(\text{Vol}=1)} \cong 0.242 \sqrt{n}$. It is also possible to show that for n great, the hypersphere has non-zero volume only if $R > R_{(\text{Vol}=1)}$, which is proportional to the square root of n , according to the constant $1/\sqrt{2\pi e}$.

Property 2: *Vast majority of the volume lies near the equator*

The "Pole North" is an arbitrarily chosen vector on the hypersphere, while the "equator" is the intersection of the hypersphere with the hyperplane perpendicular to the Pole North. It is seen that the volume of the n -dimensional sphere accumulates near the equator. Chosen a vector as a Pole North, assume that the equatorial plan has equation $x_n = 0$. Consider the equatorial slab bounded by the hyperplanes $x_n = -\beta_0$ and $x_n = \beta_0$, so that it is defined as $\text{Slab}(x_n, \beta_0) \equiv \{x \in R^n : -\beta_0 \leq x_n \leq \beta_0\}$. It is possible to show that for $n \rightarrow \infty$ the fraction of volume of $S_n(R)$ contained in $\text{Slab}(x_n, \beta_0)$ is equal to

$$\frac{\text{Vol}[\text{Slab}(x_n, \beta_0)]}{\text{Vol}[S_n(R)]} = \frac{1}{\sqrt{2\pi}} \int_{-\beta_0}^{\beta_0} e^{-\frac{t^2}{2}} dt \quad (3)$$

Note that while the radius of the sphere grows as \sqrt{n} , the width of the slab is constant. Therefore, in high dimensions all the volume is concentrated around an equatorial slab which represents a little region with respect to the sphere. It here also underlined that we have chosen arbitrarily the Pole North, identified by the axis x_n .

Property 3: *Vast majority of the volume lies around a very thin shell near the boundary*

Let us now consider the volume $\text{Vol}[S_n(R, \epsilon)]$ of a thin shell of width ϵ along the surface of an hypersphere of radius R . It is given as the difference between the volumes of the n -dimensional spheres of radius R and $R - \epsilon$, that is $\text{Vol}[S_n(R, \epsilon)] = \text{Vol}[S_n(R)] - \text{Vol}[S_n(R - \epsilon)]$. To show the phenomenon of the volume concentration near the boundary, consider the ratio

$$\lambda_n = \frac{Vol[S_n(R-\varepsilon)]}{Vol[S_n(R)]} = \frac{K_n(R-\varepsilon)^n}{K_n R^n} = \left(1 - \frac{\varepsilon}{R}\right)^n \quad (4)$$

for every $0 < \varepsilon < R$, this ratio tends to zero as $n \rightarrow \infty$, which means that the center is essentially void, and that every spherical shell, no matter how thin, will contain essentially the whole volume $Vol[S_n(R)]$.

Consider now the ratio of the volume of the thin shell $Vol[S_n(R, \varepsilon)]$ to the whole volume of the outer sphere $Vol[S_n(R)]$, which gives $\gamma_n = Vol[S_n(R, \varepsilon)]/Vol[S_n(R)] = 1 - \lambda_n$. Clearly, $\gamma_n \rightarrow 1$ when $n \rightarrow \infty$, which means that for high-dimensional spheres almost all the volume lies around a thin shell near the boundary.

Summarizing we have seen that: (i) in high dimensions the sphere of non-zero volume has a radius R proportional to \sqrt{n} ; (ii) chosen arbitrarily a Pole North, almost all the volume concentrates around an equatorial slab $\Xi_2 \equiv Slab(x_n, \beta_0)$, whose width does not depend upon n ; (iii) the n -dimensional sphere at the center is void, and almost all the volume concentrates around a very thin shell $\Xi_1 \equiv S_n(R, \varepsilon)$ near the boundary. As a consequence the samples fall over the region $\Xi = \Xi_1 \cup \Xi_2$ as depicted in Figure 1a.

2.2 Reliability Analysis in very high dimensional spaces

Until now, we have discussed about the n -dimensional sphere, which is symmetrical around the origin, so that each axis can be considered as a North Pole. However, in the framework of Structural Reliability Analysis, we introduce a LSS, and the symmetry of the sphere is lost. In this case, the region of probabilistic interest is close to the intersection between the region Ξ and the LSS $g(\mathbf{u})=0$.

Taking account of the statements described above, two important considerations can be made: (i) since the samples belong to the very thin shell, the LSS can be well approximated by an hyperplane; (ii) the North Pole is not fully arbitrary, but it must represent an "important direction", whose choice is a crucial step. Indeed, we must consider only the samples belonging to the equatorial slab containing the LSS. If the important direction is well chosen, the region of probabilistic interest, can be given by a very narrow equatorial slab. Clearly, the simplest and effective choice for the important direction is represented by the "design point direction" and the orientation of the equatorial slab is given by the FORM solution. Therefore, although in very high-dimensional spaces the samples fall far away from the design point, the FORM is likely to give very good approximations of the failure probability in all the cases where the "design point direction" is really an "important direction" and where the departure of the LSS from the FORM solution is weak in the region of probabilistic interest as above defined.

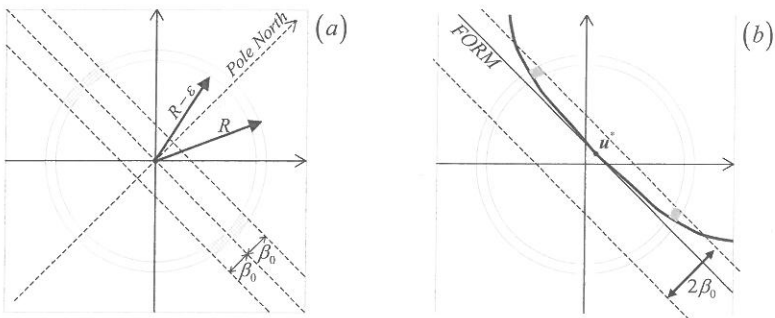


Figure 1. (a) n -dimensional sphere, (b) FORM in very high-dimensional spaces

3 FORM FOR STOCHASTIC DYNAMIC ANALYSIS

The FORM approach requires the preliminary discretization of the stochastic input into a set of standard normal random variables. Several formulations for this purpose are available, see Der

Kiureghian (Der Kiureghian 2000) for a brief review. For a zero-mean, Gaussian excitation process, all representations have the form $F(t, \mathbf{u}) = \sum s_i(t) u_i = \mathbf{s}(t) \cdot \mathbf{u}$, $i = 1, 2, \dots, n$, where n is a measure of the resolution of the discretization, $\mathbf{u} = \{u_1, u_2, \dots, u_n\}^T$ is an n -vector of standard normal random variables, $\mathbf{s}(t) = \{s_1(t), s_2(t), \dots, s_n(t)\}^T$ is an n -vector of deterministic shape functions dependent on the covariance function of the process.

Consider the response of a dynamical system to the excitation $F(t, \mathbf{u})$. Owing to the random variables \mathbf{u} , the response is stochastic and we denote it as $X(t, \mathbf{u})$. For a specified threshold x and time t , we define the tail probability as $P_f = \text{Prob}[X(t, \mathbf{u}) \geq x]$. To apply the tools of the structural reliability theory, we define the Limit State Function (LSF) $g(x, t, \mathbf{u}) = x - X(t, \mathbf{u})$, so that the failure probability with respect to the limit state $P_f = \text{Prob}[g(x, t, \mathbf{u}) \leq 0]$ is equal to the tail probability.

The problem of stochastic dynamic analysis in the time-domain is a typical case of Reliability Analysis in high-dimensional spaces, since n usually is greater than 400–500. Numerical experimentation has shown that in many cases of practical interest FORM gives good approximation of the tail probability; these results can be well explained in view of the considerations presented in section 2.2.

However FORM has some known drawbacks: (i) the evaluation of the design point is usually a quite complicated task in very high dimensional spaces, (ii) FORM gives only an approximation, and we don't have any information about the obtained level of accuracy.

The first shortcoming can be overcome through the adoption of suitable Response Surface Methods based on the Model Correction Factor Method (MCFM), recently proposed. The most important drawback is the second one, and it can be overcome by introducing a suitable Linear Response Surface Method based on the Support Vector Method (SVM) and that will be described in the next section.

4 THE PROPOSED LINEAR RESPONSE SURFACE

The basic idea of the Response Surface Methodology (Faravelli 1989, Bucher & Burgund 1990) is the approximation of the target Limit State Function (LSF) $g(x, t, \mathbf{u})$, usually complicated and implicit, with an approximate model $y_{\text{app}} = g_{\text{app}}(\mathbf{u})$, called Response Surface (RS). Once the RS is built, it is no longer necessary to run demanding nonlinear dynamic computations, but we can use the surrogate model. Clearly, because the RS works well, it is necessary that it approximates well the Limit State Surface (LSS) $g(x, t, \mathbf{u}) = 0$.

To this aim, we can consider the Reliability problem as a Classification Approach (Hurtado & Alvarez 2003), according to which we are not interested to the value $y = g(x, t, \mathbf{u})$ of the LSF, but to its sign $z = \text{sign}[g(x, t, \mathbf{u})]$, so that the points \mathbf{u}_i belonging to the safe region have the value $z_i = +1$, and the points \mathbf{u}_i belonging to the failure region have the value $z_i = -1$. It is easy to see that the building of a surrogate model $y_{\text{app}} = g_{\text{app}}(\mathbf{u})$ such that it satisfies only the sign constraints $z = \text{sign}[g(x, t, \mathbf{u})]$, is equivalent to the building of a RS which directly models the LSS.

A powerful classification approach when applied to Structural Reliability problems is given by the Support Vector Method (SVM), which will be described in the next subsection.

4.1 A Linear Response Surface based on the Support Vector Method

Let be known a set of m sampling points $\mathbf{u}_1, \mathbf{u}_2, \dots, \mathbf{u}_m$, while y_1, y_2, \dots, y_m and z_1, z_2, \dots, z_m be the corresponding values of the LSF $y_i = g(x, t, \mathbf{u}_i)$ and signs $z_i = \text{sign}[g(x, t, \mathbf{u}_i)]$, respectively.

Suppose that the target LSS is linear, $g(x, t, \mathbf{u}) = x - \mathbf{a} \cdot \mathbf{u}$, then the sampling points \mathbf{u}_i are linearly separable. Consider the approximated LSS $g_{\text{app}}(\mathbf{u}) = b - \mathbf{w} \cdot \mathbf{u}$, where \mathbf{w} determines the orientation of the plane, while the scalar b determines the offset of the plane from the origin. Clearly, when the number of samples converges toward infinity $m \rightarrow \infty$, then the linear classification function becomes coinciding with the target LSS, i.e. $\mathbf{w} \rightarrow \mathbf{a}$, $b \rightarrow x$. Conversely, for a limited number of points, there are infinite possible planes that classify the points correctly. Intuitively, a hyperplane that passes too close to the sampling points will be less likely to generalize well for the unseen data, while it seems reasonable to expect that a hyperplane that is farthest from all points will have better generalization capabilities. Given a set of m sampling points, the *margin* is de-

defined as the minimum distance between points belonging to different classes. Therefore, the optimal separating hyperplane is the one maximizing the margin.

Recall from the elementary geometry that the distance δ_i of a point \mathbf{u}_i from the hyperplane $g_{\text{app}}(\mathbf{u})=0$ reads as $\delta_i=|b-\mathbf{w}\cdot\mathbf{u}_i|/\pm\mathbf{w}\pm$; noticing that $g_{\text{app}}(\mathbf{u})=b-\mathbf{w}\cdot\mathbf{u}=0$ is invariant under a positive rescaling, we choose the solution for which the function $y_{\text{app}}=g_{\text{app}}(\mathbf{u})$ becomes one for the points closest to the boundary, i.e. $|b-\mathbf{w}\cdot\mathbf{u}_i|=1$. This couple of hyperplanes $g_{\text{app},s}(\mathbf{u})=b-\mathbf{w}\cdot\mathbf{u}=1$, $\forall \mathbf{u}\in g(\mathbf{u})>0$ and $g_{\text{app},s}(\mathbf{u})=b-\mathbf{w}\cdot\mathbf{u}=-1$, $\forall \mathbf{u}\in g(\mathbf{u})\leq 0$, are called *canonical hyperplanes* (or *support hyperplanes*). The distance from the closest point to the boundary is $\rho=1/\pm\mathbf{w}\pm$, and the margin becomes $M=2/\pm\mathbf{w}\pm$, as shown in Figure 2.

Maximizing the margin is equivalent to minimize $\pm\mathbf{w}\pm^2/2$, giving rise to the following Quadratic Programming (QP) problem

$$\begin{cases} \min_{\mathbf{w},b} & \frac{1}{2}\|\mathbf{w}\|^2 \\ \text{s.t.} & z_i(b-\mathbf{w}\cdot\mathbf{u}_i)\geq 1 \quad i=1,2,K,m \end{cases} \quad (5)$$

where the inequality constraints are equivalent to $b-\mathbf{w}\cdot\mathbf{u}_i\geq 1$, $\forall \mathbf{u}_i\in g(\mathbf{u}_i)>0$, and $b-\mathbf{w}\cdot\mathbf{u}_i\leq -1$, $\forall \mathbf{u}_i\in g(\mathbf{u}_i)\leq 0$. It is here noted that (5) is a standard convex optimization problem, so the uniqueness of the solution is guaranteed and moreover there are many robust algorithms that can effectively solve it.

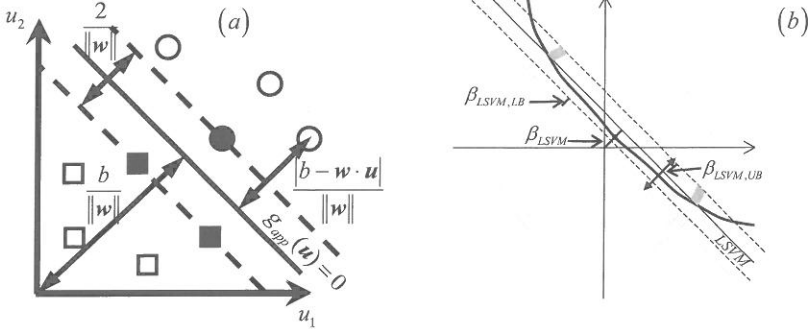


Figure 2. (a) Linear SVM, (b) L SVM Response Surface

In Figure 2a we represented with filled markers the *support vectors*, which are the points lying on the support hyperplanes $b-\mathbf{w}\cdot\mathbf{u}_i=\pm 1$. They only contribute to defining the optimal hyperplane, so that the complete sampling set could be replaced by only the support vectors, and the separating hyperplane would be the same.

Suppose now that the LSS is non-linear, so that it is not possible to identify an hyperplane, which can classify correctly all the sampling points. To this aim, we relax the constraints of (5) by introducing the slack variables $\xi_i\geq 0$ giving rise to $b-\mathbf{w}\cdot\mathbf{u}_i\geq 1-\xi_i$, $\forall \mathbf{u}_i\in g(\mathbf{u}_i)>0$, and $b-\mathbf{w}\cdot\mathbf{u}_i\leq -1+\xi_i$, $\forall \mathbf{u}_i\in g(\mathbf{u}_i)\leq 0$. The variables ξ_i give a measure of the departure from the condition of correct classification, more in particular when $0<\xi_i\leq 1$ the point is not well classified but it falls inside the margin, while when $\xi_i>1$ the point is not well classified and it falls outside the margin; finally, clearly, if $\xi_i=0$ the point is correctly classified. Under this hypothesis, the optimal separating hyperplane is the one having the maximum margin with the minimum classification error.

In Figure 2b we represented the non-linear LSS and its approximation by using the Linear SVM-based (L SVM) Response Surface. It is noted that the reliability index of the L SVM is simply given as $\beta_{\text{L SVM}}=b/\pm\mathbf{w}\pm$, while the support hyperplanes have the reliability indices $\beta_{\text{L SVM, LB}}=(b-1)/\pm\mathbf{w}\pm$ and $\beta_{\text{L SVM, UB}}=(b+1)/\pm\mathbf{w}\pm$.

4.2 Outline of the proposed approach

In each Response Surface method a crucial issue is represented by the sampling plan. The first step is finding an “important direction”. This can be the design point direction, or its approximation obtained by using the MCFM-based response surfaces, as described in section 2.2; in this way we are choosing the North Pole, and consequently the orientation of the equatorial slice. To determine the width of the equatorial slab, we define a set of points \mathbf{u}_k , $k=1,2,\dots,m_1$, along the design point direction, whose mutual distance is ρ , and evaluate their LSF $y_k = g(x, t, \mathbf{u}_k)$. The application of the LSVM to this set of points gives the first model, represented by the LSVM and its support hyperplanes, which define a first equatorial slab; note that the procedure does not use any information except the chosen important direction. This first model gives an approximation of the tail probability $P_{f,LSVM} = \Phi(-\beta_{LSVM})$, together with its flexible lower and upper bounds $P_{f,LSVM,LB} = \Phi(-\beta_{LSVM,UB})$ and $P_{f,LSVM,UB} = \Phi(-\beta_{LSVM,LB})$, respectively.

After that, an iterative procedure is developed such that: (i) generate a set of random points, (ii) evaluate the LSF only of the points belonging to equatorial slab, (iii) calculate a new LSVM, whose updated equatorial slab is likely to have a less width. The procedure stops when the equatorial slab is so thin that the flexible bounds are considered acceptable.

The proposed approach has several attractive properties: (i) it gives very good approximations of the tail probability, almost coinciding with the exact solutions, when an enough number of sample points is chosen; (ii) if a reduced number of points is chosen, it gives informations about the level of accuracy obtained, (iii) its convergence is not affected by the presence of multiple design points, (iv) it works well even if the LSF is not smooth.

5 NUMERICAL EXAMPLE

Consider a Bouc-Wen hysteretic oscillator defined by the differential equations

$$\begin{aligned} \ddot{X} + 2\zeta_0\omega_0\dot{X} + \omega_0^2[\alpha X + (1-\alpha)Z] &= F(t) \\ \dot{Z} &= -\delta|\dot{X}||Z|^{r-1}Z - \gamma|Z|^r\dot{X} + A\dot{X} \end{aligned} \quad (6)$$

where $\omega_0=8.36$ rad/sec and $\zeta_0=3\%$ are natural frequency and the damping ratio, respectively, α controls the degree of hysteresis, and r, A, δ and γ are parameters defining the shape of the hysteresis loop. The excitation is defined as $F(t) = -ma_g(t)$, where $a_g(t)$ denotes the base acceleration modeled as a white-noise process of intensity $S=0.0117$ m²/sec³. We select $\alpha=0.5$, $r=3$, $A=1$ and $\delta=\gamma=1/(2\sigma_0)$, wherein $\sigma_0=m^2\pi S/(ck)$ is the mean-square response of the linear system, obtained setting $\alpha=1$. The time step $\Delta t=0.02$ sec is used and the response at time $t=10$ sec is considered; consequently, for the case under exam, we have $n=500$ random variables.

The result is calculated for normalized threshold values x/σ_0 from 0.5 to 3 with increments of 0.5. At first a close approximation of the design point direction has been evaluated, by using the MCFM-based response surface (Alibrandi, submitted). Then, we considered along this direction a preliminary set of 51 points whose mutual distance is $\rho = 0.1$; we applied the LSVM and we found a solution very close to FORM, as shown in Figure 3a.

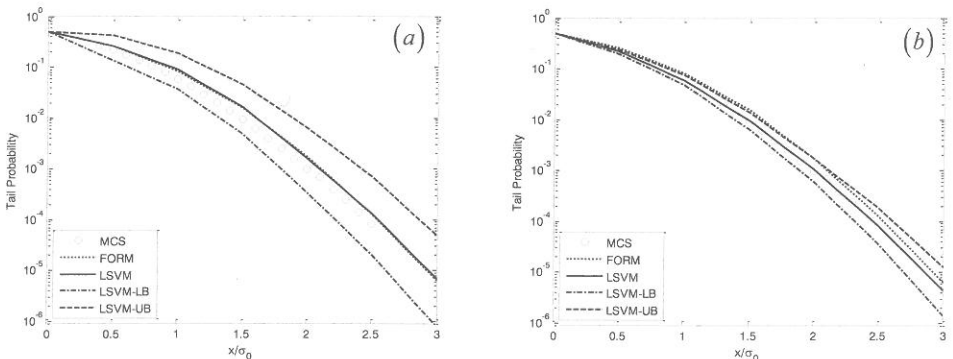


Figure 3. Tail Probability of the Bouc-Wen example (a) first model (b) after 20 iterations

Note that the LSVM adopts only the points on the important direction, so in principle it could be quite different from FORM. Moreover, the procedure allows to detect the confidence limits of the approximation. Then we have applied the iterative procedure described in section 4.2, and it is seen that after evaluating $m = 2,000$ points (20 iterations of 100 points each one), the LSVM gives an excellent agreement with the MCS with 100,000 samples; moreover the flexible bounds are clearly much more tight, as shown in Figure 3b.

6 CONCLUDING REMARKS

In this paper we have adopted a novel response surface strategy for nonlinear stochastic dynamic analysis. At first, through the analysis of the geometry of very high-dimensional spaces, we have shown that FORM may work well in many cases of practical interest. Then, we have introduced a Linear Response Surface based on the Support Vector Method that starting from the design point direction, allows to obtain an improved approximation, keeping knowledge of the achieved level of accuracy, through the introduction of suitable lower and upper bounds related to the support hyperplanes of SVM. Further research will be devoted to the analysis of MDOF systems with different degree and kind of nonlinearities.

REFERENCES

- Alibrandi, U. submitted. A Response Surface Method for Stochastic Dynamic Analysis.
- Alibrandi, U. & Der Kiureghian, A., 2010. The Model Correction Factor Method in NonLinear Stochastic Dynamic Analysis, *6th Computational Stochastic Mechanics Conference*, Rhodes, Greece.
- Alibrandi, U. & Der Kiureghian, A., 2012. A Gradient-Free Method for Determining the Design Point in Nonlinear Stochastic Dynamic Analysis, *Probabilistic Engineering Mechanics*, 28: 2-10.
- Au, S.K & Beck, J.L., 2001. Estimation of small failure probabilities in high dimensions by subset simulation, *Probabilistic Engineering Mechanics*, 16: 263-277
- Bucher, C., 2009. Asymptotic sampling for high-dimensional reliability analysis, *Probabilistic Engineering Mechanics*, 24:504-510
- Bucher, C. & Burgound, U., 1990. A fast and efficient response surface approach for structural reliability problems, *Structural Safety*, 7: 57-66.
- Der Kiureghian, A., 2000. The geometry of random vibration and solutions by FORM and SORM, *Probabilistic Engineering Mechanics*, 15: 81-90.
- Der Kiureghian, A. & Fujimura, K., 2009. Nonlinear stochastic dynamic analysis for performance-based earthquake engineering, *Earthquake Engng Struct. Dyn.*, 38: 719-738.
- Der Kiureghian, A. & Li, C-C., 1996. Nonlinear random vibration analysis through optimization, *Proceedings of the seventh IFIP WG 7.5 Conference on optimization of structural systems*, Boulder, Colorado.
- Ditlevsen, O. & Arnbjerg-Nielsen, T., 1994. Model correction factor method in structural reliability analysis, *Journal of Engineering Mechanics*, 120(1): 1-10.
- Ditlevsen, O. & Madsen, H.O., 1999. *Structural Reliability Methods*, Wiley.
- Faravelli, L., 1989. Response-surface approach for reliability analysis, *Journal of Engineering Mechanics*, 115: 2763-2781.
- Fujimura, K. & Der Kiureghian, A., 2007. Tail-equivalent linearization method for nonlinear random vibration, *Probabilistic Engineering Mechanics*, 22: 63-76.
- Garrè, L. & Der Kiureghian, A., 2010. Tail Equivalent Linearization Method in frequency domain and application to marine structures, *Marine Structures*, 23: 322-338.
- Hurtado, J.E. & Alvarez, D.A. 2003. A classification approach for reliability analysis with stochastic finite element modeling, *Journal of Structural Engineering* 129: 1141-1149.
- Koo, H., Der Kiureghian, A. & Fujimura, K., 2005. Design-point excitation for non-linear random vibration, *Probabilistic Engineering Mechanics*, 20: 136-147.
- Lutes, L.D. & Sarkani, S., 2004. *Random vibrations: analysis of structural and mechanical systems*, Burlington (MA), Elsevier.
- Mckenna, F., Fenves, GL & Scott MH., 2003. Open system for earthquake engineering simulation. *Pacific Earthquake Engineering Research Center, University of California, Berkeley, CA*, <http://opensees.berkeley.edu>.
- Pradlwarter, H.J., Schueller, G.I., Kotsourelakis P.S. & Charmpis D.C., 2007. Application of line sampling simulation method to reliability benchmark problems, *Structural Safety*, 29: 208-221
- Roberts, J.B. & Spanos, P.D., 1991. *Random Vibration and Statistical Linearization*, Wiley, Chichester.

FORM in high dimensions for stochastic dynamic analysis

S. D. Koduru

Post-doctoral Fellow, University of Alberta, Edmonton, Canada

A. Der Kiureghian

Taisei Professor of Civil Engineering, University of California, Berkeley, CA

ABSTRACT: Reliability problems involving large numbers of random variables pose special difficulties in various computational reliability methods – the so-called “curse of dimensionality.” We investigate the high-dimension reliability problem in the context of the first-order reliability method (FORM) for the particular class of nonlinear stochastic dynamic problems. Previous researchers have claimed that FORM is not appropriate for this class of problems because of the curse of dimensionality. We show that the accuracy of FORM depends more on the nature of the nonlinear system, which can be assessed by physical considerations before solving the reliability problem, than on the dimension of the problem. Furthermore, it is shown that even for problematic cases useful results can be obtained for reliability problems of practical interest. It is also shown that the accuracy of FORM does not deteriorate when the dimension of the problem increases due to the use of a finer discretization of the input stochastic process.

1 INTRODUCTION

The first-order reliability method (FORM) is well established as an approximate method of analysis for structural reliability problems defined in terms of a well behaved limit-state function. The accuracy of the approximation lies in the fact that the first-order approximation (linearization) of the limit-state function is performed at a point in a transformed standard normal space, where the probability density is maximal among all points within the failure domain. Based on this, it has been argued that the neighborhood of this point, commonly known as the design point, provides the dominant contribution to the failure probability integral (Ditlevsen & Madsen 1996), thereby explaining the reason for the effectiveness of the first-order approximation.

Due to its success in solving ordinary structural reliability problems, in recent years FORM has been used to solve more challenging problems involving random processes or fields. Since FORM requires a formulation in terms of random variables, these types of problems require that input random processes or fields be discretized and represented in terms of a finite set of random variables. Depending on the fineness of the discretization, the number of random variables of the problem can be large, i.e., in hundreds or thousands. It has been argued that in such cases the neighborhood of the design point does not necessarily provide the dominant contribution to the probability integral (Katafygiotis & Zuev 2008, Valdebenito et al. 2010). In fact, in high dimensions, even though the design point remains the most likely (maximal probability density) point in the failure domain, its neighborhood may make negligible contribution to the failure probability. This is because in high dimensions the incremental volume increases exponentially with distance from the origin so that failure regions far from the origin in the standard normal space may contain the bulk of the probability, even though the probability density there is small.

In this paper we investigate FORM solution of nonlinear stochastic dynamic problems involving large number of random variables (exceeding one thousand). We show that the accuracy

of FORM strongly depends on the physical characteristics of the system in a manner that is predictable by the knowledgeable user. We also show that even for problematic cases, useful approximations can be obtained by FORM for some important reliability measures. Furthermore, we show that the degree of fineness of the resolution has little influence on the FORM estimate, even when the number of random variables is doubled or quadrupled.

2 FORM SOLUTION OF STOCHASTIC DYNAMIC PROBLEMS

Consider the response $X(t)$ of a nonlinear system to a zero-mean Gaussian excitation, which is represented in the discretized form $F(t) = \sum_{i=1}^N s_i(t)u_i$, where u_i are a set of independent standard normal random variables and $s_i(t)$ are a set of basis functions characterizing the correlation structure of the process (Der Kiureghian 2000). The stochasticity in the response is due to the random variables $\mathbf{u} = (u_1, \dots, u_N)$ and we indicate this by writing the response as $X(t, \mathbf{u})$. To determine the tail probability $\Pr[x_0 < X(t, \mathbf{u})]$ at a selected time t , we solve the reliability problem defined by the limit-state function

$$G(t, \mathbf{u}) = x_0 - X(t, \mathbf{u}) \quad (1)$$

The FORM solution of this problem requires finding the design point $\mathbf{u}^* = \arg \min\{\|\mathbf{u}\| \mid G(t, \mathbf{u}) = 0\}$ and linearizing the limit-state function at \mathbf{u}^* , i.e., employing the approximation $G(t, \mathbf{u}) \cong x_0 - \nabla_{\mathbf{u}}X(t, \mathbf{u}^*)(\mathbf{u} - \mathbf{u}^*)$, where $\nabla_{\mathbf{u}}X(t, \mathbf{u})$ is the response gradient. The FORM approximation of the probability of interest is then given as $\Pr[x_0 < X(t, \mathbf{u})] \cong \Phi[-\beta(x_0, t)]$, where $\beta(x_0, t) = \|\mathbf{u}^*\|$ denotes the reliability index. For a linear system, one can show (Fujimura & Der Kiureghian 2007) that $X(t, \mathbf{u})$ is a linear function of \mathbf{u} and, therefore, the above approximation is indeed exact. For a nonlinear system, the accuracy of the approximation clearly depends on the degree of nonlinearity of the system. In view of the high-dimension problem described above, the question arises whether the accuracy of the FORM approximation also depends on the fineness of the discretization employed, i.e., on the number of random variables, N used to discretize the input excitation. We investigate these issues by way of two example systems in the following section.

The above problem characterizes the reliability of the system at a point in time. In practice, one is more interested in the reliability of the system over an interval of time, i.e., the probability $\Pr[x_0 < \max_{t \in T} X(t, \mathbf{u})]$ for some selected time interval T . As described in Fujimura & Der Kiureghian (2007), this problem can be solved as a series system reliability problem

$$\Pr[x_0 < \max_{t \in T} X(t, \mathbf{u})] \cong \Pr[\cup_{t_i \in T} \{x_0 < X(t_i, \mathbf{u})\}] \quad (2)$$

in which t_i are a set of closely spaced time points within the interval of interest. It can be seen that the "components" of the series system are the point-in-time reliability problems defined in Eq. 1. Hence, the tail-probability problem in Eq. 1 is a fundamental problem for solving other reliability measures of interest in stochastic dynamic analysis. As shown in Fujimura & Der Kiureghian (2007), FORM solution of the above problem is given in terms of the multinormal probability function involving the design points of the individual point-in-time problems.

3 INVESTIGATION OF NONLINEAR SYSTEMS

We consider two nonlinear systems: an elastic Duffing oscillator and an inelastic oscillator following the Bouc-Wen hysteretic law (Wen 1976). In order to gain insight into the behavior of each system, we examine the projections of the failure domain in two-dimensional subspaces in the standard normal space. To simplify the problem, we consider the input excitation as a white-noise process discretized in time domain. This is characterized by a sequence of time points $t_i = i \times \Delta t$, $i = 0, 1, \dots, N$, where Δt is a small time increment, and the basis functions $s_i(t_j) = \sigma \delta_{ij}$, where δ_{ij} is the Kronecker delta and $\sigma = \sqrt{2\pi S_0 / \Delta t}$, in which S_0 is the intensity of the white noise.

3.1 Duffing Oscillator

The Duffing oscillator is defined by the differential equation

$$m\ddot{X}(t) + c\dot{X}(t) + k[X(t) + \gamma X^3(t)] = F(t) \quad (3)$$

We consider parameter values originally considered by Koo et al. (2005) and also used by Katafygiotis & Zuev (2008): mass $m = 1000$ kg, damping $c = 200\pi$ Ns/m, stiffness $k = 1000(2\pi)^2$ N/m, and nonlinearity coefficient $\gamma = 1$ m⁻². The intensity of the discretized input white noise is set to $S_0 = 10^6$ N²s/rad. We consider the time instant $t = 12$ s and the threshold $x_0 = 3\sigma_0$, where $\sigma_0^2 = \pi S_0/(ck)$ represents the stationary mean-square response of the linear oscillator, i.e., for the case with $\gamma = 0$. Koo et al. (2005) have shown that the response of the Duffing oscillator is effectively stationary by the time $t = 12$ s. We consider the time step $\Delta t = 0.01$ s so that the number of random variables used in discretizing the input process is $N = 1 + t/\Delta t = 1201$.

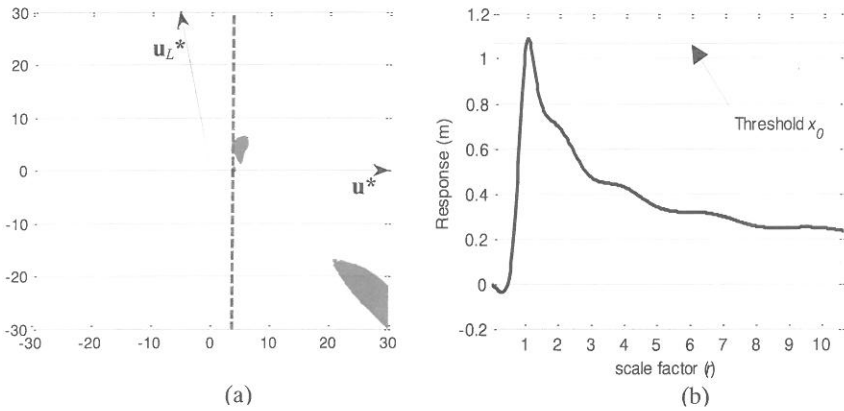


Figure 1: (a) Failure domain in the plane of $\pi(\mathbf{u}^*, \mathbf{u}_L^*)$ for the instantaneous failure at $t = 12$ s; (b) Duffing oscillator response at $t = 12$ s along the design point direction

Katafygiotis & Zuev (2008) considered visualization of the above problem in the two-dimensional plane $\pi(\mathbf{u}^*, \mathbf{u}_L^*)$, where \mathbf{u}^* is the vector defining the design point of the system in Eq. 3 and \mathbf{u}_L^* represents the design point vector for the corresponding linear oscillator (i.e., with $\gamma = 0$). Figure 1a shows this plane with the failure domain shaded. As can be seen, the failure domain in this plane is disjointed and the FORM approximation (shown in thick broken line) grossly overestimates it. Indeed, the FORM approximation of the problem yields a probability of failure of 8.3×10^{-5} , while the “exact” result obtained by Monte Carlo simulation is 3.0×10^{-5} with 10^5 samples. To understand the reason for this behavior, in Figure 1b we show a plot of the response at $t = 12$ s as a function of the ratio $r = \|\mathbf{u}\|/\|\mathbf{u}^*\|$, where \mathbf{u} is a vector coincident with the design-point vector \mathbf{u}^* , i.e., the response $X(12s, r\mathbf{u}^*)$. This plot is similar to one used earlier by Katafygiotis & Zuev (2008). Note that for any choice of \mathbf{u} we have a deterministic input, and the ones selected along the vector \mathbf{u}^* have time histories proportional to the design-point excitation with r being the scale factor. The remarkable observation in Figure 1b is that, as the excitation is scaled up, the response at time $t = 12$ s is far from monotonically increasing. After an initial rise up to the specified threshold value of x_0 for $r = 1$, the response $X(12s, r\mathbf{u}^*)$ rapidly drops to values far below x_0 . This has to do with the rapidly stiffening behavior of the selected Duffing oscillator. (Its stiffness increases by a cubic law in terms of the displacement.) As the excitation is scaled, the peak response occurs at an earlier time and, as the oscillator stiffens, the response at time $t = 12$ s falls below the threshold value. This explains why the failure domain in Figure 1a is disjointed.

It is clear that FORM is not a good solution method for solving the point-in-time reliability problem for the selected Duffing oscillator. But let us see if FORM can be used to solve the reliability problem defined in Eq. 2. We select the interval $T = (12s, 24s)$ so that the reliability problem is that of determining the probability that the peak of the stationary response over a period of 12 seconds will exceed the threshold x_0 . This problem has $N = 2401$ random variables and the series system in Eq. 2 has 1201 “components.” In Figure 2 we examine the system (composite) failure domain $\cup_{t_i \in T} \{x_0 < X(t_i, \mathbf{u})\}$ in four different planes $\pi(\mathbf{u}_j^*, \mathbf{u}_{Lj}^*)$, where the index j corresponds to the time-point “components” at $t = 12, 12.5, 12.7$ and $13.5s$. It can be seen that the composite failure domain gradually regularizes so that by the time instance $13.5s$, it is a fully joined domain. This behavior is a consequence of the stiffening nature of the Duffing oscillator. As the excitation is scaled, i.e., points are taken farther away from the origin in the standard normal space, a peak in the response occurs at an earlier time that exceeds the specified threshold. Hence, later time-point “components” are all expected to have fully joined failure domains.

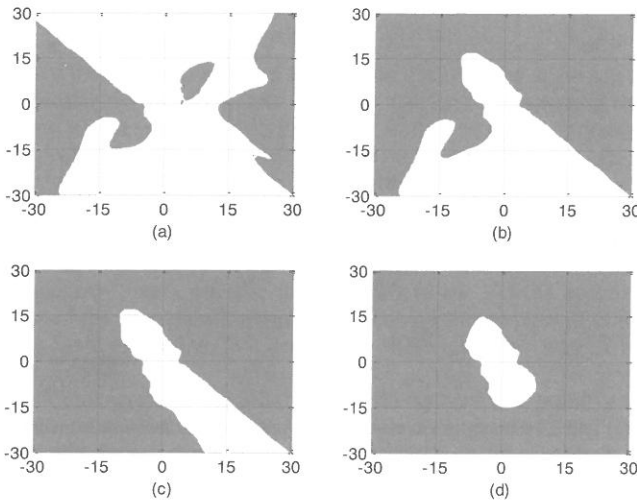


Figure 2: Failure domains for the first-passage probability over duration $T = (12s, 24s)$ in planes $\pi(\mathbf{u}_j^*, \mathbf{u}_{Lj}^*)$ for (a): $t = 12s$, (b): $t = 12.5s$, (c): $t = 12.7s$ and (d): $t = 13.5s$

In constructing a FORM approximation for the series system, we linearize the failure surface for each time-point “component.” Clearly, when the safe domain is closed and convex as in Figure 2d, the linearization at each design point is active only over a small neighborhood of the design point. Because of this, one can expect that the FORM approximation will provide reasonably accurate results for such cases. Indeed, the FORM approximation of the failure domain in the plane $\pi(\mathbf{u}_j^*, \mathbf{u}_{Lj}^*)$ for time point $t = 13.5s$, shown in Figure 3a, indicates a fair approximation of the actual failure domain shown in Figure 2d. To numerically examine this further, in Figure 3b we show estimates of the probability $\Pr[x_0 < \max_{t \in T} X(t, \mathbf{u})]$ obtained by FORM (solid line) along with Monte Carlo simulation results (dots with dashed lines indicating one-standard deviation confidence interval) for increasingly longer time intervals T , starting from $T = (12s, 12s)$, which is identical to the point-in-time problem described earlier, to $T = (12s, 24s)$. It can be seen that the relative error in the FORM approximation gradually decreases as a longer time interval is considered. The bulk of this error is related to the poor approximation of the composite failure domain for a short initial interval.

In summary, while FORM is not well suited for systems such as the Duffing oscillator which produce disjointed failure domains, even for such problems FORM produces fairly accurate results for the reliability problem defined over an interval of time. Indeed, the instantaneous reli-

bility problem is not of practical interest; it is only a means for obtaining the reliability over an interval of time, which is the problem of real practical interest. The above analysis shows that, even for the Duffing oscillator that has a peculiar stiffening behavior, FORM provides a reasonable solution for this reliability problem of practical interest.

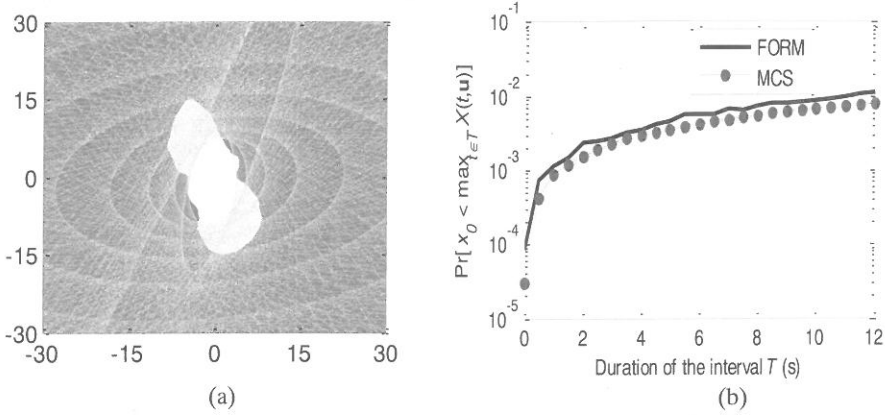


Figure 3: (a) FORM approximation of the failure domain in the plane $\pi(\mathbf{u}_j^*, \mathbf{u}_{Lj}^*)$ at $t = 13.5s$ for the first-passage probability over duration $T = (12s, 24s)$ for the Duffing oscillator; (b) Comparison of FORM system-reliability approximation with the Monte Carlo sampling (MCS) result

3.2 Hysteretic Oscillator

Consider a nonlinear oscillator characterized by the Bouc-Wen hysteresis law:

$$m\ddot{X}(t) + c\dot{X}(t) + k[\alpha X(t) + (1 - \alpha)Z(t)] = F(t) \quad (4)$$

$$\dot{Z}(t) = -\gamma|\dot{X}(t)| |Z(t)|^{n-1}Z(t) - \eta|Z(t)|^n\dot{X}(t) + A\dot{X}(t) \quad (5)$$

where m , c and k are as defined for the Duffing oscillator, $\alpha = 0.5$ is a nonlinearity parameter ($\alpha = 1$ corresponds to the linear case), $Z(t)$ is the hysteretic component of the response, and $n = 1$, $A = 1$ and $\gamma = \eta = 1/(2\sigma_0)$, where $\sigma_0^2 = \pi S_0 m^2 / (ck)$ is the mean-square response of the linear oscillator, i.e., for $\alpha = 1$. In this case, the input excitation is considered as $F(t) = -mA(t)$, where $A(t)$ is the base acceleration with a constant power spectral density $S_0 = 1 \text{ m}^2/(\text{rad.s}^3)$. This oscillator was earlier studied by Koo et al. (2005). It is important to note that, in contrast to the Duffing oscillator, the hysteretic oscillator has a softening behavior.

As in the previous case, we first consider the point-in-time reliability problem at $t = 12s$ for the threshold $x_0 = 3\sigma_0$. Using $\Delta t = 0.01s$, the problem has $N = 1 + t/\Delta t = 1201$ random variables. Figure 4a shows the failure domain in the plane $\pi(\mathbf{u}^*, \mathbf{u}_L^*)$, where again \mathbf{u}^* is the design point for the system in Eqs. 4 and 5 and \mathbf{u}_L^* represents the design point for the corresponding linear ($\alpha = 1$) oscillator. In contrast to Figure 1a for the Duffing oscillator, the failure domain of the hysteretic oscillator is well behaved and appears to be amenable for a FORM approximation. In fact, in the plane considered in Figure 4a, deviations of the tangent plane from the true limit-state surface on the two sides of the design point tend to cancel out. Insight into the good behavior of the hysteretic oscillator is gained by examining the response $X(12s, r\mathbf{u}^*)$ as a function of the scale parameter r , as shown in Figure 4b. It can be seen that the response at $t = 12s$ almost linearly increases with the scale parameter r . (The near linearity of this curve is the basis for the well known "equivalent displacement rule" (Chopra 2007) in deterministic inelastic dynamic analysis.) This has to do with the softening behavior of the hysteretic oscillator – as forcing function is scaled upward, the displacement at all times tends to increase. These observations suggest that one can expect FORM to provide good approximations of the point-in-time reliability problem for a hysteretic system. Indeed, the FORM approximation of the point-in-time failure probability for this case is $\Pr[x_0 < X(12s, \mathbf{u})] \cong 2 \times 10^{-4}$, which practically coincides with the "exact" value computed by Monte Carlo simulation.

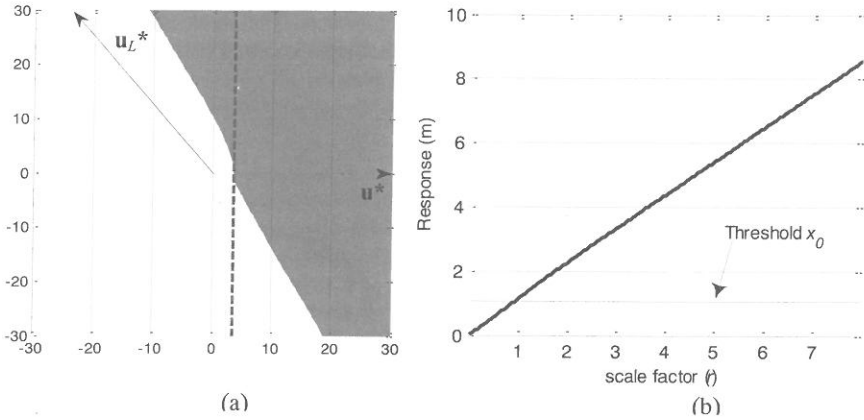


Figure 4: (a) Failure domain in the plane $\pi(\mathbf{u}^*, \mathbf{u}_L^*)$ at $t = 12\text{s}$; (b) Bouc-Wen oscillator response at $t = 12\text{s}$ along the design point direction

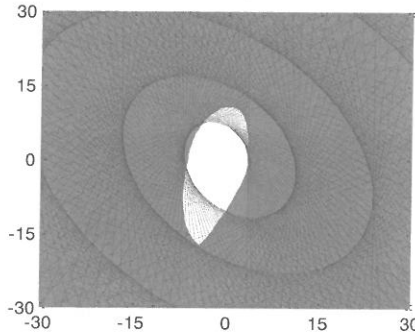


Figure 5: System reliability approximation of the failure domain in the plane $\pi(\mathbf{u}_j^*, \mathbf{u}_{Lj}^*)$ at $t = 12\text{s}$ for the Bouc-Wen oscillator

Next, we consider the reliability problem $\Pr[x_0 < \max_{t \in T} X(t, \mathbf{u})]$ with $T = (12\text{s}, 24\text{s})$. Figure 5 shows the true and FORM-approximated failure domains in the plane $\pi(\mathbf{u}^*, \mathbf{u}_L^*)$. While the two domains are not identical, their probability contents are nearly the same. Indeed, solution of the series system problem by FORM yields $\Pr[x_0 < \max_{t \in T} X(t, \mathbf{u})] \cong 0.0172$, while the “exact” result obtained by Monte Carlo simulation is $\Pr[x_0 < \max_{t \in T} X(t, \mathbf{u})] = 0.0131$. Noting that in reliability analysis order-of-magnitude accuracy is what we expect, the FORM approximation of the hysteretic oscillator appears to be good both for the point-in-time and time-interval reliability problems.

4 EFFECT OF HIGH DIMENSION

As mentioned earlier, several investigators have argued that the design point in FORM analysis loses its significance in higher dimensions, and that the FORM approximation is expected to deteriorate with increasing number of random variables. For example, Valdebenito et al. (2010) have used idealized limit-state functions to show how the FORM approximation rapidly deteriorates with increasing dimension of the random space. For this reason, they have argued against the use of FORM for high-dimensional problems. This argument suggests that in reliability problems involving random processes or fields, the FORM approximation should deteriorate as

the discretization is made finer and a larger number of random variables are used to formulate the problem. We explore this problem in this section.

For the Bouc-Wen oscillator of the previous section, we consider three different discretizations of the input excitation $F(t)$ corresponding to the time steps $\Delta t = 0.02s, 0.01s$ and $0.005s$. For the point-in-time reliability analysis at $t = 12s$, these respectively correspond to $N = 601, 1,201$ and $2,401$ random variables. Figure 6a shows plots of the reliability index $\beta = \Phi^{-1}(1 - p)$, where $p = \Pr[x_0 < X(12s, \mathbf{u})]$, on a normal probability chart as a function of the normalized threshold x_0/σ_0 . The dots in this figure are “exact” results obtained by 10^5 Monte Carlo simulations with the gray dashed lines indicating the one-standard deviation confidence interval, while the three coinciding lines are the FORM approximations based on the three time steps with varying number of random variables. It is remarkable that there is virtually no distinction between the three FORM approximations, even though the number of random variables varies by a factor of 4. Figure 6b shows similar results for the interval reliability problem $\Pr[x_0 < \max_{t \in T} X(t, \mathbf{u})]$ with $T = (12s, 24s)$, where the numbers of random variables for the three time steps now are $N = 1,201, 2,401$ and $4,801$. Again, we find the three FORM approximations to nearly coincide and to be in close agreement with the “exact” Monte Carlo results.

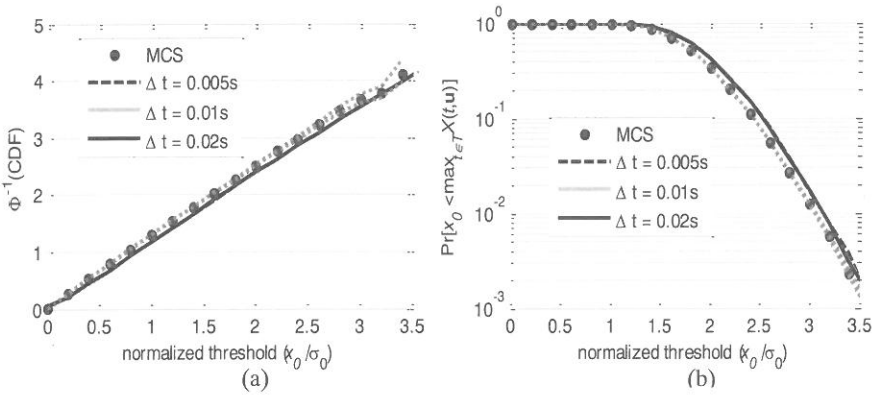


Figure 6: Comparison of the FORM and Monte Carlo Sampling (MCS) results with varying numbers of random variables for (a) point-in-time reliability at $t = 12s$, and (b) first-passage probability for $T = (12s, 24s)$

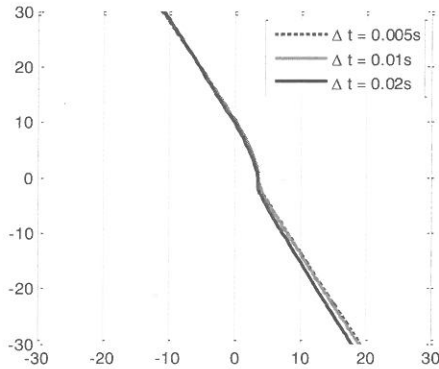


Figure 7: Comparison of the limit-state surfaces for different discretizations in the plane $\pi(\mathbf{u}^*, \mathbf{u}_L)$ for the instantaneous failure at $t = 12s$

The above observations suggest that FORM approximations are independent of the fineness of the discretization of random processes or fields, provided, of course, that the discretization is

sufficiently fine to accurately represent the underlying continuum problem. The idea that higher dimensions necessarily deteriorate the accuracy of the FORM approximation is incorrect. One can conjecture that with increasing fineness of the discretization, the influence of each random variable diminishes and the limit-state surface in the higher dimensions becomes more flat. As a simple demonstration of this, in Figure 7 we compare the limit-state surfaces of the above point-in-time problem in the planes $\pi(\mathbf{u}^*, \mathbf{u}_t^*)$ for each discretization scheme. It can be seen that the surface becomes more flat for finer time steps. This effect, which was first mentioned in Der Kiureghian & Fujimura (2008), has also been observed for finite-element reliability problems with discretized random fields in Koduru (2008).

In summary, while for certain problems the FORM approximation may deteriorate in high dimensions, this is not necessarily the case when the random variables result from discretization of random processes or fields. Hence, discounting FORM as a solution method for all high-dimensional reliability problems is unwise.

5 CONCLUSIONS

The applicability of FORM to solve nonlinear stochastic dynamic problems is demonstrated. As any approximate numerical method, assessing the suitability of FORM requires an understanding of the physical nature of the underlying system. We have shown that the accuracy of the FORM approximation is strongly dependent on the nature of nonlinear problem at hand, and not necessarily on the dimensionality of the standard normal space that arises primarily from the discretization of a random process or field. For the type of practical nonlinear problems investigated, the error in the probability computation with FORM remained independent of the number of random variables employed in the discretization of the input process.

ACKNOWLEDGEMENT

The first author gratefully acknowledges the funding provided by Natural Science and Engineering Research Center (NSERC) of Canada through Post-doctoral Fellowship.

REFERENCES

- Chopra, A. K., 2007. *Dynamics of Structures-Theory and applications to earthquake engineering*. Prentice-Hall, N.J.
- Der Kiureghian, A., 2000. Geometry or random vibrations and solutions by FORM and SORM. *Probabilistic Engineering Mechanics*, 15 (1), 81-90
- Der Kiureghian, A. & Fujimura, K., 2008. Nonlinear stochastic dynamic analysis by tail-equivalent linearization. *Keynote in Proceedings of Asian-Pacific Symposium on Structural Reliability and Its Applications*, Hong Kong, 19-20 June 2008
- Ditlevsen, O., & Madsen, H.O., 1996. *Structural Reliability Methods*, Wiley, U.K.
- Fujimura, K., & Der Kiureghian, A., 2007. Tail-equivalent linearization method for nonlinear random vibration. *Probabilistic Engineering Mechanics*, 22(1), 63-76
- Katafygiotis, L., & Zuev, K.M., 2008. Geometric insight into the challenges of solving high-dimensional reliability problems. *Probabilistic Engineering Mechanics*, 23: 208-218
- Koduru, S.D., 2008. *Performance-based Earthquake engineering with the first-order reliability method*. PhD Dissertation, University of British Columbia, Vancouver, Canada
- Koo, H., Der Kiureghian, A., & Fujimura, K., 200. Design-point excitation for non-linear random vibrations. *Probabilistic Engineering Mechanics*, 20: 136-147
- Valdebenito, M. A., Pradlwarter, H.J., & Schueller, G. I., 2010. The role of the design point for calculating failure probabilities in view of dimensionality and structural nonlinearities. *Structural Safety*, 32: 101-111
- Wen, Y.-K. 1976. Method for random vibration of hysteretic systems. *Journal of Engineering Mechanics Division*, 102 (EM2): 249-263

Discretization of stochastic processes in time domain by *sinc* basis functions and application in TELM analysis.

M. Broccardo, A. Der Kiureghian.
University of California Berkeley, USA.

ABSTRACT: This paper investigates methods for discrete representation of band-limited stochastic processes. The approach employs a unified framework for such representations by use of concepts of Hilbert space and general decomposition of a signal into basis functions. The proposed representation, in general, allows reducing the number of random variables used in the simulation of stochastic processes. Direct application of the representation is employed for Tail-Equivalent Linearization Method (TELM) analysis. An example of a single degree of freedom hysteretic oscillator subjected to a Gaussian band-limited white noise simulated by use of *sinc* basis functions is presented. The accuracy and efficiency of the representation are compared with those of current discretization methods.

1 INTRODUCTION

Structural Engineering problems often require consideration of nonlinear behavior of structures at high reliability levels. In such applications, the interest is focused on the tail of the response probability distribution rather than on its mean and standard deviation.

Fujimura and Der Kiureghian (2007) developed the Tail-Equivalent Linearization Method (TELM) to tackle this class of problems. The approach, which is based on the First-Order Reliability Method (FORM), defines an equivalent linear system for each considered response threshold by equating its tail probability with the first-order approximation of the tail probability of the nonlinear response. TELM requires discretization of the input process and its representation in terms of a finite set of standard normal random variables. Since the computational time of the method depends on the number of random variables, TELM may become computationally demanding when this number is too large. For this reason, formulations that reduce the number of random variables are of interest. The present work serves two purposes. The first is to critically review commonly used methods for representing stochastic processes in time and frequency domains. The second is to develop a unified framework for such representation by use of concepts of Hilbert space and general decomposition of a signal into basis functions. Issues of periodicity of the signal and efficiency of the representation, as measured in terms of the number of required random variables, are discussed. Finally an example that makes use of *sinc* basis functions is presented and is incorporated into TELM analysis. It is shown that the time required to solve the non-linear random vibration problem with TELM is significantly reduced if this representation of the input stochastic process is employed.

2 REVIEW OF TIME- AND FREQUENCY-DOMAIN DISCRETIZATION

A general function can be represented as an infinite linear combination of a set of basis functions:

$$f(t) = \sum_{n=1}^{\infty} s_n(t)c_n. \quad (1)$$

A stochastic process can be derived from the above representation by considering the function as a particular realization of a sample space. The developed approach considers the coefficients, c_n , as a series of random variables. Thus, we write the stochastic process as

$$F(t) = \mu(t) + \sum_{n=1}^{\infty} s_n(t) C_n, \quad (2)$$

where C_n are zero mean, independent random variables and $\mu(t)$ defines the mean function of the process. The choice of the basis functions $s_n(t)$, together with the variances of C_n , determine the autocorrelation function of the process. Furthermore, when C_n are Gaussian random variables, the process is Gaussian. Note that this representation allows separating the "randomness" of the process (inherent in the coefficients C_n) from its time evolution (represented by $s_n(t)$). In this paper we focus on zero-mean stationary Gaussian processes so that we can rewrite (2) as:

$$F(t) = \mathbf{s}(t) \cdot \sigma \mathbf{u}, \quad (3)$$

where $\mathbf{s}(t) = [s_1(t) \dots s_N(t)]^T$ is the vector of basis functions and $\mathbf{u} = [u_1 \dots u_N]^T$ is a vector of statistically independent standard normal random variables. This representation employs truncation of the series after N terms, which is necessary for computational purposes.

2.1 Time-domain discretization

The choice of the basis functions not only determines the covariance structure of the process but also the discretization method. In Der Kiureghian (2000), for example, a filtered white noise process is represent by

$$F(t) = [\eta(t) * W(t)]U(t) = \int_0^t \eta(t - \tau)W(\tau)d\tau, \quad (4)$$

where $*$ denotes convolution, $U(t)$ is the unit step function, $\eta(t)$ the impulse-response function (IRF) of a stable linear filter, and $W(t)$ a white-noise process. In the time-domain discretization, for a selected time step Δt and initial time $t_0 = 0$, $W(t)$ is approximated with the following rectangular wave process:

$$\widehat{W}(t) = \frac{1}{\Delta t} \int_{t_{n-1}}^{t_n} W(\tau)d\tau, \quad t_{n-1} < t < t_n, \quad n = 1, 2, \dots, N. \quad (5)$$

The resulting process is band-limited at frequency $\bar{\omega} = \pi/\Delta t$ [rad/s] and has variance $\sigma^2 = 2\pi S/\Delta t$, where S is the double-sided spectral density of the white noise. Defining the standard normal random variables as $u_n = \widehat{W}_n(t_n)/\sigma$, (5) can be written in the form:

$$\widehat{W}(t) = \mathbf{s}(t) \cdot \sigma \mathbf{u}, \quad (6)$$

$$s_n(t) = 1, \quad t_{n-1} < t \leq t_n \\ = 0, \quad \text{otherwise.} \quad (7)$$

The discrete version of (3), $\widehat{F}(t)$, is obtain by replacing $W(t)$ with $\widehat{W}(t)$

$$\widehat{F}(t) = [\eta(t) * \widehat{W}(t)]U(t) = \mathbf{s}(t) \cdot \sigma \mathbf{u} \quad (8)$$

$$s_n(t) = \int_{t_{n-1}}^{t_n} \eta(t - \tau)d\tau, \quad t_{n-1} < t \leq t_n, \quad n = 1, 2, \dots, N \\ = 0 \quad t \leq t_n. \quad (9)$$

2.2 Frequency-domain discretization

An alternative to the time-domain discretization is the frequency-domain discretization proposed by Shinozuka (1975-91) and Deodatis (1991), which is based on the original work of Rice (1954). The representation is the canonical Fourier series with random coefficients with sine and cosine as selected basis functions. The discretization of the frequency domain is obtained by selection of a discretization step $\Delta\omega$ and a band-limit $\omega_K = \bar{\omega}$. The process is written as:

$$\widehat{F}(t) = \sum_{k=1}^K \sigma_k [u_k \sin(\omega_k t) + \bar{u}_k \cos(\omega_k t)] = \mathbf{s}(t) \cdot \Sigma \mathbf{u} \quad (10)$$

$$\mathbf{s}(t) = [s_1(t), \dots, s_K(t); \bar{s}_1(t), \dots, \bar{s}_K(t)], \quad (11)$$

where $\mathbf{u} = [u_1, \dots, u_K, \bar{u}_1, \dots, \bar{u}_K]^T$, $s_k(t) = \sin(\omega_k t)$, $\bar{s}_k(t) = \cos(\omega_k t)$ and Σ is the diagonal matrix containing the variances $\sigma_k^2 = 2S(\omega_k)\Delta\omega$, in which $S(\omega)$ is the double-sided spectral density of the process. If $S(\omega) = S$, then $\hat{F}(t) = \hat{W}(t)$. In contrast to the time-domain discretization that leads to a band-limited process, the frequency domain discretization leads to a periodic process. For a selected $\Delta\omega$, (10) produces a process with period $T = 2\pi/\Delta\omega$.

4 FUNCTIONAL SPACE INTERPRETATION

In this section we introduce some basic and intuitive concepts underlying functional spaces, which are helpful to extend our discrete representation of a random process. Functional spaces are not the main focus of the paper, so we choose a simple intuitive and not rigorous approach. Moreover, we restrict ourselves to band-limited Gaussian white-noise processes. This is not restrictive, because other processes can be easily derived from white noise by filtering either in time or frequency domain; moreover, the band limit is not a real restriction, since one can never achieve pure white noise in practice. It is assumed that the reader is familiar with the concepts of a vector space \mathbb{R}^N , Euclidian norm, and orthogonality. When the dimensionality of the vector space \mathbb{R}^N is pushed to infinity, each vector can be viewed as a function. We equip this new space with norms which define the length of our function. Because the dimensionality is not finite, we restrict the function to have a finite norm. The notions of inner product and orthogonality can be extended to this space by the usual limit of the Riemann sum pushed to an integral. In lieu of this concept, the inner product of two vectors is viewed as the integration between two functions with finite norm and the concept of orthogonality is easily extendable. Two functions are said to be orthogonal if their inner product is zero. A vector space equipped with an inner product is said to be an inner product space.

Functions $f_1(t), \dots, f_N(t)$ are linearly independent if $\sum_{n=1}^N c_n f_n(t) = 0$ is true only if $c_n = 0$ for all n . The span of a set of functions is the subspace consisting of all linear combinations of the functions in the set. A set of functions is a base for a space or subspace when the functions are linearly independent and their span covers the whole space or subspace. A set of orthonormal functions is a set of functions which are orthogonal with unitary norm. We reserve the letter s_n for each element of the orthonormal base. Given an orthonormal base, each coefficient c_n can be easily computed as the orthogonal projection of the function onto each element of the base s_n , i.e. $c_n = \langle f(t), s_n(t) \rangle$, where $\langle \cdot, \cdot \rangle$ denotes the standard inner product between two functions, i.e. $\int_0^t f(t)s(t)dt$. Equation (1) can be viewed as the expansion of the function $f(t)$ into a set of orthonormal basis functions.

A complete inner product space is named a Hilbert space. The concept of completeness is beyond the scope of this paper, but both representations described above can be cast in the Hilbert space framework. As an example, the space of the square integrable functions over a period $[0, T]$ is a Hilbert space; it is easy to show that the set of sines and cosines in (10) represents a complete set of orthonormal basis for such functions. Each realization of a periodic banded white noise of period T can be described by the above expansion and the coefficients of the Fourier series are the orthogonal projections of the realization into each sine and cosine.

It should be intuitively clear that any valid set of basis functions can be used to describe the (square integrable) realizations of a stochastic process and, thus, to describe the process itself by randomizing the coefficients. In particular, given a set of orthonormal basis (we don't really need orthonormal but it is convenient), we can easily describe Gaussian processes, choosing the random coefficients to be Gaussian random variables. A vector in a finite space or a function in the Hilbert space can be described completely if all the coordinates of the expansion (1) are provided. In application, we truncate the infinite series after a sufficiently large N . If we consider only a finite number of basis functions, we constrain our work into a subspace V , which is the span of the finite set of these basis functions, and the approximate realization is the orthogonal projection of the real realization into this subspace. This has an important consequence because it guarantees to be the best approximation of the real realization for the given basis.

5 THE *SINC* BASIS FUNCTIONS

As mentioned in the previous section, in general any basis can be used to describe a particular Hilbert space. In this section we present the *sinc* function as a particular basis to describe a Gaussian process. The use of the *sinc* basis function to represent band-limited white noise was first proposed by Grigoriu (1993). This choice is suggested by the theory of signal processing, in which *sinc* functions are used to reconstruct band-limited signals from a set of equally spaced samples. In this paper we investigate if the *sinc* function offers a valid set of basis functions to describe a Gaussian process and the advantages that we gain in implementing this representation in TELM analysis.

5.1 The *sinc* function

The original *sinc* function is defined as $\text{sinc}(t) = \sin(\pi t) / \pi t$. In this paper we use a scaled version, which is denoted as $\text{sinc}_{\Delta t}$ and is defined as

$$\text{sinc}_{\Delta t}(t) = \frac{\sin(\pi t / \Delta t)}{\pi t / \Delta t}. \quad (12)$$

Given a function $f(t)$ that is band-limited at $\bar{\omega}$ and a set of equally spaced samples $f(\Delta t), \dots, f(n\Delta t)$ such that the sampling rate $\Delta t \leq \pi / \bar{\omega}$, the original function can be reconstructed from its samples by the following series:

$$f(t) = \sum_{n=0}^{\infty} f(n\Delta t) \text{sinc}_{\Delta t}(t - n\Delta t). \quad (13)$$

Equation (13) is also known as Whittaker–Shannon interpolation formula or *sinc* interpolation and its proof can be found in, e.g., Vertelli and Kovacevic (1995). What is interesting to observe is that (13) can be viewed independently of (1) and be used in general to simulate a continuous band-limited white noise process. The advantage of this formulation over the classical time-domain formulation is that the sampling rate (which is the sampling simulation rate for a stochastic process) is completely separated from the analysis integration step, so that we can control directly and independently the band-width of the process. The advantage over the frequency-domain formulation is that the coefficients of the series are just samples of the original function, or in the case of a stochastic process they are the simulated samples, and the spectrum of the realization is continuous, not discrete.

5.2 Orthonormality

To prove the orthonormality of the *sinc* functions we make use of the Parseval identity, i.e. $\langle f^H(t), g(t) \rangle = 1/2\pi \langle F^H(\omega), G(\omega) \rangle$, where the superscript *H* denotes the Hermitian conjugate and $F(\omega)$ and $G(\omega)$ are the Fourier transforms of $f(t)$ and $g(t)$, respectively. Moreover the Fourier transform of the *sinc* function is the rectangular function i.e.

$$F[\text{sinc}(t)] = \Pi_{\pi} \quad (14)$$

$$F[\text{sinc}_{\Delta t}(t)] = \Delta t \Pi_{\pi / \Delta t}, \quad (15)$$

where $F[\] = \langle \cdot, e^{-i\omega t} \rangle$ is the linear Fourier transform operator and Π_{π} is the rectangular function defined as $\Pi_{\pi} = 1$ for $-\pi \leq \omega \leq \pi$ and $\Pi_{\pi} = 0$ otherwise. Equation (15) is directly derived from equation (14) by use of the scaling property of the Fourier transform. In the case of equation (14), the orthonormality condition is verified by:

$$\begin{aligned} \langle \text{sinc}(t - n), \text{sinc}(t - m) \rangle &= \langle \text{sinc}(t) * \delta(t - n), \text{sinc}(t) * \delta(t - m) \rangle \\ &= \frac{1}{2\pi} \langle \Pi_{\pi} e^{in\omega}, \Pi_{\pi} e^{-im\omega} \rangle = \frac{1}{2\pi} \langle \Pi_{\pi} e^{i(n-m)\omega} \rangle = \text{sinc}(n - m) = \delta[n - m]. \end{aligned} \quad (16)$$

On the other hand, when we introduce the scale factor Δt , $\langle \text{sinc}_{\Delta t}(t - \Delta tn), \text{sinc}_{\Delta t}(t - \Delta tm) \rangle = \Delta t$ so that we have to normalize our base function by $\sqrt{\Delta t}$ i.e. $s_n(t) = 1/\sqrt{\Delta t} \text{sinc}_{\Delta t}(t - n\Delta t)$ and the orthonormality is verified by repeating the passages of (16).

5.3 The coefficients of the series

In this subsection we compute the coefficients of the orthonormal series expansion

$$f(t) = \sum_{n=1}^{\infty} \langle f(t), s_n(t) \rangle s_n(t), \quad (17)$$

where $s_n(t) = 1/\sqrt{\Delta t} \operatorname{sinc}_{\Delta t}(t - n\Delta t)$. Again using the Parseval identity and considering $\bar{\omega}$ as the band-limit of $f(t)$ we obtain

$$\langle f(t), s_n(t) \rangle = \frac{1}{2\pi} \langle F^H(\omega), \sqrt{\Delta t} \Pi_{\frac{\pi}{\Delta t}} e^{i\omega n\Delta t} \rangle = \frac{\sqrt{\Delta t}}{2\pi} \langle F^H(\omega), e^{i\omega n\Delta t} \rangle = \sqrt{\Delta t} f(n\Delta t). \quad (18)$$

Examining (17) and (18), it is evident that (13) can be considered a Hilbert space framework. Moreover (13) can be read also as an orthogonal but not orthonormal expansion if we consider as base function just $\operatorname{sinc}_{\Delta t}(t - i\Delta t)$.

5.4 The autocorrelation of the process

In this subsection we verify that the *sinc* expansion provides a valid autocorrelation function for a band-limited white noise. In this case we have a closed-form solution for the autocorrelation function that is well known to be again the *sinc* function. For a white-noise process $W(t)$ that is band-limited at $\bar{\omega}$, we can write:

$$W(t) = \sum_{n=0}^{\infty} C_n \operatorname{sinc}_{\Delta t}(t - n\Delta t), \quad (19)$$

where $\Delta t \leq \pi/\bar{\omega}$ and C_n are zero-mean and unit-variance, statistically independent random variables. The autocorrelation function can be written as

$$\begin{aligned} \Phi(t, t') &= E[W(t), W(t')] \\ &= \sum_{n=0}^{\infty} \sum_{m=0}^{\infty} E[C_n C_m] \operatorname{sinc}_{\Delta t}(t - n\Delta t) \operatorname{sinc}_{\Delta t}(t' - m\Delta t) \\ &= \sum_{n=0}^{\infty} E[C_n^2] \operatorname{sinc}_{\Delta t}(t - n\Delta t) \operatorname{sinc}_{\Delta t}(t' - n\Delta t) \\ &= \sum_{n=0}^{\infty} \operatorname{sinc}_{\Delta t}(t - n\Delta t) \operatorname{sinc}_{\Delta t}(t' - n\Delta t). \end{aligned} \quad (20)$$

The series (20) converges to $\operatorname{sinc}_{\Delta t}(\tau)$, where $\tau = t - t'$. To prove it, we represent the function $\operatorname{sinc}_{\Delta t}(t - t')$ for a fixed t' with the orthogonal expansion (13):

$$\begin{aligned} \operatorname{sinc}_{\Delta t}(t - t') &= \sum_{n=0}^{\infty} \operatorname{sinc}_{\Delta t}(n\Delta t - t') \operatorname{sinc}_{\Delta t}(t - n\Delta t) \\ &= \sum_{n=0}^{\infty} \operatorname{sinc}_{\Delta t}(t' - n\Delta t) \operatorname{sinc}_{\Delta t}(t - n\Delta t), \end{aligned} \quad (21)$$

where in the second line we have used the symmetry property of the *sinc* function. Thus the autocorrelation function can be written as $\Phi(t, t') = \operatorname{sinc}_{\Delta t}(t - t') = \operatorname{sinc}_{\Delta t}(\tau)$.

6 TELM ANALYSIS WITH SINC BASIS FUNCTION

In the previous section we have established that the *sinc* expansion can be used to represent a band-limited white noise. In this section we investigate the extension of TELM analysis based on *sinc* functions. For a review of TELM analysis in the time domain the reader should consult Fujimura and Der Kiureghian (2007), while TELM analysis in the frequency domain can be found in Garrè and Der Kiureghian (2009). The extension of TELM in the context of *sinc* expansion or in general in the context of any orthonormal or orthogonal basis is rather straightforward. The governing equation of a stable system, subject to a stochastic input, can be written as:

$$L[X(t)] = F(t), \quad (22)$$

where $L[\]$ is a differential operator. If the system is linear, the response can be obtained by convolving its IRF with the input excitation:

$$X(t) = [h(t) * \hat{F}(t)] = \sum_{n=1}^N \int_0^t \sigma h(t - \tau) s_n(\tau) d\tau u_n = \mathbf{a}(t) \cdot \mathbf{u}, \quad (23)$$

where $h(t)$ is the IRF of the linear system and $a_n = \int_0^t \sigma h(t - \tau) s_n(\tau) d\tau$. As mentioned earlier, filtering can be used to describe colored white noise. If the system is nonlinear, a numerical solution can be used to compute the response $X(t)$ for a given \mathbf{u} . Given the representation in (3), the response $X(t)$ is either an explicit or implicit function of the standard normal variables, i.e. $X(t) = X(t, \mathbf{u})$. Given a response threshold of interest x , at a specific time t_x , the tail probability is defined as $\Pr[x < X(t_x, \mathbf{u})]$. Reliability theory is then used to compute the tail probability by defining a limit-state function $g(x, t_x, \mathbf{u}) = x - X(t_x, \mathbf{u})$ and rewriting the probability statement as $\Pr[g(x, t_x, \mathbf{u}) < 0]$. In the standard normal space the design point \mathbf{u}^* , which is the point belonging to limit-state surface $g(x, t_x, \mathbf{u}) = 0$ with minimum distance from the origin, is then computed. The importance of the design point, whose norm is the reliability index, is described in Koo et al. (2005). Once \mathbf{u}^* is determined, TELM employs FORM to obtain the first-order approximation of the tail probability. If the system is linear, the limit-state surface is a hyperplane with gradient $\mathbf{a}(t)$ and the design point is given in closed form as

$$\mathbf{u}^* = \frac{x}{\|\mathbf{a}(t_x)\|} \frac{\mathbf{a}(t_x)^T}{\|\mathbf{a}(t_x)\|} \quad (24)$$

Given the design point, the gradient of the hyperplane can be determined by reversing (24):

$$\mathbf{a}(t_x) = \frac{x}{\|\mathbf{u}^*\|} \frac{\mathbf{u}^{*T}}{\|\mathbf{u}^*\|} \quad (25)$$

In the nonlinear case, first the design point is computed then the limit-state surface is expanded in Taylor series at the design point:

$$g(x, t_x, \mathbf{u}^*) = x - [X(t_x, \mathbf{u}^*) + \nabla_{\mathbf{u}^*} X(t_x, \mathbf{u}^*) \cdot (\mathbf{u} - \mathbf{u}^*) + \text{h. o. t.}] \quad (26)$$

The first-order approximation of $\Pr[g(x, t_x, \mathbf{u}) < 0]$ is then obtained by keeping the linear terms, resulting in $\Pr[g(x, t_x, \mathbf{u}) < 0] \cong \Phi[-\|\mathbf{u}^*\|]$, where $\Phi[\]$ is the standard normal cumulative probability function. This corresponds to linearizing the limit-state function at the design point, enforcing $\mathbf{a}(t_x) \equiv \nabla_{\mathbf{u}^*} X(t_x, \mathbf{u}^*)$ and defining a tail-equivalent linear system (TELS), as described below. Up to this point, the formulation is applicable to any valid basis functions that describe the input Gaussian process.

In the conventional time-domain TELM formulation, denoting by M the total number of discrete time points in the integration scheme, the IRF $h(t)$ of the TELS is determined by solving the set of equations

$$\sum_{m=1}^M h(t_x - t_m) s_n(t_m) = a_n(t_x), \quad n = 1, \dots, N. \quad (27)$$

To solve this system, the time sampling rate has to be equal to the time integration step, i.e. $N = M$. In other words, the response analysis is dictating the band limit of the represented process. In nonlinear analysis, the time discretization step has to be sufficiently small in order to guarantee convergence and, consequently, a large number of random variables has to be used to represent the input process. Usually this large number of random variables is useful in representing the high frequency content in the excitation, which may not be important relative to the resonant frequencies of the filter and the structure. In the *sinc* formulation there is no such constraint and the solution lies in the subspace of the selected band-limited signals. Thus, we can either obtain the solution of (27) as a min-norm solution of the over-determined system, i.e. $M > N$, or, better in terms of efficiency, we can compute directly the samples of the IRF enforcing $M = N$ and then reconstruct the IRF using again the *sinc* interpolation formula, i.e.,

$$\sum_{m=1}^N h(t_x - t_m) s_n(t_m) = a_n(t_x), \quad n = 1, \dots, N \quad (28)$$

$$h(t) = \sum_{m=1}^N h(m\Delta t) \text{sinc}_{\Delta t}(t - m\Delta t). \quad (29)$$

Once the IRF of the TELS is obtained, methods of linear random vibration analysis are used to compute the statistic of interest for the selected response threshold x .

7 NUMERICAL INVESTIGATION

In this example we examine the computational efficiency gained in TELM analysis by use of the *sinc* formulation. The efficiency of TELM is related to the time used to determine the design point \mathbf{u}^* in the constrained nonlinear optimization problem:

$$\mathbf{u}^* = \operatorname{argmin}\{\|\mathbf{u}\| \mid g(x, t_x, \mathbf{u}) = 0\}. \quad (30)$$

The scheme adopted here is the improved HLRF algorithm proposed by Zhang and Der Kiureghian (1995), which requires computation of the nonlinear response $X(t_x, \mathbf{u})$ and its gradient $\nabla_{\mathbf{u}}X(t_x, \mathbf{u})$. The gradient is computed by the DDM algorithm proposed by Zhang and Der Kiureghian (1993). The computationally most expensive part of the improved HLRF algorithm is that of the gradient, which strongly depends on the number of random variables.

The proposed example is a single-degree-of-freedom oscillator described by the non-degrading hysteretic Bouc-Wen model, which was also investigated by Fujimura and Der Kiureghian (2007). The excitation is due to base motion and is described by $F = -m\ddot{U}_g$, where m is the mass of the oscillator and \ddot{U}_g is a white noise with spectral density $S = 1[\text{m}^2/\text{rad s}^3]$. The mass, damping and stiffness are selected so as to have the fundamental period of 1[Hz] and 5% damping for small-amplitude oscillations. The response threshold $x = 3\sigma_0$ is selected, where σ_0 is the RMS of the corresponding linear oscillator. Figure 1 shows the design-point excitation and response, as well as the IRF and FRF of the TELS. These are for two different sampling rates, which result in band limits of 50[Hz] and 2.5[Hz]. Table 1 shows the reduction in computational time achieved by implementation of the *sinc* expansion with varying sampling rates. It can be seen that accurate results are achieved by sampling rate as large as 0.2[s] with a 20 fold reduction in the number of random variables. Of course this is possible here because the oscillator is not affected by large frequencies, as is evident in the FRF in Figure 1d.

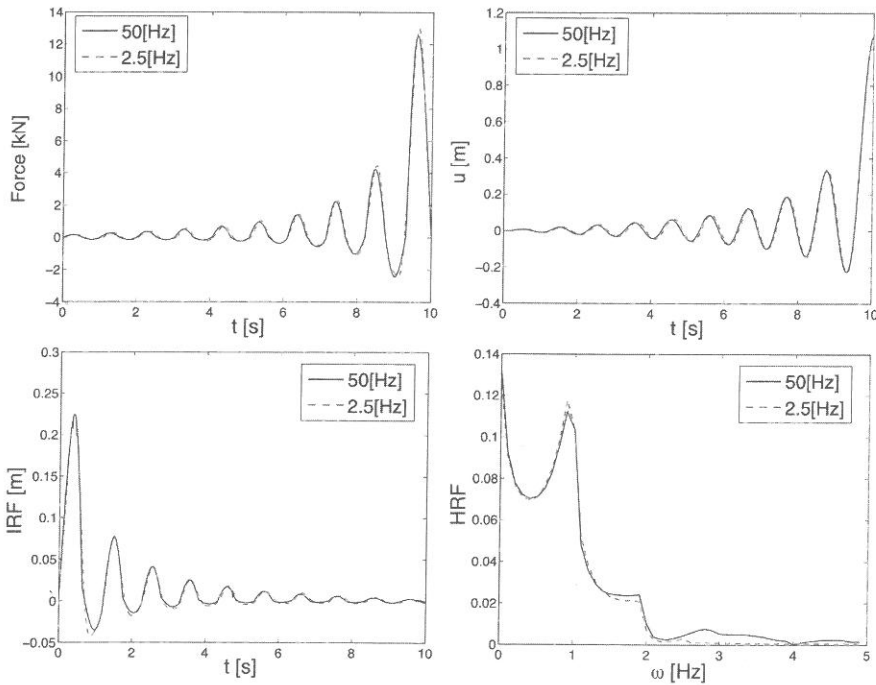


Figure 1: a) Design-point excitation, b) design-point response, c) IRF, d) FRF

Table 1. Efficiency of the TELM based on *sinc* basis functions, time integrations step 0.01[s]

Sampling rate [s]	Band limit [Hz]	N. random variables	Reliability index	Computational time [s]
0.01	50.0	1000	3.122	836
0.02	25.0	500	3.135	321
0.05	10.0	250	3.122	291
0.10	5.0	100	3.122	113
0.20	2.5	50	3.133	51

8 CONCLUSION

In this paper we investigate an alternative method to discretize stochastic processes and its application in TELM analysis. We move from the concept of Hilbert space to represent general signals as expansion of basis functions. From this representation we generate a stochastic process by randomizing the coefficients of the series expansion. In particular, we study the representation of band-limited white noise. Other processes can be modeled through filtering. We employ *sinc* functions as the set of orthonormal basis, but any other valid set of basis can be used. Next, we extend TELM analysis to the *sinc* representation. The advantage of this formulation, as compared to the usual time-domain TELM formulation, is evident by the complete separation and control of the band limit of the process from the time integration step used in the response analysis. For problems in which the high frequency content in the input excitation is not important, the number of random variables used to describe the process can be significantly reduced. The advantage compared to the frequency-domain formulation lies in complete avoidance of the issue of periodicity; furthermore, the represented spectrum is continuous.

A drawback of the *sinc* expansion is that the function does not die off and this reduces its efficiency. This is the reason why the authors are currently exploring other basis functions, including a lower order Lagrange polynomial expansion, to further improve the efficiency.

9 REFERENCES

- Der Kiureghian, A., 2007. The geometry of random vibrations and solution by FORM and SORM. *Probabilistic Engineering Mechanics*, 15(1): 81-90
- Fujimura, K., Der Kiureghian, A., 2007. Tail-Equivalent linearization method for nonlinear random vibration. *Probabilistic Engineering Mechanics*, 22: 63-77
- Garrè, L., Der Kiureghian, A., 2009. Tail-Equivalent linearization method in frequency-domain and application to marine structures. *Marine Structures*, 23: 322-338
- Grigoriu, M., Balopoulou, S., 1993. A simulation method for stationary Gaussian random functions based on the sampling theorem. *Probabilistic Engineering Mechanics*, 8: 239-254
- Koo, H., Der Kiureghian, A., Fujimura, K., 2005. Design point excitation for nonlinear random vibration. *Probabilistic Engineering Mechanics*, 20(2): 136-147
- Rice, S.O., 1954. Mathematical analysis of random noise. *Selected Papers on Noise and Stochastic Processes*, (Edit by Nelson Wax), Dover 133-294.
- Shinozuka, M., 1972. Digital simulation of random process. *Journal of Sound and Vibration*, 25: 191-204
- Shinozuka, M., Deodatis, G. 1991. Simulation of stochastic process by spectral representation. *American Society of Mechanical Engineers*, 25: 191-204
- Vertelli, M., Kovacevic J., 1995 Wavelets and subband coding *Prentice Hall PTR*.
- Zhang, Y., Der Kiureghian, A., 1993. Dynamic response sensitivity of inelastic structures. *Computer Method in Applied Mechanics and Engineering*, 108: 23-36
- Zhang, Y., Der Kiureghian, A., 1993. Two improved algorithms for reliability analysis in reliability in reliability and optimization of structural systems. *Rackwitz R, Augusti G, Borri A, editors. Proceeding of the 6th IFIP WG 7.5 working conference on reliability and optimization of structural systems.*

Author index

- Alibrandi, U. 237
Anders, A. 25, 33
Ando, K. 57
- Berggreen, C. 183
Bourinet, J.-M. 83
Breitung, K. 41
Broccardo, M. 261
Bucher, C. 49, 223
- Der Kiureghian, A. 191, 245, 261
Dimentberg, M.F. 223
Dimitrov, N. 183
Dubourg, V. 83
- Faber, M. 199
Friis-Hansen, P. 183
Fu, G. 127
Furuta, H. 57, 215
- Gardoni, P. 143
Gidaris, I. 17
Ginda, G. 119
- Haukaas, T. 1
Hera, A. 223
- Ishibashi, K. 57, 215
- Kechejian, H. 231
Kimiæifar, A. 111
Koduru, S.D. 245
Konakli, K. 207
Kostandyan, E.E. 135
Kutz, N. 75
- Liu, L. 127
Lund, E. 111
- Maes, M.A. 9
Mahsuli, M. 1
Mardfekri, M. 143
Marmo, F. 103
Márquez-Dominguez, S. 167
Mašlak, M. 119
Michalski, A. 65
- Naess, A. 9, 223
Nakatsu, K. 57, 215
Nielsen, J.S. 175
Nielsen, S.R.K. 151, 159
Nishijima, K. 25, 33
- Ohanyan, V. 231
- Papaioannou, I. 65, 91
Pozzi, M. 191
- Qin, J. 199
- Sessa, S. 103
Sichani, M.T. 151, 159
Song, J. 75
Sørensen, J.D. 111, 135, 167, 175
Straub, D. 65, 91
Sudret, B. 83
- Taflanidis, A.A. 17
Takahashi, K. 57, 215
Thoft-Christensen, P., 159
Thomsen, O.T. 111
- Umekage, T. 215
- Valoroso, N. 103
- Wolff, S. 49
- Yen, P. 127
You, J. 127
- Zonta, D.
Zwirgmaier, K. 91

This volume contains 32 papers by renowned international experts on the latest advances in structural reliability and optimization methods, probabilistic models, engineering risk analysis and decision making, reliability-based optimal design, and applications in various engineering domains, including infrastructure systems, wind turbines, bridges, natural hazards, and seismic analysis.

All contributions were presented at the 16th Working Conference of the International Federation of Information Processing (IFIP) Working Group 7.5 on Reliability and Optimization of Structural Systems, which was held at the American University of Armenia, Yerevan, June 24-27, 2012. Working Group 7.5's purposes are to promote modern theories and methods of structural and system reliability and optimization; to stimulate research, development and application of structural and system reliability and optimization theories; to further the dissemination and exchange of information on reliability and optimization of structural systems; and to encourage education in structural and system reliability and optimization theories.

This book is intended for civil and mechanical engineers working and researching in structural and system optimization and risk and reliability analysis, as applied to structural, mechanical and infrastructural systems.

